

# Influence of Spray Jet Technology on Bond Strength of Asphalt and Pavement Life

by  
Eugenie Pienaar

Thesis presented in fulfilment of the requirements for the degree of Master  
of Engineering in Civil Engineering in the Faculty of  
Engineering at Stellenbosch University



**Supervisor:** Dr Chantal Rudman

**Co-supervisor:** Prof Kim Jenkins

March 2020



UNIVERSITEIT • STELLENBOSCH • UNIVERSITY  
jou kennisvenoot • your knowledge partner

### Plagiaatverklaring / Plagiarism Declaration

- 1 Plagiaat is die oorneem en gebruik van die idees, materiaal en ander intellektuele eiendom van ander persone asof dit jou eie werk is.  
*Plagiarism is the use of ideas, material and other intellectual property of another's work and to present is as my own.*
- 2 Ek erken dat die pleeg van plagiaat 'n strafbare oortreding is aangesien dit 'n vorm van diefstal is.  
*I agree that plagiarism is a punishable offence because it constitutes theft.*
- 3 Ek verstaan ook dat direkte vertalings plagiaat is.  
*also understand that direct translations are plagiarism.*
- 4 Dienooreenkomstig is alle aanhalings en bydraes vanuit enige bron (ingesluit die internet) volledig verwys (erken). Ek erken dat die woordelike aanhaal van teks sonder aanhalingstekens (selfs al word die bron volledig erken) plagiaat is.  
*Accordingly all quotations and contributions from any source whatsoever (including the internet) have been cited fully. I understand that the reproduction of text without quotation marks (even when the source is cited) is plagiarism.*
- 5 Ek verklaar dat die werk in hierdie skryfstuk vervat, behalwe waar anders aangedui, my eie oorspronklike werk is en dat ek dit nie vantevore in die geheel of gedeeltelik ingehandig het vir bepunting in hierdie module/werkstuk of 'n ander module/werkstuk nie.  
*I declare that the work contained in this assignment, except where otherwise stated, is my original work and that I have not previously (in its entirety or in part) submitted it for grading in this module/assignment or another module/assignment.*

<b>Studentenommer / Student number</b>	<b>Handtekening / Signature</b>
Eugenie Pienaar <b>Voorletters en van / Initials and surname</b>	March 2020 <b>Datum / Date</b>

## ABSTRACT

Tack coats promote bonding between pavement layers. This allows the pavement structure to behave as a single unit whilst providing adequate strength. The lack of poor bonding leads to a pavement structure comprising of multiple independent (thin) layers. This in turn will be unable to withstand traffic-imposed loading potentially resulting in pavement distress. The occurrence contributes to fatigue distress such as cracking as well rutting significantly reducing pavement life.

Various studies have shown that interface bonding between pavement layers (provided by tack coats) has a significant effect on pavement performance. Some of these studies also investigated pavement response due to external factors such as traffic loading, existing road surface conditions and temperature. However, it is also reported that intrinsic factors (e.g. tack coat application method) of the tack coat are found to contribute to the degree of bonding achieved. Various conventional methods are available for application of the tack coat. Alternatively, Spray Jet technology developed by the Wirtgen Group is a more modern method used to apply tack coats. The technology enables the immediate construction of the asphalt surfacing once the tack coat is sprayed onto the surface.

Preliminary research shows the economical advantages of the use of the technology but some logistical disadvantages still remain when used in larger projects. Some of the intermediate disadvantages however can be outweighed by the long term benefits provided by the technology. The advantages creates the drive to employ the technology currently in smaller projects such as municipal roads. It also promotes the use of the technology on an international level.

The technology is investigated by means of a two-phase project in collaboration with Pisa University. The study includes laboratory work, linear-elastic analysis and mechanistic design as part of the first phase (preliminary research study). The second phase (current study) includes the simulation of the conditions from the first phase through Finite Element Modelling in order understand the results obtained and behaviour observed. The purpose of the analyses is mainly to develop an understanding of the influence of shear strength on the pavement life and which factors influence the shear developed within the tack coat. This will provide insight on the potential advantages or disadvantages of the use of the technology.

Both academic institutions considered representative pavement structures and conditions during analyses performed during *Phase 1*. This phase consists of two components: linear-elastic analysis and laboratory testing. A linear-elastic analysis was completed by Pisa and Stellenbosch University where two types of laboratory experiments were completed by Pisa University. Although, the results vary in terms of degree of stress observed in the pavement, all results favoured the application by means of tack coat compared to other methods. Extended research is required to provide a broader understanding however. The preliminary analysis highlights the influence of material stiffness and layer thickness and its relation with shear generation with certain regions of the pavement structure. The combinations of these two parameters are found to have a significant impact on the pavement life with regards to fatigue and serviceability. From the analyses, the material stiffness was identified as the most critical parameter.

For the current research, contradictory results were obtained from the two different simulated models. The conditions of these models were set-up to replicate conditions of the Leutner shear testing device and pavement analysis of national pavement structures with some alterations. The *Leutner Shear Test* model confirmed the favourable outcome for the use of Spray Jet technology. The simulated FEM model used for the *Pavement Analysis* showed that tack coat application is unnecessary. The results suggest that pavement performance can be improved by simply adhering to better compaction of granular layers to withstand the same loading conditions. It should be noted that these results were obtained with a structure with poor subgrade conditions which largely influences the outcome of the analysis. Similar as for preliminary research, the *Leutner Shear Test* model emphasised the influence of material stiffness on the type of bonding achieved under certain conditions. For the *Pavement Analysis* model, the layer thickness is recognised as the most crucial parameter having a great influence on predicted pavement life (fatigue life). The advantages of the use of Spray Jet Technology and the favourable results recommends the implementation of the technology where additional research would accentuate its use.

## ABSTRAK

Kleeflae bevorder die binding tussen plaveisellae wat lei tot samehangende gedrag van die plaveiselstruktuur. Dit lei tot genoegsame sterkte van die plaveiselstruktuur. Die gebrek aan behoorlike binding in 'n plaveiselstruktuur veroorsaak dat die plaveisellae lae as veelvoudige, onafhanklike lae optree. Wanneer hierdie lae blootgestel word aan verkeerslading kan dit lei tot die ewekansige verswakking van die struktuur. Hierdie gedrag dra by tot vermoeidheidsverswakking soos kraakvorming en spoorvorming wat plaveisellewe aansienlik verkort.

Verskeie studies beklemtoon dat koppelvlak binding tussen die plaveisellae, wat deur die kleeflaag verskaf word, 'n noemenswaardige impak het op die werkverrigting van die plaveisel. Sommige van hierdie studies het ook ondersoek ingestel op die impak van eksterne faktore soos verkeerslading, bestaande padoppervlak kondisies en temperatuur op plaveiselwerkverrigting. Nogtans, is dit ook bevind dat interne faktore soos die aanwendingsmetode van die kleeflaag, ook bydrae tot die verkrygbare binding onder sekere kondisies. Verskeie tegnologieë word gebruik in hierdie verband, waarvan die spuitbalk tegnologie, ontwikkel deur die Wirtgen Groep, 'n moderne metode is wat in hierdie hoedanigheid gebruik word. Die tegnologie gee die geleentheid dat onmiddellike konstruksie van die asfaltlaag, nadat die kleeflaag op die oppervlak geplaas is.

Voorafgaande navorsing toon die ekonomiese voordele van die gebruik van die tegnologie maar logistiese uitdaging in terme van aanwending van die tegnologie op groter projekte is geïdentifiseer. Ten spyte hiervan, is dit gevind dat die intermediêre uitdagings oorheers word deur die langtermyn voordele wat deur die tegnologie gebied word. Hierdie voordele voorsien die dryfkrag om die implikasies in terme van plaveisel werkverrigting te beklemtoon in munisipaliteit verwante padprojekte. Dit bevorder ook die gebruik van hierdie tegnologie op 'n internasionale vlak.

Die tegnologie is ondersoek deur middel van 'n twee fase projek in samewerking met Universiteit van Pisa. Die eerste fase van die studie (voorafgaande navorsingsprojek) sluit in laboratoriumwerk, lineêrelastiese analyses en meganistiese ontwerp. Die tweede fase (huidige studie) behels die simulاسie van kondisies ondersoek gedurende die eerste fase om die resultate verkry en waarnemings wat gemaak is te bekragtig. Die doel van die analyses is om die invloed van skuifsterkte op plaveisellewe te verstaan en faktore wat die skuifskuur van die koppelvlak beïnvloed, te identifiseer.

Beide akademiese instellings het verteenwoordigende plaveiselstrukture oorweeg vir die analyses wat uitgevoer is gedurende *Fase 1*. Hierdie fase bestaan uit twee komponente: 'n lineêrelastiese analise en laboratoriumtoetse. 'n Lineêrelastiese analise is uitgevoer deur beide Stellenbosch en Pisa Universiteit waar twee tipes laboratoriumtoetse deur Pisa Universiteit voltooi is. Alhoewel, die resultate vanuit die verskillende analyses verkry verskil in terme van ordegrootte, was alle resultate ten gunste van die gebruik van die tegnologie in vergelyking met ander konvensionele metodes wat tans gebruik word. Meer uitgebruide toetse word verlang om genoegsame inligting te verskaf wat hierdie waarneming kan bevestig. Die voorafgaande analyses beklemtoon die invloed van materiaalstyfheid en laagdikte en die verwantskap met ontwikkeling van skuifskuur binne sekere gedeeltes van die plaveiselstruktuur. Die kombinasie van hierdie twee faktore toon 'n groot invloed op die resultate verkry in terme van plaveisellewe (vermoei- en dienslewe). Oor die algemeen, is die materiaalstyfheid as die mees kritiese veranderlike geïdentifiseer.

Vir die huidige navorsing, is resultate verkry teenstrydig tussen die twee gesimuleerde modelle. Die modelkondisies is van so aard dat dit werklike kondisies voorstel van die Leutner skuiftoets en plaveisel analise van gekose verteenwoordigende plaveiselstrukture. Sommige aanpassings is aangebring tot die modelle. Die *Leutner Skuifskuur Toets* bevestig die waarnemings gemaak gedurende die lineêr-elastiese analise(s) waar die resultate ten gunste is vir die gebruik van die spuitbalk tegnologie. Die tweede model, *Plaveisel Analise* model, toon dat die gebruik van 'n kleeflaag onnodig is en dat dieselfde sterkte kapasiteit bereik kan word deur genoegsame kompaksie van die granulêre lae in die plaveiselstruktuur onder dieselfde kondisies. Hierdie resultate is verkry vanuit 'n model wat bestaan uit swak grondlaag kondisies wat aansienlik die resultate kan beïnvloed. Soortgelyk aan die lineêr-elastiese analyses, het die *Leutner Skuifskuur Toets* die invloed van materiaalstyfheid en laagdikte op die tipe binding verkry onder sekere kondisies beklemtoon. Vir die *Plaveisel Analise* model, is slegs die laagdikte geïdentifiseer as die mees kritiese veranderlike met die grootste invloed op die beraamde plaveisellewe (vermoëlewe spesifiek). Die voordele van die gebruik van die spuitbalk tegnologie en die voordelige resultate beklemtoon die implementering van die tegnologie alhoewel addisionele navorsing verlang word om hierdie bevinding te bevestig.

## ACKNOWLEDGEMENTS

Firstly, I would like to thank Helpmekaar Studiefonds (HSF) for funding my postgraduate studies allowing the opportunity to further my studies.

***“No one becomes successful without lots of hard work, support from others, and a little luck.” – R. Conway***

I have crossed paths with many people who have become important figures during my postgraduate journey who has played a significant role in my individual growth and academic career. I am truly thankful for each and every one who has contributed to all my success achieved. Thank you for always believing in me especially during times when I did not believe in myself. Thank you for all of the support and lesson learnt. I would like to express my profound gratitude to each of these important figures.

***“You can do anything as long as you have the passion, the drive, the focus, and the support.” – S. Bryan***

I would like to thank my thesis advisors Prof Kim Jenkins and Dr Chantal Rudman. You have become my “Engineering parents” during my postgraduate studies – providing a friendly working environment. Thank you for always being available whenever I had a question about my research or writing. I am grateful that you have contributed to setting the foundation of my academic career and enhanced my interest in the field of pavement engineering.

- Prof, thank you for sharing all of your insightful knowledge and wisdom. Your kindness and wisdom have taught us all valuable lessons and has peaked my interest in the particular research field. I am eternally grateful for everything you have taught me during my studies.
- Dr Rudman, you have been my “mother” figure during this period. Thank you for your endless support, guidance and patience. There is not enough words to be said to express my gratitude. You have taught me a lot of valuable (life) lessons.

A great component of the research would not have been possible without the assistance of Dr Johan Gerber. Thank you for your endless guidance and patience for the FEM component of the research. Your time, input and insights have been of significant value for the current research study.

Acknowledgement is also given to Lorenzo Bianchi and Alessandro Marradi from the Department of Civil and Industrial Engineering at University of Pisa, Italy, for the collaboration of research during the first phase of the research project by means of pavement analyses and laboratory work. A component of the current research would not have been possible without their corroboration in terms of preliminary testing and findings. In line with the research, I would also like to show my gratitude towards Prof Jenkins and Marco Garofalo (from the Wirtgen Group) for allowing me the opportunity to be part of the research study.

***“God has blessed me with an amazing family, friends and work colleagues that have been my joy, support, and my sanity. I don’t know what I would do without them.” – J. Loren***

The completion of the thesis would not have been possible without my support structure at the university. To all my colleagues (especially the *Pavement Specials*) and fellow post graduates – thank you for your continuous support and encouragement. You have become my second family. It has been

quite the journey and I am thankful for sharing the experience with you all. You have made it an unforgettable experience which I will always treasure.

To all my friends, the old and the new that has crossed my path – who has supported and encouraged me during very difficult and trying times – Thank you for always believing in me and always pushing me to deliver my best.

***“Be strong, be fearless and be beautiful. And believe that anything is possibly when you have the right people there to support you.” – M. Copeland***

To my father, my sister and my grandmother. Thank you for being my rocks – always there to motivate me and support me during the high and the low points. I am truly grateful for all your endless love and support which has carried me through my studies. Without you, I would not have been able to achieve all my successes in life. Great appreciation is also shown for other family members providing support and motivating me in difficult times.

***Mom, You are an angel as beautiful as can be. Who sits upon a cloud and watches over me. My mother will guide me from heaven up above. She is my guardian angel sending me her love. You left beautiful memories, your love is still my guide. Although I cannot see you, I know you're always by my side.***

To my late mother. Thank you for teaching me perseverance, gratitude and kindness. Your courage continues to be an inspiration. Your courage has always guided me especially throughout my academic career - helping me to never give up no matter the difficulty of the circumstance I found myself in. You have always motivated me to give my best and work hard to achieve my goals – to keep pursuing my passions no matter how hard it would be or how long it would take. This thesis is dedicated to you mom! It saddens me that you are not able to experience the joy thereof with me.

***“In my deepest, darkest moments, what really got me through was prayer. What I’ve discovered is that intimate connection and communication with my Creator will always get me through because I know my support, my help, is just a prayer away.” – I. Vanzant***

This achievement would not have been possible without our Creator, God Almighty blessing me with good health and the ability to undertake the research study. I have been blessed with the knowledge and perseverance to complete the research study satisfactorily.

# TABLE OF CONTENTS

<b>PLAGIAATVERKLARING / PLAGIARISM DECLARATION</b>	<b>I</b>
<b>ABSTRACT</b>	<b>II</b>
<b>ABSTRAK</b>	<b>IV</b>
<b>ACKNOWLEDGEMENTS</b>	<b>VI</b>
<b>LIST OF FIGURES</b>	<b>XII</b>
<b>LIST OF TABLES</b>	<b>XX</b>
<b>LIST OF ABBREVIATIONS</b>	<b>XXIV</b>
<b>LIST OF SYMBOLS</b>	<b>XXVI</b>
<b>GLOSSARY OF TERMS</b>	<b>XXX</b>
<b>CHAPTER 1: INTRODUCTION</b>	<b>1</b>
1.1 Background .....	1
1.2 Problem Statement and Research Need.....	1
1.3 Objectives .....	2
1.4 Limitations .....	3
1.5 Report structure.....	3
<b>CHAPTER 2: LITERATURE REVIEW</b>	<b>5</b>
2.1 Introduction .....	5
2.2 Tack coats.....	5
2.2.1 Introduction .....	5
2.2.2 Tack coat materials .....	6
2.2.3 Tack coat application .....	17
2.2.4 Tack coat application methods.....	21
2.3 Characterisation of interlayer bond strength .....	28
2.3.1 Interlayer bonding evaluation .....	29
2.3.2 Factors influencing interlayer shear bonding .....	47
2.3.3 Influence on residual pavement life .....	58
2.3.4 Impact of factors on interlayer strength .....	61
2.4 Pavement Analysis and Design .....	61
2.4.1 Pavement structure and design philosophy .....	62
2.4.2 South African Mechanistic-Empirical Design Method .....	63
2.5 Finite Element Method .....	71
2.5.1 Introduction .....	71
2.5.2 Pavement design.....	71
2.5.3 Interlayer bonding .....	71
2.6 Synthesis of literature review .....	73

<b>CHAPTER 3: PRELIMINARY RESEARCH</b>	<b>75</b>
<hr/>	
3.1 Research Overview .....	75
3.2 Preliminary Research: Stellenbosch University .....	77
3.2.1 Research background .....	77
3.2.2 Analysis approach .....	77
3.2.3 Results and findings .....	82
3.2.4 Shear stresses .....	82
3.2.5 Stresses in layers.....	88
3.2.6 Strains .....	90
3.2.7 Pavement life .....	93
3.2.8 Conclusions .....	98
3.3 Preliminary Research: Pisa University .....	99
3.3.1 Research background .....	99
3.3.2 Empirical Testing.....	99
3.3.3 Linear-Elastic Analysis.....	104
3.4 Comparative Study of Preliminary Linear-Elastic Analysis.....	116
3.4.1 Introduction .....	116
3.4.2 Loading Parameters .....	117
3.4.3 Pavement Structure considerations .....	118
3.4.4 Performance Analysis .....	121
3.5 Significance of bonding and tack coat application .....	132
3.5.1 Introduction .....	132
3.5.2 Emulsion tanker versus Spray Jet paver .....	132
3.5.3 Effect of bonding condition on Fatigue Life.....	133
3.6 Synthesis of preliminary research.....	134
<b>CHAPTER 4: METHODOLOGY</b>	<b>136</b>
<hr/>	
4.1 Introduction .....	136
4.2 Leutner Shear Test Method .....	137
4.2.1 Introduction .....	137
4.2.2 Model set-up.....	138
4.2.3 Parts .....	139
4.2.4 Properties .....	142
4.2.5 Assembly .....	149
4.2.6 Boundary conditions and constraints .....	150
4.2.7 Meshing Techniques and Element Types .....	157
4.2.8 Analysis .....	160
4.2.9 Acquisition of results .....	161
4.2.10 Synthesis of analysis .....	163
4.3 Pavement analysis .....	164
4.3.1 Introduction .....	164
4.3.2 Model set-up.....	166

4.3.3 Parts and properties .....	167
4.3.4 Boundary and loading conditions .....	170
4.3.5 Meshing techniques.....	174
4.3.6 Acquisition of results .....	176
4.3.7 Synthesis of analysis .....	177
4.4 Synthesis of methodology .....	179
<b>CHAPTER 5: RESULTS AND INTERPRETATION</b>	<b>180</b>
<hr/>	
5.1 Introduction .....	180
5.2 Leutner Shear Test Model.....	181
5.2.1 Introduction .....	181
5.2.2 Shear stress distribution .....	182
5.2.3 Interface bonding.....	186
5.2.4 Critical pavement parameters .....	189
5.2.5 Tack coat properties .....	193
5.2.6 Test Configuration: Gap Width .....	196
5.2.7 Summary of Results .....	196
5.2.8 Model 1 versus Preliminary Research .....	197
5.3 Pavement Analysis Model.....	200
5.3.1 Introduction .....	200
5.3.2 Interface bonding.....	202
5.3.3 Normal stresses and normal strains .....	204
5.3.4 Horizontal strains.....	205
5.3.5 Vertical strains .....	208
5.3.6 Pavement life prediction .....	210
5.3.7 Conclusion.....	214
5.3.8 Model 2 versus preliminary laboratory work .....	214
5.4 Finite Element Model Comparison: Model 1 versus Model 2 .....	215
5.4.1 Introduction .....	215
5.4.2 Testing conditions.....	216
5.4.3 Shear stresses .....	217
5.5 Synthesis of Results Interpretation.....	218
<b>CHAPTER 6: CONCLUSIONS AND RECOMMENDATIONS</b>	<b>220</b>
<hr/>	
6.1 Conclusions .....	220
6.1.1 Preliminary Research .....	220
6.1.2 Laboratory study.....	222
6.1.3 Leutner Shear Test Model.....	222
6.1.4 Pavement Modelling using FEM .....	223
6.2 Recommendations .....	225
6.2.1 Leutner Shear Model .....	225
6.2.2 Pavement Analysis Model.....	226
6.2.3 Expanded Laboratory Testing .....	226

<b>REFERENCES</b>	<b>227</b>
<b>APPENDICES</b>	<b>234</b>
<hr/>	
Appendix A: Stellenbosch Preliminary Analysis Results .....	235
Appendix A1: Shear Stresses .....	236
Appendix A2: Normal Stresses.....	239
Appendix A3: Strains.....	241
Appendix A4: Pavement Life.....	243
Appendix B: Pisa Preliminary Analysis Results.....	245
Appendix B1: Preliminary laboratory and field-testing results .....	246
Appendix B2: Linear-Elastic Analysis Results .....	248
Appendix C: Preliminary Comparative Analysis.....	249
Appendix C1: Experimental Frameworks.....	250
Appendix C2: Sensitivity Analysis.....	252
Appendix D: Finite Element Model Set Up .....	254
Appendix D1: Creation of Model 1 .....	255
Appendix D2: Analysis Steps for Model 1 .....	257
Appendix D3: Boundary Conditions and Constraints for Model 1 .....	260
Appendix D4: Meshing an Mesh Controls for Model 1 .....	262
Appendix D5: Element Types for Model 1 .....	270
Appendix D6: Boundary Conditions for Model 2.....	275
Appendix D7: Element Types for Model 2 .....	276
Appendix E: Finite Element Analysis.....	277
Appendix E1: Leutner Shear Model .....	278
Appendix E2: Pavement Analysis Model .....	283
Appendix F: Stress distribution in pavements with Burmister Theory .....	287

## LIST OF FIGURES

<b>Figure 1.5a:</b> Chapter layout .....	3
<b>Figure 2.2.1a:</b> Slippage failure .....	5
<b>Figure 2.2.2.1a:</b> Bitumen binder and cutback bitumen used as tack coat materials .....	6
<b>Figure 2.2.2.1b:</b> Bitumen emulsions used as tack coat materials .....	7
<b>Figure 2.2.2.4a:</b> Emulsion process .....	13
<b>Figure 2.2.2.4b:</b> Illustration of cationic and anion.....	14
<b>Figure 2.2.2.4c:</b> Bitumen emulsion setting.....	14
<b>Figure 2.2.2.4d:</b> Application of Elasto-Tack with spray paver .....	16
<b>Figure 2.2.2.4a:</b> Uniform tack coat coverage .....	17
<b>Figure 2.2.3.1b:</b> Tack coat application procedure .....	17
<b>Figure 2.2.3.2a:</b> Breaking and setting of bitumen emulsion .....	18
<b>Figure 2.2.3.2b:</b> Bitumen emulsion bond development.....	18
<b>Figure 2.2.3.3a:</b> Tack coat coverage .....	19
<b>Figure 2.2.3.4a:</b> Pick-up by haul truck tyres .....	20
<b>Figure 2.2.4.1a:</b> Tack coat application equipment .....	21
<b>Figure 2.2.4.1b:</b> Application of tack coat with hand sprayer.....	22
<b>Figure 2.2.4.2a:</b> Distribution truck setup.....	22
<b>Figure 2.2.4.2b:</b> Spray bar assembly.....	22
<b>Figure 2.2.4.2c:</b> Distribution truck setup.....	23
<b>Figure 2.2.4.2d:</b> Proper nozzle setting.....	23
<b>Figure 2.2.4.2e:</b> Uniform tack coat application with double and triple overlapping .....	24
<b>Figure 2.2.4.2f:</b> Correct spray bar height.....	24
<b>Figure 2.2.4.2g:</b> Incorrect spray bar height .....	24
<b>Figure 2.2.4.3a:</b> Spray bar valve arrangement .....	25
<b>Figure 2.2.4.3b:</b> Spray paver with material transfer vehicle .....	25
<b>Figure 2.2.4.4a:</b> Emulsion break process.....	26
<b>Figure 2.2.4.4b:</b> Spray Jet technology by Vögele.....	26
<b>Figure 2.2.4.4c:</b> Evaporation of water .....	26
<b>Figure 2.2.4.4d:</b> Spray Jet Technology components.....	27
<b>Figure 2.2.4.4e:</b> Spray Jet spray nozzles .....	27
<b>Figure 2.2.4.5a:</b> Uniform tack coat coverage .....	28
<b>Figure 2.3a:</b> Tyre suction phenomenon.....	28
<b>Figure 2.3b:</b> Separation modes.....	28
<b>Figure 2.3c:</b> Shear-tensile separation .....	29
<b>Figure 2.3.1a:</b> Working schemes of destructive methods used for interlayer testing .....	29
<b>Figure 2.3.1b:</b> Destructive test method categories.....	30
<b>Figure 2.3.1.1a:</b> Torque meter.....	31
<b>Figure 2.3.1.2a:</b> Leutner shear test.....	32
<b>Figure 2.3.1.2b:</b> Leutner shear test .....	33
<b>Figure 2.3.1.2c:</b> Shear force-displacement curve for Leutner test.....	33
<b>Figure 2.3.1.2d:</b> Setup of LPDS test device.....	33
<b>Figure 2.3.1.2e:</b> Schematisation of Double Shear Test.....	34
<b>Figure 2.3.1.2f:</b> Schematization and illustration of DST device.....	35

<b>Figure 2.3.1.3a:</b> Direct shear test with loading versus Directs Shear test without loading .....	35
<b>Figure 2.3.1.3b:</b> Shear Fatigue Test .....	36
<b>Figure 2.3.1.3c:</b> Shear stress-displacement curve for Shear Fatigue Test.....	36
<b>Figure 2.3.1.3d:</b> ASTRA shear test device .....	37
<b>Figure 2.3.1.3e:</b> ASTRA direct shear test device with normal load .....	37
<b>Figure 2.3.1.3f:</b> Shear stress-displacement curve for Direct Shear Test .....	38
<b>Figure 2.3.1.4a:</b> Direct tensile test .....	39
<b>Figure 2.3.1.4b:</b> Pull-Off Device .....	39
<b>Figure 2.3.1.4c:</b> Schematic of ITT device .....	40
<b>Figure 2.3.1.4d:</b> ITS calculation parameters .....	40
<b>Figure 2.3.1.4e:</b> Testing device .....	41
<b>Figure 2.3.1.4f:</b> Specimen shapes .....	41
<b>Figure 2.3.1.4g:</b> Load-displacement curves .....	41
<b>Figure 2.3.1.4h:</b> Testing device.....	41
<b>Figure 2.3.1.4i:</b> Wedge Splitting Test Setup .....	42
<b>Figure 2.3.2.1a:</b> Bonding strength of different asphalt on steel surface.....	48
<b>Figure 2.3.2.1b:</b> Bonding strength of different asphalt on asphalt surface .....	48
<b>Figure 2.3.2.1c:</b> Variation of bonding strength for different surface types .....	49
<b>Figure 2.3.2.1d:</b> Three types of interlayer surfaces.....	50
<b>Figure 2.3.2.1e:</b> Shear resistance for two bitumen mixtures .....	51
<b>Figure 2.3.2.1f:</b> Macrotecture and microtexture .....	51
<b>Figure 2.3.2.1g:</b> Interlayer bonding with contamination condition .....	52
<b>Figure 2.3.2.2a:</b> Effect of curing time on peak shear stress .....	53
<b>Figure 2.3.2.2b:</b> Variation in interlayer shear strength .....	54
<b>Figure 2.3.2.2c:</b> Effect of curing time on peak shear stress.....	55
<b>Figure 2.3.2.2d:</b> Temperature dependency on peak shear stress .....	55
<b>Figure 2.3.2.3a:</b> Sample layer configuration.....	56
<b>Figure 2.3.2.3b:</b> Force-deformation curves with standard deviation for gap width configurations.....	57
<b>Figure 2.3.2.3c:</b> In-layer and interlayer shear testing.....	57
<b>Figure 2.3.2.3d:</b> Schematic diagram of modified Leutner load frame .....	58
<b>Figure 2.3.3a:</b> Average interface shear strength results for location.....	59
<b>Figure 2.3.3b:</b> Average interface shear strength of gradient service time.....	60
<b>Figure 2.3.3c:</b> Stress-displacement curves of gradient service time .....	60
<b>Figure 2.3.3d:</b> Average interface shear strength and fail displacement on rutting and upheaval specimens .....	60
<b>Figure 2.3.3e:</b> Stress-displacement curves of upheave and rutting specimens .....	61
<b>Figure 2.4.1a:</b> Typical pavement structure.....	62
<b>Figure 2.4.2.1a:</b> Schematic representation of the main components.....	63
<b>Figure 2.4.2.1b:</b> Illustration of SAMDM analysis procedure .....	64
<b>Figure 2.4.2.3a:</b> Wheel load distribution.....	67
<b>Figure 2.4.2.3b:</b> Wheel configuration.....	67
<b>Figure 2.4.2.3c:</b> Tensile strain at bottom of asphalt layer.....	68
<b>Figure 2.4.2.3d:</b> Critical parameter and location for granular layers .....	69
<b>Figure 2.4.2.3e:</b> Crack Propagation asphalt layer.....	70
<b>Figure 2.5.2a:</b> Near pavement surface stresses induced by tyre loading.....	71

<b>Figure 2.5.3a:</b> Near pavement surface stresses induced by tyre loading.....	72
<b>Figure 2.5.3b:</b> Shear stress distribution.....	72
<b>Figure 2.5.3c:</b> Schematic geometry of FE models.....	73
<b>Figure 2.5.3d:</b> Schematic geometry of FE models .....	73
<b>Figure 3.1a:</b> Experimental framework for research study.....	75
<b>Figure 3.1b:</b> Schematic representation of the research study .....	76
<b>Figure 3.1c:</b> Chapter layout.....	76
<b>Figure 3.2.1a:</b> Phase 1 Experimental Design .....	77
<b>Figure 3.2.2.2a:</b> Three frictions defined for linear-elastic analysis .....	80
<b>Figure 3.2.2.3a:</b> Case combinations.....	81
<b>Figure 3.2.3a:</b> Structure of result discussion .....	82
<b>Figure 3.2.4a:</b> Shear stress results measured Below Wheel .....	83
<b>Figure 3.2.4b:</b> Shear stress development for Case1 T1 loading condition .....	83
<b>Figure 3.2.4c:</b> Analysis location points .....	84
<b>Figure 3.2.4d:</b> Comparative analysis of testing parameters for HF condition.....	86
<b>Figure 3.2.4e:</b> Comparative analysis of testing parameters for MF condition .....	86
<b>Figure 3.2.4f:</b> Comparative analysis of testing parameters for LF condition .....	87
<b>Figure 3.2.5.1a:</b> Critical location and parameter for granular layers .....	88
<b>Figure 3.2.5.1b:</b> Deviator stress.....	88
<b>Figure 3.2.5.2a:</b> Normal stress development for Case 1 Tyre 1 (MPa).....	88
<b>Figure 3.2.5.3a:</b> Stress block indicating stress directions .....	89
<b>Figure 3.2.5.3b:</b> Deviator stresses for Below Wheel (kPa) .....	90
<b>Figure 3.2.6.2a:</b> Strain for asphalt layer .....	90
<b>Figure 3.2.6.2b:</b> Horizontal strains for T1 and T2 loading conditions (Microstrain) .....	91
<b>Figure 3.2.6.2c:</b> Strain for asphalt layer.....	91
<b>Figure 3.2.6.3a:</b> Subgrade layer strain.....	92
<b>Figure 3.2.6.3b:</b> Vertical strains for T1 and T2 loading conditions (Microstrain).....	92
<b>Figure 3.2.7.1a:</b> Critical parameters and locations.....	93
<b>Figure 3.2.7.4a:</b> T1 Pavement life Below Wheel estimates .....	97
<b>Figure 3.2.7.4b:</b> T2 Pavement life Below Wheel estimates.....	97
<b>Figure 3.2.8a:</b> Dissipation of externally applied stress in layered pavement system .....	98
<b>Figure 3.3.1a:</b> Pisa University research regime .....	99
<b>Figure 3.3.2.2a:</b> Leutner shear test specimens.....	99
<b>Figure 3.3.2.2b:</b> Samples for laboratory testing.....	99
<b>Figure 3.3.2.2c:</b> Interlayer shear strength results for simulated samples.....	100
<b>Figure 3.3.2.3a:</b> Trial field samples.....	102
<b>Figure 3.3.2.3b:</b> Interlayer shear strength results for simulated samples .....	103
<b>Figure 3.3.2.3c:</b> Water within samples .....	103
<b>Figure 3.3.2.3d:</b> Failure surface of samples.....	104
<b>Figure 3.3.3.2a:</b> Contact area on XY plane .....	105
<b>Figure 3.3.3.2b:</b> Contact area on XY plane .....	105
<b>Figure 3.3.3.6a:</b> Pisa University shear stress results .....	108
<b>Figure 3.3.3.6b:</b> Pisa University horizontal strains at Side and Centre points.....	109
<b>Figure 3.3.3.6c:</b> Pisa University vertical strains at Side and Centre points .....	110
<b>Figure 3.3.3.7a:</b> Horizontal and vertical strains.....	111

<b>Figure 3.3.3.7b:</b> Pavement Life centre point measurements .....	112
<b>Figure 3.3.3.7c:</b> Pavement Life side point measurements .....	112
<b>Figure 3.3.3.8a:</b> Additional pavement structure considerations.....	113
<b>Figure 3.3.3.9a:</b> Minimum Pavement Life for Case A .....	115
<b>Figure 3.4.7.2b:</b> Minimum Pavement Life for Case B .....	115
<b>Figure 3.3.3.9c:</b> Minimum Pavement Life for Case C.....	116
<b>Figure 3.4.1a:</b> Subjects of interest for comparative analysis.....	116
<b>Figure 3.4.2.1a:</b> Wheel on XZ plane.....	117
<b>Figure 3.4.3.1a:</b> Analysis locations .....	119
<b>Figure 3.4.3.2a:</b> Asphalt layer thickness and modular ratio .....	120
<b>Figure 3.4.3.2b:</b> Interface 1 Maximum Shear stresses .....	120
<b>Figure 3.4.4.3a:</b> Shear stress results for SU Tyre 1 and Pisa University research at Interface 1.....	122
<b>Figure 3.4.4.3b:</b> Shear stress results for SU Tyre 2 and Pisa University research at Interface 1.....	122
<b>Figure 3.4.4.3c:</b> Horizontal strain results for SU Tyre 1 and Pisa University research at Interface 1....	124
<b>Figure 3.4.4.3d:</b> Horizontal strain results for SU Tyre 2 and Pisa University research at Interface 1 ...	124
<b>Figure 3.4.4.3e:</b> Vertical strain results for SU Tyre 1 and Pisa University research .....	126
<b>Figure 3.4.4.4a:</b> Pavement life for fatigue failure mode .....	129
<b>Figure 3.4.4.4b:</b> Pavement life for serviceability failure mode .....	130
<b>Figure 3.5.3a:</b> Effect of interlayer bonding on linear-elastic Fatigue Life .....	133
<b>Figure 3.6a:</b> Load spreading abilities of pavements .....	134
<b>Figure 3.6b:</b> Load spreading ability of different base layers .....	134
<b>Figure 4.1a:</b> Two material models replicated in FEM analysis .....	136
<b>Figure 4.2.1a:</b> Material model 1 experimental plan.....	137
<b>Figure 4.2.1b:</b> Material model components.....	138
<b>Figure 4.2.2a:</b> Model 1 components according to simulation modules.....	138
<b>Figure 4.2.3.1a:</b> Schematic illustration of the Leutner Shear Test .....	139
<b>Figure 4.2.3.1b:</b> Leutner Shear Test FEM replication .....	139
<b>Figure 4.2.3.1c:</b> Leutner test device gap width .....	140
<b>Figure 4.2.3.1d:</b> Datum plane and partition .....	140
<b>Figure 4.2.3.2a:</b> Set-up of a part.....	141
<b>Figure 4.2.3.2b:</b> Create Part.....	141
<b>Figure 4.2.4.1a:</b> Material property definition.....	142
<b>Figure 4.2.4.2a:</b> Poisson's ratio.....	143
<b>Figure 4.2.4.3a:</b> Material property definition inputs.....	145
<b>Figure 4.2.4.3b:</b> Typical 50/70 SAPREF Unaged Binder .....	146
<b>Figure 4.2.4.4a:</b> Definition of section .....	147
<b>Figure 4.2.4.4b:</b> Definition of section properties .....	147
<b>Figure 4.2.4.4c:</b> Core sample properties .....	147
<b>Figure 4.2.4.4d:</b> Shear ring properties.....	148
<b>Figure 4.2.5a:</b> Model set-up procedure for Model 1 – Assembly module .....	149
<b>Figure 4.2.5b:</b> Assembled model .....	150
<b>Figure 4.2.6.1a:</b> Step Editor .....	150
<b>Figure 4.2.6.2a:</b> Degrees of freedom.....	151
<b>Figure 4.2.6.2b:</b> FEM replication with reference points.....	151
<b>Figure 4.2.6.2c:</b> Magnified view of arrows indicating degrees of freedom.....	152

<b>Figure 4.2.6.2d:</b> FEM replication with reference points.....	152
<b>Figure 4.2.6.2e:</b> Boundary conditions.....	153
<b>Figure 4.2.6.3a:</b> Model set-up procedure for Model 1 –Interaction module.....	154
<b>Figure 4.2.6.3b:</b> Model set-up procedure –Interaction module .....	155
<b>Figure 4.2.6.3c:</b> Tie constraint between shear ring and core sample .....	156
<b>Figure 4.2.6.3d:</b> Tie constraint between shear ring and core sample.....	156
<b>Figure 4.2.6.3e:</b> Rigid body constraints at reference points .....	157
<b>Figure 4.2.7.1a:</b> Model set-up procedure for Model 1 –Mesh module .....	157
<b>Figure 4.2.7.2a:</b> Mesh process.....	158
<b>Figure 4.2.7.2b:</b> Two meshes with different element shapes .....	158
<b>Figure 4.2.7.2c:</b> Meshing techniques.....	158
<b>Figure 4.2.7.3a:</b> Mesh controls dialog box .....	159
<b>Figure 4.2.7.3b:</b> Hex shaped elements .....	159
<b>Figure 4.2.7.3c:</b> Meshing techniques.....	159
<b>Figure 4.2.8a:</b> Model set-up procedure – Job module .....	160
<b>Figure 4.2.8b:</b> Dialog box for job definition.....	160
<b>Figure 4.2.8c:</b> Job monitor .....	161
<b>Figure 4.2.9a:</b> Acquired result locations.....	162
<b>Figure 4.2.9b:</b> Results acquired at Model 1 locations .....	162
<b>Figure 4.2.9c:</b> Shear stresses .....	163
<b>Figure 4.2.10a:</b> Experimental plan for Model 1.....	163
<b>Figure 4.2.10b:</b> Phase 2: Experimental plan for Model 1 .....	164
<b>Figure 4.3.1a:</b> Material model 2 experimental plan.....	165
<b>Figure 4.3.2a:</b> Model 2 components according to simulation modules.....	166
<b>Figure 4.3.3a:</b> Model 2 components according to simulation modules.....	167
<b>Figure 4.3.3b:</b> Sketch of geometry of part.....	167
<b>Figure 4.3.3c:</b> Partitioning .....	168
<b>Figure 4.3.3d:</b> Partitioning.....	169
<b>Figure 4.3.3e:</b> Pavement structure properties .....	170
<b>Figure 4.3.4.1a:</b> Analysis step basic tab for Model 2.....	170
<b>Figure 4.3.4.1b:</b> Analysis step incrementation tab for Model 2.....	171
<b>Figure 4.3.4.2a:</b> Model set-up procedure for Model 2– Load module.....	171
<b>Figure 4.3.4.2b:</b> Sketch of geometry of part.....	171
<b>Figure 4.3.4.3a:</b> Axle load distribution and configuration.....	172
<b>Figure 4.3.4.3b:</b> Idealisation of load application in Abaqus .....	173
<b>Figure 4.3.4.3c:</b> Load are partition .....	173
<b>Figure 4.3.4.3d:</b> Load definition.....	173
<b>Figure 4.3.4.3e:</b> Replicated loading conditions .....	174
<b>Figure 4.3.4.3f:</b> Illustration of all prescribed conditions .....	174
<b>Figure 4.3.5a:</b> Model set-up procedure for Model 2 –Mesh module.....	174
<b>Figure 4.3.5b:</b> Mesh generation for Model 2 .....	175
<b>Figure 4.3.5c:</b> Model 2 mesh .....	175
<b>Figure 4.3.6a:</b> Results acquired at Model 2 locations .....	176
<b>Figure 4.3.6b:</b> Locations for acquisition of results .....	176
<b>Figure 4.3.6c:</b> Displacements.....	177

<b>Figure 4.3.7a:</b> Experimental plan for Model 2.....	178
<b>Figure 4.3.7b:</b> Experimental plan for Model 2.....	178
<b>Figure 5.1a:</b> Subjects of interest for discussion of results .....	180
<b>Figure 5.2.1a:</b> Analysis approach for Leutner Shear Test Model.....	181
<b>Figure 5.2.2.1a:</b> Shear stress distribution over sample cross section .....	182
<b>Figure 5.2.2.2a:</b> Path 1 Cross Section Shear Distribution .....	182
<b>Figure 5.2.2.2b:</b> Path 2 Cross Section Shear Distribution .....	183
<b>Figure 5.2.2.2c:</b> Path 3 Cross Section Shear Distribution .....	183
<b>Figure 5.2.2.2d:</b> Path 3 location for assembly .....	184
<b>Figure 5.2.2.2e:</b> Path 4 Cross Section Shear Distribution .....	184
<b>Figure 5.2.2.2f:</b> Path 5 Cross Section Shear Distribution.....	185
<b>Figure 5.2.2.2g:</b> Path 3 location for assembly .....	185
<b>Figure 5.2.3.1a:</b> Shear stress results for increase in wearing course thickness .....	186
<b>Figure 5.2.3.2a:</b> Shear stresses .....	188
<b>Figure 5.2.3.2b:</b> Axial load results for increase in wearing course thickness .....	188
<b>Figure 5.2.4.1a:</b> Pane glass and featherbed illustration .....	189
<b>Figure 5.2.4.1b:</b> Comparison of shear stress according to modular ratio .....	190
<b>Figure 5.2.4.2a:</b> Schematization of constructed pavement layers .....	191
<b>Figure 5.2.4.2b:</b> Shear stress comparison according to wearing course and tack coat stiffness.....	192
<b>Figure 5.2.5.1a:</b> Tack coat stiffness influence for wearing course thickness for MR1 for $T_{WC1}$ and $T_{WC2}$ .....	193
<b>Figure 5.2.5.1b:</b> Tack coat stiffness influence for wearing course thickness for MR1 for $T_{WC3}$ .....	194
<b>Figure 5.2.5.2a:</b> Shear distribution for $E_{TC1}$ and $E_{TC2}$ .....	194
<b>Figure 5.2.5.2b:</b> Shear stress between layers.....	195
<b>Figure 5.2.6a:</b> Shear stress between layers.....	197
<b>Figure 5.2.8a:</b> Structure of comparative studies .....	197
<b>Figure 5.3.1a:</b> Analysis approach for Pavement Analysis model .....	201
<b>Figure 5.3.2a:</b> Distress modes at pavement interface.....	202
<b>Figure 5.3.2.1a:</b> Model 2 interface shear stress .....	202
<b>Figure 5.3.2.1b:</b> Shear distress mode .....	202
<b>Figure 5.3.2.2a:</b> Critical pavement locations .....	205
<b>Figure 5.3.4.1a:</b> Model 2 horizontal strain .....	206
<b>Figure 5.3.5.1a:</b> Model 2 vertical strain.....	208
<b>Figure 5.3.6a:</b> Critical strains for SAMDM approach for LE analysis and Model 2 .....	210
<b>Figure 5.3.6.1a:</b> Model 2 fatigue life .....	210
<b>Figure 5.3.6.2a:</b> Model 2 serviceability life.....	212
<b>Figure 5.4.3a:</b> Model 1 versus Model 2 shear stress comparison .....	218

## Appendix A

<b>Figure A1:</b> Shear stress results measured at Edge.....	236
<b>Figure A2:</b> Deviator stress results measured at Edge .....	239
<b>Figure A3:</b> T1 Pavement life Edge estimates .....	244
<b>Figure A4:</b> T2 Pavement life Edge estimates .....	244

## Appendix C

<b>Figure C1:</b> Experimental design for Stellenbosch University .....	250
<b>Figure C2:</b> Experimental design for Pisa University .....	251

## Appendix D

<b>Figure D1:</b> Two-dimensional plane in modelling space .....	255
<b>Figure D2:</b> Three-dimensional plane in modelling space .....	255
<b>Figure D3:</b> Extruded solid feature .....	256
<b>Figure D4:</b> Sketch of geometry of part .....	256
<b>Figure D5:</b> Analysis step basic tab for Model 1 .....	257
<b>Figure D6:</b> Analysis step incrementation tab for Model 1 .....	258
<b>Figure D7:</b> Model set-up procedure for Model 1 – Step module .....	259
<b>Figure D8:</b> Definition of boundary conditions .....	260
<b>Figure D9:</b> Surface-based tie algorithm .....	261
<b>Figure D10:</b> Definition of rigid body in constraint editor .....	261
<b>Figure D10:</b> Structured mesh .....	262
<b>Figure D12:</b> Swept mesh .....	263
<b>Figure D13:</b> Free mesh generated with tetrahedral elements .....	263
<b>Figure D14:</b> Bottom-up hexahedral meshed part .....	264
<b>Figure D15:</b> Mesh generation .....	266
<b>Figure D16:</b> Four phases of bottom-up meshing technique .....	267
<b>Figure D17:</b> Mesh generation .....	267
<b>Figure D18:</b> Bottom-up meshing methods .....	268
<b>Figure D19:</b> Bottom-up meshing .....	268
<b>Figure D20:</b> Compatible mesh .....	269
<b>Figure D21:</b> Element Type dialog box for Model 1 .....	270
<b>Figure D22:</b> Fully integrated integration points for quadrilateral elements .....	271
<b>Figure D23:</b> Integration points for quadrilateral elements with reduced integration .....	271
<b>Figure D24:</b> Linear element .....	272
<b>Figure D25:</b> Geometrical features and deformation mode of cohesive element .....	272
<b>Figure D26:</b> Cohesive elements sharing nodes with other elements .....	273
<b>Figure D27:</b> Local directions for 3D cohesive elements .....	274
<b>Figure D28:</b> Sketch of geometry of part .....	275
<b>Figure D29:</b> Sketch of geometry of part .....	275
<b>Figure D30:</b> Element Type dialog box for Model 2 .....	276

## Appendix E

<b>Figure E1:</b> Minimum, Average and Maximum shear stress results for increase in $T_{WC1}$ .....	278
<b>Figure E2:</b> Progressive shear stress change according to wearing course thickness ( $T_{WC}$ ) .....	280
<b>Figure E3:</b> Tack coat stiffness influence for wearing course thickness for MR2 .....	280
<b>Figure E4:</b> Shear stress variation in tack coat thickness (%) .....	281
<b>Figure E5:</b> Tack coat thickness influence for $E_{TC1}$ and $E_{TC2}$ (%) .....	281
<b>Figure E6:</b> Property differences measured for Model 2 interface shear stress .....	283
<b>Figure E7:</b> Loading condition differences measured for Model 2 interface shear stress .....	283

**Figure E8:** Loading condition differences measured for Model 2 horizontal strain ..... 284  
**Figure E9:** Property differences measured for Model 2 horizontal strain..... 284  
**Figure E10:** Loading condition differences measured for Model 2 vertical strain ..... 284  
**Figure E11:** Property differences measured for Model 2 vertical strain ..... 285  
**Figure E12:** Loading condition differences measured for Model 2 fatigue life ..... 285  
**Figure E13:** Property differences measured for Model 2 fatigue life ..... 285  
**Figure E14:** Loading condition differences measured for Model 2 serviceability life ..... 286  
**Figure E15:** Property differences measured for Model 2 serviceability life ..... 286

**Appendix F**

**Figure F1:** Burmister Graph (Vertical and Horizontal Stresses) for Poisson Ratio of 0.25 and Layer Thickness of  $h=a/2$  ..... 288  
**Figure F2:** Burmister Graph (Vertical and Horizontal Stresses) for Poisson Ratio of 0.25 and Layer Thickness of  $h=a$ ..... 289  
**Figure F3:** Illustration of stress locations of interest ..... 290  
**Figure F4:** Vertical stresses for analyses combinations (kPa) ..... 291  
**Figure F5:** Horizontal stresses for analyses combinations (kPa)..... 292

## LIST OF TABLES

<b>Table 2.2.2.2a:</b> Prior limitation versus Superpave testing and specification features.....	8
<b>Table 2.2.2.2b:</b> PG binder nomenclature .....	9
<b>Table 2.2.2.2c:</b> Bitumen binder advantages and disadvantages.....	9
<b>Table 2.2.2.3a:</b> Cutback classification.....	10
<b>Table 2.2.2.3b:</b> Cutback bitumen advantages and disadvantages .....	11
<b>Table 2.2.2.3c:</b> Cutback bitumen versus bitumen emulsion .....	12
<b>Table 2.2.2.4a:</b> Emulsion production procedure.....	13
<b>Table 2.2.2.4b:</b> Emulsion description .....	14
<b>Table 2.2.2.4c:</b> Bitumen emulsion classification .....	15
<b>Table 2.2.2.4d:</b> Bitumen emulsion advantages and disadvantages .....	15
<b>Table 2.2.3.3a:</b> Recommended tack coat application rates .....	19
<b>Table 2.2.4.2a:</b> Application factors.....	23
<b>Table 2.2.4.4a:</b> Process of bitumen emulsion break .....	26
<b>Table 2.3.1a:</b> Destructive and non-destructive tests.....	30
<b>Table 2.3.1.5a:</b> Comparison of Torque Bond, Leutner and LPDS Test.....	43
<b>Table 2.3.1.5b:</b> Comparison of DST, Shear Fatigue Test and ASTRA Direct Shear Box Test.....	44
<b>Table 2.3.1.5c:</b> Pull-Off Device and Wedge Splitting Test .....	46
<b>Table 2.3.2.3a:</b> Shear testing results .....	57
<b>Table 2.4.2.1a:</b> Attributes of the South African Mechanistic-Empirical Design Method .....	65
<b>Table 2.4.2.3a:</b> Structural Analysis and prediction of individual layer life for asphalt layer .....	68
<b>Table 2.4.2.3b:</b> Structural Analysis and prediction of individual layer life for subgrade .....	68
<b>Table 2.4.2.3c:</b> Structural Analysis and prediction of individual layer life for granular layer .....	69
<b>Table 2.4.2.3d:</b> Structural Analysis and prediction of individual layer life for cemented layer .....	70
<b>Table 3.2.2.1a:</b> Axle loading and tyre pressures.....	77
<b>Table 3.2.2.2a:</b> Friction conditions .....	79
<b>Table 3.2.2.3a:</b> Material properties and pavement layer thickness.....	80
<b>Table 3.2.2.3b:</b> Pavement structure considerations .....	81
<b>Table 3.2.4a:</b> Shear stresses at Below Wheel location for Case 1 (kPa).....	84
<b>Table 3.2.4b:</b> Shear stresses at Below Wheel location for Case 2 (kPa).....	84
<b>Table 3.2.4c:</b> Shear stresses at Below Wheel location for Case 3 (kPa) .....	85
<b>Table 3.2.4d:</b> Shear stresses at Below Wheel location for Case 4 (kPa).....	85
<b>Table 3.2.7.2a:</b> Fatigue life results for Below Wheel location (MESAs) .....	94
<b>Table 3.2.7.3a:</b> Serviceability Results for Below Wheel location (MESAs) .....	95
<b>Table 3.3.2.2a:</b> Series and attributes used for laboratory testing.....	100
<b>Table 3.3.2.2b:</b> Average bonding strength .....	100
<b>Table 3.3.2.3a:</b> Trial field attributes .....	102
<b>Table 3.3.2.3b:</b> Average bonding strength for trial field samples .....	103
<b>Table 3.3.3.4a:</b> Types of national networks .....	106
<b>Table 3.3.3.5a:</b> Pavement structure considerations .....	107
<b>Table 3.3.3.5b:</b> Pavement structure considerations .....	107
<b>Table 3.3.3.8a:</b> Adjusted parameters (Bianchi et al., 2018b) .....	114
<b>Table 3.3.3.8b:</b> Comparison of testing conditions.....	114
<b>Table 3.3.3.9a:</b> Asphalt Concrete Overlay Equivalent results .....	114

<b>Table 3.3.3.9b:</b> AC Overlay and Tack Coat cost comparison .....	115
<b>Table 3.4.2.1a:</b> Loading conditions for SU and Pisa University .....	117
<b>Table 3.4.2.2a:</b> Friction conditions for SU and Pisa University.....	118
<b>Table 3.4.2.2a:</b> Friction conditions for SU and Pisa University.....	118
<b>Table 3.4.3.2a:</b> Modular ratio of SU and Pisa University pavement structures .....	119
<b>Table 3.4.3.2b:</b> Asphalt layer thickness for SU and Pisa University research (in mm) .....	120
<b>Table 3.4.3.2c:</b> Modular ratio and surfacing thickness rankings .....	121
<b>Table 3.4.4.2a:</b> Cover thickness for SU and Pisa University research (in mm) .....	121
<b>Table 3.4.4.3a:</b> SU versus Pisa University shear stress results .....	123
<b>Table 3.4.4.3b:</b> SU versus Pisa University horizontal strain results.....	125
<b>Table 3.5.7.2a:</b> SU versus Pisa University horizontal strain results.....	126
<b>Table 3.4.4.4a:</b> Transfer functions used for Pavement Life estimations.....	128
<b>Table 3.5.7.2b:</b> SU versus Pisa University Fatigue Life Results.....	129
<b>Table 3.4.4.4c:</b> SU versus Pisa University Serviceability Life Results.....	130
<b>Table 3.4.4.4d:</b> Sensitivity analysis for asphalt fatigue SU results .....	131
<b>Table 3.4.4.4e:</b> Sensitivity analysis for subgrade failure SU results .....	131
<b>Table 3.4.4.4f:</b> Transfer function and strain relation .....	132
<b>Table 3.5.2a:</b> ISS values for different application methods.....	132
<b>Table 4.2.3.1a:</b> Layer thickness combinations for Model 1.....	141
<b>Table 4.2.4.3a:</b> Elastic behaviour types for Model 1 .....	145
<b>Table 4.2.4.4a:</b> Section features of elements for Model 1 .....	148
<b>Table 4.2.6.2a:</b> Summary of degrees of freedom.....	152
<b>Table 4.2.6.2b:</b> Summary of boundary conditions .....	154
<b>Table 4.2.6.3a:</b> Definition of rigid point constraints at reference points.....	157
<b>Table 4.3.3a:</b> Layer thickness combinations for Model 2.....	168
<b>Table 4.3.3b:</b> Elastic behaviour types for Model 2 .....	169
<b>Table 4.3.3c:</b> Section features of elements for Model 2 .....	169
<b>Table 4.3.4.3a:</b> Axle loading and tyre pressures.....	172
<b>Table 5.2.8.1a:</b> Trial field testing results for Series I .....	198
<b>Table 5.3.2.2a:</b> LE Analysis versus replicated model shear stresses .....	204
<b>Table 5.3.3.1a:</b> Model 2 normal stresses (MPa).....	205
<b>Table 5.3.3.2a:</b> Model 2 normal strains (Microstrain).....	205
<b>Table 5.3.4.2a:</b> LE Analysis versus replicated model for horizontal strains .....	207
<b>Table 5.3.5.2a:</b> LE Analysis versus replicated model for vertical strains.....	209
<b>Table 5.3.6.1a:</b> LE Analysis versus replicated model for fatigue life .....	212
<b>Table 5.3.6.2a:</b> LE Analysis versus replicated model for serviceability life .....	214
<b>Table 5.3.8a:</b> Comparison of testing properties .....	215
<b>Table 5.4.2a:</b> Model 1 versus Model 2 testing conditions .....	216
<b>Table 5.4.3a:</b> Model 1 versus Model 2 testing conditions .....	218

## Appendix A

<b>Table A1:</b> Shear stresses at Edge location for Case 1 .....	236
<b>Table A2:</b> Shear stresses at Edge location for Case 2 .....	236
<b>Table A3:</b> Shear stresses at Edge location for Case 3 .....	237

<b>Table A4:</b> Shear stresses at Edge location for Case 4 .....	237
<b>Table A5:</b> Case 1 difference ( $\Delta\%$ ) for shear stress results (%) .....	237
<b>Table A6:</b> Case 2 difference ( $\Delta\%$ ) for shear stress results (%) .....	237
<b>Table A7:</b> Case 3 difference ( $\Delta\%$ ) for shear stress results (%) .....	238
<b>Table A8:</b> Case 4 difference ( $\Delta\%$ ) for shear stress results (%) .....	238
<b>Table A9:</b> Deviator stresses for High Friction condition (kPa) .....	239
<b>Table A10:</b> Deviator stresses for Medium Friction condition (kPa) .....	239
<b>Table A11:</b> Deviator stresses for Low Friction condition (kPa) .....	239
<b>Table A12:</b> Difference ( $\Delta\%$ ) for deviator stress results (%) for Below Wheel .....	240
<b>Table A13:</b> Difference ( $\Delta\%$ ) for deviator stress results (%) for Edge .....	240
<b>Table A14:</b> Case 1 to 4 Horizontal strains for High Friction condition (Microstrain) .....	241
<b>Table A15:</b> Case 1 to 4 Horizontal strains for Medium Friction condition (Microstrain) .....	241
<b>Table A16:</b> Case 1 to 4 Horizontal strains for Low Friction condition (Microstrain) .....	241
<b>Table A17:</b> Case 1 to 4 difference results ( $\Delta\%$ ) for horizontal strains (%) .....	241
<b>Table A18:</b> Case 1 to 4 Vertical strains for High Friction condition (Microstrain) .....	242
<b>Table A19:</b> Case 1 to 4 Vertical strains for Medium Friction condition (Microstrain) .....	242
<b>Table A20:</b> Case 1 to 4 Vertical strains for Low Friction condition (Microstrain) .....	242
<b>Table A21:</b> Case 1 to 4 difference results ( $\Delta\%$ ) for vertical strains (%) .....	242
<b>Table A22:</b> Fatigue Life results for Edge location (MESAs) .....	243
<b>Table A23:</b> Case 1 to 4 difference results ( $\Delta\%$ ) for Fatigue Life (%) .....	243
<b>Table A24:</b> Serviceability Life results for Edge location (MESAs) .....	243
<b>Table A25:</b> Case 1 to 4 difference results ( $\Delta\%$ ) for Serviceability Life (%) .....	243

## Appendix B

<b>Table B1:</b> Laboratory testing results .....	246
<b>Table B2:</b> Field testing results .....	247
<b>Table B3:</b> Case 1 to 4 difference results ( $\Delta\%$ ) for Pisa University shear stresses (%) .....	248
<b>Table B4:</b> Case 1 to 4 difference results ( $\Delta\%$ ) for Pisa University horizontal strains (%) .....	248
<b>Table B5:</b> Case 1 to 4 difference results ( $\Delta\%$ ) for Pisa University vertical strains (%) .....	248

## Appendix C

<b>Table C1:</b> Sensitivity analysis for asphalt fatigue Pisa University results .....	252
<b>Table C2:</b> Sensitivity analysis for subgrade failure Pisa University results .....	252
<b>Table C3:</b> SU and Pisa University $\Delta_{Life}$ behaviours .....	252

## Appendix D

<b>Table D1:</b> Summary and illustration of top-down meshing techniques .....	262
<b>Table D2:</b> Summary and illustration of bottom-up meshing techniques .....	264
<b>Table D3:</b> Element types .....	264
<b>Table D4:</b> Illustration of element shapes .....	265

## Appendix E

<b>Table E1:</b> Shear stress results (in MPa) for wearing course thickness of 30mm ( $T_{WC1}$ ).....	278
<b>Table E2:</b> Shear stress results (in MPa) for wearing course thickness of 50mm ( $T_{WC2}$ ).....	279
<b>Table E3:</b> Shear stress results (in MPa) for wearing course thickness of 100mm ( $T_{WC3}$ ).....	279
<b>Table E4:</b> Axial force (in kN) results for wearing course thickness of 30mm ( $T_{WC1}$ ) .....	279
<b>Table E5:</b> Axial force (in kN) results for wearing course thickness of 50mm ( $T_{WC2}$ ) .....	279
<b>Table E6:</b> Axial force (in kN) results for wearing course thickness of 100mm ( $T_{WC3}$ ) .....	280
<b>Table E7:</b> Average estimation of modular ratio for $T_{WC1}$ combinations .....	282
<b>Table E8:</b> Interface shear stress from LE analysis for T1 loading condition (MPa).....	282
<b>Table E9:</b> Estimations for HF condition for $T_{WC1}$ (%) .....	282
<b>Table E10:</b> Shear stress results for Model 2 i.e. Pavement Structure (in kPa) .....	283

## Appendix F

<b>Table F1:</b> Burmister graph estimations for stresses for T1 loading condition (kPa) .....	290
<b>Table F2:</b> Burmister graph estimations for stresses for T2 loading condition (kPa) .....	290
<b>Table F3:</b> Burmister graph results for T1 loading condition .....	291
<b>Table F4:</b> Burmister graph results for T2 loading condition .....	291

## LIST OF ABBREVIATIONS

Symbol	Description
2D	Two-dimensional
3D	Three-dimensional
AASHTO	American Association of State Highway and Transportation Officials
AC	Asphalt Concrete/ Asphalt Cement (Bitumen)
AC	Asphalt Concrete
ASTRA	Ancona Shear Testing Research and Analysis
BC	Binder course layer
BC	Boundary condition(s)
CBR	California Bearing Ratio
CEEC	China Energy Engineering Corporation
CRS	Cationic Rapid Set
CTB	Cement-treated Base
dof	Degree of freedom
DST	Double Shear Test
ECR	Electronic Contact Resistance
ESAL	Equivalent Single Axle Load
FDOT	Florida Department of Transport
FEM	Finite Element Method
FWD	Falling Weight Deflectometer
HF	High Float
HF	High Friction
HMA	Hot Mix Asphalt
IBT	Interface Bond Test
ISS	Interlayer Shear Strength
ITS	Indirect Tensile Strength
ITT	Indirect Tensile Test
LE	Linear-elastic
LF	Low Friction
LISST	Louisiana Interlayer Shear Strength Tester
LPDS	Layer Parallel Direct Shear (test)
LTCQT	Louisiana Tack Coat Quality Test
LVDT	Linear Variable Differential Transformers
MC	Medium Curing
MEPDG	Mechanistic Empirical Pavement Design Guide
MESAs	Million Equivalent Standard Axle(s)
MF	Medium Friction
MR	Modular ratio
MS	Medium Set
MTS	Material Testing System
MTV	Material Transfer Vehicle

NCHRP	National Cooperative Highway Research Program
NDT	Non-destructive tests
Nlgeom	Geometric nonlinearity
ODB	Output database
PBST	Portable Bond Strength Tester
PCC	Portland Cement Concrete
PG	Performance Graded
PMAE	Polymer-Modified bitumen emulsions
PN	Pavement Number
PU	Pisa University
QS	Quick Set
RC	Rapid Curing
RP	Reference point
RS	Rapid Set
SAMDM	South African Mechanistic-Empirical Design Method
SAPREF	South African Petroleum Refineries
SBG	Subgrade
SC	Slow Curing
SN	Structural Number
SR	Shear ring
SS	Slow Set
SU	Stellenbosch University
TC	Tack coat
TF	Transfer function
UNB	Unbound Course
UPOD	UTEP Pull-Off Device
UTEP	University of Texas at El Paso
WC	Wearing course layer
SBR	Styrene Butadiene Rubber

## LIST OF SYMBOLS

Symbol	Description
$N_x$	Number of load repetition to failure by fatigue cracking
$N_z$	Number of 12t ESALs to produce permanent deformation at top of subgrade layer
$\Delta_{Analysis}$	Percent difference of analysis results
$\Delta_{Life}$	Percent difference of pavement life
$\Delta_{MR}$	Percent difference according to Modular Ratio
$\epsilon_x$	Horizontal tensile strain at bottom of asphalt layer
$\epsilon_z$	Vertical strain measured at top of the subgrade layer
$\tau_{max}$	Maximum shear stress
$\tau_{min}$	Minimum shear stress
$E_{base1}$	Base layer stiffness of 2500MPa
$E_{base1}$	Lower base layer stiffness of 400MPa (Case 1 and Case 3)
$E_{base2}$	Base layer stiffness of 1000MPa
$E_{base2}$	Higher base layer stiffness of 1500MPa (Case 2 and Case 4)
$T1_{result}$	Result obtained for T1 loading condition (Axle load of 40kN and tyre pressure of 750kPa)
$T2_{result}$	Result obtained for T2 loading condition (Axle load of 70kN and tyre pressure of 900kPa)
$t_{Asphalt1}$	Lower asphalt layer thickness of 50mm (Case 1 and Case 2)
$t_{Asphalt2}$	Higher asphalt layer thickness of 100mm (Case 3 and Case 4)
$t_n$	Nominal traction in normal direction (vertical)
$t_s$	Nominal traction in local shear direction (horizontal direction)
$t_t$	Nominal traction in local shear direction (horizontal direction)
$x_{CP}$	Results obtained at centre point
$x_{FEM}$	Parameter calculated by means of Finite Element Method analysis
$x_{HF}$	Parameter calculated within high friction (HF) conditions
$x_{LE}$	Parameter calculated by means of Finite Linear-Elastic analysis
$x_{LE}$	Results from preliminary linear-elastic analysis
$x_{LF}$	Parameter calculated within low friction (LF) conditions
$x_{Model1}$	Result from FEM analysis for Leutner model
$x_{Model2}$	Result from FEM analysis for Pavement Analysis model
$x_{PU}$	Parameter calculated within Pisa University research
$x_{SP}$	Results obtained at side pint
$x_{SU}$	Parameter calculated within Stellenbosch University research
$x_{lab}$	Results from Pisa University laboratory testing
$\gamma_{ij}$	Shear strains
$\epsilon_D$	Strain in lateral direction (cross section)
$\epsilon_L$	Strain in longitudinal direction
$\epsilon_{ii}$	Normal strains
$\epsilon_n$	Nominal strain in normal direction (vertical direction)

$\varepsilon_s$	Nominal strain in local shear direction (horizontal direction)
$\varepsilon_t$	Nominal strain in local shear direction (horizontal direction)
$\sigma_{ii}$	Normal stresses
$\sigma_{ij}$	Shear stresses (also indicated as $\tau_{ij}$ )
$\tau_{MR1}$	Shear stress achieved for MR1 defined modular ratio (MR = 1)
$\tau_{MR2}$	Shear stress achieved for MR2 defined modular ratio (MR = 2.5)
$\tau_{avg}$	Average shear stress
$\Delta(\%)$	Percent difference
$\Delta E_{TC}$	Percent difference according to tack coat stiffness
$\Delta T_{TC}$	Percent difference according to tack coat layer thickness
$\Delta T_{WC}$	Percent difference according to wearing course thickness
$\Delta D$	Change in diameter
$\Delta L$	Change in length
A	Area calculated as $A = \pi r^2$ with r equal to the load radius
a	Load radius
AK	Standard shear spring compliance
ALK	Reduced shear spring compliance
C	Cationic
c, d	Constants
$C_{term}$	Cohesion for material codes
D	Elasticity tensor
E	Young's Modulus of Elasticity
$E_{Asphalt}$	Asphalt layer stiffness
$E_{base}$	Base layer stiffness
$E_{nn}$	Stiffness modulus in normal direction (vertical direction)
$E_{SR}$	Leutner shear ring stiffness
$E_{ss}$	Stiffness modulus in local shear direction (horizontal direction)
$E_{TC}$	Tack coat layer stiffness
$E_{TC1} / E_{TC1}$	Tack coat layer stiffness of 1MPa
$E_{TC2} / E_{TC2}$	Tack coat layer stiffness of 0.21MPa
$E_{tt}$	Stiffness modulus in local shear direction (horizontal direction)
$E_{WC}$	Wearing course layer stiffness
sF	Axle load
F	Stress ratio
G	Shear Modulus
G	Complex Modulus
h	Hardness
h	Top layer thickness
M	Modified
MR1	Low modular ratio of 1
MR2	High modular ratio of 2.5
N	Number of equivalent standard axles to safeguard against shear failure
$N_{eff}$	Effective fatigue life ( <i>crack progression</i> )

$N_f$	Fatigue life
$N_{min}$	Minimum Pavement Life
P	Polymer
$p$	Tyre pressure
r	Load radius
S	Solvent
S11	Abaqus equivalent of $\sigma_1$ or $\sigma_{11}$ (horizontal stress)
S12	Abaqus equivalent of $\sigma_{12}$ or $\tau_{11}$ (shear stress on horizontal plane)
S22	Abaqus equivalent of $\sigma_2$ or $\sigma_{22}$ (horizontal stress)
S33	Abaqus equivalent of $\sigma_3$ or $\sigma_{33}$ (vertical stress)
SF	Shift factor for crack propagation
t	(Pavement) Layer thickness
T	Waiting duration
T1	Tyre 1 (Single wheel type)
T2	Tyre 2 (Super single wheel type)
$t_{Asphalt}$	Asphalt layer thickness
$t_{base}$	Base layer thickness
$t_{TC}$	Tack coat thickness
$T_{TC1}/TTC1$	Tack coat thickness of 0.2mm
$T_{TC2}/TTC2$	Tack coat thickness of 0.5mm
$T_{TC3}/TTC3$	Tack coat thickness of 1mm
$t_{WC}$	Wearing course layer thickness
$T_{WC}$	Wearing course layer thickness
$T_{WC1}/TWC1$	Wearing course layer thickness of 30mm
$T_{WC2}/TWC2$	Wearing course layer thickness of 50mm
$T_{WC3}/TWC3$	Wearing course layer thickness of 100mm
U1	Translational degree of freedom in direction 1 (x-direction)
U2	Translational degree of freedom in direction 2 (y-direction)
U3	Translational degree of freedom in direction 3 (z-direction)
UR1	Rotational degree of freedom about direction 1 (x-direction)
UR2	Rotational degree of freedom about direction 2 (y-direction)
UR3	Rotational degree of freedom about direction 3 (z-direction)
V	Shear force
$V_{avg}$	Average shear force
$V_{max}$	Maximum shear stress
$V_{min}$	Minimum shear force
$\alpha$	Friction parameter
$\alpha, \beta$	Constants
$\epsilon$	Normal Strain/ Total elastic strain/ Horizontal tensile strain at bottom of layer (microstrain)
$\epsilon_b$	Strain-at-break
$\epsilon_t$	Horizontal tensile strain at bottom of asphalt layer
$\nu$	Poisson's ratio

$\sigma$	Total normal stress/ tyre pressure subjected in normal direction
$\sigma_1$	Stress in vertical direction/ Major principle stresses acting in middle of granular layer
$\sigma_1 - \sigma_3$	Deviator stress
$\sigma_3$	Stress in horizontal direction/ Minor principle stresses acting in middle of granular layer
$\sigma_t$	Horizontal stress
$\tau$	Shear stress
$\gamma$	Shear strain
$\phi_{term}$	Angle of internal friction for material codes
$\omega$	Angular frequency
$D$	Diameter
$L$	(Original) length

## GLOSSARY OF TERMS

Term		Description
<b>Adhesion</b>	-	Action or process of adhering to a surface or object i.e. sticking together of particles of different substances
<b>Ambient</b>	-	Immediate surroundings
<b>Anionic</b>	-	Negatively charge element
<b>Anisotropic</b>	-	Physical property having different value when measured in different directions (no symmetry planes)
<b>Asphalt</b>	-	Mixture of bituminous binder and aggregate, with/ without mineral filler
<b>Assembly module</b>	-	Abaqus CAE module where parts are assembled to form a <i>part instance</i>
<b>Binder</b>	-	Material used to hold aggregate particles together
<b>Bitumen</b>	-	Black viscous mixture of hydrocarbons obtained naturally or as residue from petroleum distillation
<b>Bitumen emulsion</b>	-	Mixture of bitumen and water with <i>emulsifier</i>
<b>Bleeding/ flushing</b>	-	Shiny, black surface film of asphalt on road surface caused by upward movement of bitumen in pavement surface
<b>Break</b>	-	Separation of bitumen emulsion into free bitumen and water which occurs as a results of coagulation ( <i>see coalescence</i> ). Colour change from brown to black occurs
<b>Breaking time</b>	-	Duration of separation of water and bitumen droplets
<b>Cationic</b>	C	Positively charged element
<b>Coalescence</b>	-	Process by which two or more droplets merge during contact from single droplets
<b>Cohesion</b>	-	Sticking together of particles of the same substance
<b>Cold mix(ing)</b>	-	Mixture of bituminous binder and aggregate with/ without filler produced warm or cold in a mixing plant suitable for stockpiling, spreading and compaction
<b>Constraint</b>	-	Relationship between particular degrees of freedom that is enforced during simulation
<b>Curing</b>	-	Development of mechanical properties of bitumen based on evaporation of solvent. Process during which a chemical reaction occurs which results in a harder, tougher, more adhesive substance
<b>Cutback bitumen</b>	-	Bitumen dissolved in solvents such as kerosene, petrol and diesel
<b>Cutter</b>	-	Solvent used to cutback bitumen
<b>De-bonding</b>	-	<i>See delamination</i>
<b>Delamination</b>	-	Loss of large discrete area of wearing course layer (“de-bonding” of pavement layers)
<b>Diluent</b>	-	Substance used to decrease viscosity of a liquid
<b>Diluted</b>	-	Thinning or weakening of liquid with addition of water or solvent
<b>Distillation</b>	-	Action of purifying a liquid by process of heating or cooling

<b>Electronic Contact Resistance</b>	ECR	Resistance to current flow at a contact interface due to surface conditions
<b>Empirical</b>	-	Based on observation or experience rather than theory or pure logic
<b>Emulsifier</b>	-	Compound that lowers surface tension between two liquids i.e. soap
<b>Emulsifying agent</b>	-	<i>See Emulsifier</i>
<b>Emulsion</b>	-	Mixture of asphalt concrete or performance grade type binders emulsified in water with/ without other additives i.e. solvents, polymers
<b>Emulsion residue</b>	-	Bitumen that remains after evaporation of water
<b>Finite Element Method</b>	FEM	Numerical method solving problems of engineering and mathematical physics
<b>Flocculation</b>	-	Process by which fine particulates are caused to aggregate (clump together) into a floc
<b>Homogeneous</b>	-	A material of uniform composition throughout that cannot be mechanically separated into different material
<b>Hot Mix Asphalt</b>	-	Combination of bitumen binder and aggregate
<b>Hysteresis</b>	-	Phenomenon where value of physical property lags behind changes in the effect causing it
<b>Increment</b>	-	Interval of an analysis step
<b>Incrementation</b>	-	Division of analysis time into increments
<b>Interaction module</b>	-	Abaqus CAE module used to define interaction between regions of models or model and surroundings
<b>Interlocking</b>	-	Being jointed together
<b>Isotropic</b>	-	Physical property having same value when measured in different directions (infinite number of symmetry planes passing through one point)
<b>Job module</b>	-	Abaqus CAE module used for submission of model created for analysis
<b>Kerosene</b>	-	Light fuel oil obtained by distilling petroleum
<b>Lift</b>	-	A layer or course of paving material
<b>Load module</b>	-	Abaqus CAE module used to define conditions such as loads and boundary conditions
<b>Macrotexture</b>	-	Deviation of pavement surface from true planar surface
<b>Mechanistic</b>	-	Relation to theories which explain phenomena in purely physical or deterministic terms
<b>Mechanistic</b>	-	Relation to theories which explain phenomena in purely physical or deterministic terms
<b>Mesh</b>	-	Parts arranged into finite elements
<b>Mesh module</b>	-	Abaqus CAE model which controls mesh generation of model (parts or assembly)
<b>Microtexture</b>	-	Deviation of aggregate from a true planar surface
<b>Milled</b>	-	Process of removing part of pavement surface
<b>Non-ionic</b>	-	Not dissociating into ions

<b>Orthotropic</b>	-	Materials have two orthogonal symmetry planes for the elastic properties
<b>Overlay</b>	-	Paving method of applying a new layer of asphalt to a deteriorating surface
<b>Oxidised</b>	-	Exposure of bitumen/ asphalt to oxygen after which it becomes stiffer and more brittle
<b>Part instance</b>	-	Copy of original part to be used for analysis
<b>Part module</b>	-	Abaqus CAE module used to create and manage parts of a model
<b>Partition</b>	-	To divide into parts
<b>Pavement life</b>	-	Number of loading repetitions pavement can withstand before failure
<b>Performance Graded</b>	PG	Superpave pavement grading system developed to address pavement performance at various temperatures
<b>Pocked</b>	-	Pavement with irregular surface i.e. potholes
<b>Poisson's ratio</b>	$\nu$	Ratio of lateral (horizontal) to vertical deformation of a material subject to an axial load
<b>Property module</b>	-	Abaqus CAE module where material and section properties are defined
<b>Residual bitumen</b>	-	Remaining bitumen after emulsion has set, typically 57 to 70% of undiluted emulsion
<b>Roller</b>	-	Vehicle used to compact road building materials i.e. gravel, soils and asphalt
<b>Screed</b>	-	Flattening of road material by paver
<b>Seed</b>	-	Markers/ points used in Abaqus CAE along edges of unmeshed assembly to indicate the desired density of the mesh
<b>Set</b>	-	When all water has evaporated, leaving the residual bitumen
<b>Setting</b>	-	Time taken by bitumen to separate from water
<b>Setting time</b>	-	Speed at which water evaporates and bitumen particles separate from water
<b>Slippage (cracks)</b>	-	Crescent or half-moon shape cracks generally having two ends pointed into direction of traffic
<b>Solid (parts)</b>	-	Information which defines solid regions – 2D planar, 3D and axisymmetric
<b>Step</b>	-	Captures changes of model i.e. boundary conditions or model interaction
<b>Step module</b>	-	Abaqus CAE module used to create and define analysis steps
<b>Streaks</b>	-	Presence of alternating stripes of aggregate or bitumen
<b>Super single (tyre)</b>	-	Single wide-based tyres
<b>Surfactants</b>	-	Compounds that lower surface tension
<b>Sweep path</b>	-	Direction in which nodes of mesh are copied along edge of part
<b>Tack coat</b>	-	Spray application of thin membrane of asphalt binder acting as cohesive bond

<b>Temperature susceptibility</b>	-	Change in viscosity of bitumen binder with change in temperature
<b>Thermoplastic</b>	-	Material prone to <i>temperature susceptibility</i> i.e. viscosity varies with change in temperature
<b>Top-down meshing</b>	-	Meshing technique generated in downward direction from geometry of part/ region to individual mesh nodes and elements
<b>Tracking</b>	-	Pick-up of tack coat material by vehicle tyres
<b>Traction</b>	-	Force used to generate motion between a body and a tangential surface (through use of shear force)
<b>Traction separation</b>	-	Material response to model de-bonding
<b>Undiluted</b>	-	Liquid without the addition of water or solvent to thin/ weaken a liquid
<b>Viscosity</b>	-	Description of fluid's resistance to flow i.e. its consistency
<b>Visualisation module</b>	-	Abaqus CAE module used to provide graphical display of <i>finite element models</i> and results
<b>Volatile</b>	-	Ease at which a substance evaporates
<b>Wearing course</b>	-	Top layer of road surface that is worn down by traffic

## CHAPTER 1: INTRODUCTION

---

### 1.1 Background

The loss of bonding, or a weak bond between pavement layers, can result in various forms of distress. The types of distress anticipated typically include slippage cracking, difficulty of compaction, premature fatigue and top down cracking (Ghaly et al., 2014). Various research initiatives have shown that the lack of proper interlayer bonding due to a poor tack coat, results in a significant decrease of pavement layer performance. This phenomenon is attributed to the stress and strain regime within the layers of the pavement structure. It is, therefore, essential to understand the material characteristics and their interaction within a pavement structure, along with interlayer bonding conditions, in order to achieve adequate pavement life.

A variety of methods of tack coat application exists, with varied effects on pavement life. The use of “Spray Jet” technology for tack coat application is claimed to improve the efficiency of pavement projects, compared to the use of conventional emulsion spray tankers. Some advantages of the use of Spray Jet technology for tack coat application are attributed to the “non-requirement” of filler on the polymer emulsion tack coat to protect it from jobsite traffic and its (sometimes) logistical use in road projects. It is also found to improve the safety and environmental impacts in municipal roads. In addition, recent preliminary results reported the benefits associated of higher shear strength between the wearing course and base, manifesting in better bonding and ultimately resulting in a significant longer pavement life.

Unfortunately, the use of the technology in a large project setting has an adverse effect, given the volume of spraying required which would lead to a more frequent refilling of the paver. In turn, additional emulsion tanks will be required, which could also be an excessive hindrance concerning visibility on site. Last-mentioned would realise in instances where tanks with a capacity of 7000L or more would be required for a project (Wirtgen Group, 2017). Apart from these logistics, the financial aspect of acquiring the technology is also of concern. This stems from the fact that the purchase price of emulsion tanks are significantly lower compared to Spray Jet technology. However, it should be recognised that some of the immediate disadvantages might be out-weighed by long term benefits provided by the technology. Hence, the factors impacting the full life-cycle of such alternatives should be considered. It is, therefore, important to understand these aspects; i.e. the impact of technology on pavement performance and the full cost over the whole term of the pavement life.

### 1.2 Problem Statement and Research Need

Current construction practices in most countries do not specify the method of application of the tack coat, leading to variable performance of the upper pavement structure. The correlation between different tack coat application methods and the resultant interlayer bond requires investigation.

Previous research, using the Leutner Shear Test, indicates that conventional spray tanker application of tack coats that are trafficked by construction vehicles provides an interlayer shear strength that is low and is significantly exceeded with Jet Spray application of the tack coat by the paver, avoiding traffic on the tack before asphalt paving. This would suggest that only investigating the influence of bond strength would be insufficient in understanding the extent of influence of tack coat application by means of Spray Jet technology.

Therefore, a research study proposes to investigate the benefits of the use of the Spray Jet technology for tack coat application relative to conventional applications, through laboratory work and subsequent analysis of variables. The study explores the influence of shear strength on pavement life and the factors that contribute to the shear bond within the bond layer (tack coat). Investigating the bond strength due to tack coat application, and its relation to pavement life, will accomplish a better understanding of the technology. The application of the technology is studied at two levels; i.e. macro and micro phase, which will augment the understanding thereof. The macro stage investigates the significance of bond strength by means of tack coat application and its relation to pavement life. The focus of the micro level investigates factors which influence the strength that the bond coat can provide to the pavement as a whole.

Numerical analyses such as finite element (FE) modelling is considered a necessity in the investigation. The FE is needed to simulate a shear bonding in a laboratory test and to replicate the response of the interlayer material within a pavement structure. The replication of the Leutner Shear Test (using previous results), together with FE, will allow evaluation of different subject matters – tack coat material, interlayer bonding strength and durability. The optimisation of such a tack coat application is fundamental in understanding the differences. The combination of operational advantages and pavement performance implications for road projects creates the awareness of the use of Spray Jet technology on an international level.

### 1.3 Objectives

The goal of this study is to investigate the influence of tack coats constructed with Spray Jet technology on the interlayer bond, and hence the pavement life relative to those constructed using conventional technologies. This will provide a detailed understanding of how the shear deformation, as well as the resistance to shear, develops within the tack coat (bond coat), and what properties influence the bond behaviour. The goal will be achieved through the following primary objectives:

- (a) Determining, through analysis, whether Spray Jet Technology provides a significantly different shear bond when compared to traditional methods.
- (b) Preliminary evaluation of the extent to which interlayer bonding influences pavement response and performance properties, using Mechanistic Empirical Linear Elastic Modelling.
- (c) Simulation of the Leutner Shear test by developing a Finite Element Model to replicate the progression of shear, particularly within the bond (tack coat) layer. This will allow a detailed understanding of how shear deformation develops within the bond and which properties influence the bond behaviour.
- (d) Simulation of pavement structures by developing a Finite Element Model to replicate pavement structures used for preliminary evaluation. These will include the material properties of the tack coat layer used to evaluate bond influence and to understand which factors influence Fatigue Life. These preliminary Finite Element Models are based on a linear-elastic analysis although it is recognised that the bituminous material of tack coat displays visco-elastic behaviour.
- (e) Evaluate the extent of influence of variables within the pavement structure, i.e. material stiffness, layer thickness on the bond strength (shear stresses) and the performance properties for both simulated models, to identify which variables have the most influence on pavement behaviour.
- (f) Comparison of simulated models with preliminary evaluation to evaluate correlation between analysis approaches. This will highlight influential variables such as material stiffness and loading

on pavement performance. Subsequently, establishing whether the addition of a tack coat layer is deemed essential to enhance pavement performance.

## 1.4 Limitations

The following aspects limit the scope of this project:

1. It allows for a certain time period, resulting in simplification of some testing conditions to allow shorter computational time in order to produce sufficient results for the objective of the research. Consequently, these conditions may not be an accurate representation of actual conditions.
2. Variability exists in results from different testing methods, based on different (theoretical) approaches used to acquire the results. This allows for a comparative analysis in terms of sensitivity of parameters, which may not provide conditions for a just comparison of results.
3. Detailed information available for tack coat properties was limited. A number of assumptions were made to incorporate these properties in the analyses from previous laboratory testing, completed with bitumen emulsion, with similar material characteristics.
4. Both Mechanistic Empirical and Finite Element Method analyses are based on linear-elastic analysis where tack coats are Visco-Elastic-Plastic.
5. The full Leutner load-displacement data per test was not available. The available results only consisted of readings acquired at failure of specimens where no intermediate results (i.e. measurement of load at other time steps) are available.
6. It is uncertain whether the construction traffic rode on the conventional tack coat to give a realistic simulation of what happens on site.

## 1.5 Report structure

The purpose of the study is to evaluate the interlayer bond within pavement structures to establish the effectiveness of tack coat application in terms of pavement life. This will be achieved over a series of chapters where different fundamental components of the research is discussed as illustrated in Figure 1.5a. Chapter 1 provides the background about interlayer bonding and its influence on pavement life. The objectives and limitations for the current research study are also provided in this chapter.

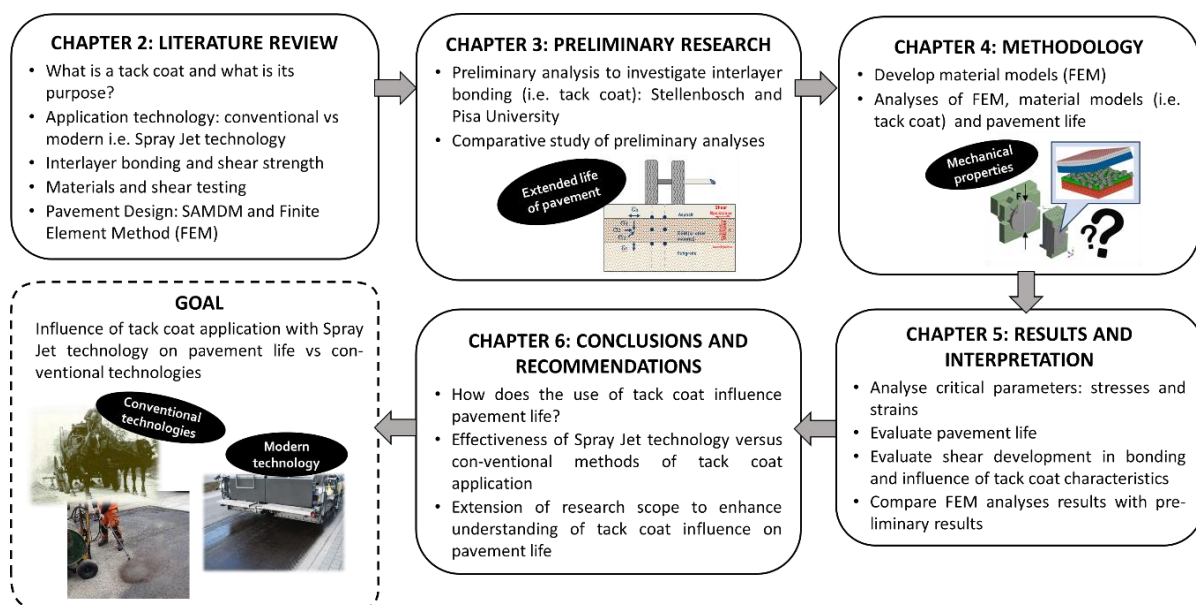


Figure 1.5a: Chapter layout

**Chapter 2** provides an introduction to the practicality of tack coats and how they contribute to pavement design in terms of shear strength. Topics addressed include various materials used for tack coats as well as various application methods, i.e. Spray Jet technology and other conventional methods. The chapter also explores the influence of shear bonding and the different shear tests used to evaluate the component, with focus on the Leutner Shear Test. Influential factors in different capacities are studied, followed by its contribution to residual pavement performance. Different elements of pavement design are also discussed. Discussions in Chapter 2 occur in relation to previous studies (where appropriate) to substantiate findings made in the different capacities.

**Chapter 3** is an introduction to the current research which provides a summary of the preliminary research carried out in collaboration with Pisa University. The different testing conditions, assumptions made, and results acquired accordingly are discussed in the relevant sections of this chapter. A comparative analysis of the two preliminary research studies is also completed to highlight distinctive differences whilst addressing different elements thereof.

**Chapter 4** describes the procedures followed to set-up the two material models used for FE analyses in this study. The experimental plan, together with the assumptions made with regard to the testing conditions and input parameters, is provided in Chapter 4. The methods used for acquisition of results for both these models are discussed, together with the critical criteria used for the interpretation of the results in Chapter 5.

**Chapter 5** contains the results obtained for the two material models analysed according to different testing conditions described in Chapter 4. The results are interpreted according to different criteria (critical parameters) for each of the two models. This addresses the objectives of each model. Results focused on the evaluation of shear stresses, strains and prediction of pavement life influenced by a variety of variables. This chapter also allows the correlation between results of material models and results acquired from preliminary analyses.

**Chapter 6** summarises the conclusions for the respective analyses, which include preliminary research undertaken by the Stellenbosch- and Pisa University. The findings from the analyses carried out with two material models, in accordance with the objective of the current research study, are addressed. The chapter also provides recommendations for further studies. This includes improvements to existing testing conditions of the respective analyses performed.

## CHAPTER 2: LITERATURE REVIEW

---

### 2.1 Introduction

Chapter 2 studies a variety of subject matters, contributing to the scope of the research study. Firstly, an introduction is given to tack coats in terms of their functions and applications in practice. Various technologies are also investigated with the main focus of tack coat application by means of Spray Jet technology. Insight is provided into the importance of interlayer bonding and the different factors which influence the bond with regard to shear strength, developed in respective layers of the pavement structure.

The macro stage of the research scope addresses numerical finite element modelling. A brief discussion on Mechanistic-Empirical analysis is also provided. This component of the research will be used to replicate the evaluation of shear development that occurs in a tack coat (interlayer bond). A discussion of the type of analysis is provided, focusing on composition of different components relevant to the research study. Previous research conducted in different capacities is also presented parallel to the relative subject matters where appropriate.

### 2.2 Tack coats

#### 2.2.1 Introduction

A tack coat is a sprayed application of an asphalt binder upon an existing asphalt or concrete pavement prior to an overlay, or between layers of new asphalt concrete (AC). The thin membrane of asphalt binder acts as a glue between the respective layers. This creates a monolithic structure which performs as a unit instead of as unbound, independent layers (Federal Highway Administration, 2016). Where consecutive pavement layers are not “properly” bonded, the structure could potentially fail prematurely, as these independent layers are not designed to accommodate traffic-imposed bending stresses (Pavement Interactive, 2011). Additionally, independent pavement layers with no tack coat allow the opportunity of water infiltrating the pavement structure, causing a decline in its structural integrity (Surface King, 2015).

Poor bonding is the direct result of inadequate tack coat practices resulting in delamination or “de-bonding”, slippage cracking (Figure 2.2.1a), sliding and shoving of surface layers. The type of failure illustrated in Figure 2.2.1a is frequently observed at locations such as intersections where braking and acceleration take place. Structural distress, such as fatigue cracking and potholes, is also a cause of concern. Ultimately, poor bonding reduces the life of the pavement structure.



**Figure 2.2.1a:** Slippage failure (Federal Highway Administration, 2016)

Various studies have been performed to evaluate the practice of using tack coats. Literature reviewed includes research by Ghaly et al. (2014) and Wang et al. (2017). Their research involved series of different controlled laboratory shear testing and included analysing different characteristics. Research by Wang et al. (2017) specifically addressed the shear testing to establish its influence on interlayer bonding. Other factors (i.e. tack coat types, application rate) contributing to these characteristics were also investigated in the study. The findings

concluded in these studies allow for an understanding of pavement failure mechanisms related to interlayer bonding characteristics. The results acquired in both instances were in favour of tack coat application, especially in terms of bond strength.

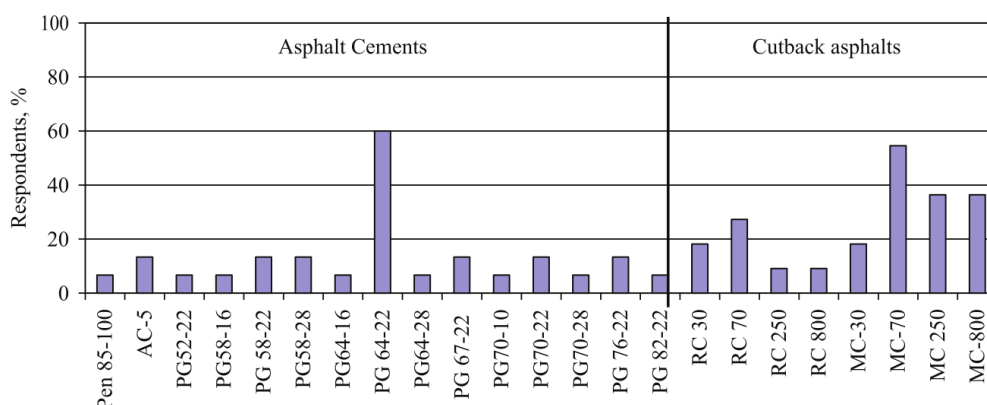
Federal Highway Administration (2016) reports a 50% decrease in pavement life with only 10% bond loss, where 60 to 75% bond loss was reported in pavement structures where there is no bonding. Jaskula & Rys (2017) have shown an improvement on fatigue life for different percentages of bond, increasing pavement life up to 7 times. The interlayer bonding and development of shear is of particular interest for the current study. Therefore, a discussion of the interlayer bonding conditions and shear at interface is provided in Section 2.3.

## 2.2.2 Tack coat materials

### 2.2.2.1 Introduction

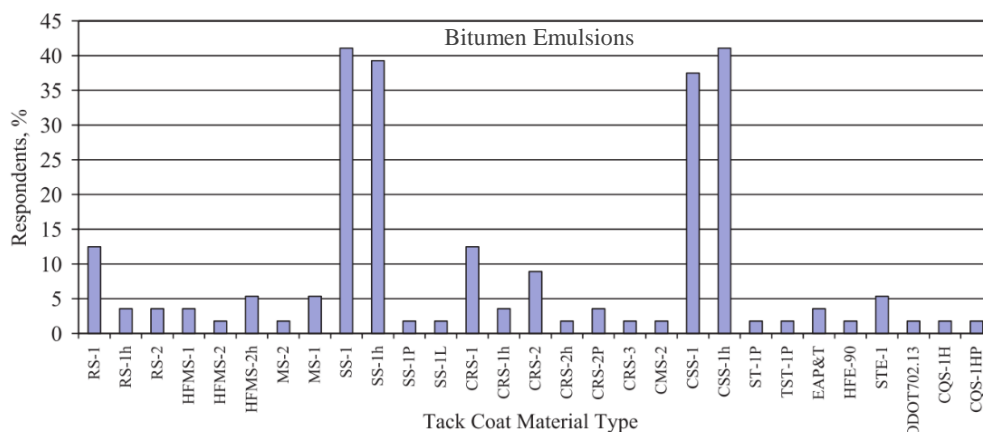
Various types of materials are used for tack coats. The choice of tack coats to be used, depends on the preference of the contractor (i.e. time, efficiency and logistics), functionality of the road (traffic capacity), material availability and properties, as well as financial implications on projects. Climatic conditions also have an influence on the selection. Federal Highway Administration (2016) suggests that appropriate tack coat material selection should be based on a combination of material properties and availability. For a tack coat to be applied, it must be in a liquid form. This can be achieved by heating it, mixing with a solvent to make a cutback or mixing it with an emulsifying agent (such as soap) to produce an asphalt emulsion (Gierhart & Johnson, 2017). Thus, three types used as tack coat materials are hot bituminous binders, cutback bitumen (bitumen-solvent base) and/ or bitumen emulsions (bitumen-water base).

Research conducted by Mohammad et al. (2012), involves a worldwide survey where 72 responses were evaluated to establish the type and grade of commonly used tack coat materials. The survey indicated that 100% of the responding agencies used bitumen emulsions, whereas only 27% and 20% used bituminous binders and cutback bitumen respectively. The different types and grades of commonly used tack coat materials are each illustrated in Figures 2.2.2.1a and 2.2.2.1b. In each of these figures, the tack coat binder type is indicated on the horizontal axis.



**Note:** Asphalt Cement = Bitumen (binder), Asphalt = Bitumen, Pen = Penetration Grade, AC = Asphalt Cement, PG = Performance Graded, RC = Rapid Curing, MC = Medium Curing

**Figure 2.2.2.1a:** Bitumen binder and cutback bitumen used as tack coat materials (Mohammad et al., 2012)



**Note:** For Nomenclature, refer to Table 2.2.2.4c

**Figure 2.2.2.1b:** Bitumen emulsions used as tack coat materials (Mohammad et al., 2012)

The survey responses indicate that bitumen emulsions are the most common types of tack coat materials used, followed by bitumen binders and lastly, cutback bitumen. In addition, the most common gradings of the respective types used are PG 64-22 (bitumen binder), MC-70 (cutback bitumen) and SS-1 and CSS-1h bitumen emulsions. It should be noted that the survey was conducted in the United States and preference of the type and grades commonly used may vary, given the different climatic conditions and road design standards of different countries.

In a South African context, the Committee of State Road Authorities (1994) suggests the use of an anionic stable grade emulsion where a cationic spray grade emulsion should be considered as an alternative only. The bitumen emulsion mix is usually diluted with water in a 1:1 ratio. Hence, achieving full coverage of the underlying layer with a thin residual bitumen film (South African Bitumen Association, 2011). A bitumen content of 60% is recommended for these emulsions with a net bitumen content of 30% in the tack coat. Emulsions such as the SS60 produced by Colas are preferably used as a tack coat material in South Africa (Petersen & Knipe, 2009). However, in a paper published by Molenaar et al. (2009) found that Styrene Butadiene Rubber (SBR) modified bitumen with a 3.5% latex can be considered as an alternative tack coat material in South Africa.

The three types of tack coat materials are individually discussed in 2.2.2.2 to 2.2.2.4. These three tack coat types introduced in subsequent sections are each limited in terms of its disadvantages, especially hot bitumen binders and cutback bitumen. Hence, asphalt emulsions are more commonly used in the field. Malicki & Górszczyk (2012) conducted research in which they investigated the problem of different tack coat materials and how they contribute to the strength and durability of interlayer bonding in an asphalt layer system. The study showed the significant influence that the various material coats could have. The type of material is also known to contribute to the interlayer bonding strength. This phenomenon will be discussed in Section 2.3.

### 2.2.2.2 Hot bituminous binders

#### **Function**

As described in Jenkins & Rudman (2018a), penetration grade bitumen is manufactured by means of two processes: straight-run distillation or blending of two base components i.e. one hard binder and one soft binder. The penetration grade bitumen is either used as the primary binder or base bitumen for cutback bitumen, or bitumen emulsions. Cutback bitumen and bitumen emulsions comprise of a certain percentage of bituminous binder, but the residual bitumen rate and application rate are the

same (Mohammad et al., 2012). Furthermore, cutback and emulsions are mixtures of binder with solvents, emulsifiers with or without additives. In some areas, (hot) bituminous binders are used as tack coat materials depending on the climatic conditions.

The grade of asphalt binder selected is typically the same as the binder incorporated into the Hot Mix Asphalt (HMA) (RAHA Bitumen, 2016d). Hence, the material would meet requirements of performance graded (PG) binders. Bituminous binders are also classified according to the penetration grade or viscosity grade, but are limited in their ability to fully characterise bitumen binder use for HMA pavements (nuroil, 2014). The Superpave grading system addresses the limitations found for the penetration and viscosity grade systems. Current South African specifications are being adapted to a PG specification framework for bituminous binders, based on engineering properties. This adaptation ensures optimal pavement performance especially under higher traffic categories (van de Ven et al., 2004). A summary of the different limitations and the improvement by means of the PG system is provided in Table 2.2.2.a.

**Table 2.2.2.a:** Prior limitation versus Superpave testing and specification features (After nuroil, 2014)

Attributes	Limitation of previous grading systems	Superpave grading system
<b>Pavement performance</b>	Penetration and ductility tests and empirical, and not directly related to HMA pavement performance	Maintained at higher temperatures than cutbacks and emulsions to remain fluid enough to spray through distributor
<b>Temperatures</b>	Tests are conducted at only one standard temperature, ignoring the ambient temperature	Constant test criteria, variable temperatures to meet changes considering binder grade selected for specific climatic condition
	Range of temperatures not accurately covered	Entire range of pavement temperatures experienced are covered
<b>Grading</b>	Different characteristics of binders within the same grading category are neglected	Grading is more precise and less overlap between grades
<b>Modified binders</b>	Modified binders are not suited for the grading system	Tests and specifications intended to include modified and unmodified binders
<b>Binder age</b>	Test methods only consider short term bitumen binder aging, where long-term aging is a significant factor	Three critical binder ages simulated and tested: <ul style="list-style-type: none"> <li>• Original binder prior to aggregate addition</li> <li>• Aged binder after HMA production and construction</li> <li>• Long-term aged behaviour</li> </ul>

**Classification**

PG binder nomenclature (in the form PG XX-YY) incorporates the temperature extremes under which HMW pavement must perform to resist rutting, fatigue and thermal cracking. The grade is determined by indicating the high temperature (XX) and the low temperature (-YY) performance. The low temperature attribute is represented by a negative sum due to the low temperature being a negative number. The various attributes of the nomenclature are explained in Table 2.2.2.2b.

**Table 2.2.2.2b:** PG binder nomenclature (After Texas Department of Transportation, 2015)

Attribute		XX	-YY
Classification	Temperature Performance	High	Low
	Grading system (increments of 6°C)	58, 64, 70, 76 and 82	-16, -22, -28 and -34
	Designation	7-day average high pavement temperature	Low pavement temperature

**Advantages and disadvantages**

The use of bitumen binder as a tack coat material is not that common, compared to cutback and emulsions, based on its material properties. The advantages and disadvantages for the use of the binder as tack coat material are summarised in Table 2.2.2.2c accordingly. These attributes are compiled from literature reviewed from Gierhart & Johnson (2017) and Zhang (2017) respectively.

**Table 2.2.2.2c:** Bitumen binder advantages and disadvantages (After Gierhart & Johnson, 2017; Zhang, 2017)

Advantages	Disadvantages
<ol style="list-style-type: none"> <li>Higher interlayer shear strength</li> <li>Decrease in construction duration as no set/curing time is required</li> </ol>	<ol style="list-style-type: none"> <li>To be maintained at higher temperatures than cutbacks and emulsions to remain fluid enough to spray through distributor</li> <li>High temperature required for application leads to safety concern of construction workers</li> <li>More energy is required to heat the binder</li> <li>Higher interface bonding is required compared to cutbacks and emulsions</li> </ol>

Studying the various attributes listed, it is evident that the interlayer shear strength produced by the bituminous binder can be considered both an advantage and disadvantage – high interlayer shear strength is favourable, although greater strength is required equivalent to other options for tack coat material (unfavourable).

**Hot bitumen binders in practice**

These types of binders are typically used for night time road construction, as water is not needed for break and set times. According to Federal Highway Administration (2016), excellent performance was reported in projects where bituminous binder was used. The most general of these binders used are PG 58-28, PG 64-22, PG 67-22 and PG 76-22 where a modified binder (PG 76-22M) has also been found to perform well in bonding two pavement layers (Zhang, 2017). In some instances, the bituminous

binder used can be polymer modified. Applying hot bitumen binders as tack coats are very common in South Africa in the construction of chip seals.

### 2.2.2.3 Cutback bitumen

#### **Production**

Cutback bitumen is a blend of penetration grade bitumen and controlled amounts of petroleum solvent (“cutter”) used to temporarily reduce the viscosity of the bitumen. The reduction allows the bitumen to penetrate pavements more effectively. After its application, the petroleum solvent evaporates and leaves behind binder residue on the pavement surface (J. Wang et al., 2017) which binds the aggregate. Similar occurrence applies to bitumen emulsions. Three types of solvents are used, namely slow curing (SC), medium curing (MC) and rapid curing (RC) of which the MC and RC are the most commonly used in South Africa (RAHA Bitumen, 2016c). The type of solvent used will determine the curing rate of the bitumen when exposed to air. The curing is related to the evaporation rate of the solvent used which influences the setting time of the bitumen. The viscosity is dependent on the proportion of solvent added to the mixture.

#### **Classification**

A curing rate and viscosity are designated for cutback bitumen in order to distinguish between the different types of products in this material group. The classification comprises two attributes (curing rate and viscosity) and is represented by a symbol or number as indicated in Table 2.2.2.3a. The time for curing and viscosity of the cutback bitumen can be controlled by the dilution of the solvent and the volatility of the solvent added (The Constructor, 2017).

**Table 2.2.2.3a:** Cutback classification (After Texas Department of Transportation, 2015)

Attribute		Classification			
Curing (rate)	Describes volatility of solvent used	Types		Volatility	Solvent
		SC	slow curing	low	petrol/ gas
		MC	medium curing	intermediate	kerosene
		RC	rapid curing	high	diesel oil
Viscosity	Assigned a number between 30 and 3000	<i>Examples:</i> <ul style="list-style-type: none"> <li>• 30 contains approximately 35 to 40% solvent</li> <li>• 3000 contains approximately 5% solvent</li> </ul>			

#### **Advantages and disadvantages**

Despite the benefit of the added solvent to reduce viscosity, the evaporation of the solvents (volatile chemicals) produces emissions that are harmful to the environment. Additionally, the utilisation of these solvents requires higher amounts of energy to manufacture. This is a more expensive process compared to the production of bitumen emulsion (J. Wang et al., 2017). The various advantages and disadvantages of cutback bitumen are summarised in Table 2.2.2.3b, as acquired from various literature sources reviewed. Literature reviewed includes studies carried out by Ghaly et al. (2014) and Wang et al. (2017), Moreover, other resources from RAHA Bitumen (2016b) and Pavement Interactive (2012) were also used to assist with the compilation in Table 2.2.2.3b.

**Table 2.2.2.3b:** Cutback bitumen advantages and disadvantages (After Ghaly et al., 2014; Wang et al., 2017; RAHA Bitumen, 2016b; Pavement Interactive, 2012)

Advantages	Disadvantages
<ol style="list-style-type: none"> <li>1. Fluid at lower temperatures, i.e. 10 to 120°C</li> <li>2. Remains fluid for a long period after application, permitting latitude between distribution and application of rock</li> <li>3. Some cutter remains in the cutback seal to conform to some movement in underlying pavement layers</li> <li>4. Cutback can have self-healing characteristics with minimal cracking</li> <li>5. Robust in applications where larger aggregate is covered by fines</li> <li>6. Mixtures made with unheated aggregates and some cutback</li> </ol>	<ol style="list-style-type: none"> <li>1. Does not obtain ultimate strength until most of solvent has evaporated</li> <li>2. Rock can be displaced under heavy traffic and high temperatures during its curing period</li> <li>3. Rain can float cutback to the top of the rock and tracking can occur</li> <li>4. Potential fire hazard</li> <li>5. Contributes to air pollution due to evaporation of solvent and is dangerous to human health</li> <li>6. Excessive moisture on existing layer can hinder good adhesion</li> </ol>

***Cutback bitumen in practice***

Cutback bitumen ensures that the material regains its original hardness and property after setting. The penetration grade bitumen is a thermoplastic material as it is prone to temperature susceptibility. The fluidity required at time of placement is achieved by raising the temperature, whereas the cutback bitumen is added when fluidity is required at a lower temperature (The Constructor, 2017). Therefore, cutback bitumen is ideally used for cold weather bituminous road construction and maintenance (Mathew & Rao, 2007).

The use of the material as a tack coat is limited due to health and safety risks, but permitted for priming bases and patching mixes. Typical cutback bitumen used is MC 30 and RC 250 (RAHA Bitumen, 2016c). Cutback bitumen is more workable compared to penetration grade bitumen. It also requires less heat (energy) to liquefy and eases its use at lower temperatures. However, compared to bitumen emulsion described in 2.2.2.4, cutback bitumen is considered less favourable, given the advantages presented by bitumen emulsion materials used for tack coats. A comparison of these two materials is provided in Table 2.2.2.3c based on measurable aspects, such as composition, manufacturing and health and safety implications. The comparative aspects given in the table are compiled from Afsar (2012) and RAHA Bitumen (2016b) respectively.

**Table 2.2.2.3c:** Cutback bitumen versus bitumen emulsion (After Afsar, 2012; RAHA Bitumen, 2016b)

Attribute	Cutback bitumen	Bitumen emulsion
<b>Residual bitumen</b>	80% residual bitumen.	40 to 65% residual bitumen.
<b>Application</b>	<ul style="list-style-type: none"> <li>• Cannot be applied at very low temperatures, requiring additional fuel cost.</li> <li>• Dry pavement is required for application. Extends duration of project as more time is required for drying of surface.</li> </ul>	<ul style="list-style-type: none"> <li>• Easily applied at low temperatures and saves fuel cost.</li> <li>• Can be applied on wet surfaces with no requirement of dry surface for application.</li> </ul>
<b>Safety</b>	Not safe to use. It is flammable due to high energy products (ingredients) and poses potential health risk.	Safe to use and has no side effects.
<b>Environment</b>	<ul style="list-style-type: none"> <li>• Volatile chemicals (solvents) evaporate into atmosphere and emissions contribute to air pollution (not environment friendly).</li> <li>• Non-water solvent results in high energy diluent wastage in atmosphere.</li> </ul>	Water (solvent) evaporates into atmosphere (environment friendly).
<b>Manufacturing and cost</b>	Requires high amount of energy to manufacture and is expensive.	Requires low amount of energy and is less expensive (compared to cutback bitumen). In general, it is cheaper than any other binding material with the same material properties.

#### 2.2.2.4 Bitumen emulsion

##### **Production**

Bitumen emulsions are mixtures of bitumen emulsified in water. It consists of bitumen, water, an emulsifying agent (emulsifier) and may include additives such as latex, polymers, acids and stabilizers to further modify the physical characteristics of the emulsion. The three ingredients are mixed in a high-speed mixer called a colloid mill (Asphalt Institute & Asphalt Emulsion Manufacturers Association, 2008).

The blending of the bitumen and water is aided with the emulsifying agent. The combination of the emulsifier (soap) and high shear, breaks bitumen up into small droplets which remain dispersed in water (RAHA Bitumen, 2016a). The particles of the emulsifier surround the bitumen particles (droplets) and break the surface tension that holds them together (Figure 2.2.2.4a left). Bitumen emulsions used as tack coat material consist of approximately 67% bitumen binder and 33% water (For Construction Pros, 2014).

Apart from material properties of the respective ingredients, the process is influenced by environmental conditions such as ambient temperature, humidity and wind movement (Yaacob et al., 2013). The process of emulsion production is demonstrated in Figure 2.2.2.4a (right) with a description of the four components in the figure provided in Table 2.2.2.4a.

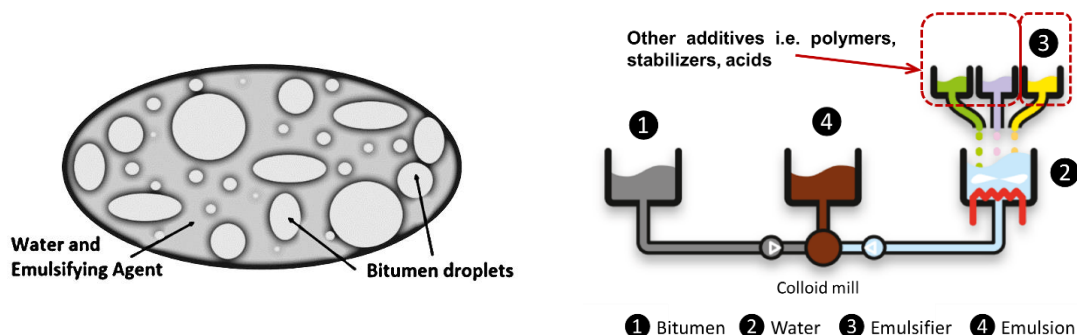


**Figure 2.2.2.4a:** Emulsion process (After Dillard, 2015) (After Akzo Nobel, 2010)

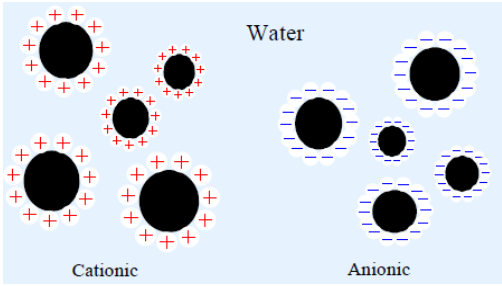
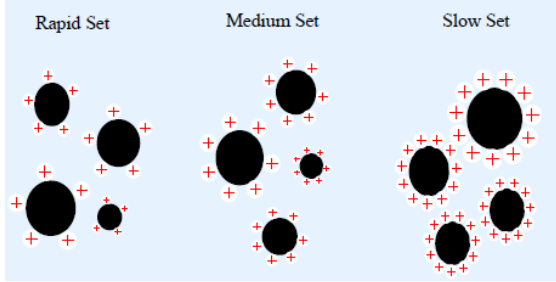
**Table 2.2.2.4a:** Emulsion production procedure (After Johnson, n.d.)

Diagram symbol	Ingredient	Characteristics
①	Bitumen	<ol style="list-style-type: none"> <li>1. Basic ingredient.</li> <li>2. Makes up 50 to 75% of emulsion (Asphalt Institute &amp; Asphalt Emulsion Manufacturers Association, 2008).</li> <li>3. Some properties have significant effect on final product.</li> <li>4. No exact correlation between property and ability to emulsify bitumen.</li> <li>5. Properties of bitumen affect performance of residual asphalt on the road.</li> </ol>
②	Water	Mineral and other materials in water possibly affects production of stable emulsions.
③	Emulsifier	<ol style="list-style-type: none"> <li>1. Chemical used greatly influences properties of bitumen emulsion.</li> <li>2. Keeps bitumen particles in suspension and controls breaking time (according to Texas Department of Transportation (2015)), suspension allows for application at lower temperatures).</li> <li>3. Determines whether emulsion is cationic, anionic or non-ionic.</li> <li>4. Note: Chemical compatibility of emulsifying agent with bitumen is of great importance to produce stable emulsion.</li> </ol>
④	Emulsion	In the mill, the bitumen is sheared into microscopic particles. The size of these particles influences the physical properties of emulsions.

**Classification**

Bitumen emulsions are classified by their type (ionic charge) (Figure 2.2.2.4c), speed of break (Figure 2.2.2.4d), viscosity of emulsion, stiffness/ hardness of residue binder as well as the presence of additives. A description of the various components that form part of the classification is provided where appropriate in Table 2.2.2.4b. Classifications are indicated subsequently in Table 2.2.2.4c.

**Table 2.2.2.4b:** Emulsion description

Attribute	Description
<p><b>Ionic charge</b></p>	<p>“C” is designated for cationic (positive charge) emulsion. Not using a “C” describes anionic (negative charge) emulsion.</p>  <p><b>Figure 2.2.2.4b:</b> Illustration of cationic and anion (Yaacob et al., 2013)</p>
<p><b>Speed of emulsion break</b></p>	<p><b>Description</b></p> <p>The number of charge particles surrounding the bitumen droplets (Figure 2.2.2.4c) decides the setting of the bitumen. As the quantity (of charge) decreases, the repulsive forces between droplets minimize and ease flocculation. Similarly, droplets with lesser surface charge upon contact with aggregate surface will ease flocculation and coalescence (Yaacob et al., 2013). The phenomena describe the behaviour of droplets to clump together and to merge into one droplet.</p>  <p><b>Figure 2.2.2.4c:</b> Bitumen emulsion setting (Yaacob et al., 2013)</p> <p>Emulsion break and set times are influenced by the application rate, climatic conditions, ambient temperature, surface and application temperature (Federal Highway Administration, 2016). Also, the use of diluted emulsion would require more time to break, compared with an undiluted emulsion, given the increase in amount of water.</p>

**Table 2.2.2.4c:** Bitumen emulsion classification

Attribute		Classification
Speed of emulsion break	Classification	HF – high float: gelling property that prevents runoff after application. RS – rapid set. MS – medium set. SS – slow set. QS – quick set (for use in slurry seals).
Emulsion viscosity		1 – low viscosity. 2 – high viscosity.
Stiffness/ hardness		“h” suffix: indicates stiffer/ harder emulsion residue.
Additives		“P” suffix: additive added i.e. polymer. “S” suffix: solvent added.

**Advantages and disadvantages**

An advantage of this type of tack coat material is flexibility, given that its physical properties can be modified to optimize storage, curing, mixing, traffic return and bonding strength (Section 2.3). As mentioned, additives can be used to enhance the physical properties of both the emulsion and the cured asphalt (Johnson, 2018a). Bitumen emulsions are considered ideal binders for hill road construction, where heating of the bitumen or aggregate can be difficult (Mathew & Rao, 2007).

Extensive benefits exist for bitumen emulsions of which a few of the key advantages are shown alongside its disadvantages in Table 2.2.2.4d. It should be noted that the benefits are dependent on the type of bitumen emulsion used as an effective treatment for a specific road need (RAHA Bitumen, 2016a).

**Table 2.2.2.4d:** Bitumen emulsion advantages and disadvantages (Federal Highway Administration, 2016) (Johnson, 2018a)

Advantages	Disadvantages
<ol style="list-style-type: none"> <li>1. Application uniformity</li> <li>2. Ideal for remote locations in absence of hot mix plants</li> <li>3. No/ minimal hydrocarbon emissions</li> <li>4. Reduces overall life cycle costs</li> <li>5. Improves skid resistance, reduces hydroplaning and improves visibility</li> </ol>	<ol style="list-style-type: none"> <li>1. Emulsion break and set time</li> <li>2. Tracking potential</li> <li>3. Transfer of tack coat material to adjacent pavement though construction vehicles or equipment</li> </ol>

Bitumen emulsions are the most well-known and broadly used materials for tack coat (Johnson, 2018b). The main advantage of the bitumen emulsion is attributed to its ability to be applied at lower temperatures (beneficial for cold mixing) compared to cutback bitumen or hot bitumen binders. Furthermore, it is an environmentally friendly material containing no harmful volatile solvents. These materials are also safer to use as they are inflammable and do not pose a health risk to workers (Chen & Huang, 2010). It is also known that bitumen emulsions produce greater interface bonding strength than cutback bitumen (J. Wang et al., 2017).

### **Bitumen emulsions in practice**

The general practice is to use slow setting (SS) emulsion, diluted with water, before application (Ergon Asphalt and Emulsions, 2006). According to Federal Highway Administration (2016), the most common tack coat materials used are bitumen emulsions, i.e. (anionic) slow setting or “SS” emulsions: SS-1, SS-1h, CSS-1 and CSS-1h. Other increasingly-used materials are rapid setting or “RS” emulsions such as RS-1, RS-2, CRS-1 and CRS-2, as well as polymer-modified bitumen emulsions (PMAE), such as SS-1hP. PMAE emulsions are particularly used for spray paver applications (Federal Highway Administration, 2016). The addition of polymers or modifiers increases the adhesion and service life of the tack coat (Texas Department of Transportation, 2015). In many European countries, cationic rapid setting (CRS), or a specially designated low viscosity medium setting emulsion (MS-1), is used and applied undiluted (Surface King, 2015).

Tosas has played an instrumental role in bitumen emulsions developed and supplied formulated to perform in the mining and road construction sectors for more than 40 years (Tosas, 2018). In-situ Engineering Technical Solutions (IETS) are formulated to perform well in environmental conditions where 70-100 grade base bitumen is used in the emulsification process. Because of the chemical and physical properties, no leaching of matter will occur after emulsion is applied and “cured” in dust control application. The PG 70-100 bitumen remains as a binder that “bonds” dust and soil particles. The product does not contain any cutters, extender oils and volatile components. Consequently, no volatiles are released in the atmosphere or into the soil during or after application (Tosas, 2018).

In addition, Tosas developed Elasto-Tack to create a superior bond between the existing surface and the ultra-thin friction course (UTFC). The material is applied using integrated spray pavers, as those discussed in Section 2.2.4, that are capable of laying a tack coat prior to placing the asphalt layer. The emulsion is modified with a Styrene Butadiene Rubbers (SBR) polymer to improve the residual binder



**Figure 2.2.2.4d:** Application of Elasto-Tack with spray paver (Tosas, 2019)

properties, bond strength and adhesion at the interface (Tosas, 2019). The purpose of the addition is attributed to shear force acting on the interface between the substrate and asphalt overlay being higher than those experienced with thicker asphalt layers. When applying Elasto-Tack, it will start to boil underneath the UTFC mix as shown in Figure 2.2.2.4d. This process causes bubbles to burst leaving an elastic bond between the existing surface and newly laid UTFC. More technical details with regards to the product is provided in Tosas (2019).

## 2.2.3 Tack coat application

### 2.2.3.1 Introduction

Tack coats should be applied as a thin coat, uniformly distributed across the entire pavement surface (Figure 2.2.3.1a) and should cover approximately 90% of the surface area. However, an optimum application rate of 90 to 95% is preferred, according to Wang et al. (2017). This allows tack coat distribution consistency in bonding strength along the pavement surface. The quantity of the tack coat is also critical, as too little tack coat could result in inadequate bonding, i.e. delamination (de-bonding), whereas over-application can form a slip lane (Asphalt Institute & Asphalt Emulsion Manufacturers Association, 2008). In addition, materials can



**Figure 2.2.2.4a:** Uniform tack coat coverage (RAHA Bitumen, 2016a)

be drawn into an overlay, which has a negative impact on the mixing properties. This could possibly create the potential for excessive flushing or bleeding in thin overlays (Pavement Interactive, 2011).

The tack coat is sprayed as a thin film on the existing layer surface, after which the succeeding pavement layer (surfacing) is constructed. Interlocking develops when the tack coat wets the surface of the existing pavement layer, fills the pores and solidifies. A low viscosity tack coat penetrates and follows surface irregularities better, compared to a high viscosity tack coat (Ghaly et al., 2014). This would suggest that a lower viscosity tack coat provides better interlocking. Many factors affect the tack coat performance and interlayer bond strength. These components are investigated in Section 2.3.

Figure 2.2.3.1b illustrates the procedure of tack coat application as recommended in the National Cooperative Highway Research Program (NCHRP) *Report 712*. The first step in achieving proper tack coat application is attributed to the calibration of the equipment used. In addition, trial tack coat application is required if the distributor

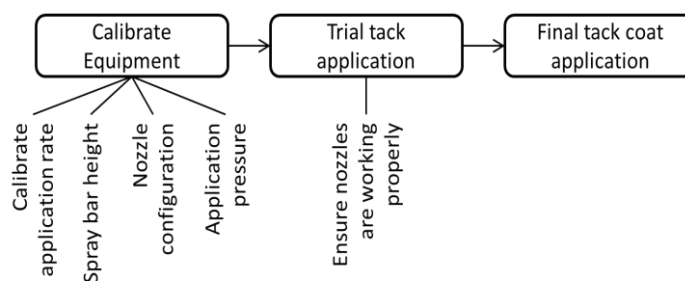


**Figure 2.2.3.1b:** Tack coat application procedure (Mohammad et al., 2012)

has not been used for some time, which will also ensure that the nozzles are working properly. The application rate should also be calibrated in both longitudinal and transverse directions.

The fundamental aspects of successfully applied applying tack coats are listed here:

1. Clean and dry roadway surface prior to tack coat application free from any loose material that may prevent bonding;
2. Traffic and equipment i.e. rollers and trucks should be kept off tacked surfaces to avoid tracking;
3. Uniform application, including all vertical surfaces of joints and structures;
4. Ensure all equipment functions properly and is set up correctly;
5. Selection of proper application rate for the tack material used, together with existing surface conditions;
6. Allow tack to set prior to paving to ensure best possible bond between layers.

### 2.2.3.2 Tack coat breaking and setting

It has been demonstrated that bitumen emulsions (2.2.2.4) are preferred over both hot bituminous binders (2.2.2.2) and cutback bitumen (2.2.2.3). The emulsion should break before placement of the tack coat. However, according to Surface King (2015), there is currently no complete agreement with regard to the requirement of tack coat to be allowed to break and set (Figure 2.2.3.2a) before placing the HMA layer. Generally, bitumen emulsions used for tack coats will break and be fully cured shortly after placement (Asphalt Institute & Asphalt Emulsion Manufacturers Association, 2008).

As the bitumen emulsions are applied on aggregates, the water starts to evaporate which causes the bitumen to separate from the water. When the emulsion breaks, the colour of the material changes from brown to black after which the water evaporates (Asphalt Institute & Asphalt Emulsion Manufacturers Association, 2008). The breaking rate is dependent on environmental conditions and grade of emulsions selected. After the water has evaporated, the physical properties of residual bitumen are regained, resulting in a strong adhesive bond. The bitumen spreads over the aggregate surface, acting as a binding material and slowly attains its strength (RAHA Bitumen, 2016a) as shown in Figure 2.2.3.2a. The procedure explained is demonstrated by means of Figure 2.2.3.2b.

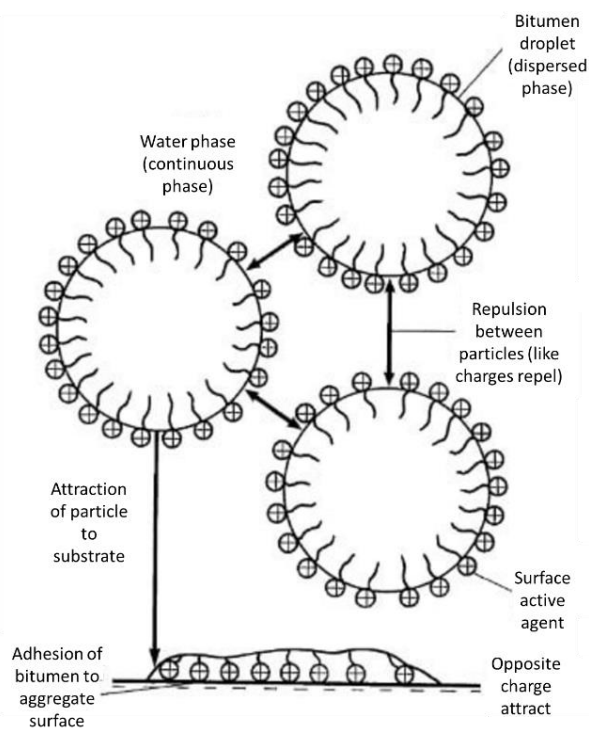


**Figure 2.2.3.2a:** Breaking and setting of bitumen emulsion (The Constructor, 2017)

The breaking rate is dependent on environmental conditions and grade of emulsions selected. After the water has evaporated, the physical properties of residual bitumen are regained, resulting in a strong adhesive bond. The bitumen spreads over the aggregate surface, acting as a binding material and slowly attains its strength (RAHA Bitumen, 2016a) as shown in Figure 2.2.3.2a. The procedure explained is demonstrated by means of Figure 2.2.3.2b.

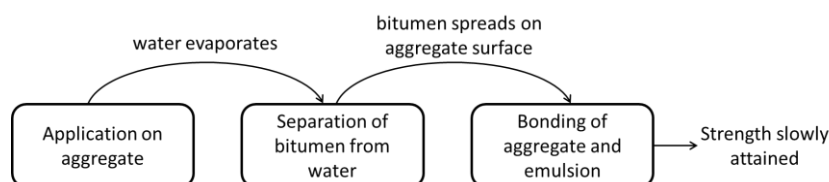


**Figure 2.2.3.2b:** Bitumen emulsion bond development

Factors that affect breaking and curing rates of bitumen emulsions, are summarised from the Asphalt Institute & Asphalt Emulsion Manufacturers Association (2008):

1. *Water absorption*;
2. *Aggregate moisture content* – wet aggregate slows the curing process as it increases the time required for evaporation;
3. *Weather conditions* – temperature, humidity and wind velocity influence the evaporation rate, emulsifier migration, and water release characteristics;
4. *Mechanical forces* – roller pressure as well as slow moving traffic forces water from the mix, helping to attain mixture cohesion, cure and stability;
5. *Surface area* – greater aggregates accelerate emulsion breaking;

6. *Surface chemistry* – intensity of aggregate surface charge and emulsifier charge could impact setting rate;
7. *Emulsion and aggregate temperature* – at high temperature, emulsion breaking accelerates;
8. *Emulsifier type and amount* – the surfactant will establish the emulsion breaking characteristics
9. *Application (and dilution) rate.*

### 2.2.3.3 Tack coat uniformity

Optimal application of tack coat (Figure 2.2.3.3a), will achieve proper interlayer bonding strength. According to Federal Highway Administration (2016), the best opportunity for pavements to achieve performance is presented by adhering to good design and construction practices. Comprehensive details concerning tack coat practices are provided in Federal Highway Administration (2016).

The design phase involves an evaluation of the existing surface, selection of appropriate tack coat material (Section 2.2.2) and the proper residual bitumen rate. To achieve uniformity in surface coverage, various aspects of application should be controlled. These aspects include the current condition of the existing surface (new, old or milled), the application rate and tack coat dilution (Mohammad et al., 2012).



**Figure 2.2.3.3a:** Tack coat coverage (Federal Highway Administration, 2016)

### **Application rates and dilution**

The application rate alternates, based on the type and condition of the pavement receiving the tack coat (Pavement Interactive, 2011). The *Basic Asphalt Emulsion Manual* reports typical application rates of 0.25 to 0.7l/m<sup>2</sup>. General recommendations for tack coat application rates on different common surfaces are summarised in Table 2.2.3.3a. The higher the application rate, the longer it will take (for the emulsion) to break and set (Federal Highway Administration, 2016). In addition, characteristics of the distributor vehicle to be discussed in Section 2.2.4, also affect the application rate.

**Table 2.2.3.3a:** Recommended tack coat application rates (Federal Highway Administration, 2016)

Surface Type	Application rate (l/m <sup>2</sup> )	Approximate bar rate (l/m <sup>2</sup> )	
		Undiluted	Diluted (1:1)
New Asphalt	0.09 – 0.2	0.14 – 0.32	0.3 – 0.63
Existing Asphalt	0.18 – 0.32	0.3 – 0.5	0.54 – 1
Milled surface	0.18 – 0.36	0.3 – 0.54	0.54 – 1.1
Portland Cement Concrete (PCC)	0.14 – 0.2	0.2 – 0.36	0.45 – 0.72

In practice, three types of application rates are identified: low, intermediate and highest. Low application rates (0.09 to 0.2l/m<sup>2</sup>) are recommended for new pavement structures, whereas intermediate rates (0.21 to 0.4l/m<sup>2</sup>) are recommend for resurfacing of existing, relatively smooth surfaces. The upper limit application rate (0.41l/m<sup>2</sup> and above) is for old, oxidised, cracked, pocked or milled HMA

and Portland Cement Concrete (PCC) pavement surfaces (Asphalt Institute & Asphalt Emulsion Manufacturers Association, 2008). Dry, aged surfaces require more tack coat compared to surfaces experiencing “fattiness” or flushing. Fattiness or flushing will increase with the amount of residual bitumen required for milled surfaces, attributed to the increased specific surface area (Mohammad et al., 2012).

Under certain circumstances, tack coats are diluted with water to increase the total liquid volume, while maintaining the volume of bituminous binder. It assists with achieving uniformity without excessive amounts of bituminous binder. Premature emulsion break can occur due to excessive dilution. Pavement Interactive (2011) indicates that dilution increases emulsion break and set time and points out the importance of water being added to the emulsion, and not vice versa, as it would cause the tack to break. The diluted emulsions require greater application rates to obtain the same residual bitumen coverage.

The low viscosity of emulsion, compared to penetration bitumen, it is not possible to spray emulsion at more than approximately 0.6 to 0.7l/m<sup>2</sup>, without the binder tending to flow (CSIR, 2007). It should be noted that distributors have a limitation of spraying 0.6l/m<sup>2</sup> as a minimum application rate.

#### 2.2.3.4 Other tack coat challenges

Pavement Interactive (2011) identifies three tack coat aspects which should be considered noteworthy, although not deemed critical, with reference to tack coat application, viz. the timing, tracking and traffic. The timing involves the break and set (bitumen emulsion) or cure (cutback bitumen) allowed for the placement of the specific tack coat material and whether sufficient time was allowed in the process.

##### **Tracking**

A persistent problem associated with tack coat application is tracking. The phenomenon occurs when construction vehicles drive on the applied tack coat and remove the tack coat material from the pavement surface as it is picked-up by vehicle tyres (Figure 2.2.3.4a). The material removed is deposited on adjacent pavement surfaces. It has been found that deposited material has little effect and wears away quickly, but in extreme cases may distort pavement surfaces or hinder a driver’s ability to navigate (Pavement Interactive, 2011). The occurrence is encouraged by inappropriate practices of tack coat application (J. Wang et al., 2017).



**Figure 2.2.3.4a:** Pick-up by haul truck tyres (Mohammad et al., 2012)

Various methods to address tracking include:

1. *Tack coat application.* Application of tack coat to pavement surface underneath paver just ahead of the screed, using a special paver fitted with a tack coat spray bar (Mohammad et al., 2012).
2. *Specialised vehicles.* A material transfer vehicle (MTV) can be used to address the pick-up of tack coat material. This must be used with a second tank to solve the problem (J. Wang et al., 2017).
3. *Set and break time.* The tracking of emulsion is reduced as the water leaves the emulsion. Similarly, an emulsion that has set would be less prone to tracking than an emulsion that is broken. Johnson (n.d.) recommends a waiting period to allow sufficient time for the bitumen to set as it would further reduce tracking issues, although additional time leads to a delay in paving.

4. *Modified tack coats*. Use of modified tack coat materials without stickiness or pick-up problems also referred to as “trackless” or non-track materials. The emulsions are formulated with stiffer base binders with or without chemical modifications i.e. polymer modified (Federal Highway Administration, 2016) and are manufactured to harden quickly, while comprising minimal adhesion. The addition of asphalt lift placed over the tack would cause the hardened tack coat to be re-activated by heat. The circumstance results in a stronger bond between the new overlay and the existing surface. However, compared to traditional emulsions, some set time is still required until it is reduced. Hence, these materials should actually be referred to as “reduced-tracking” materials (Gierhart & Johnson, 2017).

### **Traffic**

Traffic should not be allowed on tack coats as exposure to traffic provides the potential for reduced skid resistance, especially during wet weather. If the necessity exists for a tacked surface to be opened to traffic, it should be covered with sand to provide friction and prevent pick-up of the tack coat material. A typical rate of 2.2 to 4.4 kg/m<sup>2</sup> is recommended by Pavement Interactive (2011) for applying sand cover aggregate.

## **2.2.4 Tack coat application methods**

### **2.2.4.1 Introduction**

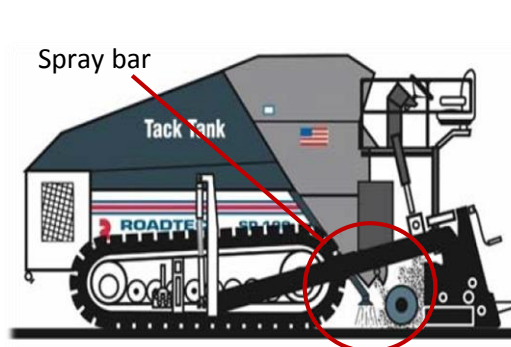
There are three types of tack coat application methods as shown in Figures 2.2.4.1a and 2.2.4.1b:

1. Conventional distributor truck
2. Special paver with tack coat tank and spray bar
3. Manual application with hand spray

A summary of the various components of each of these methods is provided in 2.2.4.2 to 2.2.4.5 respectively. Preliminary research completed for the current study (Section 3.2) highlights the importance of tack coats. This was completed by investigating the effectiveness of such a layer in terms of pavement durability. Factors impacting the tack coat, such as layer thickness and material stiffness, were investigated. (Different variables were included for the preliminary research and the current study, although the method of application is not eminent in the simulated models and linear-elastic analyses completed).



**Tack coat distributor truck**



**Paver with tack coat tank and spraybar**

**Figure 2.2.4.1a:** Tack coat application equipment (Asphalt Institute & Federal Highway Administration, 2016; ArrMaz, 2012)



**Figure 2.2.4.1b:** Application of tack coat with hand sprayer (Yaacob et al., 2014)

### 2.2.4.2 Tack coat distributor truck

The distributor truck is used to apply the tack coat on the prepared surface. A disadvantage of this method of application is that it is responsible for tracking (2.2.3.4). Various studies, such as research conducted by Wang et al. (2017), showed that typical application rates had little effect on interface shear strength. It was also found that rates higher than the recommended application rates resulted in slightly lower interface strength.

The distributor truck consists of a heated tank for storing the tack coat material at desired application temperatures, as different tack coat materials require different working temperatures. A spray bar is fitted with nozzles, which distributes the tack coat at the relative application rate which is maintained at the back of the truck. The width of the spray bar is 4.3m to cover a single lane. The application rate is monitored and adjusted by means of a computerised system inside the truck – it is adjusted by altering the truck speed as well as nozzle size type and size (J. Wang et al., 2017). An illustration of such a setup is shown in Figure 2.2.4.2a. An enlarged version of the spray bar is provided in Figure 2.2.4.2f.

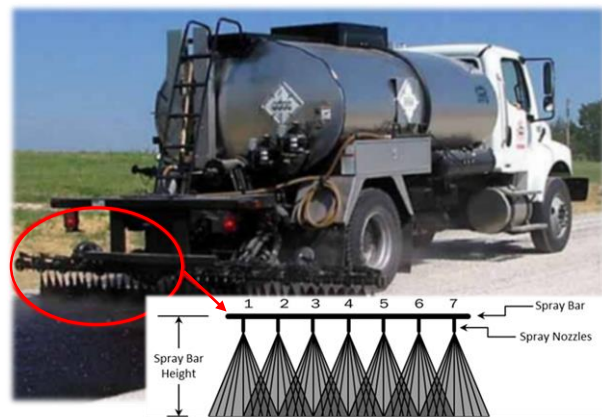
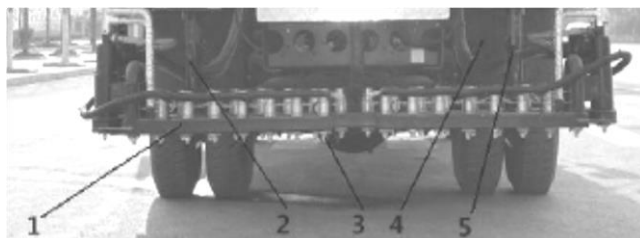


**Figure 2.2.4.2a:** Distribution truck setup (After Wang et al., 2017)



**1** – Air reservoir nozzle assembly, **2** – Rear spray bar hook, **3** – Spraying bar, **4** – Adjusting chain

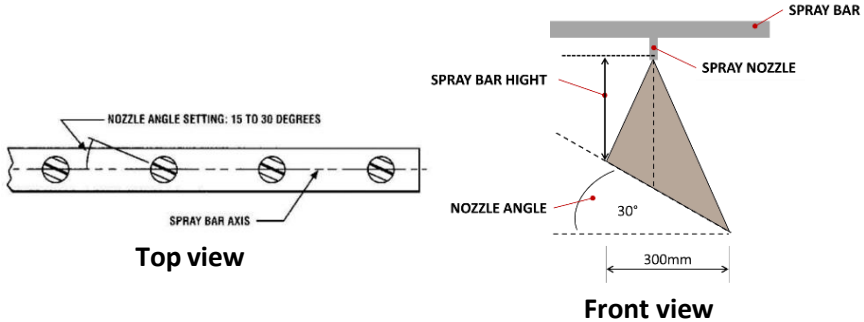
**Figure 2.2.4.2b:** Spray bar assembly (CEEC Trucks Industry, 2001)

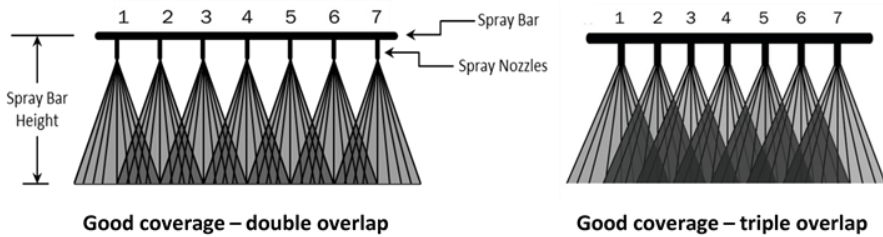
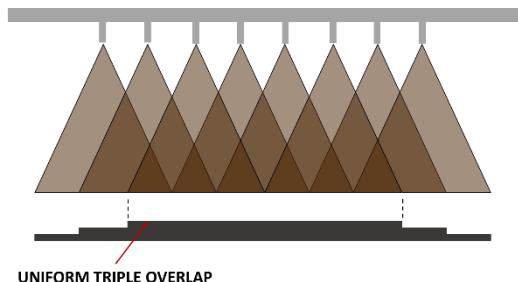
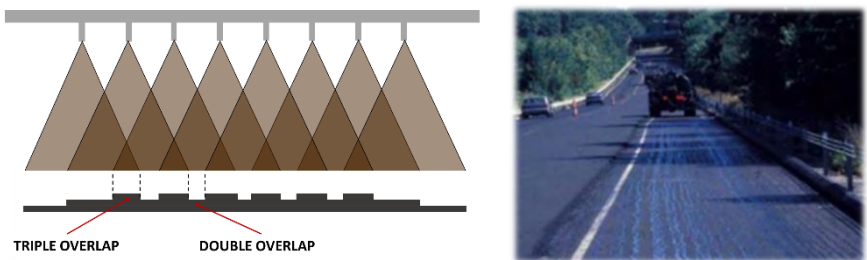
The setup of a tack coat distributor truck consists of two important components: control (liquid temperature), i.e. volume meter and thermometer, and calibration of the components mentioned previously, i.e. spray nozzles (Figure 2.2.4.2b). Temperature control and calibration of different mechanical parts of the distributor are of cardinal importance in achieving uniform tack coat application (Asphalt Institute & Federal High-way Administration, 2016). It should be noted that the configuration of the elements shown in Figure 2.2.4.2b will

differ slightly between the different types of distributor trucks used. In a South African context, a distributor and spray bar is commonly used in application of chip seals and are less common concerning asphalt materials.

It has been reported that the paving quality and good interlayer bonding are ensured by proper tack coat application (Al-Qadi et al., 2012). Furthermore, the significance of uniformity and amount of application in achieving the objective have been mentioned previously. These two factors were found to be significant in achieving uniform tack coat placement (2.2.3.3). However, several vehicle-related adjustments and settings are also important. The adjustments include the different elements of the distributor truck setup, shown in Figures 2.2.4.2a and 2.2.4.2b respectively. The different factors, together with their relative specifications, are summarised in Table 2.2.4.2a, compiled from literature from Mohammad et al. (2012) and van Zyl (2018).

**Table 2.2.4.2a:** Application factors (After Mohammad et al., 2012; van Zyl, 2018)

Factor	Specification
<p><b>Uniformity of nozzle spray patterns</b></p>	<p>The nozzle spray patterns should be identical along the distribution spray bar to prevent the spray of bitumen emulsion interfering with adjacent nozzles. This can be achieved if all nozzles are set at the same angle (approximately 30°) as shown in Figure 2.2.4.2c. A lack of a uniform angle will result in some areas of the pavement having a thicker or thinner coverage.</p>  <p><b>Figure 2.2.4.2c:</b> Distribution truck setup</p>
<p><b>Size of nozzles</b></p>	<p>A small nozzle size is required for tack coat application. The combination of a too small nozzle with too much pressure results in a spider web coating on the surface (Figure 2.2.4.2d).</p>  <p><b>Figure 2.2.4.2d:</b> Proper nozzle setting</p>

<p><b>The height of the spray bar</b></p>	<p>Mohammad et al. (2012) reports that best tack coat application results are acquired from double or triple overlapping (Figure 2.2.4.2e). The spray patterns overlap one another in a way that every portion of the pavement surface is sprayed by two or three nozzles.</p>  <p><b>Figure 2.2.4.2e:</b> Uniform tack coat application with double and triple overlapping</p> <p>It is important for the spray bar height to remain constant and provide uniform coverage (Figure 2.2.4.2f).</p>  <p><b>Figure 2.2.4.2f:</b> Correct spray bar height</p> <p>With the application of tack coat, the truck becomes lighter and the spray bar rises. Consequently, a constant bar height should be maintained. If the spray is too low, the low spray results in streaks as illustrated in Figure 2.2.4.2g.</p>  <p><b>Figure 2.2.4.2g:</b> Incorrect spray bar height</p>
	<p><b>Pressure of application</b></p>
<p><b>Temperature of tack coat</b></p>	<p>Tack coat equipment should be able to maintain the temperature of the material to ensure its flowability. For slow-setting emulsions a temperature between 24 and 54°C is recommended. Excessive heating might lead to emulsion break while still in the distributor.</p>

### 2.2.4.3 Tack coat paver

The second method is a tack coat distributor truck used for tack coat application. However, the design has been upgraded by developing a special paver with a tack coat tank and spray bar. In contrast to the previous method of application, this method includes a variety of advantages. It is time and cost effective, and with no construction of tack, no tracking occurs. In addition, uniform tack coat application is achieved (ArrMaz, 2012). However, the technology used could possibly experience functional problems during paving (J. Wang et al., 2017).

The tack coat is applied, followed by placement of a HMA pavement layer. The combination of spraying and laydown has been found to produce a high-quality mat with strong bond between the layers (similar to spray jet technology developed by Wirtgen Group). Similar to a distributor truck, the liquid is distributed by means of a computer-controlled system through self-cleaning valves (Figure 2.2.4.3a) and the flow rate is controlled by an on-board microprocessor (RoadTec, 2008). The liquid material (tack) is circulated regularly in the system to maintain the material at a proper temperature. An example of the technology is the spray paver developed by RoadTec.

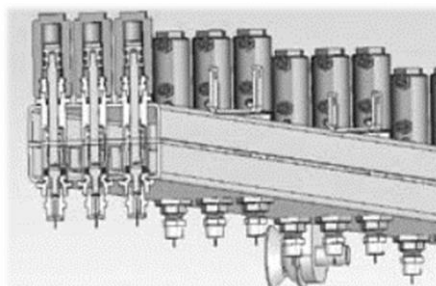


**Figure 2.2.4.3a:** Spray bar valve arrangement (RoadTec, 2008)

The placement of the HMA layer is completed by means of a MTV (Figure 2.2.4.3.b). It eliminates thermal segregation in the mix and allows construction of very thin layers, i.e. 0.5 inches (approximately 13mm). The combination of the spray paver and the MTV (shuttle buggy) allows continuous road construction, which provides a more sufficient project with a smooth road surface.



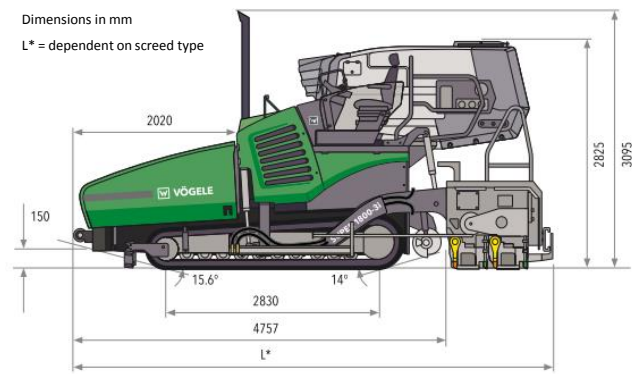
**Figure 2.2.4.3b:** Spray paver with material transfer vehicle (RoadTec, 2008)

The use of the specific technology produces a series of advantages. As mentioned, the technology is capable of constructing ultra-thin layers and the speed at which it operates allows for construction with minimum traffic disruption. Given that no tack is placed in front of the train, traffic can move more freely whilst preventing tracking onto adjacent streets and sidewalks. The technology provides effective surface treatment for high-volume, high-speed roadways (RoadTec, 2008). In South Africa, the use of spray pavers are becoming increasingly common in the construction of UTFCs.

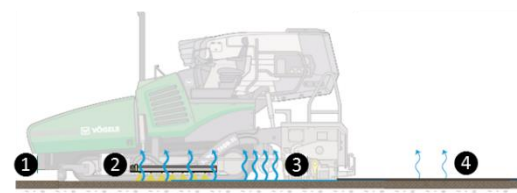
The importance of sufficient break and set time before wearing course construction commences have been emphasised previously. However, technology, such as the Spray Jet technology, developed by the Wirtgen Group, allows application of the next layer immediately after tack coat is applied. Preliminary research conducted in this regard has produced favourable results in terms of bonding and pavement life, which also serve as the basis of the current research study. A discussion of the technology addressing relative subject matters is covered in 2.2.4.4.

**2.2.4.4 Spray Jet technology**

Standard practice of binder and surface courses involves conventional pre-spraying of emulsion (process described in 2.2.3.2). From the description, it is evident that a considerable amount of time and equipment is required to fulfil the necessary tasks. In this capacity, the Spray Jet technology (by Vögele) was developed by the Wirtgen Group. It can be considered “trackless” and is an innovative technology which helps to ensure complete surface coverage with tack coat (Al-Qadi et al., 2012). The technology (Figure 2.2.4.4a) has proved to be advantageous as it is time efficient and projects can occur on a continuous basis (Vögele, 2018) without any interruptions in construction work, i.e. emulsion break/ set time (Figure 2.2.4.4b). A description of the different elements labelled number one to four in Figure 2.2.4.4b is provided in Table 2.2.4.4a.



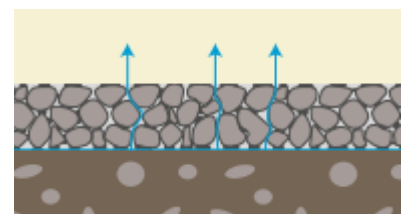
**Figure 2.2.4.4b:** Spray Jet technology by Vögele (Vögele Wirtgen Group, 2018)



**Figure 2.2.4.4a:** Emulsion break process (After Vögele Wirtgen Group, 2018)

**Table 2.2.4.4a:** Process of bitumen emulsion break (After Vögele Wirtgen Group, 2018)

Diagram symbol	Description
①	Existing surface – prepared base layer consists of either milled material or new binder course material that is freshly laid.
②	Spray paver applies the bitumen emulsion at temperatures between 70° and 80°C ( <b>tack</b> ).
③	Commencement of binder or wearing course. Emulsion breaks immediately as HMS causes the water to evaporate.
④	Remainder of water evaporates through open pores of the asphalt overlay (Figure 2.2.4.4c). With the Spray Jet Technology, emulsion break occurs faster when the bituminous layer is placed on top of the tack coat. From research completed by Jenkins (2000) it was found that 50% of the moisture in the emulsion penetrates the bituminous layer on top once the bitumen emulsion is sprayed onto the surface. Given the small thickness of the bitumen emulsion and tack coat conclusions made by Jenkins (2000) , excess water will be minimal.



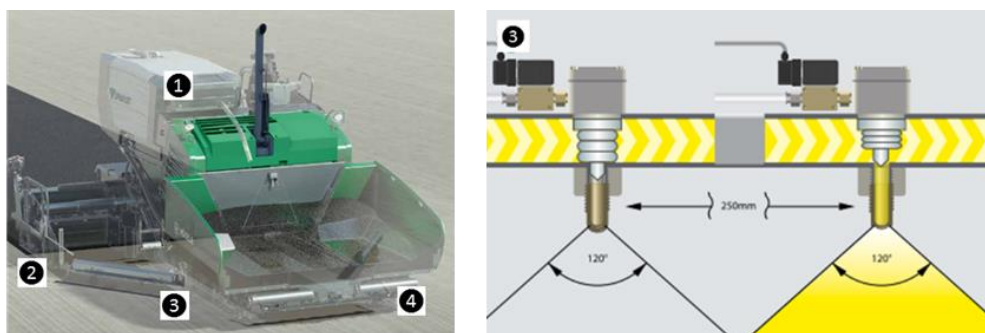
**Figure 2.2.4.4c:** Evaporation of water

Figure 2.2.4.4d illustrates the main components of the Spray Jet module. The setup of the technology will subsequently be discussed, according to each of these components. These discussions are compiled from the product brochure, Vögele Wirtgen Group (2018).



**Figure 2.2.4.4d:** Spray Jet Technology components (After Vögele Wirtgen Group, 2018)

1. *Spray bars.* The Spray Jet is equipped with five spray bars. The front spray bar is located between the machine's crawler tracks behind the push-rollers and has six spray nozzles. Articulated spray bars are installed on each side of the paver with seven nozzles each. Lastly, there are short spray bars with two nozzles provided behind the crawler track. The arrangement of the spray bars allows full coverage of the existing surface with the bitumen emulsion. Application occurs at various rates and is dependent on the type of emulsion used.
2. *Nozzles.* The spray nozzles are open and closed pneumatically (labelled number one in Figure 2.2.4.4e). In contrast to other application technologies, the spray of emulsion is operated in pulsed mode, where the frequency of the spray pulse is adjusted. The frequency is automatically adjusted as a function of the speed rate, paving speed and pave width. The spray nozzles are located at items number two to four in Figure 2.2.4.4e.



**Figure 2.2.4.4e:** Spray Jet spray nozzles (After Vögele Wirtgen Group, 2018)

3. *Nozzle pressure.* The emulsion is applied at very low maximum pressure of 300kPa. The combination of the pressure and nature of the nozzles produces a "clean" spread of emulsion.
4. *(Standard) Emulsion tank.* It is 2 100 litres in capacity with temperature sensors fitted in the tank, which control the emulsion temperature, prevent the emulsion from burning and turn off heating when the emulsion is below a specified limit. It also includes a heating system which can heat the emulsion when the supply of material is too cold.
5. *Additional emulsion tank* (Figure 2.2.4.4d). Provides additional 5 000 litres, increasing the amount of bitumen emulsion that can be carried to 7 100 litres. The temperature of the additional emulsion tank is controlled by means of a stand-alone heating unit. If the emulsion in the standard emulsion tank reaches a level below 1 000 litres, the emulsion is automatically delivered

### 2.3 Characterisation of interlayer bond strength

from the additional tank into the standard tank. If the paver is equipped with the additional emulsion tank, material mix is supplied by a material feeder, which transfers the material from a bin within the additional tank to the paver's conveyors.

#### 2.2.4.5 Hand Spraying

Typically, tack coat material is placed by a tack truck or distributor tank. In some instances, manual application could be required such as at joint faces (Figure 2.2.4.5a). Care should be taken to assure that a uniform coat of tack is applied to the existing surface. However, this method is generally not recommended and Pavement Preservation and Recycling Alliance (2018) advises that the use of this method should be minimised whenever possible.

The reason for this suggestion is that this method does not allow a consistent bond application to be achieved compared to distributors that allow computer controlled application rates. This method typically results in insufficient material in some areas and too much in other areas. However, this method of application is better than no tack coat being applied. It is therefore suggested that care should be taken with this method in order to assure the uniform application of the tack coat. Compared to the other application methods, the use of hand a hand spray and tack cart is the most common and widely used method in South Africa for asphalt paving.



**Figure 2.2.4.5a:** Uniform tack coat coverage (Pavement Interactive, 2013)

### 2.3 Characterisation of interlayer bond strength

Section 2.2 highlights the significant contribution of interlayer bonding by means of tack coat application. The section also illustrates the practical impact of the lack of or poor bonding condition of such a layer on pavement structures, resulting in a variety of premature failures. Identified failures include delamination and cracking, which are causes of concern for the residual performance of a pavement structure. The different types of interlayer bonding are demonstrated in Figures 2.3a to 2.3c.

Bonding failures at the interface can be categorised into three separation modes: shear, tensile and a mixed shear tensile mode (Figure 2.3a). The pure shear condition occurs in the transverse or longitudinal direction generated by traffic, or a combination of traffic and temperature-induced (temperature variation in pavement) shear stresses (Rahman et al., 2017). The shear stresses are generated by the horizontal loads induced by

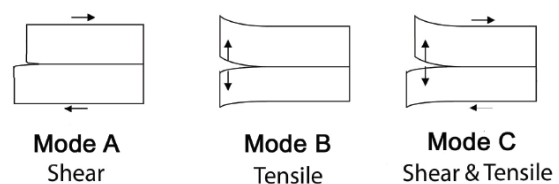


**Figure 2.3b:** Separation modes (Sutanto,

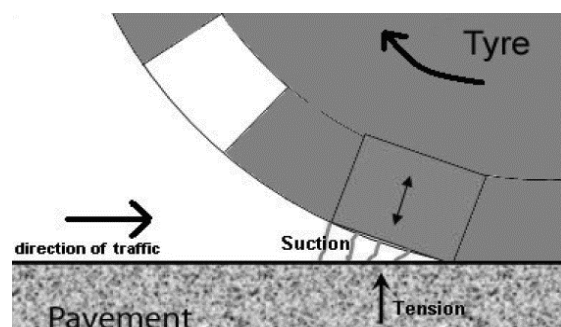


**Figure 2.3a:** Tyre suction phenomenon (Sutanto, 2009)

### 2.3 Characterisation of interlayer bond strength

the vehicles, such as acceleration and deceleration. Sutanto (2009) reports that the tensile separation mode is caused by vertical tensile stresses due to the suction of the tyre. Hence, adhesion is generated at the contact area between the pavement and the tread block of the tyre (Figure 2.3b).

The mixed shear-tensile separation mode occurs in pavement structures composed of thin surfacing layers (shear-tensile occurs beneath the thin surfacing) as demonstrated in Figure 2.3c. When a low shear strength is achieved beneath the thin surfacing, it reduces the ability to transfer horizontal loadings to the pavement layers below. The horizontal loadings are concentrated in the surfacing (asphalt) layer and may cause buckling of the thin surfacing layer at the front of the tyre (Sutanto, 2009). However, this type of failure in actual pavement structures has not been covered in literature. This would suggest that the occurrence would rarely be found in pavement structures. It will only occur as a combined effect of the following listed conditions:

1. Excessive horizontal loading;
2. Poor horizontal load transfer to subsequent layers as a result of low interface shear strength;
3. Buckling within thin surfacing;
4. No separation of interface in shear mode, such that interface tensile adhesion still exists.

For the objective of this research, shear and tensile mode separation is of particular interest. This section will explore the different approaches or methods used to evaluate interlayer bonding, and investigates the factors which influence the interlayer strength. The section is concluded with a study on the effect of interlayer bonding and shear strength on pavement performance.

#### 2.3.1 Interlayer bonding evaluation

According to Di Benedetto et al. (2013), many methods and equipment have been developed for testing the interlayer bond of pavement layers. However, a lack of correlation and harmonization exists amongst these methods. Hence, there is no internationally recognised test or procedure established. The distinctive differences in procedures are attributed to the loading conditions, specimen geometry as well as test temperature (Di Benedetto et al., 2013). This section presents the different testing procedures and methods which will be discussed in subsequent sections.

The recognised test methods can be divided into two categories, i.e. destructive tests (Figure 2.3.1a) and non-destructive tests (NDT) on existing pavements. The different elements of both tests are summarised and compared in Table 2.3.1a according to the method approach and different testing methods or techniques. The characteristics summarised are a compilation of literature reviewed by Rahman et al. (2017) and Di Benedetto et al. (2013).

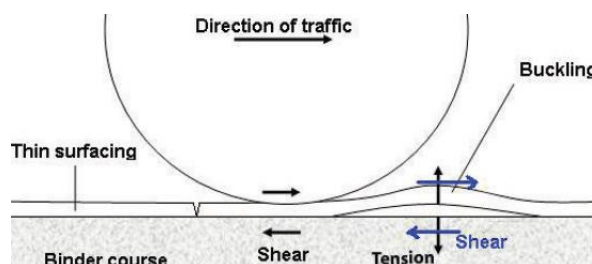


**Figure 2.3c:** Shear-tensile separation (Sutanto, 2009)

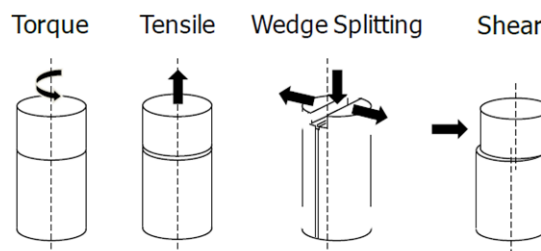


**Figure 2.3.1a:** Working schemes of destructive methods used for interlayer testing (Di Benedetto et al., 2013)

## 2.3 Characterisation of interlayer bond strength

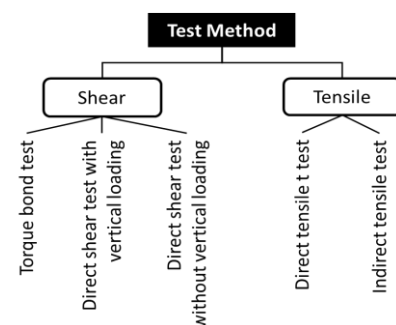
**Table 2.3.1a:** Destructive and non-destructive tests (After Rahman et al., 2017; Di Benedetto et al., 2013)

	Destructive tests	Non-destructive tests
Method Approach	<ul style="list-style-type: none"> <li>Require laboratory testing of specimens considering at least two layers of pavement structures.</li> <li>Specimen brought to failure at loading or displacement rate.</li> <li>Drawbacks:               <ol style="list-style-type: none"> <li>Destructive for part of pavement;</li> <li>Time consuming;</li> <li>Causes traffic delays.</li> </ol> </li> </ul>	<ul style="list-style-type: none"> <li>Directly performed in the field without destroying pavement layers.</li> <li>Techniques are based on wave propagation of frequencies higher than 20Hz into the pavement structure.</li> <li>Testing method is considered more reliable. Samples are not destroyed, allowing it to be subjected to a number of non-destructive tests to eliminate risk of oversight or inaccuracy.</li> </ul>
Testing methods and techniques	<p>Based on configuration or loading procedures, the test methods are grouped into four categories (illustrated in Figure 2.3.1a):</p> <ol style="list-style-type: none"> <li>Torque tests;</li> <li>Tensile pull-off tests (direct tensile tests);</li> <li>Wedge splitting tests (indirect tensile tests);</li> <li>Direct shear tests, including and excluding normal (vertical) loading.</li> </ol>	<p>The procedures differ according to the methods used for wave impulse generation and the acquisition system. The most common techniques used include:</p> <ol style="list-style-type: none"> <li>Portable Seismic pavement Analysis;</li> <li>Colibrì test;</li> <li>Hammer test;</li> <li>Falling Weight Deflectometer (FWD);</li> <li>Grand-penetrating radar (GPR);</li> <li>Infrared thermography.</li> </ol>

The non-destructive tests will not be studied as it is beyond the scope of current research, but reference can be made to Di Benedetto et al. (2013). The experimental devices currently used will however be described where relevant. (The different testing methods can be categorised into the two main recognised modes of failure, i.e. shear and tensile, as presented in Figure 2.3.1b).

### 2.3.1.1 Torque bond testing

This method measures the peak shearing torque applied on core samples to cause de-bonding of a surface system from its substrate (Di Benedetto et al., 2013). According to Rahman et al. (2017), the procedure has been adopted for testing the bond strength between a thin surfacing layer and underlying layer. The torque is applied to the top of the specimen (100 and 150mm in diameter) composed of a twisting failure mechanism in the bond layer. The torque is applied to the plate bonded to the surface of core sample, through a handheld torque wrench (Figure 2.3.1.1a). The torque is applied until shear failure occurs

**Figure 2.3.1b:** Destructive test method categories

### 2.3 Characterisation of interlayer bond strength

in the bond layer or when a torque of 300Nm is exceeded (Rahman et al., 2017). Bond strength is calculated accordingly – the maximum measured torque moment at failure.

This testing method allows comparison between in-situ and laboratory prepared specimens. The in-situ specimen collected, is cored up to just below the surfacing layer in order to ensure failure at the interface. Laboratory specimens are cut and extracted where double-layered cores are

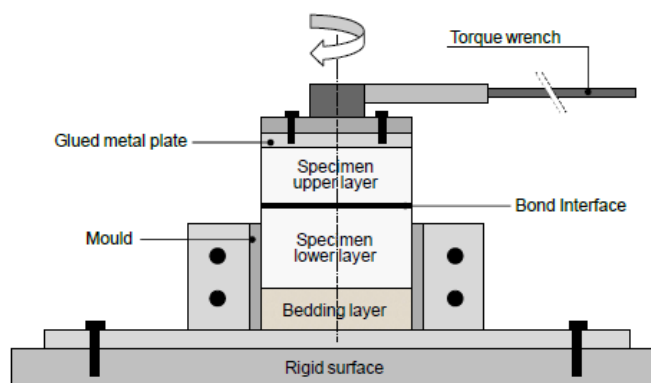


**Figure 2.3.1.1a:** Torque meter (Di Benedetto et al., 2013)

clamped or glued to a firm base. For the torque test, a steel plate is glued on top of the specimen, which acts as an adapter between the sample and a wrench used to measure the torque moment, as illustrated in Figure 2.3.1.1a (Di Benedetto et al., 2013). An extensive list of devices used for torque bond testing is provided in Rahman et al. (2017). The devices used include the Tack Coat Evaluation Device (TCED) and the monotonic torque test developed, used by Diakhaté et al. (2011).

Experimental studies from literature reviewed by Di Benedetto et al. (2013) and Rahman et al. (2017) have presented several shortcomings in the conventional torque bond test used. The shortcomings are summarised as follows:

1. Fixed specimen diameter.
2. Applicability – mostly just applicable in field testing and limited to uppermost interface in the pavement.
3. Axial bending occurs.
4. Relatively high forces are applied to “twist off” the surfacing. A limitation of the tests involves its unfeasibility, when the torsional resistance of the respective material layers is lower than the interlayer bonding resistance.
5. Non-uniform shear stress distribution at the interface between the two layers, as the shear stress varies from zero at the centre, to a maximum value at the peripheral of the cored specimen. Non-uniform failure occurs initiated at the peripheral propagating towards the centre of the core.
6. Torque rate variability attributed to the manual operation of the torque wrench leads to inaccurate results. Sutanto (2011) conducted a study to develop an automatic bond test. Results showed that at a constant torque rate of 600N/min, shear strength measured with the automatic torque test is higher than the shear strength measured using the manual torque bond test. In general, the automatic torque bond test produced 20 -30% higher values in comparison with the manual torque bond test (Rahman et al., 2017). The behaviour is attributed to the drawback of the manual operated testing device.

The drawback of the testing method resulted in a newly-developed automatic version of the testing method. Although anticipated higher torque moments were acquired with the automatic version, limitations in the newly-developed devices remained unsolved (Rahman et al., 2017).

## 2.3 Characterisation of interlayer bond strength

### 2.3.1.2 Direct shear tests without normal loading

Rahman et al. (2017) regards direct shear testing as the most commonly used method to investigate interface problems. This is attributed to its “smooth” operation and suitability as devices used are not operator-dependent. Furthermore, devices are found to provide consistent results with exceptional circumstances. The shear testing device was originally constructed for soil mechanic purposes, which has been developed in different countries over time. Direct shear tests with normal loading are categorised as “experimentally complex”, given its complexity with normal and shear load application (Sutanto, 2009). Hence, tests without these loading applications were developed to simplify the experimental setup. In general, direct shear tests, without normal loading rate, are considered suitable laboratory-based tests for routine testing of bonding attributed to the following listed considerations (from Sutanto (2009)) :

1. Absence of normal load applied to the specimen simplifies the experimental setup;
2. Simplified preparation of specimens, as only cored specimens are used;
3. The shear load is applied in a pre-defined shear plane – prevents failure in asphalt layer;
4. Shorter testing duration;
5. Acquisition of test results in good precision.

Examples of shear testing devices without vertical (normal) loading include the Leutner shear test, Layer Parallel Direct Shear (LPDS) test (modified Leutner) and the Double Shear Test (DST). This section discusses the different characteristics and configuration of the Leutner and modified Leutner devices, given the similarities between these shear tests. Additionally, an overview of the DST is provided to demonstrate the difference between the shear testing devices commonly used. Reference can be made for a comprehensive list in Rahman et al. (2017).

#### ***Leutner and the modified Leutner shear test***

The Leutner test designed by Leutner (1979), is a favoured testing device used, given its simple configuration and easy performance. It is regarded the most common “pure” interlayer shear test equipment (setup shown in Figure 2.3.1.2a). The simple arrangement of the testing device allows rapid testing for investigation of interlayer bonding of pavement layers (Di Benedetto et al., 2013). The test involves the application of a shear displacement (to double-layered specimens) at a constant rate, across a pre-defined plane. It also monitors the resultant shear force, as well as the applied displacement providing force-shear displacement curve at the investigated plane (Di Benedetto et al., 2013).

The testing frame is fitted into an ordinary fitting frame, allowing testing on a  $150\pm 2$ mm diameter core (cylindrical) specimen. The sample is composed of at least two layers with the bond layer between them (Sutanto, 2009). These samples can either be taken from a pavement structure or produced in the laboratory. A constant rate of shear displacement is applied to the double-layered specimen until interface failure occurs. The load is applied to the top layer while the bottom layer is constrained to produce displacement between the layers (Rahman et al., 2017). The loading mode of the Leutner test is strain-controlled (J. Wang et al., 2017).



**Figure 2.3.1.2a:** Leutner shear test (Di Benedetto et al., 2013)

### 2.3 Characterisation of interlayer bond strength

The testing device consists of a range of clamping and loading devices, i.e. upper and lower shearing rings (Figure 2.3.1.2b) to accommodate a variety of specimen diameters. The displacement rate of the test is  $50\pm 3$ mm/min at a standard testing temperature of  $20\pm 1$ °C. According to Sutanto (2009), the standard displacement rate will allow the test to be performed in a Marshall or California Bearing Ratio (CBR) loading device, widely available in most road testing laboratories.

The adhesion quality between the asphalt layers is best described by the maximum shear load in an interlayer bonding. Shear strength of an interlayer bonding is expressed as the ratio of the maximum shear load to the initial area of the specimen. The relationship between shear force and displacement is illustrated in Figure 2.3.1.2c. Additional information that this curve can provide is the evolution into dissipated energy, which is a valuable analysis tool for understanding behaviour (Di Benedetto et al., 2013).

Despite the popularity of the test, it should be recognised that the test also comprises of limitations, such as the possibility of load eccentricity, causing additional momentum and non-uniform distribution of interface stresses. Another disadvantage is the absence of normal loading that represent wheel loading in real conditions. Hence, no traffic load is simulated during shear bond evaluation.

A modified version of the Leutner test developed, is the Layer Parallel Direct Shear (LPDS) testing device (Figure 2.3.1.2d) which is very similar to the Leutner test (Figure 2.3.1.2a) with the following differences:

1. 2mm gap with allowed between shear rings (varies in devices used today);
2. Specimen clamping – one part of core is laid on circular u-bearing and constrained by means of a semi-circular pneumatic clamp;
3. Accommodation of specimens with different diameters are attributed to the adjustable clamp of the testing device and allows testing on prismatic specimen (width of 150mm and 130mm in height).

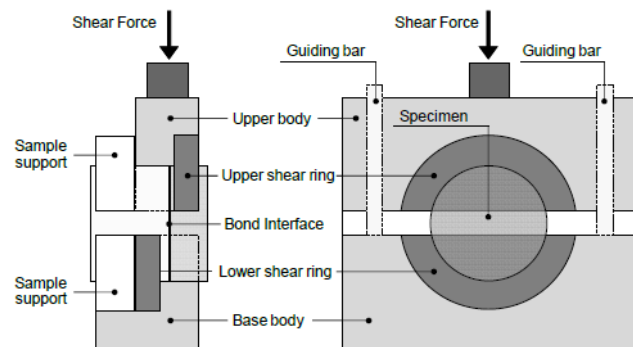


**Figure 2.3.1.2b:** Leutner shear test (Di Benedetto et al., 2013)

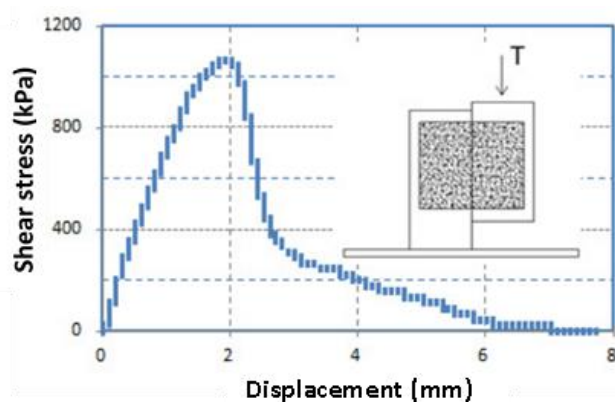


**Figure 2.3.1.2c:** Shear force-displacement curve for Leutner test (D'Andrea & Tozzo, 2012)

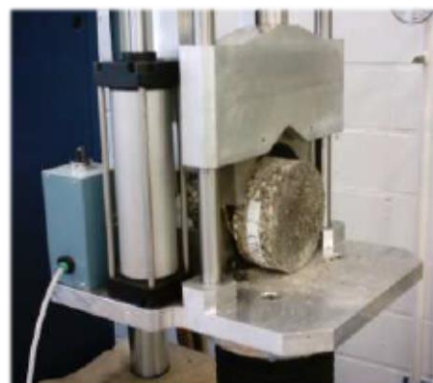


**Figure 2.3.1.2d:** Setup of LPDS test device (Di Benedetto et al., 2013)

### 2.3 Characterisation of interlayer bond strength

The modified Leutner was employed by Florida Department of Transport (FDOT). The testing device is mounted on a Material Testing System (MTS) which allows temperature control during testing. The test is also undertaken on specimens (150mm in diameter) cored from the pavement or laboratory-prepared. However, the shear force is measured at a displacement rate of 50.8mm/min (Di Benedetto et al., 2013). Wang et al. (2017) describe the test as strain-controlled that is widely used in Swiss and Italian pavements. The preference of this testing device to the conventional Leutner is due to its versatile geometry and more defined clamping mechanism. It is also favourable as it allows determination of interlayer and in-layer shear properties (Rahman et al., 2017).

Comparing this method with the shear box testing method, different stress-deformation curves were obtained, even though experimental results were comparable. Rahman et al. (2017) attribute the occurrence to the shear mechanism and stress conditions imposed during testing. Shortcomings of the test include the exclusion of the combined impact of horizontal and vertical loading, while dilatancy effects, eccentricity effects, testing temperature limitations and specimen thickness are also causes for concern, as great variability exists in results at higher temperatures, according to Rahman et al. (2017).

Sholar et al. (2004) developed a similar testing device as an alternative. A standard gap width of 4.8mm is accommodated between shearing platens in order to accommodate cores not extracted perpendicular to the pavement surface (Di Benedetto et al., 2013). The maximum shear force at failure is recorded from the test by means of software which also measures the shear stress generated at this instance.

#### **Double Shear Test**

The Double Shear Test (DST) is a type of shear interface fatigue test. It was initially developed by the University of Limoges (Diakhaté et al., 2011) to investigate crack propagation within asphalt surfacing under loading focusing on the shear fatigue behaviour of tack coats. In contrast to other shear tests, for the DST, a prismatic sample composed of three asphalt layers (AC #1 to AC #3 in Figure 2.3.1.2e) with a tack coat applied to the interlayer interface, is used. Figure 2.3.1.2e demonstrates the configuration of the test, including the two external asphalt layers (AC #1 and AC #3) held in position with steel clamps while the central layer (AC #2) is subjected to a displacement (loading) to produce a shear force. The samples used for testing have a volumetric dimension of 70×120×50mm<sup>3</sup> (Sutanto, 2009). Six metal (steel) plates are glued onto the specimen attached to the device to ensure shear failure occurs at the predefined shear planes. Furthermore, the gap between the plates are adjustable between 4 and 10mm.

The DST loading involves the testing of a specimen subjected to monotonic or repeated loading until failure (Sutanto, 2009). The loading is applied through a servo-hydraulic machine (Figure 2.3.1.2f) that allows controlled displacement on controlled force (Di Benedetto et al., 2013).

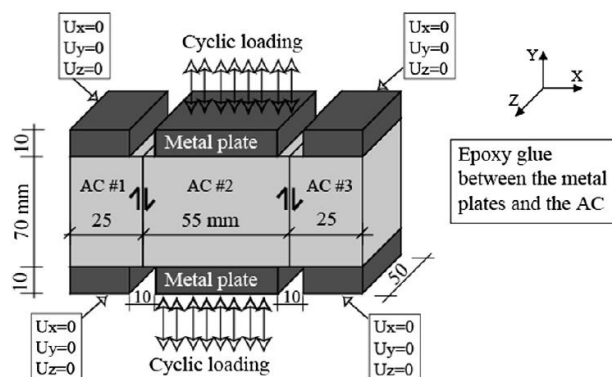


**Figure 2.3.1.2e:** Schematisation of Double Shear Test (Diakhaté et al., 2011)

## 2.3 Characterisation of interlayer bond strength

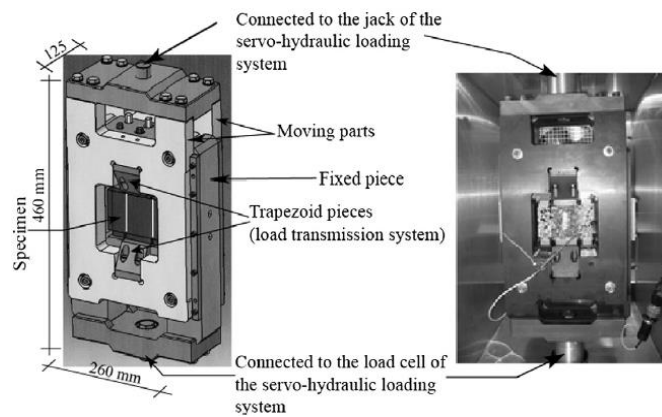


**Figure 2.3.1.2f:** Schematization and illustration of DST device (Diakhaté et al., 2011)

Many authors have reported that dynamic loading is a better presentation of the simulation when compared to monotonic loading (Rahman et al., 2017). This attributed to a more representative simulation of loading conditions and evaluation of interface shear fatigue behaviour. However, it is the opinion of Leng et al. (2008), that a more precise assessment of interlayer bond characteristics is made possible through monotonic testing. The authors' argument is based on the complexity introduced by dynamic loading and its operational difficulty. The monotonic tests are simpler to use for evaluation of tack performance, while shear resistance if visco-elastic behaviour of the material is not a concern (Rahman et al., 2017).

### 2.3.1.3 Direct shear tests with normal loading

Literature studied in Rahman et al. (2017) reveals that the use of shear bond strength data, acquired from shear testing without normal loading (described in 2.3.1.2 and shown in Figure 2.3.1.3a), would result in the overdesign of pavements. Despite complexity in terms of setup, direct shear tests with loading (Figure 2.3.1.3a) are considered suitable for fundamental research due to their ability to assess the effect of normal load and dilatancy (Sutanto, 2009). Many testing devices of this type, and similar to other devices, are available and have been developed over the years. This section discusses the different elements of two types of tests used with normal loading – the Shear Fatigue Test and the Direct Shear Box Test. References listed in Rahman et al. (2017) can be consulted for a comprehensive list of devices used for the specific type of shear testing.

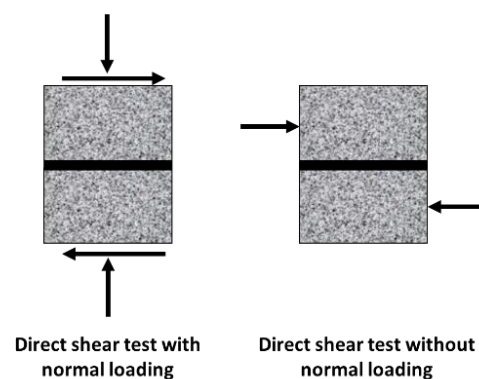
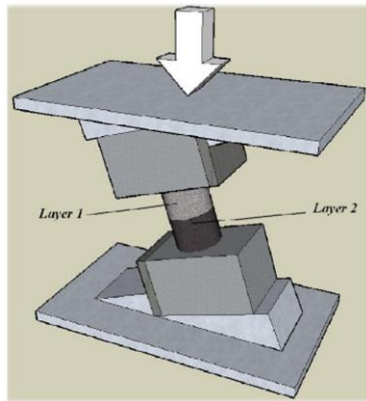


**Figure 2.3.1.3a:** Direct shear test with loading versus Directs Shear test without loading

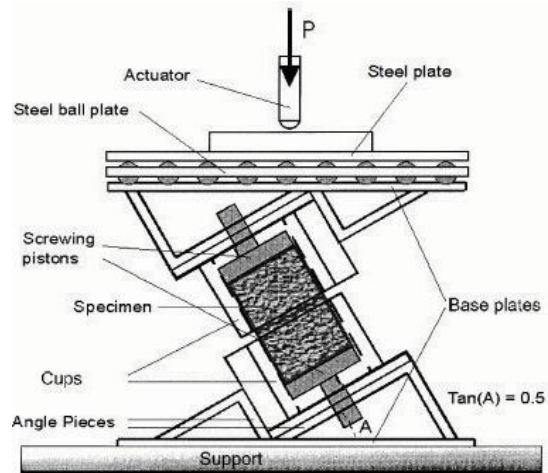
### **Shear Fatigue Test**

The Shear Fatigue Test developed by Romanoschi & Metcalf (2001) incorporates the aspect of interface failure induced by multiple loads caused by repetitive loading (Figure 2.3.1.3b left). The normal load is applied close to the joint surface of the two asphalt layers (interface, i.e. tack coat) after which it is broken through the joint surface by applying a lateral displacement of the faces with a load inclination of  $25.5^\circ$  from the applied side (Raposeiras et al., 2013). Figure 2.3.1.3b (right) provides an illustration of this setup. The vertical load is applied with a frequency of 5Hz. The position of the shear plane at  $25.5^\circ$  produces a shear stress equivalent to half of the normal stress (Sutanto, 2009).

## 2.3 Characterisation of interlayer bond strength



Shear Fatigue Test (Raposeiras et al., 2013)

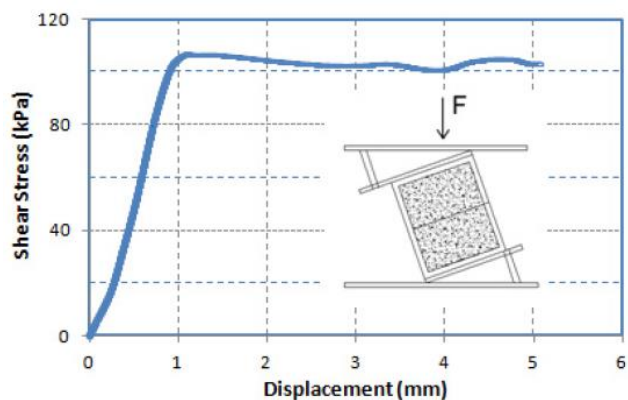


Schematic diagram (Romanoschi, 1999)

**Figure 2.3.1.3b:** Shear Fatigue Test

According to Romanoschi (1999), this approach is applied to simulate the condition in wearing course interlayers under wheel load, for which vertical and horizontal loading comply, to a ratio of 0.5 (at the pavement surface). Romanoschi & Metcalf (2001) found it difficult to determine the fatigue failure point. Hence, the number of load cycles that produced an increase of permanent shear deformation of 1mm was used as a parameter for a comparative evaluation of the interface fatigue properties.

An example of result output is presented in Figure 2.3.1.3c. It illustrates the results acquired from fatigue testing completed by Wheat (2007). The study focused on the evaluation of shear behaviour of differently composed specimens, considering different testing conditions. Testing conditions included the change in the loading mechanism of the test and different properties of the tack coat, such as application rate and tack coat quantity. The author concluded that the shear strength of the interface is not influenced by either the tack coat application rate or interface material type.

**Figure 2.3.1.3c:** Shear stress-displacement curve for Shear Fatigue Test (D'Andrea & Tozzo, 2012)

Before testing, samples are kept in a temperature-controlled chamber at the desired temperature for a period of 24 hours (J. Wang et al., 2017). The specimens are then placed into two metal split cups. Screwing pistons (Figure 2.3.1.3b right) accommodate the adjustment of specimen position, allowing an approximate 5mm distance between the two cups. Furthermore, the two steel cups are fixed onto two sets of metal angle pieces that are welded to base plates. A steel ball plate is placed on top of the upper baseplate to allow relative horizontal movement, while the bottom baseplate is fixed to the hydraulic frame.

### Direct Shear Box Test

From the description of the previous testing device, it is general knowledge that varieties of direct shear box tests have been designed and used for shear testing. Each of these devices comprises of its own unique qualities and favourable outcome. A popular direct shear box test used is the Ancona Shear Testing Research and Analysis (ASTRA) apparatus (Figure 2.3.1.3d). The testing device was developed in Italy at the Università Politecnica delle Marche (Canestrari et al., 2005) and is similar to devices used in soil mechanics. This testing device deviates from the direct shear box test originally developed by Uzan et al. (1978), used to evaluate the stiffness parameter ( $K$ ) for different test conditions (Di Benedetto et al., 2013).



**Figure 2.3.1.3d:** ASTRA shear test device (Di Benedetto et al., 2013)

The device accommodates testing of multi-layered bitumen system performance under laboratory conditions. It can test both prismatic and cylindrical specimens. The first-mentioned is composed of a cross-sectional area of  $100 \times 100 \text{ mm}^2$  with cylindrical specimens varying in diameter between 94 and 100mm (Canestrari et al., 2005). According to the working scheme in Figure 2.3.1.2e, the sample is placed in two half-boxes and separated by the unconfined interlayer shear zone. Canestrari et al. (2005) provide the following statements to motivate the setup:

1. Assurance of shear force applied in the weakest horizontal plane (where major of shear displacement occurs);
2. To avoid influence of two mixed aggregates on the interlayer shear resistance.

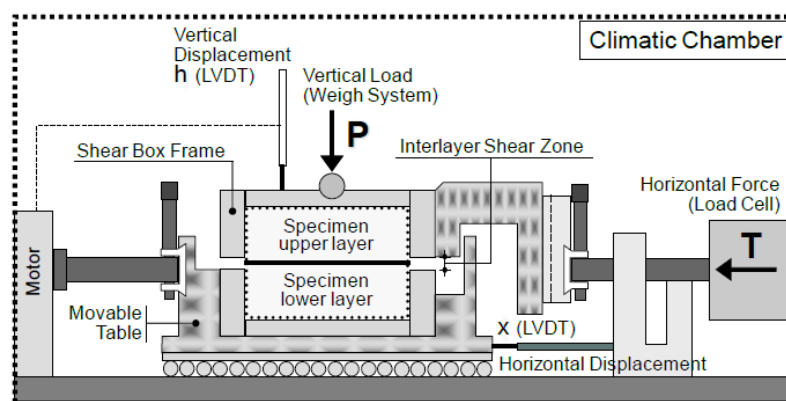


**Figure 2.3.1.3e:** ASTRA direct shear test device with normal load (Di Benedetto et al., 2013)

A constant vertical load is applied perpendicular to the interface surface plane (Figure 2.3.1.3e) during the test carried out at a constant displacement rate of 2.5mm/min. The load is applied by means of a lever and weight system. Subsequently, a load cell connected to the upper frame continuously reads and records the horizontal force. Simultaneously, two transducers or Linear Variable Differential Transformers (LVDTs) are used to measure the vertical and horizontal displacement (Canestrari et al., 2005). The entire apparatus is placed in a climatic chamber with temperature and relative humidity

### 2.3 Characterisation of interlayer bond strength

control. The test returns a data set that allows calculation of maximum shear stress at failure, together with the dilatancy (geometrical parameter) (Di Benedetto et al., 2013). Figure 2.3.1.3f shows a typical curve for shear stress versus horizontal displacement. Results presented in this figure were obtained in research done by Chen & Huang (2010), studying the effect of surface characteristics on bonding properties of tack coats.

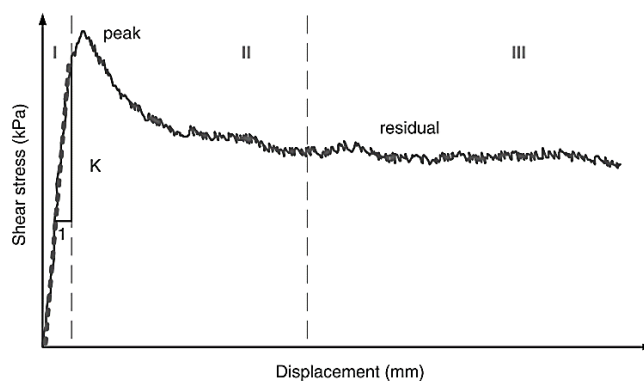


**Figure 2.3.1.3f:** Shear stress-displacement curve for Direct Shear Test (Chen & Huang, 2010)

The figure is divided into three zones: linear, transitional and residual (*Zone I, II and III*). Initially, the shear stress increases (approximately linearly) at a rapid rate until the peak value is reached. This trend has an initial slope that is representative of the shear rate which is used to determine the tangential modulus ( $K$ ) by means of a linear regression analysis. The parameter does not refer to an actual modulus value, as it is expressed in  $\text{kPa/mm}$  (Chen & Huang, 2010). Subsequently, *Zone II* shows the peak value that describes the cumulative strength of the material bonding the two halves of the shear plane, and the shear resistance of the matching surfaces, i.e. the interlayer shear stress. In *Zone III*, the shear stress remains relatively constant, with the increased displacements falling to a residual value (Chen & Huang, 2010).

#### 2.3.1.4 Direct and Indirect Tensile Tests

The direct and indirect tensile tests are both bond tests used to determine tensile bond properties between two bonded asphalt layers. The direct tensile test is available in in-situ and laboratory variants, while the indirect tensile test is only available in a laboratory variant (Sutanto, 2009). The tensile failure mode is one of the separation modes in a real pavement structure, illustrated in Figure 2.3.1.4a. Despite its occurrence, previous research has shown that tensile separation, employed by these two tests, is rarely found in reported cases of bond failure. These tests are found to be limited in terms of the type of results acquired. Each test is discussed subsequently, where its different characteristics and limitations will be addressed. Examples of testing devices used in each capacity will be provided where relevant.

##### **Direct Tensile Test**

The direct tensile (or pull-off) test entails the application of a tensile stress to a double-layered specimen with interface layer (Figure 2.3.1.4a). The top surface is glued to a steel plate that is pulled off in the normal (vertical) direction leading to the breaking of the interface. For the laboratory variant, the bottom surface is glued to the fixed steel plate (Di Benedetto et al., 2013). Similar to other tests, the obtained result is the maximum load obtained during testing.

### 2.3 Characterisation of interlayer bond strength

The limitations of the direct tensile test according to Di Benedetto et al. (2013) and Sutanto (2009) are summarised as follows:

1. Possibility of eccentric load transmission due to an inclined resting piston;
2. The constrained transverse strains in area of load application due to the glued plate results in stress concentrations;
3. Inability to determine tensile strength when it exceeds the tensile strength of the asphalt. The test proves to be unfeasible when the tensile resistance of the material exceeds the interlayer bonding resistance. This is similar to the phenomenon experienced during torque bond testing (2.3.1.1);
4. Inability to assess the effect of aggregate interlocking. During testing, it is impossible to evaluate the aggregate interlock produced during compaction. Hence the behaviour in terms of dilatancy cannot be studied.

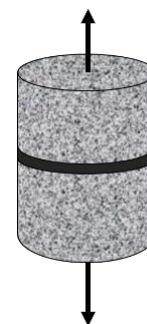


**Figure 2.3.1.4a:** Direct tensile test

Popular direct tensile tests used include Louisiana Tack Coat Quality Test (LTCQT), UTEP Pull-Off Device (UPOD), Interface bond test (IBT) as well as the Schenck-Trebel test. The main shortcoming of conventional UPOD devices (Figure 2.3.1.4b) is attributed to its manual operation, allowing potential human error. This could lead to a non-uniform loading rate due to the eccentric loading effect often experienced, producing less reliable results (Rahman et al., 2017). The UPOD device issue was addressed with the LTCQT design and developed during research by Mohammad et al. (2012). The authors considered the technology as a “viable” method to assess tack coat quality. In addition, the response of various tack coats could be compared (Rahman et al., 2017).

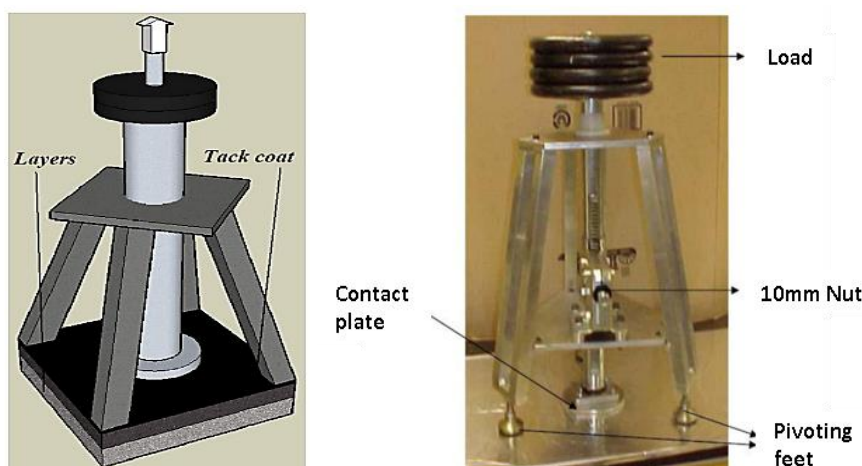


**Figure 2.3.1.4b:** Pull-Off Device (Raposeiras et al., 2013) (Wheat, 2007)

Hakimzadeh et al. (2012) attempted to develop a new tensile-mode IBT to evaluate interface behaviour between two asphalt layers. This test is based on a fracture-energy parameter used as indication of the bond quality achieved by the interlayer (tack coat) (Rahman et al., 2017). Although the use of the method is easy, researchers found crack propagation to be stable only at a testing temperature of  $-12^{\circ}\text{C}$  (Hakimzadeh et al., 2012). The Schenck-Trebel test was designed as an alternative, or modernised version of other testing devices. However, the device requires clamps to either be tightened or directly attached to the material, causing variations in eccentricities. The

## 2.3 Characterisation of interlayer bond strength

shortcomings of the testing devices of this category were overcome by using indirect tensile testing devices (J. Wang et al., 2017).

**Indirect Tensile Test**

The Indirect Tensile Test (ITT) involves a cylindrical specimen loaded with compressive load parallel to, and along the vertical diametrical plane (shown in Figure 2.3.1.4c left). The loading is applied through a steel loading strip that is curved at the interface, having a radius equal to the radius of the specimen. Once the loading is applied, a uniform tensile stress is generated perpendicular to the direction of the load applied (along the vertical diametrical plane). Eventually the loading causes the specimen to fail by splitting or rupturing along the vertical diameter (Figure 2.3.1.4c right). Typical testing devices used are capable of applying at least 25kN at a constant displacement rate of 50.8mm/min. Furthermore, it can measure the load accurately to 0.05kN and the displacement to 0.1mm (BSM Laboratories, 2016).

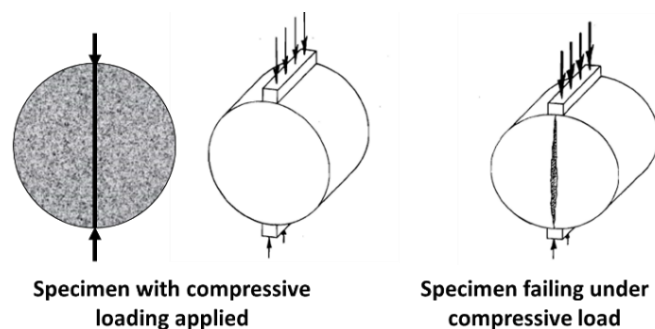


**Figure 2.3.1.4c:** Schematic of ITT device (After Anagnos & Kennedy, 1972)

The Indirect Tensile Strength (ITS) is determined with Equation 2.3.1.4a, incorporating the load measured ( $P$ ) as well as the height ( $h$ ) and the diameter ( $D$ ) of the specimen (Figure 2.3.1.4d).

$$ITS = \frac{2P}{\pi hD} \quad (2.3.1.4a)$$

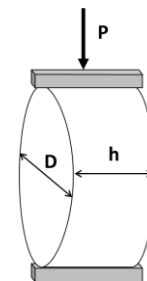


**Figure 2.3.1.4d:** ITS calculation

Where:

- ITS = Indirect Tensile Strength (N/mm<sup>2</sup> or MPa)
- P = Maximum applied load (N)
- h = Average height of specimen (mm)
- D = Diameter of the specimen (mm)

A new indirect tensile wedge splitting test was introduced by Tschegg et al. (1995). The test consists of opening a crack in a dual layer specimen until complete separation of the two layers occurs per illustration in Figure 2.3.1.4e. The experiments are performed with specimens produced for laboratory tests and with cores removed from road pavements. The test accommodates a variety of specimen shapes as shown in Figure 2.3.1.4f. The groove and the starter notch can be prepared easily by using different equipment (stones, saws or metal pieces).

## 2.3 Characterisation of interlayer bond strength

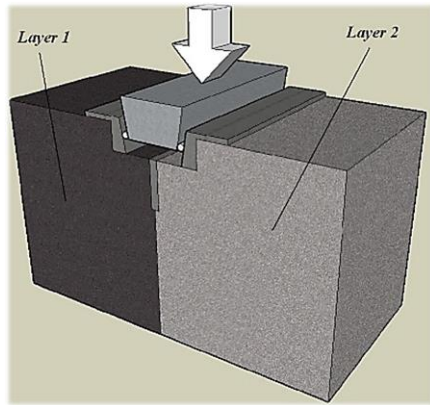


**Figure 2.3.1.4f:** Testing device (Raposeiras et al., 2013)

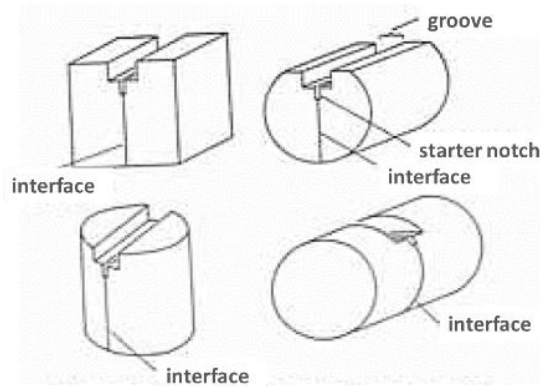


**Figure 2.3.1.4e:** Specimen shapes (Tschegg et al., 1995)

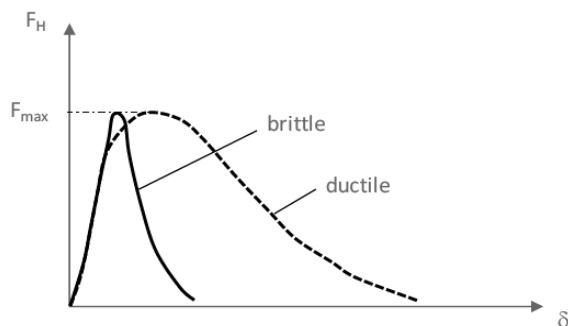


**Figure 2.3.1.4g:** Load-displacement curves (Tschegg et al., 1995)

From the test it is possible to record load-displacement curves of heterogeneous materials from stable crack propagation until failure (separation) occurs. Sufficient data, such as the maximum strength ( $F_{max}$ ), is available to characterise the fracture properties. The advantage of the testing device developed, is the possibility to differentiate between brittle and ductile behaviour (Figure 2.3.1.4g).

The obtained result is a load-displacement ( $F_H$ - $\delta$ ) curve which enables the evaluation of the fracture mechanical properties. The curve is obtained by measuring the displacement with gauges placed at the ends of the starter notch (Figure 2.3.1.4f) and clamped to the specimen. The two load-displacement curves are obtained accordingly (Tschegg et al., 1995). An example of the wedge splitting test setup is provided in Figure 2.3.1.4h. The device consists of five components (labelled a – e in the figure).

The representation of each of the labelled components is as follows:

- Fixture to attach displacement gauges on specimen with four screws;
- Load-displacement pieces with six needle bearings;
- Wedge;
- Inductive displacement gauge;
- Mechanical adjustment for zero point of displacement ( $\delta$ ).

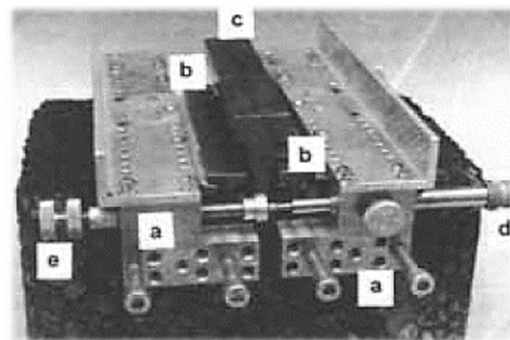


**Figure 2.3.1.4h:** Testing device (Tschegg et al., 1995)



**Table 2.3.1.5a:** Comparison of Torque Bond, Leutner and LPDS Test

	<b>Torque Bond Test</b>	<b>Leutner</b>	<b>Layer Parallel Direct Shear (LPDS) Test</b>
<b>Reference(s)</b>	<ul style="list-style-type: none"> <li>Section 2.3.1.1</li> <li>Figure 2.3.1.1a</li> </ul>	<ul style="list-style-type: none"> <li>Section 2.3.1.2</li> <li>Figures 2.3.1.2a to 2.3.1.2d</li> </ul>	<ul style="list-style-type: none"> <li>Section 2.3.1.2</li> <li>Figure 2.3.1.2d</li> </ul>
<b>Significance and use</b>	Torque force moment is measured at failure	<ul style="list-style-type: none"> <li>Measurement of maximum shear load and corresponding displacement</li> <li>Evaluate appropriateness of tack coat material</li> </ul>	In-layer and Interlayer shear properties measured to evaluate material quality and tack coat properties
<b>Procedure</b>	Torque force applied to core sample with torque wrench until failure occurs	Vertical shear load applied to two-layered specimen at a displacement rate of 50mm/min at a temperature of 20°C	Vertical shear load applied to specimen with strain-control mode, at a displacement rate of 50.8mm/min at temperature of 20°C
<b>Specimen</b>	<ul style="list-style-type: none"> <li>Cylindrical core sample: 100 and 150mm in diameter</li> <li>Laboratory prepared and extracted from pavement structure</li> </ul>	<ul style="list-style-type: none"> <li>Cylindrical core sample: 100 and 150mm in diameter</li> <li>Laboratory prepared and extracted from pavement structure</li> </ul>	<ul style="list-style-type: none"> <li>Cylindrical core sample: 100 and 150mm in diameter</li> <li>Laboratory prepared and extracted from pavement structure</li> <li>Specimen needs to be glued to plate</li> </ul>
<b>Results</b>	Bond strength – higher bonding strength acquired with automatic torque bond testing device than with manual testing device	<ul style="list-style-type: none"> <li>Maximum shear load (<math>F_{Max}</math>)</li> <li>Corresponding maximum displacement (<math>\delta</math>)</li> </ul>	<ul style="list-style-type: none"> <li>Maximum shear load (<math>F_{Max}</math>)</li> <li>Corresponding maximum displacement (<math>\delta</math>)</li> </ul>
	Inconsistency in results due to operation – higher torque moments are acquired for the automatic torque bond testing	<ul style="list-style-type: none"> <li>Inaccurate results – eccentricity during testing causes additional momentum and non-uniform distribution of interface stresses</li> </ul>	<ul style="list-style-type: none"> <li>Although it allows evaluation of in-layer and interlayer shear properties, the combined effect of vertical and horizontal loading is not considered</li> </ul>

## 2.3 Characterisation of interlayer bond strength

		<ul style="list-style-type: none"> <li>Inaccurate simulation of pavement conditions as no traffic load is simulated during shear bond evaluation</li> </ul>	<ul style="list-style-type: none"> <li>Furthermore, the ignorance of dilatancy effects, eccentricity effects and testing temperature allow accurate evaluation to a certain extent</li> <li>Greater variability is noticeable in results when testing a high temperatures</li> </ul>
<b>Remark(s)</b>	Developed by Highway Agency, United Kingdom	<ul style="list-style-type: none"> <li>No normal load applied</li> <li>Developed by Leutner (1979)</li> </ul>	<ul style="list-style-type: none"> <li>Modified Leutner test</li> <li>Shear-plane may be along interface or within layers</li> </ul>

*Note: Displacement rate and sample size varies according to different testing device models used.*

**Table 2.3.1.5b:** Comparison of DST, Shear Fatigue Test and ASTRA Direct Shear Box Test

	<b>Double Shear Test (DST)</b>	<b>Shear Fatigue Test</b>	<b>ASTRA Direct Shear (Box) Test</b>
<b>Reference(s)</b>	<ul style="list-style-type: none"> <li>Section 2.3.1.2</li> <li>Figures 2.3.1.2e and 2.3.1.2f</li> </ul>	<ul style="list-style-type: none"> <li>Section 2.3.1.3</li> <li>Figures 2.3.1.3b and 2.3.1.3c</li> </ul>	<ul style="list-style-type: none"> <li>Section 2.3.1.3</li> <li>Figures 2.3.1.3d to 2.3.1.3f</li> </ul>
<b>Significance and use</b>	Study the shear fatigue behaviour of tack coats	Study interface fatigue properties	Shear resistance property used to evaluate tack coat properties
<b>Procedure</b>	<ul style="list-style-type: none"> <li>External layers of sample are held in position by steel clamps while central layer is subjected to loading (displacement), producing a shear force</li> <li>Monotonic or repeated loading subjected to specimen</li> </ul>	<ul style="list-style-type: none"> <li>Normal load applied to joint surface of sample broken through by application of lateral displacement of faces with load inclination of 25.5°</li> <li>Load applied at frequency of 5Hz</li> <li>Loading rate of 3mm/min</li> </ul>	<ul style="list-style-type: none"> <li>Horizontal load applied along interface at constant displacement rate of 2.5mm/min</li> <li>Constant vertical load applied at top of specimen</li> </ul>

## 2.3 Characterisation of interlayer bond strength

<b>Specimen</b>	<ul style="list-style-type: none"> <li>Prismatic sample composed of three asphalt layers with volumetric dimension of <math>70 \times 120 \times 50 \text{mm}^3</math> with tack coat applied to interlayer interface</li> <li>Six steel plates glued to specimen – assure failure occurs at pre-defined shear planes</li> </ul>	Dual layer system with interface layer	<ul style="list-style-type: none"> <li>Cylindrical core sample: 94mm to 100mm in diameter</li> <li>Prismatic core sample: <math>100 \times 100 \text{mm}^2</math></li> <li>Laboratory prepared and extracted from pavement structure</li> </ul>
<b>Results</b>	<ul style="list-style-type: none"> <li>Applied shear load</li> <li>Corresponding displacement (<math>\delta</math>)</li> </ul>	<ul style="list-style-type: none"> <li>Shear stress</li> <li>Corresponding displacement (<math>\delta</math>)</li> </ul>	Shear stress at failure ( $\tau_{\max}$ )
	<ul style="list-style-type: none"> <li>Better results are provided through dynamic loading as it simulates loading conditions better than monotonic loading. According to some literature, a precise assessment of interlayer bonding characteristics is made possible through monotonic testing</li> <li>Dynamic loading also allows better evaluation of interface shear fatigue behaviour</li> </ul>	<ul style="list-style-type: none"> <li>Accurate simulation as it incorporates both vertical loading conditions induced by traffic</li> <li>Assists in “direct” evaluation of pavement durability.</li> <li>Results output (curve) differs to results acquired from other tests (Figure 2.3.1.3c compared to Figures 2.3.1.2c and 2.3.1.3f)</li> </ul>	<ul style="list-style-type: none"> <li>Incorporates climatic and traffic conditions although it is incorporated under laboratory conditions and may not necessarily describe physical conditions experienced on site</li> <li>Effect of dilatancy taken into consideration in contrast with LPDS test (Table 2.3.1.5a).</li> </ul>
<b>Remark(s)</b>	Developed by University of Limoges	Developed by Romanoschi & Metcalf (2001)	<ul style="list-style-type: none"> <li>Variation in applied normal load supplies sufficient data for Mohr Coulomb failure envelope</li> <li>Developed in Italy at the Università Politecnica delle Marche</li> </ul>

**Note:** Displacement rate and sample size varies according to different testing device models used.

## 2.3 Characterisation of interlayer bond strength

Table 2.3.1.5c: Pull-Off Device and Wedge Splitting Test

	UTEP Pull-Off Device	Wedge Splitting Test
<b>Reference(s)</b>	<ul style="list-style-type: none"> <li>Section 2.3.1.4</li> <li>Figure 2.3.1.4b</li> </ul>	<ul style="list-style-type: none"> <li>Section 2.3.1.4</li> <li>Figures 2.3.1.4e to 2.3.1.4i</li> </ul>
<b>Significance and use</b>	<ul style="list-style-type: none"> <li>Tensile strength of tack coat material measured to determine bonding properties</li> <li>Evaluates appropriateness of the tack coat material</li> </ul>	<ul style="list-style-type: none"> <li>Maximum horizontal force and specific fracture energy determined to characterise fracture mechanical properties (brittle vs. ductile) of interlayer bonding</li> <li>Properties used to evaluate appropriateness of tack coat material</li> </ul>
<b>Procedure</b>	Torque force applied to detached plates or contact plates and tack coated pavement (sample)	Vertical load ( $F_M$ ) applied through wedge to two-layered specimen with groove and starter notch along interface (at constant rate) until failure
<b>Specimen</b>	Cylindrical specimen	<ul style="list-style-type: none"> <li>Cubic or cylindrical specimen with interlayer in middle and starter notch at interface</li> <li>Differently shaped specimen</li> </ul>
<b>Results</b>	Tensile stress at failure	<ul style="list-style-type: none"> <li>Maximum horizontal force (<math>F_H</math>)</li> <li>Corresponding maximum displacement (<math>\delta</math>)</li> </ul>
	Inconsistency (less reliable) in results as the device is manually operated which could lead to a non-uniform loading rate due to eccentric loading effect often experienced	<ul style="list-style-type: none"> <li>Accurate simulation as it incorporates both vertical and horizontal loading conditions induced by traffic</li> <li>Maximum tensile strength does not sufficiently characterise mechanical properties of materials such as brittle and ductile fracture behaviour – fracture energy is derived from results in this capacity</li> <li>Limited results are obtained – it produces a stress distribution that does not represent field conditions</li> </ul>
<b>Remark(s)</b>	Developed by University of Texas at El Paso (UTEP)	Developed by Tschegg et al. (1995)

### 2.3.2 Factors influencing interlayer shear bonding

References in various technical literature have been made regarding influencing parameters that have an impact on the interface bonding between pavement layers. For example, in research by Malicki & Górszczyk (2012), the authors investigated the problem of different tack coat materials and how they contribute to the strength and durability of interlayer bonding in an asphalt layer system. The authors found that these attributes specifically showed the significant influence of tack coat materials on interlayer shear strength. Other research by Jaskula & Rys (2017) highlighted the improvement (of almost 6 times) on fatigue life for different percentages of bonding life.

As reported by Malicki & Górszczyk (2012), various factors influence the level of interlayer bonding; the main factor relating to the execution of work quality (site traffic). In addition, the weather during application plays a role in the final properties of the tack coat. Different types of hot mix asphalt require different amounts of a tack coat. The thickness of layer should also be taken into consideration as a too thick layer may weaken the interlayer bonding.

Several methods are used to establish the extent of influence, which include laboratory testing (Section 2.3.1), non-destructive testing and theoretical analysis using field data. The comprehensive research enables an understanding of the major factors influencing the interlayer shear strength (ISS). Some of the main factors identified are listed in the following points:

- Binder Age;
- Temperature;
- Pavement type and mixture;
- Surface characteristics;
- Application rate and curing time of bitumen emulsion;
- Position of interface;
- Speed of vehicles travelling – describes the loading impact on pavement;
- Compaction energy and method;
- Stiffness of pavement foundation (subgrade);
- Climatic conditions;
- Rheological properties of the tack coat material: viscosity, softening point, penetration, etc.

Some of these components are found to be interrelated and have a cumulative effect on the outcome of results. In addition to the factors related to the material used for the interlayer, testing conditions of the devices used, also contribute to the outcome of the analysis. Hence, Section 2.3.2 explores the factors listed, as well as attributes of testing devices, which impact evaluation of shear resistance. The different elements responsible for impacting interlayer shear strength are discussed subsequently in 2.3.2.1 to 2.3.2.3. Only fundamental factors listed will be addressed, given the extensive potential factors identified in literature.

Firstly, aspects related to surface characteristics are discussed, followed by the different tack coat characteristics, such as application rate, material type, and dosage used for pavement construction. The simulation of traffic loads in shear testing are also addressed. The section is concluded by investigating the impact of testing conditions on the outcome of shear testing. The discussion is concluded with reference to Leutner testing only, given its applicability to the current research study.

## 2.3 Characterisation of interlayer bond strength

## 2.3.2.1 Surface characteristics

Surface characteristics can be broken down into different components, including surface type, surface roughness and texture and surface state (moisture and dust). The surface characteristics were evaluated in research by Wei et al. (2015), Huang et al. (2015), Raposeiras et al. (2013) and Wang et al. (2017) respectively. This section provides a brief discussion of the different elements related to surface characteristics and how they influence interlayer bond strength.

**Surface type**

Huang et al. (2015) undertook a study to assess the effect of surface characteristics, tack coat material and application rate on interface bonding stress. The bonding performance of four different types of tack coat was assessed on different interfaces considering various surface types, including steel and asphalt. A variety of application rates were also considered during evaluation. Three samples were tested for each test condition defined by tack coat material and application rate. For the purpose of the study, testing was completed with the Portable Bond Strength Tester (PBST). The results acquired from testing are shown in Figures 2.3.2.1a and 2.3.2.1b for a steel and asphalt surface.

The bonding stress is recorded on the vertical axis relative to application rate shown on the vertical results. Results are portrayed in these figures according to the different tack coat materials used, i.e. bitumen emulsion, cutback or hot bituminous binder (2.2.2.2 to 2.2.2.4). Results presented in these figures are the average values obtained from triplicate samples tested.

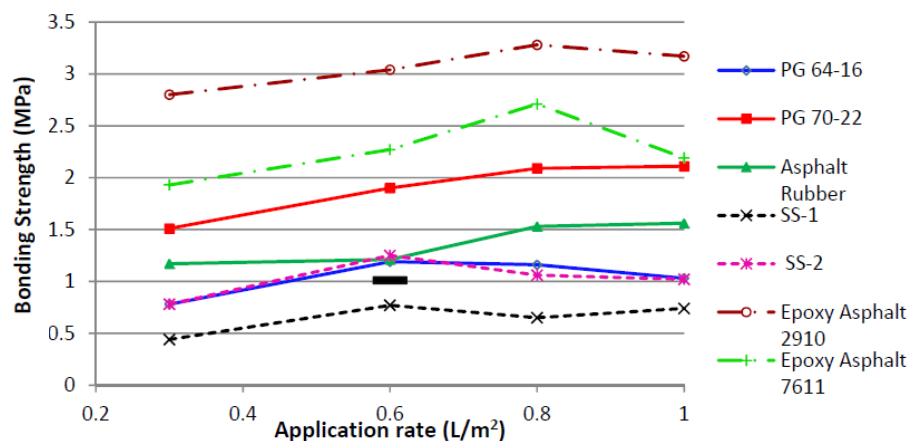


Figure 2.3.2.1a: Bonding strength of different asphalt on steel surface (Huang et al., 2015)

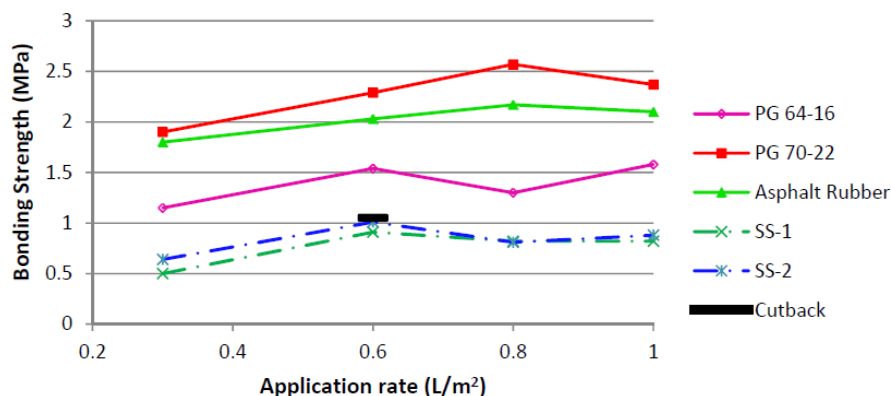


Figure 2.3.2.1b: Bonding strength of different asphalt on asphalt surface (Huang et al., 2015)

### 2.3 Characterisation of interlayer bond strength

Studying the trends of the curves in Figure 2.3.2.1a, it is noticeable that initially an increase in bonding strength occurs for all tack coat types evaluated. This behaviour is attributed to the fact that tack coat materials are required to first fill voids of layers, acting as a binding material (Wei et al., 2015). Succeeding behaviour shows a rapid decrease in the bonding strength with an increase in the tack coat application rate, suggesting that higher application rates do not guarantee stronger bonding between layers.

From the results an optimum application rate between 0.6 and 0.8L/m<sup>2</sup> is observed. The author reports that application rates between 0.6 and 0.8L/m<sup>2</sup> caused the structural asphalt to reach saturation on the surface. As these two attributes are increased simultaneously, an excess of tack coat material becomes available, causing it to act as a lubricant (Wei et al., 2015). Consequently, excessive asphalt exists in the form of free asphalt, if additional asphalt is applied, supporting the phenomenon that no increase in bonding strength occurs with an increase in the application rate (Huang et al., 2015).

Figure 2.3.2.1b excludes samples composed of epoxy asphalt (from Figure 2.3.2.1a) as it is rarely used in asphalt interlayers (Huang et al., 2015). The behaviour observed concerning the different materials correlated with the bonding strength recorded of asphalt on a steel surface. The figure also highlights the significance of using a hot bituminous binder (2.2.2.2) for tack coat material, rather than a bitumen emulsion (2.2.2.4).

Research performed by Wei et al. (2015) agreed with the variation of interface shear strength with the change in residual application rate (Figure 2.3.2.1c). However, a different optimum dosage was achieved for the different surface types. Wei et al. (2015) argue that the effects of microstructure features affect the optimum dosage, which is responsible for the behaviours observed. Every road structure has an optimum tack coat dosage, depending on the structure of the bottom layer within the structure. The volume of voids in different structures differ, which result in variations of optimum dosage for each structure. Relating this to aggregate surface, optimum conditions will be influenced by water absorption characteristics.

The maximum optimum dosage for the different surface types is 0.6, 0.8 and 1kg/m<sup>2</sup> where maximum bonding strength ranges between 1.15 to 1.35MPa. For research by Huang et al. (2015) maximum bonding strengths exceeding 2.5MPa (117% increase) were observed. In this studying a maximum shear strength of 3.3MPa (187% difference) was obtained for results presented for asphalt on a steel surface.

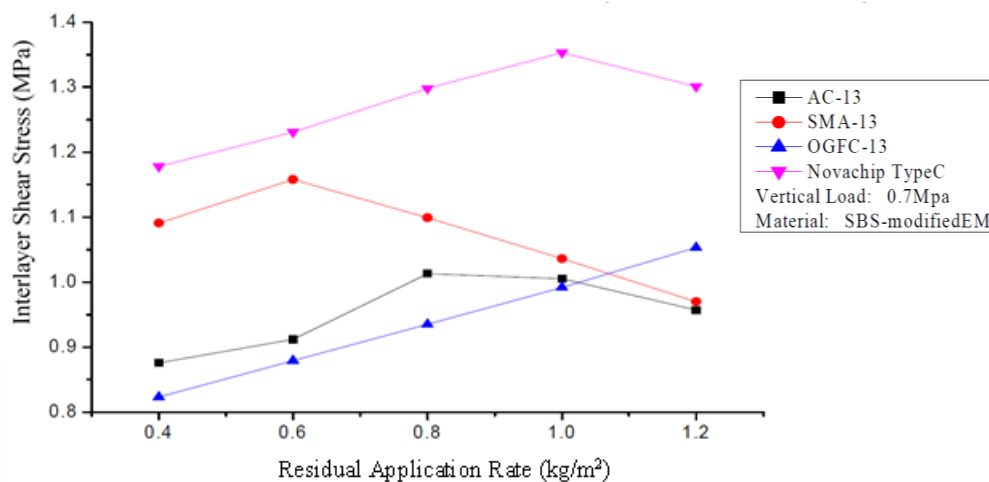
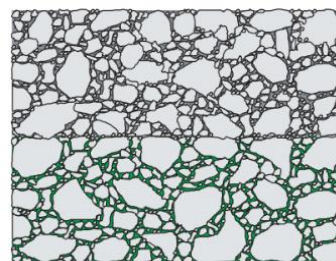


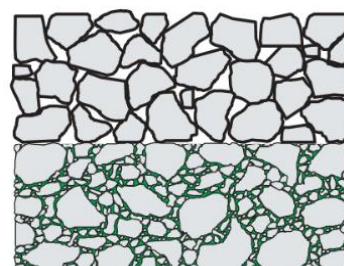
Figure 2.3.2.1c: Variation of bonding strength for different surface types (Wei et al., 2015)

### 2.3 Characterisation of interlayer bond strength

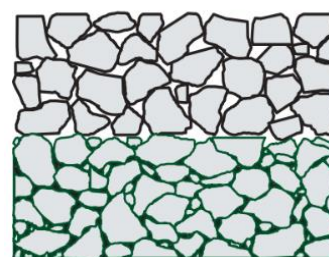
Three surface types were identified in Chen & Huang (2010), as demonstrated in Figure 2.3.2.1d. Figure 2.3.2.1d (i) depicts an instance where both the upper and lower layers are paved with dense-graded mixtures, resulting in adequate bonding between the layers. Better adhesion is achieved due to extensive contact areas between the interlayer surfaces. The shear properties of these surfaces describe the adhesion which is acquired. An example of a porous mix asphalt is given in Figure 2.3.2.1d (ii) with an air content of 20%, manifesting weaker shear resistance as a result of lack of adhesion of the upper layer. With a reduction in the contact areas between the interlayer surfaces (Figure 2.3.2.1d (iii)), the peak shear strength will comprise of the lowest shear strength compared to Figures 2.3.2.1d (i) and (ii).



(i)



(ii)



(iii)

#### **Surface roughness and texture**

The surface type and its impact on interlayer bonding strength is usually scrutinized according to the material type and application rate (Figures 2.3.2.1a, b and d). Despite these being the main attributes associated, Raposeiras et al. (2013) included the surface roughness and texture as another potential factor. A list of studies entailing the evaluation of this is also included in research by Raposeiras et al. (2013) titled, *Test Methods and Influential Factors for Analysis of Bonding between Bituminous Pavement Layers*.

Through the literature provided, a significant observation is made in terms of the surface roughness. It was found that milled surfaces provide higher bonding strength, indicating minimal effect of the absence of tack coat. In contrast, non-milled surfaces, together with the absence of tack coat, show a severe decrease in the bonding strength. It should be noted that when smooth surface conditions are maintained, milled sections show the best results, according to Raposeiras et al. (2013).

The surface roughness and texture vary according to the type of bituminous mixture used. A case of this occurrence is evident in Raposeiras et al. (2012), who postulate that a bituminous mixture, with higher macrotexture values, produces better strength values (Figure 2.3.2.1e). Results are representative of two different bitumen mixtures referred to as *AC16D* (left) and *AC22* (right) according to European Standards. Another area of interest of the study was tack coat dosage. The authors recommend that a tack coat dosage and optimal layer should be based on the macrotexture value of the bituminous mix.

For the results shown in Figure 2.3.2.1e, optimal dosage varied between 250 and 500g/m<sup>2</sup> (0.25 to 0.5kg/m<sup>2</sup>). These dosages are seemingly smaller than the optimal dosages found in research by Wei et al. (2015) where optimal dosages varied between 0.6, 0.8 and 1kg/m<sup>2</sup>. Considering the highest rate determined from Raposeiras et al. (2012) and the highest rate from Wei et al. (2015) research, a change of 300% (increase) is noticeable.

**Figure 2.3.2.1d:** Three types of interlayer surfaces (Chen & Huang, 2010)

## 2.3 Characterisation of interlayer bond strength

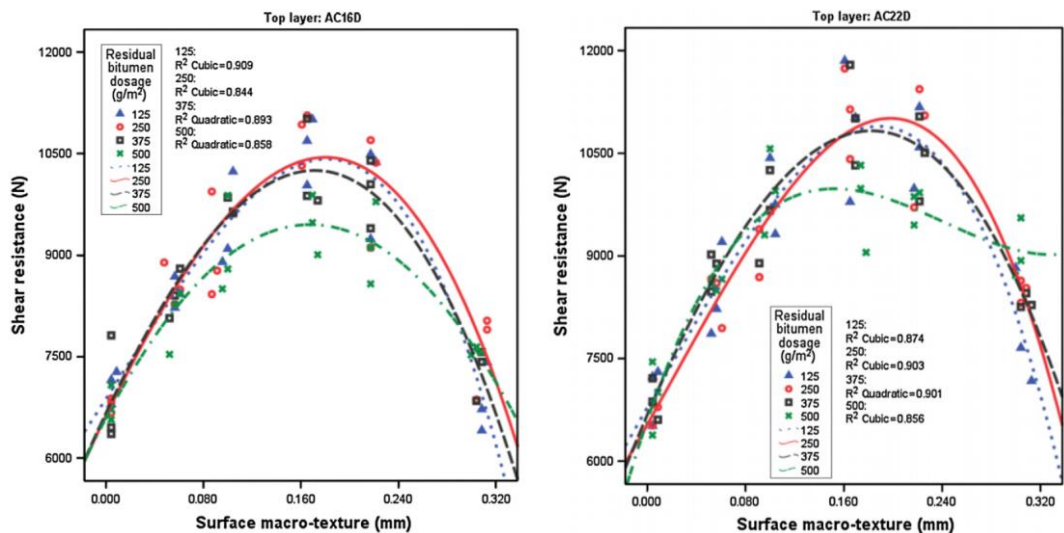


Figure 2.3.2.1e: Shear resistance for two bitumen mixtures (Raposeiras et al., 2012)

Macrotecture (Figure 2.3.2.1f) is described as a family of wave-shaped road surface characteristics that consist of partly desired and undesired properties, i.e. surface roughness. It is measured in millimetres (0.5 to 50) mainly attributed to coarse aggregate size, shape, angularity and distribution (Chen & Huang, 2010). The phenomenon is important as the road texture affects the interaction between the road surface and the tyre footprint. Hence, inadequate macrotecture due to improper construction practice or wear has a negative influence on shear properties. The main function of macrotecture is that it supplies rapid drainage for pavements. The main benefit is attributed to hysteresis and avoidance of hydroplaning (Serigos, 2013).

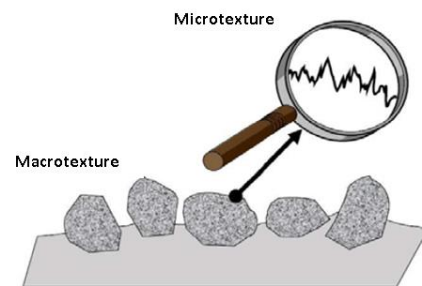


Figure 2.3.2.1f: Macrotecture and microtecture (Fontes et al., 2006)

### Surface state

Adhering to typical construction practices, the upper pavement layer cannot be constructed immediately after the tack coat is sprayed. Tack coat application by means of Spray Jet Technology (2.2.4.4) is the exception to this occurrence, where these layers are placed immediately after one another. During construction, trucks may contribute to dust on the constructed layers that cannot be cleaned. Additionally, breakdown of these vehicles may result in oil spilling on the tack coat. Oil spillage and dust, relative to the interlayer, are found to harm the bonding condition (Wei et al., 2015).

### Presence of dust and moisture

Apart from the material type and texture of the surface, the surface conditions play a big role in the bonding strength achieved. Studies by Mohammad et al. (2008), and Raab & Partl (2004) addressed surface conditions such as moisture and dust. The research of Raab & Partl (2004) revealed that the presence of tack coat provides a form of adherence in the presence of water or moisture. As anticipated, a weaker bonding condition is experienced when there is water on the tack coat surface. In contrast, Mohammad et al. (2008) noted a difference in results between clean and dusty surfaces, where no change in results was observed between wet and dry surfaces.

### 2.3 Characterisation of interlayer bond strength

Research completed by Santagata et al. (2009) addressed influence of dust on interface strength. The authors found that the presence of dust when tack coat is spread i.e. emulsion, improves the bonding characteristics at an early stage rather than acting as a disadvantage. In addition, a study by Mohammad et al. (2011) showed that no significant difference were found statistically between samples tested relative to dry and wet conditions. Results produced showed that a small amount of water can be flushed away Hot Mix Asphalt (HMA) mat and will have “inconsequential” effect on the tack coat quality.

The observations made in both the studies point out the large contribution that surface state, roughness (macrotexture) and the mixture type has on bond strength produced. A higher macrotexture is recommended for lower layers. The elements mentioned should also be considered in correlation with binder dosage, as the dosage varies for each surface macrotexture (Raposeiras et al., 2013). The extent of the impact of these factors, specifically on tack coats, was investigated at three contamination levels in a research study by (Wei et al., 2015). Testing was performed at a temperature below 20°C, with a normal pressure load of 0.35MPa. The recorded interlayer shear stress is shown in Figure 2.3.2.1g. The contamination level (pollution rate) is indicated on the horizontal axis. Interlayer shear stress was measured at rates of 0.1, 0.2 and 0.4kg/m<sup>2</sup>.

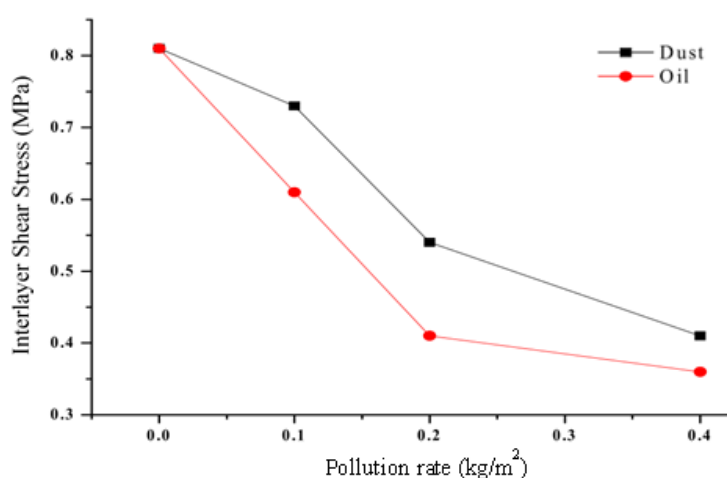


**Figure 2.3.2.1g:** Interlayer bonding with contamination condition (Wei et al., 2015)

Figure 2.3.2.1g illustrates the difference of the impact of oil spills and dust on the interlayer shear stress. A significant variation in the results is noticeable, until a pollution rate of 0.4kg/m<sup>2</sup> is reached, where a decrease in the difference in results is noticeable. The trends in both curves highlight the negative impact of the factors on the bonding strength where it is evident that oil is more influential. The behaviours are attributed to the existence of the factors spoiling the continuity of the binder, causing poor cohesion in the material (Wei et al., 2015).

#### 2.3.2.2 Tack coat characteristics

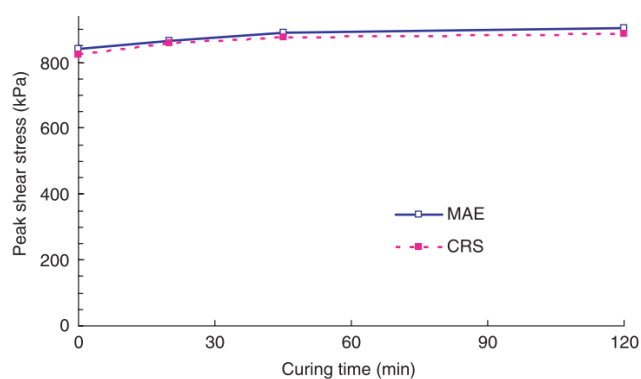
Three types of tack coat materials were introduced in Section 2.2.2 where bitumen emulsions are favoured materials used for tack coats. In a survey conducted by Mohammad et al. (2008), it was confirmed that different tack coat materials used, lead to different bonding strengths. From various studies conducted to evaluate interlayer bonding strength, the tack coat material was identified as a crucial factor. The behaviour is motivated by the different rheological properties of the materials, showing great dependency on factors such as temperature (related to viscosity) and the dosage used at a particular application rate. Consequently, these factors have an impact on the material response during shear testing, implicating the shear stresses generated. The attributes identified, related to the tack coat material, are subsequently discussed.

### Breaking and curing time

The different types of bitumen emulsion used as tack coat material acquire different curing times due to various emulsifying agents (2.2.2.4) used. Wang et al. (2017) report that a majority of tack coats require one to two hours to “fully” cure. Literature studied from various authors in Wang et al. (2017) concluded the following in terms of curing and shear strength:

1. 1 and 3 hour curing times has a similar impact on interlayer bond strength (Destrée et al., 2015).
2. Shear strength increases with curing time (Sholar et al., 2004) which is counter inclusive to findings by Destrée et al. (2015) described in point 1
3. Good versus poor compaction of layer(s) constructed before and after tack coat plays a major role on shear strength obtained. Better bonding is accomplished with good compaction, because of increased contact points. In general, although curing time contributes to results, it is shown to have a minimal effect on the interlayer shear strength (Papagiannakis & Tashman, 2006).

Results from Chen & Huang (2010) are presented in Figure 2.3.2.2a. The graph illustrates the effect of curing time on shear stress. The results in the figure were obtained under a normal stress loading of 552kPa at a temperature of 25°C. The behaviour in the graph correlates with the findings made in research completed by Wang et al. (2017) – increase in curing time produces minimal increase shear strength values. The study also highlighted that adequate bonding can be achieved with little curing time. Observations in terms of the curing time are explained through the reaction that occurs once the bitumen emulsion is placed (sprayed) on the pavement during construction. The process is described in 2.2.3.2 and illustrated in Figures 2.2.3.2a and 2.2.3.2b.



**Note:** MAE = Modified Asphalt Emulsion (Bitumen emulsion),  
CRS = Cationic Rapid-Setting emulsion (2.2.2.4).

**Figure 2.3.2.2a:** Effect of curing time on peak shear stress (Chen & Huang, 2010)

### Application rate

Results provided in Figures 2.3.2.1a and 2.3.2.1b (from Huang et al. (2015)) and Figure 2.3.2.1c (from Wei et al. (2015)) indicate the effect of the application rate on interlayer bonding. A decrease occurs in the shear strength until an optimum is achieved, after which a decrease in the bonding occurs. Typical application rates are supplied in 2.2.3.3. Similar to curing, the application rate does not dominantly influence the interlayer bonding properties, but is mostly influenced by factors such as temperature and surface characteristics (2.3.2.1).

Extensive research has been conducted on this attribute, as provided in the research study by Wang et al. (2017) titled, *Application of Tack Coat in Pavement Engineering*. Raposeiras et al. (2012) and Mohammad et al. (2002) observed that the existence of optimal tack coat application rates where shear strength reached a maximum value. Apart from the conclusions drawn from the respective research studies considered in Wang et al. (2017), overall behavioural patterns were prominent in the results. This included the identification of optimum application rates to provide good interface

### 2.3 Characterisation of interlayer bond strength

bonding at low (construction) cost. However, establishment of an optimal application rate value has not been studied, according to Wang et al. (2017).

#### Temperature

Bae et al. (2010) investigated the characteristics of interface shear bonds of tack coats, relating to temperature. Two tack coats were considered, i.e. trackless material and a cationic rapid-setting bitumen emulsion (CRS-1). The emulsion that was used, comprises of PG 58-28. For the trackless material, only results for high temperature could be established (PG 82). The asphalt mixtures are composed of PG 64-22 binder.

Testing was executed with the Louisiana Interlayer Shear Strength Tester (LISST) for three application rates (0.14, 0.28 and 0.7L/m<sup>2</sup>) considering eight temperatures ranging between -10°C and 60°C, in intervals of 10°C. The shear stresses recorded under different conditions are demonstrated in Figure 2.3.2.2b. It is important to note that the limitation in results is attributed to specimens that collapsed under their own weights. For the trackless material, this is noted for testing at 50° and 60°C at a 0.14L/m<sup>2</sup> application rate. Temperatures were selected to not exceed the binder PG grading range. For the bitumen emulsion, this occurred for testing at 50°C for a 0.14 and 0.28L/m<sup>2</sup> application rate. In addition, no results were available for testing completed at 60°C (Bae et al., 2010).

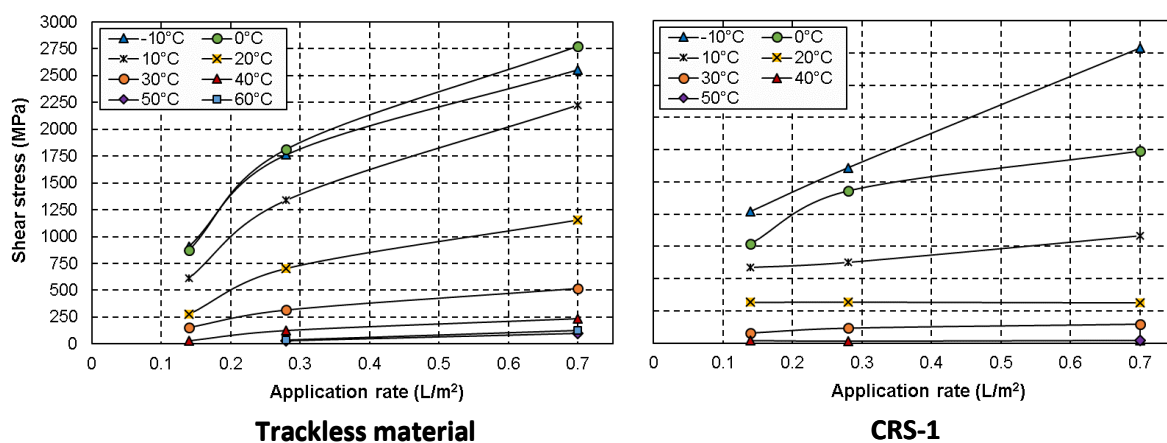


Figure 2.3.2.2b: Variation in interlayer shear strength (Bae et al., 2010)

The phenomenon exhibited by these graphs, where specimens collapsed under their own weights before shearing, is motivated by the absence of shear resistance of the material. This occurred mostly at low application rates for the CRS-1 material. Consequently, it is shown that the trackless material has a greater shear resistance than that of CRS-1 material at high temperatures. Similarly, for an increase in both the application rate and temperature, an increase in shear strength is observable. This contradicts findings made in research by Mohammad et al. (2002) where weaker bonding, with increased application rates at lower testing temperatures, was experienced.

For the bitumen emulsion (Figure 2.3.2.2b right), the interlayer shear strength (ISS) increases gradually with the increase in application rate at testing temperatures from 20°C and higher. However, a constant increase is noticed for the trackless material at higher temperatures. For the trackless material (Figure 2.3.2.2b left), an increase in ISS occurs for testing temperatures between 60° and 0°C, after which it decreases towards -10°C. Validation of the behaviour is given by the poor elongation properties of the material at low temperatures. Different behaviour is observed for CRS-1, where a constant decrease occurs with the decrease in testing temperature. In general, the trackless material produces greater ISS results (Bae et al., 2010).

## 2.3 Characterisation of interlayer bond strength

Canestrari & Santagata (2005) performed a series of laboratory tests, using the ASTRA testing device (2.3.1.3), to study performance-related characteristics of tack coat emulsions. The testing program consists of one bitumen mixture type prepared as multi-layered samples composed of 50/70 penetration grade bitumen, combined with siliceous and calcareous aggregates. Furthermore, 5.8% bitumen content was prescribed with a compaction density of  $2.285\text{g/cm}^3$  corresponding to a void content of 7.1% (Canestrari & Santagata, 2005). The tack coat consists of a cationic emulsion composed of 60% bitumen.

Testing was completed considering a combination of various temperatures and normal stress levels. Shear stress was evaluated for five testing temperatures and three normal stresses. The experimental results gave insight into failure properties of the material. The shear stresses measured for each of the combinations are given in Figure 2.3.2.2c.

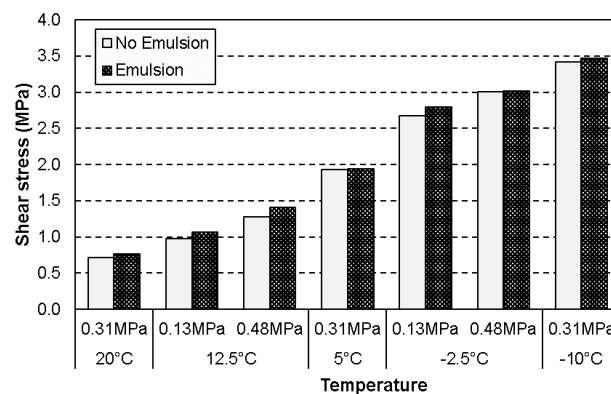


**Figure 2.3.2.2c:** Effect of curing time on peak shear stress (Canestrari & Santagata, 2005)

Studying the results in Figure 2.3.2.2c, an anticipated increase in shear resistance with the decrease in temperature was observed by the authors. The change in shear corresponds to results reported in Figure 2.3.2.2b. Shear stress results captured for 0.13MPa and 0.48MPa, at -2.5 and 12.5°C, are illustrated in Figure 2.3.2.2d. Results are shown for the samples with no emulsion, and with an emulsion of  $0.5\text{kg/m}^2$ . Based on parallel trends of these graphs, the authors hypothesised that shear reduction shows temperature susceptibility of the bituminous material from the sample tested.

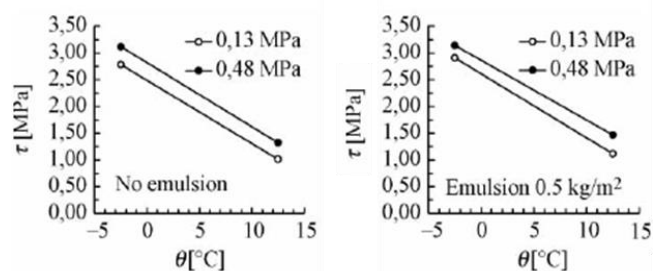


**Figure 2.3.2.2d:** Temperature dependency on peak shear stress (Canestrari & Santagata, 2005)

The correlation between temperature and ISS observed by Bae et al. (2010) and Canestrari & Santagata (2005) is also confirmed by Hu et al. (2017). The author also explains the contradictive behaviour found in Mohammad et al. (2002), due to the following attributes:

1. The flowability of the tack binder is important with respect to the interface strength. The viscosity (which describes the resistance to flow of a material) of the binder improves ISS at high temperatures.
2. The brittle behaviour of a binder enhances deformation resistance ability of the material at lower temperatures.

3. Changes in results are attributed significantly to a combination of testing temperature, tack coat dosage and the rheological performance of the material.
4. Increase dosage is recommended to improve interface shear properties at low temperatures.

### 2.3.2.3 Gap width of Leutner Shear Test

In Section 2.3.1, the Leutner test is categorised as the most popular “pure” shear testing device used to assess interlayer bonding in asphalt pavements. As discussed in the overview of the testing methods in 2.3.1.2, it is evident that the testing equipment has been adjusted since the design of the original patent developed by R. Leutner in 1970. Also, decades of research studied show how these adjustments influence the outcome of testing. One of these components is the gap width. Standards gap widths are applied, depending on the testing device manufacturer. A typical gap width of 2mm is adhered to (Di Benedetto et al., 2013), while research conducted by Sutanto (2009) considered testing with a 5mm gap width.

The influence of the width came under scrutiny by the European Committee of Standards; hence, a laboratory study was developed to investigate the influence of varying the gap width between 0 and 5mm. The research study by Raab et al. (2010) includes the evaluation of load-deformation properties for the different gap widths, where the focus is placed on stiffness values and maximum shear stress that corresponds to shear deformation. In-layer and interlayer shear properties were also evaluated in the study. For the purpose of testing, 0, 2.5 and 5mm gap widths were applied. For the Leutner testing, a displacement rate of 50mm/min was applied at a standard temperature of 20°C. For every gap width, a selection of five to seven cores were tested (Raab et al., 2010). The composition of these cores is shown in Figure 2.3.2.3a where samples consist of four layers as indicated. Some of the testing was completed with standard Leutner and some with LPDS (2.3.1.2).

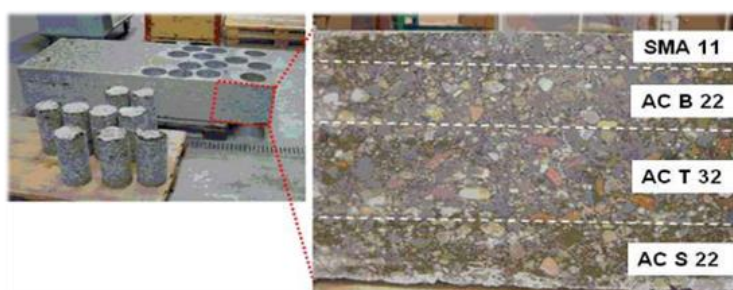


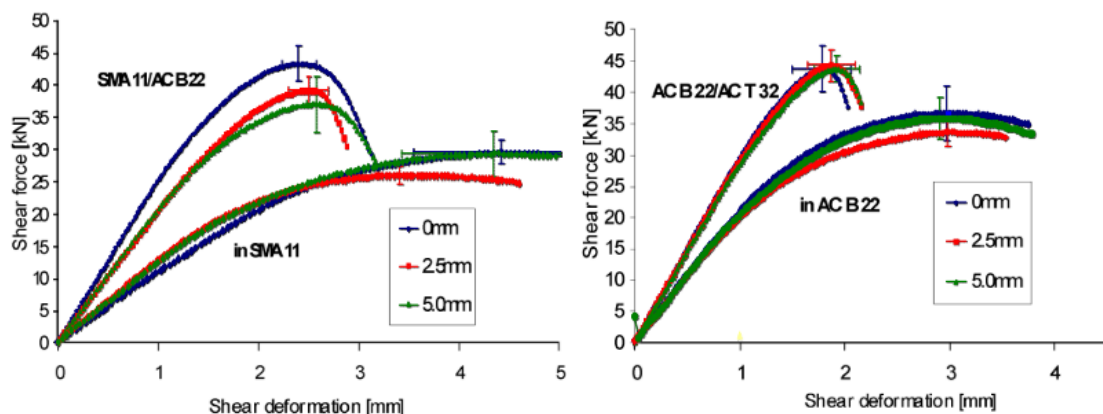
**Figure 2.3.2.3a:** Sample layer configuration (Raab et al., 2010)

Successful shear testing was accomplished for the interlayer of each core. Concerning interlayer testing, tests were carried out on lower layers while surface layers were glued to concrete cores to “enlarge” the samples, hence, accommodating testing of layer thicknesses below 30mm. Results for both layer and in-layer are summarised in Table 2.3.2.3a and presented in Figure 2.3.2.3b for samples at indicated interlayers. The results shown include the average obtained values for shear forces, stresses, as well as deformation (displacement) for the different gap width configurations. Where results are indicated with an “in” prefix, it refers to the in-layer results obtained.

## 2.3 Characterisation of interlayer bond strength

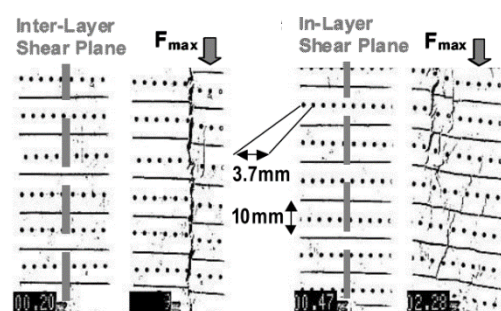
**Table 2.3.2.3a:** Shear testing results (Raab et al., 2010)

Shear Plane	Gap Width [mm]	Force [kN]	Stress [MPa]	Deformation [mm]
SMA 11/AC-B 22	0	43.2	2.4	2.3
	2.5	39.2	2.5	2.4
	5	37.0	2.1	2.5
AC-B 22/AC-T 32	0	43.6	2.5	1.8
	2.5	44.3	2.5	1.9
	5	43.6	2.5	1.9
AC-T 32/AC-S 22	0	26.0	1.5	0.9
	2.5	27.6	1.6	1.0
	5	19.3	1.1	0.8
In SMA 11	0	29.5	1.7	4.4
	2.5	26.0	1.5	3.2
	5	29.3	1.7	4.2
In AC-B 22	0	36.6	2.1	3.0
	2.5	33.6	1.9	3.0
	5	35.8	2.0	2.9
In AC-T 32	0	39.8	2.3	2.4
	2.5	40.6	2.3	2.2
	5	42.0	2.4	2.4

**Figure 2.3.2.3b:** Force-deformation curves with standard deviation for gap width configurations (Raab et al., 2010)

In Figure 2.3.2.3b, behaviour of interlay adhesion between surface and binder course is stiffer and less ductile. Therefore, the graphs for interlayer results show less deformation compared to the in-layer results. For the purpose of the current research, only results related to interlayer bonding are of significant interest, although in-layer results are used for comparative purposes only. For comprehensive results and observations, reference can be made to the research paper published by Raab et al. (2010), titled *Effect of Gap Width on Interlayer Shear Bond Results*.

It should be noted that the interlayer is governed by adhesion between two planes. According to Raab et al. (2010), it is implied that the whole plane has to be moved at once to produce shear failure. The difference between interlayer and in-layer testing is demonstrated in Figure 2.3.2.3c, relative to the shear plane of the samples. For each set of the results the left-hand side figure shows the situation at the start of the test and the figure on the right shows results when cracks start to appear.

**Figure 2.3.2.3c:** In-layer and interlayer shear testing (Raab et al., 2010)

### 2.3 Characterisation of interlayer bond strength

In summary, the study concluded the following, with reference to interface bonding, from the testing completed:

1. Increase in gap width leads to a decreasing maximum shear force and shear stiffness;
2. Material characteristics:
  - Samples composed of layers with similar material characteristics showed that the change in gap width has a minimal impact on the interlayer shear results.
  - In contrast, when samples are composed of layers with different material characteristics (for the two mixtures), they do not have any influence on the interlayer shear results.
  - When good interlock is achieved, minimal impact of gap width on results is observed. In case of poor interlayer bonding, the gap width may influence the testing outcome. This motivates a standardisation, opting for narrow gap width tolerances.
3. Increase in gap width results in a shear plane that is less defined where failure tends to occur at the weakest point, instead of at the exact interface. Raab et al. (2010) reports that a gap width of 5mm can possibly produce results that reflect combined in-layer and interlayer properties.
4. A gap width not exceeding 2.5mm is recommended to optimise the testing process (relates to point with regard to standardisation).

Failure of specimens used in preliminary research by Collop et al. (2009) indicated that large aggregate particles at the edge of the specimen, located close to the interface, were crushed. These occurrences took place when high interface shear strengths were generated while there was misalignment between the shear plane and the Leutner load frame. The struggle with aligning the interface to the shear plane, especially with a specimen with a rough surface, led to the modification of the loading frame to accommodate a gap with of 5mm. A schematic diagram of the modified test is given in Figure 2.3.2.3d.

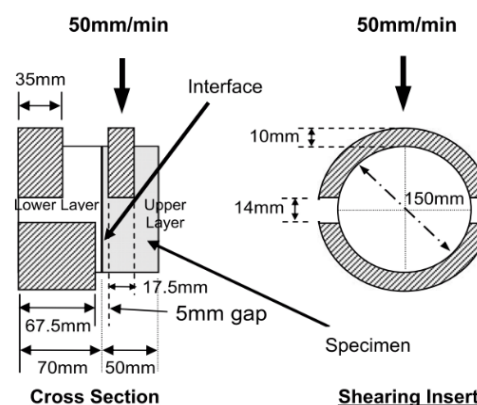


**Figure 2.3.2.3d:** Schematic diagram of modified Leutner load frame (Collop et al., 2009)

Although the configuration was evaluated by Raab et al. (2010) and was deemed unsuitable, the research by Collop et al. (2009) contradicted this. The researchers found that the modification of the test setup reduced the crushing at the edge of the specimen to a large extent. From the testing done, a profound smaller variability in the results obtained was produced from the modified Leutner test.

#### 2.3.3 Influence on residual pavement life

Adhesion provided by tack coats are found to play a virtual role in pavement performance. Factors such as service time and fatigue are known in pavement distress. Therefore, these attributes should also be considered. Wan et al. (2018) studied the relationship between interface shear characteristics and residual pavement performance. Only flexible pavements were considered in the research study. The experimental program of the study entailed the investigation of shear properties in terms of service time, traffic loading and distress. A total of 120 cylindrical specimens, 100mm in diameter, were used for testing, composed of an approximate 30mm thick wearing course layer and a binder

### 2.3 Characterisation of interlayer bond strength

course. The 120 samples were allocated to three different research groups which would address each of the elements to be evaluated in this study – location, service time and distress.

The first-mentioned group includes testing of 72 samples: three identical samples were collected from three locations from eight sections, subjected to distress for seven years. The sections were selected based on the type of traffic loading (heavy, middle and mild) for rutting, no rutting and shoulder location. The subsequent research group (service time) consisted of 40 samples of eight identical specimens collected at five locations. The five locations are described as each with a different service time from 0 to 4 years. These samples will be used to establish service time dependency. Finally, four specimens were cored from a rutting and upheaval area which will be used to investigate the effect of the distress type on the interface shear performance (distress research group).

#### **Research group 1: Shear characteristics and traffic loading frequency**

The 72 specimens collected from the different locations are samples exposed to the same environmental conditions, but subjected to different loading conditions. Areas where rutting occurs are the locations with highest traffic loading, whereas the mild traffic loading areas are located at the shoulder positions. The shear strength recorded at these locations enable an understanding of the impact of traffic loading on the interface adhesion, during the service life of the specific pavement structure. The average shear strength (stress) measured at the prescribed locations are presented in Figure 2.3.3a. The results are provided according to the eight different sections for the three different distress types.

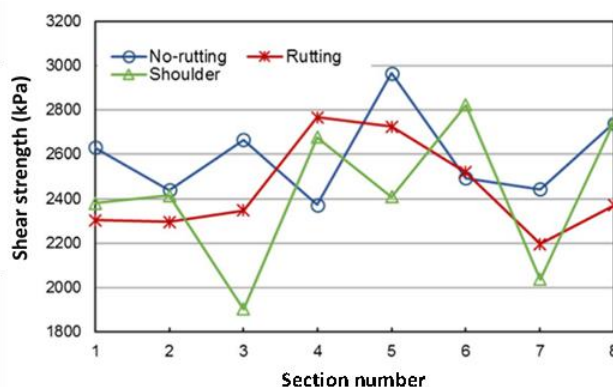


**Figure 2.3.3a:** Average interface shear strength results for location (Wan et al., 2018)

As anticipated, from Figure 2.3.3a the shear strength results for the no rutting locations were higher than locations where rutting was observed. This behaviour confirms that a heavier traffic loading and rutting cause greater decrease in shear strength, ultimately leading to the failure of the structure. Better endurance is maintained by a tack coat with higher shear strength, as it is capable of withstanding higher shear stress under actual service conditions (Wan et al., 2018).

**Research group 2: Shear characteristics and service time dependency** The 40 specimens tested in this research group were used to verify the ageing tendency of shear characteristics of the interlayer. The shear strength determined through testing is presented in a histogram in Figure 2.3.3b for all four service years of specimen. The histogram provides the average results of all the results acquired. A decrease in the shear strength is prominent for service year zero to three, suggesting a decrease in the bonding quality with the increase in service time. Subsequently, an increase in shear strength is indicated for a four-year service time.

2.3 Characterisation of interlayer bond strength

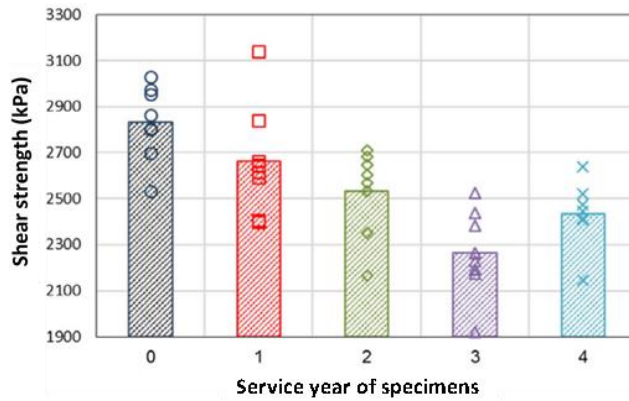


Figure 2.3.3b: Average interface shear strength of gradient service time (Wan et al., 2018)

The shear strength results in Figure 2.3.3c are slightly higher compared to the results shown in Figure 2.3.3b. In general, the results highlight the pavement’s vulnerability to distress in the following service time, since the interlayer has aged to a certain extent (Wan et al., 2018). Shear properties decrease to a certain degree, until it reaches a point where the pavement has a risk of being damaged after four years of service. The nature of these results and displacements (Figure 2.3.3c) allows the evaluation of the residual performance of the pavement interlayer as well as the risk of distress.

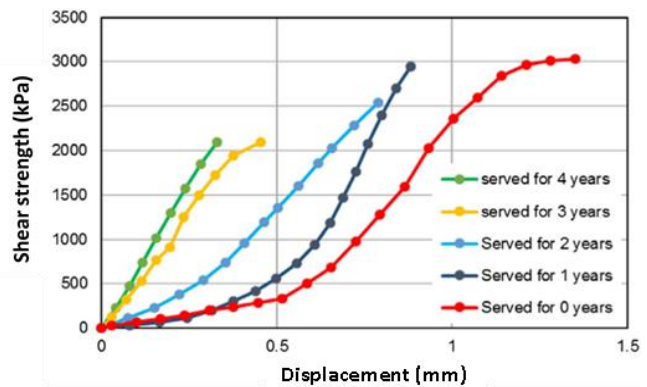


Figure 2.3.3c: Stress-displacement curves of gradient service time (Wan et al., 2018)

**Research group 3: Shear characteristics and distress type dependency**

The average shear strength results are shown in Figure 2.3.3d for the eight specimens of the final group. Eight specimens were tested from upheaval and rutting location. For the four specimens at the rutting location, the shear characteristics were better than for the upheaval specimens according to Figure 2.3.3d. Similar as for Research Group 2, the stress-displacement results are illustrated in Figure 2.3.3e. The curves for the upheaval specimens shown in this figure adhere to an almost linear shape suggesting rigid fractures. In addition, the rutting areas have better shear characteristics at the interface compared to upheaval areas (Wan et al., 2018). Consequently, it is noted that the pavement distress is related to the shear characteristics of the interlayer to a certain extent.

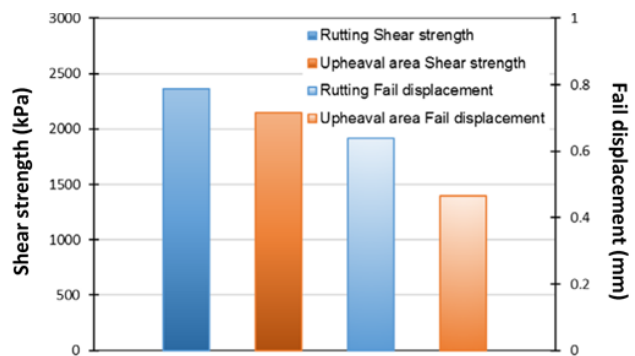
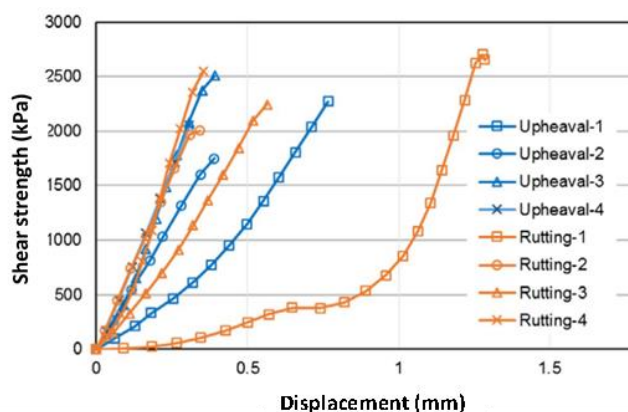


Figure 2.3.3d: Average interface shear strength and fail displacement on rutting and upheaval specimens (Wan et al., 2018)



**Figure 2.3.3e:** Stress-displacement curves of upheave and rutting specimens (Wan et al., 2018)

The significance of bonding contribution has become a fundamental topic in research concerning everyday construction (Raab & Partl, 2009), which questions the long term behaviour of bonding properties. Research summarised by (Wan et al., 2018) evaluated various indicators which aid in answering the questions to a limited extent. The knowledge through the research can be expanded with research conducted by Raab & Partl (2009). The conducted study investigates the impact of the long-term properties of the lower layers. Research entailed shear testing performed with the Layer Parallel Shear Test or LPDS (2.3.1.2).

From the testing completed, it was found that compaction induced by traffic, together with the settlement after construction, has a positive impact on bonding properties. Unfortunately, in rehabilitation or old construction situations, an improvement cannot be expected, given that these structures depend on their surface life. Furthermore, a decrease of 50% in shear strength at lower interfaces was observed that could possibly lead to complete damage of the pavement structure. The research provided great insight concerning shear (bonding) properties as it showed that interlayer shear properties are subjected to change over the life cycle of the pavement. Hence, continuous monitoring of development as a function of factors, such as traffic and climatic history, is recommended by Raab & Partl (2009).

### 2.3.4 Impact of factors on interlayer strength

The section studies the different factors that influence the shear strength results obtained by shear testing. These factors include the surface characteristics and tack coat characteristics. Furthermore, the discussion of these factors is found to be interrelated. However, literature is in agreement that the factor that has the greatest impact, is the temperature, as it is linked with the viscosity (material behaviour), describing the material response under certain conditions. Hereafter, the tack characteristics such as dosage and application rate are found to have an impact, followed by the surface characteristics. The tack coat characteristics determine the extent of influence from the surface characteristics.

## 2.4 Pavement Analysis and Design

The current study focuses on the interlayer bonding provided by tack coat, i.e. shear strength. The extent of interlayer bonding was evaluated in preliminary research (Section 3.2) by means of Mechanistic-Empirical design. In addition, models will be simulated (finite element models) to replicate actual pavement conditions to enhance the understanding of the findings made during the preliminary research. Mechanistic-Empirical (ME) Design and Finite Element Method (FEM) are the

modelling tools used to measure and compare the influence of tack coat. The different components of ME Design are discussed in Section 2.4, while the FEM approach is covered in Section 2.5.

### 2.4.1 Pavement structure and design philosophy

Pavement structures for flexible pavements vary according to local design standards. A representation of a typical flexible pavement structure, according to South African standards, is shown in Figure 2.4.1a. The pavement consists of three layers, the bituminous surfacing, base and the sub-base. The sub-base layer improves the ability of the top layers to carry heavy traffic loading. Because of the cemented layer, the neutral axis shifts, leading to tension in the sub-base and compression in the base. Hence, the layer is incorporated in areas where roads are subjected to large volume of traffic on a regular basis. Otherwise, the pavement structures exclude a sub-base layer. The subgrade supports all of the upper layers and is crucial to the overall structure.

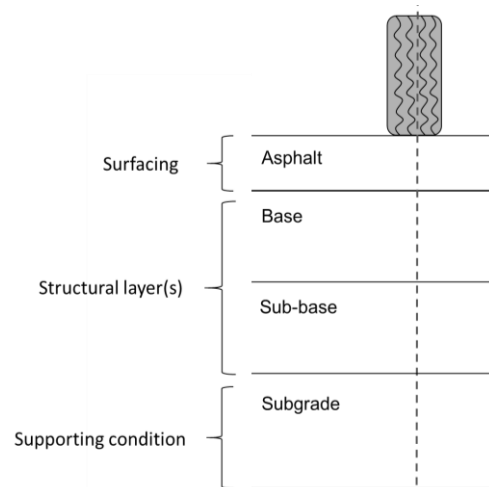


**Figure 2.4.1a:** Typical pavement structure

When the pavement structure is subjected to loading, permanent deformation develops in the area of the wheel tracks. For all well-designed pavement, a uniform distribution of the permanent deformation is expected between the different pavement layers (Croney & Croney, 1998). Theyse et al. (1996) are in disagreement and found that opposite behaviour does occur. The wheel loads result in compressive stresses where bituminous materials will be subjected to tensile stresses as the wheel load passes. The magnitude of these stresses is determined by the material stiffness of the particular layer (Young's Modulus of Elasticity) and will be at a maximum at the bottom of a material layer. For the granular materials used in the lower layers (base and sub-base), significant tensile stresses are not expected, as they will relax under loading while reducing the effective elastic modulus of the materials.

An increase in the viscosity of the bituminous pavement material results in an increase in material stiffness over a certain period. This will result in a minimal impact of deformation with time while subject to loading induced by traffic. Furthermore, as the bituminous layers harden, they will attract tensile stress from traffic loading (Croney & Croney, 1998). The structure failure of the pavement is typically initiated by fatigue cracking in these layers.

Various approaches exist for pavement design, including empirical and theoretical approaches. For analytical pavement design, the philosophy is attributed to the way in which the structure is treated. According to Sutanto (2009), the philosophy suggests that the pavement structure be treated the same as any other civil engineering structure, and should adhere to the following procedure:

1. Specification of loading;
2. Consideration of available materials to be used for construction;
3. Estimations of dimensions and material properties of the respective layers;
4. Performance of a structural analysis (according to preferred approach i.e. theoretical or empirical);
5. Analysis of critical stress, strains or deflections with allowable values;
6. Design adjustment until desired requirements are achieved;
7. Design consideration based on economic feasibility aspects.

The simplest approach for the analysis is a linear-elastic approach, which allows the prediction of stress, strains and the deflection induced by wheel load. The method in which these critical parameters are estimated, depends on the type of analysis method used, i.e. software based on empirical research or methods based on a theoretical approach, i.e. the Burmister theory. Alternatively, more modern approaches, such as the use of finite element modelling, can be used for the solution of pavement design-related problems. The approach allows the evaluation of strains and stresses of multi-layered system at any point within the structure, while also accommodating non-linear (elastic) and plastic behaviour.

### 2.4.2 South African Mechanistic-Empirical Design Method

There are many structural capacity estimation methods available, such as the AASHTO Structural Number (SN) Method, Pavement Number (PN) Design Method as well as the South African Mechanistic-Empirical Design Method (SAMDM). Many variations exist of these design methods, such as the Mechanistic Empirical Pavement Design Guide (MEPDG). Given the scope of the current research, the section studies SAMDM, providing insight into the approach used by this method in addressing the different failure mechanisms in pavement structures, such as fatigue and rutting.

#### 2.4.2.1 Background

Various components of the South African Mechanistic-Empirical Design Method (SAMDM) have been developed since the 1970s, with the latest version, still widely used in South Africa, having been published in 1996. This design approach includes material and pavement behaviour, design traffic, service levels and other relevant components (Theyse et al., 1996). It also addresses the mechanistic analysis procedure. A schematic representation of the main components of SAMDM is given in Figure 2.4.2.1a.

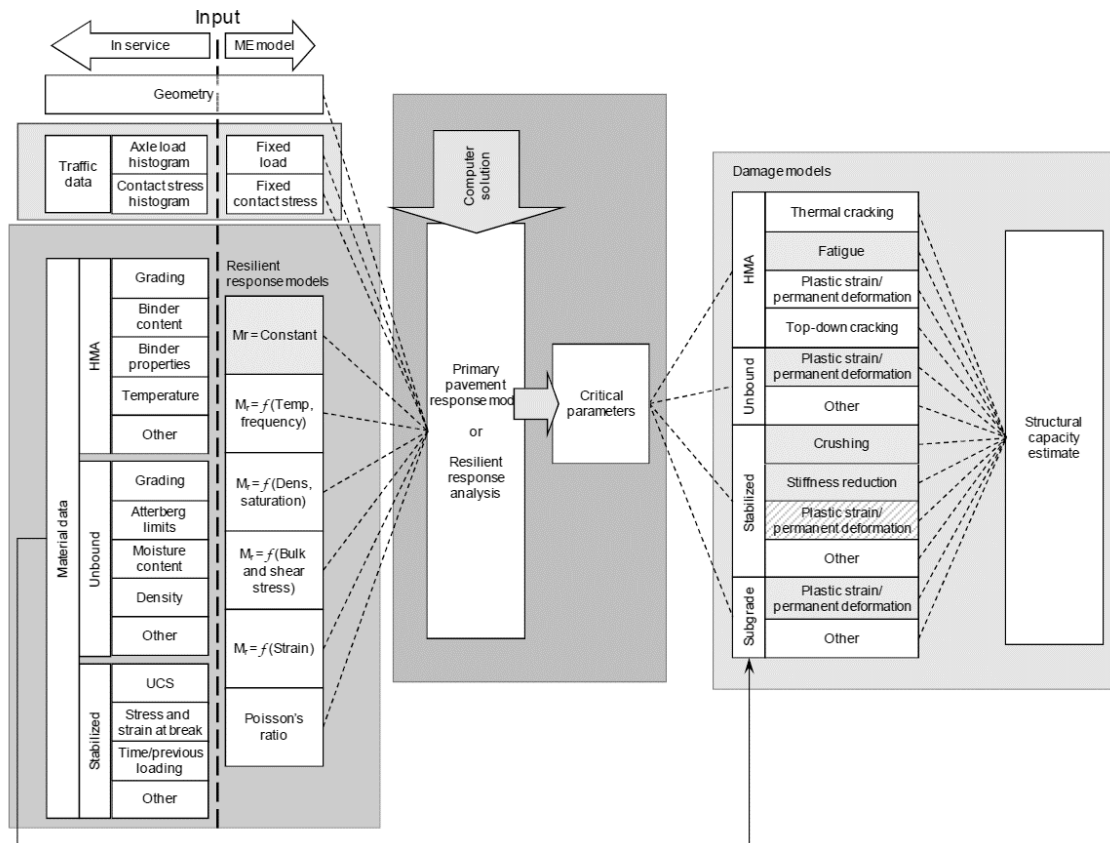


Figure 2.4.2.1a: Schematic representation of the main components (Theyse et al., 2011)

Figure 2.4.2.1b shows a simplified illustration of the SAMDM analysis procedure. This includes material and load characterisation, while parameters such as the layer thickness and elastic material properties for each layer in the pavement structure, are also included. The step is succeeded with a structural analysis which typically involves a linear-elastic, static analysis of the multilayer system, resulting in the pavement response to the loading conditions. These responses are expressed in stresses ( $\sigma$ ) and strains ( $\epsilon$ ). Subsequently, the stresses and strains are used as input data to locally developed transfer functions for representative material types, hence, relating to the stress-strain condition to the number of loads that a specific pavement structure can sustain before reaching a certain terminal condition (Theyse et al., 1996). A synthesis of the method is provided in Table 2.4.2.1a, compiled from a combination of various literature sources, including the South, Theyse et al. (1996) and Theyse et al. (2011).

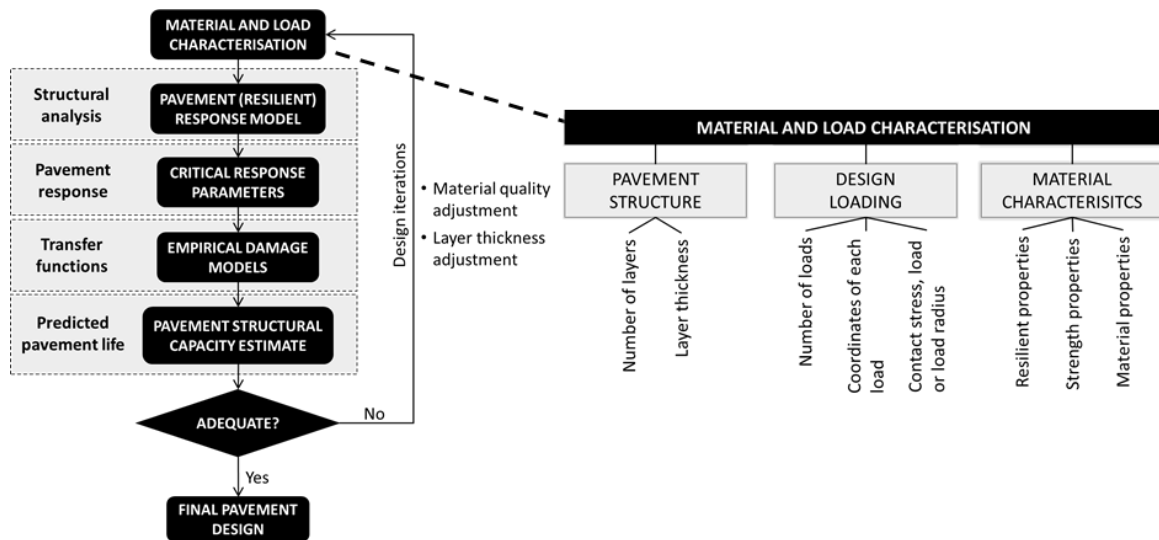


Figure 2.4.2.1b: Illustration of SAMDM analysis procedure (After Theyse et al., 2011)

**Table 2.4.2.1a:** Attributes of the South African Mechanistic-Empirical Design Method

<b>Assumptions</b>	<ol style="list-style-type: none"> <li>1. Linear-elastic with static load.</li> <li>2. Assume that consistent set of conditions apply for the duration of structural life of pavement.</li> </ol>
<b>Advantages</b>	<ol style="list-style-type: none"> <li>1. Suited for new and rehabilitation design.</li> <li>2. Evaluates the adequacy of individual pavement layers and the pavement system.</li> <li>3. Calibrated for South African conditions and materials.</li> <li>4. Accommodates different pavement types and pavement compositions.</li> <li>5. Accommodates changes in operating conditions i.e. axle loads.</li> </ol>
<b>Disadvantages</b>	<ol style="list-style-type: none"> <li>1. Developed for new pavement design and adapted to rehabilitation design with difficulty.</li> <li>2. Perceived to be biased towards certain pavement types.</li> <li>3. Overly sensitive to small variation input.</li> <li>4. Input parameters not well related to routine engineering parameters.</li> <li>5. Damage models outdated.</li> <li>6. Relatively complex, only suited to computer application.</li> <li>7. Inconsistent results, stronger and thicker layer (especially subbase) do not always lead to an increase in structural capacity.</li> </ol>
<b>Data required for analysis and inputs</b>	<ol style="list-style-type: none"> <li>1. Load, i.e. traffic loading conditions.</li> <li>2. Material characterisation for each layer – material stiffness (E) and Poisson's ratio (<math>\nu</math>).</li> <li>3. Layer thickness for each layer.</li> </ol>
<b>Incorporation of climate, ageing and durability</b>	<ol style="list-style-type: none"> <li>1. Method focuses significantly on effect of load magnitude on structural capacity ignoring effects of construction and environmental conditions.</li> <li>2. Field variables such as density, temperature and moisture content of pavement layers are significantly unquantified.</li> <li>3. Evaluation of pavement life accounts for moisture condition/ climatic condition during granular material damage model (transfer function) as well as the terminal rut depth i.e. for subgrade and selected layers.</li> <li>4. Provision for crack propagation by means of a shift factor (SF) for both asphalt and cemented material layers.</li> </ol>

<b>Calibration of theoretical input or laboratory results vs. field performance</b>	<ol style="list-style-type: none"> <li>1. Damage models are not well calibrated for the appropriate critical response parameters appropriate to each material type as certain significant variables were not considered – only elastic response was considered suggesting that materials are not assessed according to true performance potential.</li> <li>2. For granular material – the shear failure calibrated/ validated for the calculation of this parameter in the middle of the layer even if it is not the position with the highest safety factor.</li> </ol>
<b>Accuracy</b>	Inconsistency in results as stronger and thicker layers do not always produce higher structural capacity.
<b>Sensitivity</b>	<ol style="list-style-type: none"> <li>1. Sensitive to small variations in input and significant difference in structural capacity estimates found with small changes in input.</li> <li>2. Overly sensitive to small changes in resilient response parameters.</li> </ol>
<b>Reliability</b>	<p>Measure of design reliability is incorporated into the evaluation of pavement life from transfer functions:</p> <p>Design reliability (coefficients incorporated for category road reliability level in combination with material aspects such as crushing/grading of material) into transfer functions i.e. <math>a</math>, <math>b</math>, <math>c</math>, <math>\alpha</math> and <math>\beta</math>.</p>
<b>Other relevant information</b>	<p>Method is under revision to address shortcomings/ problems raised for the 1996 version. The desired objectives of the modified version include:</p> <ul style="list-style-type: none"> <li>• Density, saturation and stress-dependent model for unbound materials;</li> <li>• Temperature and load rate dependent model for hot mix asphalt.</li> </ul> <p>In addition, various of these objectives are related to the response models for the materials:</p> <ul style="list-style-type: none"> <li>• 3D stress dependency;</li> <li>• Hypo-elastic models calibrated from static test results;</li> <li>• Perfect plasticity models calibrated from static test results;</li> <li>• Contact non-linearity at pre-defined cracks.</li> </ul> <p>Dynamic analysis including effects of stiffness, damping and inertia.</p>

### 2.4.2.2 Material characterisation

SAMDM incorporates standard South African road building materials, i.e. asphalt, cemented and granular materials. For the first-mentioned, a Poisson ratio of 0.44 was defined and 0.35 for cemented and granular materials from previous laboratory testing. For the stiffness of these three materials, an extensive range of values has been specified. The stiffness of the material can vary, based on a variety of variables, such as the condition (at a relative temperature) of the material and the variation (type) of the certain material group. The different suggested stiffness moduli (E) for the materials are summarised in (Theyse et al., 2011).

### 2.4.2.3 Structural analysis and pavement life prediction

A typical structural analysis is carried out with a static, linear-elastic multilayer analysis software. For the analysis, standard South African loading conditions are considered: 40kN dual wheel load at 350mm (175mm to centre) spacing between centres, with a contact pressure of 520kPa (or 750kPa). The axle loading is equally distributed for all wheels as indicated in Figure 2.4.2.3a. The wheel configuration is demonstrated in Figure 2.4.2.3b.

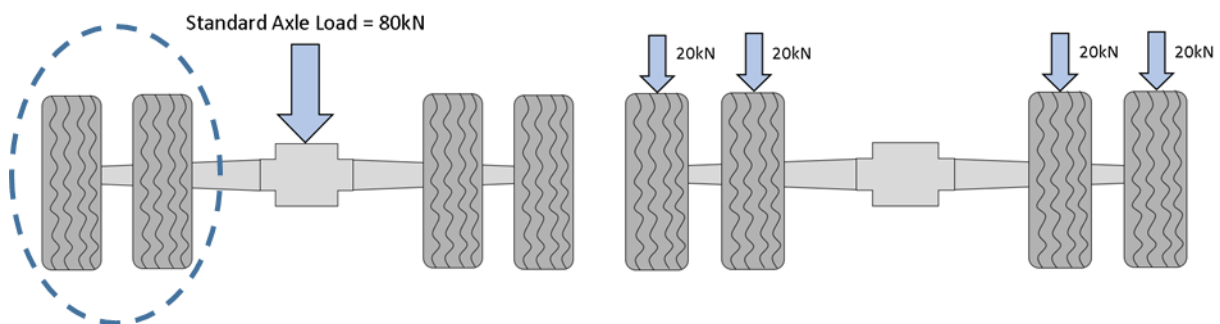


Figure 2.4.2.3a: Wheel load distribution

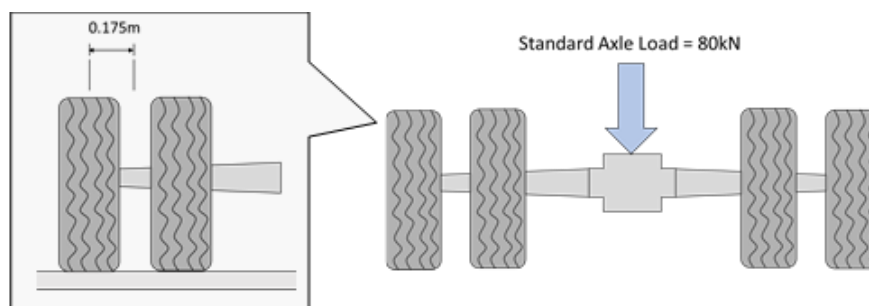
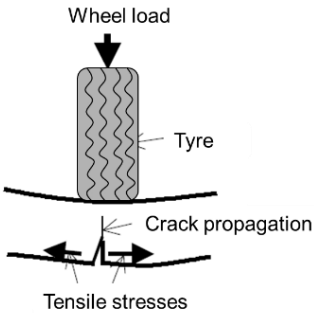


Figure 2.4.2.3b: Wheel configuration

Theyse et al. (1996) reports that pavement life predictions are made up of two components – prediction of individual layer life for each layer, and the ultimate pavement life of the layered system. It uses the estimated individual layer life to establish which layer would fail first under certain loading conditions.

The combined sequence, in which these individual layers fail, is the ultimate pavement life which describes the service life of the pavement structure until failure. Hence, this section focuses on the individual layer life predicted for every material type (layer) made of different characteristics, prone to certain failure modes. The structural analysis and pavement life prediction for the individual layers are summarised according to the different materials accommodated by SAMDM in Tables 2.4.2.3a to 2.4.2.3d. Information provided in this table is a compilation of Theyse et al. (1996) and Jenkins & Rudman, (2018b).

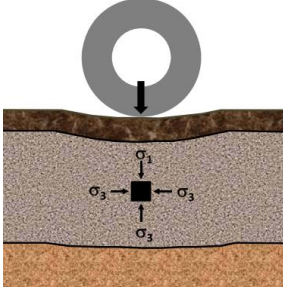
**Table 2.4.2.3a:** Structural Analysis and prediction of individual layer life for asphalt layer

Structural Analysis	Individual layer life
<p>The maximum horizontal tensile strain at the bottom of the asphalt layer (Figure 2.4.2.3c) is used as the critical parameter to estimate fatigue life (same for cemented layer).</p>  <p><b>Figure 2.4.2.3c:</b> Tensile strain at bottom of asphalt layer(Walubita &amp; Van de Ven, 2000)</p>	$N_f = 10^{\alpha \left(1 - \frac{\log \epsilon_t}{\beta}\right)} \quad (2.4.2.3a)$ <p>Where:</p> <p><math>N_f</math> = Fatigue life  <math>\alpha, \beta</math> = Constants given in Table 5.6 from Jenkins &amp; Rudman, (2018b)  <math>\epsilon_t</math> = Horizontal tensile strain at bottom of asphalt layer</p>

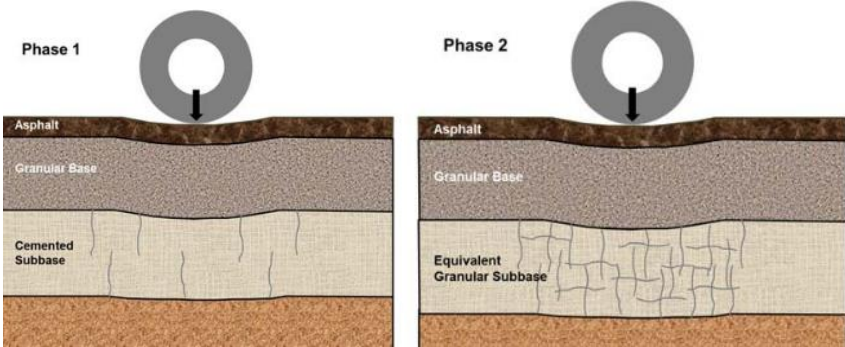
**Table 2.4.2.3b:** Structural Analysis and prediction of individual layer life for subgrade

Structural Analysis	Individual layer life
<p>The maximum vertical compressive strains are measured at the top of the subgrade layer for either a 10mm or 20mm terminal rut depth. The strain is used in the transfer function, represented by Equation 2.4.2.3b to predict life of this layer.</p>	$N_{PD} = 10^{(a - \log(\epsilon_v))} \quad (2.4.2.3b)$ <p>Where:</p> <p><math>N_{PD}</math> = Standard axles to set level of permanent deformation  <math>a</math> = Constants given in Table 5.14 from Jenkins &amp; Rudman, (2018b)  <math>\epsilon_b</math> = Vertical compressive strain at top of layer (microstrain)</p>

**Table 2.4.2.3c:** Structural Analysis and prediction of individual layer life for granular layer

Structural Analysis	Individual layer life
<p>The layer is prone to fail under shearing conditions. Therefore, the shear stresses are measured in this instance and compared to the shear strength in terms of friction angle (<math>\phi</math>) and cohesion (C), using the Mohr-Coulomb model (Equation 2.4.2.3c). The shear stresses in the middle of the layer are considered (Figure 2.4.2.3d)</p>  <p><b>Figure 2.4.2.3d:</b> Critical parameter and location for granular layers (Jenkins &amp; Rudman, 2018b)</p> <p>The shear strength state is known as the safety factor (Equation 2.4.2.3c). The element is used in the transfer function to estimate the structural capacity of the granular layer by means of Equation 2.4.2.3d.</p>	$F = \frac{\sigma_3 \phi_{term} + C_{term}}{(\sigma_1 - \sigma_3)} \quad (2.4.2.3c)$ <p>Where:</p> <p>F = Stress ratio</p> <p><math>\sigma_3, \sigma_1</math> = Major and minor principle stresses acting in middle of granular layer</p> <p><math>\phi_{term}</math> = Angle of internal friction for material codes given in Table 5.8 from Jenkins &amp; Rudman, (2018b)</p> <p><math>C_{term}</math> = Cohesion for material codes given in Table 5.8 from Jenkins &amp; Rudman, (2018b)</p> $N = 10^{(\alpha F + \beta)} \quad (2.4.2.3d)$ <p>Where:</p> <p>N = Number of equivalent standard axles to safeguard against shear failure</p> <p><math>\alpha, \beta</math> = Constants given in Table 5.8 from Jenkins &amp; Rudman, (2018b)</p> <p>F = Stress ratio defined in Equation 2.4.2.3b</p>

**Table 2.4.2.3d:** Structural Analysis and prediction of individual layer life for cemented layer

Structural Analysis	Individual layer life
<p>The cemented layers are analysed for effective fatigue as well as crushing of the material at the top of the layer, assuming the cracks start at the bottom of the layer and propagate to the top of the layer (Phase 1 in Figure 2.4.2.3e right).</p>  <p><b>Figure 2.4.2.3e:</b> Crack Propagation asphalt layer (Jenkins &amp; Rudman, 2018b)</p> <p>The most terminal condition is reached when that the cracking state of the material exhibits similar effective stiffness as an unbound granular layer. When the cemented layer has reached the equivalent granular state (Phase 2 in Figure 2.4.2.3e right), the granular materials transfer function is used to estimate the layer life.</p> <p>The transfer function used to determine fatigue in this layer is represented by Equation 2.4.2.3e, in which the two elements in this equation are determined with Equations 2.4.2.3f and 2.4.2.3g (as represented by Equation 2.4.2.3h).</p>	$N_{eff} = SF \cdot N \quad (2.4.2.3e)$ <p>Where:</p> <ul style="list-style-type: none"> <li><math>N_{eff}</math> = Effective fatigue life (<i>crack progression</i>)</li> <li>SF = Shift factor for <i>crack propagation</i> given in Table 5.12 from Jenkins &amp; Rudman, (2018b) – Eq. 2.4.2.3e</li> <li>N = Fatigue life (<i>Crack initiation</i>) – Equation 2.4.2f</li> </ul> $SF = 10^{0.00285t - 0.293} \quad (2.4.2.3f)$ <p>Where:</p> <ul style="list-style-type: none"> <li>SF = Shift factor for crack propagation given in Table 5.12 from Jenkins &amp; Rudman, (2018b)</li> <li>t = Pavement layer thickness (cemented layer)</li> </ul> $N = 10^{c \left(1 - \frac{\epsilon}{d\epsilon_b}\right)} \quad (2.4.2.3g)$ <p>Where:</p> <ul style="list-style-type: none"> <li>c, d = Constants given in Table 5.12 from Jenkins &amp; Rudman, (2018b)</li> <li><math>\epsilon</math> = Horizontal tensile strain at bottom of layer (microstrain)</li> <li><math>\epsilon_b</math> = Strain-at-break with recommended values given in Table 5.11 from Jenkins &amp; Rudman, (2018b)</li> </ul> $N_{eff} = SF \cdot 10^{c \left(1 - \frac{\epsilon}{d\epsilon_b}\right)} \quad (2.4.2.3h)$

## 2.5 Finite Element Method

### 2.5.1 Introduction

The Finite Element Method (FEM) is a numerical method used for solving problems of engineering and mathematical physics. Barna A. Szabó (2015) describes it as a numerical problem constructed by piecing together elements by means of finite element analysis (FEA) software. Various conditions are applied at nodes within the model, which satisfy equations of static equilibrium for the entire model (Barna A. Szabó, 2015). The method has been found useful with complicated geometries, loadings and material properties where analytical solutions cannot be obtained. However, the author raises the concern that there is no assurance of an underlying mathematical problem being well-posed, or that requirements of consistency or stability, are met.

It should be noted that the definition allows a broad opportunity of applications. It can be used in pavement analysis-related problems to evaluate stresses and strains that are used to evaluate durability (Section 2.5.2). Alternatively, it can be used to replicate laboratory conditions to evaluate elements related to the durability of a given pavement structure (Section 2.5.3). This section will explore both the subject matter in light of FEM to illustrate its application in the different scenarios. The discussion of Sections 2.5.2 and 2.5.3 provide background to the models developed for the purpose of the current research study. This section briefly discusses application of shear tests for interlayer bonding simulated as FEM models. Elaboration of the method and its applications are discussed in further chapters.

### 2.5.2 Pavement design

As opposed to empirical curves (nomographs) used to evaluate stresses and strains for pavement life prediction, actual road conditions can be simulated by means of FEM (Figure 2.5.2). The incorporation of such elements enables the simplification of complex problems experienced with limited linear-elastic software. As mentioned, the stresses and strains can be measured at any point along the structure where FEM provides an extensive series of capabilities, producing more accurate results.

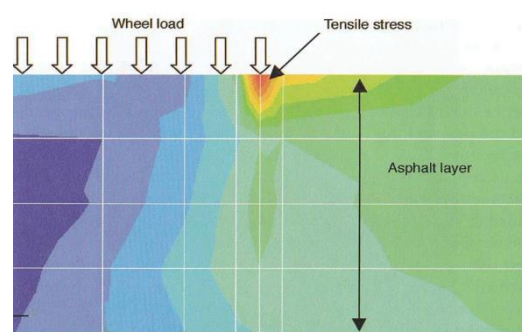


**Figure 2.5.2a:** Near pavement surface stresses induced by tyre loading (Sutanto, 2009)

### 2.5.3 Interlayer bonding

Górszczyk & Malicki, (2012) investigated various factors influencing interlayer bonding by replicating the Leutner shear testing devices (2.3.1.2) by means of FEM using ANSYS software. Comparative monotonic Leutner tests and fatigue tests were also carried out in the research study. Numerical analyses, i.e. finite element method (FEM), were performed for determining the distribution of shear stresses in a specimen. Furthermore, these analyses were performed to evaluate the range of shear stresses required to describe the work of a bonding in a tested specimen.

A geometric model was constructed (replicating the Leutner device) for specimens ranging in diameters with the various material properties (of different materials considered for the tack coat). An illustration of the Leutner testing devices and its FEM replication is provided in Figure 2.5.3a. The

FEM replication is indicated on the right-hand side. The Coulomb friction model was used to describe contact conditions.

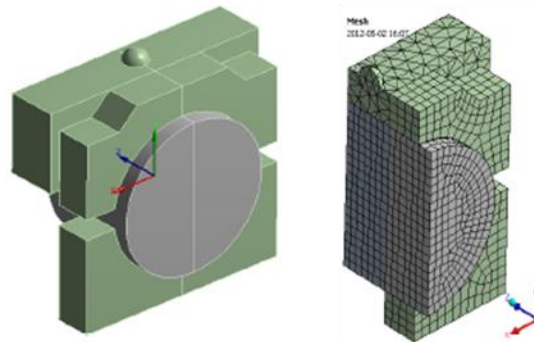


**Figure 2.5.3a:** Near pavement surface stresses induced by tyre loading (Malicki & Górszczyk, 2012)

The problem was solved by means of a non-linear approach. The approach was adhered to due to the change in material stiffness of the whole system as a result of contact between the device and the specimen. The researchers observed partial sliding and separation between the surfaces of the device and the asphalt mixture specimens. Solutions were computed by iterative Newton-Raphson procedure (Malicki & Górszczyk, 2012). The stress distribution is demonstrated in Figure 2.5.3b, showing accumulation of stresses at specimen edge (left) and its continuous distribution in the area of the cutting plane (right).

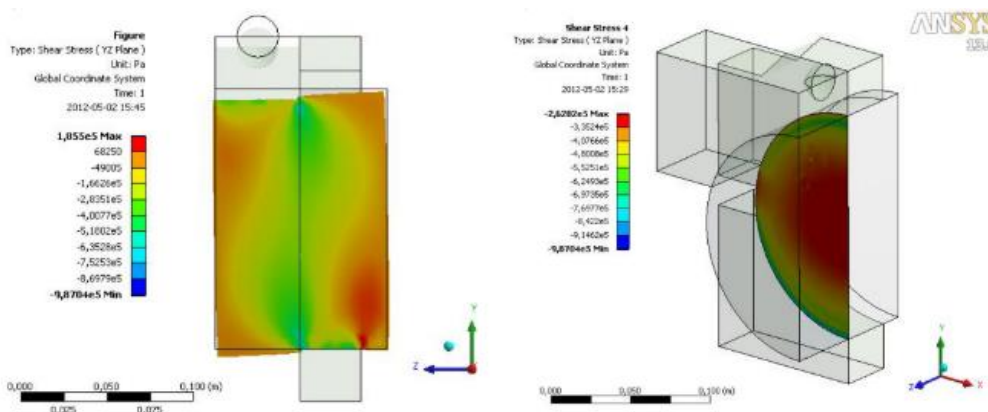


**Figure 2.5.3b:** Shear stress distribution (Malicki & Górszczyk, 2012)

The nature of the results suggests that the boundary conditions of the specimen significantly affect the stress distribution during testing. The observation may be attributed to the specimen's material and the specimen's small diameter. Hence, damage most likely started at the specimen edge at the point of the local stress accumulation (Malicki & Górszczyk, 2012)

Kim et al. (2011) studied the interlayer behaviour of double-layer asphalt specimens taken from a roadway, using the co-axial shear test (CAST) as well as the Layer Parallel Direct Shear (LPDS) test (2.3.1.2). In addition, finite element (FE) simulations were also completed. Abaqus software was used for all the simulations. Three-dimensional continuum elements were used for the FE simulation where symmetry was applied to shorten computation time. Only a quarter size part of the setup was modelled (Figure 2.5.3c). For all of the simulations, a 1kN loading amplitude was applied as a consistent loading condition (Kim et al., 2011).

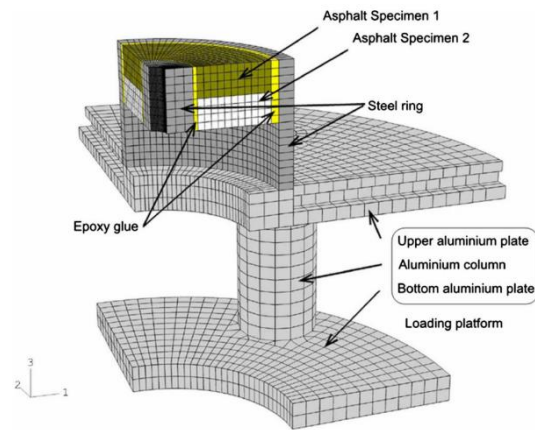


**Figure 2.5.3c:** Schematic geometry of FE models (Kim et al., 2011)

The stress distributions of the specimens for fully bonded (left) and no-bonding (right) interlayer conditions are illustrated in Figure 2.5.3d. For the models with “full” bonding, continuous stress distributions over the depth of the specimen can be observed. Contradictive behaviour is observed for the no-bonding specimens where stress discontinuity occurred (Kim et al., 2011). These specimens (FE models) produced high concentrated tension and compression stresses in comparison with the “full” bond models. Given that bonding and friction properties were not directly incorporated into the simulation, tensile stresses occurred at the bottom of each layer, causing greater deformations and sliding at the interfaces according to Kim et al. (2011). In general, the replication of the testing devices provided favorable results with the exception of the incorporation of components describing the interface properties.

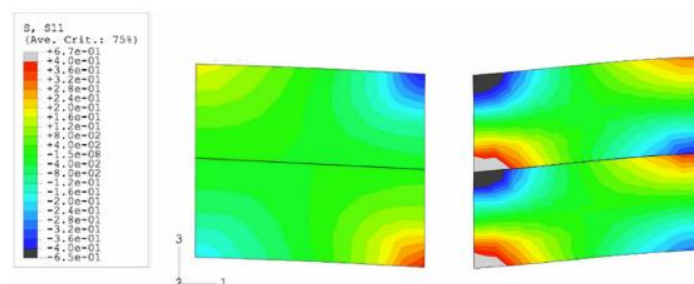


**Figure 2.5.3d:** Schematic geometry of FE models (Kim et al., 2011)

## 2.6 Synthesis of literature review

When pavement layers are not properly bonded, the layers exhibit independence, resulting in alteration of stress distribution profiles. Hence, it is imperative to design pavement structures in which the layers are properly bonded, where all layers act in unison. Chapter 2 introduced the importance of tack coats and identified different types of materials used for this purpose. Crucial components of the material were also investigated in this chapter. Furthermore, Chapter 2 gave recognition to the different test methods used to assess the interlayer bonding (provided by tack coats). In combination with the different testing methods, the dependence of factors of interlayer bonding were also studied. From these discussions the following points were identified:

1. The physical testing conditions (testing device configuration) impact the results obtained.
2. The type of test used for evaluation depends on the required output given the limitation(s) for operating certain devices, i.e. manual versus automatic operation, or sample sizes used for testing.

## *2.6 Synthesis of literature review*

3. Various literature reviewed suggests that the temperature is the factor which has the greatest impact, as it directly influences the other factors investigated, such as tack coat dosage and macrotexture. Furthermore, it greatly contributes to the material response, which determines the material behaviour under certain conditions.

The implication of the bonding component in terms of pavement design was also considered to provide insight to pavement analysis and the different approaches used. The combination of the topics discussed in this chapter allows full understanding of the different mechanisms of tack coat applications that relate to the quality of bonding achieved. It also allows the incorporation of this component in terms of pavement design. The elements provide a good foundation in preliminary research, setting the groundwork for research conducted in the current study.

## CHAPTER 3: PRELIMINARY RESEARCH

### 3.1 Research Overview

The different aspects of shear testing, interlayer bonding (i.e. tack coat) and the different technologies used, were discussed in Chapter 2. The lack of proper interlayer bonding results in significant decrease of pavement durability as a result of change in stress and strain distribution in the pavement structure. Therefore, it is important to understand the properties of the material in terms of its behaviour in the pavement structure, together with interlayer bonding conditions.

A research study was undertaken to investigate Spray Jet technology in terms of interlayer bonding for which Leutner tests and a series of analyses were conducted. In these tests, a significant increase in shear strength results was revealed when compared to conventional technologies. These preliminary tests and analyses form the basis of the current research study. Figure 3.1a shows the experimental framework of the research for each of the phases and the relative outcomes. The experimental plan consists of two phases in which research was conducted, in parallel with Pisa University for the first phase (preliminary). The current research study forms the *Phase 2* component of the experimental plan. The objective of the two-phase approach is to allow for the understanding of the variation in friction resistance and its impact on pavement life.

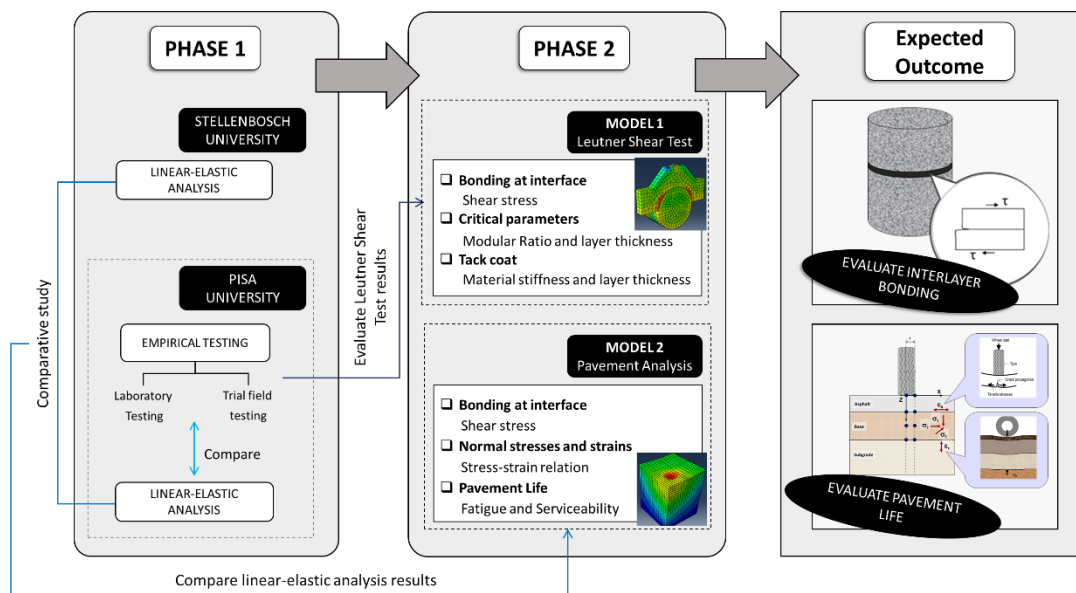


**Figure 3.1a:** Experimental framework for research study

*Phase 1* entails the preliminary analyses performed in parallel with Pisa University, based on Mechanistic Design (discussed in Chapter 2). The *Phase 2* component of the research is composed of an analysis of typical pavements through Finite Element (FE) modelling. This phase of the research includes investigation of the interlayer bonding by means of Spray Jet application through evaluation of mechanistic properties. *Phase 1* was performed to specifically analyse pavement life through a linear-elastic analysis, considering different variables. These variables include support condition, pavement layer thickness, different material properties and shear resistance factors. The first phase will enable the articulation of how these factors, and the magnitude of the shear resistance provided by the Spray Jet, are opposed to other values.

In the first phase emphasis was placed on the importance of tack coat application and its correlation to pavement life (Figure 3.1b). During *Phase 2* the analysis particularly focused on the FEM component and allowed evaluation of different variables influencing shear resistance on a fundamental level.

*Phase 1* research confirmed expected behaviour and showed prominent similarities between the two studies, with minor exceptions in the findings. The respective studies highlighted key components that play an important role in the efficiency of a good bonding condition within a pavement structure. The findings created the opportunity for further investigation by means of finite element method (FEM) analyses (*Phase 2*). Therefore, understanding the extent of how the aspects investigated contribute to the durability of a pavement, are of significant importance.

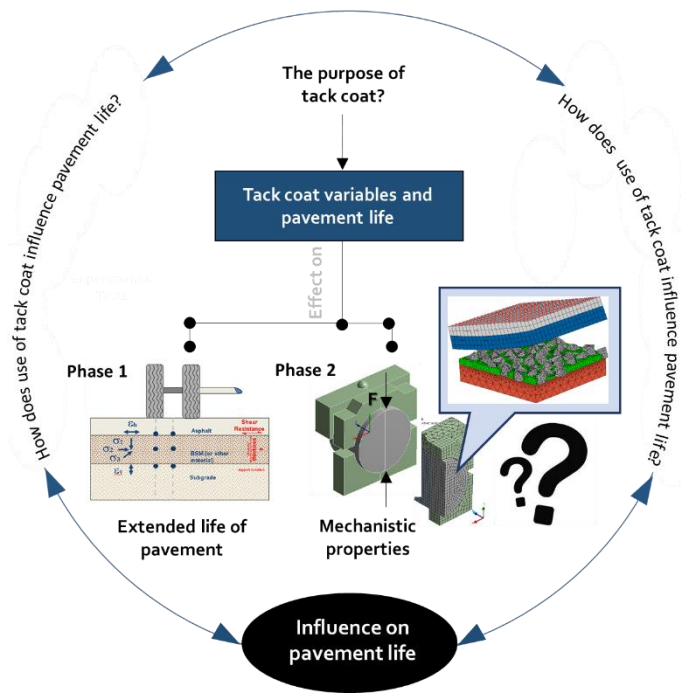


**Figure 3.1b:** Schematic representation of the research study

The different components of the research carried out are divided into two chapters with the relative sections and are structured as demonstrated in Figure 3.1c. The preliminary analyses (*Phase 1*), together with the findings made, will be discussed in Chapter 3. These sections will also provide insight on the preliminary empirical testing performed by Pisa University. The finite element analysis component of the research is introduced and discussed comprehensively in Chapter 4.

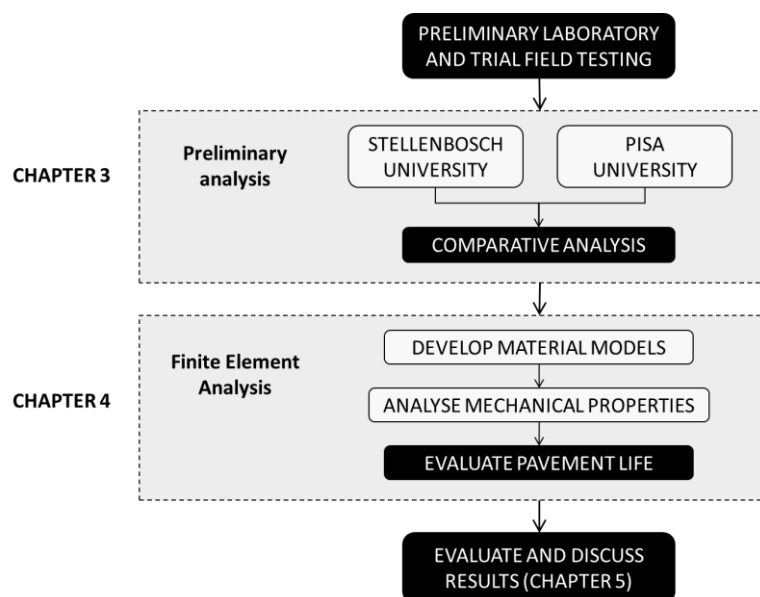


**Figure 3.1c:** Chapter layout

### 3.2 Preliminary Research: Stellenbosch University

#### 3.2.1 Research background

The purpose of Phase 1 is to establish an understanding of friction variation and its influence on pavement life (Figure 3.1b). The objective of this preliminary research was achieved by a set of liner-elastic analyses conducted using BISAR software based on Mechanistic Design. The analyses takes a series of variables into consideration. This includes material properties, different pavement layer thicknesses, as well as shear resistance factors (shear compliance) for the surfacing, base and subgrade layer.

Figure 3.2.1a demonstrates the experimental design of the different variables incorporated into the analysis. This section firstly outlines the methodology in summarising the different testing conditions, which are loading and material properties according to the different variables considered. Subsequently, a summary of the results is provided, and significant observations made are emphasised.

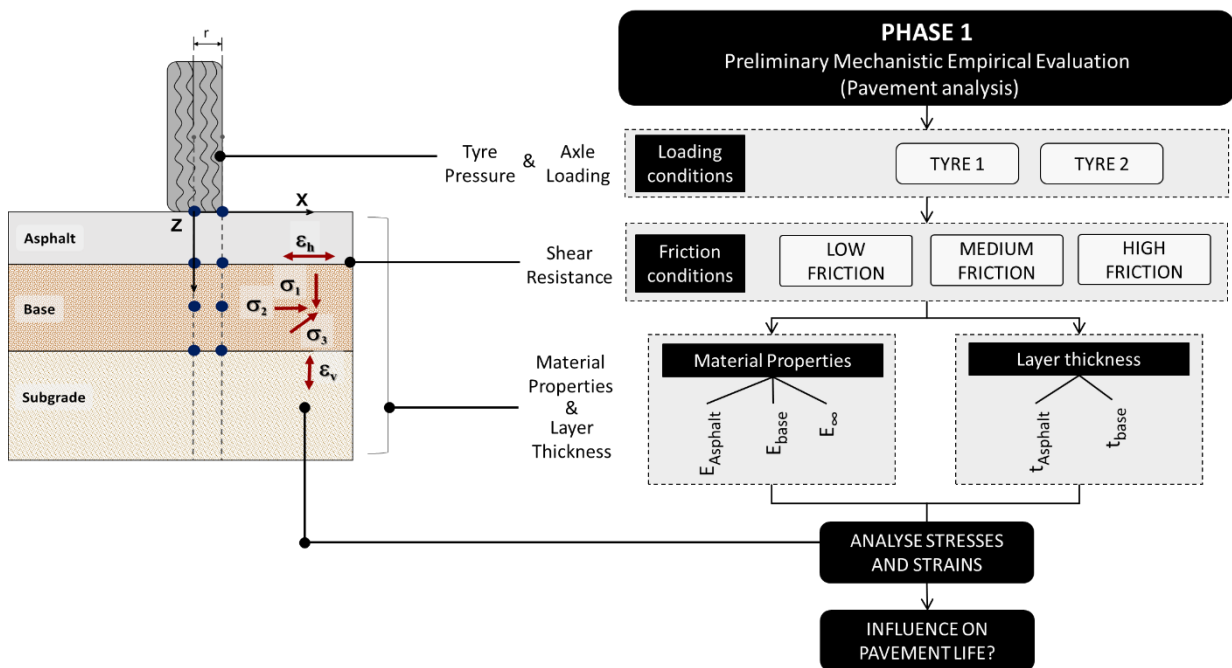


Figure 3.2.1a: Phase 1 Experimental Design

#### 3.2.2 Analysis approach

##### 3.2.2.1 Loading conditions: Axle loading and tyre pressure

In terms of loading, two-axle loading and tyre pressures were considered for the analyses. The loads included in the analyses are summarised in Table 3.2.2.1a. In this section, the two loading conditions in Figure 3.2.1a will be referred to as T1 and T2 respectively.

Table 3.2.2.1a: Axle loading and tyre pressures

Load	Tyre type	Axle load (kN)	Tyre pressure (kPa)	Load radius (m)
T1	Super single	40	750	0.13
T2	Super single	70	900	0.157

It should be noted that the analyses were performed based on a half-axle approach. The two axle loads selected for the analyses were 80 and 140kN. With the half-axle approach, the two loads used would then be 40 and 70kN respectively (as indicated in Table 3.2.2.1a). A different tyre pressure is expected for greater axle loading. Tyre pressure for a standard 80kN axle is recommended to be 750kPa, with the greater axle loading comprising of an increased tyre pressure of 900kPa. The respective load radius is also indicated in the relative table.

The pavement structure shown in Figure 3.2.1a, illustrates the points of analysis. The points are referred to as *Below Wheel* and *Edge* (at load radius distance). This point (*Edge*) has two variations, given two different radii specified for the two different loading conditions *T1* and *T2*. The *Edge* location serves as a comparison for configuration of other wheel types, even though *Below Wheel* is the critical location. The two radii are determined through substituting the combination of the load and tyre pressure, summarised in Table 3.2.2.1a into Equation 3.2.2.1a. By re-arranging the equation, the radius (also referred to as load radius) for *T1* and *T2* loading condition was determined.

$$\sigma = \frac{F}{A} \quad (3.2.2.1a)$$

Where:

- $\sigma$  = Tyre pressure subjected in normal direction (750 or 900kPa)
- $F$  = Axle load (40 or 70kN which are half-axle loads for 80kN and 140kN axles)
- $A$  = Area calculated as  $A = \pi r^2$  with  $r$  equal to the load radius

### 3.2.2.2 Friction condition and shear resistance

Three friction conditions are specified – High, Medium and Low. The incorporation of relative conditions and their interpretation differ, depending on the type of analysis software used to perform the analyses. BISAR does not adhere to the traditional approach of a friction coefficient, where 0 defines full slip (low friction) and 1 describes the interface of two layers subjected to full friction conditions.

In BISAR, the ability to account for full or partial slip is incorporated by means of a shear spring compliance. This should not be confused with the application of a friction coefficient. The incorporation of the shear spring compliance can be attributed to the mathematics behind the BISAR model, which assumes continuous relations for all parameters. The application of the well-known friction coefficient would require a mathematical model that is able to cope with discontinuities (step functions) (Shell, 1998).

The shear spring compliance approach involves representing the interface between two horizontal pavement layers as an infinitely thin layer of which the strength is described by means of a spring compliance. This approach assumes that shear stresses at the interface cause a relative horizontal displacement of the 2 layers proportional to the stresses acting on the interface (Shell, 1998), as illustrated by Equation 3.2.2.2a (definition of the standard shear spring compliance). The standard shear spring compliance ( $AK$ ) is measured in  $m^3/N$ . A mathematical relation is also developed with the equation for the friction parameter (not equal to friction coefficient) defined in Equation 3.2.2.2b. The reduced shear spring compliance,  $ALK$  (measured in  $m$ ) is defined by Equation 3.2.2.2c.

$$AK = \frac{\text{relative horizontal displacement of layers}}{\text{stresses acting at the interface}} \quad (3.2.2.2a)$$

## 3.2 Preliminary Research: Stellenbosch University

$$\alpha = \frac{AK}{AK + \frac{1+\nu}{E}a} \quad (3.2.2.2b)$$

Where:

- $\alpha$  = Friction parameter with  $0 \leq \alpha \leq 1$  where  $\alpha = 0$  means full friction and
- AK = Shear spring compliance ( $m^3/N$ )
- E = Modulus of layer above interface (Pa)
- $\nu$  = Poisson's ratio of specific layer
- a = Radius of the load (m) [equivalent to r parameter used in Equation 3.2.2.1a]

$$ALK = \frac{\alpha}{1 - \alpha}a \quad (3.2.2.2c)$$

Where:

- ALK = Reduced shear spring compliance (m)

Either values of Equation 3.2.2.2a or c can be used as input values for the BISAR program. The value of  $\alpha$ , also known as interface friction, is used in all computations. The  $\alpha$  parameter is derived from the input provided, that is the input of AK or ALK in the software for analysis (Shell, 1998). The purpose of the interface friction ( $\alpha$ ) is fundamental to this analysis as it does not function as a material property, but is dependent on the diameter of the applied load. For the two defined loading conditions T1 and T2, two different diameters are used given the two different radii estimated per Equation 3.2.2.1a. This would result in two different values for  $\alpha$  which need to be applied for one ALK or AK value as physical characteristic for a specific layer interface. Based on the definition of  $\alpha$ , it is incorrect to express a percentage of slip as a proportion of the spring compliance for full slip. Shell (1998) recommends a numerical variation in ALK from 0 to 100 times the radius of the loaded area, which covers the range from full friction to (practically) full slip (equivalent of  $\alpha = 0.99$ ).

For interpretation of the results, the different friction conditions will be referred to as HF or full bond (High Friction), MF or partial slip (Medium Friction) and LF or full slip (Low Friction) respectively. The terms will be used interchangeably to describe the bond strength between the different pavement layers. The various inputs for the shear compliance used (Table 3.2.2.2a) is determined in accordance with the estimations discussed in this section as represented by Equations 3.2.2.2a to c.

**Table 3.2.2.2a:** Friction conditions

Load	Shear spring compliance (m)		
	LF	MF	HF
T1	13	6.51	NA
T2	15.7	7.87	NA

**Note:** HF = High Friction (full bond), MF = Medium Friction (partial slip) and LF = Low Friction (full slip)

The estimated shear spring compliance summarised in Table 3.2.2.2a is acquired according to the recommendation of the ALK value by Shell (1998). The authors recommend a value between 0 and 100 times the load area for specifically the MF and LF friction conditions. The three different friction conditions are illustrated in Figure 3.2.2.2a according to decrease in friction. Figure 3.2.2.2a shows the proportion of the shear spring compliance applied. It is applied at both interlayers (interface): *Interface 1* is

between the asphalt and base layer and *Interface 2* is between the base and the subgrade layer. For certain circumstances, the subgrade will also be referred to as the supporting condition.

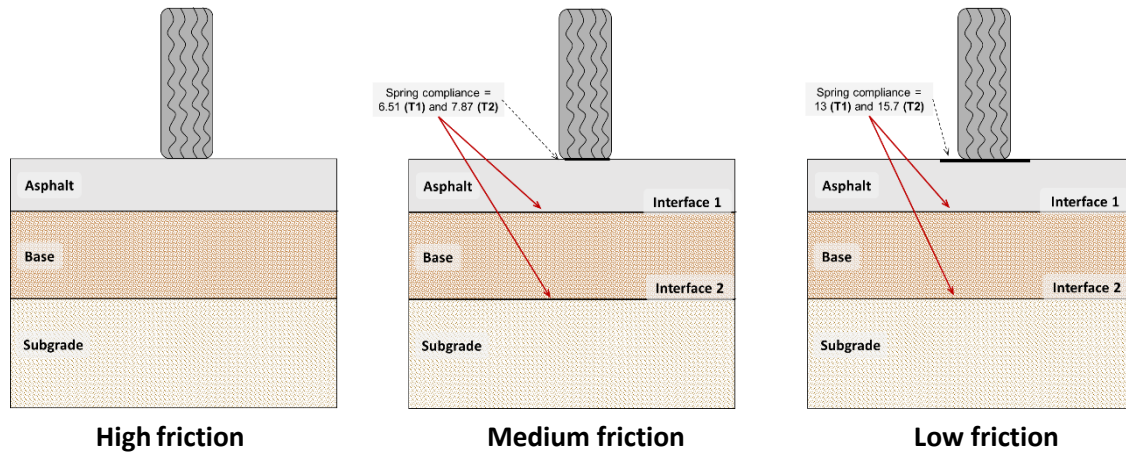


**Figure 3.2.2.2a:** Three frictions defined for linear-elastic analysis

**High Friction**

High Friction (*HF*) defines the “full bond” between the pavement layers, or an instance of full friction. For this specific condition, the friction condition is defined as “Full friction” in specific software program. MF and LF specifications should be considered carefully based on the approach followed by relative analysis software.

**Medium Friction**

Medium Friction (MF) or partial slip was defined as 50% of the load radius defined for *T1* and *T2* in Table 3.2.2.1a. Thus, the shear compliance for the MF is determined as 50 multiplied with the radius of *T1* and *T2* and obtained as 6.51m and 7.87m for *T1* and *T2* accordingly.

**Low Friction**

In terms of a friction coefficient, in BISAR, Low friction (LF) (or full slip) is represented by a value of 1. Therefore, the shear compliance for this friction condition is determined as 100% of the load radius specified in Table 3.2.2.1a. The shear compliance for this friction condition was determined as 100 multiplied with the radius of *T1* and *T2* loading conditions and obtained as 13m and 15.7m accordingly.

**3.2.2.3 Pavement structure considerations**

The experimental design for the analysis is illustrated in Figure 3.2.1a for two-wheel loads for which a range of material properties ( $E_{Asphalt}$ ,  $E_{base}$  and  $E_{\infty}$ ) and layer thickness ( $t_{Asphalt}$ ,  $t_{base}$ ) were specified as indicated in Table 3.2.2.3a. In turn, for each of the loading conditions, three friction conditions were specified i.e. High Friction (*HF*), Medium Friction (*MF*) and Low Friction (*LF*). The nature of the loading and friction conditions was described in 3.2.2.1 and 3.2.2.2 respectively.

**Table 3.2.2.3a:** Material properties and pavement layer thickness

Pavement structures	Asphalt		Base		Subgrade
	$E_{Asphalt}$ (MPa)	$t_{Asphalt}$ (mm)	$E_{base}$ (MPa)	$t_{base}$ (mm)	$E_{\infty}$ (MPa)
Case 1	2500	50	400	200	150
Case 2	2500	50	1500	200	150
Case 3	2500	100	400	200	150
Case 4	2500	100	1500	200	150

3.2 Preliminary Research: Stellenbosch University

Four analyses were performed on a half-axis (with super single wheel) approach which consists of measurements at two points at various locations along the depth of the pavement layers. Each of the components mentioned is categorised as *Case 1*, *Case 2*, *Case 3* and *Case 4*. The four combinations selected are interrelated as shown in Figure 3.2.2.3a with the components subsequently illustrated in Table 3.2.2.3b. The pavement structures is not an entirely representative of a typical South African pavement, although it still allows for comparative studies in collaboration with Pisa University.

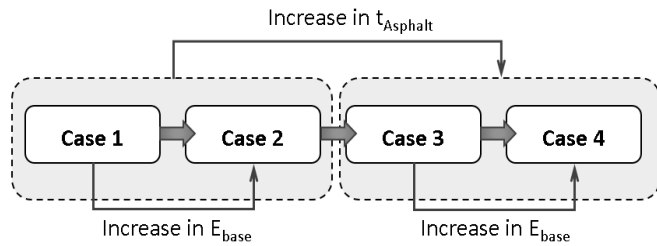


Figure 3.2.2.3a: Case combinations

Table 3.2.2.3b: Pavement structure considerations

Case 1	Case 2
$E_{base} = 400\text{MPa}$ with $t_{Asphalt} = 50\text{mm}$	$E_{base} = 1500\text{MPa}$ with $t_{Asphalt} = 50\text{mm}$
Case 3	Case 4
$E_{base} = 400\text{MPa}$ with $t_{Asphalt} = 100\text{mm}$	$E_{base} = 1500\text{MPa}$ with $t_{Asphalt} = 100\text{mm}$

### 3.2.3 Results and findings

The results obtained from the analyses performed will be discussed, with regards to different criteria, according to each of the combinations specified (*Case 1 to 4*). The criteria considered include the following aspects:

1. Normal Stress, Strain and Principal Normal Stresses;
2. Principal Shear Stresses and Strain;
3. Displacements;
4. Energy measured – Strain Energy and Dissipation Energy.

To achieve the objective of the analysis, it is evident that the first two mentioned criteria (normal and shear stresses and strains) are fundamental to the research. Investigating these criteria will lead to understanding the bond strength and the consequent evaluation of pavement life. The discussion of results occurs in a comparative nature to evaluate the effect of different testing conditions on results, together with the evaluation of pavement life in alignment with the structure demonstrated in Figure 3.2.3a.

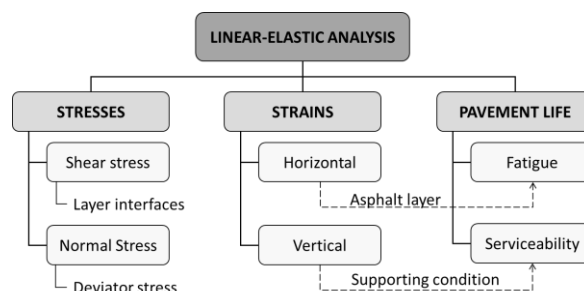


**Figure 3.2.3a:** Structure of result discussion

Within the linear-elastic analysis, it is possible to obtain a variety of a results, such as the criteria mentioned previously. Results are acquired in terms of stresses and strains for the variety of testing conditions described in Section 3.2.2. The conditions include three bonding conditions. The extent of the influence of the bonding can be highlighted by inspecting all results for both research studies, from *HF* and *LF* conditions expressed as a ratio as shown in Equation 3.2.3a. This variable is only used as an indicator only to show the change in specific parameter with the change in the bonding condition.

$$\Delta [\%] = \frac{x_{HF} - x_{LF}}{x_{HF}} \quad (3.2.3a)$$

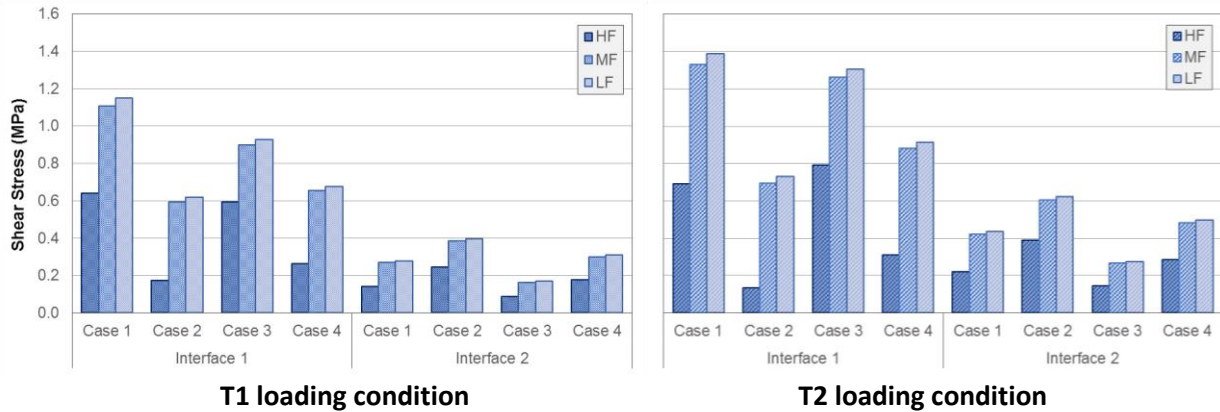
Where:

- $x_{HF}$  = Parameter calculated within high friction (HF) conditions
- $x_{LF}$  = Parameter calculated within low friction (LF) conditions

### 3.2.4 Shear stresses

Shear stress ( $\tau$ ) is the parameter which describes the bond strength between pavement layers and is the value dependent on the different defined friction conditions. Therefore, the shear stresses measured at the different interfaces are emphasised in this discussion. The shear stresses (or principal stresses) measured at the interfaces at each defined depth (*Interface 1* and *Interface 2*) comprise of those measured *Below Wheel* and *Edge* positions respectively (Figure 3.2.4a). Each of these sets of results consists of conditions illustrated according to the two defined loading conditions (*T1* and *T2*) relative to each friction condition for *Case 1 to 4*. The software used for the analyses allowed for analyses at points above and below the depth relative to the interlayer. The results for only the *Below Wheel* location are shown in Figure 3.2.4a. It is the most critical location, hence being the most conservative approach. The results for *Edge* position is shown in Figure A1 in Appendix A. Similar trends were observed for these results but significant lower shear stresses were achieved.

3.2 Preliminary Research: Stellenbosch University



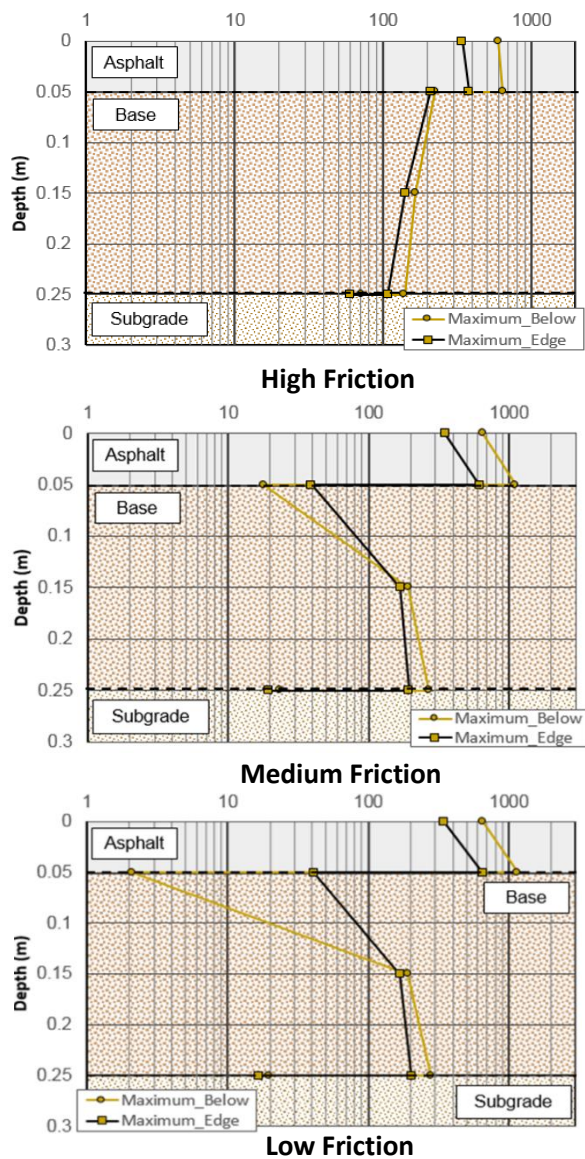
**Note:** Interface 1 = Asphalt/Base, Interface 2 = Base/Subgrade. Case 1 and 2: Interface 1 at 0.05m, Interface 2 at 0.25m. Case 3 and 4: Interface 1 at 0.1m, Interface 2 at 0.3m

**Figure 3.2.4a:** Shear stress results measured Below Wheel

The shear stresses are evaluated at the interface, but provision is also made for considering points just above and below the particular interface as shown in Figure 3.2.4b. The figure shows the results obtained for *Case 1 T1* loading condition. The three graphs in this figure illustrate the three defined friction conditions. The change in shear stress for the three friction conditions provides a good indication of the shear stress distribution in the pavement structure, especially at the two interfaces. It also describes the development of shear within the respective layers in turning, representing the quality of bonding that exists.

From the graphs provided in this figure, together with the material properties defined, maximum shear stresses can be expected at *Interface 1*. The phenomenon is attributed to the combination of the stiff asphalt layer with a material stiffness ( $E_{\text{Asphalt}}$ ) of 25 00MPa with the base layer at this particular depth compared to the base layer and the subgrade layer (at *Interface 2*).

In terms of the defined base layer stiffness ( $E_{\text{base}}$ ), the combinations with a stiffer base layer (1 500 MPa as opposed to 4 00MPa) i.e. *Case 2* and *4*, yield smaller shear stresses as those obtained for *Case 1* and *3*. In addition to the stiffness, these results also suggest an increase in the shear stress with the decrease in the friction present between the pavement layers. The pavement layers are subjected to a greater shear stress with the



**Note:** Shear stress indicated in kPa on the horizontal axis

**Figure 3.2.4b:** Shear stress development for Case1 T1 loading condition

3.2 Preliminary Research: Stellenbosch University

increase in tyre pressure (from  $T1$  to  $T2$  loading condition). This behaviour becomes prominent when studying Figure 3.2.4a from left to right.

The shear stresses are summarised in Tables 3.2.4a to 3.2.4d according to the four different analyses at the defined locations demonstrated per Figure 3.2.4c. These tables summarise shear stresses for the *Below Wheel* location as it is regarded as the more dominant for this analysis. The shear stresses measured at the *Edge* location is summarised in Tables A1 to A4 in Appendix A1. Moreover, subsequent sections will also only study results acquired at this location. In relation to Figures 3.2.4a, *Interface 1* is between points 3/4 and 5/6 and *Interface 2* is between points 9/10 and 11/12.

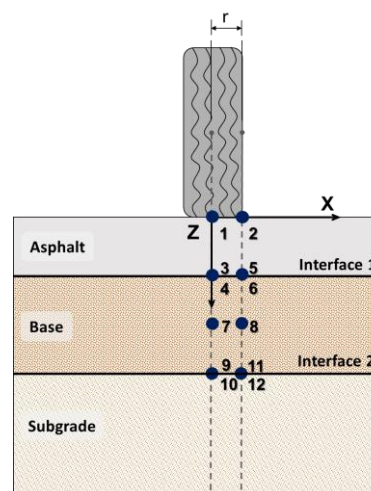


Figure 3.2.4c: Analysis location points

Compiling the shear stresses along the depth of the pavement structure will provide an overview of stress distribution. Subsequently, this will allow the inspection of influence of the different variables on the results obtained from the analysis such as the loading condition, base layer stiffness ( $E_{base}$ ) and asphalt layer thickness ( $t_{Asphalt}$ ).

Table 3.2.4a: Shear stresses at Below Wheel location for Case 1 (kPa)

Point	Depth (m)	T1 loading			T2 loading		
		HF	MF	LF	HF	MF	LF
1/2	0	600.4	656	652.2	756.5	786.2	777.3
3/4	0.05	639.2	1108	1150	690.9	1329	1387
5/6	0.05	224	17.9	0.38	267.7	1	23.9
7/8	0.15	164.9	191.3	192.2	236.5	266.4	267.1
9/11	0.25	139.8	269.1	278.6	220.4	422	435.3
10/12	0.25	72.09	23.19	20.18	114.3	35.51	31.2

Note:  $T1$  loading = 750kPa tyre pressure with 40kN half-axle load,  $T2$  loading = 900kPa tyre pressure with 70kN half-axle load, HF = high friction, MF = medium friction and LF = low friction

Table 3.2.4b: Shear stresses at Below Wheel location for Case 2 (kPa)

Point	Depth (m)	T1 loading			T2 loading		
		HF	MF	LF	HF	MF	LF
1/2	0	203.6	75.4	64.6	320.7	91	73.83
3/4	0.05	175.5	595.4	620.8	133.6	693.2	729.5
5/6	0.05	168.6	114.9	130.6	157.6	223.7	245.5
7/8	0.15	181.9	199.9	200.1	252	256.2	256.3
9/11	0.25	245.5	384.3	396.3	389	603.7	621.7
10/12	0.25	41.5	21.7	17.45	66.5	33	26.7

**Table 3.2.4c:** Shear stresses at Below Wheel location for Case 3 (kPa)

Point	Depth (m)	T1 loading			T2 loading		
		HF	MF	LF	HF	MF	LF
1/2	0	398.8	523.3	531.6	600.9	789.7	800.6
3/4	0.1	594.2	898.2	928.7	790.7	1262	1306
5/6	0.1	163	14.01	0.44	223.5	8.6	10.4
7/8	0.2	100.8	105.8	105.2	156.6	160.8	159.6
9/11	0.3	89.1	163.7	169.8	145.8	267.5	276.2
10/12	0.3	45.8	15.87	13.72	75.29	24.98	21.81

**Table 3.2.4d:** Shear stresses at Below Wheel location for Case 4 (kPa)

Point	Depth (m)	T1 loading			T2 loading		
		HF	MF	LF	HF	MF	LF
1/2	0	137.3	203.6	204.8	235.5	315.4	316.3
3/4	0.1	263.4	653.8	677.2	312.2	879.9	914
5/6	0.1	203.4	92.3	108.8	247.4	176.2	199.7
7/8	0.2	138.5	139.7	138.9	208.9	197.5	196.2
9/11	0.3	176	297.8	308.5	286.5	482.5	498.7
10/12	0.3	29.42	18.1	14.7	48.3	28.2	22.9

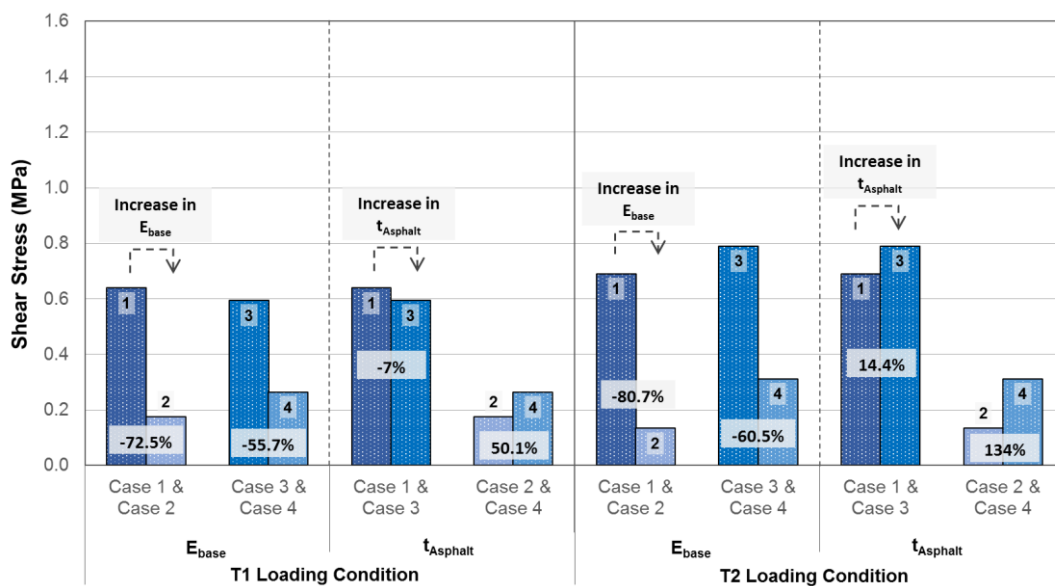
These results are also expressed by means of Equation 3.2.3a representing the ratio of change in full and no (poor) bonding condition. Shear stress results obtained for every combination were substituted into the equation to evaluate the influence of the bonding condition on the pavement structure. The estimated  $\Delta[\%]$  values are summarised in Tables A5 to A8 in Appendix A1. The  $\Delta[\%]$  parameter is not of main concern of the research, but confirmed the following behaviours observations when considering Tables 3.2.4a to 3.2.4d:

1. The no (poor) bonding condition i.e. *LF*, yields greater shear stresses than for the full bonding i.e. *HF* condition i.e. decrease in shear stress with increase in friction (from *LF* to the *HF* condition)
2. Significant variation in shear stresses are observed in the transition from the interface layer to subsequent pavement layers. The behaviour is expected as subsequent layers are composed of lower stiffness moduli values.
3. Maximum shear stresses are observed at the interlayers where friction is present
4. Pavements with asphalt layer thickness of 100mm (*Case 3* and *4*), shows significant decrease in change in shear stresses occurring at the bottom of the asphalt layer at points 3 and 5 in Figure 3.2.4c
5. Points 4 to 11 in Figure 3.2.4c represent points within the pavement structure where analyses were performed within the base layer:
  - a. *Case 1* and *2*: decrease in shear stress occurs with increase in  $E_{\text{base}}$  at top of the base layer at points 4 and 6. Subsequently, the shear stress increase with the depth of the pavement.
  - b. *Case 3* and *4*: decrease in shear stress occurs with increase in  $E_{\text{base}}$ . Comparing the results in terms of pavement depth, it is possible to observe that this behaviour occurs at a depth greater and equal to 100mm where the shear stress distribution is changing

3.2 Preliminary Research: Stellenbosch University

For this analysis, four pavement structures were analysed which can be divided into two sets of subgroups as illustrated in Figure 3.2.2.3a based on  $E_{base}$  and  $t_{Asphalt}$ . For the first-mentioned, the subgroup consists of *Case 1/3* combination with  $E_{base}$  of 400MPa and the *Case 2/4* with  $E_{base}$  of 1500MPa which is seemingly stiffer. The other subgroup consists *Case 1/2* combination with  $t_{Asphalt}$  of 50mm and *Case 3/4* combination consisting of a thicker asphalt layer with  $t_{Asphalt}$  of 100mm which is double the layer thickness for *Case 1/2* combination.

The results show that the interface conditions, represented by the three different friction conditions together with variables such as loading,  $E_{base}$  and contribute to the stress and strain generation in the pavement structures. A comparative is provided for the  $t_{Asphalt}$ ,  $E_{base}$  and loading in Figures 3.24d to 3.2.4f for all of the bonding conditions measured at the dominant location. Results are compiled according to the two defined loading conditions, *T1* and *T2* at *Interface 1*. In some instances, similar behaviours was observed with the exception of the full bonding condition (*HF*).



Note: Case 1, Case 2, Case 3 and Case 4 conditions as illustrated per Table 3.2.2.3b

Figure 3.2.4d: Comparative analysis of testing parameters for HF condition

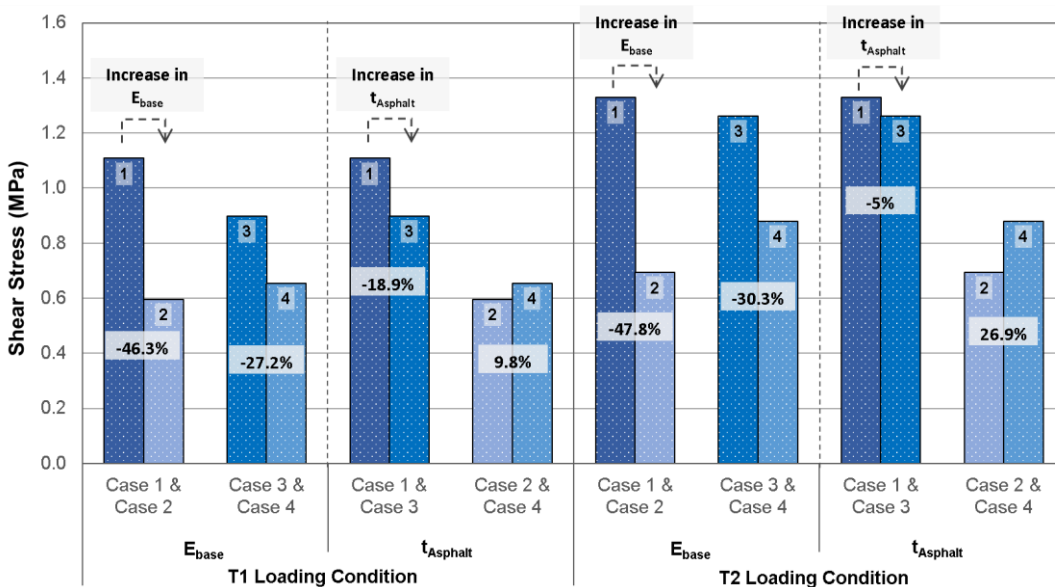


Figure 3.2.4e: Comparative analysis of testing parameters for MF condition

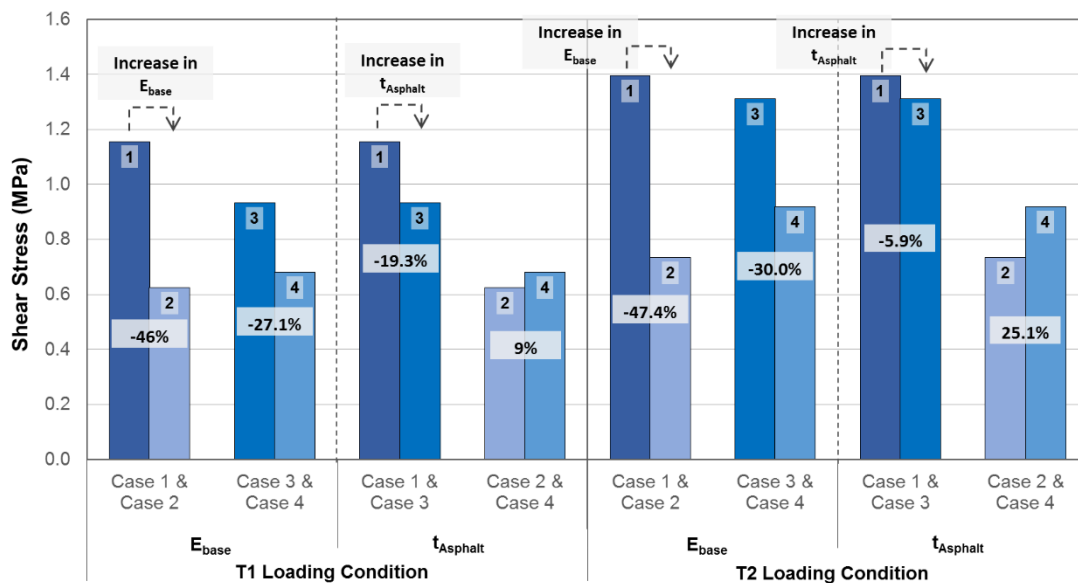


Figure 3.2.4f: Comparative analysis of testing parameters for LF condition

In relation to summarised results in Tables 3.2.4a to 3.2.4d, it is apparent that the shear stresses increase with the weakening in the bonding condition. This type of behaviour is expected as a weaker bonding condition will result in increased stress generation at the interlayer. Maximum shear stresses of 0.79MPa, 1.3MPa and 1.4MPa was obtained for HF, MF and LF conditions respectively.

The results suggest that the interface conditions represented by *HF*, *MF* and *LF* conditions, together with the variable such as loading and material stiffness, contribute to stress generation in the pavement structures. Figures 3.2.4d to 3.2.4f show a slightly higher change in subgroup results in comparing *HF* condition results to the other two bonding conditions. Figures 3.2.4e and 3.2.4f show similar trends in terms of change in subgroup results varying only up to 2% between the two bonding conditions. However, when comparing these sets of results with Figure 3.2.4d, it comprises of a 107% variation in the results. Additionally, opposite trend in results for Case 1/3 combination for  $t_{Asphalt}$  results for *T2* loading condition.

Using Figure 3.2.4 d as a reference, the following behaviours can be observed to indicate the impact the variables have on the results obtained from the analysis:

1. Change in base layer stiffness,  $E_{base}$ :
  - a. The different cases can lead to a 72.5% ( $t_{Asphalt} = 50$  mm) and 55.7% ( $t_{Asphalt} = 100$  mm) decrease in bonding with the increase in  $E_{base}$  for the *T1* loading condition. Similar for the *T2* loading condition, a decrease of 80.7% ( $t_{Asphalt} = 50$  mm) and 60.5% ( $t_{Asphalt} = 100$  mm) decrease in bonding with the increase in  $E_{base}$ .
2. Change in asphalt layer thickness,  $t_{Asphalt}$ :
  - a. For the *T1* loading condition, a decrease of 7% ( $E_{base} = 400$  MPa) and increase of 50.1% ( $E_{base} = 1500$  MPa) is observed in terms of the bonding results for the change in  $t_{Asphalt}$ .
  - b. For the *T2* loading condition, an increase of 14.4% up to a significant value of 134% is noticeable for the two different defined stiffness.

According to Figures 3.2.4d to 3.2.4f, the magnitude of change in results decreases with the increase in asphalt layer thickness suggesting that the change of thickness has less of an impact compared to the base layer stiffness.

### 3.2.5 Stresses in layers

#### 3.2.5.1 Introduction

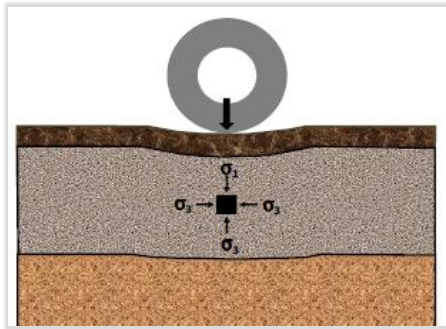


**Figure 3.2.5.1a:** Critical location and parameter for granular layers (Jenkins & Rudman, 2018)

Due to repetitive wheel motion on a road, granular materials undergo deformation due to densification and gradual shear (Theyse et al., 1996). The concept of a safety factor was introduced by Theyse et al. (1996) which incorporates shear failure by looking at principal stresses in the middle of the layer (Figure 3.2.5.1a). This is a disadvantage as the highest shear does not necessarily occur at this location (Jenkins & Rudman, 2018a). This statement has been proved by shear stress results measured at various depths of pavement structures analysed.

The safety factor was developed based on Mohr-Coulomb theory for static loading represented by material strength as a ratio of the applied stress during shear. Last-mentioned is known as deviator stress. It is determined as the difference between the major principal stress ( $\sigma_1$ ) and minor principal stress ( $\sigma_3$ ) applied stresses in x and z directions according to convention used in axi-symmetric analyses as indicated in Figure 3.2.5.1b. The two stresses used for estimations ( $\sigma_1$  and  $\sigma_3$ ) are also referred to as normal stresses.

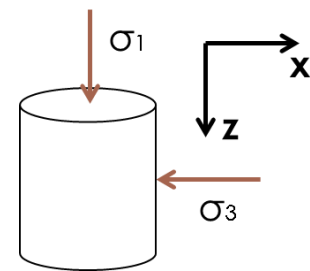


**Figure 3.2.5.1b:** Deviator stress

#### 3.2.5.2 Normal stresses

The maximum normal stresses ( $\sigma$ ) were obtained from the analyses for all of the different combinations considered. Similar trends were noticed when studying the results relative to the respective pavement layers. An example of the normal stress distribution is given for *Case 1 T1* for all three friction conditions in Figure 3.2.5.2a. Figure 3.2.5.2a illustrates the normal stresses relative to a weakening in interlayer bonding i.e. from High Friction (HF) to Low Friction (LF) condition.

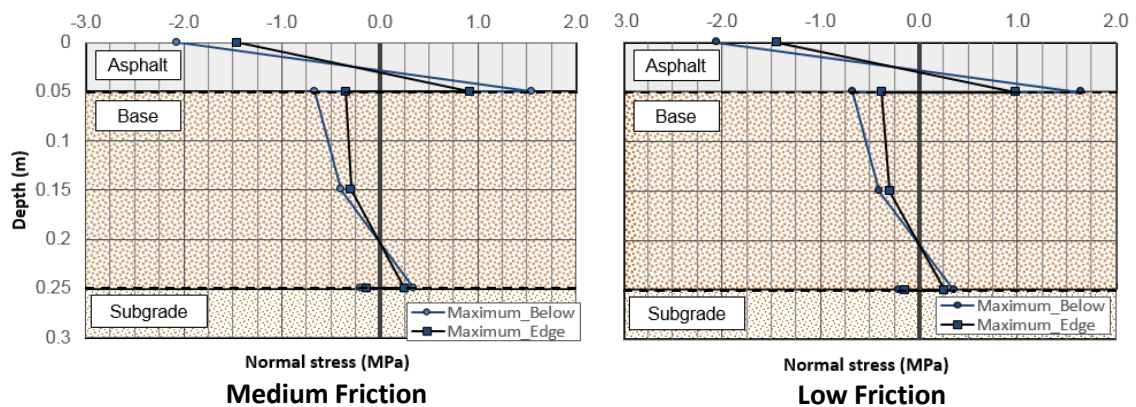


**Figure 3.2.5.2a:** Normal stress development for Case 1 Tyre 1 (MPa)

Using Figure 3.2.5.2a as a reference, the following aspects are observed:

1. The figures illustrate the characteristic influence of material stiffness when studying the normal stresses measured with the depth of the pavement structure. The surfacing has the highest material stiffness of 2500MPa compared to the 400 or 1500MPa base layer followed by the subgrade composed of a material stiffness of only 150MPa.
2. In the surfacing, a sporadic change occurs in normal stress from a compressive to tensile nature at *Interface 1* between surfacing and base layer. Subsequently, normal stresses change from tensile to compressive stresses and slightly increases before change to tensile stresses at *Interface 2*. This is the interface between the base layer and the subgrade. Compressive stresses are experience in the subgrade.
3. The decrease in friction describes an instance where less adhesion exist between the pavement layers causing an increase in stresses and strains distributed to the lower pavement layers. The more critical loading condition, *T2*, comprising of a higher axle load and tyre pressure, shows similar behaviour with the exception of the increase in normal stresses.

The normal stresses obtained are used for estimation of deviator stress ( $\sigma_1 - \sigma_3$ ) in the middle of the base layer. These points are represented by points 7 and 8 in Figure 3.2.4c. As been stated, results for the dominant location will be of concern for this research. The deviator stresses are studied subsequently in 3.2.5.3.

### 3.2.5.3 Deviator stresses

The formulation of the deviator stress is illustrated in Figure 3.2.5.1a, based on stresses measured in the two respective directions. This was completed in accordance to convention adhered to in the analysis software.

The vertical stresses are obtained in the z-direction, whereas horizontal stresses are measured in both the x and y directions as shown in Figure 3.2.5.3a. For the estimation of the deviator stress, the maximum stress obtained between the x and y-direction served as the horizontal stress component ( $\sigma_2$  and  $\sigma_3$ ). It should be noted that for the analyses performed, z was positive in a downward direction as shown on the axis on the right-hand side of Figure 3.2.5.3a.

The deviator stress ratio is a component which describes or represents the distortion of a body, implying that an increase in this parameter should be deemed critical for a pavement. Therefore, increase in deviator stress can cause failure of the specific (granular) layer which could ultimately lead to the failure of the entire pavement structure.

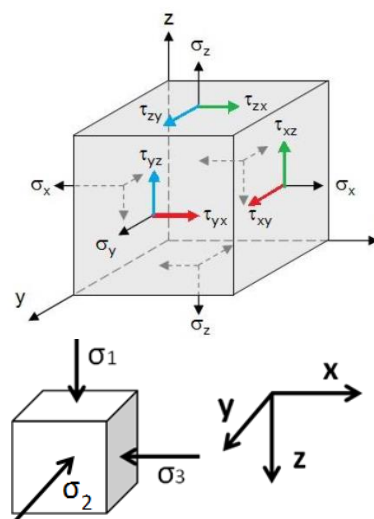


**Figure 3.2.5.3a:** Stress block indicating stress directions

The estimated deviator stresses are shown in Figure 3.2.5.3b for all specified analysis conditions including three types of bonding conditions and two loading conditions, *T1* and *T2*. The deviator stress values determined at the *Edge* location is summarised in Tables A9 to A11 in Appendix A2 according to the *HF*, *MF* and *LF* conditions. In addition, an illustration of these deviator stresses are given in Figure A2 in Appendix A2. The role of interlayer bonding was also investigated with Equation 3.2.3a. These

results are summarised in Tables A12 and A13 respectively in Appendix A2. The study of results in Figure 3.2.5.3b concludes the following:

1. The well-known phenomenon of greater load – greater stresses/ strains – is illustrated in the results given that the component is dependent on stresses generated within the pavement structure.
2. Increase in deviator stress (in magnitude) with the decrease in friction with the exception of *Case 3* and *4* for the *T2* loading condition where contradictory behaviours are observed.
3. Deviator stress observations made with respect to loading and friction conditions as well as other testing conditions coincide with the previous observations made in these capacities:
  - a. In terms of magnitude, ignoring the sign convention, all deviator stresses increase with increase in  $E_{base}$  with the exception of *Case 3* and *4* for both *MF* and *LF* conditions for *T2* loading condition
  - b. In the example of *Case 3* and *4*, results are justified by a combination of increase in  $t_{Asphalt}$  where this layer is composed of a stiffness 2 to 6 times the magnitude of  $E_{base}$ .
4. Based on the defined properties for *Case 4*, it is categorised as the “strongest” pavement structure of the four analysed. It shows a decrease in deviator stress (magnitude) with the increased loading condition. This type of behaviour implies that the pavement can withstand increased loads where smaller loads results in an increase in deviator stress.

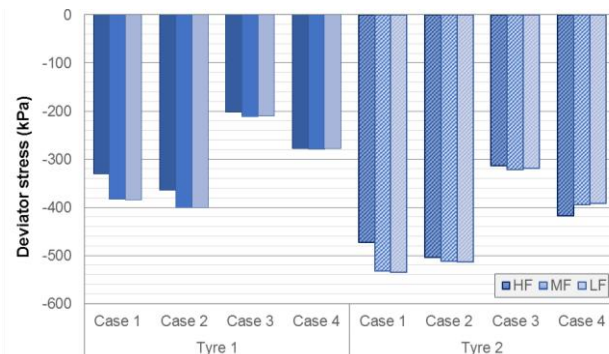


**Figure 3.2.5.3b:** Deviator stresses for Below Wheel (kPa)

### 3.2.6 Strains

#### 3.2.6.1 Introduction

The strains measured at critical locations within the pavement structure are fundamental in evaluating its pavement life. The fatigue and serviceability life are deemed crucial given the scope of the research. These two models are representative of failure evaluation within the asphalt and subgrade layer respectively. The strains measured in these layers include horizontal strains measured at the bottom of the asphalt layer (fatigue) and vertical strains at the top of the subgrade layer (serviceability). Observable differences in behaviour will be discussed in the relevant subsequent section.

#### 3.2.6.2 Horizontal strains

Asphalt layers bend under load application (similar to beam behaviour) which induce cracks at the bottom of the layer, which propagate up to the surface of the pavement (Jenkins & Rudman, 2018a). In typical behaviour, the upper part of the layer will undergo compression, whereas tensile strains will occur at the bottom of the asphalt layer (point A in Figure 3.2.6.2a). Hence, horizontal (tensile) strains at the bottom of the asphalt

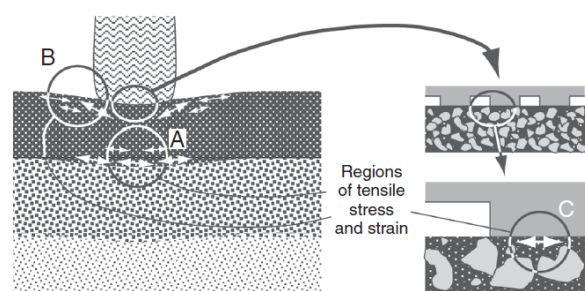
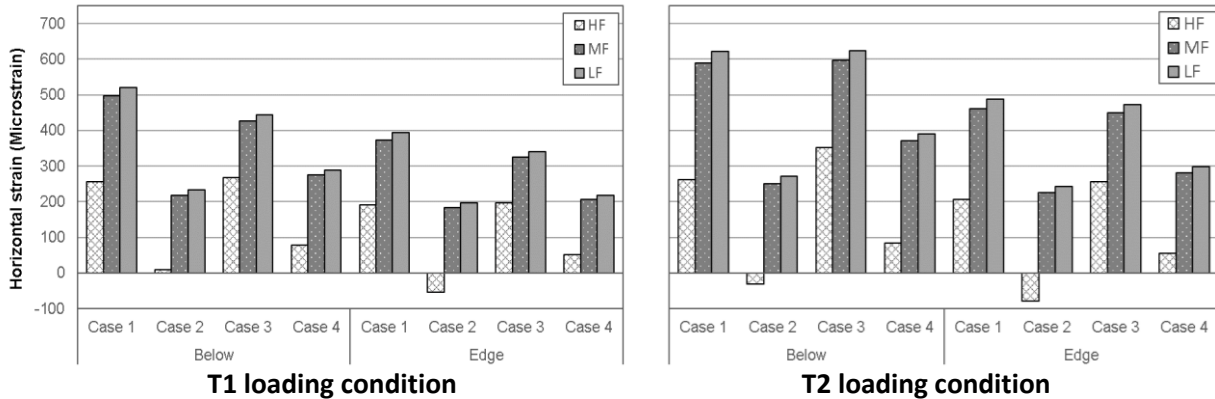


**Figure 3.2.6.2a:** Strain for asphalt layer (Thom, 2014)

layer are of interest, as they represent the resistance to crack formation. These horizontal strains are of relative importance for the research given its influence on pavement life estimation. The strains obtained for all the different combinations analysed are illustrated in Figure 3.2.6.2b for *T1* loading condition (left) and *T2* loading condition (right). Results are provided for all loading and friction conditions for all four combinations analysed. Reference can be made to Tables A14 to A16 in Appendix A3 for a summary of strains measured according to the three different friction conditions – *HF*, *MF* and *LF*.



**Note:** Negative strains = compressive strains, Positive strains = tensile strains.

**Figure 3.2.6.2b:** Horizontal strains for T1 and T2 loading conditions (Microstrain)

Observations from the two figures in Figure 3.2.6.2b are listed as follows:

1. The strains for different friction conditions approximated are – *HF*: 9 to 351 $\mu\epsilon$ , *MF*: 183 to 297 $\mu\epsilon$  and *LF*: 219 to 623 $\mu\epsilon$
2. Overall, the results indicate a decrease in horizontal strain at the bottom of the asphalt layer with increase in friction i.e. stronger bonding condition between pavement layers. Observing trends in comparing friction condition results, a significant change in *HF* condition results are visible in relation with *MF* and *LF* condition. This is mostly attributed to the application of bonding given that *MF* and *LF* conditions were defined as a percentage of the load area according to *T1* and *T2* respectively (refer to 3.2.2.2).
3. Small variation in strains are observed for *Case 3* and *Case 4* compared to *Case 1* and *Case 2*. It should be noted that *Case 3* and *Case 4* involve the analyses of a pavement structure with  $t_{Asphalt}$  of twice as thick (100mm) compared to *Case 1* and *Case 2* with  $t_{Asphalt}$  of 50mm.
  - a. An increase in  $t_{Asphalt}$  causes an increase in the loading time leading to smaller strains at the bottom of the asphalt layer (Figure 3.2.3.2c).
  - b. A thick layer with an increased loading time causes a small gradual increase in strains with distribution of loading. This would explain the observed behaviour for these cases.
  - c. Type of behaviour described in points a and b is beneficial as the pavement structure will be able to withstand subjected loading better which is beneficial in terms of its pavement life.

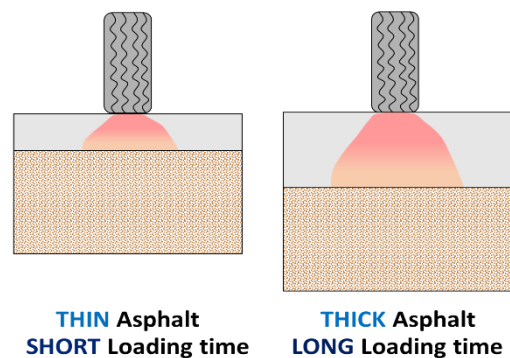


**Figure 3.2.6.2c:** Strain for asphalt layer

4. Smaller strains occur at *Edge* location compared to the *Below Wheel* location
5. The figure demonstrates negative (compressive) strains measured for *Case 2* at *Edge* location for *T1* loading condition. Similar behaviour is noticeable for *Below Wheel* and *Edge* locations for *T2* loading condition.
6. Some of the results (compressive strains) do not coincide with the definition of strains used for estimation of pavement life for the surfacing layer. This would mean that the surfacing layer of a specific pavement structure (*Case 1* to *4*) would fail immediately when subjected to loading.
7. Combining the behaviour described in points 3 and 7, it is evident that the  $t_{Asphalt}$  and  $E_{base}$  contributes extensively in the strains measured. According to the results, it would seem as  $E_{base}$  is the more prominent contributing variable in the analysis.
8. The behaviour described in points 3 and 7 are also highlighted when evaluated according to the  $\Delta[\%]$  parameter by means of Equation 3.2.3a. The change in this parameter allows understanding of strain development with weaker bonding condition between respective pavement layers. The results obtained for these percentages are provided in Table A17 in Appendix A3.

### 3.2.6.3 Vertical strains

The vertical compressive strains measured at the top of the subgrade layer are important for the serviceability life component of a pavement structure. The subgrade layer is analysed for permanent deformation in the layer, manifesting as rutting on the pavement surface (Jenkins & Rudman, 2018a), which is calculated using these strains. The occurrence described is illustrated in Figure 3.2.6.3a.

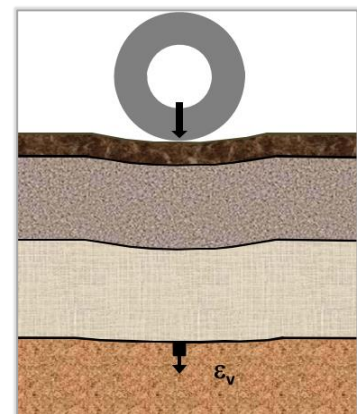


**Figure 3.2.6.3a:** Subgrade layer strain (Jenkins & Rudman, 2018a)

The vertical strains from all different combinations investigated during the linear-elastic analysis are shown in Figure 3.2.6.3b. The figures shown in Figure 3.2.6.3b are similar to the illustration of the results for the purpose of the horizontal strains, where results were grouped according to all locations analysed. Results (in microstrain,  $\mu\epsilon$ ) are represented according to the different defined conditions. Similar to the horizontal strains, the strains measured are summarised in Appendix A3 in Tables A18 to A20 relative to the different bonding conditions.

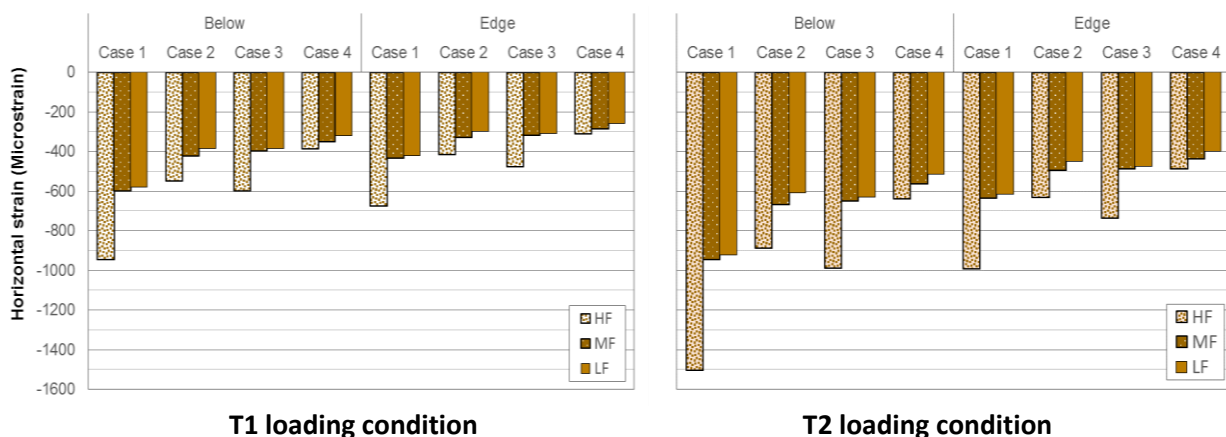


**Figure 3.2.6.3b:** Vertical strains for T1 and T2 loading conditions (Microstrain)

Studying these figures in Figure 3.2.6.3b, the following behaviour is observed for *Case 1* to *4* and the two analysis locations i.e. *Below Wheel* and *Edge* which includes the following:

1. The figure illustrates a decrease in strains with a weaker interlayer bonding i.e. decrease in friction – from *HF* to *LF* condition
2. Strains for different friction conditions approximated are – *HF*: 312 to 1505 $\mu\epsilon$ , *MF*: 300 to 950 $\mu\epsilon$  and *LF*: 260 to 920 $\mu\epsilon$
3. Larger change in strain when comparing results for *HF* to the *MF* and *LF* conditions. Justification for this observation is based on the incorporation of the bonding element when the analysis was performed. Friction incorporated as proportion of the loading area. This phenomenon is prominent when studying all of the results i.e. shear stresses and horizontal strains
4. Smaller strains are measured at *Edge* location compared to *Below Wheel* location. This agrees with phenomenon of the load distribution which was also observed for horizontal strains in Figure 3.2.6.2b.
5. Anticipated strains of greater magnitude occurs for T2 loading condition with a difference of 560 $\mu\epsilon$  (59%) compared to T1 loading condition
6. An increasing difference occurs in strains between *Case 1* and *2* compared to *Case 3* and *4*:
  - a. An increase in  $E_{\text{base}}$  (*Case 1* to *2* and *Case 3* to *4*) showed a decrease in strain in the subgrade layer of approximately 42% for *Below Wheel* and 39% for *Edge* results
  - b. The increase in  $t_{\text{Asphalt}}$  (*Case 1* to *3* and *Case 2* to *4*) illustrates a decrease in vertical strain motivated motivated by behaviours illustrated in Figure 3.2.6.2c – thicker asphalt layer, smaller increase in strains with distribution of loading.
  - c. From a visual inspection, it would appear that  $E_{\text{base}}$  is the most influential in the analysis.
7. The  $\Delta[\%]$  parameter was also used with the results to show the effect of friction between the pavement layers. The estimated values are captured in Table A21 in Appendix A3. The behaviour described in the previous points correlate with the results obtained for this parameter acquired with Equation 3.2.3a.

The horizontal and vertical strains are used to estimate the pavement life. An elaborative discussion is provided in Section 3.2.7. This section investigates the contribution of the strains on pavement life. Furthermore, it addresses the impact of the different attributes considered during analyses.

### 3.2.7 Pavement life

#### 3.2.7.1 Introduction

The pavement life emphasises the strains measured in the respective critical layers – horizontal strains in the surfacing layer and vertical strains in the subgrade layer. These two aspects are categorised as the fatigue cracking model and serviceability life of a specific pavement structure. An illustration of these two aspects is provided in Figure 3.2.7.1a following the discussion of each aspect in subsequent section of Section 3.2.7.

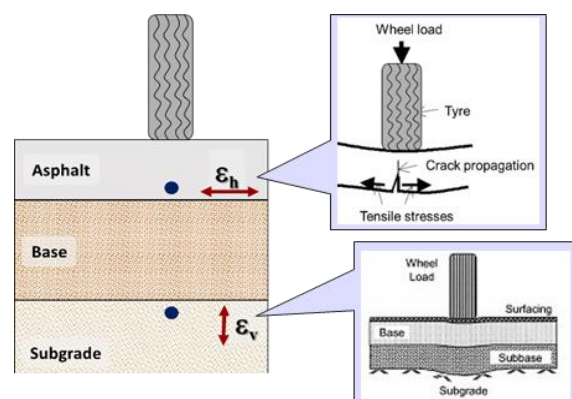


Figure 3.2.7.1a: Critical parameters and locations

### 3.2.7.2 Fatigue Life of Asphalt

The fatigue life was determined for *Case 1* to *4* for all of the applicable conditions. The fatigue life (cracking model) was derived based on a standard 50/70 Bitumen Type at 15°C and is represented by Equation 3.2.7.2a as derived from Shell nomographs. In this instance, the measured horizontal strains at bottom of asphalt layer shown in Figure 3.2.6.2b were used to determine the pavement fatigue life at both *Below Wheel* and *Edge* locations.

$$N = 4.92 \times 10^{-13} (\epsilon)^{-5} \quad (3.2.7.2a)$$

Where:

N = Number of load repetitions to failure by fatigue cracking

$\epsilon$  = Horizontal tensile strain at bottom of asphalt layer (at points 3 and 5 in Figure 3.2.4c)

The estimated fatigue life are summarised in Table 3.2.7.2a at the domination location, *Below Wheel*, for all the different analysis conditions. The results are organised according to the defined loading and friction conditions. Results acquired for *Edge* location are summarised similarly in Table A22 in Appendix A4.

**Table 3.2.7.2a:** Fatigue life results for Below Wheel location (MESAs)

Analysis conditions	T1 loading			T2 loading		
	HF	MF	LF	HF	MF	LF
<b>Case 1</b>	0.44	0.02	0.01	0.40	0.01	0.01
<b>Case 2</b>	>100	1.00	0.72	-	0.50	0.33
<b>Case 3</b>	0.36	0.04	0.03	0.09	0.01	0.01
<b>Case 4</b>	>100	0.31	0.24	>100	0.07	0.05

**Note:** Pavement life estimates are capped at 100MESAs (100 per Million Equivalent Standard Axle(s)) as this is considered an upper limit for long life

From the results given in Table 3.2.7.2a, the following summarised behaviours are noticeable:

1. Absence of Fatigue Life estimates relates to compressive strains acquired (Figure 3.2.6.2b), as opposed to tensile strains that are found at the bottom of the asphalt layer.
2. Fatigue Life estimates exceeding the capped value of 100MESAs represent a “infinite” pavement life suggesting that the relative pavement structure would fail over a seemingly long period i.e. pavement structure has an “infinite” life period.
3. Studying the results in parallel with horizontal strains measured previously, it is evident that a shorter pavement life is predicted for maximum (greater) horizontal strains. In contrast, strains of smaller magnitude would produce a longer pavement life as pavement endures less strain.
  - a. Greater load subjected to pavement structure leads to increase in stress development in the respective pavement layers. The trend is noticeable comparing *T1* loading results with *T2* loading results which is composed of a 950kPa tyre pressure and 70kN axle loading.
  - b. A weakening in bonding, studying the results from *HF* to *LF* condition where strains increase significantly, shows that a weaker degree of bonding does shorten the pavement life significantly. It is evident for both loading conditions irrespective of properties such as  $E_{base}$  and  $t_{Asphalt}$ .

- c. The anticipated behaviours in b is confirmed for the results for *LF* (full slip) condition, as lower bonding exists between the layers. This leads to greater strains in turn shortening the pavement life of a specific pavement structure.
  - d. As observed in previous sets of results, estimated values for *MF* and *LF* condition are in close approximation compared to *HF* condition.
4. Studying results in context of analysis conditions yield expected results:
    - a. *Case 4* produced the maximum pavement life consisting of  $t_{\text{Asphalt}}$  of 100mm and  $E_{\text{base}}$  of 1500MPa.
    - b. A stiffer base layer increases Fatigue Life. From visual inspection this parameter is the most influential parameter.
    - c. An increase in  $t_{\text{Asphalt}}$  leads to greater strains which causes a reduction in Fatigue Life.
  5. Estimations with Equation 3.2.3a for the  $\Delta[\%]$  parameter was also completed with Fatigue Life results incorporating the different degrees of bonding. These results provide more insight to the influence of bonding. Reference can be made to Table A23 in Appendix A4 to understand magnitude of changes.

### 3.2.7.3 Serviceability Life of Subgrade

The Serviceability Life was also determined for *Case 1* to *4* for all of the pre-defined conditions at *Below Wheel* and *Edge* locations. The vertical strains measured at the top of the subgrade layer (compressive strains) were substituted into the transfer function represented by Equation 3.2.7.3a to predict the permanent deformation as described in Chapter 2 in accordance to Theyse et al. (2007).

$$N_{PD} = 10^{(a - \log(\varepsilon_v))} \quad (3.2.7.3a)$$

Where:

- $N_{PD}$  = Number of equivalent standard axles to set level of permanent deformation
- $\varepsilon_v$  = Vertical compressive strain at top of subgrade (at points 10 and 12 in Figure 3.2.4c) (in Micro-strain)
- $a$  = Constant from Theyse et al. (2007)

The constant ( $a$ ) is determined in accordance with Theyse et al. (2007), assuming a 10mm terminal rut depth at 95% reliability level for a Category A road. Based on these assumptions the relative constant is equal to 33.7. The estimated serviceability for each of the four pavement structures analysed, is summarised in Table 3.2.7.3a according to the two defined loading conditions *T1* and *T2*, together with the three defined bonding conditions, *HF*, *MF* and *LF*. Results for *Edge* location is given in Table A24 in Appendix A4.

**Table 3.2.7.3a:** Serviceability Results for Below Wheel location (MESAs)

Analysis conditions	T1 loading			T2 loading		
	HF	MF	LF	HF	MF	LF
<b>Case 1</b>	0.01	0.84	1.15	< 1	0.01	0.01
<b>Case 2</b>	1.96	26.5	72.65	0.02	0.28	0.72
<b>Case 3</b>	0.83	50.89	69.14	0.01	0.38	0.5
<b>Case 4</b>	63.99	>100	>100	0.44	1.54	3.75

Anticipated behaviour manifested in these results and include the following:

1. Studying the results of the vertical strains illustrated in Figure 3.2.6.3b, it is apparent that small strains produce longer pavement life compared to strains of greater magnitude.
  - a. An example of this behaviour is the results obtained for Case 1 with T2 loading for the HF condition. A strain exceeding  $1500\mu\epsilon$  was obtained resulting in a significantly reduced pavement life of only 8 cycles was obtained for this combination.
  - b. Due to nature of T2 loading condition, seemingly shorter Serviceability Life estimates were achieved especially for Case 1 which is considered the “weakest” of the four structures analysed.
  - c. Significant variation in Serviceability Life in terms of magnitude is visible when comparing overall T2 loading results with T1 loading results.
  - d. A decrease in friction suggesting a weaker adhesion is prone to produce smaller strains with load spreading. Behaviour contradicts the behaviours observed for the Fatigue Life failure for the different bonding conditions. This illustrates that weaker bonding lengthens Serviceability with the decrease in strains. Similar observation as for Fatigue Life results which entails close approximation of MF and LF condition results compared to the HF condition. Note that this observation should be taken in context that this is a linear-elastic analysis.
  - e. The function of the subgrade is very important as failure of this layer could most likely cause the failure of a pavement structure. Therefore, minimizing the strains experienced in these layers is imperative.
2. Serviceability Life estimates exceeding the capped value of 100MESAs represent a “infinite” pavement life suggesting that the relative pavement structure would fail over a seemingly long period i.e. pavement structure has an “infinite” life period.
3. Studying results in relation with analysis conditions, certain expected behaviour is noticeable:
  - a. Maximum overall Serviceability Life was achieved by Case 4 composed of  $E_{\text{base}}$  of 1500MPa and  $t_{\text{Asphalt}}$  of 100mm.
  - b. Increase in  $E_{\text{base}}$  produced a decrease in strain extending Serviceability Life
  - c. Pavement structure with thicker asphalt layer of 100mm compared to 50mm, adheres to similar behaviour.
  - d. As observed in previous critical conditions (stresses and strains), the change in base layer stiffness has the most impact on the results.
4. The main objective of the linear-elastic analyses carried out is to understand the effect of bonding (tack coat) between layers. The influence was captured by the  $\Delta[\%]$  parameter using the measured Serviceability Life estimates. The behaviours in results justify observation in listed points 1 to 3 and is shown in Table A25 in Appendix A4.

#### 3.2.7.4 Effects of interface condition on pavement life

The horizontal strains at the bottom of the asphalt layer suggest that, for the fully bonded condition (HF), the strains vary in the tension domain. For other interface conditions (MF and LF or partial and full slip), these strains start to transition to the compressive domain. In addition, the maximum vertical strains measured at the top of the subgrade layer suggest an increase in the strains where full bond is lost (with a decrease in friction i.e. from HF to MF and then LF conditions respectively). It can also be

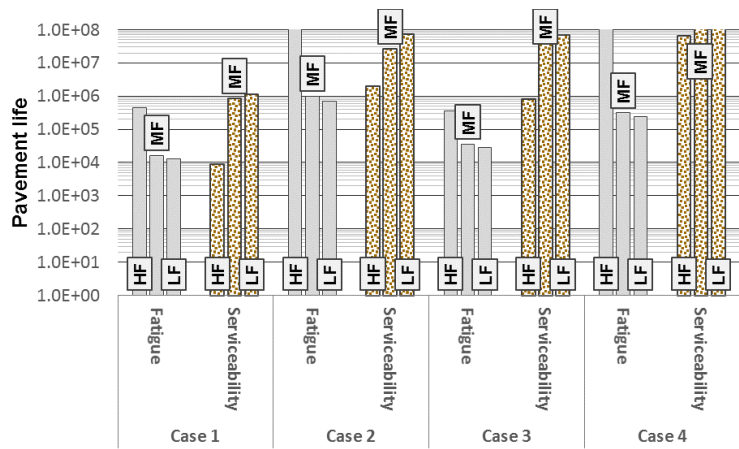
3.2 Preliminary Research: Stellenbosch University

concluded that the loss of bonding between the asphalt and base layer affects the magnitude in strains more than the bond between the base and the subgrade layer. This is attributed to the stiffness of the asphalt and base layer with the change in layer thickness ( $t_{Asphalt}$ ) throughout the analyses.

These components serve as sub-objectives in helping to establish the pavement life for pavement structures in order to provide an understanding of its behaviour. It also emphasises the effectiveness of using Spray Jet technology that promotes bond strength, affecting pavement life. The estimation of the pavement life has been discussed in terms of fatigue failure and serviceability in the previous two sections of Section 3.2.7, which addresses the acquisition of the results provided previously. Figures 3.2.7.4a and b provide an illustration of these results for  $T1$  and  $T2$  loading conditions measured at *Below Wheel* location. An illustration of these results are given in Figures A2 and A3 respectively in Appendix A4.

The effect of the interface conditions was studied in context of Figures 3.2.7.4a and b, which is based on the pavement life estimates determined by transfer functions represented by Equations 3.2.7.2a and 3.2.7.3a respectively. These functions are used to determine both serviceability and fatigue life for the four pavement structures. The observations made from these illustrations include:

1. The interface with tack coat (*HF* condition) leads to a longer Fatigue Life than the interface without a tack coat (*MF* and *LF* conditions), whereas an opposite trend is noticeable for Serviceability Life. A 97% decrease in pavement life is observed when comparing results for *HF* to *LF* condition.
2. The Serviceability Life is longer (in most instances) for  $T1$  results (Figure 3.2.7.4a), with the exception of *Case 2* and *4* (with greater base stiffness compared to *Case 1* and *3*).
3. Contrary behaviour occurs for  $T2$  results – *Case 1* and *2* comprise a longer fatigue life and *Case 3* and *4* mostly have a longer serviceability life with exception of *HF* condition (fatigue) for *Case 4*.
4. Overall Fatigue and Serviceability Life values are within a close range, with a few exceptions.
5. Based on a difference in loading conditions,  $T2$  (Figure 3.2.7.4b) produces fatigue and serviceability life estimates that are smaller in comparison with those obtained for  $T1$  (Figure 3.2.7.4a). This



**Note:**  $T1$  = Tyre pressure of 750kPa and half-axle load of 40kN. Pavement life values are capped at 100 MESAs as this is considered an upper limit for long life

**Figure 3.2.7.4b:**  $T1$  Pavement life Below Wheel estimates

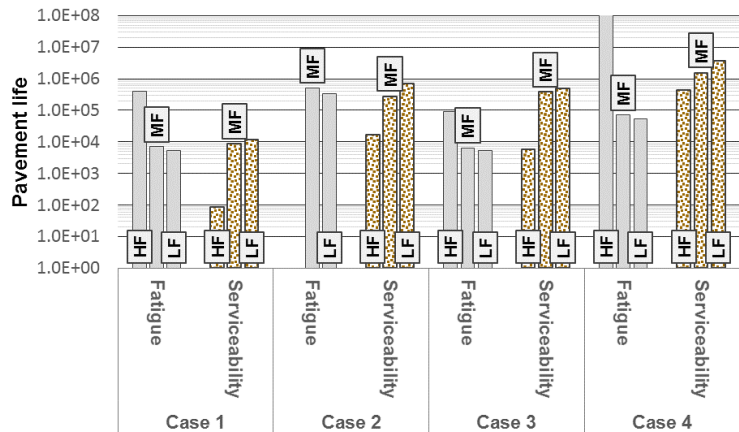


**Figure 3.2.7.4b:**  $T2$  Pavement life Below Wheel estimates

can be expected as  $T2$  involves a pavement structure subjected to a greater axle load and tyre pressure, resulting in an instance where pavement deteriorates more, leading to a shorter pavement life.

### 3.2.8 Conclusions

Different critical parameters were studied from analysing four different pavement structures. This was done by performing a linear-elastic analysis followed by a mechanistic design approach. It enables the evaluation of variables contributing to shear resistance. The behaviours observed during the processing of results showed that the interface conditions are significantly influenced by the different aspects considered. Hence also contributing to stress and strain development within the flexible pavement structures.

The evaluation of the different components, with reference to the varying pavement structures, allowed the understanding of its different attributes such as the stress development within the structure, the bonding conditions and the pavement life. This attribute classifies the pavement as either “good” or “bad” whilst describing whether the structure can endure a significant number of loading cycles before failing, or fails immediately (or its successful duration) after being subjected to a specific loading condition. The evaluation of the pavement life specifically allows understanding of the shear resistance provided.

Overall behaviour (considering trends) exhibited in the relative figure is attributed to load distribution relative to location where the load is applied. The load is transferred from the wheel to a single point on the pavement after which it is distributed along the depth of the pavement structure. A visual representation of this phenomenon is presented in Figure 3.2.8a. The figure captures all of the observations made from the results such as stresses – shear and normal (and deviator stresses) as well as strains – vertical and horizontal.

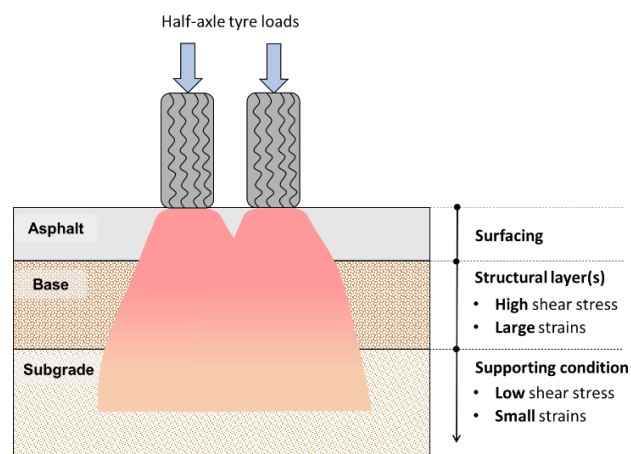


**Figure 3.2.8a:** Dissipation of externally applied stress in layered pavement system (After Theyse et al., 2011)

From the observations made, especially in terms of extended pavement life, the addition of tack coat is highly recommended as it is beneficial to the shear resistance. This would mean that the pavement structure has a better response to shear when subject to different loading conditions. However, the main objective of the research is to emphasise the application of tack coats by means of Spray Jet technology. Preliminary research by Pisa University includes laboratory testing and a linear-elastic analysis similar to Stellenbosch University. This would allow a better illustration of the efficiency of the technology in terms of bonding. Preliminary testing and analyses carried out by Pisa University is discussed subsequently in Section 3.3 followed by a comparative study in Section 3.4 performed for the linear-elastic analyses carried out by Pisa and Stellenbosch University respectively. The importance of bonding quality and application method in light of results from preliminary research completed by respective institutions will be addressed in Section 3.5.

### 3.3 Preliminary Research: Pisa University

#### 3.3.1 Research background

To improve the understanding of the benefits of a Spray jet module, empirical tests were conducted in line with theoretical modelling. For the theoretical analysis, the focus is based on the improvement of Interlayer Shear Strength (ISS) at the interface of two different asphalt layers with the use of technology. The research regime is provided in Figure 3.3.1a and will be discussed in Sections 3.3.2 and 3.3.3 respectively. Testing and analysis found to produce relevant results.

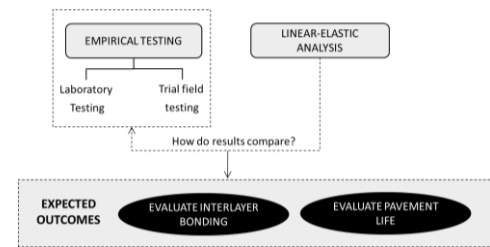


**Figure 3.3.1a:** Pisa University research regime

#### 3.3.2 Empirical Testing

##### 3.3.2.1 Introduction

In the first part of the study by Pisa University, empirical tests were conducted using the Leutner Shear tester (Chapter 2), which evaluates ISS. Two different types of empirical tests were conducted. Samples were either prepared in a laboratory or samples were acquired from trial field testing.

##### 3.3.2.2 Laboratory Testing

Various specimens were tested with the Leutner Shear Test method (Chapter 2) to evaluate the Interlayer Shear Strength (ISS) as it is important in describing the bonding conditions of a pavement structure. The specimen is composed of two layers: one layer which is used as a support, which simulates the binder layer, whereas the second layer is used to simulate the wearing course (Figure 3.3.2.2a).



**Figure 3.3.2.2a:** Leutner shear test specimens (Bianchi et al., 2018a)

The tack coat (interface where shear strength is applied by the Leutner tester), consists of a cationic emulsion (2.2.2.4) with 55% Electronic Contact Resistance (ECR) applied at different rates – 0.31 and 0.83l/m<sup>2</sup>. Some of the specimens tested consisted of a tack coat with a filler where a quantity of 0.31l/m<sup>2</sup> was added to the mixture. This was used as baseline to establish whether the addition would show improvement in terms of bonding strength at the interface. All of the specimens used for testing are made up of penetration graded bitumen 50/70 using a particular mixture. These specimens are cylindrically shaped with a diameter of 40mm produced at high temperatures of 135°C±5°C.

Six different conditions were selected for shear testing (A1, A, B1, B2, D1 and D2) involving different values for the different parameters – emulsion rate, filler rate (where applicable), curing time as well as the method of application. Two sets of cores were tested (Figure 3.2.2b) where one set consists of tack coat sprayed by Spray Jet, and the other with tack coat applied by the traditional emulsion tank. These cores are of the same type of pavement profile. The samples (cores) were obtained from

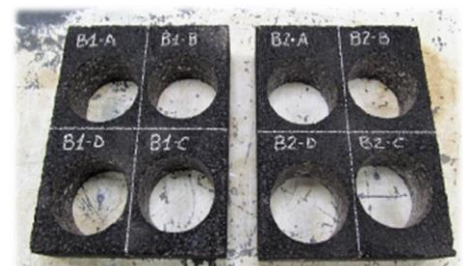


**Figure 3.3.2.2b:** Samples for laboratory testing (Vögele Wirtgen Group, 2017)

square blocks of Hot Mix Asphalt (HMA) from a Benninghoven asphalt plant which includes a binder and wearing course (Vögele Wirtgen Group, 2017). The samples were compacted using a laboratory roller compactor to simulate compaction by rollers on construction sites. For each of the specified conditions, four specimens (A to D) were used for testing (shown in Figures 3.3.2b and c). The time delay between tack coat application and shear strength (curing time) is another important variable to be considered. The attributes of the six conditions are summarised in Table 3.3.2.2a.

**Table 3.3.2.2a:** Series and attributes used for laboratory testing (Bianchi, 2018)

Series	Application method	Emulsion rate (l/m <sup>2</sup> )	Filler rate (l/m <sup>2</sup> )	Curing time (hours)
A1	Emulsion tanker	0.31	No filler	48
A2	Emulsion tanker	0.83	No filler	48
B1	Emulsion tanker	0.31	0.31	48
B2	Emulsion tanker	0.83	0.31	48
D1	Spray Jet paver	0.31	No filler	0
D2	Spray Jet paver	0.83	No filler	0

**Note:** 1l/m<sup>2</sup> ≈ 0.962g/m<sup>2</sup>

The results obtained for the laboratory tests conducted are provided in Table B1 in Appendix B1 with reference to maximum load applied, displacement achieved as well as the measured ISS. The testing at the interface provided the ISS for every specimen (Figure 3.3.2.2c), which was used to estimate an average bonding strength for each of the six defined conditions as shown in Table 3.3.2.2b.

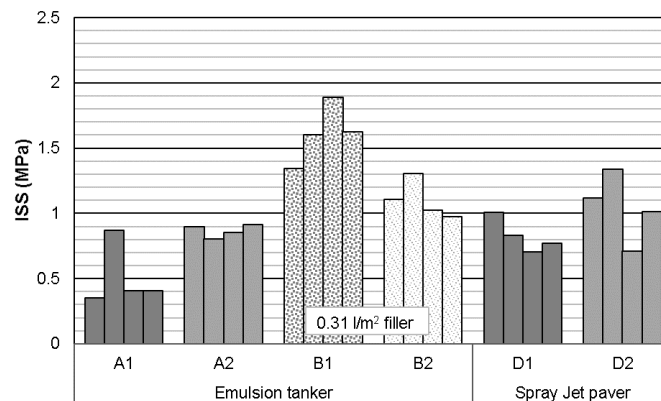


**Figure 3.3.2.2c:** Interlayer shear strength results for simulated samples (Bianchi, 2018)

**Table 3.3.2.2b:** Average bonding strength (Bianchi, 2018)

Series	Average ISS (MPa)
A1	0.51
A2	0.87
B1	1.62
B2	1.10
D1	0.83
D2	1.05

Series A1 to B2 simulate pavement structures under different conditions with tack coats applied by emulsion tanks. Series D1 and D2 simulate pavements with tack coats applied by the Spray Jet paver. The following conclusions were drawn from these results:

1. There are positive and negative correlations between tack coat rate and bonding conditions:
  - a. The positive correlation entails Series A1, A2, D1 and D2, with increase in tack coat application rates showing beneficial results in terms of ISS – higher shear strength achieved at interface
  - b. Series B1 and B2 illustrate contradictive behaviour where the increase in tack coat application rates result in a decrease in ISS
  - c. The behaviour observed in a and b confirms findings reported by Al-Qadi et al. (2012) which suggested that tack coat quantity, exceeding optimum tack coat, causes slippage at the interface and in turn causes greater displacements (refer to Table B1 in Appendix B1).
2. There is a positive correlation between presence of filler at the interface and ISS. Studying the results for B1 and B2, greater ISS results are noticeable compared to the ISS results of the other four series.
3. Extended curing time is useful for increasing ISS at the interface, as expected, although it should be noted that too long curing times have a negative impact on the interface bonding.

The results obtained in the preliminary laboratory testing are considered unsatisfactory as more results were necessary to understand the peak shear resistance achieved and shear development for each sample tested. This objective can be achieved by means of stress-strain curves which will provide a description of the development of stresses and strains within each of the samples during Leutner testing. In addition, these results can be implemented in transfer functions used to evaluate pavement life. This was completed in preliminary research performed by Stellenbosch University (*Phase 1*) and Pisa University.

The findings made from the laboratory tests provided insight into the importance of a strong interlayer bond. However, it is also fundamental to evaluate and understand the extent of the bonding at the interface by means of the type of application used, viz. the conventional method (emulsion tank) or Spray Jet technology. More effective conclusions can be drawn by extending tests conducted (Section 3.3.2.3) to investigate the bonding strength from the two different application methods. The comprehensive set of results acquired accordingly would provide a more justifiable comparison of the ISS values.

### 3.3.2.3 Trial Field Testing

A more realistic study of the ISS was required despite the benefits of tack coat application through Spray Jet technology displayed from the laboratory tests carried out in Section 3.3.2.2 Hence, the research from Section 3.3.2.3 was extended to include the set-up of trial field testing. The trial section was divided into five strips that are 20m in length and 4.5m in width. The binder used for the tack coat is a 55-45 cationic emulsion. The difference between the properties of the samples used for trial field testing, and samples used for the previous laboratory testing, are attributed to the filler content, application method and the quantity of tack coat used. The attributes of the five strips (referred to as I to V) used are summarised in Table 3.3.2.3a with an illustration of the five different strips provided in Figure 3.3.2.3a (left).

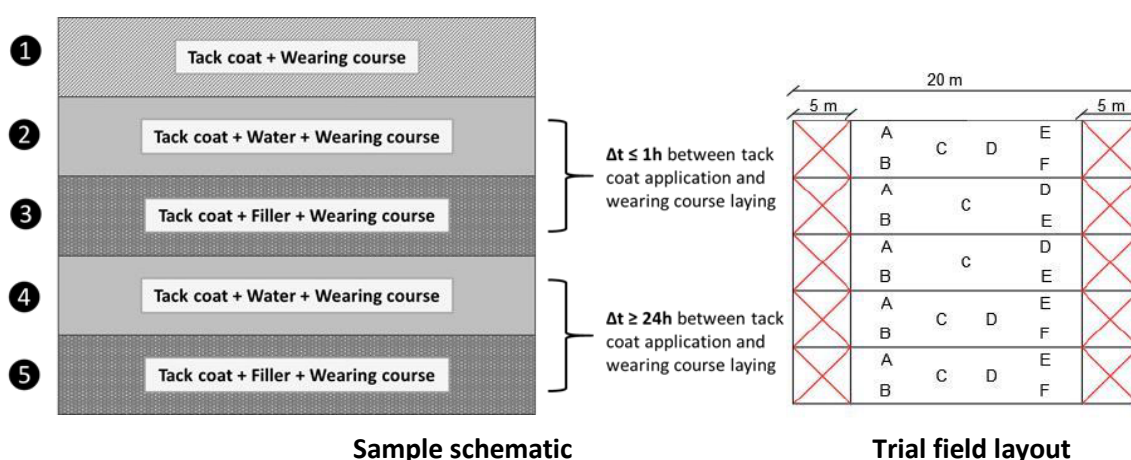
**Table 3.3.2.3a:** Trial field attributes (After Bianchi, 2018)

Strip	Application method	Emulsion rate (l/m <sup>2</sup> )	Filler rate (l/m <sup>2</sup> )	T (hours)	Description
I	Spray Jet paver	0.26	No filler	0 (*)	Tack coat + Wearing course
II	Emulsion tanker	0.62	No filler	0.5	Tack coat + Water + Wearing course
III	Emulsion tanker	0.62	0.31	0.5	Tack coat + Filler + Wearing course
IV	Emulsion tanker	0.31	No filler	24	Tack coat + Water + Wearing course
V	Emulsion tanker	0.31	0.31	24	Tack coat + Filler + Wearing course

**Note:** T = waiting duration, 1l/m<sup>2</sup> ≈ 0.962g/m<sup>2</sup>

\* Tack coat and wear course layering simultaneously, therefore T = 0 hours.

The five different sample strips are demonstrated in Figure 3.3.2.3a. Five days after the trial field was implemented, the different samples (cores) were used in subsequent laboratory tests in enhancing the understanding of the difference in tack coat application methods, while focusing on the interface shear strength of the tack coat applied.

**Figure 3.3.2.3a:** Trial field samples (After Bianchi, 2018)

Five or six cores (samples A to E or A to F) were extracted for every strip adhering to the layout given in Figure 3.3.2.3a (right). The first and last five meters of the trial field were excluded to retrieve consistent results (Bianchi, 2018). Similar to the first series of tests conducted, the shear strength (ISS) of these cores were evaluated through Leutner testing. Similar to Section 3.3.2.2, results acquired with regards to the normal load applied, displacement and ISS for each of the samples are provided in Table B2 of Appendix B1. The measured ISS is illustrated in Figure 3.3.2.3b for each sample considered, followed by the estimated average ISS as determined per strip in Table 3.3.2.3b.

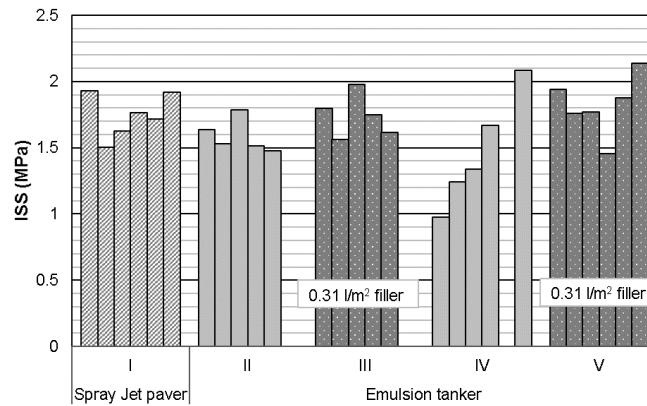


**Figure 3.3.2.3b:** Interlayer shear strength results for simulated samples (After Bianchi, 2018)

**Table 3.3.2.3b:** Average bonding strength for trial field samples (After Bianchi, 2018)

Strip	Average ISS (MPa)
I	1.74
II	1.59
III	1.74
IV	1.46
V	1.82

Studying these results, it should be noted that certain specimens were either not tested (specimen 4E) where others (specimen 1-C and 1D) were tested one week later. The following listed aspects provide a brief list of the observations made from the results obtained in this capacity.

1. A quantity of water was found at every interface. It was found that water within the specimens, irrespective of application method (emulsion tank or Spray Jet), showed similar behaviour (Figure 3.3.2.3c).



**Figure 3.3.2.3c:** Water within samples (After Bianchi, 2018)

2. For Strip V, it is found that the presence of filler decreases the quantity of water at the interface for every specimen.
3. Samples from Strip I were difficult to separate through Leutner testing, showing more complex behaviour and increasing adhesive bond between these layers. Samples tested from the remaining four strips presented contradicting behaviour with the exception of specimen 4-D.
4. The Spray Jet technology cores showed an increased irregular surface (at the failure surface), compared to the cores from the emulsion tank, as demonstrated in Figure 3.3.2.3d. The occurrence suggests that aggregate interlock is more pronounced for the Spray Jet samples.

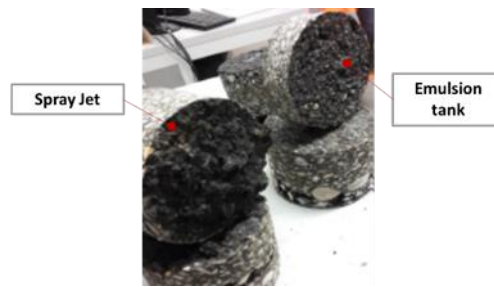


**Figure 3.3.2.3d:** Failure surface of samples (Vögele Wirtgen Group, 2017)

### 3.3.2.4 Conclusions

The testing conducted during this phase was motivated by understanding the importance of use of tack coats to improve pavement life. The phenomenon was evaluated by a series of laboratory tests of tack coats sprayed with Spray Jet technology, and an emulsion tanker, to indicate the effect of the various application methods. Weighing the components inspected i.e. application method and ISS values, the following is concluded that application by Spray Jet paver showed great potential in all respects compared to emulsion tankers:

1. Results showed that Spray Jet paver would require smaller quantity of bitumen emulsion for construction to achieve the same performance, than application with emulsion tank would have produced
2. Spray Jet paver is beneficial given the homogeneous distribution of bitumen emulsion
3. Addition of filler showed different behaviours when comparing laboratory-prepared samples (which are less important) to the trial field. This behaviour is anticipated given the impossibility of reaching precision of application in the laboratory compared to that on a construction site. Therefore, the Spray Jet paver is recommended, as it avoids the use of filler that is rarely applied homogeneously and reduces construction cost.

More testing is required to motivate the reason for high ISS values achieved through this method of application. However, according to Vögele Wirtgen Group (2017), it seemed as though the main factor was the physical reaction which occurs at the interface after the wearing course is constructed. Overall, results were good and encouraging, but more tests are required to provide a comprehensive understanding of the advantages of using the new technology.

## 3.3.3 Linear-Elastic Analysis

### 3.3.3.1 Introduction

The theoretical analysis is research completed subsequent to research study by Stellenbosch University in Section 3.2. In the present study, the relationship between bonding conditions and pavement life was also analysed considering different pavement structures i.e. *Case 1* to *4*. In contrast with the structures selected for SU research, *Case 1* to *4*, was selected from the Italian catalogue. This catalogue accommodates different conditions in terms of traffic, material and subgrade i.e. California Bearing Ratio (CBR) and layer thickness. A synthesis of analyses and calculations performed are provided in 3.3.3.2 to 3.3.3.3. The research performed for this study also consisted of a linear-elastic analysis performed using winJULEA software. It differs from the software used in the Stellenbosch University study where BISAR software was used to perform the series of analyses.

### 3.3.3.2 Loading conditions

The linear-elastic analyses performed in this capacity considered every pavement as a multilayer elastic model, based on Burmister's theory under static loading conditions. The loading used for the analyses was defined as the maximum loading allowed on Italian roads, which comprises of a 12t double-axle load. Similar to the research completed at Stellenbosch, a single wheel load was considered resulting in a 30kN load per wheel applied (Figure 3.3.3.2a) over a circular area of 37 500mm<sup>2</sup>.

The analyses were carried out considering two 30kN loads at 400mm distance (Figure 3.3.3.2b). Similar to the research by Stellenbosch University, results were obtained at various depths depending on the analysis combination. The most critical points to be considered, from the analytical point of view, were the points located at every interface, as it is representative of the bonding conditions between pavement layers.

Analyses were also performed at the *Below Wheel* location mentioned in the Stellenbosch research; however, for the research conducted by Pisa University, this will be referred to as *Side points*. As opposed to the *Edge* location also used previously, this research analysed results between the two wheels referred to as *Centre point*. The selection of these locations for the analyses can be justified based on the knowledge that the most critical values for every parameter will not always occur at the *Below Wheel* locations.

### 3.3.3.3 Friction conditions

Two different friction conditions were specified for the current research study to describe the interface bonding between the pavement layers namely high friction (*HF*) and low friction (*LF*). In accordance with the analysis software used, the high friction or full bond friction condition was set as "0" slip. For the *LF* condition, none or a very poor bond exists between pavement layers and is therefore set as "100 000" slip. These two friction conditions fulfil the same purpose as the *HF* and *LF* conditions defined for Stellenbosch University research, with the exception of its definition and incorporation of this component in the relative software used to carry out the analyses.

Apart from its incorporation, it is important to note that only two friction conditions were defined in Pisa University research compared to the additional condition (medium friction or *MF*). This was defined for the linear-elastic analysis conducted in research undertaken by Stellenbosch University (3.2.2.2). As mentioned in this section, the option of a medium-based friction condition allows a better illustration of the development of bonding between the respective layers by not just inspecting instances where very good or poor bonding arises.

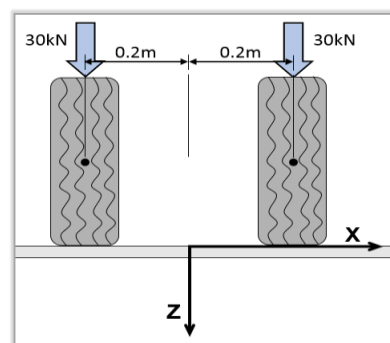


Figure 3.3.3.2a: Contact area on XY plane (Bianchi et al., 2018b)

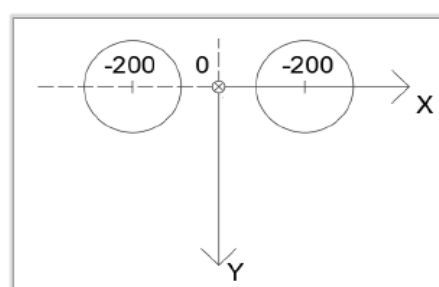


Figure 3.3.3.2b: Contact area on XY plane (Bianchi et al., 2018b)

### 3.3.3.4 Traffic conditions

In contrast with Stellenbosch research, traffic conditions were considered, as the different elements of the roads were found to be fundamental to the analysis. Hence, six different classified national road networks from the Italian catalogue were used in this capacity, which will allow the investigation of interlayer bonding on a more practical level. The 6 different road networks in question, referred to as Type A to Type F, are summarised in Table 3.3.3.4a.

**Table 3.3.3.4a:** Types of national networks (After Bianchi et al., 2018b)

Network type	Description	Speed limit
<b>Type A</b>	The only type users have to pay to drive through and the most important one, made to connect all the Italian territories; reserved only to motorways	130 km/h
<b>Type B</b>	A dual carriageway with at least two lanes for each direction, and paved shoulder. Cross-traffic and at-grade intersections are not allowed	110 km/h
<b>Type C</b>	A single carriageway road	maximum allowed speed of 90 km/h
<b>Type D</b>	Dual carriageway urban road with sidewalk	maximum allowed speed of 70 km/h
<b>Type E</b>	Single carriageway urban road with sidewalk	maximum allowed speed of 50 km/h
<b>Type F</b>	Road that cannot be classified as Type A to E	<ul style="list-style-type: none"> <li>• Highway: 50km/h</li> <li>• Urban road: 90 km/h</li> </ul>

### 3.3.3.5 Pavement structure considerations

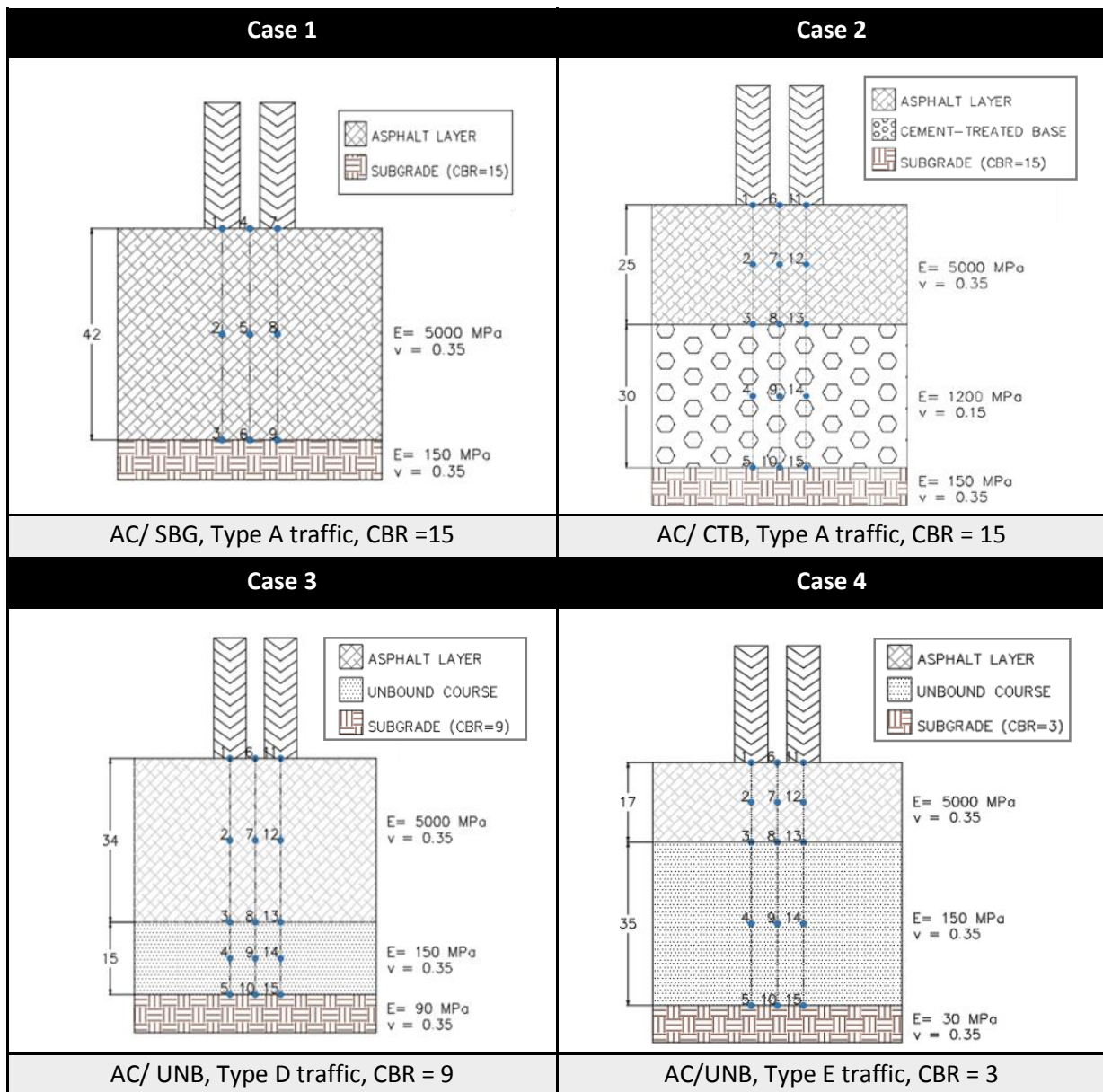
In addition to the 6 types of roads classified, the Italian catalogue showed different solutions in terms of materials, number of axle loads during pavement life by commercial vehicles (> 3t), together with subgrade conditions with a (subgrade) CBR value of 3, 9 or 15. The combination of parameters discussed previously in 3.3.3.2 to 3.3.3.4 was considered. From each combination, sets of analysis combinations (*Case 1* to *Case 4*) were selected based on the values that reflect “more real” conditions of Italian roads. In addition, these combinations would allow evaluation of the importance of good tack coat application with regards to Italian roads, where maintenance operations are more common and urgent (Bianchi et al., 2018b).

The different testing conditions of the four pavement structures analysed (*Case 1* to *Case 4*) are summarised in Table 3.3.3.5a according to the different attributes of the relative pavement structure. These pavement structures are presented in Table 3.3.3.5b accordingly. In these figures, the layer thicknesses are indicated in centimetres as opposed to millimetres.

**Table 3.3.3.5a:** Pavement structure considerations

Test condition	Case 1	Case 2	Case 3	Case 4
Pavement Structure	<ul style="list-style-type: none"> <li>Asphalt layer</li> </ul>	<ul style="list-style-type: none"> <li>Asphalt layer</li> <li>Cement-treated base layer</li> </ul>	<ul style="list-style-type: none"> <li>Asphalt layer</li> <li>Unbound base layer</li> </ul>	<ul style="list-style-type: none"> <li>Asphalt layer</li> <li>Unbound base layer</li> </ul>
Traffic condition	Type A with 45 million passages by commercial vehicles	Type A with 45 million passages by commercial vehicles	Type D with 20 million passages by commercial vehicles	Type E with 1.5 million passages by commercial vehicles
CBR	15	15	9	3

**Table 3.3.3.5b:** Pavement structure considerations



**Note:** AC = Asphalt Concrete, SBG = Subgrade, CTC = Cement-treated Base and UNB = Unbound Course

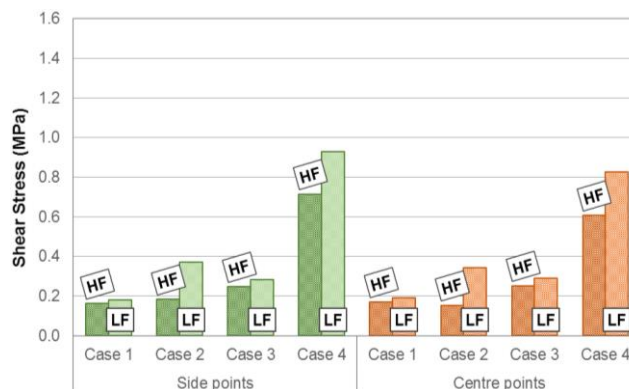
### 3.3.3.6 Results and findings

The nature of the results obtained in the two research studies by Pisa and Stellenbosch will be scrutinized in parallel in Section 3.4.

#### Shear stresses

The shear stresses measured at the location specified in 3.3.3.2, are presented in Figure 3.3.3.6a for all four combinations analysed; *Case 1* to *4*. Apart from the change in shear stress magnitude, compared to SU shear stress results, similar behaviours are noticeable comparing results yielded from *HF* and *LF* conditions respectively.

In contrast to the Stellenbosch University (SU), Pisa University (PU) performed their analyses at *Centre points* and *Side points* (equivalent of SU *Below Wheel* location). Considering the composition of the different pavement structures, the following observations were made based on the results shown for the two locations in this figure:



Note: Refer to Table 3.3.3.5b for description of the structures

**Figure 3.3.3.6a:** Pisa University shear stress results (After Bianchi et al., 2018b)

1. *Centre points* results are lower than *Side points* results with the exception of *Case 1* and *3*. This is possibly attributed to  $t_{\text{Asphalt}}$  as these pavements have seemingly thicker asphalt layers than *Case 2* and *4*.
2. The no (poor) bonding condition i.e. *LF*, yields greater shear (expected) stresses than for the full bonding i.e. *HF* condition i.e. decrease in shear stress with increase in friction (from *LF* to the *HF* condition)
3. Change in properties:
  - a.  $E_{\text{base}}$  and base layer thickness,  $t_{\text{base}}$ :
    - Case 4 has the greatest  $t_{\text{base}}$  value (35mm) with an  $E_{\text{base}}$  of only 150MPa compared to Case 3 with the same  $E_{\text{base}}$ , but  $t_{\text{base}}$  of 15mm. In relation with the shear stress results, the thickness has a significant impact on shear stress for these two structures.
    - Overall, it is suggested that the increase in the layer stiffness leads to a decrease in shear stress. However, the pavement structure with the cemented base (*Case 2*), has a slightly thicker layer compared to *Case 3*, but is almost 10 times stiffer with  $E_{\text{base}}$  of 1200MPa.
    - *Case 1*, composed of only an asphalt and subgrade layer experienced the least shear stresses at the interface.
  - b.  $t_{\text{Asphalt}}$ : Increase in this parameter results in a decrease in shear stress which is related to stress distribution illustrated in Figure 3.2.6.2c.
  - c. **CBR**: In this instance, it is apparent that the stiffness of the layer of the subgrade does influence the stress generation in the structure. However, the CBR related to the material quality is the dominating factor. The increase in the CBR value shows a material of better quality. Linking this with the trends observed in Figure 3.3.3.6a, the better material provides better stability in structure, hence better stress distribution. With increase in CBR, a decrease in shear stress occurs.

- d. **Traffic/ loading condition:** Similar as to point c – an increase in the loading subjected leads to a decrease in the shear stresses generated at the interface.
  - e. The behaviours described in a to d are based on visual inspection of Figure 3.3.3.6a. No clear distinction concerning influence of these parameters were possible in these results as there was no variable which remained constant for the different pavement structures in *Case 1* to 4. A combination of variables influence the results. Hence, it is difficult to allow a valid evaluation in this context.
4. Results were also evaluated according to Equation 3.2.3a using the  $\Delta[\%]$  parameter which confirms behaviours listed in points 2 and 3:
    - a. Confirms that shear stress is always higher in LF conditions.
    - b. Moreover, presence of good interface bonding does not affect the shear stress at the interface in the same way. Last mentioned is dependent on the change in variables discussed in point 3d.
    - c. Not dominant factor in this research, however estimations are summarised in Table B3 in Appendix B2.

### Horizontal strains

The horizontal strains measured in this analysis, are illustrated in Figure 3.3.3.6b for both locations considered for the analysis. Except for the extent of change in the horizontal strains from *HF* to *LF*, similar behaviour as for SU research results (Figure 3.2.6.2b) is prominent in Figure 3.3.3.6a.

The behaviours observed are summarised subsequently. As established previously, there is not sufficient results to evaluate influence of material properties and layer thickness. Therefore, comments based on visual inspection of results.

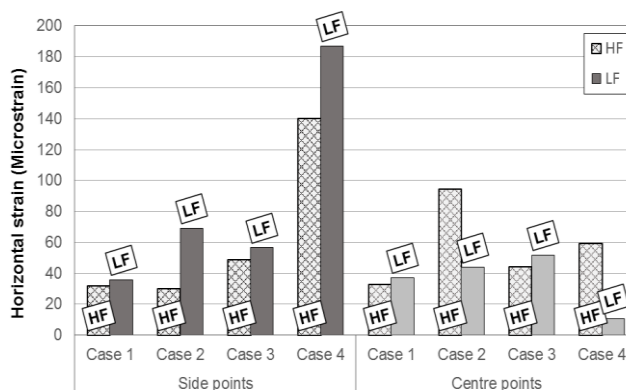


**Figure 3.3.3.6b:** Pisa University horizontal strains at Side and Centre points (Bianchi et al., 2018b)

1. The loading and friction conditions have more impact in measuring strains as opposed to shear stresses:
  - a. With a decrease in friction, greater strains emerge within the pavement structure – LF results greater than HF condition. This is attributed to weaker bonding between layers alongside loads subjected where a sporadic distribution of these loads occur.
  - b. Inversely, better interlayer bonding conditions produce smaller strains with the exception of *Case 2* and *4* at *Centre points* location
  - c. Ironically, *Case 1* to *4* represent cases where a decrease of loading occurs where an increase in strains are noticeable. Last-mentioned is evidence that the behavioural patterns cannot be limited to one variable as they work co-inherently.
2. Studying the results for *Side points* and *Centre points*, a similar trend is observed given that maximum stress is achieved at contact point of the wheel and surfacing layer, assuming an evenly-

spread distribution of stresses (and strains), with a decrease in the parameter in lower pavement layers. The phenomenon was demonstrated in Figure 3.2.8a.

3. The horizontal strains are measured at the bottom of the asphalt layer meaning the properties of this layer will govern. Comparing the trends in increase of strains, it is apparent that the change in  $t_{\text{Asphalt}}$  makes a significant contributions in the strains experienced at this point.
4. Behavioural trends coincide from behaviours observed in analysing results with  $\Delta[\%]$  parameter of which results are captured in Table B4 in Appendix B2. The greatest estimated was acquired for *Case 2* composed of a cemented base layer compared to *Case 3* and *4* with a unbound granular layer and *Case 1* exists of only a surfacing and subgrade layer.

### Vertical strains

The vertical strains yielded from the analysis of the four different combinations (*Case 1* to *4*), are shown in Figure 3.3.3.6c according to the *Side points* and *Centre points* locations respectively for both defined friction conditions. Studying the strains captured in this figure, the different aspect observed can be summarised as follows:

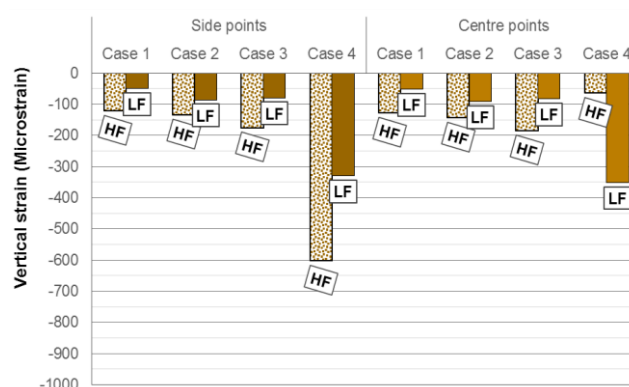


**Figure 3.3.3.6c:** Pisa University vertical strains at Side and Centre points (Bianchi et al., 2018b)

1. Influence of change in the friction and loading conditions:
  - a. From *HF* to *LF* condition, a decrease in vertical strain is noticeable expect for *Case 4* at *Centre points* location. This behaviour is in contrast with behaviour observed with horizontal strains. Justification is provided from the material quality of this layer linked with the CBR value. The material quality has an impact on the load distribution, hence, strain and stress generation in this layer.
  - b. Similar to horizontal strains, *Case 1* to *4* represent cases of decrease in loading conditions where an increase in strains are observed.
  - c. As expected, the maximum vertical strains were measure for *Case 4* attributed to the composition of this structure. It is composed of a subgrade layer allocation a poor condition CBR rating and low material stiffness of 30MPa. Concerning the magnitude in strains – greater strains are noticeable for the *LF* condition compared to *HF* condition. This was observed at the *Centre points* location only.
2. Similar trends are visible for *Side points* and *Centre points* location with the exception of *Case 4*, Firstly significant strains are measured for this pavement structure compared to results of *Case 1* to *3*. Furthermore, contradictory behaviour is noticed at *Centre points* location as mentioned in point 1a.
3. Figure 3.2.8a shows an idealistic representation of a well-balanced pavement structure. However, the results in Figure 3.3.3.6c do not conform to this illustration. This would highlight that the behaviour patterns cannot be studied in isolating one parameter as observations are attributed to different variables in conjunction.

- a. It is important to take notice these behaviours as previous results have accentuated the influence of cemented layer material properties on the shear stresses (to some extent) and especially the horizontal strains studied previously.
  - b. The most critical component in the analysis of vertical strains would be the material quality of the material represented by the CBR value. In example, the greatest strains were achieved for *Case 4* consisting of a low material stiffness of 30MPa with a CBR value as low as 3.
4. Observations from these results showed expected impact brought upon by variety of material properties defined for the analyses. The impact of interlayer bonding is promoted with the evaluation of the  $\Delta\%$  parameter. The results confirms previous summarised points and is provided in Table B5 in Appendix B2.

### 3.3.3.7 Pavement life

The Pavement Life is defined as the highest number of repetitive loads a pavement structure can resist under specific load conditions which was inspected in two ways for this analysis: fatigue cracking and permanent deformations. The two failure mechanisms form the fatigue and serviceability component of Pavement Life and focusses on strains in the asphalt and subgrade layer as shown in Figure 3.3.3.7a. The strains obtained in 3.3.3.6 are used in subsequent calculations to assist with pavement life estimations.

#### **Fatigue Life of asphalt and Serviceability Life of subgrade**

For research completed by Pisa University, the Fatigue Life was estimated by a transfer function developed by Giannini-Camomilla, represented by Equation 3.3.3.7a for the pavement structures considered.

$$N_x = \frac{-0.234 \sqrt{\epsilon_x}}{\sqrt{142}} \cdot 10^6 \quad (3.3.3.7a)$$

Where:

$N_x$  = Number of 12t ESALs to failure by fatigue cracking

$\epsilon_x$  = Horizontal tensile strain at bottom of asphalt layer (Figure 3.3.3.7a)

In this instance the pavement life regarding subgrade failure was determined by means of Equation 3.3.3.7b, a transfer function by Dormon-Metcalf.

$$N_z = \frac{-0.21 \sqrt{\epsilon_z}}{\sqrt{1.16 \cdot 10^{-2}}} \quad (3.3.3.7b)$$

Where:

$N_z$  = Number of 12t ESALs to produce permanent deformation at top of subgrade layer

$\epsilon_z$  = Vertical strain measured at top of the subgrade layer (Figure 3.3.3.7a)

**Note:** ESALs = Equivalent Standard Axle Loadings

The estimated values for fatigue and serviceability are illustrated in Figures 3.3.3.7b and 3.3.3.7c for *Centre points* and *Side points* results respectively.

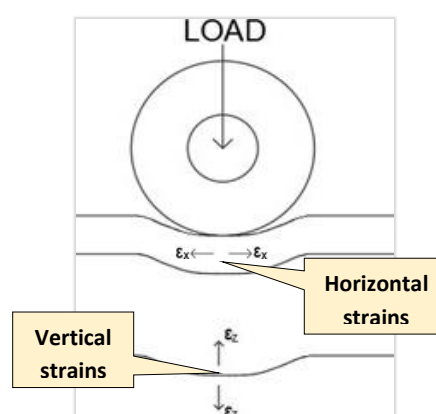


**Figure 3.3.3.7a:** Horizontal and vertical strains (Bianchi et al., 2018b)

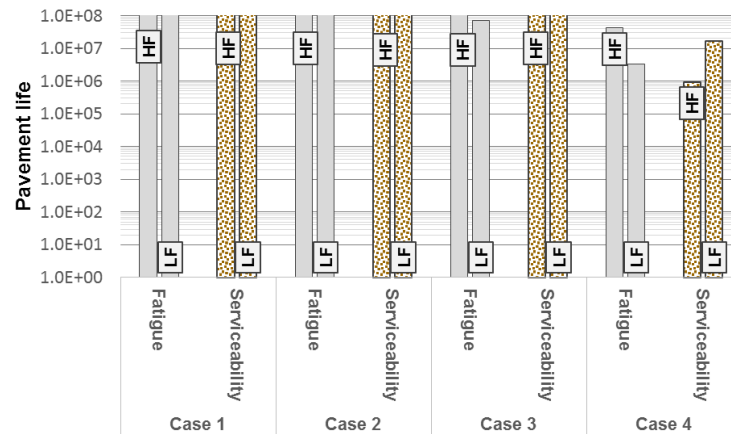


**Figure 3.3.3.7b:** Pavement Life centre point measurements (After Bianchi et al., 2018b)

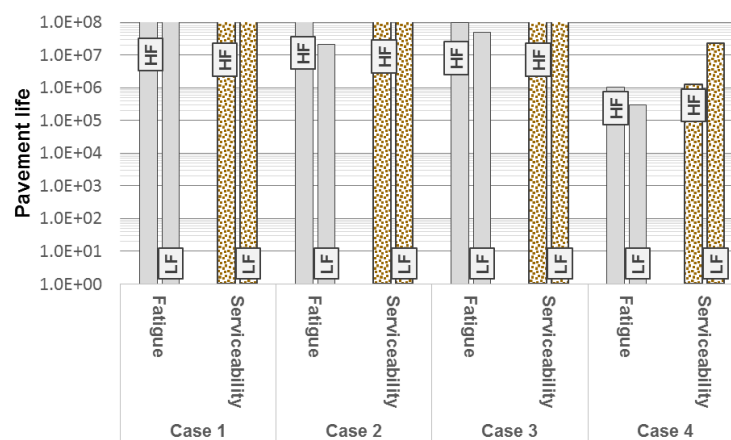


**Figure 3.3.3.7c:** Pavement Life side point measurements (After Bianchi et al., 2018b)

Observing Figures 3.3.3.7b and 3.3.3.7c, the following aspects are concluded:

1. Compared to the pavement life estimates of the analyses performed in the Stellenbosch research study, it was apparent that the pavement life estimates in the Pisa research study is significantly higher.
  - a. Estimates reached pavement life values of  $> 10^8$  (100 MESAs), which can mainly be attributed to the asphalt layer thickness and the change in other testing conditions, i.e. material properties and the loading conditions considered for the analyses.
  - b. The significance of influence of material properties such as the modular ratio (layer material stiffness) and layer thickness will be emphasised during the discussion of the comparative analyses in Section 3.4.
  - c. The analyses explored features such as different  $t_{\text{Asphalt}}$  values producing set pavement life and its influence from an economic standpoint.
  - d. A material component not evaluated in Section 3.2 for SU research is the subgrade quality (CBR). Pisa University found this element to be influential to a certain extent. It was found to affect the behaviour of the pavement under different loading conditions.
  - e. Consequently, the previous two points listed, created the opportunity for additional analyses. The technicalities of these analyses will be discussed in the subsequent section.

2. Trends of the estimates relates with the expected behaviour of increase in strains producing shorter pavement period. More stresses and strains are generated in the pavement reducing the period in which a given structure can be functional.
  - a. For the majority of the combinations, serviceability was more critical than fatigue failure as more significant vertical strains were recorded in the analyses. Hence, the subgrade layer is the most critical and may results into a pavement structure failing due to subgrade failure i.e. experience permanent deformation.
  - b. In exceptional cases where horizontal strains are more critical, a signification reduction occurs in fatigue life and the asphalt layer is the most critical. Hence, the pavement structure experiences fatigue failure.

### 3.3.3.8 Additional analyses

Results have showed that significant stresses and strains decrease pavement life and opposite effect is expected for components of smaller magnitude. In a design context, the conservative approach would be to consider minimum pavement life ( $N_{min}$ ) assuming a shorten design or structural period. Additional research was conducted to enhance the understanding of the relationship between  $N_{min}$ ,  $t_{Asphalt}$ , bonding conditions at the interface and subgrade quality – CBR.

For the purpose of the analyses objective, three types of pavement are considered – two flexible pavements and a semi-rigid pavement. These pavements were selected and are labelled as *Case A* to *Case C*, as illustrated in Figure 3.3.3.8a. The two flexible pavements include similar characteristics to some of the previous four pavements considered (*Case 1* to *4* shown in Table 3.3.3.5b), whereas the semi-rigid pavement is a newly introduced pavement structure suggested by the Italian catalogue.

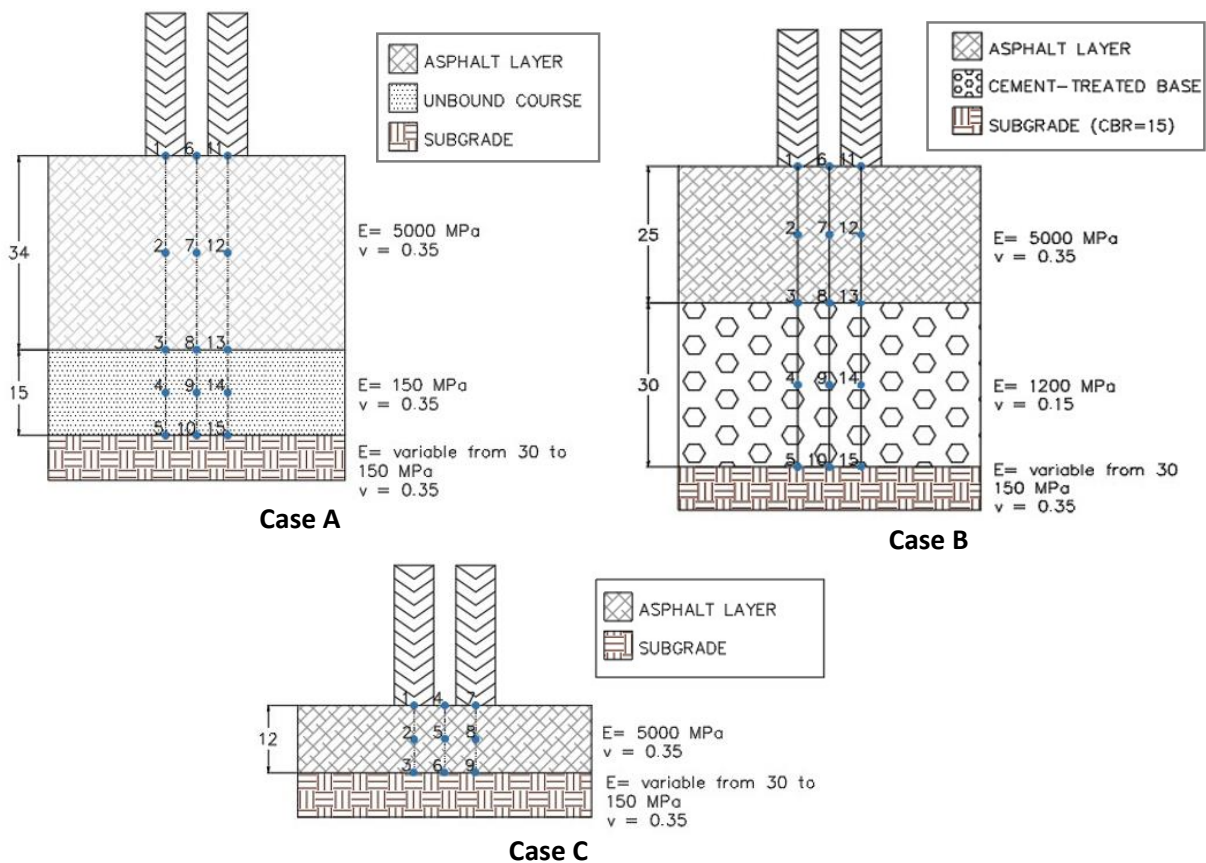


Figure 3.3.3.8a: Additional pavement structure considerations (Bianchi et al., 2018b)

The critical parameters such as shear stresses and strains – vertical and horizontal, are determined for each of the structures shown in Figure 3.3.3.8a with WinJULEA software with the adjustment parameters shown in Table 3.3.3.8a. The characteristics of the three pavement structures, *Case A* to *C* used for the additional analyses carried out, are summarised in Table 3.3.3.8b.

**Table 3.3.3.8a:** Adjusted parameters (Bianchi et al., 2018b)

Parameter	Adjustment
$t_{\text{Asphalt}}$	<ul style="list-style-type: none"> <li>Increased by 100mm or reduced by 200mm</li> <li>No modification</li> </ul>
Subgrade quality (CBR)	3, 6, 9 and 15
Bonding condition	High friction (HF) and low friction (LF)

**Table 3.3.3.8b:** Comparison of testing conditions (Bianchi et al., 2018b)

Conditions	Original			New	
	Analyses	$t_{\text{Asphalt}}$ (cm)	CBR	$t_{\text{Asphalt}}$ (cm)	CBR
Case A	Case 3	34	9	32 to 36	3, 6, 9 and 15
Case B	Case 2	25	15	23 to 27	3,6, 9 and 15
Case C	NA	NA	NA	10 to 14	3, 6, 9 and 15

### 3.3.3.9 Asphalt layer thickness and subgrade quality

An *Asphalt Concrete Overlay Equivalent* was completed to compare  $t_{\text{Asphalt}}$  to be added for *LF* conditions to produce the same pavement life than a thinner layer within *HF* conditions. These results are compiled in Table 3.3.3.9a. This aspect is fundamental for making informed decisions of tack coat application from an economic standpoint. The importance of this component is also demonstrated in terms of its application cost, including or excluding the addition of  $t_{\text{Asphalt}}$ . This is shown in Table 3.3.3.9b where a summary of the cost equivalents and changes is indicated subsequently.

**Table 3.3.3.9a:** Asphalt Concrete Overlay Equivalent results (Bianchi et al., 2018b)

Groups	AC Overlay Equivalent	$\Delta\%$ (LF → HF)	Pavement Structure
Case 1	1,6 cm	41.9 %	42 cm AC + SBG
Case 2	7 cm	97.2 %	25 cm AC + 30 cm CTB + SBG
Case 3	1,2 cm	47.3 %	34 cm AC + 15 cm UNB + SBG
Case 4	1,4 cm	67.4 %	17 cm AC + 35 cm UNB + SBG

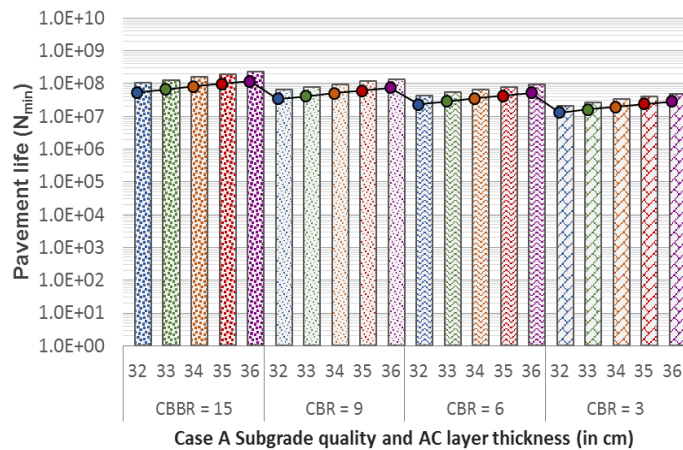
**Note:** AC = Asphalt Concrete, SBG = Subgrade, CTC = Cement-treated Course, UNB = Unbound Course

**Table 3.3.3.9b:** AC Overlay and Tack Coat cost comparison (Bianchi et al., 2018b)

Groups	AC Overlay Equivalent	Tack Coat Cost (/m <sup>2</sup> )	AC Overlay Cost (/m <sup>2</sup> )	Δ% (TC → AC)
Case 1	1,6 cm	€ 0,7	€ 3,36	380 %
Case 2	7 cm	€ 0,7	€ 14,7	2000 %
Case 3	1,2 cm	€ 0,7	€2,52	260 %
Case 4	1,4 cm	€ 0,7	€ 2,94	320%

The main theme centralizes the importance of tack coat at the interface of the surfacing layer. Hence, making it a crucial parameter contributing to pavement life. This parameter is useful in understanding the relation between bonding and pavement life. The main them centralizes the importance of tack coat application at the interface of the surfacing layer. This would make the bonding an important aspect contributing to pavement life. It is useful in understanding the relation between a good tack coat and pavement life.

Research together with Stellenbosch University (SU) shows that factors i.e. subgrade quality, could assist in improving pavement number of ESALs (Equivalent Standard Axle Loadings) that a specific pavement can withstand. The analyses performed incorporating all defined conditions produced minimum values for the pavement life ( $N_{min}$ ). The minimum pavement life defines the most critical layer of a given pavement structure – indicates which layer in the pavement system is likely to fail first. The significance of the behaviours recognised from the results presented in Figures 3.3.3.9a to 3.3.3.9c, justifies the purpose of the additional analyses performed.



**Note:** Column graphs = HF condition, Line graphs = LF condition and  $N_{min}$  = Minimum Pavement Life

**Figure 3.3.3.9a:** Minimum Pavement Life for Case A (After Bianchi et al., 2018b)

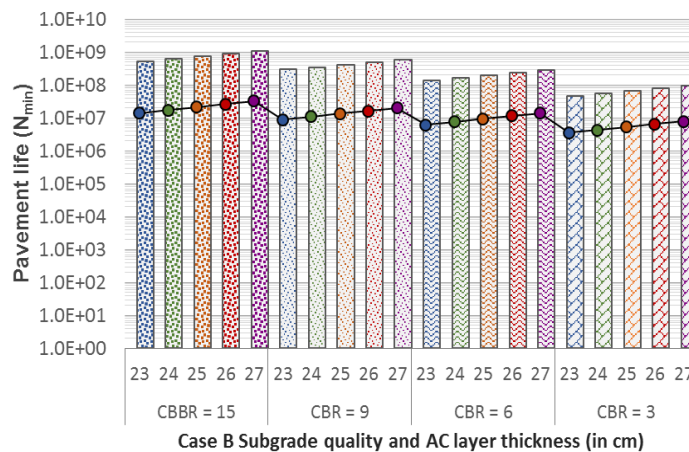


**Figure 3.3.3.9b:** Minimum Pavement Life for Case B (After Bianchi et al., 2018b)

### 3.4 Comparative Study of Preliminary Linear-Elastic Analysis

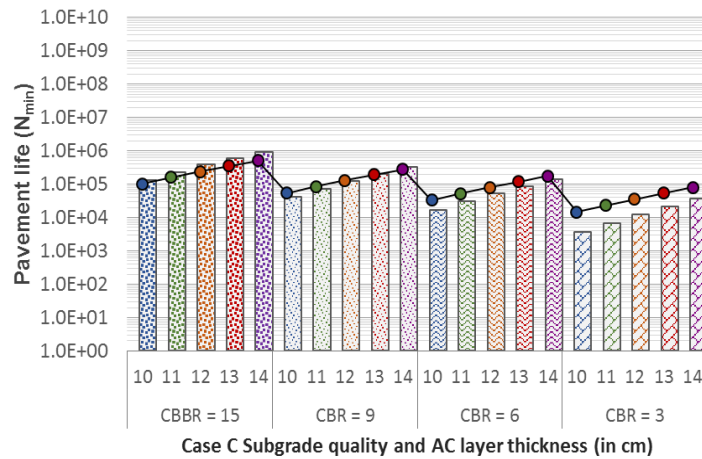


**Figure 3.3.3.9c:** Minimum Pavement Life for Case C (After Bianchi et al., 2018b)

The significance of the behaviours recognised from the results provided in Figures 3.3.3.9a to c., justifies the purpose of the additional analyses performed. This research study concluded the following from these results:

1. **Case A to Case C:** With increase in  $t_{Asphalt}$ , the more efficient tack coat application in terms of pavement life.
2. **Case C:** With a poor subgrade it is better to have LF conditions instead of HF conditions (controversial). This phenomenon is attributed to suggested catalogue value (for E) of 150MPa. If the value differs, failure occurs due to vertical strains (in the case of insufficient or bad bonding). It is thus suggested that the pavement structure (i.e. good vs. weak subgrade), and not only the bond at the interfaces, could result in pavement failure.

## 3.4 Comparative Study of Preliminary Linear-Elastic Analysis

### 3.4.1 Introduction

The different components and principal findings of the respective studies from Stellenbosch and Pisa University were discussed in Sections 3.2 and 3.3. In this section, a comparative study is completed to highlight various eccentricities according to the different elements illustrated in Figure 3.4.1a. All of the different elements scrutinized are categorised in three groups namely *loading parameters*, *pavement structure considerations* and *performance analyses*. The different parameters are quantified in Sections 3.2 and 3.3 and reference can be made to Figures C1 and C2 in Appendix C1 for a detailed experimental framework in the different capacities.

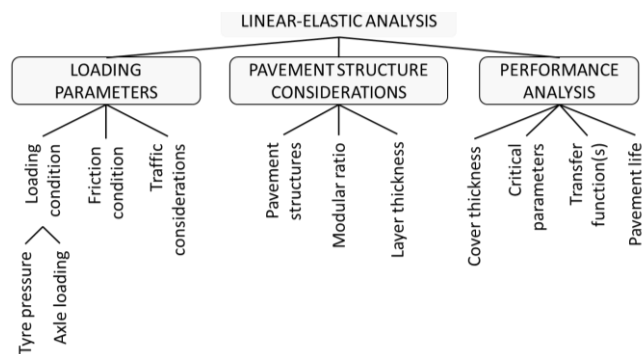


**Figure 3.4.1a:** Subjects of interest for comparative analysis

A section is devoted to each of the three categories shown in Figure 3.4.1a. Additional research by Stellenbosch i.e. normal and deviator stresses and from Pisa i.e. equivalent layer thickness are excluded from the discussion as they are not deemed relevant to the objective and scope of this research. However, it should be noted that in general, it would be important criteria to consider.

3.4 Comparative Study of Preliminary Linear-Elastic Analysis

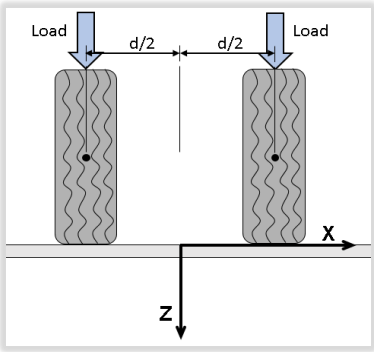
3.4.2 Loading Parameters

The loading parameters comprise of three components: loading conditions, friction conditions and traffic considerations. Given the difference in specified conditions, the discussion of the parameters occurs in a comparative nature for SU and Pisa University research. The discussion of these components is structured in a way to allow understanding of the different analyses conditions and the results obtained accordingly. It also serves as a fundamental part in evaluating the results and performance analysis completed in Section 3.4.4.

3.4.2.1 Loading conditions

The loading conditions included the axle load subjected to the pavement structure of choice, the tyre pressure applied as well as the different axle configurations adhered to during the two sets of analyses as shown in Table 3.4.2.1a.

Table 3.4.2.1a: Loading conditions for SU and Pisa University

	SU	Pisa University
Wheel load	Two different conditions, Tyre 1 and Tyre 2: <ul style="list-style-type: none"> <li>• Super single tyres                             <ul style="list-style-type: none"> <li>➢ Tyre 1: 80kN (40kN half-axle load)</li> <li>➢ Tyre 2: 140kN (70kN half-axle load)</li> </ul> </li> </ul>	One loading condition: <ul style="list-style-type: none"> <li>• Maximum allowable loading in Italy of 12 tonne double axle load</li> </ul>
Tyre pressure	Loads paired with tyre pressure: <ul style="list-style-type: none"> <li>• Tyre 1: 750kPa</li> <li>• Tyre 2: 900kPa</li> </ul>	Single wheel load of 30kN
Axle configuration	<ul style="list-style-type: none"> <li>• Single wheel load used</li> <li>• Load at 350mm distance (<math>d/2 = 175\text{mm}</math> in Figure 3.4.2.1a)</li> </ul>	<ul style="list-style-type: none"> <li>• Two 30kN loads used</li> <li>• Load at 400mm distance (<math>d/2 = 200\text{mm}</math> in Figure 3.4.2.1a)</li> </ul>
	 <p>Figure 3.4.2.1a: Wheel on XZ plane</p>	

3.4.2.2 Friction conditions

The interlayer bonding component was introduced differently in the two research studies. Quantification of the bonding condition is provided in Sections 3.2.2 and 3.3.3. Evaluation of the results shows that interpretation of the bonding component in analyses has been found to impact the outcome. Therefore, the definition of this element in the relative software used for the analysis is crucial. Furthermore, it aids with the interpretation of results accordingly. The different interpretations are presented in Table 3.4.2.2a.

## 3.4 Comparative Study of Preliminary Linear-Elastic Analysis

**Table 3.4.2.2a:** Friction conditions for SU and Pisa University

	SU	Pisa University
Definition	<ul style="list-style-type: none"> <li>• Defined by means of shear spring compliance               <ul style="list-style-type: none"> <li>➤ Taken as percentage of load area</li> </ul> </li> <li>• Three defined conditions:               <ul style="list-style-type: none"> <li>➤ HF - <i>full bond</i>: friction par. (<math>\alpha</math>) set to 0</li> <li>➤ MF - <i>partial slip</i>: at 50% of load area</li> <li>➤ LF - <i>full slip</i>: at 100% of load are</li> </ul> </li> </ul>	<ul style="list-style-type: none"> <li>• Default definition from software</li> <li>• Two defined conditions:               <ul style="list-style-type: none"> <li>➤ HF - <i>full bond</i>: set as “0” slip</li> <li>➤ LF - <i>full slip</i>: set as “100 000” slip</li> </ul> </li> </ul>

**3.4.2.3 Traffic considerations**

The main difference of the traffic considerations for both studies is based on the definition of the number of loading repetitions (N). SU research is structured in such a way that the number of loading repetitions can be determined with pavement life estimations. In contrast, Pisa University research uses these estimates as a pre-defined parameter for their analyses. The traffic conditions specified for Pisa University research consisted of 6 different classified national road networks, viz. Type A to Type F.

**3.4.3 Pavement Structure considerations****3.4.3.1 Pavement structures**

A detailed discussion of the pavement structures considered is given in Sections 3.2 and 3.3. The structures were selected based on national standards and according to defined objectives of the particular research study. SU research concentrated on the effect asphalt layer thickness ( $t_{\text{Asphalt}}$ ) and base layer stiffness ( $E_{\text{base}}$ ) also focussing on other elements such as loading with the critical element being the bonding condition. Pisa selected a variety of parameters such as layer thickness, material stiffness including the material quality represented by the CBR value. A summarised comparison of these criteria are produced in Table 3.4.3.1a with illustration of analysis locations in Figure 3.4.3.1a.

**Table 3.4.3.1a:** Friction conditions for SU and Pisa University

	SU	Pisa University
Structures	4 Standard pavement structures. Properties shown in Table 3.2.2.3b	4 pavement structures selected from the Italian catalogue. Properties shown in Table 3.3.3.5b
Approach	<ul style="list-style-type: none"> <li>• Hal-axle approach</li> <li>• 1 wheel load modelled on assumption that equivalent load distribution from 2 wheels</li> </ul>	<ul style="list-style-type: none"> <li>• Half-axle approach</li> <li>• 2 wheel loads modelled</li> </ul>
Locations	Analysis at 2 locations (Figure 3.4.3.1a): <ul style="list-style-type: none"> <li>• <i>Below Wheel</i></li> <li>• <i>Edge</i></li> </ul>	Analysis at 2 locations (Figure 3.4.3.1a): <ul style="list-style-type: none"> <li>• <i>Side points</i> (equivalent of Below Wheel)</li> <li>• <i>Centre points</i></li> </ul>

3.4 Comparative Study of Preliminary Linear-Elastic Analysis

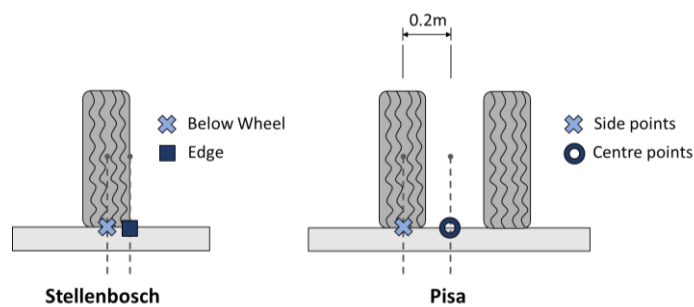


Figure 3.4.3.1a: Analysis locations

3.4.3.2 Key parameters

**Modular Ratio**

From the results gathered from preliminary analyses, it is apparent the material stiffness is a significant contributing factor in the types of behaviours observed. Hence, the importance of the modular ratio of a structure is accentuated. The modular ratio (MR) is the ratio of the stiffness of the upper layer (E<sub>1</sub>) to the stiffness of the lower layer (E<sub>2</sub>) as illustrated in Equation 3.5.4.2a, for each pavement structure in Tables 3.2.2.3b and 3.3.3.5b with the results given in Table 3.4.3.2a.

$$MR = \frac{E_1}{E_2} \tag{3.4.3.2a}$$

Where:

- MR = Modular ratio
- E<sub>1</sub> = Stiffness of upper layer
- E<sub>2</sub> = Stiffness of lower layer

Table 3.4.3.2a: Modular ratio of SU and Pisa University pavement structures

	Case 1	Case 2	Case 3	Case 4
SU	6.25	1.67	6.25	1.67
Pisa University	33.3 (*)	4.2	33.3	33.3

(\*) Structure consisting of surfacing and subgrade layers only

In comparing the modular ratios obtained, it is evident that significant higher MR-values were achieved for Pisa University research. The results reported on a maximum ratio of 33.3 compared to SU research ratio of 6.25. In other words, MR for Pisa research is approximately 5.5 times larger, with double the asphalt layer stiffness (E<sub>Asphalt</sub>), compared to SU research. Furthermore, subsequent layers comprised of stiffness values varying between 150 and 1 200MPa. For SU research these stiffness values varied between 400 and 1 500MPa. The concept of the modular ratio in this context is fundamental in the performance analyses of the two research studies.

**Layer Thickness**

Apart from the extensive range of defined layer stiffness, the variance in defined asphalt layer thickness (t<sub>Asphalt</sub>) should also be taken into consideration. The different defined thicknesses are summarised in Table 3.4.3.2b. SU pavement structures involved a thin asphalt surfacing (50 and 100mm) in comparison with Pisa University. Their layer thickness range from 170mm to 420mm respectively. These structures are three to four times the thickness specified in SU research.

3.4 Comparative Study of Preliminary Linear-Elastic Analysis

**Table 3.4.3.2b:** Asphalt layer thickness for SU and Pisa University research (in mm)

	Case 1	Case 2	Case 3	Case 4
SU	50	50	100	100
Pisa University	420	250	340	170

The different locations where results are measured are attributed to the position where the critical tensile strain is to occur. For SU research, the critical tensile strain is under the wheel i.e. *Below Wheel* location, given thin surfacing used in South Africa. In contrast, for Pisa where asphalt thicknesses of greater than 170mm are used, the critical tensile strain is between the wheels where the influence is evident where both wheels overlap. The combination of the modular ratio and the asphalt layer thickness is fundamental, as it will dictate the strains in the asphalt layer.

A graphical representation is provided in Figure 3.4.3.2a to illustrate the variation in MR and  $t_{Asphalt}$ . In this figure, the relative components are ranked in ascending order where 1 would indicate the lowest  $t_{Asphalt}$  or MR-value. The maximum shear stresses are also provided in Figure 3.4.3.2b. The combination of these graphs provides insight into the extent of influence on the results obtained from the 8 structures analysed.

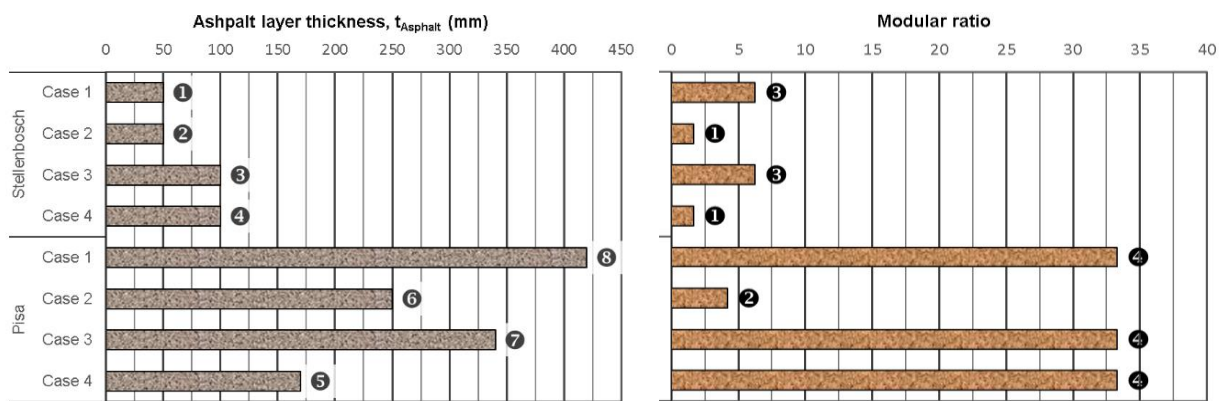
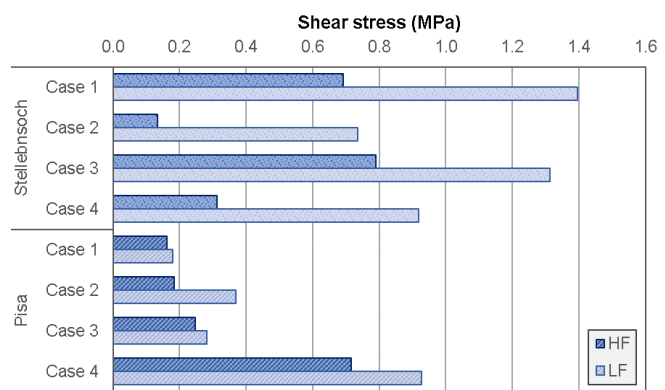


**Figure 3.4.3.2a:** Asphalt layer thickness and modular ratio

Keeping the two key parameters in mind, the most critical pavement structure would be the structure complying with the most critical combination of MR and  $t_{Asphalt}$ , viz. thicker asphalt layer and higher modular ratio.

This would not be the weakest structure per se, but one with the greatest influence in results for bonding conditions, stresses and strains. The rankings, in correlation with Figures 3.4.3.2a and 3.4.3.2b are summarised in Table 3.4.3.2c.



**Note:** Shear stresses for T2 loading condition for SU research

**Figure 3.4.3.2b:** Interface 1 Maximum Shear stresses

## 3.4 Comparative Study of Preliminary Linear-Elastic Analysis

**Table 3.4.3.2c:** Modular ratio and surfacing thickness rankings

Analyses	SU				Pisa University			
	Case 1	Case 2	Case 3	Case 4	Case 1	Case 2	Case 3	Case 4
$t_{\text{Asphalt}}$	1	2	3	4	8	6	7	5
MR	3	1	3	1	4	2	4	4

From Table 3.4.3.2c, the most crucial combinations include *Case 1, 3* and *4* for Pisa University research where the highest MR values were obtained in conjunction with greatest defined surface thickness. Furthermore, *Case 2* of Pisa University and *Case 1* and *3* of SU research are more moderate, with the second highest modular ratios specified for this group of analyses.

### 3.4.4 Performance Analysis

#### 3.4.4.1 Introduction

In order to study the performance of typical pavements, evaluation of critical parameters such as strains and stresses were done. Developed transfer functions used to estimate pavement life are also discussed alongside the estimation of pavement life produced from the analyses.

#### 3.4.4.2 Cover thickness

The material depth, or cover thickness, is the total depth of overlaying layers relative to the subgrade (also referred to as the supporting condition in SU research). It is required that the strength of the cover thickness should be sufficient for traffic-imposed stresses above this depth. In addition, these imposed stresses above this depth are assumed to have dissipated below the depth in question. Therefore, the different cover thickness for each structure analysed is considered crucial in evaluating results acquired from the analyses. The different cover depths for each of the research studies are summarised in Table 3.4.4.2a.

**Table 3.4.4.2a:** Cover thickness for SU and Pisa University research (in mm)

	Case 1	Case 2	Case 3	Case 4
SU	250		300	
Pisa University	420	550	490	520

An increasing 68% difference is evident for the minimum cover depth defined for each research study, i.e. 250mm and 420mm. Furthermore, seemingly an increase of 83.3% is found for the maximum cover thickness for SU and Pisa University research – 300mm for SU research and 550mm for Pisa University. Overall, SU research cover depth varied at a slight 20% compared to a slightly higher percentage of 31% for Pisa University research.

#### 3.4.4.3 Critical pavement parameters

A series of results obtained, such as shear stresses and strains, have been discussed according to each of the studies in Sections 3.2 and 3.3 respectively. From the discussion of the results, it can be concluded that these stresses and strains are of great importance for the purpose of the study. Testing conditions such as the material layer thickness and stiffness proved to be influential with the stresses and strains acquired from the various analyses.

3.4 Comparative Study of Preliminary Linear-Elastic Analysis

A series of results were obtained such as the shear stress and strains which have been discussed previously. From the results discussion, it can be concluded that these stresses and strains are of great importance for the purpose of the study. Testing conditions such as layer thickness and material stiffness proved to be influential with the results acquired. Hence, a section is devoted to evaluate each of these parameters individually. Comprehensive discussion of results were covered in Sections 3.2 and 3.3, where results are compared in terms of magnitude and prominent behaviours observed.

**Shear stresses**

Studying shear stress results, it was noticeable that the parameter is highly dependent on the friction condition. The shear stresses measured at *Interface 1* (between surfacing and subsequent layer) will be used for comparison purposes in this section. Only high and low friction (*HF* and *LF*) conditions are compared as Pisa University did not consider an “intermediate” friction condition i.e. medium friction (*MF*).

These shear stresses are illustrated in Figure 3.4.4.3a and 3.4.4.3b where the two friction conditions are indicated as *HF* and *LF* respectively. In addition, this figure also portrays the stresses acquired with regards to the two loading conditions specified for SU, *Tyre 1* and *Tyre 2* (*T1* and *T2*) compared to one set of Pisa research results. The results capture in the figure are the *Below Wheel* location of SU research and *Side points* location for Pisa research.

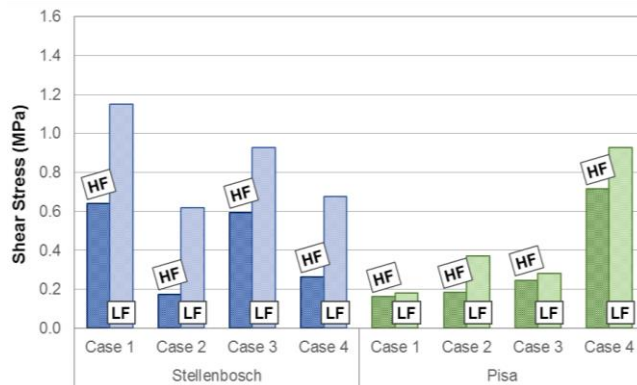


Figure 3.4.4.3a: Shear stress results for SU Tyre 1 and Pisa University research at Interface 1

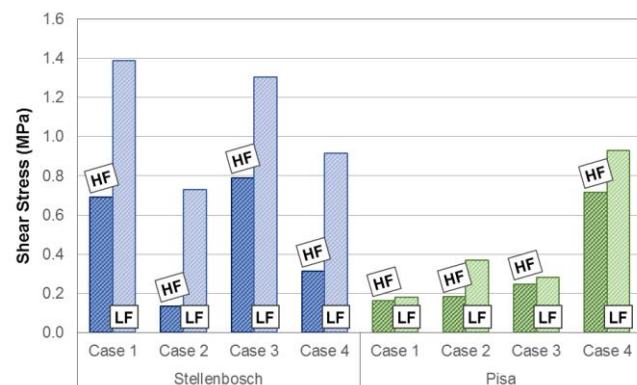


Figure 3.4.4.3b: Shear stress results for SU Tyre 2 and Pisa University research at Interface 1

The various observations from, and discussion of results are divided into different categories (Table 3.4.4.3a), such as minimum/ maximum stresses and other attributes of the analyses addressed previously. The discussion is derived from the results provided in Figure 3.4.4.3a where anticipated behaviour and consequent deviations are highlighted. Pisa University is referred to as PU in the discussion of results.

3.4 Comparative Study of Preliminary Linear-Elastic Analysis

**Table 3.4.4.3a:** SU versus Pisa University shear stress results

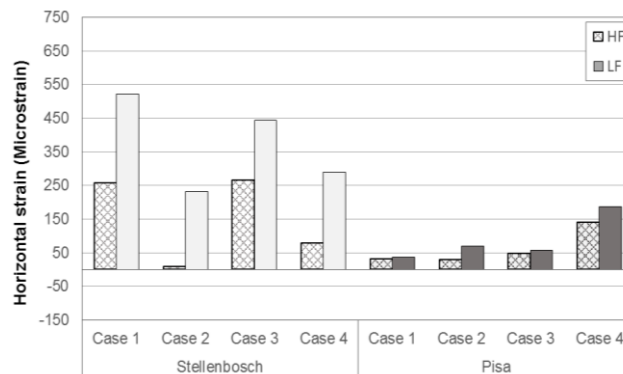
		SU		Pisa University	
HF	T1	Maximum: 0.64MPa Minimum: 0.18MPa	↓0.46	HF	Maximum: 0.72MPa Minimum: 0.16MPa ↓0.56
	T2	Maximum: 0.69MPa Minimum: 0.13MPa	↓0.56		
LF	T1	Maximum: 1.2MPa Minimum: 0.62MPa	↓0.58	LF	Maximum: 0.93MPa Minimum: 0.18MPa ↓0.75
	T2	Maximum: 1.4MPa Minimum: 0.73MPa	↓0.67		
Minimum and Maximum	HF	<b>Maximum</b> 7.8% shear stress increase from T1 to T2		HF	<b>Maximum</b> PU compared to SU research results showed a 12.5% and 4.3% increase in shear stress relative to T1 and T2 respectively
	HF	<b>Minimum</b> 27.7% shear stress decrease from T1 to T2		HF	<b>Minimum</b> PU compared to SU research results showed a 11.1% decrease in shear stress relative to T1 and 23.1% increase relative to T2 respectively
Minimum and Maximum	LF	<b>Maximum</b> 16.7% shear stress increase from T1 to T2		LF	<b>Maximum</b> PU compared to SU research results showed a 22.5% and 33.6% decrease in shear stress relative to T1 and T2 respectively
	LF	<b>Minimum</b> 17.7% shear stress increase from T1 to T2		LF	<b>Minimum</b> PU compared to SU research results showed a 71% and 75.3% decrease in shear stress relative to T1 and T2 respectively
Modular ratio		<ul style="list-style-type: none"> <li>• Decrease in shear stress with decrease in modular ratio (increase in <math>E_{base}</math> from 400 to 1 500MPa)</li> <li>• Ratio ranges between 1.67 for 400MPa <math>E_{base}</math> and 6.25 for 1 500MPa <math>E_{base}</math></li> </ul>		<ul style="list-style-type: none"> <li>• Variation of increase and decrease of shear stresses relative to decrease in modular ratio                             <ul style="list-style-type: none"> <li>➤ Double <math>E_{Asphalt}</math> of SU research at 5000MPa (SU research: 2500MPa) results in 33.3 modular ratio and 4.2 for increased <math>E_{base}</math> for Case 2</li> <li>➤ Modular ratio 5.5 to 20 times the modular ratio for SU <math>E_{base}</math> of 400 and 1500MPa respectively</li> </ul> </li> </ul>	

3.4 Comparative Study of Preliminary Linear-Elastic Analysis

Asphalt layer thickness	<ul style="list-style-type: none"> <li>Layer thickness selected at 50mm and 100mm respectively (thin surfacing):             <ul style="list-style-type: none"> <li>➤ <b>Tyre 1:</b> <ul style="list-style-type: none"> <li>7% decrease in shear stress for <i>HF</i></li> <li>19.3% decrease in shear stress for <i>LF</i></li> </ul> </li> <li>➤ <b>Tyre 2:</b> <ul style="list-style-type: none"> <li>14.4% increase in shear stress for <i>HF</i></li> <li>5.9% decrease in shear stress for <i>LF</i></li> </ul> </li> </ul> </li> <li>Decrease in shear stress with increase in layer thickness from 50 to 100mm</li> <li>Variation of increase and decrease in shear stress occurs at lower Interface 1 depth i.e. increase from 50mm to 100mm thickness</li> </ul>	<ul style="list-style-type: none"> <li>Layer thickness selected ranged between 170mm and 420mm (thick surfacing)</li> <li>Decrease in shear stress with increase in layer thickness from 170 to 420mm:             <ul style="list-style-type: none"> <li>77.3% decrease in shear stress for <i>HF</i></li> <li>80.6% decrease in shear stress for <i>LF</i></li> </ul> </li> <li>Gradual decrease in shear stress occurs at lower Interface 1 depth i.e. increase in layer thickness from 170 to 420mm</li> </ul>
-------------------------	--	--

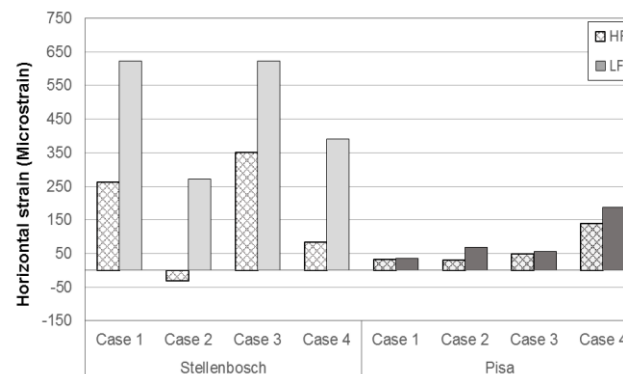
**Horizontal strains**

The definition of these strains were introduced in 3.2.6.2 and classified as critical for the surfacing layer of a pavement structure resulting in fatigue failure. The maximum horizontal strains achieved are shown in Figures 3.4.4.3c and 3.4.4.3d according to all defined conditions i.e. loading and friction.



**Note:** Negative strains = compressive strains, Positive strains = tensile strains.

**Figure 3.4.4.3c:** Horizontal strain results for SU Tyre 1 and Pisa University research at Interface 1



**Note:** Negative strains = compressive strains, Positive strains = tensile strains.

**Figure 3.4.4.3d:** Horizontal strain results for SU Tyre 2 and Pisa University research at Interface 1

3.4 Comparative Study of Preliminary Linear-Elastic Analysis

Similar to shear stress results, prominent behaviours are compiled in Table 3.4.4.3b concerning these results. Discussion of these behaviours are categorised into different groups in the relative table. Groups selected are based on the strain magnitude and addressing the two key parameters identified previously i.e. modular ratio and asphalt layer thickness.

**Table 3.4.4.3b:** SU versus Pisa University horizontal strain results

[\*] Actual minimum strain is a compressive strain which is insufficient as tensile strains are required. Strains in microstrain  $\mu(\epsilon)$ .

		SU		Pisa University	
HF	T1	Maximum: 266.9 Minimum: 9	↓257.9	HF	Maximum: 140 Minimum: 30.1 ↓109.9
	T2	Maximum: 351.1 Minimum: 84.3 [*]	↓266.8		
LF	T1	Maximum: 444.2 Minimum: 232.9	↓211.3	LF	Maximum: 187 Minimum: 35.9 ↓151.1
	T2	Maximum: 623.3 Minimum: 271.3	↓352		
Minimum and Maximum	HF	<b>Maximum</b> 31.5% horizontal strain increase from T1 to T2		HF	<b>Maximum</b> Pisa University compared to SU research results showed a 47.5% and 60.1% decrease in horizontal strain relative to T1 and T2 respectively
	HF	<b>Minimum</b> 89.3% horizontal strain decrease from T2 to T1		HF	<b>Minimum</b> Pisa University compared to SU research results showed a 70.1% and 64.3% decrease in horizontal strain relative to T1 and T2 respectively
Modular ratio	LF	<b>Maximum</b> 40.3% horizontal strain increase from T1 to T2		LF	<b>Maximum</b> Pisa University compared to SU research results showed a 57.9% and 70% decrease in horizontal strain relative to T1 and T2 respectively
	LF	<b>Minimum</b> 16.5% horizontal strain increase from T1 to T2		LF	<b>Minimum</b> Pisa University compared to SU research results showed a 84.6% and 86.8% decrease in horizontal strain relative to T1 and T2 respectively
Modular ratio		Decrease in horizontal strain with decrease in modular ratio (increase in $E_{base}$ from 400 to 1500MPa)		Variation of increase and decrease in horizontal strain relative to decrease in modular ratio	

3.4 Comparative Study of Preliminary Linear-Elastic Analysis

<b>Asphalt layer thickness</b>	<ul style="list-style-type: none"> <li>Layer thickness selected at 50mm and 100mm respectively (thin surfacing):                     <ul style="list-style-type: none"> <li><b>Tyre 1:</b> <ul style="list-style-type: none"> <li>3.9% increase in shear stress for HF</li> <li>14.8% decrease in shear stress for LF</li> </ul> </li> <li><b>Tyre 2:</b> <ul style="list-style-type: none"> <li>34% increase in shear stress for HF</li> <li>0.3% increase in shear stress for LF</li> </ul> </li> </ul> </li> <li>Decrease in horizontal strain with increase in layer thickness from 50 to 100mm</li> </ul>	<ul style="list-style-type: none"> <li>Layer thickness selected ranged between 170mm and 420mm (thick surfacing)</li> <li>Gradual decrease in horizontal strain with increase in layer thickness from 170 to 420mm:                     <ul style="list-style-type: none"> <li>77.4% decrease in horizontal strain for HF</li> <li>80.8% decrease in horizontal strain for LF</li> </ul> </li> </ul>
--------------------------------	--	--

**Vertical strains**

The essence of the vertical strains has been demonstrated in 3.2.6.3. Furthermore, it has been highlighted that these strains measured at the critical location – top of subgrade, contributes to the serviceability life of a pavement structure. The vertical strains are shown in Figures 3.4.4.3e and 3.4.4.3f including all analysis conditions. The figures are composed of the two loading conditions set of results and one set of results from Pisa University. A compilation of the prominent behaviours of these results are given in Table 3.4.4.3c subsequently. The structure allows for showing contrasting behaviours of two studies.

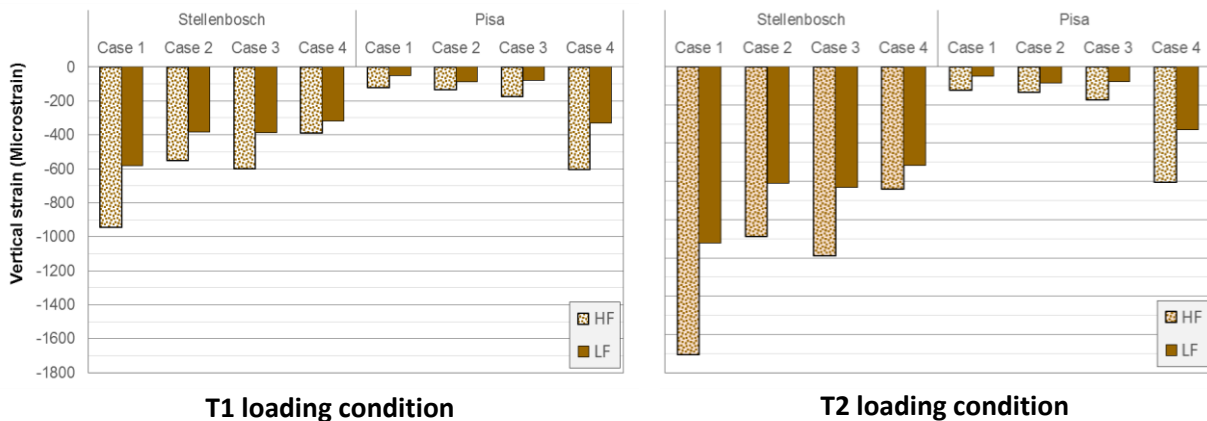


**Figure 3.4.4.3e:** Vertical strain results for SU Tyre 1 and Pisa University research

**Table 3.4.4.3c:** SU versus Pisa University horizontal strain results

		SU		Pisa University			
<b>Minimum and Maximum</b>	<b>HF</b>	<b>T1</b>	Maximum: 945.5 Minimum: 388.5	↓557	<b>HF</b>	Maximum: 603 Minimum: 122	↓481
		<b>T2</b>	Maximum: 1505 Minimum: 639.8	↓865.2		Maximum: 330 Minimum: 49.8	↓72.2
	<b>LF</b>	<b>T1</b>	Maximum: 580.5 Minimum: 318.9	↓261.6	<b>LF</b>	Maximum: 330 Minimum: 49.8	↓72.2
		<b>T2</b>	Maximum: 920.7 Minimum: 515.9	↓404.8			

3.4 Comparative Study of Preliminary Linear-Elastic Analysis

<b>Minimum and Maximum (continued)</b>	HF	<b>Maximum</b> 59.2% vertical strain increase from T1 to T2	HF	<b>Maximum</b> PU compared to SU research results showed a 36.2% and 59.9% decrease in vertical strain relative to T1 and T2 respectively
	HF	<b>Minimum</b> 64.7% vertical strain decrease from T1 to T2	HF	<b>Minimum</b> PU compared to SU research results showed a 68.6% and 80.9% decrease in vertical strain relative to T1 and T2 respectively
	LF	<b>Maximum</b> 58.6% vertical strain increase from T1 to T2	LF	<b>Maximum</b> PU compared to SU research results showed a 43.2% and 64.2% decrease in vertical strain relative to T1 and T2 respectively
	LF	<b>Minimum</b> 61.8% vertical strain increase from T1 to T2	LF	<b>Minimum</b> PU compared to SU research results showed a 84.4% and 90.3% decrease in vertical strain relative to T1 and T2 respectively
<b>Modular ratio</b>	Decrease in vertical strain with decrease in modular ratio (increase in $E_{base}$ from 400 to 1500MPa)		Variation of increase and decrease of vertical strain relative to decrease in modular ratio	
<b>Asphalt layer thickness</b>	<ul style="list-style-type: none"> <li>• Layer thickness selected at 50mm and 100mm respectively (thin surfacing):                             <ul style="list-style-type: none"> <li>➤ <b>Tyre 1:</b> 29.4% decrease in vertical strain for HF 16.9% decrease in vertical strain for LF</li> <li>➤ <b>Tyre 2:</b> 27.9% decrease in vertical strain for HF 15.2% decrease in vertical strain for LF</li> </ul> </li> <li>• Decrease in vertical strain with increase in layer thickness from 50 to 100mm</li> </ul>		<ul style="list-style-type: none"> <li>• Layer thickness selected ranged between 170mm and 420mm (thick surfacing)</li> <li>• Variation of increase and decrease in vertical strain with increase in layer thickness from 170 to 420mm:                             <ul style="list-style-type: none"> <li>79.8% decrease in vertical strain for HF</li> <li>84.9% decrease in vertical strain for LF</li> </ul> </li> </ul>	

3.4.4.4 Transfer Functions and Pavement Life

**Transfer functions**

The pavement life was determined at two critical locations by means of transfer functions. In turn, these function represent fatigue cracking and permanent deformation in the asphalt and subgrade layer respectively. For SU research, these functions were empirically derived based on the South Africa Mechanistic Design Method (SAMDM) discussed in Section 2.4.2. Furthermore, for Pisa University the functions empirically developed by Giannini-Camomilla and Dormon-Metcalfs were adhered to. For comparison, both sets of functions are shown in Table 3.4.4.4a.

## 3.4 Comparative Study of Preliminary Linear-Elastic Analysis

**Table 3.4.4.4a:** Transfer functions used for Pavement Life estimations

	SU	Pisa University
<b>Fatigue</b>	<b>Critical parameter: <i>Horizontal tensile strains measured at bottom of asphalt layer</i></b>	
	$N = 4.92 \times 10^{-13} (\varepsilon)^{-5}$ <b>(TF1)</b>	$N_x = \frac{-0.234 \sqrt{\varepsilon_x}}{\sqrt{142}} \cdot 10^6$ <b>(TF2)</b>
	<b>Where:</b> $N$ = Number of load repetitions to failure by fatigue cracking $\varepsilon$ = Horizontal tensile strain at bottom of asphalt layer	<b>Where:</b> $N_x$ = Number of load repetition to failure by fatigue cracking $\varepsilon_x$ = Horizontal tensile strain at bottom of asphalt layer
<b>Serviceability</b>	<b>Critical parameter: <i>Vertical compressive strains measured at top of subgrade layer</i></b>	
	$N_{PD} = 10^{(a-10 \log(\varepsilon_v))}$ <b>(TF3)</b>	$N_z = \frac{-0.21 \sqrt{\varepsilon_z}}{\sqrt{1.16 \cdot 10^{-2}}}$ <b>(TF4)</b>
	<b>Where:</b> $N_{PD}$ = Number of equivalent standard axles to set level of permanent deformation $\varepsilon_v$ = Vertical compressive strain at top of subgrade $a$ = Constant from Theyse et al. (2007) (33.7 with 95% reliability)	<b>Where:</b> $N_z$ = Number of 12t ESALs to produce permanent deformation at top of subgrade layer $\varepsilon_z$ = Vertical strain measured at top of the subgrade layer

**Pavement Life**

The fatigue and permanent deformation criteria were established for both studies were two different two different estimations were completed between the two studies. The results are compared for both failure mechanisms in subsequent tables, Tables 3.4.4.4b and 3.4.4.4c compiling the different observations noticed from the results. A preview of the results are also given in the respective tables where one set of Pisa results are compared to the two sets of results from SU research for T1 and T2 loading condition.

A visual representation of the estimates are captured in Figure 3.4.4.4a for Fatigue Life and Figure 3.4.4.4b for Serviceability Life. These estimations are illustrated in the number of load cycles and are capped at 100MESAs (100 per Million Equivalent Standard Axle(s)) equal to  $1 \times 10^8$  load cycles. Estimations exceeding this value represents an infinitive pavement life suggesting that a pavement structure would “never” fail or fail over a seemingly long period. Furthermore, only results for low friction and high friction, *LF* and *HF* are shown for comparison purposes.

Topics addressed includes loading, bonding state, modular ratio,  $t_{Asphalt}$  as well as sensitivity of transfer function used. Comprehensive discussion of results occurs in Sections 3.2 and 3.3. The summary is followed by a sensitivity analysis carried out comparing effectiveness of transfer function on acquired estimations represented by the  $\Delta_{Life}$  parameter.

**Table 3.4.4.4b:** SU versus Pisa University Fatigue Life Results

Preliminary analyses horizontal strains		Loading	Friction	Modular ratio	$t_{Asphalt}$	Fatigue
<p><b>T1 loading condition</b></p> <p><b>T2 loading condition</b></p> <p><b>Figure 3.4.4.4a:</b> Pavement life for fatigue failure</p>	<b>SU</b>	<p>Decrease in Fatigue Life with increase in loading condition – 20% increase in tyre pressure and 75% increase in axle load</p>	<p>Decrease in Fatigue Life with decrease in friction i.e. from <i>HF</i> to <i>LF</i></p>	<p>Increase in Fatigue Life with decrease in modular ratio – increase in <math>E_{base}</math> from 400 to 1500MPa</p>	<ul style="list-style-type: none"> <li>• Thin surfacing</li> <li>• Variation of increase and decrease in Fatigue Life with increase in <math>t_{Asphalt}</math> from 50 to 100mm</li> </ul>	TF1
	<b>Pisa University</b>	<p>Decrease in Fatigue Life with the increase in loading with exception of Case 2 composed of cemented base layer suggesting modular ratio is more influent</p>	<p>Decrease in Fatigue Life with decrease in friction i.e. from <i>HF</i> to <i>LF</i></p>	<p>Variation of increase and decrease in Fatigue Life relative to decrease in modular ratio – visible for <i>Case 2</i> with cemented base layer</p>	<ul style="list-style-type: none"> <li>• Thick surfacing</li> <li>• Variation of increase and decrease in Fatigue Life with increase in layer thickness from 170 to 420mm</li> </ul>	TF2

3.4 Comparative Study of Preliminary Linear-Elastic Analysis

Table 3.4.4.4c: SU versus Pisa University Serviceability Life Results

Preliminary analyses horizontal strains		Loading	Friction	Modular ratio	$t_{Asphalt}$	SL
<p><b>T1 loading condition</b></p> <p><b>T2 loading condition</b></p> <p><b>Figure 3.4.4.4b:</b> Pavement life for serviceability failure mode</p>	<b>SU</b>	<p>Decrease in Serviceability Life with increase in loading condition – 20% increase in tyre pressure and 75% increase in axle load</p>	<p>Decrease in Serviceability Life with decrease in friction i.e. from <i>HF</i> to <i>LF</i></p>	<p>Increase in Serviceability Life with decrease in modular ratio – increase in <math>E_{base}</math> from 400 to 1500MPa</p>	<ul style="list-style-type: none"> <li>• Thin surfacing</li> <li>• Increase in Serviceability Life with increase in layer thickness from 50 to 100mm</li> </ul>	TF3
	<b>Pisa University</b>	<p>Decrease in Serviceability Life with the increase in loading with exception of Case 2 composed of cemented base layer suggesting modular ratio is more influential</p>	<p>Decrease in Serviceability Life with decrease in friction i.e. from <i>HF</i> to <i>LF</i></p>	<p>Variation of increase and decrease in Serviceability Life relative to decrease in modular ratio - – visible for Case 2 with cemented base layer</p>	<ul style="list-style-type: none"> <li>• Thick surfacing</li> <li>• Increase in Serviceability Life with increase in layer thickness from 170 to 420mm</li> </ul>	TF4

### 3.4 Comparative Study of Preliminary Linear-Elastic Analysis

Anticipated behaviours manifested in the various figures – smaller strains produced longer pavement life compared to strains of greater magnitude having the opposite effect. The decrease in friction describing weaker adhesion, produced greater horizontal strains in terms of fatigue failure in Figure 3.4.4.4a. This shows that bonding condition at the surfacing layer is fundamental in the pavement structure. The type of behaviour contradicts the behaviour observed in Figure 3.4.4.4b for subgrade failure. Failure of the layer could (most likely) cause the failure of a pavement structure. Therefore, minimising the strains experienced in these layers would be imperative.

#### Sensitivity analysis

The extent of change in pavement life results due to the transfer function used, is unknown. Hence, a sensitivity analysis was completed for all four transfer functions used in the two studies – TF1 to TF4 in Table 3.4.4.4a. The formulation will allow an understanding of the function's influence by calculation results as a proportion of the relative study's result by means of Equation 3.4.4.4a.

$$\Delta_{Life} = \frac{x_{PU} - x_{SU}}{x_{SU}} \quad (3.4.4.4a)$$

Where:

$x_{SU}$  = Parameter calculated within Pisa University research i.e. TF2 and TF4

$x_{PU}$  = Parameter calculated within Stellenbosch University research i.e. TF1 and TF3

One set of vertical and horizontal strains are selected from each study, to be substituted into Equation 3.4.4.4a. In both studies, LF condition results were used for fatigue life estimates and HF condition results for serviceability life estimates. The selection of strains were used as they made up the most conservative results of the analyses. Given the variety of SU conditions, results compiled for the T2 loading condition were considered. The results are grouped in Tables 3.4.4.4d for SU research. The exercise is repeated for Pisa University results and is summarised in Tables C1 and C2 in Appendix C2.

**Table 3.4.4.4d:** Sensitivity analysis for asphalt fatigue SU results

Analyses	$\epsilon_h$	TF1 result	TF2 result	Difference	$\Delta_{Life}$	
Case 1	621.7	$5.30 \times 10^3$	$1.82 \times 10^3$	$3.48 \times 10^3$	65.7%	↓
Case 2	271.3	$3.35 \times 10^5$	$6.29 \times 10^4$	$2.72 \times 10^5$	81.2%	↓
Case 3	623.3	$5.23 \times 10^3$	$1.80 \times 10^3$	$3.43 \times 10^3$	65.6%	↓
Case 4	390.7	$5.40 \times 10^4$	$1.32 \times 10^4$	$4.08 \times 10^4$	75.5%	↓

**Note:** TF1 input strains as measured. TF2 input strains in microstrain

**Table 3.4.4.4e:** Sensitivity analysis for subgrade failure SU results

Analyses	$\epsilon_v$	TF3 result	TF4 result	Difference	$\Delta_{Life}$	
Case 1	1505	$8.41 \times 10^1$	$1.67 \times 10^4$	$1.66 \times 10^4$	99.5%	↑
Case 2	886.8	$1.67 \times 10^4$	$2.08 \times 10^5$	$1.91 \times 10^5$	92.0%	↑
Case 3	988.3	$5.64 \times 10^3$	$1.24 \times 10^5$	$1.18 \times 10^5$	95.5%	↑
Case 4	639.8	$4.36 \times 10^5$	$9.83 \times 10^5$	$5.47 \times 10^5$	55.6%	↑

**Note:** TF3 input strains in microstrain. TF4 input strains as measured. Estimations based on adjusted Equation 3.4.4.4a: PU relative to SU as ratio of PU

### 3.5 Significance of bonding and tack coat application

The comparison allows the individual influence of the different transfer functions. A detailed comparison of the transfer functions is carried out using pavement structures *Case 1* (SU) and *Case 3* (Pisa University) and the findings are shown in Table 3.4.4.4f.

**Table 3.4.4.4f:** Transfer function and strain relation

Critical conditions	Strains			$\Delta_{Life}$	
	SU	Pisa	$\Delta$	SU	Pisa
Asphalt fatigue	621.7	56.6	90.9%	65.7%	95.7%
Subgrade failure	1505	175	88.4%	99.5%	100 %

## 3.5 Significance of bonding and tack coat application

### 3.5.1 Introduction

The different aspects of the preliminary research is covered in Sections 3.2 and 3.3 followed by a comparison study in Section 3.4. This section will highlight the findings of these studies by discussing the following two main points in accordance with the objective of the research:

1. Significance of tack coat application by means of Spray Jet technology
2. Effectiveness of bonding state on the Fatigue Life of a given pavement structure

A discussion is devoted to each of the topics where prominent findings are studied. The discussion considers results acquired in research by both Stellenbosch and Pisa University. The first topic investigates effectiveness based on preliminary laboratory testing. The second subject of interest is highlighted by means of Stellenbosch research.

### 3.5.2 Emulsion tanker versus Spray Jet paver

The Interlayer Shear Strength (ISS) results of samples will be used in order to compare the effect of the application method on the type of strength or bonding achieved. The ISS results are summarised in Table 3.5.2a for specimens where tack coat was applied at emulsion rate of 0.31 and 0.83l/m<sup>2</sup>.

**Table 3.5.2a:** ISS values for different application methods

Emulsion rate (l/m <sup>2</sup> )	Application methods		
	Emulsion tanker	Spray Jet paver	Difference
0.31	0.51	0.83	33.9 ↑
0.83	0.87	1.05	70.9 ↑

The results are originally compiled in Table 3.3.2.2b for all the different specimen tested. However, to enable a just comparison, samples selected exclude the addition of filler. For this purpose, samples *A1*, *A2* and *D1* and *D2* as summarised in Table 3.3.2.2a are considered. For the first mentioned, an increase of 0.32MPa (62.7%) is noticeable for Spray Jet paver application compared to emulsion tanker. Similar results are found for the 0.83l/m<sup>2</sup> emulsion rate, where a 0.18MPa (20.7%) increase is obtained for the bonding measured for bond coat applied with Spray Jet paver. These results will be used as basis for calculation of the pavement life reported in Sections 3.2.7, 3.3.3.7 and 3.4.4.4. This enables the evaluation of change in friction condition considering certain variables.

### 3.5.3 Effect of bonding condition on Fatigue Life

The correlation between Fatigue Life and proportion of bonding is illustrated in Figure 3.5.3a for the purpose of quantifying the analysis performed on different combination of pavements.

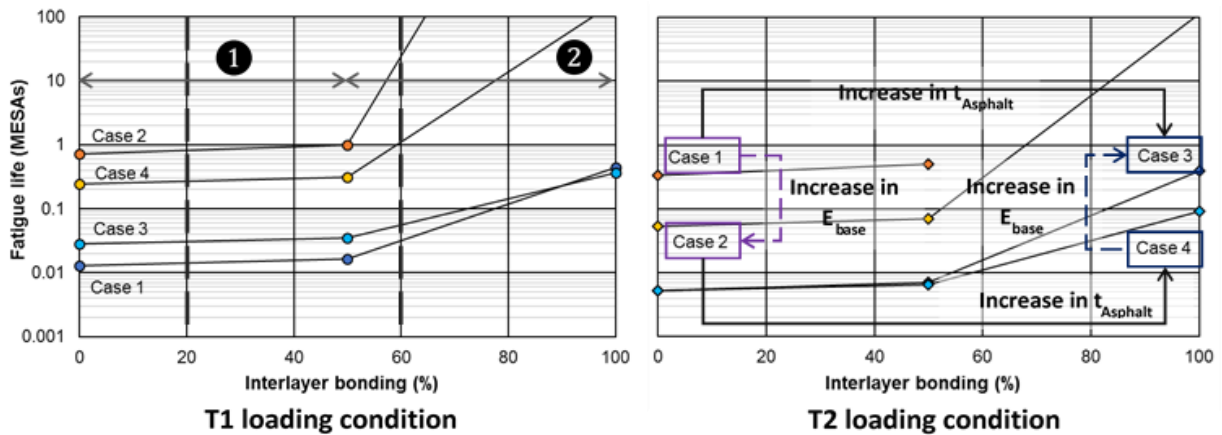


**Figure 3.5.3a:** Effect of interlayer bonding on linear-elastic Fatigue Life

The influence of defined conditions i.e. loading,  $t_{\text{Asphalt}}$ ,  $E_{\text{base}}$ , are visible in this figure where following distinctive behaviours are observed with regards to the Fatigue Life:

1. Regions
  - a. Region 1: (0 to 50% bonding) – gradual increase in Fatigue Life for all cases
  - b. Region 2: (> 50% bonding) – steep gradient is achieved
2. Bonding
  - a. Friction condition between 0 and 50% (*LF* and *MF* condition) would significantly shorten pavement life.
  - b. In contrast, stronger bonding i.e. greater than 50%, will lead to pavement life having a rapid response which is valuable in the long term.

Two reference interlayer bonding frictions are chosen to illustrate the effect of different friction conditions on pavement life occurring due to different tack coat application methods. Benchmark friction conditions were set to 20 and 60% in line with results obtained background testing in Section 3.3.2. This clarifies how the pavement life is influenced in the two parts of the graph developed labelled as Region 1 and 2 in Figure 3.5.3a. This is chosen as the reference bonding (or friction) percentage for the traditional application by an emulsion tanker.

Subsequently, a second reading is taken from the comparison using the percentage increase in friction that has been reported in Table 3.5.2a between an emulsion tanker and Spray Jet module. The results reveal that under a low friction benchmarked at 20%, a gradual increase in pavement life occurs. Results suggest that a low friction (*LF*) condition will have a minimal influence on the Fatigue Life. Benchmarking values at 60% for the high friction (*HF*) condition, shows a significant increase in the Fatigue Life as observed in Figure 3.5.3a.

For example, *T1* results at *LF* condition of 20%, change in  $E_{\text{base}}$  shows an increase of 59 and 90% in Fatigue Life for *Case 1/2* and *Case 3/4* combinations respectively. Furthermore, for the change in  $t_{\text{Asphalt}}$ , up to double Fatigue Life was determined for *Case 1/3* and *Case 2/4* respectively. From the results, it is shown that the stronger bonding has a sporadic effect on the Fatigue Life. It is also noticeable that the testing conditions have an increase influence on Fatigue Life estimates of the different pavement structures. The increase in  $E_{\text{base}}$  and  $t_{\text{Asphalt}}$  is indicated for both loading conditions – *T1* and *T2* in Figure 3.5.3a.

### 3.6 Synthesis of preliminary research

The spreading ability of loads of different pavement structures are fundamental, emphasising stress and strain generation in the different pavement layers. From critical parameters such as shear stresses and strains, both anticipated and contradictive behaviours were observable. Addressing important attributes of the pavement structures analysed deemed critical for pavement design and involves the material stiffness and layer thickness.

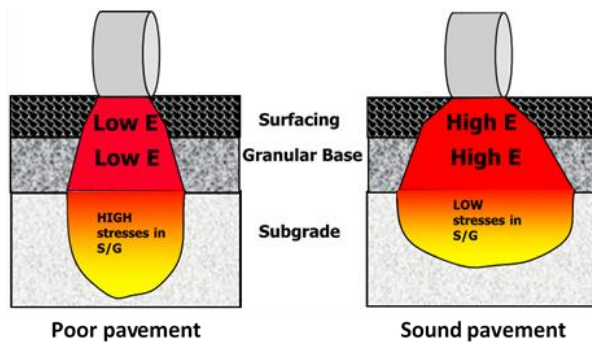


**Figure 3.6a:** Load spreading abilities of pavements (Jenkins & Rudman, 2018a)

The development of stresses and strains were illustrated in Figure 3.2.8a. This figure indicates that smaller strains are obtained in the subgrade layer compared to the other structural layers. The primary task of a pavement is to prevent stresses that are too high in the subgrade as described in Jenkins & Rudman (2018) and shown in Figure 3.6a. Hence, understanding the purpose of the layers would assist in comprehending the contribution of crucial components to pavement. The linear-elastic analyses emphasised the profound

influence of material layer stiffness which was identified as the most critical parameter in both research studies.

An example of phenomenal influence of material layer stiffness is the pavement structure analysed by Pisa University referred to as *Case 2* composed of a cemented base layer. The Cement-treated Base (CTB) material comprises of “slab-like” characteristics with beam strength similar to asphalt layer behaviour. It is incomparable to granular base layers which fail during loss of interlock when subjected to traffic loading. Also, its ability to gain strength with age even under various traffic conditions, attributes to the material’s excellent performance (Portland Cement Association, 2018). A thinner layer thickness compared to a granular base layer is probable as the CBT is a rigid material which distributes load over a large area (Figure 3.6b). The objective of such a base layer is attributed to its load spreading – it spread loads and reduces stress on the subgrade. The behaviour described was noticeable when studying stresses and strains for this structure.

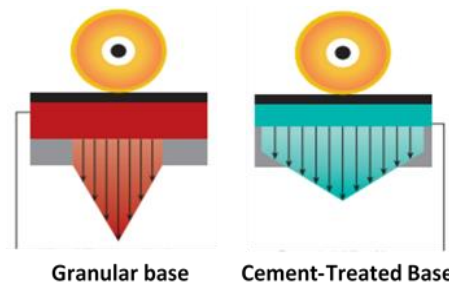


**Figure 3.6b:** Load spreading ability of different base layers (Portland Cement Association, 2018)

Overall, similar behaviours were noticeable in terms of friction conditions and the shear resistance along with additional analyses performed. It should be kept in mind, however, that the analyses were performed under different testing conditions. Despite the absence of a factors between the two studies, Stellenbosch and Pisa University research concurred the beneficial influence of tack coat on pavement life. Furthermore, it is very important to identify the role of a good quality subgrade and subbase to help improve the loading subjected to a pavement, while it also highlights the importance of modular ratio and layer thickness.

### 3.6 Synthesis of preliminary research

From the observations made particularly in terms of the extended pavement life in Section 3.5, the application of tack coat by means of Spray Jet technology was found to be highly recommended. Despite being more expensive, it could lead to better results with less maintenance costs involved. The nature of these results during *Phase 1* should be considered preliminarily as a finite element method (FEM) representation of the pavement structure to allow extended investigation of the results. Hence, describing actual road conditions as accurate as possible. The different components involved in the FEM approach is addressed in Chapter 4 which gives a broader understanding regarding the nature of results obtained during the linear-elastic analysis.

## CHAPTER 4: METHODOLOGY

### 4.1 Introduction

The main focus of the current research study has been highlighted throughout the empirical (linear-elastic) analyses carried out in Chapter 3. The influence of the interlayer bond linked to pavement structures with several variables, was investigated. From the results achieved in the previous chapters, it became apparent that further evaluation of these to understand the preliminary results, was needed.

Dovetailing conclusions from the previous chapter, the chapters to follow will include extended analyses by means of finite element method (FEM) modelling. This allows for evaluation of the behaviour at the interface in terms of the bonding condition, pending different types of applications (represented by different material properties). It will also allow advanced evaluation of stresses and strains for pavement analyses. The preliminary laboratory testing performed with Leutner shear testing will be incorporated in FEM analyses and the various testing conditions will be replicated. Two material models were created as FEM models: one representing the Leutner Shear Test (Chapter 2) and the other being a simplification of a pavement structure, subjected to a single wheel load (equivalent of half-axle approach used in preliminary analysis) as shown in Figure 4.1a.

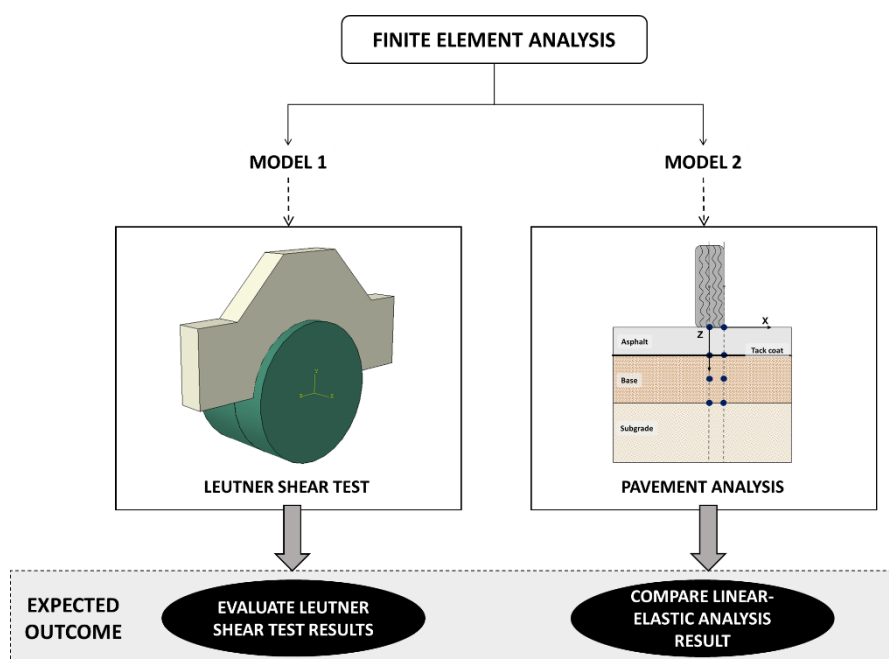


**Figure 4.1a:** Two material models replicated in FEM analysis

The sections to follow discuss each of the models replicated (Sections 4.2 and 4.3). The discussions comprise of two components, i.e. theory (mathematical model) component and the physical (real) component's characteristics as developed in Abaqus.

## 4.2 Leutner Shear Test Method

### 4.2.1 Introduction

The different components and testing conditions of the Leutner Shear Test Method was summarised from various literature reviewed in Chapter 2. The main purpose of the test is to evaluate the shear condition (shear stress) within a given sample at the interlayer interface. For current research, preliminary testing in the previous chapter provided limited results. The different components of the test were replicated as an FEM model as reported in this chapter, where testing conditions assigned replicate the behaviour of the physical testing equipment as accurately as possible. The experimental plan of the different parameters to be evaluated in the analysis are presented in Figure 4.2.1a.

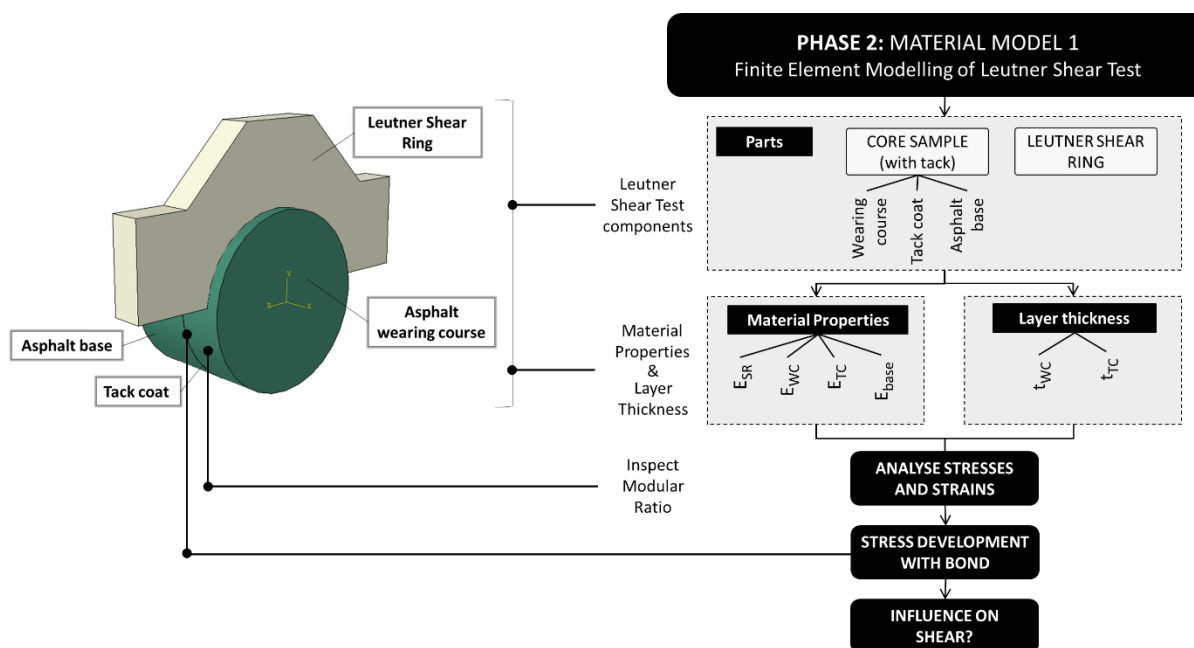


**Figure 4.2.1a:** Material model 1 experimental plan

Given the function of the test, the main objective of the material model is to evaluate the shear stresses at the interlayer surface. This objective will be achieved by evaluating a series of parameters used for the analysis to establish its effect and extent of influence on the shear stresses developed at the interlayer interface (as shown in Figure 4.2.1a):

1. Effect of change in modular ratio (3.5.4.2): the change in shear stresses according to the increase and decrease of modular ratio. A modular ratio of 1 and 2.5 is applied in the analyses
2. Different properties of the tack coat material used: material properties (stiffness) and layer thickness and the role they play in the interlayer bonding of pavement layers are evaluated. Two different material stiffness moduli and three tack coat thicknesses were considered
3. Change in wearing course layer thickness as it influences the shear development within the pavement model. Three different thickness are considered to evaluate the parameters' influence on the results

The different components of the model set-up and analyses will be discussed comprehensively in subsequent sections of Section 4.2 where all assumptions used are provided and justified. The components of the model discussed in this section are illustrated in Figure 4.2.1b.

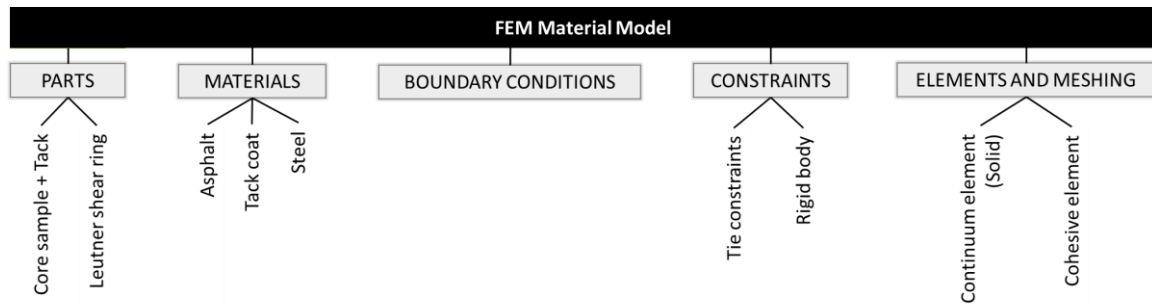


**Figure 4.2.1b:** Material model components

Firstly, a summary of the model set-up is provided which discusses all the parts of the FEM model set up, followed by its given properties (testing conditions such as material properties). Subsequently the replicated testing conditions are provided including boundary conditions and constraints used to replicate the physical characteristics of the testing conditions. The final component, before the analyses of the results, incorporates the pure mathematical components of the analyses, i.e. meshing and assignment of element types. This divides the parts into smaller integration points (nodes and elements) which are used to evaluate stresses (and strains) or any required criteria from the analysis of the particular model.

#### 4.2.2 Model set-up

The different attributes of the model are defined in different modules within the FEM software used. The components for each module in the model are shown in Figure 4.2.2a. The *Part* and the *Property* modules will be used to firstly create the different parts (define the geometry i.e. dimensions and material properties). The *Assembly* module is used to assemble the different part instances to build the model to which various boundary conditions and interactions will be assigned.

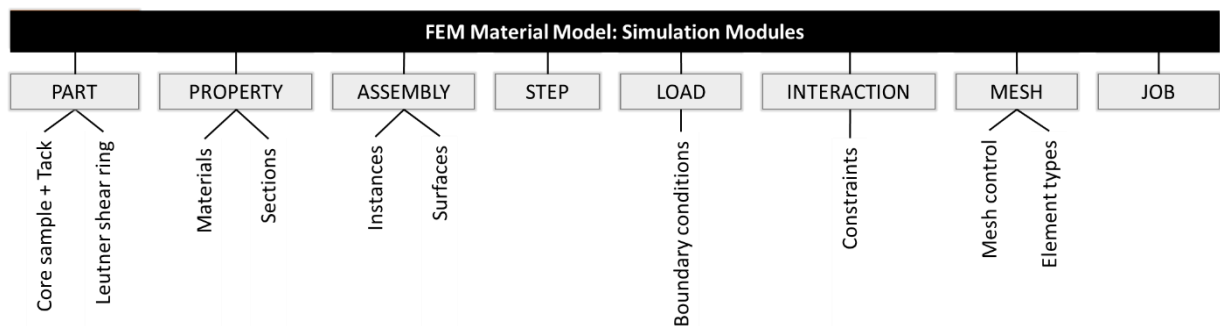


**Figure 4.2.2a:** Model 1 components according to simulation modules

Hereafter, the boundary conditions and constraints will be assigned (*Load* and *Interaction* module) which depend on the *Step* module defining the instance when these conditions are applied. Additionally, information such as increment for the analyses is defined (4.2.6.1). This allows the setting of a number of iterations used to complete the analysis. The final step is to assign elements and meshing techniques (*Mesh* module) to divide the assembled model into small integration (finite) elements and processed in the *Job* module, based on the increment previously set for the analysis. The results acquired accordingly can be interpreted and illustrated in the *Visualisation* module where a variety of results of the specific analysis can be obtained.

The set-up of the model will be discussed according to the different modules shown in Figure 4.2.2a in Sections 4.2.3 to 4.2.7.

4.2.3 Parts

4.2.3.1 FEM replication

The model used to replicate the Leutner Shear Test consists of two parts, the steel shear ring and the core sample (with a diameter of 150mm). Figure 4.2.3.1a provides a schematic of the Leutner Shear Test.

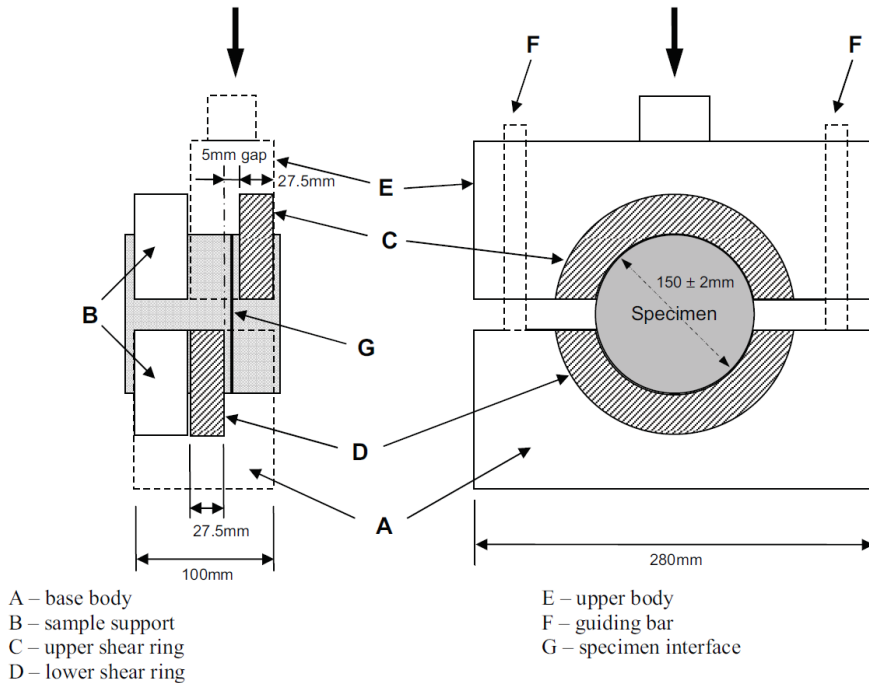


Figure 4.2.3.1a: Schematic illustration of the Leutner Shear Test (Sutanto, 2009)

Figure 4.2.3.1b illustrates the different components replicated in the FEM model. To simplify the replication in FEM, no shear rings were explicitly modelled and only the upper shearing ring (*parts C and D* in Figure 4.2.3.1a) (with a different geometry) is noticeable in the FEM replication. Furthermore, it is evident that the sample support and base body (*parts A and B* in Figure 4.2.3.1a) are not incorporated into the FEM model. Even though these elements were not physically added to the model, they are represented by means of boundary conditions and constraints. These components allow the absent elements of the Leutner Shear Test to be modelled. They are represented by constraints which will act as clamps, performing the same actions as the actual parts of the test. The movement of the testing device (displacement) is achieved by means of boundary conditions assigned to the assembled model.

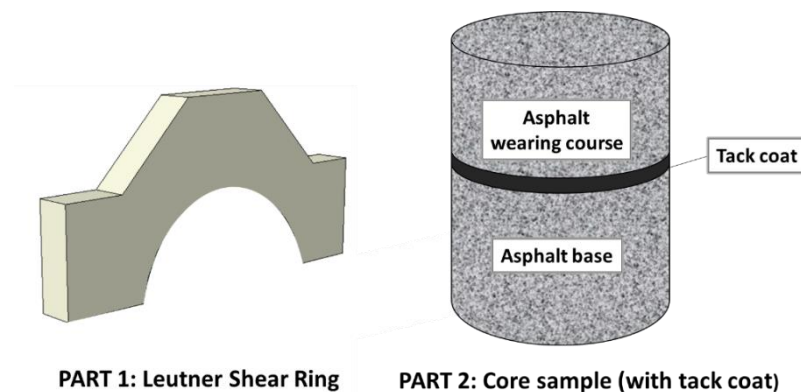
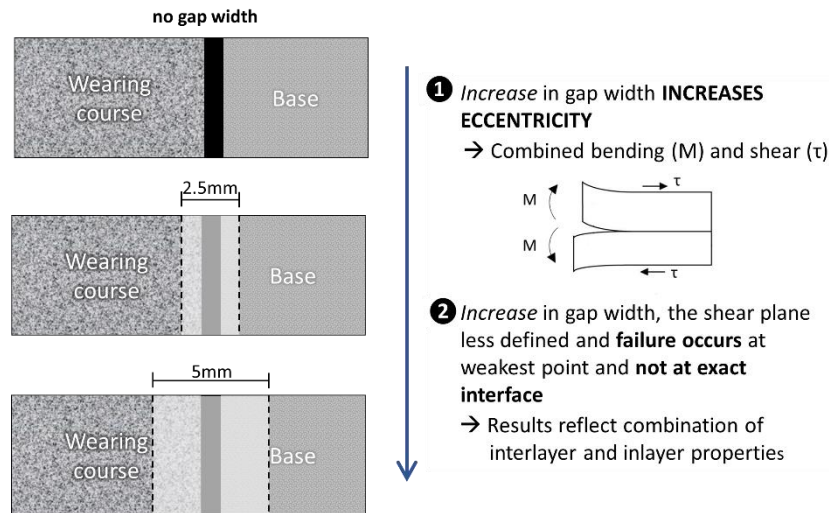


Figure 4.2.3.1b: Leutner Shear Test FEM replication

For the FEM model, a 2.5mm gap width was assumed as opposed to the 5mm indicated on the schematic shown of the test. Research was conducted to investigate the impact of the gap width on the results acquired from shear testing. Literature reviewed in Chapter 2 provided insight into the influence of the gap width on shear test results in a research study by Raab et al. (2010). They concluded that a gap width of 5mm may lead to results which reflect a combination of inlayer and interlayer properties (Figure 4.2.3.1c). In Figure 4.2.3.1c, the description of the effect of gap width on shear results is adapted from Raab et al. (2010) and Sutanto (2009). The tack coat is represented as a black strip in the figure.



**Note:** The black strip represents the tack coat and the shaded area represents the gap width

**Figure 4.2.3.1c:** Leutner test device gap width

The study found that the gap width between shear rings of the device did not influence the interlayer shear test results when materials with similar characteristics were used. In instances where two mixtures of different material characteristics are used, the gap width was found to influence the interlayer shear test results. For the materials, an increase in the gap width would result in a decrease of the maximum shear force and shear stiffness. Furthermore, from material testing carried out by Raab et al. (2010), a gap width of 2.5mm was favoured, as existing Leutner devices allow for a maximum gap width of 2.5mm (Figure 4.2.3.1c). Hence, this gap width was applied in the model. Due to the absence of the sample support, the gap width was applied symmetrically relative to the parts. This means that the upper shear ring was placed 1.25mm from the centre of the tack coat layer.

The core sample (150mm in diameter) consists of three parts or pavement layers, i.e. wearing course, the tack coat and the asphalt base. The model considers cored samples from a pavement where an asphalt overlay was completed, therefore having two subsequent asphalt material layers. The tack coat is applied to provide better bonding between the existing surfacing layers, which becomes the base layer after the wearing course had been constructed. For the core sample, only one part was created. The three respective layers are added to the model by means of partitioning. Many methods exist to execute this exercise in Abaqus; however, given the small dimension with the small tack coat thickness specified, a datum plane (Figure 4.2.3.1d) was used to apply the partitioning.

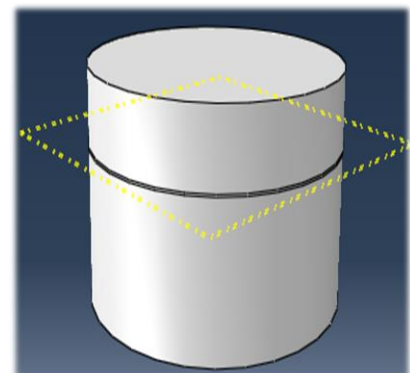


**Figure 4.2.3.1d:** Datum plane and partition (Abaqus Inc., 2017)

The different thicknesses considered for the respective layers in the analysis are summarised in Table 4.2.3.1a. For all of the different combinations considered, a constant layer thickness is used for the base layer at 60mm and the geometry of the steel ring remains unchanged. A variety of thicknesses is considered for the wearing course layer ( $t_{wc}$ ) as well as the tack coat layer ( $t_{tc}$ ), seeing that these are parameters, which influence on shear stresses, are to be evaluated from the analyses.

**Table 4.2.3.1a:** Layer thickness combinations for Model 1

Part/ Region	Thickness (mm)			
Shear ring	NA	NA		
Wearing course	$t_{wc}$	30	50	100
Tack coat	$t_{tc}$	0.2	0.5	1
Base	NA	60		

The different properties assigned to each of these layers of the core sample (and the shear ring) will incorporate the material behaviour of each of these elements. The defined material properties for the FEM model elements are summarised in Section 4.2.4 where theoretical background of the different material behaviours is also provided.

**4.2.3.2 FEM theory**

The geometry of the part (the dimensions and thickness) is completed in the *Parts* module. The set-up of the parts is completed through the process demonstrated in Figure 4.2.3.2a. Different parts – deformable, rigid, Eulerian, electromagnetic and fluid parts – can be created, each with its own set of characteristics.

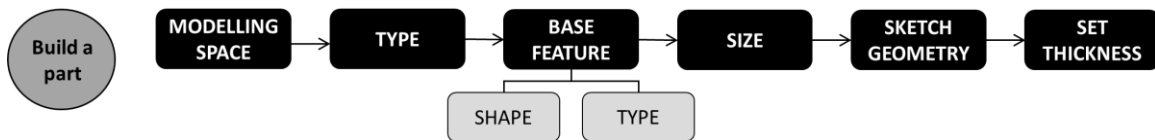


**Figure 4.2.3.2a:** Set-up of a part

The different parts created are constructed by means of a list of features while parameters are used to define the geometry of each feature (Figure 4.2.3.2b).

The model includes:

1. A *3D modelling space*
2. A *deformable* body (part type), because the model is subject to deform under loading conditions and;
3. Choosing a *solid extrusion*

The choice and selection of these features will be discussed in great detail in Appendix D1.

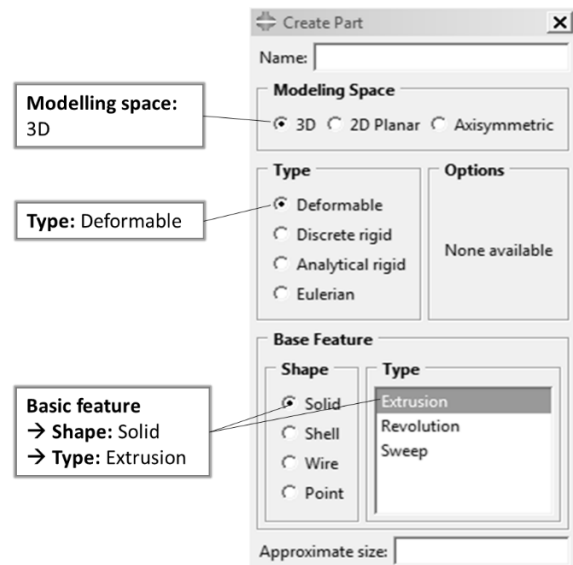


**Figure 4.2.3.2b:** Create Part (Abaqus Inc., 2017)

## 4.2.4 Properties

### 4.2.4.1 Introduction

In succession to the creation of the part, the material properties of each of the materials of the elements models are assigned. The definition of these properties is designated to the part created in The *Property* module. Distinction is made between the FEM replication and FEM theory, with reference to the two different types of material behaviour prominent in the model created. The different features used to define the material behaviour are illustrated in Figure 4.2.4.1a.

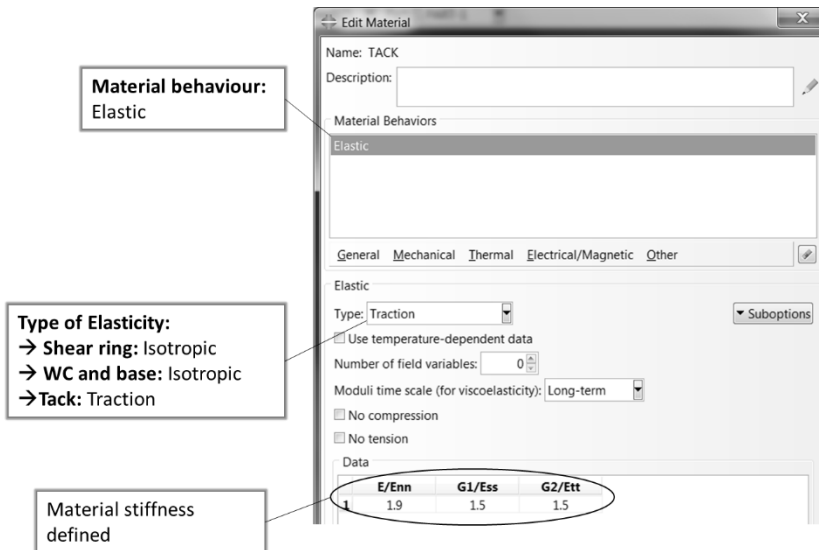


Figure 4.2.4.1a: Material property definition (Abaqus Inc., 2017)

For the entire assembly (shear ring and core sample), three different materials were defined. The core sample is composed of three layers: the wearing course (WC), the tack coat (TC) and the base layer. Given the function of the wearing course layer, it is assigned asphalt material as well as for the base layer, which was the surfacing layer of the existing pavement before the tack coat and wearing course were constructed on top of it. The tack coat comprises of bitumen emulsion and a steel shear ring is used in the Leutner testing device.

### 4.2.4.2 Elastic behaviour

The elasticity or elastic response of a material describes the ability of a material to resume its normal shape after deformation, i.e. being stretched or compressed when subjected to loading. Linear-elasticity is the simplest form of elasticity (Figure 4.2.4.1a) in the FEM software used. The linear-elastic model can define isotropic, orthotropic or anisotropic material behaviour for instances where small elastic strains are experienced. The total stress is defined through the total elastic strain (Equation 4.2.4.2a). In Equation 4.2.4.2a,  $\sigma$  represents the total stress and  $D$  is a fourth-order elasticity tensor. The strain parameter ( $\epsilon$ ) comprises of the total elastic strain.

$$\sigma = D \cdot \epsilon \quad (4.2.4.2a)$$

The classification of linear-elasticity of a material depends on the number of symmetry planes that exist to which elastic properties can be assigned. The behaviour is categorised as isotropic when an infinite number of symmetry planes pass through every point in the model. In contrast, anisotropic behaviour would describe a model where no symmetry planes exists. There are also instances where a restricted number of symmetry planes pass through every point in the model. This would describe orthotropic

behaviour – when a material has orthogonal symmetry planes for the elastic properties (Dassault Systèmes Simulia, 2014b). The number of independent components of the elasticity tensor D depends on such symmetry options.

**Isotropic**

The simplest form of linear-elasticity would be isotropic behaviour (for asphalt and steel materials used). The stress-strain relationship of such behaviour is given by Equation 4.2.4.2b. The elastic properties are defined by giving the Young’s Modulus of Elasticity (E) and the Poisson’s ratio (ν). From the definition, E is a well-known parameter which describes the stiffness of a material.

$$\begin{Bmatrix} \varepsilon_{11} \\ \varepsilon_{22} \\ \varepsilon_{33} \\ \gamma_{12} \\ \gamma_{13} \\ \gamma_{23} \end{Bmatrix} = \begin{bmatrix} 1/E & -\nu/E & -\nu/E & 0 & 0 & 0 \\ \nu/E & 1/E & \nu/E & 0 & 0 & 0 \\ -\nu/E & -\nu/E & 1/E & 0 & 0 & 0 \\ 0 & 0 & 0 & 1/G & 0 & 0 \\ 0 & 0 & 0 & 0 & 1/G & 0 \\ 0 & 0 & 0 & 0 & 0 & 1/G \end{bmatrix} \begin{Bmatrix} \sigma_{11} \\ \sigma_{22} \\ \sigma_{33} \\ \sigma_{12} \\ \sigma_{13} \\ \sigma_{23} \end{Bmatrix} \quad (4.2.4.2b)$$

Where:

- $\varepsilon_{ii}$  = Normal strains
- $\gamma_{ij}$  = Shear strains
- E = Young’s Modulus of Elasticity
- ν = Poisson’s ratio
- $\sigma_{ii}$  = Normal stresses
- $\sigma_{ij}$  = Shear stresses (also indicated as  $\tau_{ij}$ )

Poisson’s ratio is a ratio which describes the relation of horizontal deformation relative to vertical deformation of a material when subjected by an (axial) load (load P in Figure 4.2.4.2a). The estimation of Poisson’s ratio is illustrated by Equations 4.2.4.2c to 4.2.4.2e. The parameters used in these equations are illustrated in Figure 4.2.4.a assuming no confinement.

$$\varepsilon_L = \frac{\Delta L}{L} \quad (4.2.4.2c)$$

Where:

- $\varepsilon_L$  = Strain in longitudinal direction
- $\Delta L$  = Change in length
- L = (Original) length

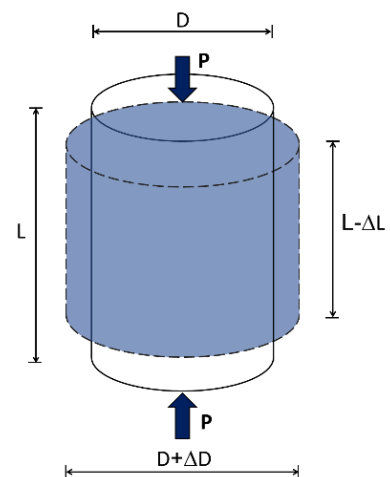


**Figure 4.2.4.2a: Poisson’s ratio**

Equation 4.2.4.2c describes the estimation of strain in the longitudinal (vertical) direction which is calculated as the ratio of the change in length (due to load P) relative to the length (original length) of the sample subjected to loading. Similar estimation is shown in Equation 4.2.4.2d relative to the diameter.

$$\varepsilon_D = \frac{\Delta D}{D} \quad (4.2.4.2d)$$

Where:

$\varepsilon_D$  = Strain in lateral direction (cross section)

$\Delta D$  = Change in diameter

D = Diameter

The ratio of Equation 4.2.4.2c (vertical strain) to Equation 4.2.4.2d (horizontal strain) results in Poisson's ratio (Equation 4.2.4.2e) as it satisfies the definition of the material parameter.

$$\nu = \frac{\varepsilon_D}{\varepsilon_L} \quad (4.2.4.2e)$$

The Shear Modulus (G), can be expressed in terms of E and  $\nu$  as shown in Equation 4.2.4.2f. These parameters can be given as functions of temperatures and other pre-defined fields, if necessary. The temperature component (for the bitumen emulsion) and displacement rate of the Leutner testing device are incorporated for the elasticity defined for the tack coat layer. Given the nature of the material used for the tack coat (Section 2.2) in the core sample, it is evident that the layer does not adhere to isotropic behaviour. Therefore, the layer is modelled as a cohesive element and complies with elasticity in terms of *traction and separation*. The constitutive response of cohesive elements using traction-separation is discussed comprehensively in Section 4.2.7, where the different element types are studied for the meshing of the model.

$$G = \frac{E}{2(1 + \nu)} \quad (4.2.4.2f)$$

Where:

G = Shear Modulus

According to Dassault Systèmes Simulia (2014b), stability criterion requires that E and G be greater than zero and that Poisson's ratio should range between -1 and 0.5, as Poisson ratio values approaching 0.5 result in nearly incompressible behaviour (rubber-like).

### ***Traction and Separation***

Cohesive elements (Section 4.2.7) are used to model bonded interfaces, such as tack coats, in the current model. Abaqus provides an elasticity definition that can be written directly in terms of the nominal tractions and nominal strains. The occurrence can be incorporated considering coupled and uncoupled behaviours. For uncoupled behaviour (core sample), each traction component depends only on its conjugate nominal strain (Dassault Systèmes Simulia, 2014b) as demonstrated by Equation 4.2.4.2g.

$$\begin{Bmatrix} t_n \\ t_s \\ t_t \end{Bmatrix} = \begin{bmatrix} E_{nn} & E_{nn} & E_{nn} \\ E_{nn} & E_{ss} & E_{nn} \\ E_{nn} & E_{nn} & E_{tt} \end{bmatrix} \begin{Bmatrix} \varepsilon_n \\ \varepsilon_s \\ \varepsilon_t \end{Bmatrix} \quad (4.2.4.2g)$$

Equation 4.2.4.2g shows the stress-strain relations for uncoupled behaviour in local element directions. The quantities  $t_n$ ,  $t_s$ , and  $t_t$  represent the nominal tractions in the normal and the local shear directions respectively whereas the  $\epsilon_n$ ,  $\epsilon_s$ , and  $\epsilon_t$  represent the corresponding nominal strains. Under these circumstances, the stability criterion of Abaqus, for uncoupled behaviour, requires that  $E_{nn}$ ,  $E_{ss}$  and  $E_{tt}$  are defined and be greater than up to this point.

**4.2.4.3 Material behaviour replicated in FEM model**

The previous section studied the different types of elastic behaviours relative to the FEM model created to replicate the Leutner Shear Test. The two types of elastic behaviour investigated were *isotropic* (linear-elastic) and *traction and separation* behaviour. In addition, it was shown that the two asphalt layers (the wearing course and base layer) and the steel shear ring comprise of isotropic behaviour. The tack coat, which bonds these two asphalt layers, acting as a type of “glue” between the respective layers, complies with traction and separation behaviour. These types of elastic behaviours are defined as shown in Figure 4.2.4.3a (similar to Figure 4.2.4.1a). The elastic behaviour in turn, forms the mechanical definition of the material property of a selected part.

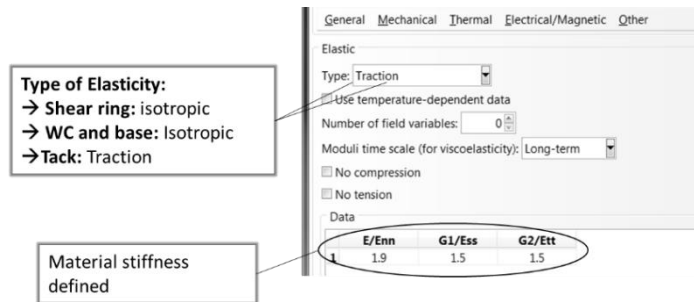


**Figure 4.2.4.3a:** Material property definition inputs (Abaqus Inc., 2017)

The different input parameters (material properties) for all of the different materials in the model are summarised in Tables 4.2.4.3a. In this table, the types of elastic behaviour are summarised according to the different parts, and the materials designated to each of these parts are also indicated in the table. It also provides information with regard to the material stiffness (E) and Poisson’s ratio (for isotropic behaviour only).

**Table 4.2.4.3a:** Elastic behaviour types for Model 1

Part/ Region	Material	Type	Stiffness (MPa)		Poisson ratio ( $\nu$ )
Shear ring	Steel	Elastic → Isotropic	2000		0.3
Wearing course	Asphalt	Elastic → Isotropic	2500		0.44
Tack coat	Bitumen emulsion	Elastic → Traction	0.21	2	NA
Base	Asphalt	Elastic → Isotropic	2500	1000	0.44

A variety of material stiffness for the base was considered as the modular ratio (MR) is a parameter which influences recorded shear stresses which should be investigated. The MR is the ratio of material stiffness of the upper layer relative to the lower layer. For this model, 2 MR values were defined i.e. 1 and 2.5 with a variance of base layer material stiffness of 1000 and 2500MPa respectively. The material stiffness for the wearing course layer is constant with a value of 2500MPa. These material properties are defined as shown in Figure 4.2.4.3a used for every material – wearing course, tack coat and the base layer. For the tack coat layer, material stiffness is define in three directions i.e.  $E_{ss}$ ,  $E_{tt}$  and  $E_{nn}$  (normal and parallel to the interface). The values were selected based on previous research and the same modulus value was defined for these three parameters.

4.2 Leutner Shear Test Method

Firstly, 1 MPa was selected as a typical stiffness value for bitumen emulsions used for the tack coat. The other stiffness modulus used for the tack coat was obtained from results acquired in research conducted by van Zyl (2018). The research titled *Bituminous Binder in South Africa and the Fatigue Performance* investigated age performance of bitumen binders. The master curve illustrated in Figure 4.2.4.3b, obtained from the research study, was used to estimate the stiffness modulus. This was achieved by converting the standard displacement rate of the Leutner Shear Test into an angular frequency, which can be used to read off the corresponding Complex Modulus (G) (as indicated in Figure 4.2.3.2b). Hereafter, the Complex Modulus is converted to a stiffness modulus as demonstrated in Equation 4.2.4.2f. Equation 4.2.4.3a shows the relation between the radius of the sample (r), the angular frequency ( $\omega$ ) and velocity (v).

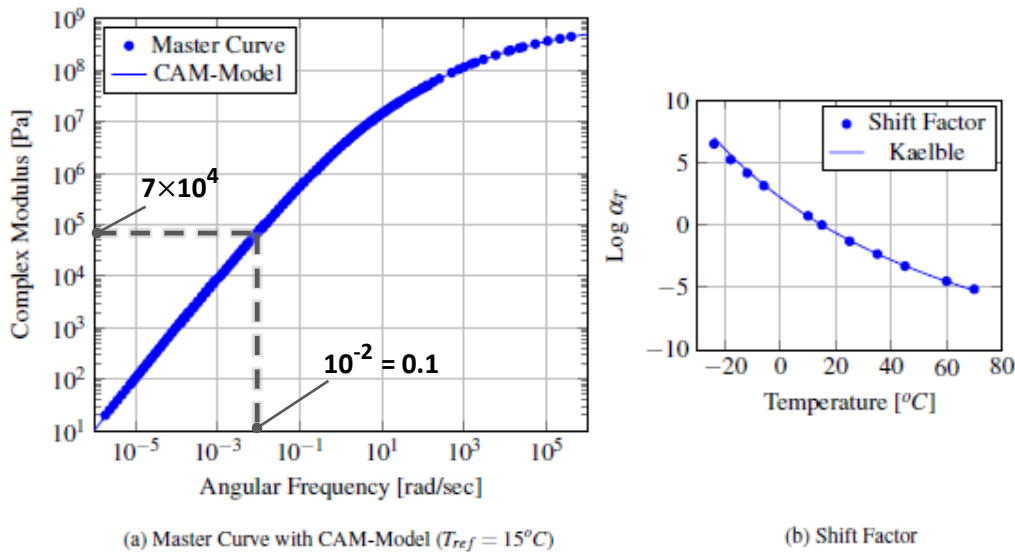


Figure 4.2.4.3b: Typical 50/70 SAPREF Unaged Binder (S. van Zyl, 2018)

$$v = r \times \omega \tag{4.2.4.3a}$$

The displacement rate of the Leutner test (50.8mm/min according to literature reviewed in Chapter 2) is converted to a velocity of  $8.47 \times 10^{-4}m/s$  to be used in the equation. The radius of the core sample amounts to 75mm (diameter of 150mm). The two estimates substituted in Equation 4.2.4.3a produce an angular velocity of approximately 0.01rad/s. Subsequently, the angular frequency is read off the horizontal axis from Figure 4.2.4.3b to the master curve, and then extends to the vertical axis to read off the corresponding Complex Stiffness. For this master curve, with an angular frequency of 0.01rad/s, a Complex Modulus of 70 000Pa (0.07MPa) is achieved.

Finally, the elastic modulus (E) of the material was obtained by substituting the acquired Complex Modulus (G) in Equation 4.2.4.2 with a Poisson ratio of 0.5 for bitumen emulsion. The nature of the equation shows the relation between the stiffness and the Complex Moduli as  $E = 3G$ . Consequently, the elastic modulus is 3 times the magnitude of the Complex Modulus, i.e. 0.21MPa. Hence, 0.21MPa was used as the second stiffness modulus of the tack coat layer (Table 4.2.4.3a).

4.2.4.4 Sections

Section assignment (Figure 4.2.4.4a) of the model uses the material properties defined previously in 4.2.4.3 which represented each material of the model. The model properties for each material is assigned to a specific section type (dependent of the type of element/ part used to define a specific

part) as shown in Figure 4.2.4.4b. Distinction was made between isotropic and traction behaviour. The material behaviour describes the differentiation between the tack coat layer in the model and the other components, i.e. the steel shear ring and the other two (asphalt) layers of the core sample. Because of its cohesive behaviour, the tack coat layer is assigned a *cohesive* type section while others are assigned a solid type section.

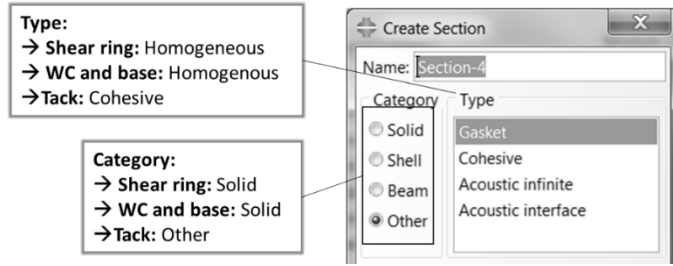


Figure 4.2.4.4a: Definition of section (Abaqus Inc., 2017)

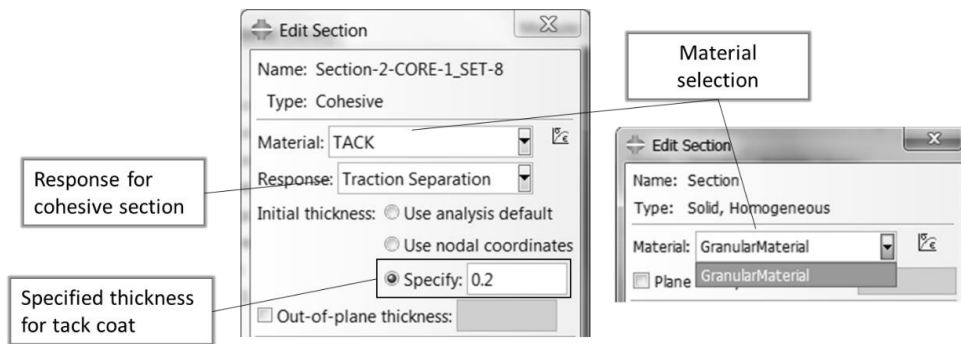


Figure 4.2.4.4b: Definition of section properties (Abaqus Inc., 2017)

For the different combinations considered (with reference to the two modular ratios), two different sections are assigned given the two different types of material properties defined. Where an MR of 1 was applied, the same section was assigned to the wearing course and base layer region of the model. For the increased MR of 2.5, an additional section was created with another asphalt defined material with a lower material stiffness (Figure 4.2.4.4c). Figure 4.2.4.4c shows a summary of the material properties is indicated. A figure with similar information is provided for the shear ring in Figure 4.2.4.4d. The regions of the respective part to which these defined properties (sections) have been assigned to, are also indicated in the respective figures.

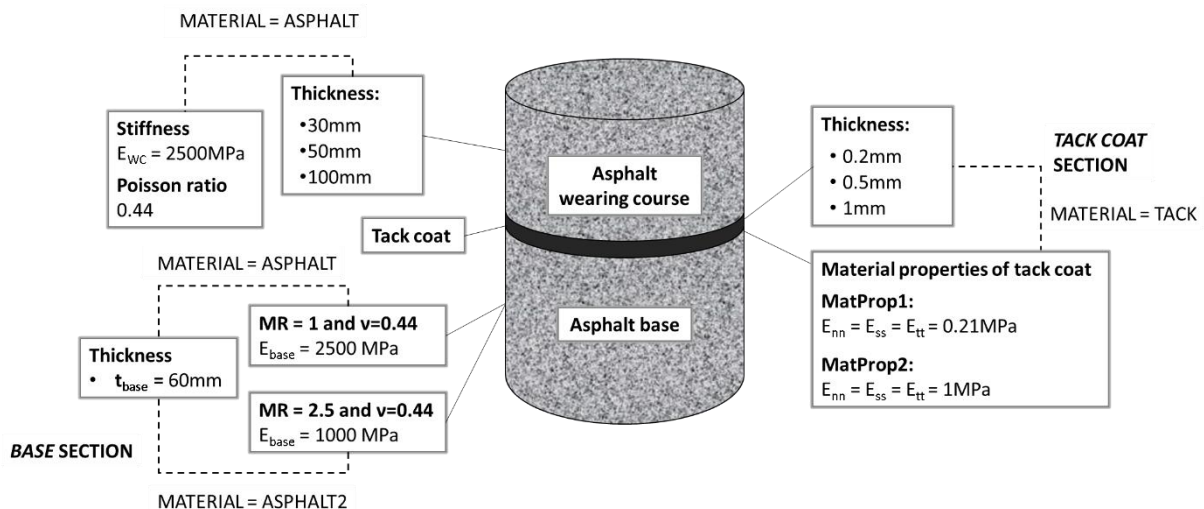
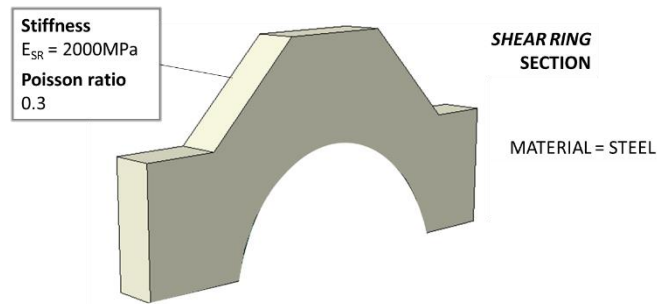


Figure 4.2.4.4c: Core sample properties



**Figure 4.2.4.4d:** Shear ring properties

Similar to part creation and material definition, a list of different features forms the section component of the model. The two features in this capacity are the *category* and the *type* relevant to the selected section category. The category and type of the different elements of the Leutner model are summarised in Table 4.2.4.4a. The relevant information is also demonstrated in Figure 4.2.4.4a and now this information is incorporated into the FEM software.

**Table 4.2.4.4a:** Section features of elements for Model 1

Part	Category	Type
Shear ring	Solid	Homogenous
Wearing course	Solid	Homogenous
Tack coat	Other	Cohesive
Base	Solid	Homogenous

### **Solid sections**

Solid sections define section properties of 3D solid regions, such as the two asphalt layers and the steel shear ring. The materials used for these regions are considered *homogenous* given that the material comprises of a uniform composition throughout, which cannot be separated mechanically into different material characteristics (Dassault Systèmes Simulia, 2014f). A material name is defined for each of the homogenous (solid) sections after which a material is assigned (Figures 4.2.4.4c and 4.2.4.4d).

### **Cohesive sections**

The modelling of bonded interfaces considers initial loading, the initiation of damage as well as the propagation of damage that eventually leads to failure at the bonded interface. The behaviour of the interface prior to damage initiation is described as linear-elastic in terms of a penalty stiffness that degrades under a combination of, or individual tensile and shear loading, but is unaffected by pure compression (Dassault Systèmes Simulia, 2014f). The cohesive sections are used to model finite thickness adhesives or negligibly thin adhesive layers for de-bonding applications.

Given the function of this layer, as well as the characteristics of the material used in these types of layers, it is evident that the section assigned to represent this section of the model does not comprise of homogenous behaviour. The region is classified as a cohesive type section. In the software used, cohesive sections (and elements) are considered special purpose elements and are categorised as *other* sections (Figure 4.2.4.4a). The features required for information of this type of section are shown in Figure 4.2.4.4b (left) and consist of the name of the section, the material response, initial thickness and out of plane thickness.

The response feature defines the constitutive behaviour of the cohesive section where three different types are available, i.e. traction separation, continuum and gasket. A *Traction Separation* response defines responses to model de-bonding, while a *continuum* response models a strain state involving direct and two transverse shear components, used to model a finite thickness adhesive layer. A *gasket* type response specifies a uniaxial stress state (Dassault Systèmes Simulia, 2016b). Mainly, two types of cohesive can be created in the FEM software – those with finite thickness, or cohesive elements with negligible thickness. The theory of the cohesive elements is explained comprehensively when addressing the meshing techniques used to divide the model into small, finite (integration) elements.

For the current model, the thickness of the region is specified to regions partitioned to represent the different layers of the core sample, as explained in 4.2.3.1 and illustrated in Figure 4.2.3.1d. However, *Traction Separation* response is used to describe the response of the tack coat section and the initial is set accordingly, depending on the thickness of the interlayer (tack coat) as partitioned in the part. The different thicknesses used to model the tack coat are 0.2mm, 0.5mm and 1mm respectively; thus, depending on the combination analysed, the initial thickness is set to 0.2mm, 0.5mm and 1mm (Figure 4.2.4.4c).

#### 4.2.5 Assembly

The respective parts have been created with the preferred geometry, after which the different material properties were assigned. With these characteristics assigned to the different regions of the different parts created within the model database, the different parts are assembled in the *Assembly* module of Abaqus. This, in turn, will form the part to which the different boundary conditions and loads will be assigned, followed by the meshing of the model in order to perform the analysis. The procedure up until this point is summarised in Figure 4.2.5a.

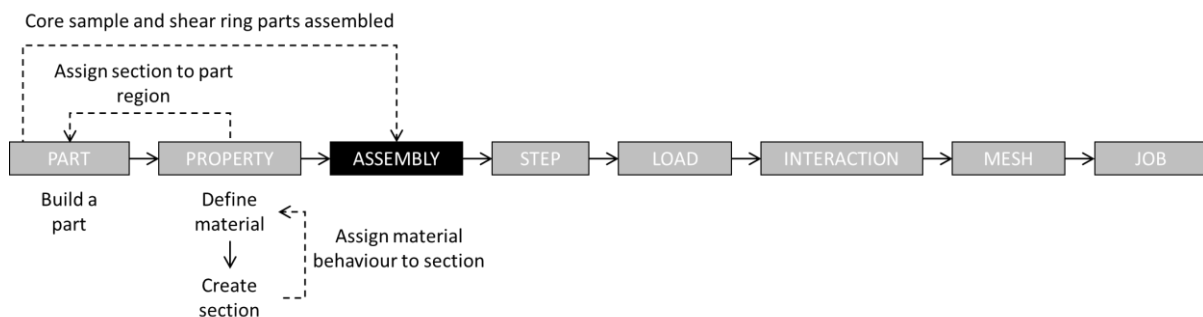
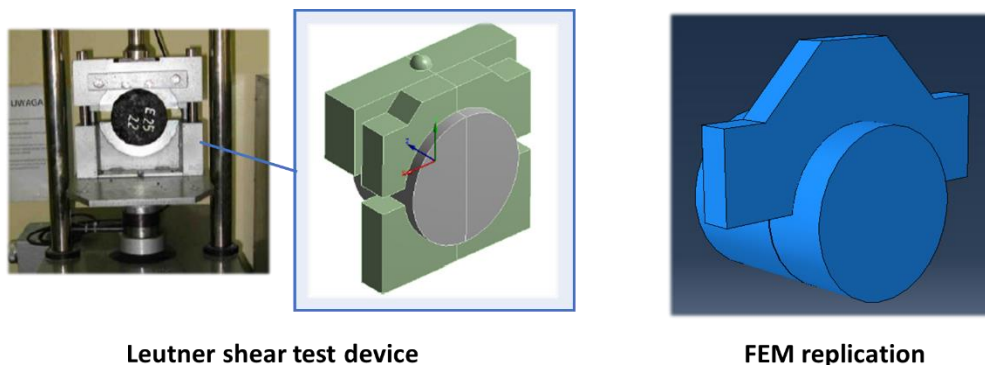


**Figure 4.2.5a:** Model set-up procedure for Model 1 – Assembly module

In Abaqus, a model contains only one main assembly, which is composed of part instances of the model (the shear ring part and core sample shown in Figures 4.2.4.4c and 4.2.4.4d). A part is originally created in its own coordinate system, which behaves in an independent manner in relation to the other parts of the model. The *Assembly* module creates instances of the parts which are then positioned or assembled in the global coordinate system to create an assembly of these parts (Dassault Systèmes Simulia, 2014f). Each of the part instances is translated (or rotated if needed) until selected faces, edges or vertices are aligned. The shear ring and core sample part instances were created after which they were translated to replicate the test set-up demonstrated in Figure 4.2.5b (left). The assembly of the FEM model is shown in Figure 4.2.5b (right).

## 4.2 Leutner Shear Test Method



Leutner shear test device

FEM replication

Figure 4.2.5b: Assembled model (After Malicki &amp; Górszczyk, 2012)

An instance maintains its association with the original part or model. Once the model is assembled, the *Interaction* and *Load* modules are used to complete the definition of the model. This is the part of the analysis setup where the boundary conditions and contact between different regions or parts are defined. Subsequently, the assembly is meshed according to the appropriate meshing technique, completing the model to be analysed. For an assembly, when a part instance is created, it can be created as either a dependent or independent part instance. When a dependent part instance is created, it references the original part meaning that the part instance shares with the geometry and mesh of the original part. An original part can be meshed, but not a (dependent) instance. When meshing is applied to such a part, the same mesh is applied to all dependent instances of the part. The advantages of dependent part instances are that they consume fewer memory resources and it is only required to mesh the part once (Dassault Systèmes Simulia, 2014f).

#### 4.2.6 Boundary conditions and constraints

##### 4.2.6.1 The Step module

According to Dassault Systèmes Simulia (2014a), an analysis is defined by dividing the problem into steps, specifying an analysis procedure for each step and prescribing loads and boundary conditions (4.2.6.2) for each step. A sequence of analysis steps is defined for the model created, which provides a convenient way to capture changes in the loading and boundary conditions of the model. The type of changes includes the interaction of different parts, removal of any additional parts or any other adjustment made to the model during the course of the analysis. The analysis software used distinguishes between two types of steps, i.e. the initial step (default) and analysis steps (user defined). The analysis steps are dependent on the condition of the analysis being performed. For the current analysis only one analysis step is used to define the different boundary conditions, which replicate the physical testing conditions of the Leutner test device.

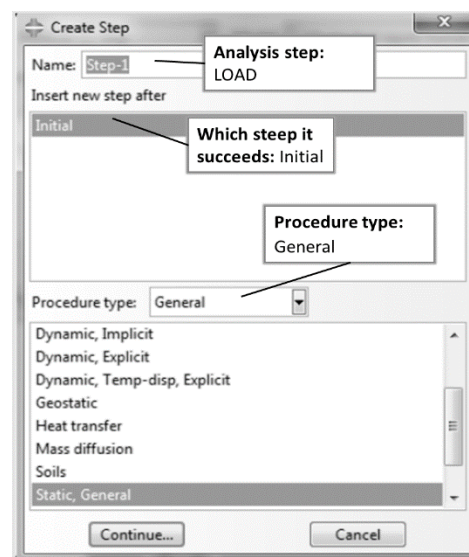


Figure 4.2.6.1a: Step Editor (Abaqus Inc., 2017)

**The initial step**

This step is created by default (Figure 4.2.6.1a) when a model is created in Abaqus. The step is created at the beginning of the step sequence of a model. Given the name of the step sequence, it describes the boundary conditions and interactions applicable at the beginning of the analysis. If a specific condition is applied throughout the analysis, i.e. boundary conditions and constraints, it is convenient to apply the conditions at this step for the analysis (Dassault Systèmes Simulia, 2016c).

**Analysis steps**

The analysis step succeeds the initial step and is associated with a specific procedure that defines the analysis type to be performed. The analysis procedure may be changed to give great flexibility in the analyses. The state of the model is updated throughout all general analysis steps (Dassault Systèmes Simulia, 2016c). Furthermore, the effects of previous history are always included in the response for each new analysis step.

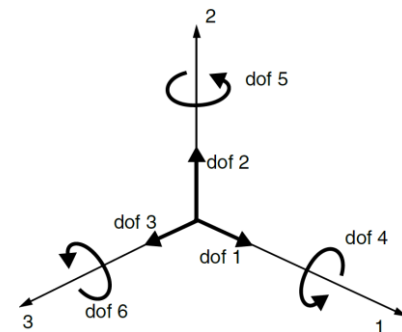
According to the description of the Leutner Test given in Chapter 2, the *Static, General* approach is considered suitable for the current analysis as indicated in Figure 4.2.6.1a. The differences between *General* and *Linear Perturbation* steps is further described in Appendix D2.

**4.2.6.2 Boundary conditions**

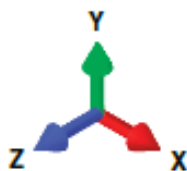
As mentioned, prescribed conditions are step-dependent objects for which analysis steps are specified (when active). A variety of components can be considered for this aspect of the model set-up. With an additional step defined for the analysis in 4.2.6.1, the prescribed conditions can be added to the model.

**Convention for prescribed conditions in Abaqus**

The boundary conditions (BCs) are applied to the regions of the model where displacements or rotations are known. These regions are constrained to remain “fixed” (no translation or rotation prohibited) during the simulation, or comprise of specified, nonzero displacements or rotations. The translation and rotation of elements of a model are described by its degrees of freedom (dof or DOF). The labelling convention used for the displacements and rotational degrees of freedom in Abaqus is illustrated in Figure 4.2.6.2a. The first three degrees of freedom (dof1 to dof3) represent translation in directions 1, 2 and 3, while the rotational degrees of freedom are represented by dof4 to dof6, as summarised in Table 4.2.6.2a. In addition, the number of the respective directions for the degrees of freedom demonstrated in Figure 4.2.6.2a coincides with the traditional directions of the global coordinate system used in Abaqus, represented by the triad shown in Figure 4.2.6.2b. The respective directions x, y and z can be linked with direction 1, 2 and 3 respectively (Table 4.2.6.2a). The translational and rotational degrees of freedom will be indicated according to the convention shown in Figure 4.2.6.2a, which imply motion of the part in the x, y or z-direction. The prescribed conditions are indicated by double-headed arrows (rotational) or three arrows (rotational and translation), as demonstrated in Figure 4.2.6.2c.



**Figure 4.2.6.2a:** Degrees of freedom (Dassault Systèmes Simulia, 2014e)

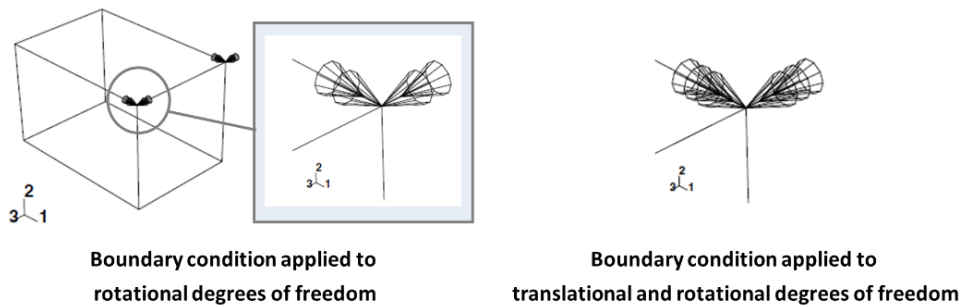


**Figure 4.2.6.2b:** FEM replication with reference points

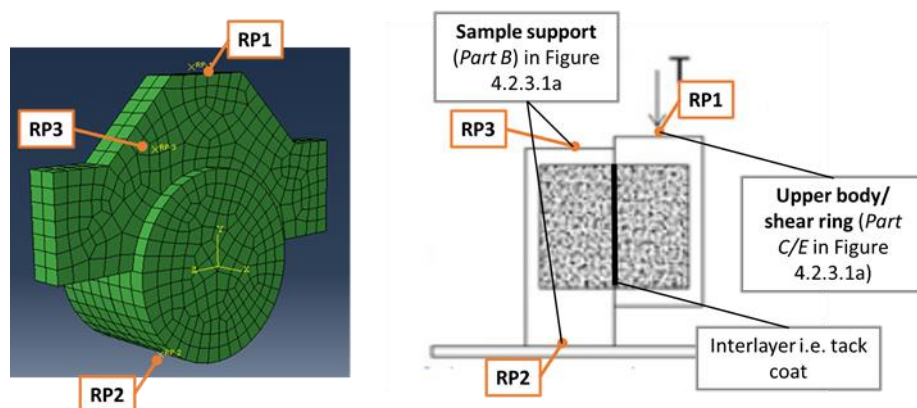
The respective directions x, y and z can be linked with direction 1, 2 and 3 respectively (Table 4.2.6.2a). The translational and rotational degrees of freedom will be indicated according to the convention shown in Figure 4.2.6.2a, which imply motion of the part in the x, y or z-direction. The prescribed conditions are indicated by double-headed arrows (rotational) or three arrows (rotational and translation), as demonstrated in Figure 4.2.6.2c.

**Table 4.2.6.2a:** Summary of degrees of freedom (Dassault Systèmes Simulia, 2014e)

DOF	Symbol	Axis	Direction
<b>Translation</b>	dof1	U1	X
	dof2	U2	Y
	dof3	U3	Z
<b>Rotation</b>	dof4	UR1	X
	dof5	UR2	Y
	dof6	UR3	Z

**Figure 4.2.6.2c:** Magnified view of arrows indicating degrees of freedom (After Dassault Systèmes Simulia, 2014f)**Model replication**

For the purpose of this model, boundary conditions are used to represent the functioning of the Leutner testing device. Critical locations are identified for the model and are referred to as reference points (RP). In context of the model set-up shown in Figure 4.2.6.2d (left), these two points in the model are constrained by acting as clamps, preventing any movement of the sample when displacement of the shear ring occurs. This type of behaviour of the model is added by means of constraints (4.2.6.3) as part of the *Interaction* module (BCs and constraints defined sequentially in the set-up of the model in Abaqus). However, to enable the configuration of these type constraints used (*tie* and *rigid*), the set-up of reference points was required.

**Figure 4.2.6.2d:** FEM replication with reference points (After Bianchi et al., 2018)

Given the nature of the testing device, three elementary points (*RP1* to *RP3*) were selected on the model, which represents three locations of motion relevant to testing conditions (Figure 4.2.6.2d). The last two points (*RP2* and *RP3*), represent the sample support of the test. The layer below the tack coat

i.e. the base layer, rests on this part represented by *RP2*. The shear displacement is applied for this layer through *RP3*, as indicated in Figure 4.2.6.2d. The first two points are “steady” and partially constrained in relation to *RP1* where displacement in the vertical direction is allowed. The load  $T$  is applied vertically at this point to move the shear ring downward in a vertical direction as demonstrated in the relative figure. The displacement of the shear ring enables the measurement of the interlayer bonding of the tack coat in terms of either shear stress or shear forces. The results obtained in this capacity will illustrate the effectiveness of the bonding. Given the nature of the analyses, different bonding conditions were also considered i.e. material properties and layer thickness (Section 4.2.4).

In comparison with the general procedure of the test as described in Chapter 2, some adjustments are made to the FEM replication to justify the comparison of the results acquired from the analysis:

1. The displacement rate of 50.8mm/min is not incorporated as a prescribed condition or in the step procedure of the model, but incorporated with the stiffness of the tack coat material as discussed per 4.2.4.3.
2. No damage parameter was selected; thus, the model does not measure shear (stress/ strength) at failure where the maximum shear is not necessarily measured.
3. The model does not measure (stress/ strength) at failure which is the point of maximum shear achieved
4. A constant displacement of 1mm is assumed for the shear ring to quantify the effect of the different testing conditions on results obtained for interlayer bonding. The displacement signifies the downward motion of the shear ring due to load  $T$ , as no loading conditions are specified for the model (correlates with the absence of damage component in the model).

A series of nodes is allocated to each of the three reference points. The nodes grouped for each of these reference points is more relevant for the discussion of the constraints of the model. Hence, an elaborative discussion is provided when the constraints of the model is discussed in 4.2.6.3. The motion of all of the nodes allocated to a reference point is controlled by the reference point itself. For this model three reference points were created to simulate the different motions of the different elements of the Leutner shear testing device. Given the behaviour of each of these elements, boundary conditions are assigned to these points, which describe the behaviour (restriction of motion in terms of displacement and rotation) of each of these points. As described in the discussion of the reference points, the boundary condition allocated to a specific reference point is representative of the motion of all of the nodes defined (group) for *RP1* to *RP3*. Alongside the configuration, shown in Figure 4.2.6.2c, the boundary conditions allocated to the Leutner model are illustrated in Figure 4.2.6.2e.

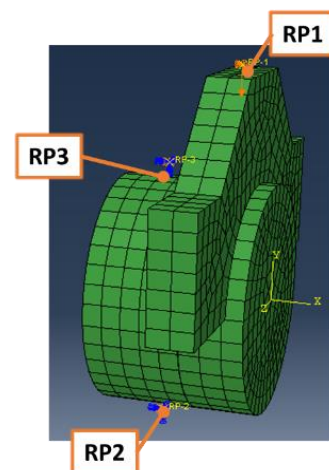


**Figure 4.2.6.2e:** Boundary conditions (Abaqus Inc., 2017)

Table 4.2.6.2b summarises the different boundary conditions shown in Figure 4.2.6.2e that are assigned to *RP1* to *RP3*. Information of summaries in this table include the region to which these points were allocated. A description of the physical model, which elucidates each of these boundary conditions, is also provided in the table. A brief illustration of the input needed is provided in Appendix D3.

**Table 4.2.6.2b:** Summary of boundary conditions

Part	Location	Boundary Condition	Description
RP1	top of steel shear ring	$U1 = U3 = 0, U2 = -1$	Only displacement in the vertical direction (U2) is permissible. Direction of displacement of the shear ring to measure the shear in the sample. A displacement of 1mm (in the negative vertical direction) was selected for the analysis.
			Displacement in the remaining direction is not permissible and is therefore constrained in these directions. Hence series of displacement and rotation relative to defined directions are set to 0.
RP2	bottom of core sample	$U1 = U2 = U3 = 0$ $UR1 = UR2 = UR3 = 0$	Point represents the sample support (Figure 4.2.3.1a) which support the sample, thus no displacement in vertical direction (U2) allowed. Displacement and rotation in all directions are not permissible and are therefore constrained in these directions. Hence, series of displacement and rotation relative to defined directions are set to 0.
RP3	top of core sample	$U1 = U3 = 0$ $UR1 = UR2 = UR3 = 0$	Displacement of the nodes (at this point) is allowed in the vertical direction (U2). The nodes are restrained from motion in the remaining direction and rotation is prohibited in all three directions (set to 0).

**4.2.6.3 Constraints**

All of the steps in the set-up process of the model completed are shown in Figure 4.2.6.3a. The focus of this section is placed on the *Interaction* module, where constrains of the model are defined.

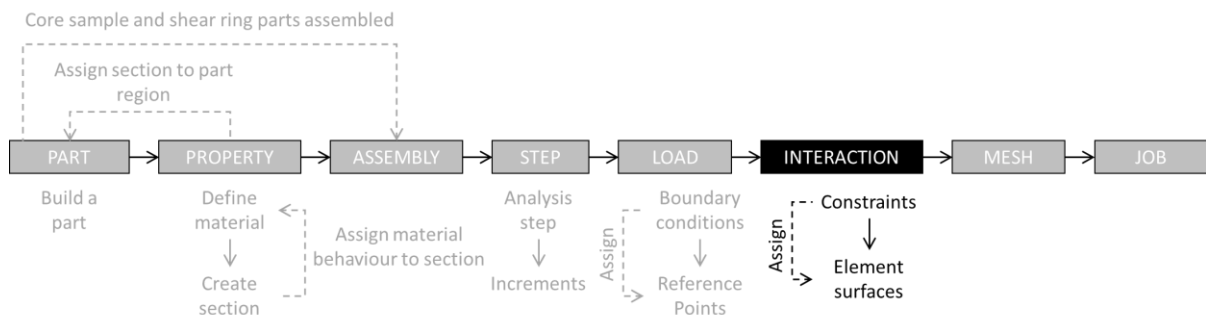


**Figure 4.2.6.3a:** Model set-up procedure for Model 1 –Interaction module

The constraints define the constrained degrees of freedom (dof) between regions of a model. There is a variety of constraint types to be used in ABAQUS, which includes *Tie*, *Rigid body*, and a variety of other options. Only the constraints relative to the current model will be discussed (Table 4.2.6.3a). A brief

theory of the appropriate constraints is provided, followed by an elaborative demonstration of its application in the FEM analysis software used to replicate physical behaviour of the Leutner Shear Test.

### **Tie constraints**

The tie constraint allows “merging” of two regions (Dassault Systèmes Simulia, 2014f) despite these regions being composed of different meshes (Section 4.2.7). This type of constraint is deemed appropriate for connecting the sample to the shear ring (Figure 4.2.6.3b), to produce harmonious movement in the vertical direction (z-direction) when the displacement boundary condition specified at RP1 becomes active during the analysis. In terms of the modelling, these two surfaces are classified as the *master* and *slave* surfaces.

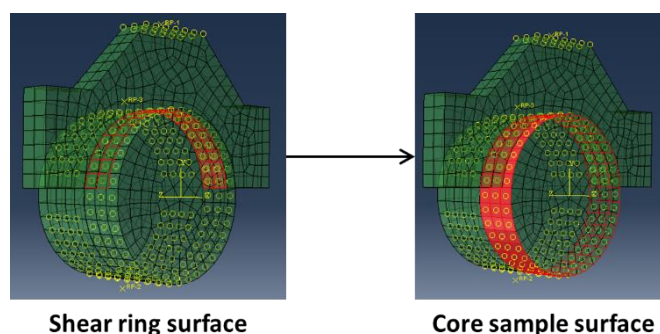


**Figure 4.2.6.3b:** Model set-up procedure –Interaction module (Abaqus Inc., 2017)

The type of tie constraint used is a surface-based tie constraint, which will enable both translational and rotational motion, as well as other active degrees of freedom equal for a pair of surfaces (Dassault Systèmes Simulia, 2014d). One surface in the constraint is designated to be the *slave* surface, whereas the other is the *master* surface. The functions (advantages) of the use of this type of constraint are listed, in accordance with Dassault Systèmes Simulia (2014d), as follows:

1. Ties two surfaces together for the duration of the simulation;
2. Can be used in mechanical and a variety of simulations;
3. It eliminates the degrees of freedom of the *slave* surface nodes that are constrained;
4. It allows for rapid transitions in mesh density within the model;
5. Each of the nodes on the *slave* surface is constrained to have the same motion as the point on the *master* surface to which it is closest;
6. It is useful for mesh refinement purposes in three-dimensional problems especially.

The surface-to surface formulation was used for the tie constraint which “links” the interacting areas of the shear ring and core sample surface shown in Figure 4.2.6.3b composed of master and slave nodes. A further discussion on the choice in *slave* and *master* nodes is provided in Appendix D3. It also includes a detailed description of the theory involved in selecting such nodes and how the constraints were defined for the Leutner model.

The tie constraint is added to the model by means of the constraint editor, where the type of constraint is selected (*Tie*) in order to proceed to the selection of regions to which these constraints are designated (Figure 4.2.6.3c). The *master* surface is selected first, followed by the *slave* surface. It should be noted that the selection of these surfaces could have an extensive impact on the accuracy of the solution acquired from the analysis. However, seeing that the *surface-to-surface* approach is used, the impact is found to be much less (Dassault Systèmes Simulia, 2014d).

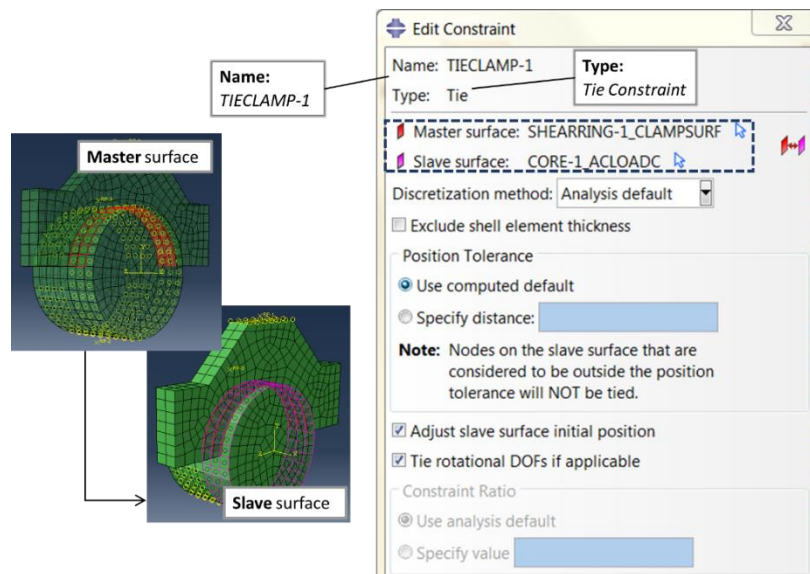


**Figure 4.2.6.3c:** Tie constraint between shear ring and core sample (Abaqus Inc., 2017)

If both the surfaces involved in the constraint are deformable surfaces, the *master* surface should be selected as the surface with the coarser mesh, for best accuracy. The meshing techniques used, and the element types assigned, are covered in the *Mesh* module, which is addressed in the subsequent section. The *master* surface is assigned to the region of the steel ring, which corresponds to the part of the core sample covered by the shear ring (red surface indicated in Figures 4.2.6.3b and 4.2.6.3c (left)). Furthermore, the *slave* surface associated with this *master* surface is assigned to the top layer of the core sample indicated by the purple region in Figure 4.2.6.3c. The other features of the tie constraint are selected as indicated in the tie constraint editor shown in Figure 4.2.6.3c (right). The surfaces used are defined individually, where specific nodes or elements are grouped together so that, when the constraints are created, these surfaces can be selected as the *master* or *slave* surface.

### **Rigid body constraint**

A rigid body constraint allows the ability to constrain the motion of regions of the assembly to the motion of a reference point (Dassault Systèmes Simulia, 2014f). The relative positions of the regions that are part of the rigid body remain constant throughout the analysis. The rigid body constraint is created by specifying the regions that are included within the rigid body for the three specified reference points, *RP1*, *RP2* and *RP3* (Figure 4.2.6.2d). The nodes associated with each of these reference points are created as node sets, where a series of nodes is grouped together to a central reference point, where a single type of motion behaviour is described for all of these nodes. The different node sets created for each reference point located on the FEM model is presented in Figure 4.2.6.3d. The creation of constraints are further described in Appendix D4.

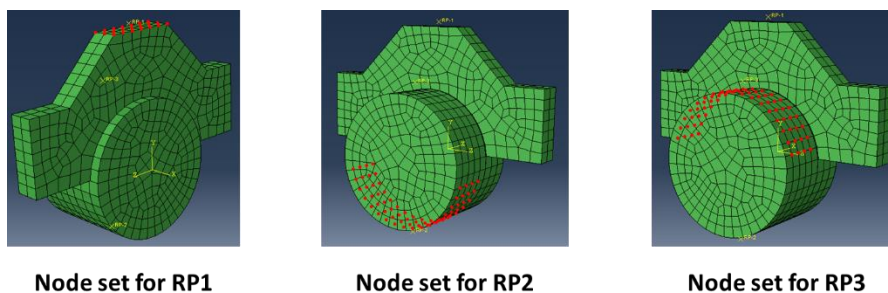


**Figure 4.2.6.3d:** Tie constraint between shear ring and core sample (Abaqus Inc., 2017)

After the selection of the region type, the regions shown in Figure 4.2.6.3d respectively are assigned to each of the rigid body constraints as indicated in the figure. This procedure completes the constraint set-up for the *Interaction* module. A summary of all of the constraint attributes (similar to summary provided for the boundary conditions in Table 4.2.6.2b) is provided in Table 4.2.6.3a accordingly. Here, the names designated to the different constraints and the various locations are also indicated. An illustration of these constraints is also provided in Figure 4.2.6.3e.

**Table 4.2.6.3a:** Definition of rigid point constraints at reference points

Location	Name	Region type	Model region
RP1	LoadPoint	Tie (nodes)	top of steel shear ring
RP2	TieACbot	Tie (nodes)	bottom of core sample
RP3	TieACtop	Tie (nodes)	top of core sample

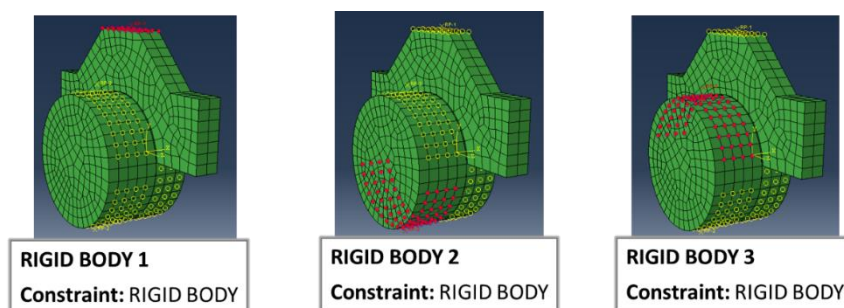


**Figure 4.2.6.3e:** Rigid body constraints at reference points (Abaqus Inc., 2017)

## 4.2.7 Meshing Techniques and Element Types

### 4.2.7.1 The Mesh module

The *Mesh* module is the final module used for the set-up of the model (by means of previous modules) to divide into finite elements for to serve as analysis points within the model (Refer to Figure 4.2.7.1a).

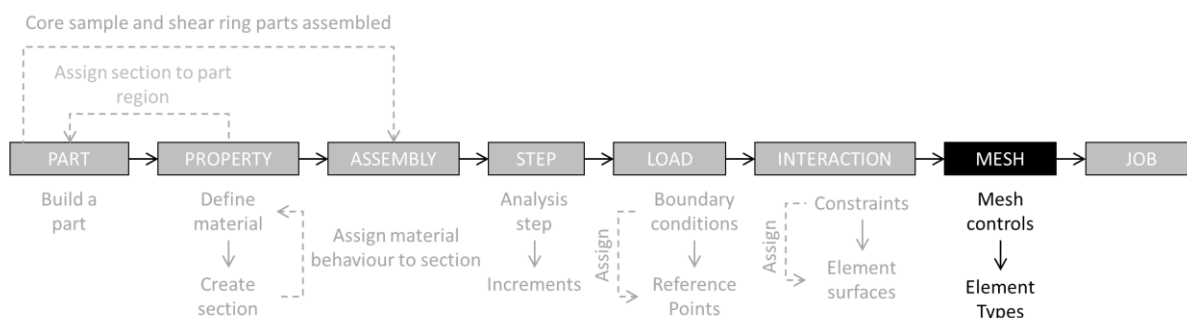


**Figure 4.2.7.1a:** Model set-up procedure for Model 1 –Mesh module

### 4.2.7.2 Basic components of the meshing module

The *Mesh* module provides the opportunity to generate meshes on the created assembly within Abaqus. Various levels of automation and control are available to produce a mesh complying with the required needs of the current analysis. Similar to the previous modules, the designation of mesh attributes to the model is feature-based, addressing information such as seeding, meshing techniques, and element types. The model is not subjected to seeding; therefore, the subject matter is not discussed in this section. Overall, the *Mesh* module provides features, including tools, to prescribe mesh density, a

variety of mesh controls and model colouring, which indicates the meshing technique assigned to the relative model region, to name a few. A demonstration of the meshing process is given in Figure 4.7.2.7a.



Figure 4.2.7.2a: Mesh process

The different steps of the meshing process are summarised according to the following listed attributes:

1. *Assign mesh attributes and set mesh controls* – Variety of tools used to specify different mesh characteristics such as mesh density, element shape and element type.
2. *Mesh generation* – Various techniques used to generate meshes. The different techniques provide different levels of control over the mesh.
3. *Mesh refinement* – Tools used to refine the mesh include seeding, model partition into simpler sub-regions, virtual topology and mesh adjustments.
4. *Mesh optimization* – Re-meshing rules are assigned to model regions which enables successive mesh refinement where each refinement is based on analysis results.
5. *Mesh verification* – Information is provided concerning the quality of elements used in the mesh.

Section 4.2.7 mainly focuses on the meshing techniques used and the element types allocated to the different regions of the model (Steps 1 to 2 listed and first three parts shown in Figure 4.2.7.2a). Reference can be made to Dassault Systèmes Simulia, (2014f) for a comprehensive explanation of the different features and capabilities of this Abaqus module.

### Mesh attributes and controls

The shape of the mesh elements can be selected as shown in Figure 4.2.7.2b, which illustrates two types of meshes. Figure 4.2.7.2b (left) shows a model which has been meshed with quadrilateral elements (Table 4.2.7.2d). In addition, Figure 4.2.7.2b (right) shows the same model meshed with triangular elements (Table 4.2.7.2d). Three different meshing techniques can be assigned i.e. free, structure or swept, and where applicable, a meshing algorithm can be selected.

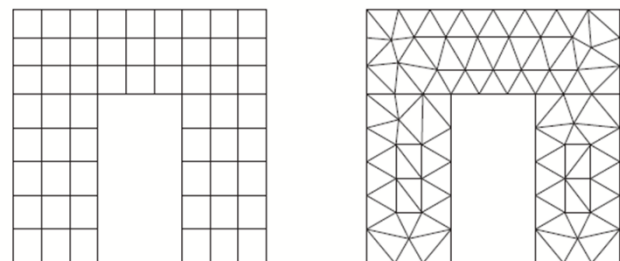


Figure 4.2.7.2b: Two meshes with different element shapes (Dassault Systèmes Simulia, 2014f)

### Mesh generation

There is a variety of meshing techniques used in Abaqus to mesh models. In some instances, the techniques used are selected, based upon its validation to a model composed of a certain topology. Otherwise, the technique used to mesh a model can be defined. These different meshing techniques provide a variety of automation levels and user controls (Dassault Systèmes Simulia, 2014f). There are two main types of meshing techniques – *top-down* and *bottom-up* each with their own conditions (illustrated in Figure 4.2.7.2c).

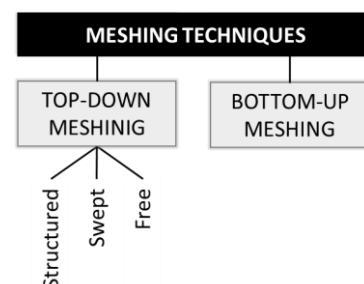


Figure 4.2.7.2c: Meshing techniques

In the current model, the *Bottom-up* meshing and *Sweep* meshing technique was used because of the technique's definition and its relation to the model conditions. In Appendix D4, a summary of the different meshes is provided. The type of meshing is dependent on the type of element used and some technique's require that successive regions are assigned the same technique i.e. the cohesive layer and the base layer. A full description of the various element types are also provided in Appendix D4. In the current study, *Hex* elements were used to generate a finer mesh.

#### 4.2.7.3 FEM model mesh controls

The *Mesh Controls* dialog box (Figure 4.2.7.3a) allows the specification of element shapes as well as the meshing technique used to generate the mesh. Given that the FEM model consists of series of regions, the mesh controls are assigned individually to each of these regions. An overview of the different meshing techniques was provided in Appendix D4. The techniques applied for the specific regions of the FEM model configured from Section 4.2.3, will be discussed in this section. This section also covered the different element types and shapes. The first feature set in the mesh control is the element shape (Table D4 in Appendix D4).

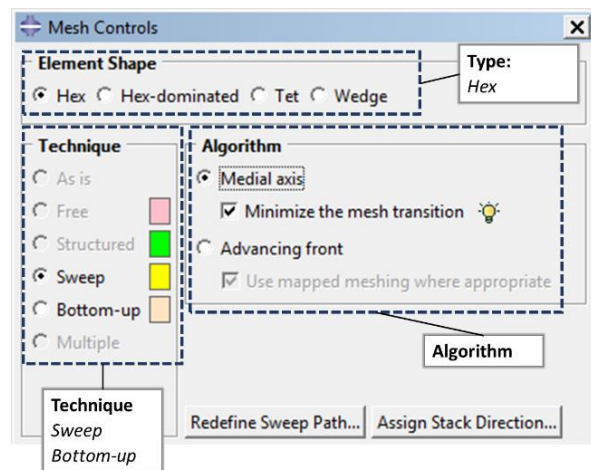


Figure 4.2.7.3a: Mesh controls dialog box (Abaqus Inc., 2017)

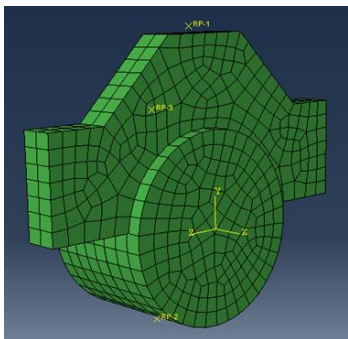


Figure 4.2.7.3b: Hex shaped elements (Abaqus Inc., 2017)

For the entire model (core sample and steel shear ring), *hex* element shapes were selected to produce a fine mesh for the geometry of the two-part instances. The element shapes applied were favoured as it is found that these elements would provide an even distribution of elements relative to the geometry of the model, as illustrated in Figure 4.2.7.3b. The meshing technique selected will determine which of the element shapes listed in Appendix D4 can be applied in a desired region of the model. Concerning the meshing techniques, two of the techniques introduced in Appendix D4 are used for the replicated model of the Leutner testing device: *sweep* and *bottom-up* meshing. The base layer and the tack coat comprise of *bottom-up* meshing where the *sweep* mesh technique is applied to the remaining regions. As demonstrated in Table D1, Abaqus uses different colours to indicate which meshing technique is assigned to a particular region. Given the code provided in this table, the techniques are illustrated in these colours as shown in Figure 4.2.7.3c (steel shear excluded from figure, but is also yellow). The description of the application of these two meshing techniques is also given in Appendix D4.

For the entire model (core sample and steel shear ring), *hex* element shapes were selected to produce a fine mesh for the geometry of the two-part instances. The element shapes applied were favoured as it is found that these elements would provide an even distribution of elements relative to the geometry of the model, as illustrated in Figure 4.2.7.3b. The meshing technique selected will determine which of the element shapes listed in Appendix D4 can be applied in a desired region of the model. Concerning the meshing techniques, two of the techniques introduced in Appendix D4 are used for the replicated model of the Leutner testing device: *sweep* and *bottom-up* meshing. The base layer and the tack coat comprise of *bottom-up* meshing where the *sweep* mesh technique is applied to the remaining regions. As demonstrated in Table D1, Abaqus uses different colours to indicate which meshing technique is assigned to a particular region. Given the code provided in this table, the techniques are illustrated in these colours as shown in Figure 4.2.7.3c (steel shear excluded from figure, but is also yellow). The description of the application of these two meshing techniques is also given in Appendix D4.

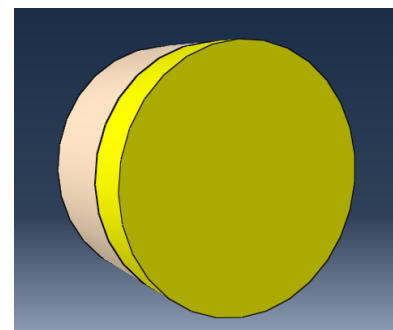


Figure 4.2.7.3c: Meshing techniques (Abaqus Inc., 2017)

#### 4.2.7.4 FEM model element types

Fundamental information for element type definition of the Leutner Model is as follows:

1. Element library – *Standard (Linear-elastic)*;
2. Family
  - Shear ring: *3D Stress*
  - Wearing course and base: *3D Stress*
  - Tack: *Cohesive*
3. Element Type – *Hexahedral (Hex) elements*;
4. Integration – *Reduced Integration* ;

The element types are assigned to the associated model region as listed. A detailed description of assigning these components is covered in Appendix D5.

#### 4.2.8 Analysis

The set-up of the model was discussed in Sections 4.2.2 to 4.2.7 relative to the different modules responsible for adding the various components that represent the physical characteristics of the Leutner test (Figure 4.2.8a). The replication in Abaqus (compared to the actual test set-up) was discussed in line with the theory background used in this capacity. With the completion of the set-up, preferred analyses can be performed with the model. The completion is enabled in the *Job* module (Figure 4.2.8a).

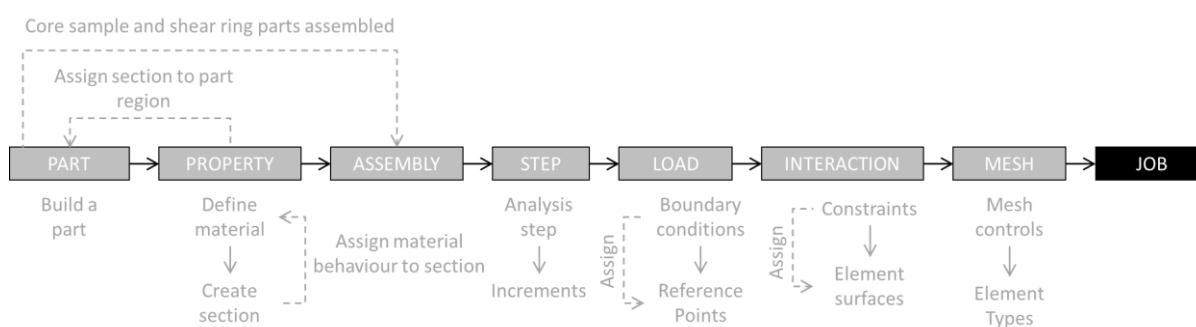


Figure 4.2.8a: Model set-up procedure – Job module

The well-known editing dialog box (Figure 4.2.8b) used for the other modules, is also used to create a “job” where the settings for the analysis can be completed. The job editor contains five tabbed pages: *Submission*, *General*, *Memory*, *Parallelization* and *Precision*. For the purpose of this analysis, only the *Submission* tabbed page is of interest. The relevance depends on the different characteristics of the analysis, i.e. whether Abaqus Standard or Explicit was used to conduct the analysis.

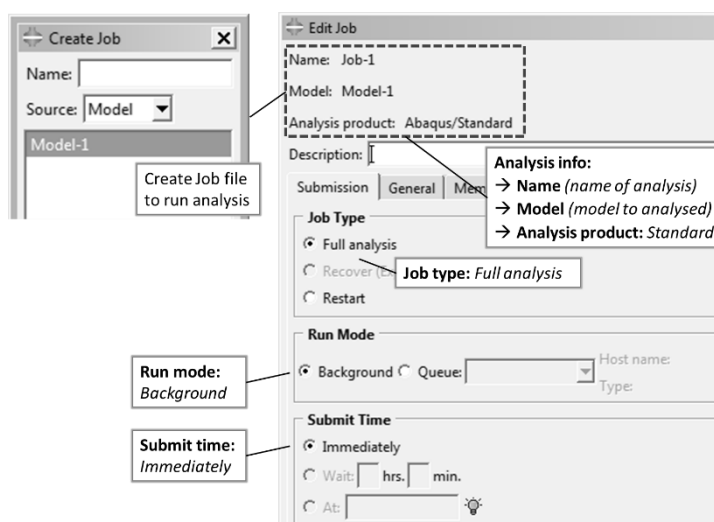
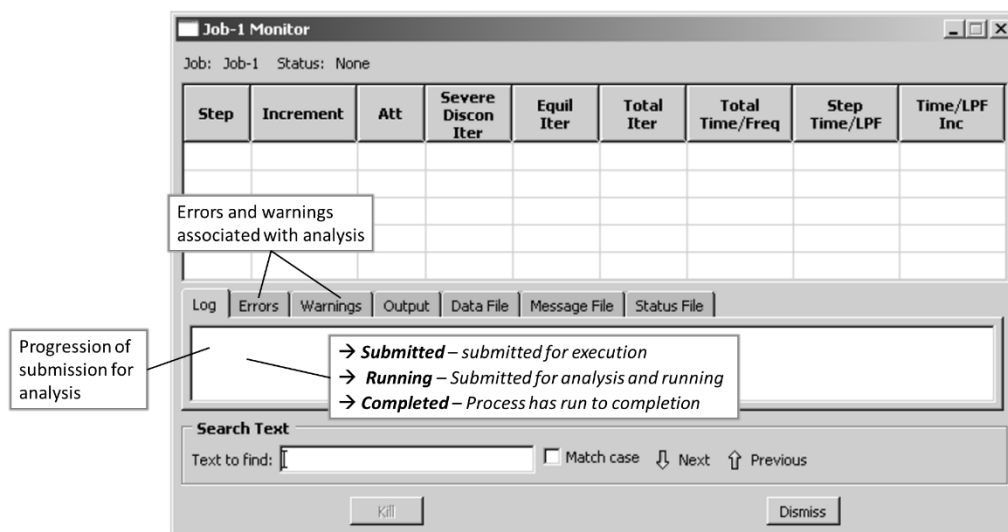


Figure 4.2.8b: Dialog box for job definition (Abaqus Inc., 2017)

The *Submission* tab is used to configure the different submission attributes of the “job” i.e. the job type, run mode and submission time. Only one analysis is performed and, therefore, to use the *queue* run mode is inappropriate. The job type used (*full analysis*) is selected, because a complete analysis is performed for the created model while generating the analysis information to an input file, subsequently writing results to the output database. The other options are used in Abaqus Explicit (*Recover*) or when data from a previous analysis is used for a specific model (*Restart*). Once the configuration of the job module is complete and the necessary information entered, the job file is submitted for analysis. During the submission, Abaqus carries out a series of validations of all the different components of the model (job monitor shown in Figure 4.2.8c). This shows the mathematics part of the analysis. It indicates the increments and different time steps which were defined in the *Incrementation* tab in the *Step* module where the analysis step was defined.



**Figure 4.2.8c:** Job monitor (Abaqus Inc., 2017)

Figure 4.2.8c will indicate any warnings or errors that might have been found during the analysis submission. If a particular region of a model is causing the error or warning in question, a node or element set will be created containing this region. This will not necessarily prevent the completion of the analysis. Conversely, in critical circumstances, i.e. where sections were not defined or defined incorrectly, Abaqus will experience convergence issues. The type of behaviour can be attributed to a variety of factors of which the main one would be concerning the increment sizes and boundaries set-up for the particular analysis (during the *Step* module). If no problem arises, the submission is completed, and the preferred results can be obtained accordingly. The results (data) can be acquired through the *Visualisation module* where illustrative representations of results can also be obtained accordingly.

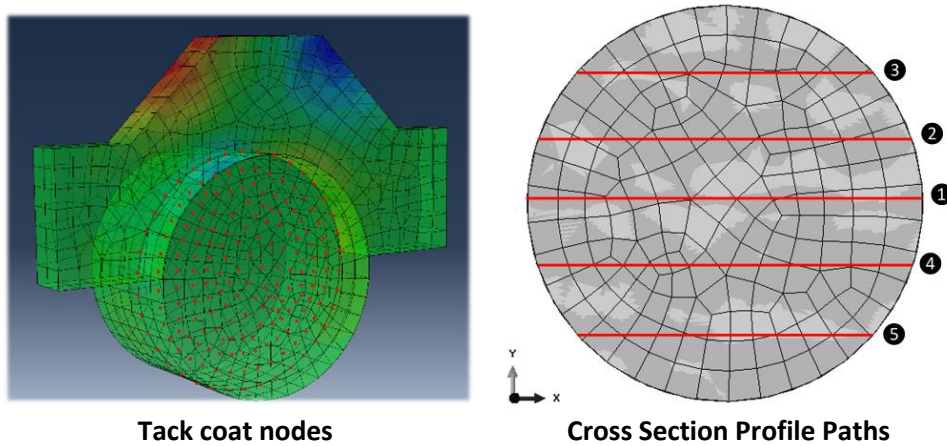
#### 4.2.9 Acquisition of results

A variety of outputs exists in Abaqus, viz. stresses (principal and such as Von Mises), displacements, reaction forces to name a few, and can be obtained from the analysed model. The objective of the research has been emphasised through the preliminary research as well as the analyses performed for this part of the research, i.e. interlayer bonding. The critical parameter, which relates to this occurrence, would be the amount shear component. It represents the shear in the tack coat layer relative to the other pavement layers which it bonds together, in essence gluing the wearing course and base layer

4.2 Leutner Shear Test Method

together. In other words, it describes the extent of bonding (adhesiveness) provided by the tack coat to the other layers.

Two approaches are used to study the effect of interface bonding. Firstly, maximum shear stresses are measured at the nodes in the tack coat layer as indicated in Figure 4.2.9a (left). Each of the set of results consists of 376 to 384 nodes. Furthermore, the shear stress profile over the cross section of the tack coat is studied to illustrate shear stress distribution over the cross sectional area of the sample. These results were selected across 5 paths on the cross sectional area spaced at 25mm from the centre as shown in Figure 4.2.9a (right). It should be noted the shear stress profile is for illustration only. Hence only one model's results are used.



**Tack coat nodes** **Cross Section Profile Paths**  
**Figure 4.2.9a:** Acquired result locations (Abaqus Inc., 2017)

For obtaining results in this model, *ODB field output* option and *Path* is used to acquire XY-data (Figure 4.2.9b). First-mentioned is used for the maximum shear stresses measured at nodes in the tack coat layer shown in Figure 4.2.9a (left). The *Path* option is used for results demonstrated in Figure 4.2.9a (right). The shear stress results are obtained at the last time step (of three seconds specified in the *Step* module). This is where maximum shear stress (S23) will be achieved in the analysis (set in *Primary Variable* tab shown in Figure 4.2.9b). This method is used to obtain shear, relative to time, from the odb (output database) and for which elements (sets) to read the data (*Deformed variable* tab is used for this setting) are needed. The results were recorded at these desired locations for all 36 combinations analysed.

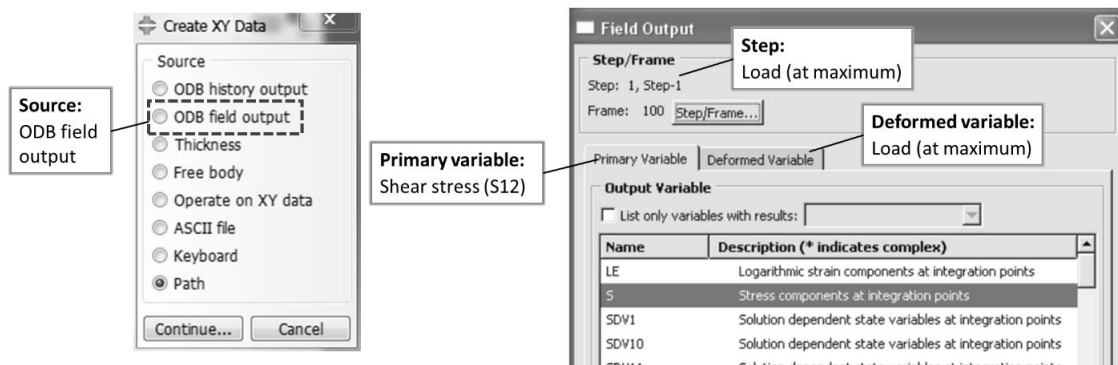


**Figure 4.2.9b:** Results acquired at Model 1 locations (Abaqus Inc., 2017)

A visual representation of the shear stress distribution (S23) obtained for one of the combinations tested, is given in Figure 4.2.9c. The example provided in this figure comprises of the following listed attributes:

1. Wearing course thickness ( $t_{TC}$ ) of 30mm;
2. Tack coat layer thickness ( $t_{TC}$ ) of 0.5mm;
3. Modular ratio (MR) of 2.5;
4. Tack coat stiffness ( $E_{TC}$ ) of 1MPa.

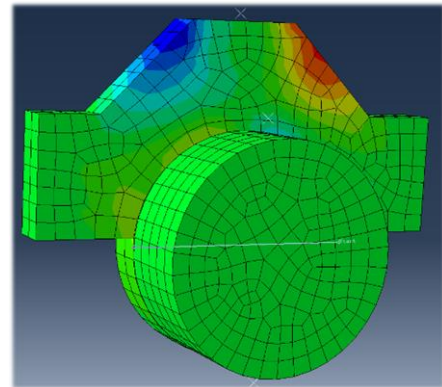
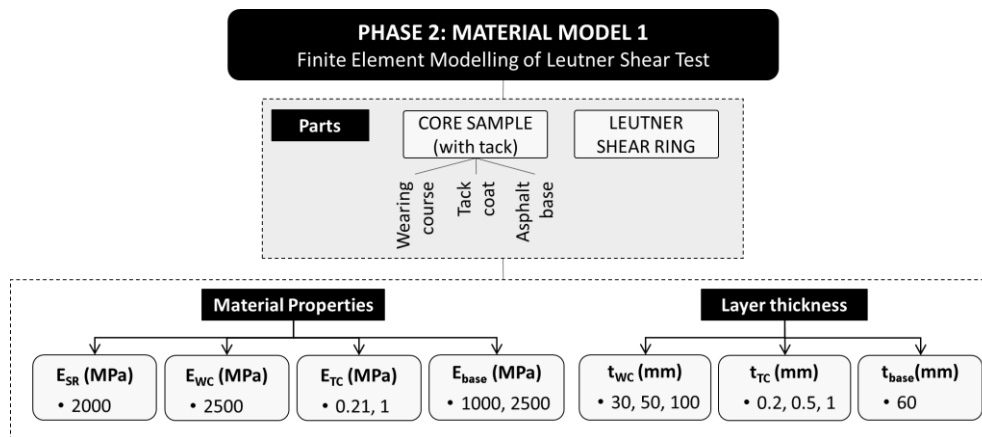


**Figure 4.2.9c:** Shear stresses (Abaqus Inc., 2017)

The results compiled from the different combinations analyses are discussed and interpreted in Chapter 5, subsequent to the discussion with regard to the set-up of the second material. This was used to analyse stresses and strains at critical locations within selected pavement structures.

#### 4.2.10 Synthesis of analysis

Figure 4.2.10a demonstrates the experimental plan with the different variables incorporated into the analysis of the Leutner test modelled. Combining all of the different material properties and geometries properties defined for the respective layers of the core sample, a total of 36 combinations was analysed.



**Note:**  $t_{WC}$  = Wearing course thickness,  $t_{TC}$  = Tack coat thickness and  $t_{base}$  = base layer thickness as given per Table 4.2.3.1a,  $E_{SR}$  = Shear ring stiffness,  $E_{WC}$  = Wearing course stiffness and  $E_{TC}$  = Tack coat stiffness as given per Table 4.2.4.3a

**Figure 4.2.10a:** Experimental plan for Model 1

The set-up of the model was achieved through different steps, where different components were added to replicate the different elements of the Leutner shear testing device. Different modules of the Abaqus software were used to implement these changes to the model. This resulted in analyses which can be used to compare the effect each of these parameters has on the bonding stresses reached in the tack coat layer. The key procedures adhered to for the set-up of this model are summarised according to each module in the set-up procedure presented in Figure 4.2.10b. For the set-up of the second material model (for the pavement analysis conducted during preliminary research as discussed in Chapter 3, Section 3.2) similar procedures are adhered to. The content of the set-up of the second model is covered in Section 4.3.

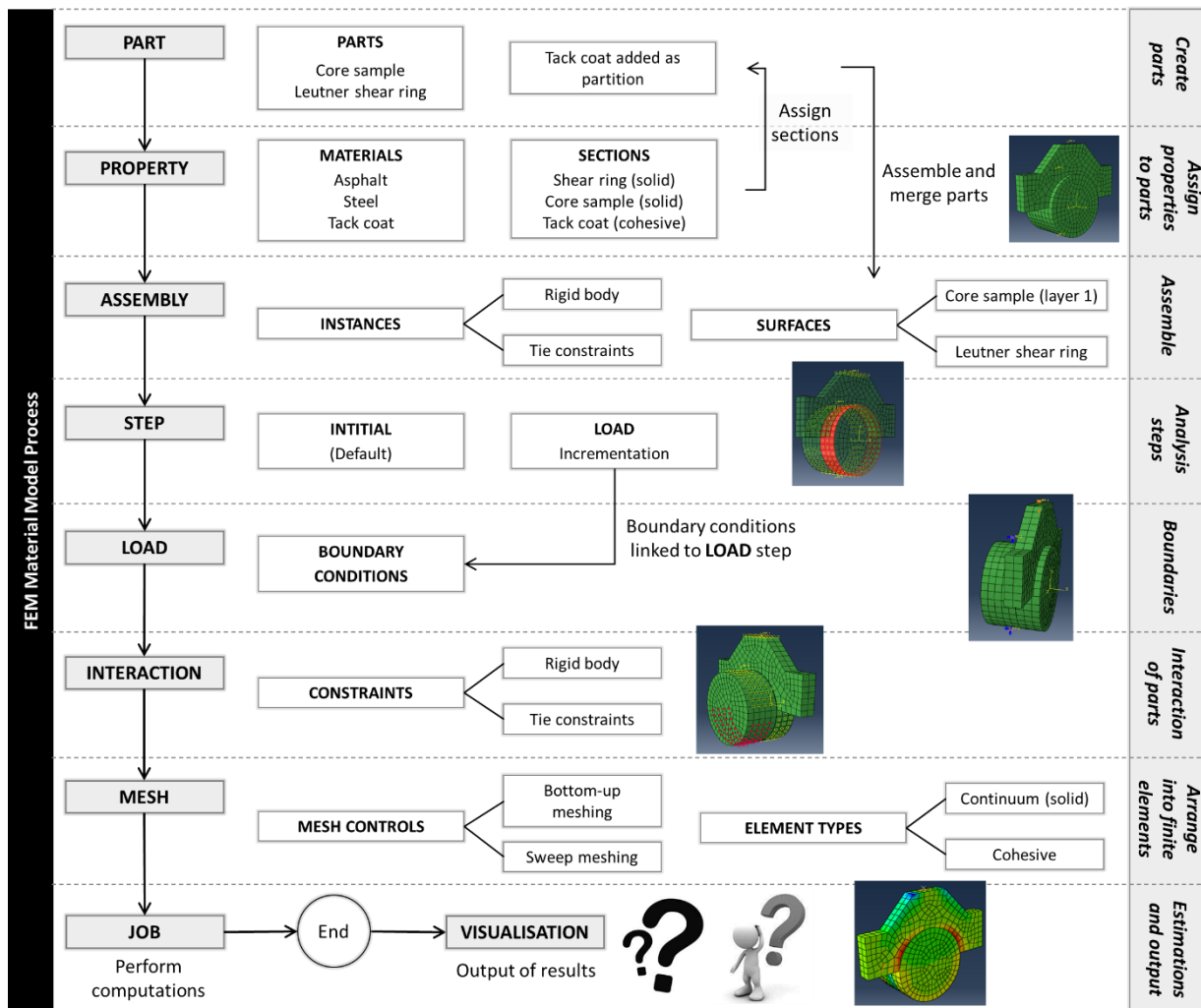


Figure 4.2.10b: Phase 2: Experimental plan for Model 1

### 4.3 Pavement analysis

#### 4.3.1 Introduction

A pavement is a structure which separates the tyres of vehicles from the underlying foundation material (Croney & Croney, 1998). Pavements are a composition of a multilayer construction of weak materials placed at the lower levels (starting from the subgrade) and progressively stronger in the above layers. Flexible pavements consist of three main layers, the bituminous surfacing, a base layer and a subbase. The weak(est) material, the soil immediately below the subbase, is the subgrade layer.

The surface of the subgrade layer is also referred to as the formation level of the pavement structure. The functionality of such a layer became prominent in the evaluation of the results in the preliminary analyses in Chapter 3, Sections 3.2 to 3.5. The analysis of stresses and strains at critical locations (Figure 3.2.7.1a) in Chapter 3 lead to the estimation of the pavement life of pavement structures examined during the linear-elastic analyses conducted. The results obtained were expressed with regards to serviceability and fatigue life of these structure. Additionally providing information concerning the number of load repetition than can be withstand by a relative layer until failure.

Even though expected behaviours were exhibited, the capabilities of a linear-elastic analysis, compared to more extensive analyses like FEM analyses, should be taken into consideration. A linear-elastic analysis provides limited information, although useful for basic estimations concerning pavement design (for mechanistic design purposes). Hence, a selected group of the structures considered for the preliminary analyses (*Case1* to *4*) will be replicated in Abaqus to enable a comparison of these estimations.

The experimental plan of this analysis resembles the experimental plan adhered to in the preliminary analysis (*Phase 1*), shown in Figure 4.3.1a. The set-up of the model, and the assumptions made in replicating the various pavement structures in Abaqus, will be addressed according to each module used to add a component to the FEM model. Some overlap exists between the models with regard to their set-up in an Abaqus module. In these instances, a brief summary is provided of the input of information. Pertinent differences will be highlighted in the discussion where appropriate.

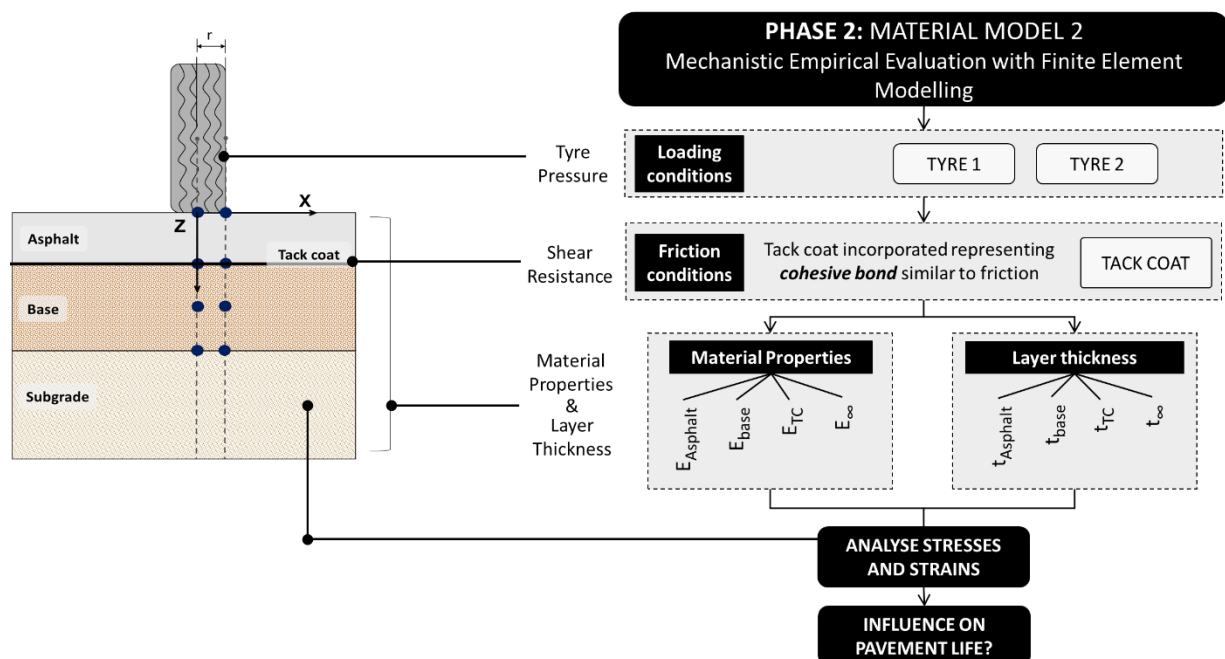


**Figure 4.3.1a:** Material model 2 experimental plan

Figure 4.3.1a denotes all the different testing conditions used for the pavement structures (*Case 1* to *4* shown in Table 3.2.2.3b) that were analysed during the preliminary tests carried out to evaluate the effect of interlayer bonding. The interlayer bonding (shear stress) was inspected through evaluating the effect of a series of variables on these results. The aspects studied included the pavement structure considerations, material properties and the layer thickness of the different materials of which the structures were composed.

To simplify the analysis, a few adjustments were made in terms of the pavements and testing conditions considered for the finite element analysis. The modifications made to the replication in FEM includes the following attributes:

1. The three friction conditions specified for preliminary analyses, i.e. high friction (HF), medium friction (MF) and low friction (LF) are not incorporated into the FEM model by means of a defined interaction. Instead, the shear resistance component incorporated as a shear spring compliance in the linear-elastic analyses completed in BISAR, will be replaced by adding the tack coat layer into the pavement structure.

2. A change was made in the pavement structure, with the inclusion of the tack coat layer within the pavement structure (between the surfacing and base layer). Adhering to the incorporation of this layer allowed the opportunity of incorporating the material properties of the tack coat layer.
3. Given the dimensionality of the problem, a pavement structure of 1×1m was used to represent a unit of the road. Boundary conditions will be incorporated to represent the deflection (deformation) conditions of the pavement structure.
4. The tyre pressure is included as specified in Section 3.2.2 with the absence of the axle load. According to the load stress and load radius demonstrated by Equation 3.2.2.1a, the combination of two of these parameters represents the third one. Hence, the axle load is expressed (in the model) in terms of a pressure and load radius.

Chapter 2 provided insight into some of the different types of pavement design approaches. Many theoretical and empirical approaches exist. It has become evident through literature that modern finite element programs can be used to evaluate more realistic stress patterns induced by wheel loads within any pavement structure. Literature reviewed by Croney & Croney (1998) denotes that the procedure entails incorporation of appropriate structural properties of the road materials (i.e. material stiffness) and the soil foundation. However, an issue arose concerning the elastic properties and the fatigue properties that are not constant throughout pavement life, and how the changes are incorporated in theory, as they were to replicate answers obtained in practice.

#### 4.3.2 Model set-up

The different elements of the models replicated in Abaqus are added, starting from the *Part* model to be analysed and created according to desired geometry (Figure 4.3.2a). The material properties are designated to a specific layer in the Property module, after which the various boundary conditions are assigned to the model. Loading conditions are defined for this model (*Load* module) representing load subjected by tyres on the pavement.

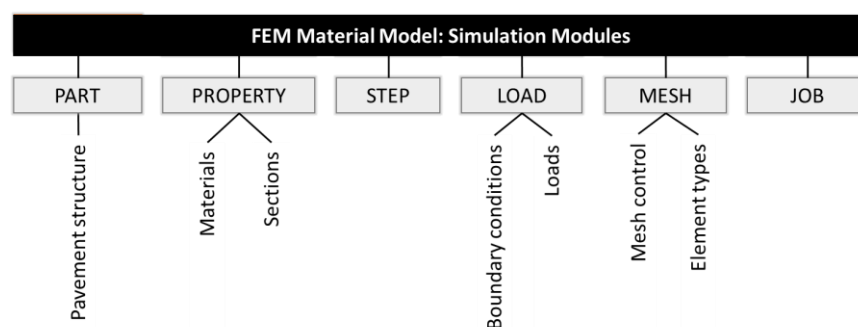


**Figure 4.3.2a:** Model 2 components according to simulation modules

Although not indicated in Figure 4.3.2a, the *Assembly* module is used in order to create a part instance to which the different loading and boundary conditions can be allocated. However, the module is not very important for this model as it consists of only one part, i.e. the pavement structure. Furthermore, all other important components of this module (i.e. dependent versus independent part instances) were covered in the discussion of the set-up of the previous model in the section devoted to the *Assembly* module (Section 4.2.5).

Subsequently, the boundary conditions are assigned to the pavement structure, preventing motion in relative directions. In contrast to the first material model, no constraints were applied. Information with regard to increments is also implanted during the *Step* module. The set-up of the model is completed

by assigning elements and meshing techniques in the *Mesh* module, followed by the analysis in the *Job* module. Lastly, results recorded from the different combinations of analyses in this instance, are interpreted and illustrated in the *Visualisation* module, where various methods can be used to demonstrate the results accordingly.

The set-up of the second material model will be discussed according to the different modules shown in Figure 4.3.2a in Sections 4.3.3 to 4.3.5. Given that a majority of the theory of certain elements used in the respective modules was discussed previously in Section 4.2, only pertinent differences will be addressed in the discussion of the model set-up. An overview for all of the modules (type of information required) was provided in discussion of model one set-up in Section 4.2. Where relevant, correlation is made between the physical characteristics of the pavement structure and its replicated version. The discussion does not exclusively distinguish between the replication and theory, but provides an overall description of the process followed to incorporate physical attributes of the road in the FEM model. Theory not discussed previously in relative modules used in Section 4.2, will be covered when required.

### 4.3.3 Parts and properties

The FEM model, replicating the configuration of the pavement structure considered for the preliminary linear-elastic analysis, is shown in Figure 4.3.3a with the relevant information. The idealisation of the pavement structure with all the required information is provided in Figure 4.3.3a (left) with the FEM replication indicated in Figure 4.3.3a (right). The depth of the pavement is modelled in the negative  $z$  direction.

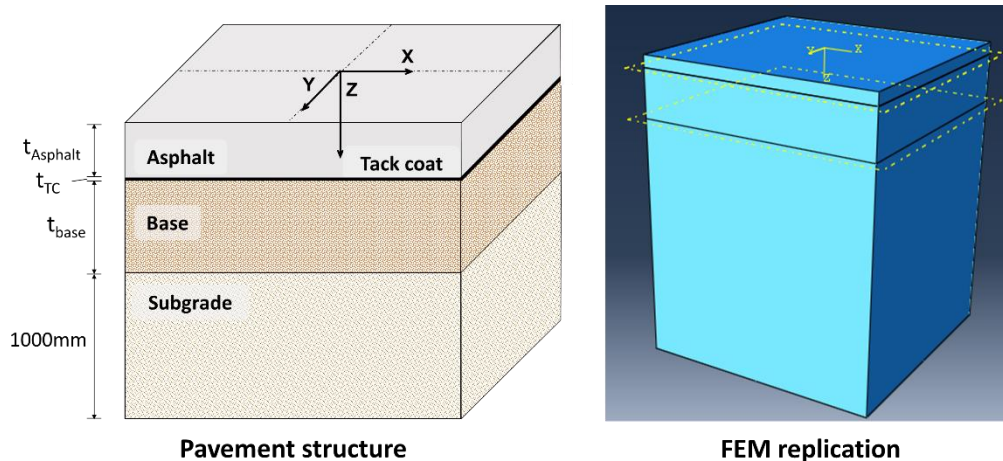


Figure 4.3.3a: Model 2 components according to simulation modules

Figure 4.3.3b shows the geometry sketch of the model – a square with a side dimension of 1000mm. Abaqus does not require the input of data in SI units, but to the preference of the user. For the purpose of the analyses performed (for both the models), dimensions were entered in mm, and forces in Newton (N), given that stresses are entered in MPa ( $N/mm^2$ ). The geometry modelled in this figure is the *surface* of the model. The depth is specified (varies between the different pavement structures) downward in the negative vertical direction (indicated in Figure 4.3.3a).

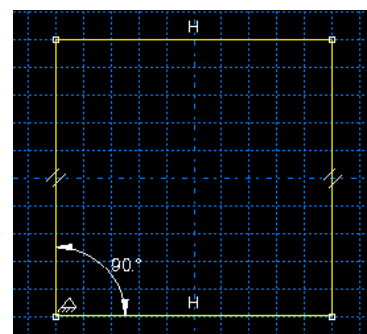
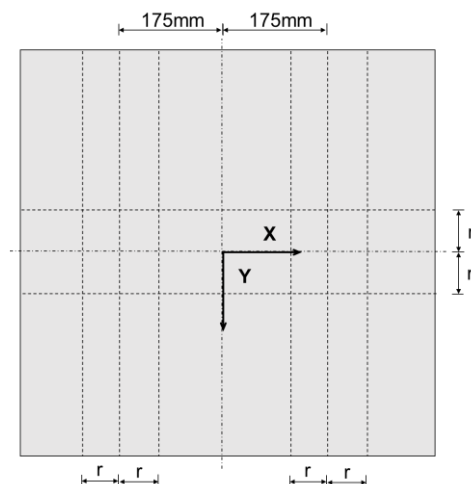


Figure 4.3.3b: Sketch of geometry of part (Abaqus Inc., 2017)

Additionally, partitions are included in the model as provided in the schematization in Figure 4.3.3c. The schematization is not drawn to scale and is used for illustration purposes only. The partition will aid in the addition of the loading to the model at the desired location. The  $r$  in these figures refer to the load radius calculated per loading condition as specified in Table 3.2.2.1a. There were two different values defined for this parameter, given the nature of the loading conditions considered. The selection of geometry is based on standard axle loadings. More information about the geometry in terms of partitioning (dimensions used) is provided in the discussion of the loading conditions Section 4.3.4.



**Figure 4.3.3c:** Partitioning

As mentioned, the four pavements analysed previously in the Stellenbosch research (Section 3.2) will be used, i.e. *Case 1* to *Case 4* illustrated in Table 3.2.2.3b. The thicknesses of the different models are summarised in Table 4.3.3a according to each of the layers. *Case 1* and *Case 3* were modelled with an asphalt layer thickness ( $t_{\text{Asphalt}}$ ) of 50mm and *Case 2* and *Case 4* pavement structures were modelled with an increased  $t_{\text{Asphalt}}$  value of 100mm. A tack coat of 0.5mm thickness was selected to enable comparison with tack coat thickness specified for *Model 1*.

**Table 4.3.3a:** Layer thickness combinations for Model 2

Region (Layer)	Thickness (mm)		
Asphalt	$t_{\text{Asphalt}}$	50	100
Tack coat	$t_{\text{TC}}$	0.5	
Base	$t_{\text{base}}$	200	
Subgrade	NA	1 000	

To shorten analyses computation, only one set of properties is used for the tack coat layer. Only one thickness ( $t_{\text{TC}}$ ) and material stiffness ( $E_{\text{TC}}$ ), defined for this layer, are used in the model (from Tables 4.2.3.1a and 4.2.4.3b). Given that the subgrade represents a type of “foundation”, the depth is typically negligible (infinite). Alternatively, in analyses where the thickness of a layer is required, 1 000mm is deemed sufficient to describe the nature of this layer in terms of its geometry. The layers are added to the model (originally created as a prism) by means of partitioning. The width (thickness) of the partitioning is the equivalent of the specific layer thickness denoted in Table 4.3.3a. Similarly, for the core sample part created in the previous analysis, the partitions created to represent the different layers are created by using a datum plane (Figure 4.3.3d).

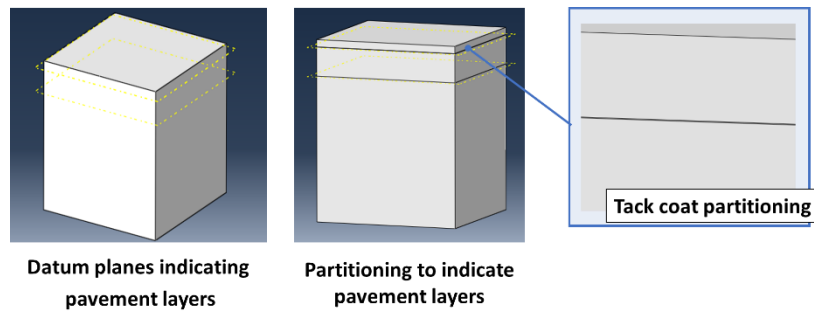


**Figure 4.3.3d:** Partitioning (Abaqus Inc., 2017)

Elastic, Isotropic behaviour is relevant for the materials used in this model, with the only exception to the previous model examined being the magnitude of the parameters specified in Table 4.3.3b. This is evident, given that a different composition of pavement structure is used compared to the core sample modelled for material model 1. The current structure is composed of four layers – asphalt (surfacing), tack coat layer, base layer and a subgrade layer, thus four different sets of material properties were defined. The surfacing material is of Asphalt (Asphalt Concrete), the tack coat is of a bitumen emulsion (bitumen emulsions discussed in Section 2.2) and the base and subgrade layers are composed of granular materials. The subgrade is the weakest layer and is allocated a seemingly lower stiffness than the base layer.

**Table 4.3.3b:** Elastic behaviour types for Model 2

Region (Layer)	Material	Type	Stiffness (MPa)		Poisson ratio ( $\nu$ )
<b>Asphalt</b>	Asphalt	Elastic $\rightarrow$ Isotropic	2500		0.35
<b>Tack coat</b>	Bitumen emulsion	Elastic $\rightarrow$ Traction	1		
<b>Base</b>	Granular	Elastic $\rightarrow$ Isotropic	400	1 500	0.35
<b>Subgrade</b>	Granular	Elastic $\rightarrow$ Isotropic	150		0.35

Seeing that the same types of elements are used in the model in comparison to the core sample modelled for the Leutner replication model, the same types of sections are applicable to the corresponding material. The surfacing, base and subgrade layers were assigned to a solid (homogenous) section feature and the cohesive element (tack coat) was assigned a “cohesive” section feature type (Table 4.3.3c). A compilation of the information summarised in Tables 4.3.3a and 4.3.3b is illustrated in Figure 4.3.3e. The material properties associated with the specific section are assigned to the corresponding pavement layer when completing a section assignment to the preferred model region, as demonstrated in Figure 4.3.3e.

**Table 4.3.3c:** Section features of elements for Model 2

Part	Category	Type
<b>Asphalt</b>	Solid	Homogenous
<b>Tack coat</b>	Other	Cohesive
<b>Base</b>	Solid	Homogenous
<b>Subgrade</b>	Solid	Homogenous

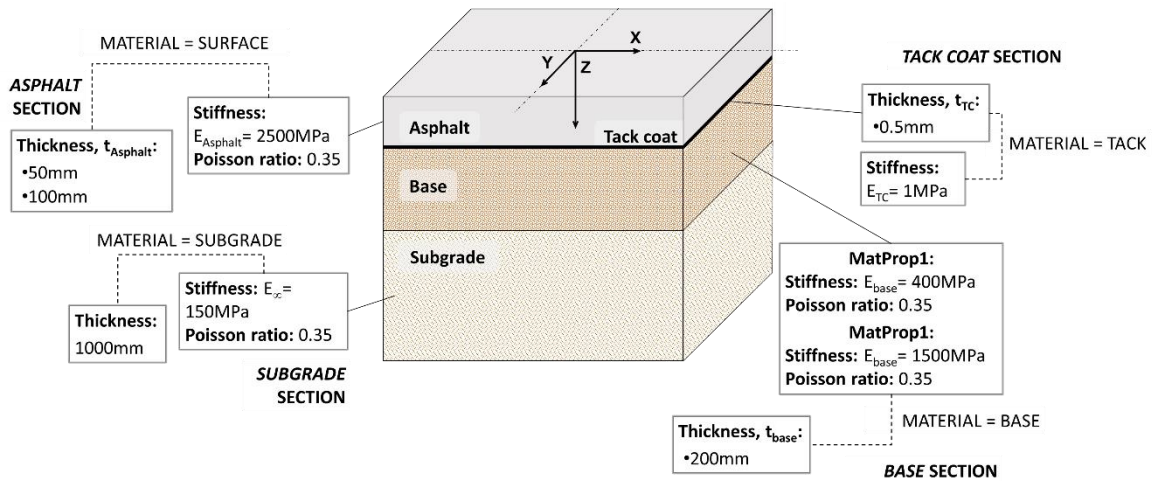


Figure 4.3.3e: Pavement structure properties

### 4.3.4 Boundary and loading conditions

#### 4.3.4.1 The Step module

The different components of this module were addressed in 4.2.6.1. For this analysis there is the default initial step (used for the boundary conditions) as well as one analysis step, which is used to define the loading subjected to the pavement structure. The *load* step succeeds the initial step and both are of *Static, General* procedure type.

Information of the analysis concerned with the *Basic* and *Incrementation* tabbed pages (introduced in Figures 4.2.6.1b and 4.2.6.2c previously in 4.2.6.1), is shown subsequently in context of the current model. The attributes of the analyses for the current model for these two analysis components are shown in Figures 4.3.4.1a and 4.3.4.1b respectively. The time-period selected for the analysis is one second, given that the results at the instant of loading is to be evaluated, and in attribution to the geometry of the model, which is pointedly simple compared to the configuration of the material model in the previous analysis. Hence, the non-linear geometric (Nlgeom) effects are considered negligible (Figure 4.3.4.1a). For the *Incrementation* tab in Figure 4.3.4.1b, the default provided values for the different increment sizes were used. Furthermore, the analysis is to be completed with the (default) maximum number of increments recommended in Abaqus, i.e. 100 increments.

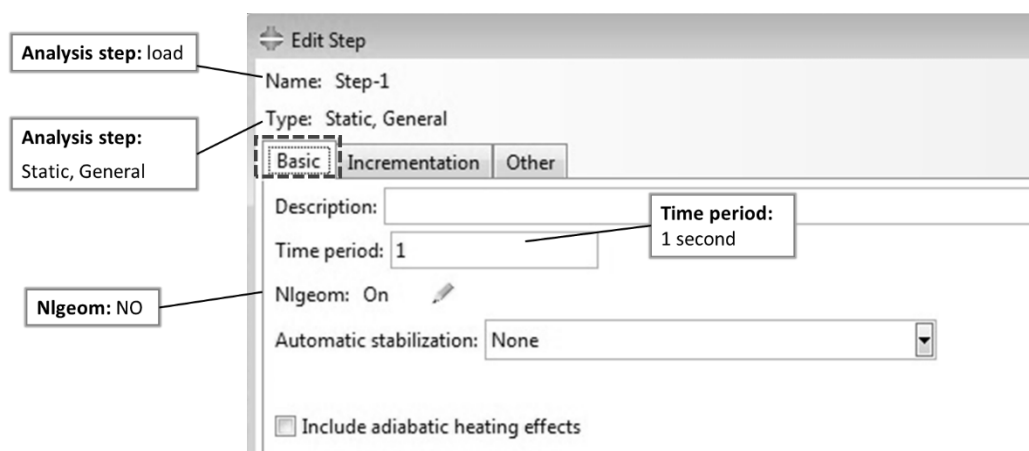


Figure 4.3.4.1a: Analysis step basic tab for Model 2 (Abaqus Inc., 2017)

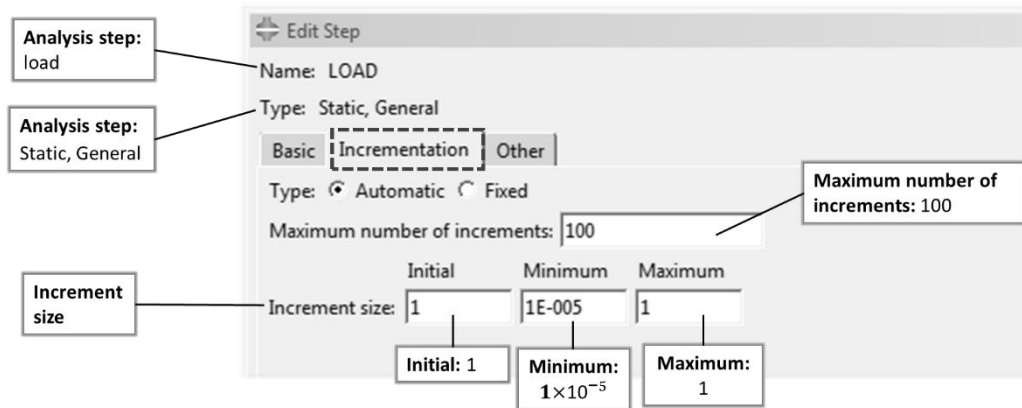


Figure 4.3.4.1b: Analysis step incrementation tab for Model 2 (Abaqus Inc., 2017)

### 4.3.4.2 Boundary conditions

The boundary and loading conditions form part of the *Load* module. The set-up of the current model up to this point, is illustrated in Figure 4.3.4.2a. The discussion of the boundary conditions is covered in this section, which denotes the different types of boundary conditions (BCs) used to replicate physical conditions of a pavement structure. The loading conditions are studied in 4.3.4.3.

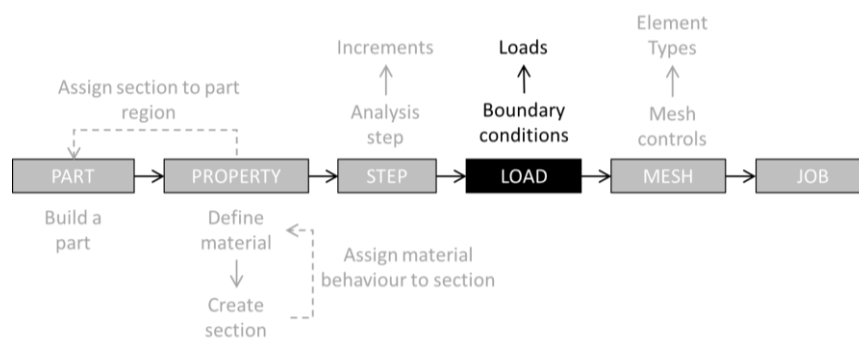


Figure 4.3.4.2a: Model set-up procedure for Model 2– Load module

Two different sets of boundary conditions are defined for the current model. These BCs are illustrated in Figure 4.3.4.2b for the replicated model in Abaqus. The definitions of these two boundary conditions are shown in Figures 4.3.4.2c and 4.3.4.2d individually.

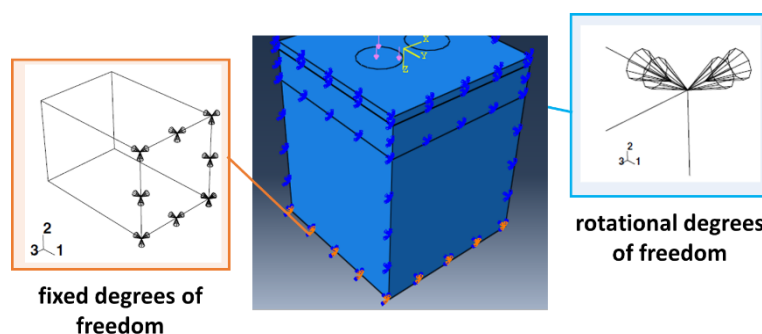


Figure 4.3.4.2b: Sketch of geometry of part (Abaqus Inc., 2017) (Dassault Systèmes Simulia, 2014f)

For this model, a fixed degree of freedom is used at the bottom representing a rigid foundation of the pavement structure. Rotational degrees of freedom are defined as indicated as displacement occurs in respective direction due to loading subjected by the tyre. A full description of these boundary conditions are given in Appendix D6.

#### 4.3.4.3 Loading conditions

##### Physical loading condition

The discussion of the loading conditions applied at this stage of the analysis is approached by a brief overview of the “physical loading condition” replicated in the finite element software. Both the loading conditions prescribed in Section 3.2, *T1* and *T2* (or *Tyre 1* and *Tyre 2*) are used for the analyses. This section also explained the acquirement of loadings to be used, where it was stated that only half-axle loads are considered, assuming a symmetrical stress distribution along the depth of the pavement structure (Figure 4.3.4.3a left).

**Table 4.3.4.3a:** Axle loading and tyre pressures

Load	Tyre type	Tyre pressure (kPa)	Load radius (m)
T1	Super single	750	0.13
T2	Super single	900	0.157

**Note:** Tyre type = super single, and load radius is indicated as *r* on Figure 4.3.4.3b. Load radius was estimated by means of Equation 3.2.2.1a as discussed per Section 3.2.2 in Chapter 3. Half-axle wheel loads are used i.e. for 80kN-axle (40kN) and 140kN-axle (70kN) for these estimations

Given the existing relationship between the axle loading and the tyre pressure, the combination of the tyre pressure and load radius (*r*) is sufficient for the analyses. Hence, only the tyre pressure is included, acting on a load area (or radius) (Table 4.3.4.3a). The wheel configuration is at a distance of 350mm from centre to centre between the two tyres (Figure 4.3.4.3a right).

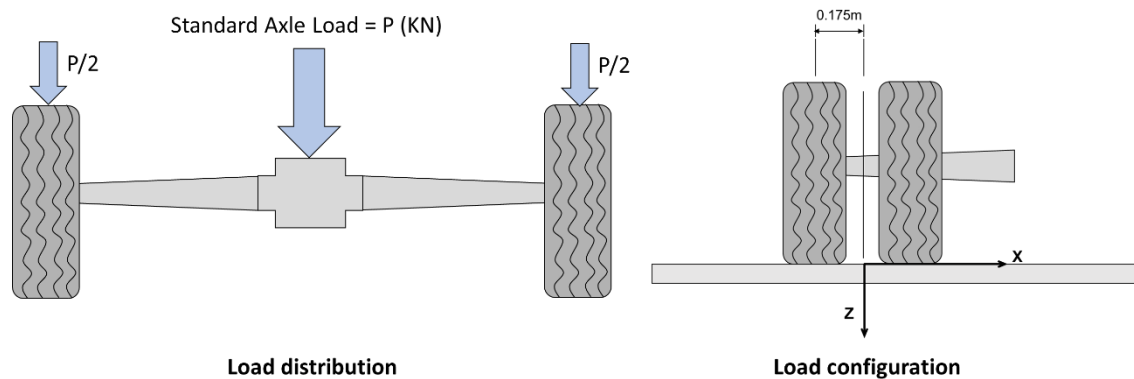


**Figure 4.3.4.3a:** Axle load distribution and configuration

The referred loading configuration in this figure is used to enable a symmetrical set-up of the model in terms of loading conditions (Figure 4.3.4.3b). It is evident in Figure 4.3.4.3b that loading is applied at only one location on the pavement surface and the loading area is twice the load radius defined for *T1* and *T2* (Table 4.3.4.3a). Dimensions are indicated according to the global coordinate system in Abaqus in Figure 4.3.4.3b (right).

4.3 Pavement analysis

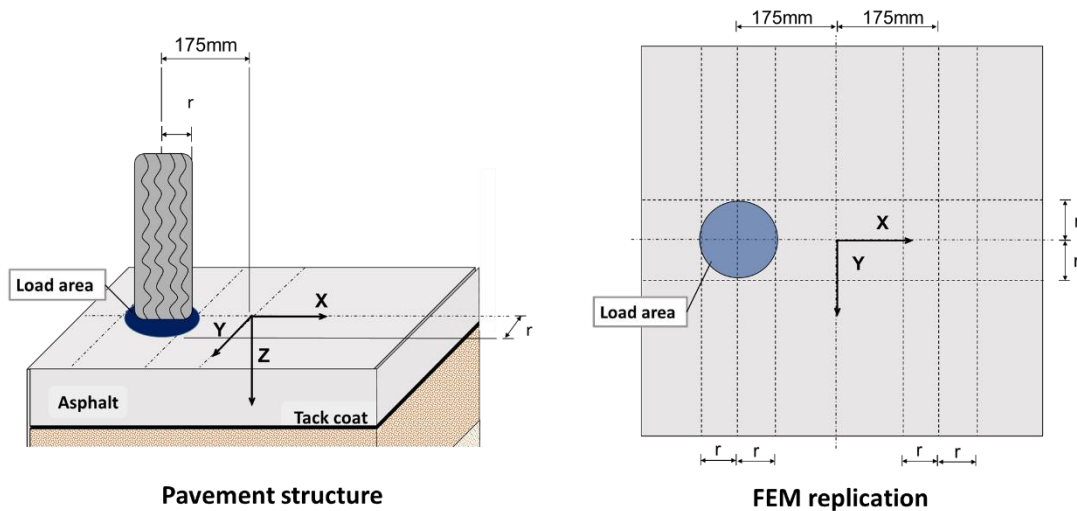


**Figure 4.3.4.3b:** Idealisation of load application in Abaqus

The load area (Figure 4.3.4.3b right), is partitioned on the surfacing layer, representing the area where the tyre is in contact with the surfacing layer – illustrated by the circular area. Two circular partitions are made on the surfacing layer (Figure 4.3.4.3c) to which the loading shall be subjected. Only one circular section is relevant, where the second was to provide a symmetric distribution of the mesh across the geometry of this surface. This application of one load is in correlation with the linear-elastic set-up where only one load was considered.

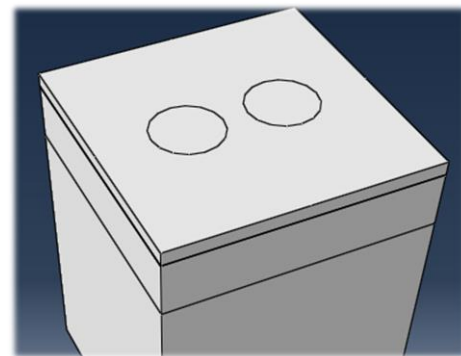


**Figure 4.3.4.3c:** Load are partition (Abaqus Inc., 2017)

**Replication of loading condition**

The load applied is categorised as *surface-based* loading in accordance with Dassault Systèmes Simulia (2014d) i.e. pressure load. General information about the loading, i.e. type, time step and region to be applied is defined in the *Load* editor (dialog box) (Figure 4.3.4.3d). All relevant data concerning the loading is supplied in this figure. The name of the load is *Tyre pressure* and is applied during the analysis step defined as *load* in 4.3.4.1. The *Mechanical* category is attributed to the *surface-based* loading condition.

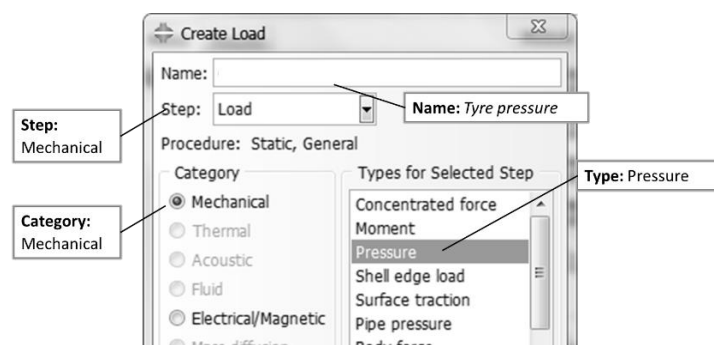
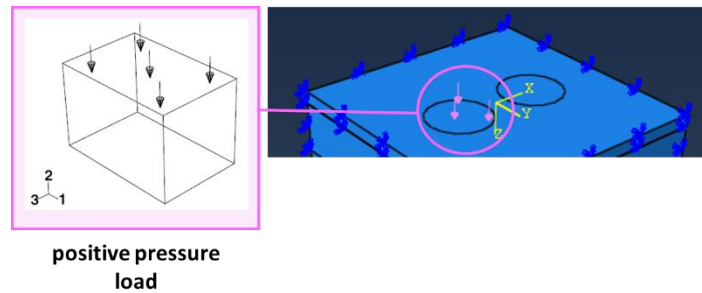


**Figure 4.3.4.3d:** Load definition (Abaqus Inc., 2017)

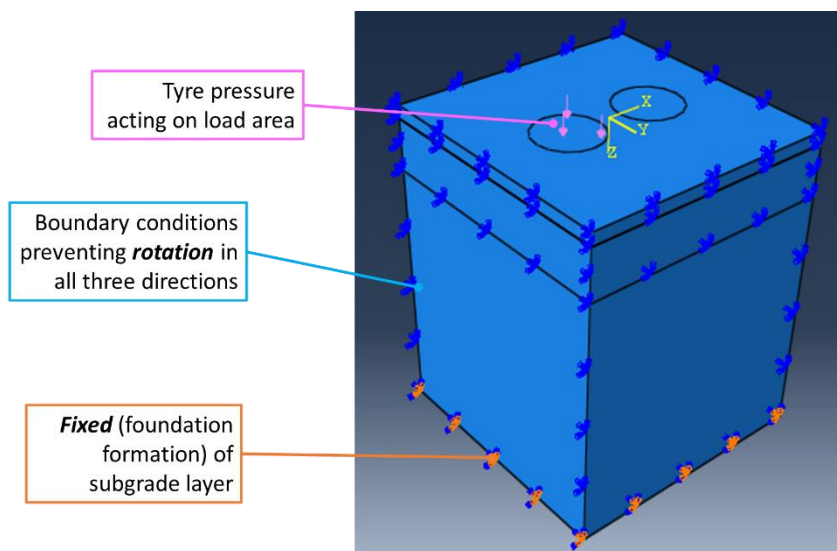
For the purpose of this analysis, it was not deemed necessary to include a footprint with non-uniformly distributed load over a non-standard shape. With the completion of the loading data, the region to which the load is applied (Figure 4.3.4.3e) is subsequently selected. For each loading case, the region indicated in Figure 4.3.4.3b (right) is selected for the load to be applied in accordance with the configurations (dimensions) shown in Figures 4.3.4.3a and 4.3.4.3b. In conclusion of the *Load module*,

Figure 4.3.4.3f denotes an illustration of all the prescribed conditions covered in 4.3.4.2 and 4.3.4.3 (loads and boundary conditions) indicated on the model replicated in Abaqus.



**Note:** The convention of degrees of freedom in direction 1, 2 and 3 do not coincide with the global coordinate system of the replicated model and is for illustration purposes only

**Figure 4.3.4.3e:** Replicated loading conditions (Abaqus Inc., 2017) (Dassault Systèmes Simulia, 2014f)



**Figure 4.3.4.3f:** Illustration of all prescribed conditions (Abaqus Inc., 2017)

### 4.3.5 Meshing techniques

Section 4.2.7 summarised the different meshing techniques and studied the characteristics of those applicable to Model 1 (Leutner test replication). For the previous model, *bottom-up* meshing (by means of extrusion) and *top-down* meshing (*swept*) were considered. This section also studied the process adhered to when part instances of a model are meshed as shown in sequence in Figure 4.3.5a and it described the important elements taken into consideration when meshing is executed.

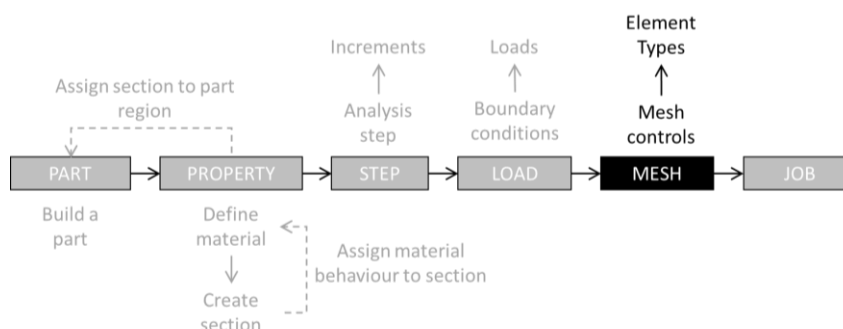


**Figure 4.3.5a:** Model set-up procedure for Model 2 – Mesh module

The model resembles the composition of the core sample (Model 1) with the exception of the geometry and the material properties. In this model cohesive elements and their definitions, the *bottom-up* meshing technique is used for the tack coat layer region of the current model and all the regions below it, representing the pavement layers below the tack coat layer. The *swept* meshing technique (*top-down* meshing) will be used for the surfacing layer (top region of the model). All of the attributes, i.e. element type and algorithm, are indicated in Figure 4.2.7.3a and are the same as for the core sample. *Hex* (hexahedral) elements are used with the meshing technique selected. The same procedure as explained in Appendix D4 were adhered to for the two respective meshing techniques used. The procedure for using the *bottom-up* meshing techniques is displayed in Figure D17 in Appendix D4, where a similar layout is given for the use of this technique for the replicated pavement structure provided in Figure 4.3.5b.

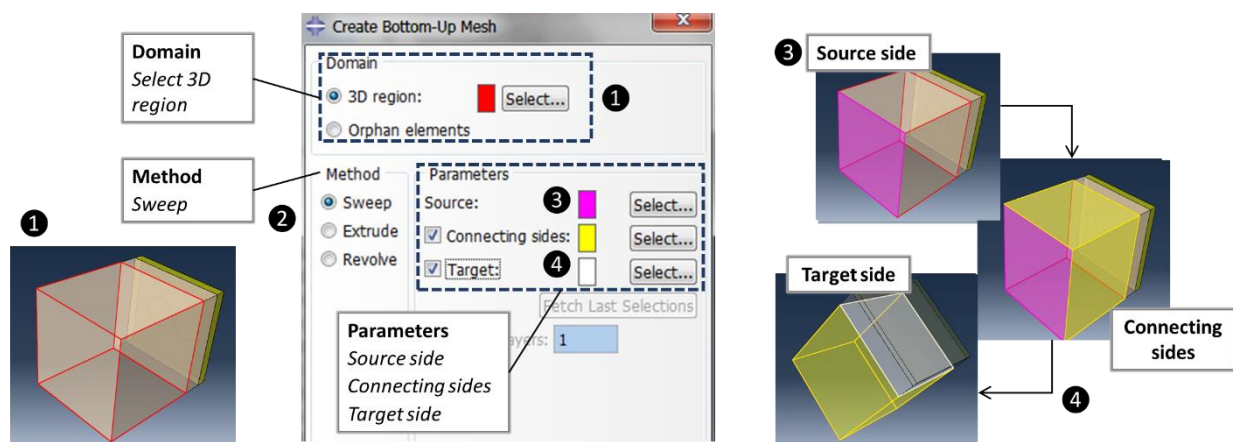


Figure 4.3.5b: Mesh generation for Model 2 (Abaqus Inc., 2017)

The *bottom-up* meshing technique was used to mesh the subgrade, base and tack coat regions individually by repeating *step 1* to *step 4* shown in Figure 4.3.5b. Subsequently, the meshing was completed for the top region. An example of the generated model mesh is given in Figure 4.3.5c. The mesh generation is indicated as the model colour changes to a light blue colour. The colour coding indicating each technique is noticeable when studying this figure. The tan-blue combination shows the area where the *bottom-up* meshing technique was used, while the plain blue region indicates the *swept* meshing region.

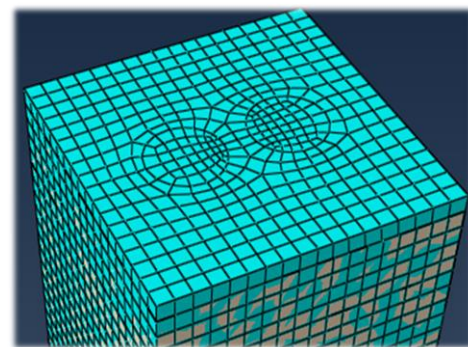


Figure 4.3.5c: Model 2 mesh (Abaqus Inc., 2017)

The following element added to the model in the *Mesh* module is the setting of the element type. The same elements used for the solid regions shown in Figure D21 (Appendix D5) apply for the solid regions defined for the current model – all the layers, except the tack coat layer. These regions are assigned eight-node linear brick elements (Figure D24 in Appendix D5) indicated as C3D8R. The reduced integration option was used for the purpose of this analysis. The same guidelines apply to the cohesive section assigned in the model.

The element types are assigned to the associated model region as listed. A detailed description of assigning these components is covered in Appendix D7.

Fundamental information for element type definition of the Pavement Analysis is as follows:

1. Element library – *Standard (Linear-elastic)*;
2. Family
  - Surface: *3D Stress*
  - Tack: *Cohesive*
  - Base: *3D Stress*
  - Subgrade: *3D Stress*
3. Element Type – *Hexahedral (Hex) elements*;
4. Integration – *Reduced Integration* ;

A different approach is used to record results for this model than that used for collection of results for the Leutner shear model in Section 4.2. These methods of results for acquisition are covered in Section 4.3.6.

#### 4.3.6 Acquisition of results

In contrast with the results for Model 1, an additional approach is included in this model to in order to record the results needed to perform the pavement life estimations. The acquisition of results in the pavement structure is completed with the assistance of Figure 4.3.6a. In contrast with Figure 4.2.9b (acquisition process for Model 1), a *path* is defined for obtaining selected results, which are desired locations, while the *ODB field output* option was used to require the necessary XY data (Figure 4.3.6a left). The *path* method specifies XY data by reading field output results (U1, U2 and U3) at locations along a path through the model. The points that make a path are selected at the critical locations directly below the wheel (Figure 4.3.6b).

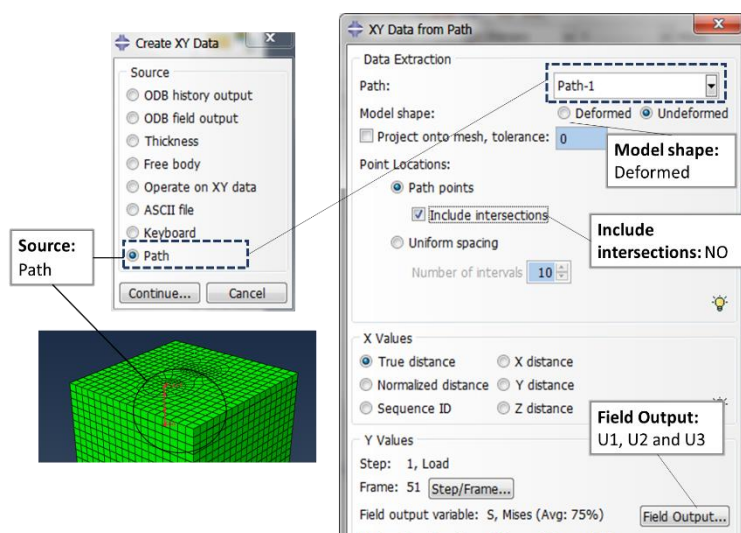


**Figure 4.3.6a:** Results acquired at Model 2 locations (Abaqus Inc., 2017)

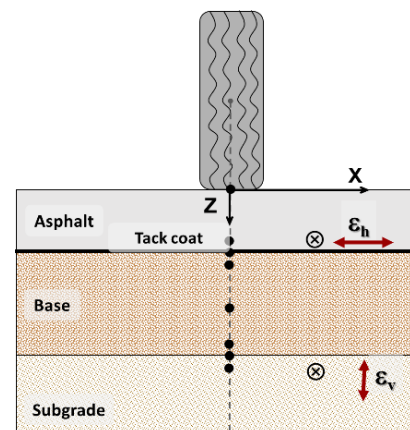


**Figure 4.3.6b:** Locations for acquisition of results

The results needed according to the two failure mechanisms (fatigue and serviceability) are indicated with an “x” in Figure 4.3.6b. Results were also recorded at points just above or below these points. In addition, for the shear stress, results were recorded at the locations of the interfaces. The desired locations are incorporated into a *path* file by entering the x, y and z coordinates of each of these points, according to their value in the global coordinate system. Hereafter, the actual reading for a relative field output can be obtained (Figure 4.3.6a right).

The purpose of the model is to evaluate critical parameters such as strains at (previously defined) critical locations within a pavement layer. For the structures selected for this particular analyses, these critical locations will be at the bottom of the surfacing layer, the mid granular (base) layer and at the top of the subgrade layer. In compiling the results, it also creates the opportunity for comparing the results obtained from these analyses with its counterparts, analysed during the linear-elastic analysis.

In Figure 4.3.6a (right), the *path* (with defined coordinates) is selected and results are recorded for the *deformed* model shape. In this instance, intersection points were excluded as a sufficient number of coordinates have been specified. Finally, the types of field output required for estimations are stresses in the three principal directions ( $\sigma_{11}$ ,  $\sigma_{22}$  and  $\sigma_{33}$  or S11, S22 and S33 as the Abaqus equivalent) as well as the shear stress measured on the horizontal plane, (the Abaqus equivalent is S12). An example of result output is given in the form of a visual representation of the displacement distribution within the model, demonstrated in Figure 4.3.6c.

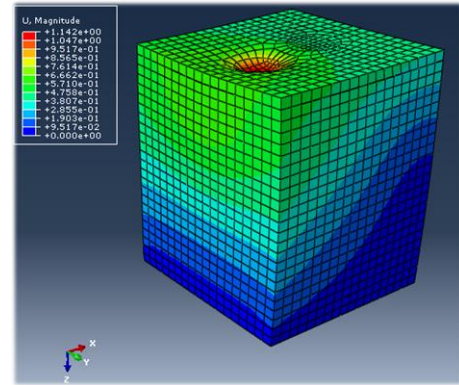


**Figure 4.3.6c:** Displacements (Abaqus Inc., 2017)

The strains are not directly recorded from the analysis; however, the stresses acquired from the analysis (S11, S22 and S33) will be used to estimate the associated strains required for the pavement life estimates. The strains are determined with Equations 4.3.6a to 4.3.6c. A constant Poisson ratio of 0.35 was assumed for all the materials. Hence, the Poisson ratio remains constant for all estimations. The Elastic Modulus (E) used, is the material stiffness of the particular layer (region) in which the estimations take place. The strains are used to determine the fatigue life (Equation 3.2.7.2a) and serviceability life (Equation 3.2.7.3a).

$$\varepsilon_x = \frac{1}{E} (\sigma_x - \nu(\sigma_y + \sigma_z)) \quad (4.3.6a)$$

$$\varepsilon_y = \frac{1}{E} (\sigma_y - \nu(\sigma_x + \sigma_z)) \quad (4.3.6b)$$

$$\varepsilon_z = \frac{1}{E} (\sigma_z - \nu(\sigma_x + \sigma_y)) \quad (4.3.6c)$$

Where:

$\varepsilon_x$ ,  $\varepsilon_y$  and  $\varepsilon_z$  = Strain in relative direction

$\sigma_x$ ,  $\sigma_y$  and  $\sigma_z$  = Stress measured in relative direction

#### 4.3.7 Synthesis of analysis

Figure 4.3.7a denotes the experimental plan with the different variables incorporated into the variety of pavement structures modelled in Abaqus. A series of loading conditions, material properties and geometric components (layer thickness variation) was introduced to evaluate the strains in the critical locations within the pavement structure, used to establish which factors have the greatest impact on the results obtained, and also which of the structures are the most beneficial with regard to the pavement

life they produce. Furthermore, a summary of the set-up procedure of Model 2 is given in Figure 4.3.7b according to the different models to define different characteristics of the model.

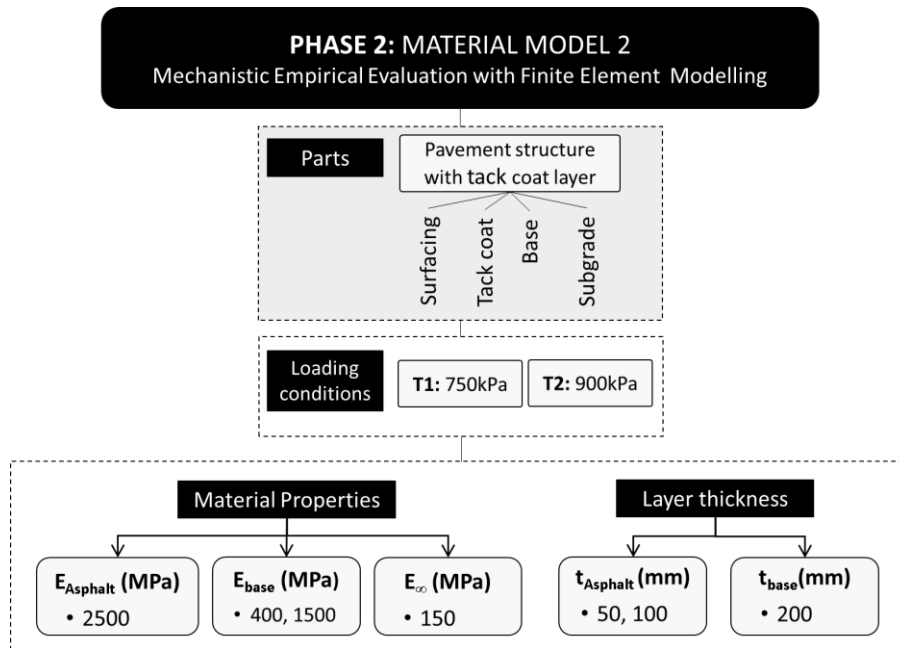


Figure 4.3.7a: Experimental plan for Model 2

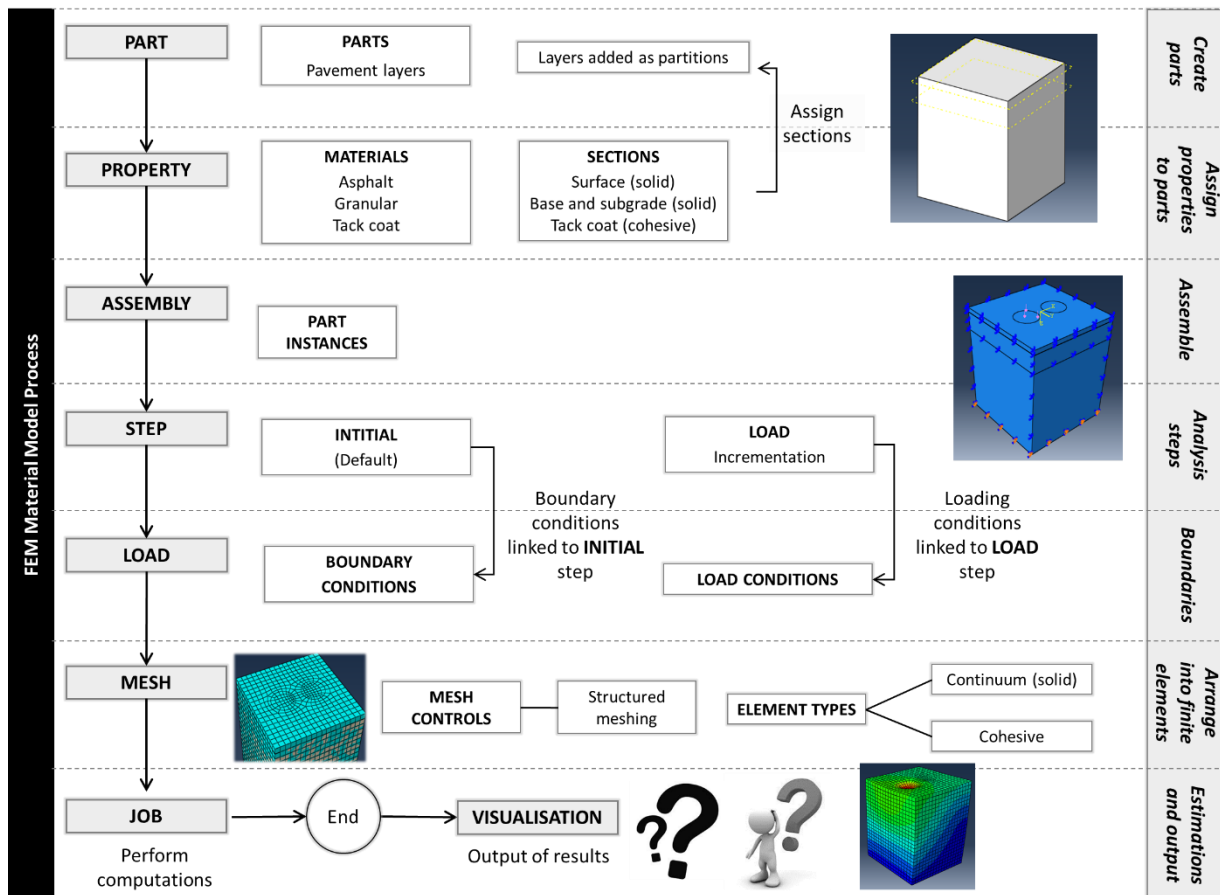


Figure 4.3.7b: Experimental plan for Model 2

#### **4.4 Synthesis of methodology**

Two different models were developed in Abaqus, each with its own objective, in turn serving as supplementary analyses to those completed during the preliminary research conducted in Chapter 3. Firstly, a model was created to replicate the Leutner shear testing device in FEM that complements the preliminary laboratory work completed by Pisa University (Section 3.3). The aim of the first model was to inspect the quality of the interlayer bonding in terms of the shear stress it produces, while investigating the influence of factors such as material properties and layer thickness. The second model comprised of a series of pavement structures created in line with Stellenbosch University's preliminary analysis (discussed in Section 3.2). These structures were replicated in FEM to evaluate stresses and strains in achieving the estimation of pavement life of these structures. The results and interpretations are provided subsequently in Chapter 5 for both the analyses.

## CHAPTER 5: RESULTS AND INTERPRETATION

### 5.1 Introduction

A variety of studies have been undertaken to gather information concerning proper interlayer bonding and its effect on pavement durability. It is well-known that the asphalt layers work separately and induce negative changes of values and stress distributions in a pavement structure (Malicki & Górszczyk, 2012). Hence, it is of significant importance that the properties of materials that are used to provide optimum interlayer bonding conditions should be investigated. The quality of interlayer bonding at the interface between the asphalt layers of flexible pavements has been found to affect the overall pavement performance. From literature reviewed in Chapter 2, importance is raised in this regard – the lack, or partial lack, of interlayer bonding causes premature failures of pavements, such as rutting, slipping of the wearing course or cracking. These defects, in turn, result in the reduction of the pavement's estimated fatigue life.

Two models were developed to address influential factors as described in Chapter 4. The areas of interest for these models depend on their objectives as indicated in Figure 5.1a. Chapter 5 is structured according to the diagram illustrated in this figure. The objective of each model is stipulated along with the discussion points to be covered in subsequent sections. For explanation purposes, the Leutner Shear Test Model will be referred to as *Model 1* and the pavement structure modelled will be referred to as *Model 2*. The content and interpretation of results is provided in Sections 5.2 and 5.3 for the respective models. A comparison of the results of each of the models relative to preliminary research is included in the respective sections. Section is concluded with a comparative study completed for the two replicated models with an overview of findings also provided to summarise prominent observations from *Phase 1* and *2* component of the research emphasising *Phase 2* component.

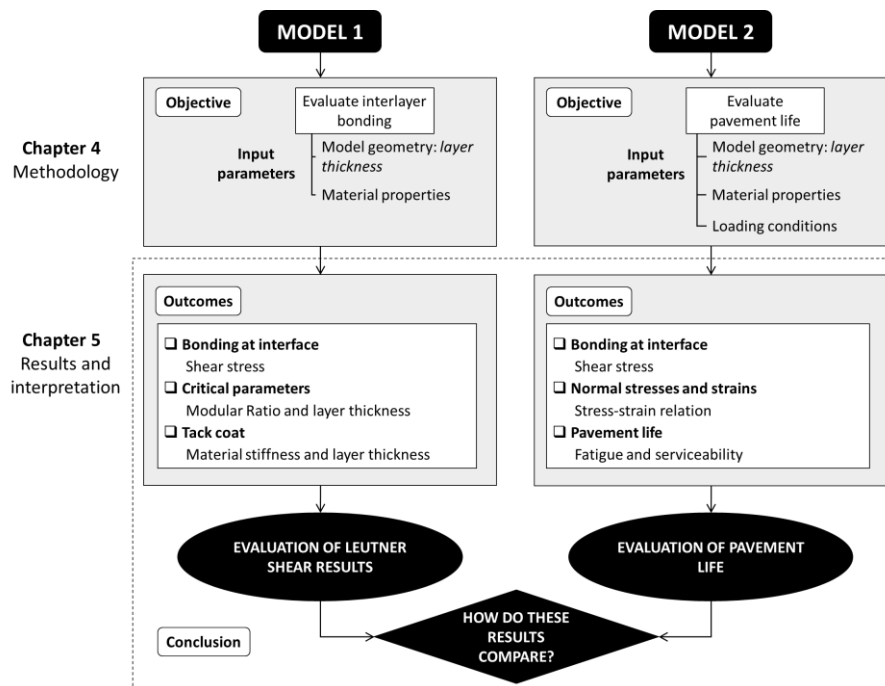
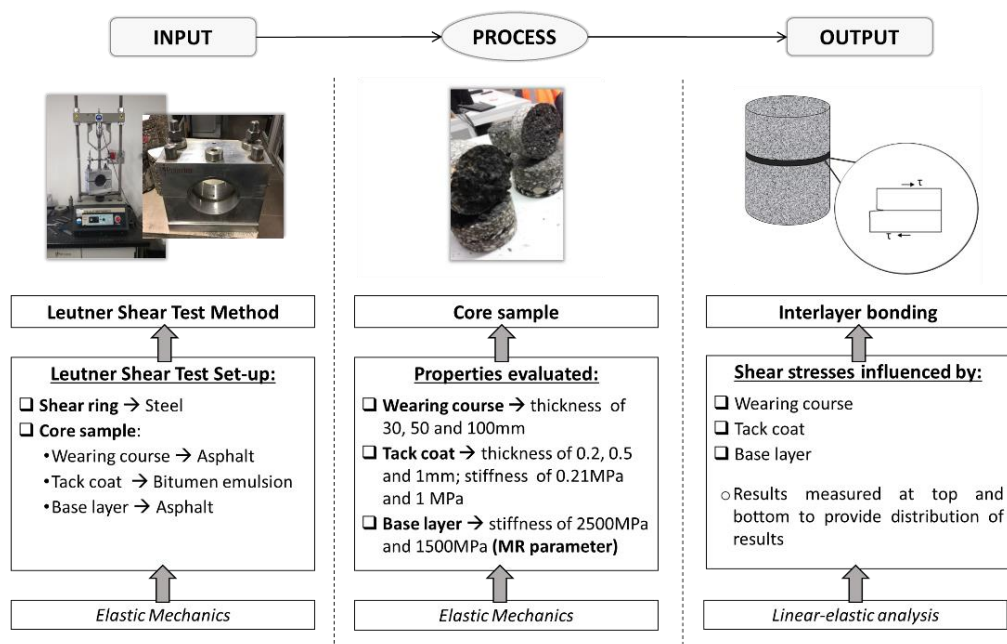


Figure 5.1a: Subjects of interest for discussion of results

## 5.2 Leutner Shear Test Model

### 5.2.1 Introduction

Selected conditions were incorporated into a finite element (FE) model simulation, which constitutes the different elements of the Leutner Shear Testing device discussed in Chapter 2. The set-up of the model was covered in Section 4.2 where all of the different components required for its set-up were discussed. Furthermore, correlation was made between the physical characteristics of the test and the replication of the finite element method (FEM) model. It should be noted that the FE replication is composed of simplified conditions compared to the traditional set-up. Consequently, reducing the number of variables for the analysis. The influence of these assumptions will be addressed where appropriate. An overview of the analysis procedure of this model is given in Figure 5.2.1a. Considering all parameters, a total of 36 analyses were performed.



**Figure 5.2.1a:** Analysis approach for Leutner Shear Test Model (Bianchi et al., 2018)

The shear stress is identified as the critical parameter given the objective of this analysis. It describes the bonding condition between the wearing course and the base layer relative to the entire pavement structure. Findings from preliminary research in Chapter 3 and various literature reviewed in Chapter 2, it is noticeable that the testing conditions influence the results recorded. These consist of physical and mechanical conditions. Physical conditions i.e. device set up and mechanical i.e. sample properties. Therefore the simplified FE model proved to be beneficial providing the opportunity to evaluate the influence of various mechanical properties. The recognised influence of these properties on bonding (shear stress) will be discussed subsequently. The different properties investigated with respect to the critical parameter (shear stress) include:

1. Change in shear stress/ load magnitude;
2. Modular ratio (MR1 and MR2) describing the increase and decrease in the material stiffness of the base layer ( $E_{base}$ ) – *modular ratio of 1 and 2.5;*
3. Wearing course layer thickness ( $t_{wc}$ ) – *thickness of 30mm, 50mm and 100mm;*
4. Material stiffness of the tack coat ( $E_{TC}$ ) – *stiffness of 0.21MPa and 1MPa;*
5. Tack coat thickness ( $t_{TC}$ ) – *thickness of 0.2mm, 0.5mm and 1mm.*

### 5.2.2 Shear stress distribution

#### 5.2.2.1 Introduction

The critical parameter which describes the effectiveness of bonding is the shear stress. Therefore, it is important to understand how this parameter varies in the analysis and at different locations of the specimen. An illustration of shear stress distribution over the sample cross section is provided in Figure 5.2.2.1a. In this figure, the different paths, as discussed in Section 4.2.9, are labelled 1 to 5. Furthermore, an indication of the order of magnitude of the shear stresses is provided for *Path 1* to *Path 5*. The figure is a representation of the shear distribution pattern at each location.

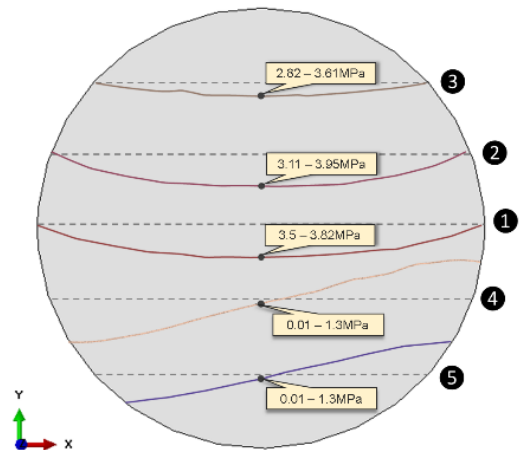


Figure 4.3.4.3a: Shear stress distribution over sample cross section

It should be noted that a recursive analysis was used for the linear-elastic analysis completed in FEM. The Leutner Shear Testing device was simplified to apply one displacement/ loading condition. In accordance with the global coordinate system in Abaqus, S23 shear stresses were used. Stress distribution patterns observed for *Path 1* to *5* will subsequently be discussed in more detail. This discussion will highlight the trends and change in shear stress distribution (in the vertical direction) at each *Path* location. Moreover, a graphical representation of these results are given in Figures 5.2.2.2a, b, c, e and f. This is a compilation of the results from the FEM analysis in Figures E1 to E5 in Appendix E.

#### 5.2.2.2 Shear Stress Curves

Figure 5.2.2.2a shows the shear stress distribution for *Path 1*. This path is in the centre of the sample ranging between 3.5 and 3.82 MPa over a cross section of 150mm. The results at this location follows a parabolic distribution with the maximum shear stresses achieved at the edges of the core sample. The “stepped” profile in the graph is attributed to the elements of the sample during mesh generation. Which is not entirely uniform distributed over the cross-section. For idealised results, the parabolic function would adhere to a smoother trend. Enlarged version of the results are provided on the left (also provided for *Path 2* to *5*).

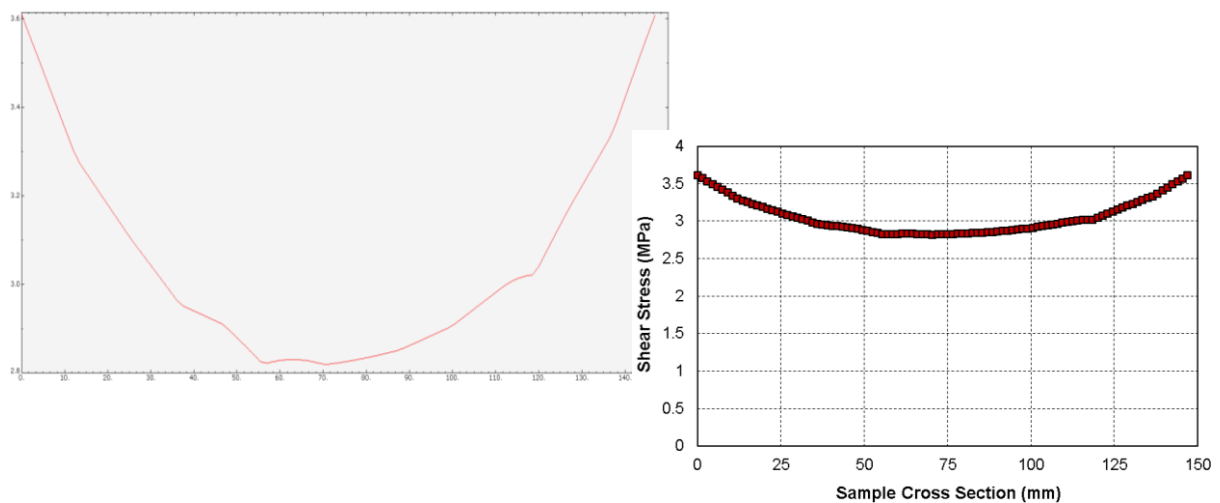
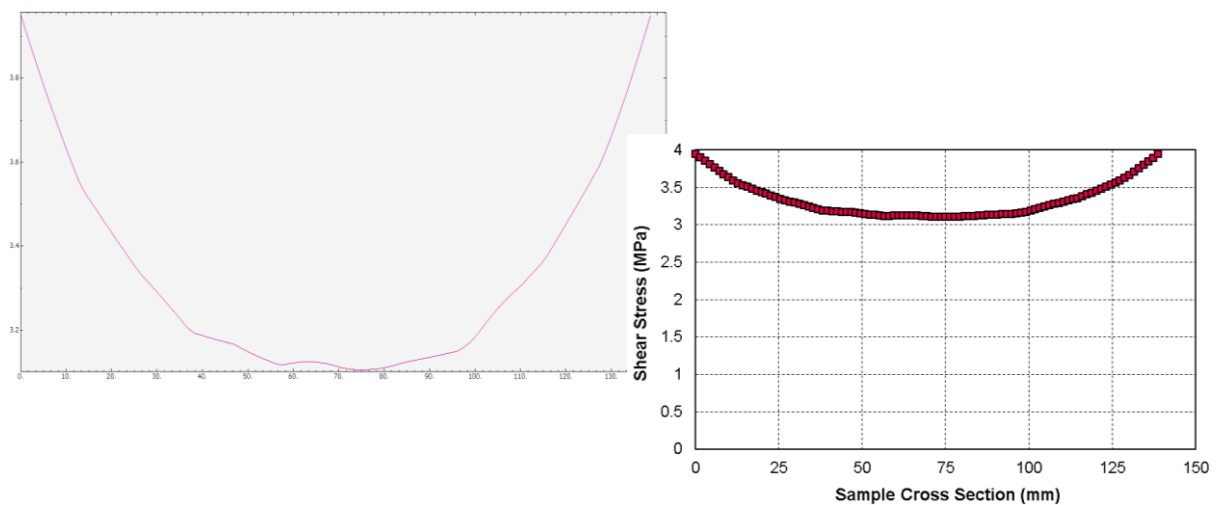


Figure 5.2.2.2a: Path 1 Cross Section Shear Distribution

## 5.2 Leutner Shear Test Model

The parabolic distribution at this location is justified by the constraints of the model. For *Path 1*, there is no defined constraint which prevents any deformation from occurring. Hence, as the load is applied in the vertical direction, the shear ring moves in a vertical direction resulting in deformation in the same direction where the maximum deformation will occur in the centre i.e. at 75mm of the cross section as seen in Figure 5.2.2.a.

*Path 2*, is located 25mm above *Path 1* and is approximately 141.4mm in length over the cross section of the core sample; the same for *Path 4*, 25mm below *Path 1*. The shear stresses generated at this location is shown in Figure 5.2.2.2b. As similar distribution is noticeable as for *Path 1* i.e. parabolic function. However, higher shear stresses are measured ranging between 3.1 and approximately 4MPa, which is slightly higher than the shear stresses at *Path 1*. Comparing *Path 2* with *Path 1*, it is evident that the graph follows a smoother trend suggesting a more evenly distribution of the stresses at this location in the sample.



**Figure 5.2.2.2b:** Path 2 Cross Section Shear Distribution

The results for *Path 3* are shown in Figure 5.2.2.2c over a cross section of approximately 112mm. On the right, a similar parabolic-like function is noticeable with an enlarged version of these results given on the left. Studying the last-mentioned preview of results, it is evident that a less smooth curve is achieved with many deformities in its distribution pattern.

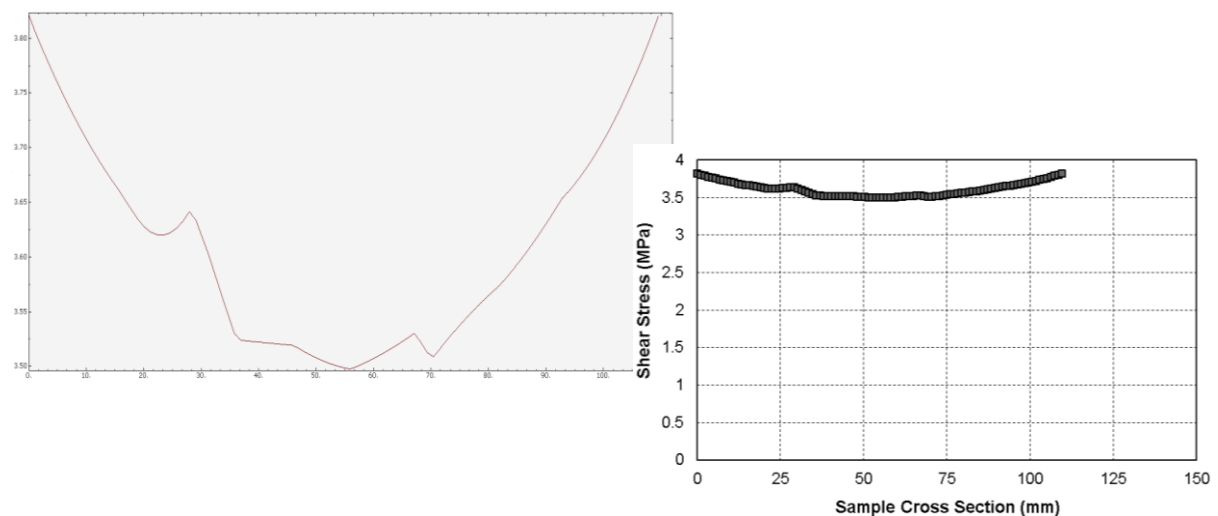


**Figure 5.2.2.2c:** Path 3 Cross Section Shear Distribution

## 5.2 Leutner Shear Test Model

In Figure 5.2.2.2c, the effect of the analysis type on the results becomes more pronounced where sporadic changes are observable in shear stresses. Shear stresses at this location range from 2.82 to 3.61MPa which is lower in order of magnitude. However, suggests significant variation in shear stress compared to *Path 1* and 2.

*Paths 1* to 3 are found to have similar distribution patterns when analysed for most variables concerning the analysis. In spite of this observation, there are contrasting distribution patterns when comparing the different groups of results. These contrasting distributions are summarised accordingly in line with studying Figure 5.2.2.2d.

1. *Path 1* and 2 in Figures 5.2.2.2a and 5.2.2.2b shows more constant distribution pattern in shear stresses adhering to a parabolic function with a small variation in shear stresses.
2. Studying the transition to *Path 3* from Figure 5.2.2.2a to Figure 5.2.2.2c, a significant change in results is observable with more variation in shear stresses and a less smooth parabolic function
3. The change in the distribution concerning the transition can be explained as follows:

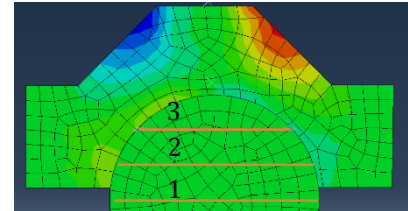


**Figure 5.2.2.2d:** Path 3 location for assembly

- a. *Path 3* is 25mm from the top of the sample and is part of the *core* part that's "connected" to the shear ring as explained in 4.2.6.3 and shown in Figure 5.2.2.2d. Thus a smoother parabolic-function is found further away from the point of "interaction" at *Path 1*.
- b. It is concluded that the stress distribution is motivated by the constrained regions of the model and the geometry which has an impact on the stress generation of the model.

The shear stress distribution at *Path 4* and 5 is shown in Figure 5.2.2.2e and 5.2.2.2f where similar trends are noticeable following a more linear pattern compared to that observed in Figures 5.2.2.2a, 5.2.2.2b and 5.2.2.2c. Transitioning from the centre of the cross section (*Path 1*) to 25 and 50mm below (*Path 4* and 5); a change in the function is visible – from parabolic to more linear. Shear stresses measured at Path 4 and 5 are significantly smaller ranging between 0.01MPa and 1.3MPa and up to 1.5MPa. The negative shear stresses measured in each instance represents shear occurring in opposite direction before transition to positive values. The results at *Path 4* slowly transition from the parabolic function observed for *Path 1*, 2 and 3 followed by a curve that is more linear in *Path 5*.

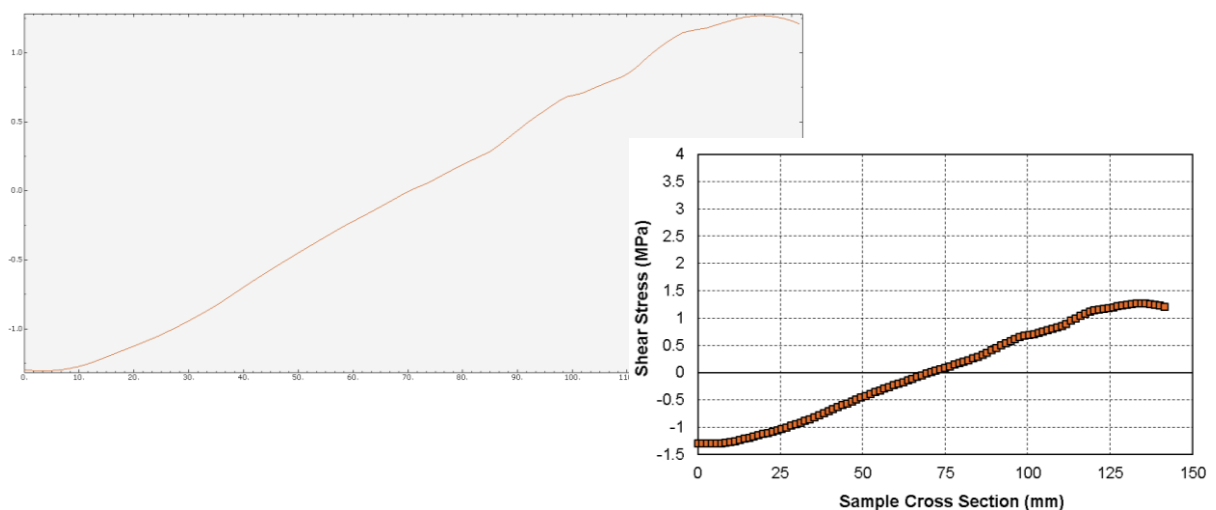


**Figure 5.2.2.2e:** Path 4 Cross Section Shear Distribution

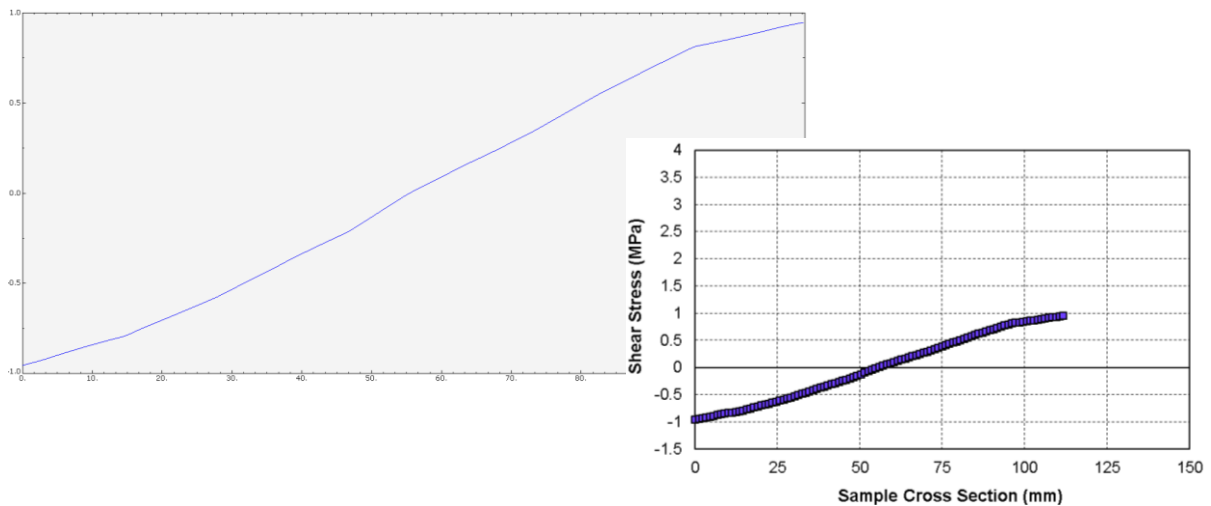


**Figure 5.2.2.f:** Path 5 Cross Section Shear Distribution

As observed, it is noticeable that the testing conditions comprises of many variables that influence the results. From the replicated model, the stress distribution at these locations is attributed to the boundary conditions and the constraints assigned. A detailed description of this constraint is given in 4.2.6.2. Furthermore, linking *Path 4* and *5* to the constraints at this region (Figure 5.2.2.g), it should be noted that the model is restrained in all degrees of freedom at this point. Hence, the shear distribution adheres to a linear function compared to the parabolic distribution pattern observed at the top half of the cross section of the specimen i.e. *Path 2* and *3*.

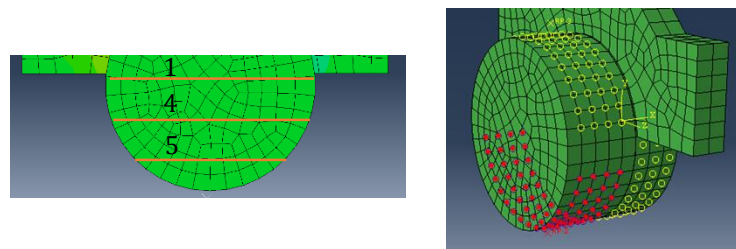


**Figure 5.2.2.g:** Path 3 location for assembly

### 5.2.2.3 Conclusion

Section 5.2.2 gave insight to the shear stress distribution over the cross section of the model within the interface layer i.e. tack coat. It shows the complexity of the shear stress generation despite of the simplicity of the Leutner Test. The distribution patterns observed agree with other research conducted where it was found that the shear progression within the sample is complex apart from the ease of performing the Leutner Test on the samples.

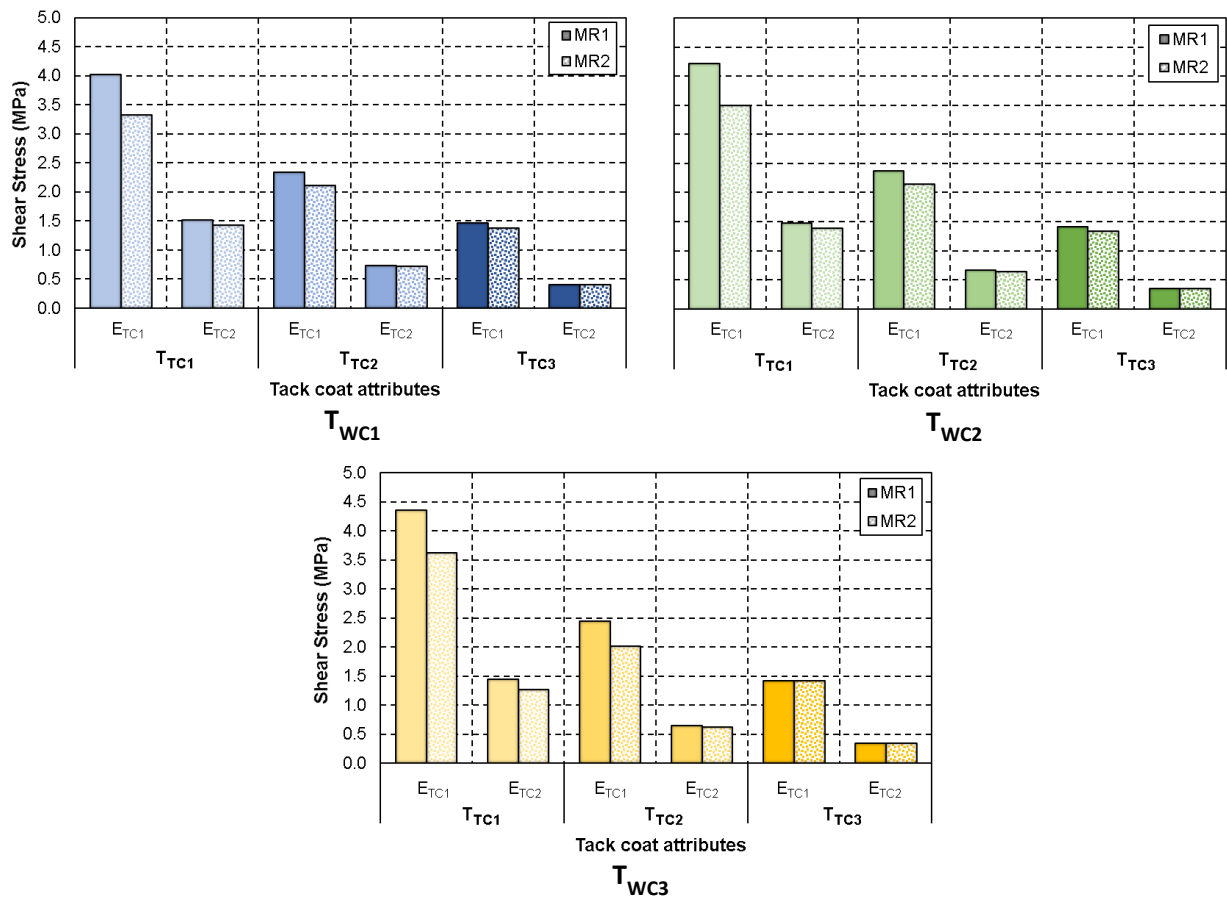
Studying the progression of these distribution patterns within the sample, it is evident that the constraints or boundary conditions of the model play a significant part in shear stress generation. Consequently, indicating that there are variables that significantly control the results from the analysis. These variables will be inspected in subsequent sections, Sections 5.2.3 to 5.2.5. Results obtained in the tack coat layer will be used for discussions in subsequent sections as mentioned in Section 4.2.9. In addition, the trends noticed is mainly justified by the condition of a linear-elastic analysis being performed where a step wise method is used to compute the results. For this instance, Leutner conditions were simplified as explained in Section 4.2.

### 5.2.3 Interface bonding

#### 5.2.3.1 Shear stresses

Keeping in mind the orientation of the coordinate system, distinction is made between positive and negative shear stresses. The sign change (negative versus positive) is only an indication that a change in shear direction has occurred. Hence, only the magnitude of the recorded stresses is of relevance. Section 5.2.2 provides an overview of the shear distribution over the cross-section of this specimen whereas Section 5.2.3 studies the magnitude of these stresses obtained in the analyses. The acquisition of the results are described in Section 4.2.9 where shear stresses were studied in the tack coat.

The minimum, average and maximum shear stress ( $\tau_{min}$ ,  $\tau_{avg}$  and  $\tau_{max}$ ), were recorded for all of the different combinations listed in Section 5.2.1 such as  $t_{wc}$ ,  $E_{TC}$  and MR. A summary of these results are given in Appendix E1. The critical bonding condition i.e. maximum shear stress is illustrated in Figure 5.2.3.1a according to the three different thicknesses specified for the wearing course layer ( $t_{wc}$ ). Furthermore, results are organised according to the defined properties  $t_{TC}$ ,  $E_{TC}$  and MR respectively.



$T_{WC1} = t_{wc1} = 30mm$ ,  $T_{WC2} = t_{wc2} = 50mm$  and  $T_{WC3} = t_{wc3} = 100mm$ ,  $T_{TC1} = t_{tc1} = 0.2mm$ ,  $T_{TC2} = t_{tc2} = 0.5mm$  and  $T_{TC3} = t_{tc3} = 1mm$ ,  $E_{TC1} = 1MPa$  and  $E_{TC2} = 0.21MPa$ , MR1 = 1 ( $E_{base} = 2500MPa$ ) and MR2 = 2.5 ( $E_{base} = 1000MPa$ )

**Figure 5.2.3.1a:** Shear stress results for increase in wearing course thickness

In these graphs, for the modular ratio (MR) and tack coat material stiffness ( $E_{TC}$ ), labelled as 1 and 2 are representative of a decrease in material stiffness. E.g.  $E_{TC1}$  represents a material stiffness of 1 MPa compared to  $E_{TC2}$  with a material stiffness of 0.21MPa. For MR1 a modular ratio of 1 is used with an increased base layer stiffness ( $E_{base}$ ) of 2500MPa. For MR2 with a modular ratio of 2.5 is used considering a lower  $E_{base}$  value of 1000MPa.

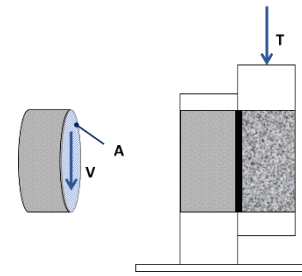
Observations from the results illustrated in Figure 5.2.3.1a are summarised:

1. Shear stresses shown in Figure 5.2.3.1a vary between an approximate minimum of 0.1MPa and maximum 4.35MPa.
2. The change in modular ratio will be discussed in detail in Section 5.2.4. From Figure 5.2.3.1a, the following aspects are noticeable:
  - a. Increase in modular ratio leads to a decrease in shear stresses for the majority of results with exceptions as listed in b, for  $E_{TC2}$  results for  $t_{TC2}$  and  $t_{TC3}$ .
  - b. Extent of change in results varies with other variables such as  $E_{TC}$  and  $t_{TC}$  specially. Studying the change in tack coat thickness ( $t_{TC}$ ), a small variation in shear stresses are visible. For example, almost no variation in shear stresses are observed for  $t_{TC3}$  compared to  $t_{TC1}$ .  $t_{TC3}$  is 1mm compared to 0.2mm represented by  $t_{TC1}$ . This observation shows the influence of tack coat thickness on the shear stress distribution in the pavement structure.
  - c. Change in results or percentage difference for the MR1 and MR2 grouped shear stresses are covered in 5.2.4.1.
3. Studying the results from  $t_{WC1}$  to  $t_{WC3}$ , shear stresses increase with the increase in the wearing course layer thickness:
  - a.  $t_{WC1}$  to  $t_{WC2}$  shows a gradual increase in shear stresses compared  $t_{WC3}$ . The expected increase is attributed to the small variation from  $t_{WC1}$  to  $t_{WC2}$  compared to  $t_{WC3}$ .  $t_{WC1}$  and  $t_{WC2}$  represent thicknesses of 30 and 50mm respectively.  $t_{WC3}$  represents a significant thicker layer of 100mm.
4. It is known that a stiffer material is beneficial for distribution of stresses in the material. This anticipated observation is confirmed when studying results for  $E_{TC1}$  compared to  $E_{TC2}$  in Figure 5.2.3.1a:
  - a. A decrease in tack coat stiffness from 1 to 0.21MPa ( $E_{TC1}$  to  $E_{TC2}$ ), shows a change in the results. However, for  $E_{TC1}$  results, more variation in shear stresses occur than with  $E_{TC2}$  results when comparing MR1 and MR2 grouped results (2 consecutive column graphs).
  - b. Comparing the grouped consecutive column graphs for  $t_{TC1}$  to  $t_{TC3}$  results, a smaller variation in shear stress becomes apparent.
5. Increase in tack coat thickness, from  $t_{TC1}$  to  $t_{TC3}$  is evident. From  $t_{TC1}$  to  $t_{TC2}$  with values from 0.2 to 0.5mm a significant decrease in shear stress occurs. In turn, comparing to  $t_{TC3}$  with a higher thickness of 1mm producing shear stresses that are approximately a third of the stresses achieved for  $t_{TC1}$ .
6. In summary, various combinations of increase and decrease in parameters produce more favourable results. This highlights the fact that different combinations of these parameters have a different impact on the results obtained. This conclusion will be explain by means of results for  $t_{WC3}$ :
  - a. In general, more significant shear stresses are recorded than for other  $t_{WC1}$  and  $t_{WC2}$
  - b. With the increase in  $t_{TC}$  leads to decrease in shear stresses where a decrease in wearing course layer thickness leads to a decrease in shear stresses
  - c. Expected decrease in shear stresses occur with the decrease in  $E_{TC}$  and  $E_{base}$  (consequent increase in MR values)

5.2 Leutner Shear Test Model

5.2.3.2 Shear forces

The shear stress results in 5.2.3.1 were converted to shear forces (V) by means of Equation 5.2.3.2a. The shear stress is the relation of the shear load applied over cross sectional area (A) of the core sample which is approximately 0.02m<sup>2</sup>. Rearranging Equation 5.2.3.2a, the shear force is determined as the product of the measured shear stress and cross sectional area. An illustration is provided in Figure 5.2.3.2a.



**Note:** V also referred to as an axial load (T)

**Figure 5.2.3.2a:** Shear stresses

$$\tau = \frac{V}{A} \tag{5.2.3.2a}$$

Where:

- $\tau$  = Shear Stress (MPa)
- F = Shear force (N)
- A = Cross section area of the core sample (with a diameter of 150mm)

Because testing conditions were simplified for the FE model, it is important to note that the load acquired, is not necessarily the load at failure of the sample. The Leutner Shear Test measures the maximum load i.e. load at failure. For the replicated model a constant displacement was added meaning that the failure load could not be measured. However, the estimation of the shear load will provide an indication of the shear load at the same time period for the different combinations analysed. This will provide a fair comparison of the effect of the different parameters.

Similar as for shear stresses, a summary of the minimum, average and maximum shear forces ( $V_{min}$ ,  $V_{avg}$  and  $V_{max}$ ) are given in Appendix E1 according to change in wearing course thickness,  $t_{wc}$ . The maximum shear forces are shown in Figure 5.2.3.2b. The shear forces are all indicated in kN. Given that the shear forces differ in a numerical sense, the same observations are made in terms of change in shear force relative to parameters such as  $E_{TC}$ , MR,  $T_{WC}$  and  $T_{TC}$ .

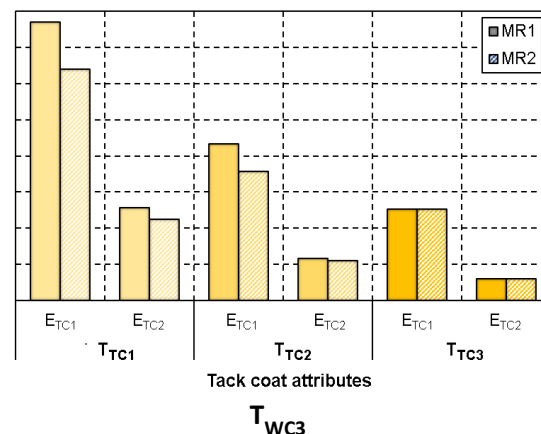
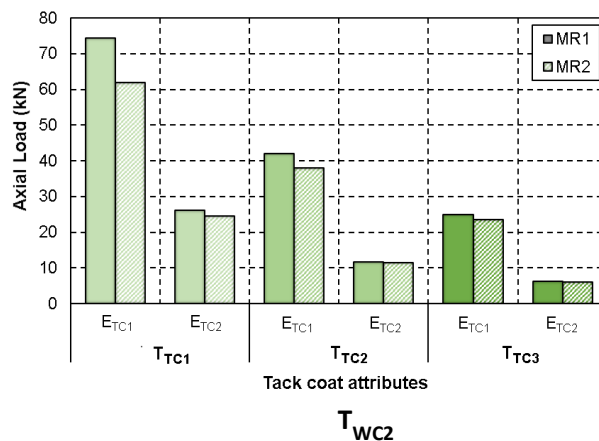
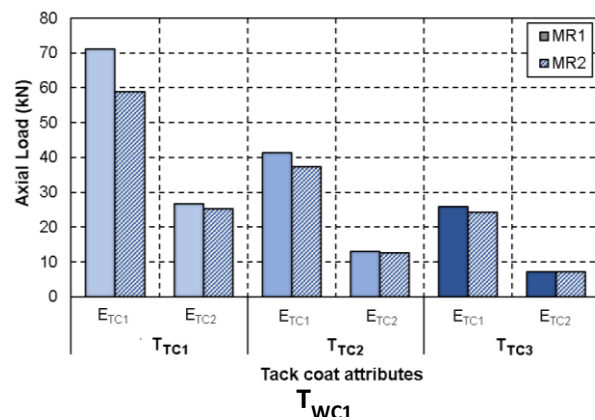


**Figure 5.2.3.2b:** Axial load results for increase in wearing course thickness

### 5.2.4 Critical pavement parameters

Preliminary research undertaken, showed that the modular ratio and top/ surfacing layer thickness contribute to the stress and strain distribution within the pavement structure. Therefore, the material stiffness of consecutive layers i.e. the modular ratio (MR) and top layer thickness ( $t_{wc}$ ) are considered critical pavement parameters. In this specific analysis, the top or surfacing layer is the wearing course layer applied on top of the tack coat.

The results from the analysis of *Model 1* are scrutinized with regards to these two parameters subsequently in 5.2.4.1 and 5.2.4.2. Other critical parameters are relative to the testing condition such as the gap width. Even though it was not evaluated in the FEM models, it should also be taken into consideration when analysing results. The respective section will study the influence of the parameter on the results obtained.

#### 5.2.4.1 Modular ratio

Jenkins & Rudman (2018a) describe the structural capacity as a function of the load spreading potential of the pavement layers, together with the quality of the subgrade on which the pavement is constructed. From the preliminary results in Chapter 3, it was evident that a weak support with a low stiffness modulus would lead to a loss of inter-particle contacts. This occurs especially in the lower parts of granular layers, with a consequent reduction in stiffness and strength under loading (Jenkins & Rudman, 2018b). In addition, with a strong and stiff support e.g. structure combination *Case 2* of Pisa University with the cemented subbase, it is noticeable that the particle contacts are enhanced, which increases the strength and stiffness of the layer.

The principle of the modular ratio (MR) was introduced in 3.4.3.2 and can be demonstrated by the principal of the glass pane on a featherbed with the action of a single load and repetitive loading (Figure 5.2.4.1a).

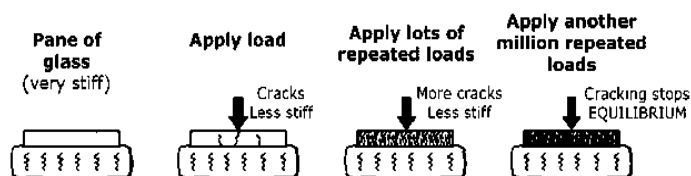


Figure 5.2.4.1a: Pane glass and featherbed illustration (Jenkins & Rudman, 2018b)

The cracking reduces the effective stiffness of the glass pane – lower effective stress reduces stress attracted by glass pane. Hereafter, more stress is transferred to the featherbed. This scenario shows correlation between stiffness (and bonding) and cracking in a pavement situation. The modular ratios used in for *Model 1* analyses are expressed in terms of Equations 5.2.4.1a and 5.2.4.1b. The maximum shear stresses were used for these estimations.

$$MR1 = \frac{E_{WC}}{E_{base1}} \quad (5.2.4.1a)$$

Where:

MR1 = Low modular ratio of 1

$E_{WC}$  = Wearing course layer stiffness of 2500MPa

$E_{base1}$  = Base layer stiffness of 2500MPa

5.2 Leutner Shear Test Model

$$MR2 = \frac{E_{WC}}{E_{base2}} \tag{5.2.4.1b}$$

Where:

MR2 = High modular ratio of 2.5

$E_{base2}$  = Base layer stiffness of 1000MPa

The core sample modelled is composed of two asphalt layers (the wearing course and the base layer) for which two modular ratios were specified. Firstly, a modular ratio of 1 (*MR1*) was defined, implying that the model was composed of two consecutive asphalt layers with the same material stiffness (Equation 5.2.4.1a). The second variation (*MR2*) was used assuming a modular ratio of 2.5, where material of the base layer consisted of asphalt material that is 2.5 times smaller in magnitude (Equation 5.2.4.1b). The wearing course layer was kept constant at a stiffness of 2 500MPa. Given the two modular ratios, a base layer stiffness of 2 500MPa (MR of 1) and 1 000MPa (MR of 2.5) was used. The shear stress results recorded during the analysis are illustrated in Figure 5.2.4.1b according to the increase in wearing course thickness ( $T_{WC}$ ). In turn, the results obtained for the two modular ratios are shown in two consecutive column graphs. These graphs illustrate the different combinations of testing conditions.

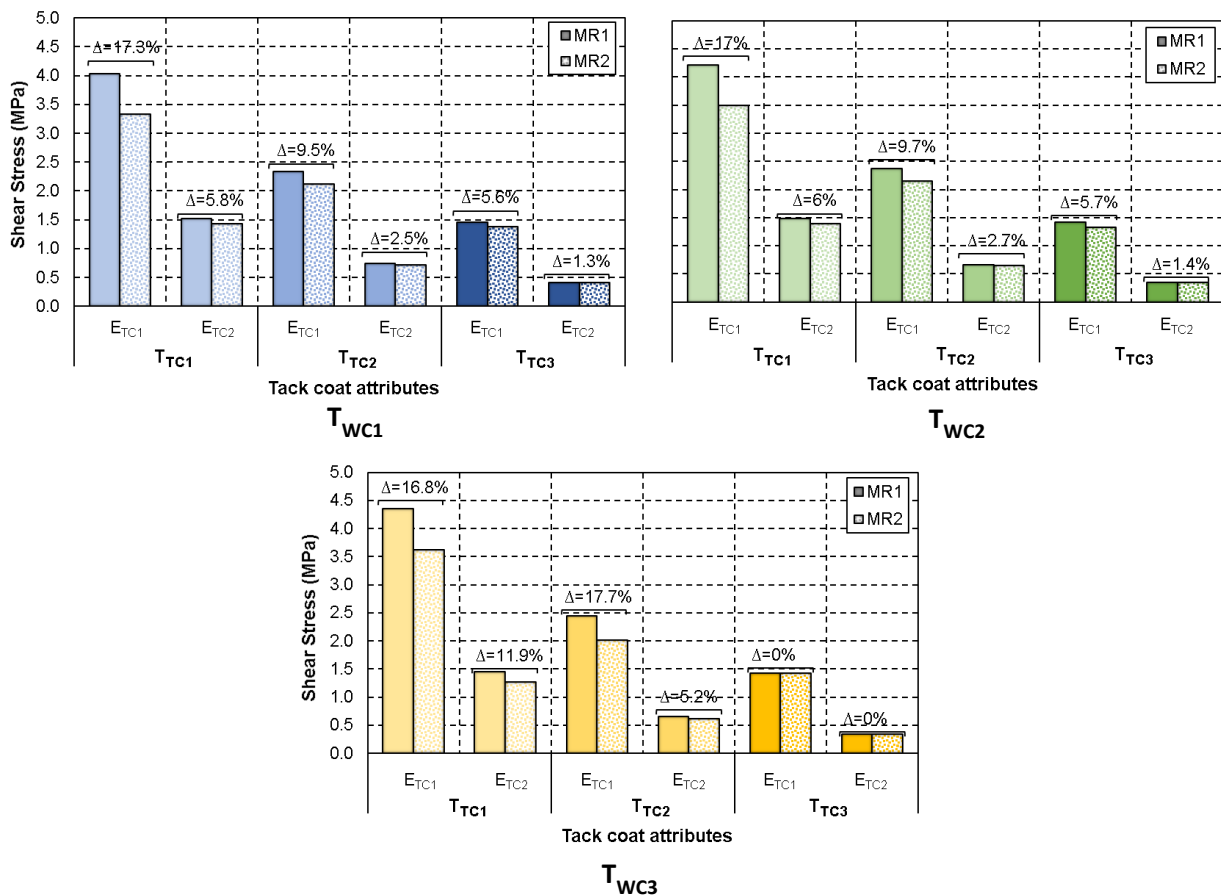


Figure 5.2.4.1b: Comparison of shear stress according to modular ratio

The effect of change in modular ratio is expressed with Equation 5.2.4.1c as a ratio of change in shear stress results of *MR1* and *MR2* to shear stress result of *MR1*. The formula is the equivalent used in Chapter 3 to indicate the difference in results in terms of the different friction conditions (Equation 3.2.3a), while the equivalent parameter used for modular ratio estimations is  $\Delta_{MR}$  in Equation 5.2.4.1c.

$$\Delta_{MR} = \frac{\tau_{MR2} - \tau_{MR1}}{\tau_{MR1}} \quad (5.2.4.1c)$$

Where:

- $\Delta_{MR}$  = Percent difference according to Modular Ratio
- $\tau_{MR1}$  = Shear stress achieved for MR1 defined modular ratio (MR = 1)
- $\tau_{MR2}$  = Shear stress achieved for MR2 defined modular ratio (MR = 2.5)

From the results, the following attributes can be observed:

1. A minimum change in modular ratio was obtained as 1.3%, where the highest difference achieved was 17.3%. For the structure composed of a wearing course layer thickness of 100mm ( $t_{WC3}$ ) with a tack coat thickness of 1mm ( $t_{TC3}$ ) an insignificant change in results is observed.
2. An increasing change in the  $\Delta_{MR}$  parameter occurs for the tack coat with the lowest material stiffness  $E_{TC2}$ , compared to a model composed of a tack coat with higher stiffness,  $E_{TC1}$ .
3. The thickest layer,  $T_{WC3}$ , is 3 times the thickness of  $T_{WC1}$  and twice the thickness specified for  $T_{WC2}$ . The change in thickness was selected to investigate the extent of influence of this parameter with a drastic increase in layer thickness.
4. In general, the results suggest that a decrease occurs in change in modular ratio parameter ( $\Delta_{MR}$ ) with the increase in wearing course thickness. The same trend is prominent for the increase in the properties of the tack coat (tack coat thickness,  $T_{TC1}$  to  $T_{TC3}$  and tack coat stiffness,  $E_{TC1}$  and  $E_{TC2}$ ).

#### 5.2.4.2 Wearing course layer thickness

A continuous program for sustaining and building of road infrastructures is regarded as common practice in both developed and developing countries (Panda et al., 2013). Attention is given to this aspect as roads play an important role in a country's growth and development. A solution to achieve sustainability in road projects is by improving existing road infrastructure to strengthen the existing surfacing layer to withstand the increase in traffic it is subjected to. The approach used involves overlaying the existing asphalt layer with another asphalt layer of appropriate material composition and thickness ( $t_{WC}$ ). The overlaying layer is referred to as the wearing course layer as indicated in Figure 5.2.2.2a.

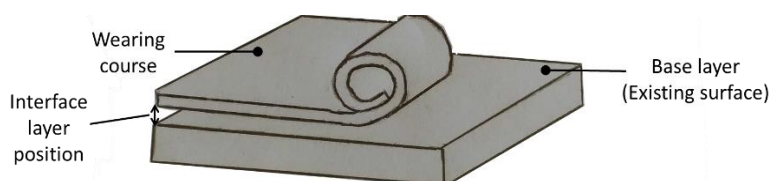
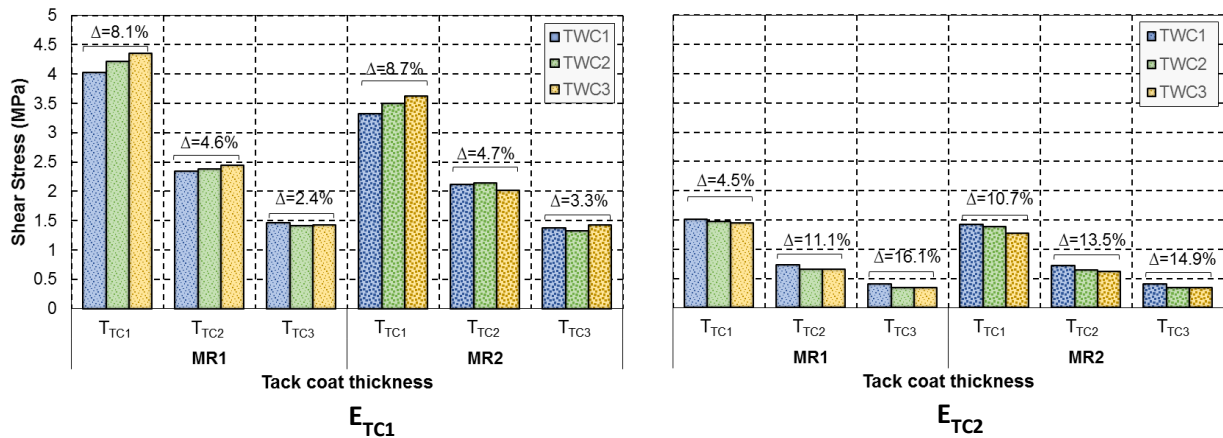


**Figure 5.2.4.2a:** Schematization of constructed pavement layers

The adhesion between the two asphalt layers is increased by placing a bitumen emulsion layer (tack coat) prior to the overlay, on the existing (or newly constructed) surface. In addition, the boundary between the two asphalt layers is where the interlayer is placed. According to Panda et al. (2013), it is believed that the pavement stress distribution has the consequential effect on the adhesion condition at the interlayer. As seen in the preliminary research by Stellenbosch University, the thickness of the top layer contributed to the stress distribution. Therefore, the thickness of this layer is of interest for the interpretation of the shear stresses measured in the core sample. Although, the stress distribution will be evaluated to the same extent as in the preliminary research, the stresses measured at the different thicknesses defined for this parameter will highlight its influence.

## 5.2 Leutner Shear Test Model

The maximum shear stresses obtained in the analysis are shown according to the different wearing course thicknesses in Figure 5.2.4.2b,  $T_{WC1}$ ,  $T_{WC2}$  and  $T_{WC3}$ . The results in the respective figures are sorted by the different parameters listed in the introduction paragraph of Section 5.2. Figure 5.2.2.2b (left) shows the results for the higher tack coat stiffness ( $E_{TC1}$ ), and Figure 5.2.2.2.b (right) represents results obtained for tack coat with a lower stiffness ( $E_{TC2}$ ). The evaluation of results in context of the variety of tack coat properties is addressed subsequently in Section 5.2.5. The variability in results are evaluated with a similar approach as was used in Equation 5.2.4.1c and is also illustrated in this figure.



**Note:**  $TWC1 = T_{WC1} = 30\text{mm}$ ,  $TWC2 = T_{WC2} = 50\text{mm}$  and  $TWC3 = T_{WC3} = 100\text{mm}$ ,  $T_{TC1} = 0.2\text{mm}$ ,  $T_{TC2} = 0.5\text{mm}$  and  $T_{TC3} = 1\text{mm}$ ,  $E_{TC1} = 1\text{MPa}$  and  $E_{TC2} = 0.21\text{MPa}$ ,  $MR1 = 1$  and  $MR2 = 2.5$  ( $E_{base} = 1000\text{MPa}$ )

**Figure 5.2.4.2b:** Shear stress comparison according to wearing course and tack coat stiffness

Studying the results shown in Figure 5.2.4.2b in terms of the wearing course thickness only (3 consecutive column graphs), the following observations are made:

1. For the tack coat material stiffness of 1MPa ( $E_{TC1}$ ), an increase in shear stress occurs only for the  $T_{TC1}$  set of results. A variation of increase and decrease in shear stresses can be noted for  $T_{TC2}$  and  $T_{TC3}$  result sets.
2. In contrast, for the tack coat with lower material stiffness ( $E_{TC2}$ ), a decrease in shear stresses occur.
3. Contribution of other parameters such as MR and tack coat thickness,  $T_{TC}$  are addressed in 5.2.4.1 and 5.2.5.2.
4. The variability in the results are evaluated and indicated in Figure 5.2.4.2b. The results are summarised as follows:
  - a. The results suggest that a 233% increase in layer thickness (70mm increase), leads to a variation in results between percentages of 2 and 16%
  - b. For  $E_{TC1}$ , results vary from 4.6 to 8.7%. Higher percentages of 10.7 to 16% was achieved for  $E_{TC2}$  results with an outlier of 4.5% recorded
5. Alternatively, progressive variation in results relative to the change in  $T_{WC}$  is determined by estimating the difference assuming an average value of shear stress for each  $T_{TC}$  group. These results are shown in Figure E2 in Appendix E1. The following is observed:
  - a. More variation in results for tack coat with lower stiffness value with change in results varying between 45 up to 54%
  - b. A smaller variation occur in results for the higher stiffness ranging between 34 up to 43%.

- c. To conclusion, the contribution of the previous identified critical parameter i.e. material stiffness, is also highlighted

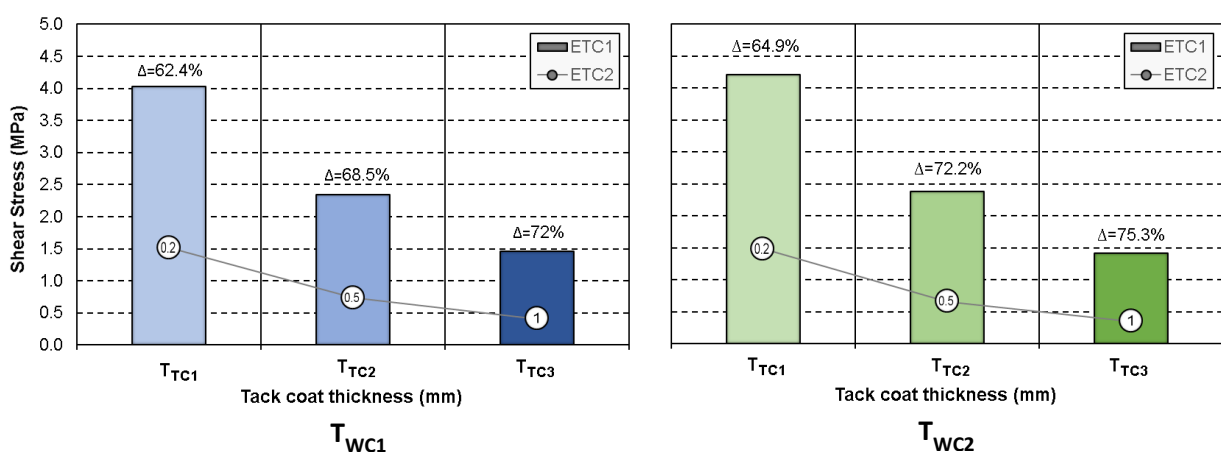
### 5.2.5 Tack coat properties

The different functions and characteristics of tack coat, i.e. materials and tack coat practices were introduced in Section 2.2 of the Literature Review. The different components of the materials used as tack coats in road construction have also been found to significantly impact the type of bonding provided (interface shear) when the pavement structure is subjected to loading once opened for traffic, as discussed in Section 2.3. Studying these two subject matters in parallel, it was found that the attributes, such as the application rate and other construction or design considerations, affect the extent of interlayer bonding achieved.

It is important to note that not all of the influential factors discussed in Chapter 2 are incorporated, given the extensive list. For this reason, it is of utmost importance to evaluate the results based on the characteristics of the tack coat, i.e. the material stiffness ( $E_{TC}$ ) and the layer thickness ( $T_{TC}$ ). Similar to Section 5.2.4, this section investigates the effect of tack coat properties on the shear stresses obtained from the FE model.

#### 5.2.5.1 Material stiffness

As discussed in Chapter 4, the material stiffness was derived from results acquired during research conducted by van Zyl (2018). From this research, a material stiffness of 0.21MPa was determined to represent a 50-70 penetration grade bitumen emulsion used as tack coat material. Furthermore, a higher stiffness of 1MPa was also used to describe the material stiffness of the tack coat material for the Leutner model (*Model 1*). Figures 2.5.3.1a summarises the shear stress results according to the three prescribed wearing course layer thicknesses,  $T_{WC1}$ ,  $T_{WC2}$  and  $T_{WC3}$ . The results in this figure are results for the lower modular ratio, MR1. Results for MR2 comply with similar observations made as for MR1 results shown in Figures 5.2.5.1a and 5.2.5.1b. The MR2 results are provided in Figure E3 in Appendix E1. In these figures it is noticeable that an increasing change in shear stress occurs with the increase in tack coat thickness.



$T_{WC1} = t_{wc1} = 30mm$ ,  $T_{WC2} = t_{wc2} = 50mm$  and  $T_{WC3} = t_{wc3} = 100mm$ ,  $T_{TC1} = t_{tc1} = 0.2mm$ ,  $T_{TC2} = t_{tc2} = 0.5mm$  and  $T_{TC3} = t_{tc3} = 1mm$ ,  $E_{TC1} = 1MPa$  and  $E_{TC2} = 0.21MPa$ ,  $MR1 = 1$  ( $E_{base} = 2500MPa$ ) and  $MR2 = 2.5$  ( $E_{base} = 1000MPa$ )

**Figure 5.2.5.1a:** Tack coat stiffness influence for wearing course thickness for MR1 for  $T_{WC1}$  and  $T_{WC2}$

5.2 Leutner Shear Test Model

An expected decrease in developed shear stress generation within the layer occurs with the increase in material stiffness. With a stiffer material, stresses of smaller magnitude are to be experienced. The same observation was made for MR2 results in Appendix E1 with the exception of shear stress values. The nature of the results obtained emphasises the contribution of material layer stiffness. From the results it could be seen that the increase and decrease of this material property have influences on the results to a certain extent. A modular ratio higher than 2.5 (MR1 case) produced smaller variations. This corresponds to the typical behaviours discussed within pavement structures concerning stress development.

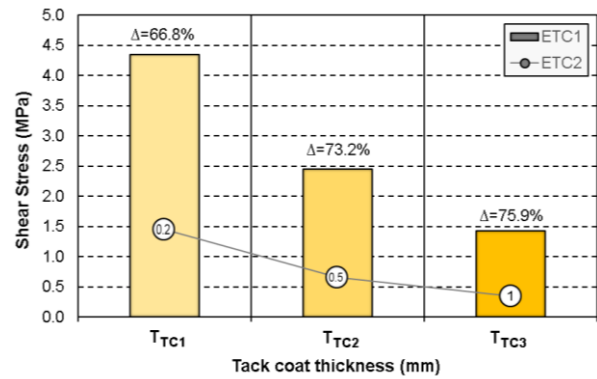


Figure 5.2.5.1b: Tack coat stiffness influence for wearing course thickness for MR1 for T<sub>WC3</sub>

5.2.5.2 Layer thickness

Influential factor impacting interlayer bonding was discussed in Section 2.2. One of these topics involved the construction of a tack coat layer where the discussion included the quantity of tack coat material and the application rate. These two factors were not explicitly incorporated into the FEM replication of the Leutner Shear Test. However, these two attributes do relate to the layer thickness placed during construction. Hence, the three different defined thickness values for the tack coat, T<sub>TC1</sub> to T<sub>TC3</sub> (0.2mm, 0.5mm and 1mm), actually represent three different combinations of application rate and material quantities. Typical tack coat thicknesses were considered for the replicated FEM model (0.2mm, 0.5mm and 1mm).

Shear stress results are organised according to the tack coat thickness, T<sub>TC</sub>, in Figure 5.2.5.2a. The shear stress results are organised according to the parameter in question (tack coat thickness) in Figure 5.2.5.2a. In this figure, the results are shown relative to the model, comprising of a tack with lower material stiffness (E<sub>TC1</sub>) in Figure 5.2.5.2a (left) and the higher tack coat stiffness, E<sub>TC2</sub>, in Figure 5.2.5.2a (right).

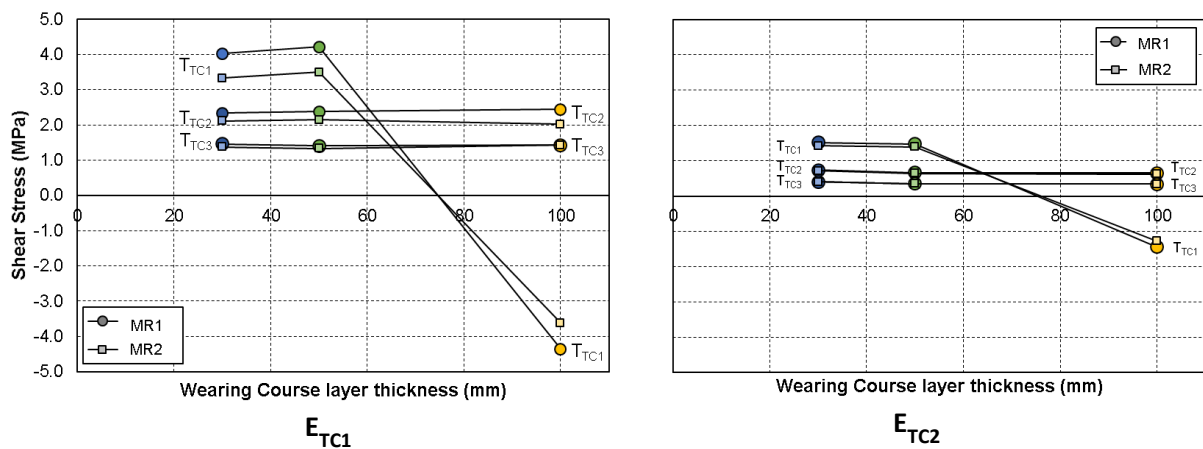
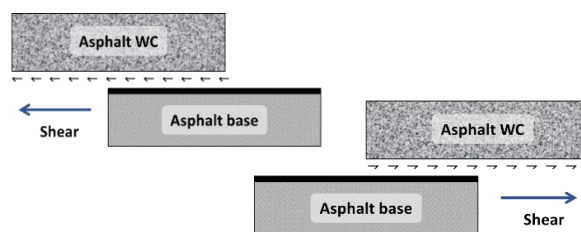


Figure 5.2.5.2a: Shear distribution for E<sub>TC1</sub> and E<sub>TC2</sub>

## 5.2 Leutner Shear Test Model

The negative and positive shear stress convention in these figures denote the variation in the shear stress, with the increase in wearing course thickness. The sign of the shear stress (negative versus positive) is merely an indication of the direction of shear, relative to the coordinate axis of the model. This is demonstrated in Figure 5.2.5.2b. Hence, for previous sets of results, the absolute shear stress values were used.



**Figure 5.2.5.2b:** Shear stress between layers

Evaluating the results shown in Figure 5.2.5.2a, the following is concluded:

1. As observed previously, higher shear stresses are obtained for the stiffer tack coat material i.e.  $E_{TC1}$ .
2. Studying results of  $T_{TC3}$  relative to  $T_{TC1}$ , shows a decrease in shear stress with increase in tack coat thickness with the exception of  $T_{TC1}$ . However,  $T_{TC1}$  results are in agreement with this observation if considering the absolute value of shear stress.
3. It is interesting to note that contrast behaviours are noticeable when comparing with  $T_{WC1}$  observations made in 5.2.4.2:
  - a.  $T_{TC1}$  and  $T_{TC2}$  which only differs with 0.3mm shows a larger decrease in shear stresses compared to  $T_{TC2}$  and  $T_{TC3}$ , with a 0.5mm gap. Aforementioned, are shear stresses with insignificant variation.
    - i.  $T_{TC1}$  and  $T_{TC2}$ : For  $E_{TC1}$ , a difference of 1.5 to 2.5MPa is visible, considering absolute values of shear stresses. For the decreased tack coat stiffness,  $E_{TC2}$ , varied with approximately 1.5MPa
    - ii.  $T_{TC2}$  and  $T_{TC3}$ : For  $E_{TC1}$ , a difference of 0.5 to 1MPa is visible, considering absolute values of shear stresses. For the decreased tack coat stiffness,  $E_{TC2}$ , varied with approximately 0.5MPa
  - b. Therefore, it is concluded that the increase in the shear stresses reach some sort of “optimum” level where the increase in tack coat thickness has a minimal contribution to the results.
4.  $T_{TC1}$  for both  $E_{TC}$  and MR groups follow a similar pattern where negative shear stresses are recorded for the thickest wearing course layer,  $T_{WC3}$ :
  - a. For the higher stiffness,  $E_{TC1}$ : from 30mm to 50mm wearing course thickness ( $T_{WC1}$  to  $T_{WC2}$ ) an increase occurs followed by a significant decrease from  $T_{WC2}$  to  $T_{WC3}$  (100mm)
  - b. For the lower stiffness,  $E_{TC2}$ : from  $T_{WC1}$  to  $T_{WC2}$ , an increase occurs for  $T_{TC2}$  and decrease occurs for  $T_{TC3}$  followed by a slight increase relative to  $T_{WC3}$ . For  $T_{TC2}$  MR2, a contrasting decrease is observed.
5.  $T_{TC2}$  and  $T_{TC3}$  result follow similar pattern consisting of positive shear stresses as described in the following points:
  - a. For the higher stiffness,  $E_{TC1}$ : from 30mm to 50mm wearing course thickness ( $T_{WC1}$  to  $T_{WC2}$ ) a decrease occurs followed by a significant decrease from  $T_{WC2}$  to  $T_{WC3}$  (100mm).
  - b. For the lower stiffness,  $E_{TC2}$ : from  $T_{WC1}$  to  $T_{WC2}$ , a decrease occurs in shear stress followed by an insignificant change relative to  $T_{WC3}$ .

## 5.2 Leutner Shear Test Model

6.  $E_{TC2}$  results shown in Figure 5.2.5.a (right) are in closer approximation compared to  $E_{TC1}$  results shown in Figure 5.2.5.a (left). This shows that with the increase in material stiffness of the tack coat together with the change in tack coat thickness results in more variance in shear stress.
7. Similar estimations as listed in points 4 and 5 in 5.2.4.2 were completed relative to change in tack coat thickness. These results are not of significant importance as it is in agreement with observations listed in these points previously. An illustration is provided in both capacities in Figures E4 and E5 in Appendix E1. Observations of these figures include the following:
  - a. More variation in results for tack coat with lower stiffness value with change in results varying between 5.8 up to 6.8% with the exception of a 1.7% difference for  $T_{WC3}$  results relative to  $T_{WC2}$ .
  - b. A smaller variation occur in results for the higher stiffness ranging between 1.2 up to 2.8%.

### 5.2.6 Test Configuration: Gap Width

Section 5.2.3 to 5.2.5 studied the mechanical conditions and its influence on the results obtained. However, it should be noted that the test configuration can also contribute to the results obtained. Even though a constant gap width was used, the influence of this aspect has been evaluated in research Sutanto. Hence, also considered a critical parameter to be considered when evaluating results.

Considering the geometry of the 100mm wearing course layer sample, the orientation of the wearing course and layer was swapped with the wearing course, being the part constricted (clamped) on the sample support section of the model for “stability” issues concerning the placing of the core sample. The gap width is of significance with the shear distribution obtained given the nature of the testing. The orientation of the sample does not, however, have an impact.

The gap width is a critical attribute of Leutner testing identified in Chapter 2. According to Sutanto (2009), the gap width provides a certain tolerance level in accommodating tests performed with specimens with skewed or “rough” interfaces. It was found that a too large gap causes excessive bending stress. This is attributed to an instance where a too large gap width is allowed and the unsupported specimen experiences a cantilever effect. Hence, the support of the sample is crucial.

For the purpose of this Leutner Shear Test model, the gap width was set to an allowable 2.5mm and the majority of the sample support was simulated by means of boundary conditions and constrains. These boundary conditions were assigned to the entire relative region supported. The boundary conditions are found to reduce the cantilever effect experienced between the interface and the wearing course layer, in turn reducing the effect of bending stresses induced in the model.

### 5.2.7 Summary of Results

This section studied the results obtained from the Leutner Test replication i.e. *Model 1*. The results were studied relative to each of the variables specified in the analysis:  $T_{TC}$  and  $E_{TC}$  (tack coat properties),  $T_{WC}$ ,  $E_{base}$  linked with MR. A summary of these parameters are shown with an example output of the results in Figure 5.2.7a.

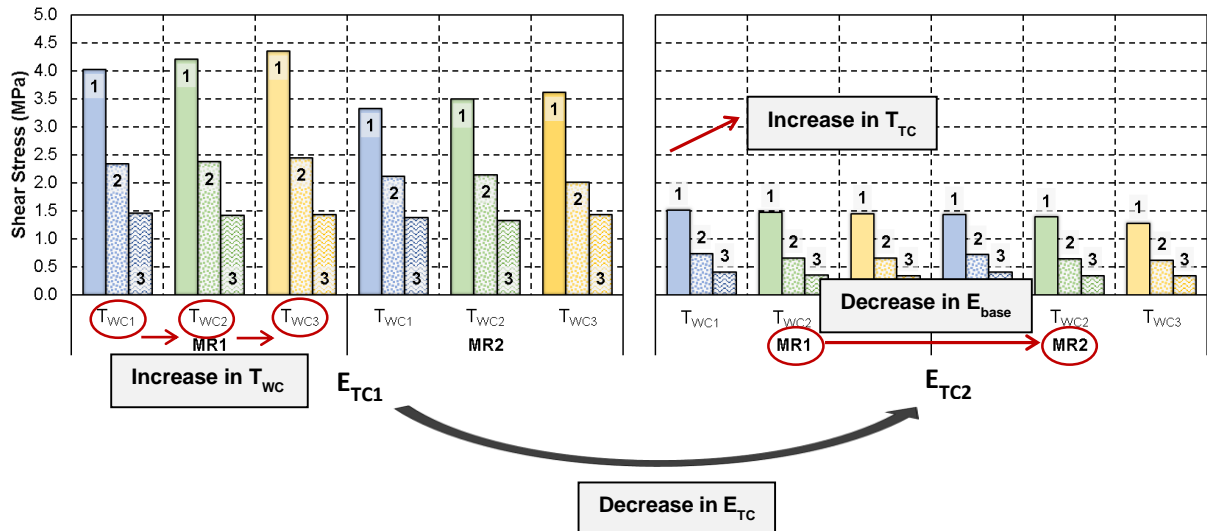


Figure 5.2.7a: Shear stress between layers

From a visual inspection of Figure 5.2.6a, it is noted that the properties of the tack coat,  $E_{TC}$  and  $T_{TC}$ , are the two most critical parameters. These parameters have a significant impact on the shear stresses generated in the bonding layer. Further inspection reveals that,  $E_{TC}$  is found to be the most critical. This is because the stiffness has a direct relationship with shear distribution. The function of the tack coat is evident. Hence, the stiffness of this material should be selected with care as it has significant influence of the composed pavement structure under certain loading conditions.

### 5.2.8 Model 1 versus Preliminary Research

The preliminary analyses completed by Stellenbosch and Pisa University and discussed in Chapter 3, provided the foundation of the *Phase 1* research. This phase provided an elementary understanding of the shear development within selected pavement structures. Pisa University expanded their scope with a series of laboratory testing with the Leutner Shear Test.

This section compares the preliminary results with those obtained for the replicated Leutner Model i.e. *Model 1*. The structure of subsequent discussions is illustrated in Figure 5.2.8a. The components evaluated are also mentioned in this figure. Firstly, results of the replicated model will be compared

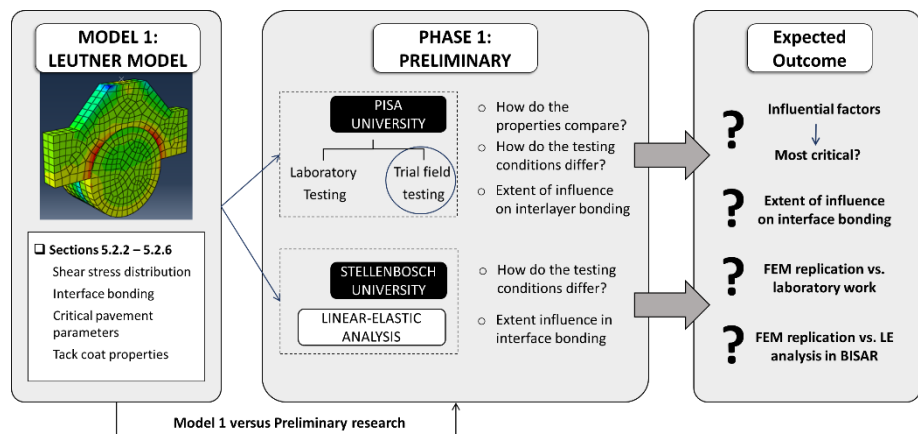


Figure 5.2.8a: Structure of comparative studies

with preliminary laboratory work carried out by Pisa University. Subsequently, a comparative study is completed for the preliminary linear-elastic analysis by Stellenbosch and *Model 1*. These comparisons are completed in 5.2.8.1 for preliminary laboratory and 5.2.8.2 for linear-elastic analysis.

### 5.2.8.1 Preliminary laboratory work

The scope of the laboratory testing was given in Section 3.3. In summary, Pisa University evaluated interlayer shear strength (ISS) with two types of testing i.e. laboratory and trial field testing. All of the differently composed samples were tested by means of Leutner Shear Testing.

For the purpose of the comparison, only one set of results of *Model 1* will be used. Results obtained for the trial field testing in 3.3.2.3 is used given the corresponding variable – wearing course thickness,  $T_{wc}$ . A summary of the results are shown in Table 5.2.8.1a where a comprehensive set of results is provided in Appendix A for all laboratory testing completed. For calculation purposes, the averaged values of the series will be used, otherwise an extensive set of combinations exist for comparison between two analyses. The results in the table are for samples where tack coat was applied with Spray Jet technology.

**Table 5.2.8.1a:** Trial field testing results for Series I (After Bianchi, 2018)

Series	Specimen	Avg load (kN)	Avg ISS (MPa)	$T_{wc}$ (mm)	Avg $T_{wc}$ (mm)	Tack quantity $l/m^2$	Equivalent thickness, $T_{TC}$ (mm)
I	A	17.8	1.74	38.3	45.57	0.26	0.25 (0.15 residual)
	B			35.1			
	C			40.3			
	D			35.1			
	E			35			
	F			49.3			

**Note:** ISS = Interlayer Shear Strength (equivalent of shear stress measured in FEM). The average wearing course thickness is the representative  $T_{wc}$  value for laboratory testing and equivalent thickness determined is the  $T_{TC}$  value for laboratory testing

The quantity of tack coat can be used to determine the equivalent thickness. One litre of tack coat material is equivalent to 1 000cm<sup>3</sup> material. In practice, this would represent a 1mm layer thick tack coat layer spread over a 1m × 1m area. The conversion is based on the assumption that bitumen emulsion has the same density as water. Hence, 1 000g/cm<sup>2</sup> is the equivalent of 1L.

Applying these guideline conversions, the tack quantity used in these prepared samples is equal to 0.25L in capacity, or represents a 0.25mm thick layer of bitumen emulsion. According to Committee of State Road Authorities (1994), 0.25mm emulsion will only provide 60% of residual bitumen i.e. 0.15mm. Hence, 0.15mm bitumen emulsion is sprayed over a 1m × 1m area as indicated in Table 5.2.8.1a. The estimated thickness is the equivalent thickness to be used as comparison with the three different tack coat thicknesses used for the FEM analyses, i.e. 0.2mm, 0.5mm and 1mm ( $T_{TC1}$ ,  $T_{TC2}$  and  $T_{TC3}$ ).

A summary of maximum shear stresses recorded for the FEM model according to change in wearing course thickness and tack coat thickness:

1. Wearing course thickness,  $T_{wc}$ :
  - a.  $T_{wc1}$ : Ranging between 0.4 and 4MPa
  - b.  $T_{wc2}$ : Ranging between 0.3 and 4.2MPa
  - c.  $T_{wc3}$ : Ranging between 0.3 and 4.4MPa

2. Tack coat thickness,  $T_{TC}$ :
  - a.  $T_{TC1}$ : Ranging between 1.3 and 4.4MPa
  - b.  $T_{TC2}$ : Ranging between 0.6 and 2.5MPa
  - c.  $T_{TC3}$ : Ranging between 0.3 and 1.5MPa

The following is observed with regard to shear stresses under two scenarios given:

1. Comparing the average wearing course of 45.57mm with the three defined wearing course thicknesses of replicated model,  $T_{WC1}$ ,  $T_{WC2}$  and  $T_{WC3}$ .
  - 56.5% decrease for  $T_{WC1}$ , 58.6% decrease for  $T_{WC2}$  and a 60.5% decrease for  $T_{WC3}$  results. These estimations are completed using the maximum shear stresses listed for  $T_{WC1}$ ,  $T_{WC2}$  and  $T_{WC3}$ .
2. The exercise is repeated relative to the tack coat thickness:
  - 60.5% decrease for  $T_{TC1}$ , 30.4% decrease for  $T_{TC2}$  and a 60.5% increase for  $T_{TC3}$  results. Similar to point 1, these estimations are completed using the maximum shear stresses listed for  $T_{TC1}$ ,  $T_{TC2}$  and  $T_{TC3}$ .

### 5.2.8.2 Linear-elastic analysis

Traditionally, interlayer bonding between two subsequent layers can be described by means of the amount of friction experienced and is represented by some form of friction coefficient. For the linear-elastic (LE) analysis completed, a significant difference in results is observed attributed to the incorporation of the interlayer attribute. This observation is justified when compared results from Stellenbosch University in Section 3.2 and Pisa University in Section 3.3. For Stellenbosch University, the component was added by means of a shear spring compliance which is taken as a proportion of the load radius. Pisa University adhered to guidelines similar to that of a friction coefficient.

For the FEM model, friction interaction was not incorporated, but instead allowed the incorporation of the properties of the tack coat as a cohesive section or region. Given the different applications, this section highlights the influence of the two different approaches used for the incorporation of interlayer bonding. This will be carried out only considering approach by Stellenbosch University.

The shear stresses recorded for the tack coat layer will be compared with the interface shear achieved in the preliminary research analysis referred to as *Interface 1*. Results of the friction conditions, high, medium and low, will be compared with the bonding applied in the FEM model. The extent of the difference between the results sets can be recorded following a mathematical approach as set out in Appendix E1. A detailed calculation example is also provided.

A summary of linear-elastic analysis shear stress results are listed as follows, according to each loading conditions:

1. Tyre 1 (T1 loading condition):
  - a. HF: Ranging between 0.6 and 0.1MPa
  - b. MF: Ranging between 0.2 and 1.1MPa
  - c. LF: Ranging between 0.2 and 1.2MPa
2. Tyre 2 (T2 loading condition):
  - a. HF: Ranging between 0.1 and 0.8MPa
  - b. MF: Ranging between 0.3 and 1.3MPa
  - c. LF: Ranging between 0.3 and 1.4MPa

Following the guidelines stipulated in Appendix E1, the following listed aspects are derived when studying the results estimated:

1. For all results, a decrease in results occur from results obtained from *Model 1*, compared to those acquired from the LE models;
2. As the bonding condition (friction) decreases, the variation in results decreases;
3. Comparing results with FEM models with an increased  $E_{base}$  value (or smaller modular ratio), a smaller change in results noticeable;
4. The same prominent observation is made in terms of the wearing course thickness given the nature of the results produced (5.2.4.2);
5. From the LE analysis, an increase in  $t_{Asphalt}$  showed similar behaviour to that described in 3: increase in results variation for *Case 1/3* combination, but a decrease in variation for the *Case 2/4* combination;
6. In addition, from the LE analysis, for an increase in  $E_{base}$ , familiar behaviour is prominent in the results

## 5.3 Pavement Analysis Model

### 5.3.1 Introduction

The performance and remaining life of asphalt pavements and its dependency on interlayer bonding state have been promoted in various studies. This includes research by Wang et al. (2017), which entailed the collection of a variety of samples that were subjected to shear testing. Research was undertaken as part of *Phase 1* research, completed in collaboration with Pisa University. Based on the findings made, the FEM analysis suggested enhancing the evaluation of stresses and strains at critical locations describing classical modes of failure in pavements, i.e. rutting (subgrade layer) and fatigue cracking (asphalt surfacing).

The calculations of strains induced in the pavement structure by a single wheel load (tyre pressure) were completed from the normal stresses measured within the three-dimensional modelling space in the x-, y- and z – directions (Section 4.3.6). Subsequent strains were used aligned with the South African Mechanistic-Empirical Design Method (SAMDM) to estimate the pavement life, addressing the different pavement distresses identified at the critical locations.

The four pavement structures used for linear-elastic analyses in BISAR were replicated as finite element models in Abaqus. Similar testing conditions were added to the duplicated versions, where some adjustments were made. The adjustments included the simplification for incorporating friction – the bonding layer, i.e. tack coat. It was modelled as part of the pavement structure and assigned material properties. Consequently, no state of bonding was described in the model through different friction states

A comprehensive summary of the analysis covering all testing combinations was provided in Section 4.3, where the different elements concerning the set-up of the model replicated was also discussed. A total of eight analyses were performed. The procedure followed for the *Pavement Analysis* model (*Model 2*) is presented in Figure 5.3.1a. For discussion and interpretation of the results of this model, it will be referred to as the *Pavement Analysis* model or *Model 2*, interchangeably.

## 5.3 Pavement Analysis Model

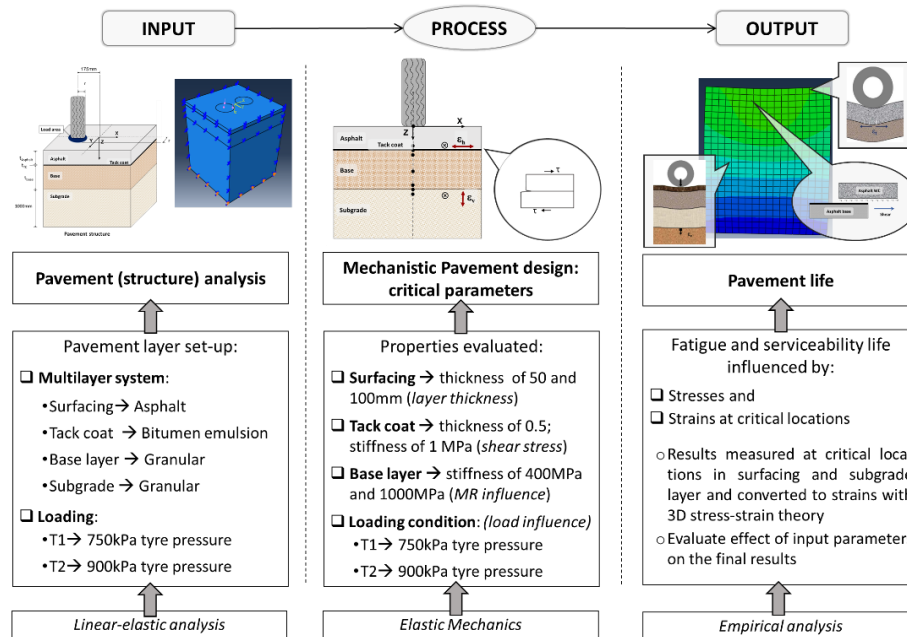


Figure 5.3.1a: Analysis approach for Pavement Analysis model

The primary objective of this model is to evaluate the durability of different pavement structures, addressing the different attributes of the testing regime shown in Figure 4.3.7a. The objective is achieved by evaluating the impact each of these attributes have on the results obtained in the different capacities i.e. normal and shear stress as well as strains. Moreover, the results recorded expand the observations and findings made from the results interpreted from the linear-elastic analysis. Similar to discussion of Model 1 results, a section is devoted to discuss each of these important attributes. These attributes are interface bonding, stresses and strains and pavement life prediction. The discussion of these attributes occurs according to specific criteria addressed. It also studies the extent of influence of each of the attributes according to:

1. Failure modes according to the shear stress results (applicable to *Interface bonding* section, Section 5.3.2);
2. Variation in surface layer thickness ( $t_{\text{Asphalt}}$ ) - *thickness of 50mm and 100mm*;
3. Variation in base layer stiffness in turn changes in the modular ratio ( $E_{\text{base}}$ ) – *stiffness of 400MPa and 1 500MPa, which represent modular ratios of 6.25 and 1.67*;
4. Increase in loading subjected to the pavement structure ( $T1$  and  $T2$ ) – *tyre pressure of 750kPa and increased tyre pressure of 900kPa (both loads considered comprise of single axle tyre loading)*.

In contrast with Section 5.2, the discussion of results will adhere to a comparative structure. Each section will summarise the pertinent observations followed by a comparison with results of the preliminary linear-elastic analysis completed in BISAR in Section 3.2.

### 5.3.2 Interface bonding

Chapter 2 reported that interface failure can be attributed to both shear and tension distress under traffic loading as illustrated in Figure a. In this figure, the direction of the traffic is indicated towards the right. Furthermore, this chapter showed that these failures can be categorised in three separate failure modes. The characteristics of these failure modes were also discussed in Chapter 2. As a result, the shear stresses relevant for this analysis is scrutinized according to these failure modes.

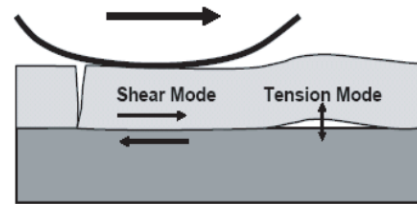


**Figure 5.3.2a:** Distress modes at pavement interface (Mohammad et al., 2012)

The different trends a observed for the different analysed combinations will be discussed. The discussion of the results is divided into two categories – *Replicated FEM model* and *Preliminary analysis and FEM replication*. The first-mentioned covers the results produced from *Model 2* (5.3.2.1) and how these results compare with preliminary findings (5.3.2.2).

#### 5.3.2.1 Finite Element Model

The shear stress results were measured at a series of points along the depth of the pavement structures evaluated as explained in Section 4.3.6. However, keeping in mind the research objective, the shear stresses were measured at the interface of the pavement structures considered, with both loading conditions, *T1* and *T2*. The shear stresses measured at the interface, for each of the combinations considered, *Case 1* to *4*, for *T1* and *T2*, are shown in Figure 5.3.2.1a accordingly. A detailed summary of results are provided in Table E10 in Appendix E2.

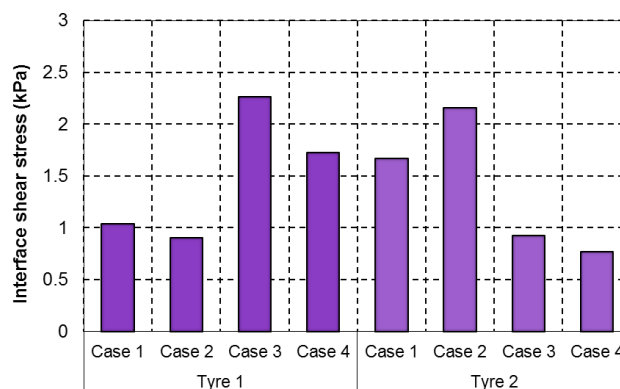


**Figure 5.3.2.1a:** Model 2 interface shear stress

The results in Appendix E2 suggest that shear stresses measured for *Model 2* are significantly small, reaching magnitudes far less than 0.01MPa. Furthermore, variations in increase and decrease in the results are evident. This type of occurrence is explained better through analysing the results with regards to the change in asphalt layer thickness and base layer stiffness. According to the definition provided for the different interface distress modes, the separation mode experienced in this instance is pure shear, with induced cracking at the bottom of the surfacing layer. Aforementioned is shown in Figure 5.3.2.1b.

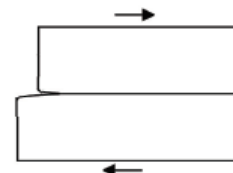


**Figure 5.3.2.1b:** Shear distress mode (After Sutanto, 2009)

The observations made from Figure 5.3.2.1a are summarised in the following points according to the different attributes of the analyses:

1. The shear stresses recorded range from 0.8 to 2.3kPa of which the maximum is the equivalent of two thousandth of an MPa.
2. Maximum shear stresses:
  - a. *T1* loading condition: Pavements with  $t_{\text{Asphalt}}$  of 100mm achieve maximum shear stress results i.e. *Case 3* and *4*.
  - b. *T2* loading condition: Pavement with  $t_{\text{Asphalt}}$  of 50mm achieve maximum shear stress results i.e. *Case 1* and *2*.
3. Influence of the change of base layer stiffness,  $E_{\text{base}}$ :
  - a. The shear stress decreases with an increase in the  $E_{\text{base}}$  with the exception of the *Case 1/2* combination for the *T2* loading condition.
  - b. The observation is motivated by the fact that the increasing material stiffness causes a very small change in stress distribution as it is a stronger material that can withstand more loads.
  - c. Similar to the parameter expressed by Equation 5.2.4.1c, change in results were determined to show the influence of the change in shear stress according to the change in the parameter. These results are shown in Figure E6 (left) in Appendix E2.
4. Influence of change in asphalt layer thickness,  $t_{\text{Asphalt}}$ :
  - a. Shear stress increase with the increase in  $t_{\text{Asphalt}}$  is noticeable for *T1* loading condition.
  - b. Contrasting behaviour is found for the more severe loading condition, *T2*.
  - c. This parameter is critical as it is the layer that “directly” transfers the load to underlying pavement layers. The combination of change in loading and asphalt layer thickness implies that the increase in the loading together with an increase in the layer thickness is less advantageous as it leads to a reduction of shear stresses generated in this layer.
  - d. Similar to the parameter expressed by Equation 5.2.4.1c, change in results were determined to show the influence of the change in shear stress according to the change in the parameter. These results are shown in Figure E6 (right) in Appendix E2.
5. The contribution of the change in results with regards to loading is implied in the aforementioned observations listed in points 2 to 4. Similar as for points 3 and 4, a visual representation of the change in results for the loading condition is given in Figure E7 in Appendix E2. In summary, it shows that a decrease in variation of shear stresses occur with the increase in  $E_{\text{base}}$  and  $t_{\text{Asphalt}}$ .

### 5.3.2.2 Preliminary Analysis versus Finite Element Model

The observations for the preliminary analysis was provided in Section 3.2 addressing elements of the LE analysis. In addition, the observations made for the replicated model was provided in 5.3.2.1. A comparison of each of the models is completed in a tabulated manner according to the different attributes i.e. loading conditions,  $t_{\text{Asphalt}}$ ,  $E_{\text{base}}$ . An exact comparison with the bonding state will be limited. Similar discussion will follow for the vertical strains, horizontal strain and pavement life estimations. The observation made for the LE-analysis will be compared to the observations for the replicated model as indicated in Table 5.3.2.2a. For the comparison purposes, for the LE analysis results, results for the HF condition will be used even though similar behaviours are noticeable.

**Table 5.3.2.2a:** LE Analysis versus replicated model shear stresses

Analyses	LE Analysis	FEM
<b>Magnitude</b>	Ranges between 0.2 and 1.2MPa (1200kPa)	Ranges between 0.8 and 2.3kPa
<b>Increase in <math>E_{base}</math></b>	<b>T1 loading</b> Decrease in shear stress	✓
	<b>T2 loading</b> Decrease in shear stress	✓ Case 1/2 exception
<b>Increase in <math>t_{Asphalt}</math></b>	<b>T1 loading</b>	
	Decrease for shear stress for <i>Case 1</i> and <i>3</i>	✓
	Increase in shear stress for <i>Case 2</i> and <i>4</i>	✓
	<b>T2 loading</b>	
	Increase for shear stress for <i>Case 1</i> and <i>3</i>	✗
	Increase in shear stress for <i>Case 2</i> and <i>4</i>	✗
<b>Increase in the loading Condition</b>	Increase in shear stresses	✓ Case 3/4 exception for <i>T2</i>

Studying Table 5.3.2.2a, a significant different in order of shear stresses can be observed. This observation is attributed to a variety of elements that can impact the results obtained of which the main is the application of interlayer bonding in the model. For the preliminary analysis in BISAR, shear spring compliance was used to represent the bonding element in the pavement. As explained in Chapter 3, this variable is determined as a proportion of the load area. For the replicated model in FEM, the tack coat properties were taken into consideration. These are two vastly different approaches – the first being a study of effectiveness of different states of bonding. The second approach, looks at the contribution of the tack coat properties to the overall performance of the pavement structure.

### 5.3.3 Normal stresses and normal strains

The normal stresses were recorded for *Model 2* in order to evaluate the normal strains in the x-, y- and z-direction, based on the three-dimensional theory discussed in Section 4.3.6. In turn, these strains are required for pavement life prediction. This section studies the stresses from the FEM analysis and the converted strains obtained accordingly. The necessary strains are used to estimate the pavement life in terms of its fatigue life or serviceability.

#### 5.3.3.1 Normal stresses

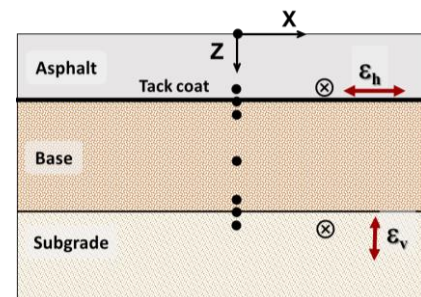
The deviator stresses ( $\sigma_1 - \sigma_3$ ) were not considered for the current analysis. Instead, the main focus was placed on the acquisition of the strains to analyse the pavement structures' ability to resist the assigned loading condition (*T1* or *T2* loading). The normal stresses obtained from the *Pavement Analysis* model are shown in Table 5.3.3.1a for both loading conditions inspected during the analysis. These stresses are the equivalent of *Below Wheel* results of LE analysis.

**Table 5.3.3.1a:** Model 2 normal stresses (MPa)

Analyses	T1 loading			T2 loading		
	$\sigma_x$	$\sigma_y$	$\sigma_z$	$\sigma_x$	$\sigma_y$	$\sigma_z$
Case 1	-0.49	-0.55	-0.2	-0.63	-0.73	-0.32
Case 2	-0.5	-0.56	-0.15	-0.65	-0.75	-0.24
Case 3	0.76	0.74	-0.11	1.01	0.99	-0.2
Case 4	0.59	0.57	-0.09	0.71	0.67	-0.16

### 5.3.3.2 Normal strains

Interpretation of horizontal and vertical strains is provided in Section 5.3.4 which also covers a comparison relative to the LE analysis results. The strains were calculated by means of Equations 4.3.6a to 4.3.6c based on three-dimensional theory – the theoretical derivation according to Jenkins & Rudman (2018a). The strains in the horizontal direction ( $\epsilon_x$  and  $\epsilon_y$ ) are obtained through Equations 4.3.6a and 4.3.6b from stresses measured at the bottom of the asphalt layer, where the vertical strain is obtained through Equation 4.3.6c from stresses measured at the top of the subgrade layer (Figure 5.3.3.2a). The strains measured in the respective directions are compiled in Table 5.3.3.2a. In this table negative strains indicate compressive strains, while positive strains indicate tensile strains.

**Figure 5.3.3.2a:** Critical pavement locations**Table 5.3.3.2a:** Model 2 normal strains (Microstrain)

Analyses	T1 loading			T2 loading		
	$\epsilon_x$	$\epsilon_y$	$\epsilon_z$	$\epsilon_x$	$\epsilon_y$	$\epsilon_z$
Case 1	-16.	-48.	-1948.5	-27.7	-80.5	-3101.5
Case 2	-1.7	-50.6	-2494.2	-32.6	-88.0	-4014.4
Case 3	255.3	245.7	-733.7	344.1	329.8	-1886.5
Case 4	213.3	202.2	-564.1	273.8	251.5	-2637.6

A fundamental concept to comprehend from the strains listed in this table, is that the nature of strains do not reflect typical types of strains in terms of magnitude. This does not coincide with expected strains in actual pavement structures, attributed to the configuration of the FEM model in Abaqus. The significant strains in the vertical (z-) direction (especially for T2), are attributed to the significant magnitude of the loading to which the structure is subjected. Last-mentioned loading, T2, consists of a 900kPa tyre pressure with a 70kN half-axle load, the equivalent of a 140kN axle load. The loading was selected very conservatively as it represents extreme loading or overloading of pavement

## 5.3.4 Horizontal strains

### 5.3.4.1 Finite Element Model

The horizontal strains were measured at the bottom of the asphalt layer. In accordance with the model configuration the results were measured 0.1mm above the layer thickness e.g. for Case 1 and 2 with  $t_{\text{Asphalt}}$  of 50mm, strains at 49.9mm were used. Similar for Case 3 and 4 with  $t_{\text{Asphalt}}$  of 100mm, strains at 99.9mm were used.

The estimation of strains was covered in 5.3.3.2. The horizontal strains are given in Figure 5.3.4.1a according to the different testing conditions. Studying these results, some expected occurrences are noticeable with regards to change in  $E_{\text{base}}$ ,  $t_{\text{Asphalt}}$  and the loading condition. Conventional design approaches have shown that pavement fatigue failure is measured at the base of the asphalt layer and are dependent on tensile strains (Figure 5.3.2.2a). These strains are measured in either the x- or y-direction of which the maximum strains provide the most conservative results in pavement design.

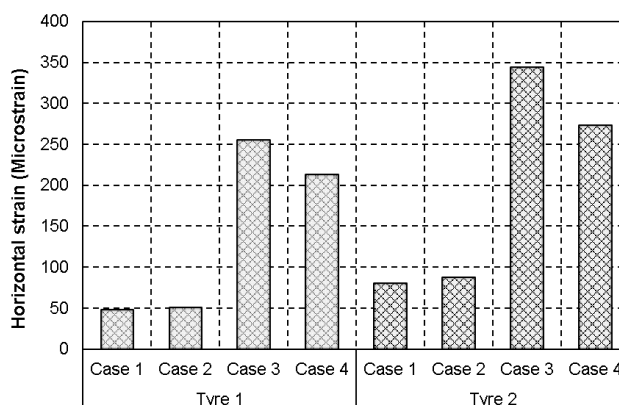


Figure 5.3.4.1a: Model 2 horizontal strain

From Figure 5.3.4.1a, the observations made in the different capacities are listed in the following points:

1. The horizontal strains measured at the bottom of the asphalt layer range from 48 to 344 $\mu\epsilon$
2. Maximum horizontal strains:
  - a. As expected, higher strains are achieved for the more critical loading condition, *T2* with strains ranging between 81 to 344 $\mu\epsilon$ .
  - b. For *T1*, strains are lower ranging between 48 and 213 $\mu\epsilon$ .
  - c. For the purpose of influence of loading, the variation in horizontal strains is evaluated similar to the parameter represented by Equation 5.2.4.1c. These results are illustrated in Figure E8 in Appendix E2. It is interesting to note more variance in strains for the structures composed of a lower  $t_{\text{Asphalt}}$  of 50mm i.e. Case 1 and 2 ranging between 68 and 74%. For the structures with a higher  $t_{\text{Asphalt}}$  of 100mm, variance of horizontal strains only vary between 28 and 35%.
3. Influence of the change in  $E_{\text{base}}$  and  $t_{\text{Asphalt}}$ :
  - a. An increase in horizontal strains occur for the *Case 1/2* combination for both the loading condition. In contrast, for the *Case 3/4* combinations for both loading conditions, a decrease occurs in the shear stresses.
  - b. In summary, a combination of increasing layer thickness for *Case 3/4* with an increase in  $E_{\text{base}}$  leads to a decrease in strains which is a favourable performance. This produces pavement structures that can withstand higher loading as it is composed of a thicker surfacing layer. Consequently allowing more loading time and gradual increase in stress distribution in the layer.
  - c. The pavements mentioned in b are composed of a stronger material used for the base layer which assists with the strain generation in the pavement. Its contribution is evident when studying the results.
  - d. Overall, aforementioned increase in  $t_{\text{Asphalt}}$  leads to an increase in strains which suggest that pavement with  $t_{\text{Asphalt}}$  of 50mm, *Case 1 and 2* are more favourable producing smaller strains. The increase in  $t_{\text{Asphalt}}$  of *Case 3 and 4* is not beneficial as it will be prone to earlier failure. In other words, these structure will undergo fatigue failure before *Case 1 and 2* pavements with a lower asphalt layer thickness.

- e. Similar to the parameter expressed by Equation 5.2.4.1c, the variation in horizontal strain is evaluated. These results are shown for the effect of change in  $t_{\text{Asphalt}}$  and  $E_{\text{base}}$  in Appendix E2 in Figure E10. A more significant variation is noticeable with the change in  $t_{\text{Asphalt}}$ , where results vary between 68 and 81%. For the change in  $E_{\text{base}}$ , variation ranges between 9 and 20% only.

#### 5.3.4.2 Preliminary Analysis versus Finite Element Model

Observations made from the horizontal strains measured from the FE analysis is summarised in 5.3.4.1. Furthermore, these observations made relative to the preliminary LE-analysis were covered in Section 3.2. Similar to shear stresses, a comparison of the models is tabulated in Table 5.3.4.2a according to the different attributes incorporated into the analyses. Direct relation regarding impact of the bonding state is limited as only one set of properties were used for the tack coat as listed in Section 5.3.1. FE results are compared with the LE analysis results for the HF condition.

**Table 5.3.4.2a:** LE Analysis versus replicated model for horizontal strains

Analyses	LE Analysis	FEM
<b>Magnitude</b>	Ranges between 232 and 623 $\mu\epsilon$	Ranges between 48 and 344 $\mu\epsilon$
<b>Increase in <math>E_{\text{base}}</math></b>	<b>T1 loading and T2 loading</b> Decrease in horizontal strain	✓ Case 1/2 exception
<b>Increase in <math>t_{\text{Asphalt}}</math></b>	<b>T1 loading</b>	
	Decrease for horizontal strain for <i>Case 1</i> and <i>3</i>	✗
	Increase in horizontal strain for <i>Case 2</i> and <i>4</i>	✓
	<b>T2 loading</b>	
	Increase for horizontal strain for <i>Case 1</i> and <i>3</i>	✓
	Increase in horizontal strain for <i>Case 2</i> and <i>4</i>	✓
<b>Increase in the loading Condition</b>	Increase in horizontal strains	✓

The comparison provided in Table 5.3.4.2a shows results of the two models are in agreement for the majority of the criteria grouped in these tables. The most concerning aspect is the order of the strains obtained in the two analyses. The strains were estimated based on three-dimensional theory described previously in Chapter 4. Together with the change in testing conditions, it is expected that the outcome of stresses will be different. This would highlight the important role the variables and conditions play in the analysis.

A positive aspect of these results would be that similar behaviours are observed in terms of the increase and decrease in material properties and loading. Furthermore, the observations made in this instance is less severe than those of the shear stresses summarised in Table 5.3.2.2a. This observation would suggest that there is a significant difference in the shear stress results measured at the interface between the surfacing and the base layer. Consequently indicating that the issue arises with the application of binding between the two analysis i.e. preliminary in BISAR and the FE model.

### 5.3.5 Vertical strains

#### 5.3.5.1 Finite Element Model

The vertical (compressive) strains are known to be measured at the top of the subgrade layer. Similar to the configuration for the horizontal strains discussed in 5.3.4.1, these strains were measured at 0.1mm below the top of the subgrade layer. Subsequently, for *Case 1* and *2*, results are recorded at 250.6mm depth. In addition, for the *Case 3* and *4* combination, the vertical strains are recorded at 300.6mm. The vertical strains are provided in Figure 5.3.5.1a according to the different testing conditions.

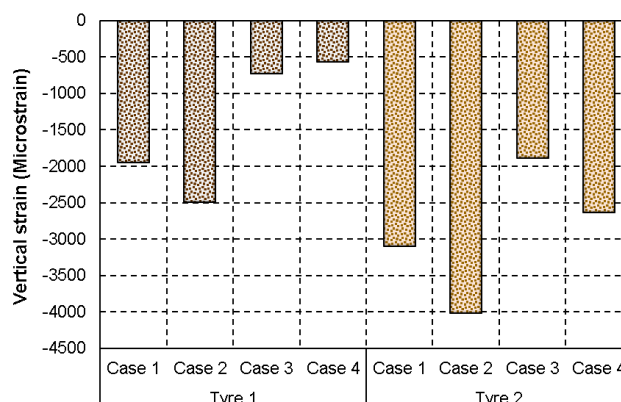


Figure 5.3.5.1a: Model 2 vertical strain

The observations made from Figure 5.3.5.1a are summarised in the following points according to the different attributes of the analyses including loading, material properties,  $E_{\text{base}}$  and  $t_{\text{Asphalt}}$ :

1. Maximum vertical strains:
  - a. Firstly, it is important to note that the nature of strains measured at this point within the pavement structure does not reflect realistic strains measured in pavements through a variety of testing equipment. The equipment includes the Falling Weight Deflectometer (FWD) used to measure deflections, which can be converted to strains.
  - b. Expected higher strains were found at the top of the subgrade layer for the more al loading condition, *T2* with strains ranging between approximately 1887 to 4014 $\mu\epsilon$ . For the *T1* loading condition strains are lower ranging between approximately 564 and 2494 $\mu\epsilon$ .
  - c. A more significant variance in strains is observable for the *T2* loading condition. Estimations were carried out similar to Equation 5.2.4.1c achieving results of 61 and 79% for this loading condition. For the lower loading condition, *T1*, a variation of only 59 and 16% was achieved. A visual representation of these results is given in Figure E10 in Appendix E2.
2. Influence of the change of base layer stiffness:
  - a. The vertical strain decreases with an increase in  $E_{\text{base}}$  with the exception of the *Case 3/4* combination for the *T2* loading condition.
  - b. Adhering to the assessment of results with Equation 5.2.4.1c, remarkable variation in results, according to change in  $E_{\text{base}}$ , is obtained for the *T2* loading condition where results differ from 29 up to 39%. All the estimations are shown in Figure E11 (left) in Appendix E2.
3. Influence of change in asphalt layer thickness:
  - a. Vertical strains decrease with the increase in  $t_{\text{Asphalt}}$  is noticeable for both loading conditions with more severe changes observed for *T1* loading condition of 62 to 77% compared to the 34 to 39% difference for the loading condition. This conclusion is also based on the Equation 5.2.4.1c approach and is shown in Figure E11 (right) in Appendix E2.
  - b. Linking with the change according to the loading condition explained in 2b, it is suggested that an increased loading shows less variability in the results.

## 5.3 Pavement Analysis Model

It is interesting to note the contrasting behaviour when comparing vertical strains results with the horizontal strains illustrated in Figure 5.3.4.1a. This is evident when comparing the corresponding combination's set of results. For example, Case 1 and 2 structure produced the minimum horizontal strains, but increasing vertical strains when studying Figure 5.3.5.1a. For example, for Case 1 and 2 combination smaller horizontal strains compared to Case 3 and 4 combination. Comparing this observation to the vertical strains, it can be noted that, Case 1 and 2 combinations produced more significant strains than the Case 3 and 4 combination.

The observations made in this capacity can be attributed to the distribution of the stresses and strains to the underlying layers. For the "weaker" composed pavement structures i.e. Case 1 and 2 little strain is carried by the surfacing layer and the majority of the strains is carried by the subgrade layer. Opposite for the stronger structures, Case 3 and 4, the majority of the strain is carried at the bottom of the asphalt layer with less strain carried by the subgrade layer.

Section 3.6 pointed out that the lower layer (i.e. subgrade) is more sensitive to loading. It was been reported in Jenkins & Rudman (2018a) that the topic of the subgrade is important and is described as a "key determinant" in the overall pavement deflection. The prominent approach to evaluate the failure of relative layers is by means of the pavement life which will be study in subsequent sections according to fatigue and serviceability in Section 5.3.6.

## 5.3.5.2 Preliminary Analysis versus Finite Element Model

The observation with respect to vertical strains acquired from the FE analyses is summarised in 5.3.5.1. The corresponding analysis for the LE preliminary research discussed in 3.2.6.3. This section provides a comparison of these two analyses which is provided in Table 5.3.5.2a according to defined conditions.

**Table 5.3.5.2a:** LE Analysis versus replicated model for vertical strains

Analyses	LE Analysis	FEM
<b>Magnitude</b>	Ranges between 319 and 921 $\mu\epsilon$	Ranges between 564 and 4014 $\mu\epsilon$
<b>Increase in <math>E_{base}</math></b>	<b>T1 loading</b>	
	Decrease in vertical strain for Case 1 and 2	✘
	Decrease in vertical strain for Case 3 and 4	✔
	<b>T2 loading</b>	
	Decrease in vertical strain for Case 1 and 2	✘
	Decrease in vertical strain for Case 3 and 4	✘
<b>Increase in <math>t_{Asphalt}</math></b>	<b>T1 loading</b> Decrease in vertical strain	✔
	<b>T2 loading</b> Decrease in vertical strain	✔
<b>Increase in the loading condition</b>	Increase in vertical strain	✔

Similar to Table 5.3.4.2a, the order of strains obtained from the FEM model is very significant compared to those obtained for the preliminary analyses completed. Furthermore, these strains, of the FEM model, do not reflect realistic strains achieving extreme values of  $4014\mu\epsilon$ . Motivation for this observation also links with the analysis conditions. As observed previously, upper layer layers significantly impact the subgrade layer. The contrasting behaviour noticed for the interface bonding in Section 5.3.2 has been carried through the pavement to the subgrade layer.

**5.3.6 Pavement life prediction**

The different attributes of SAMDM were discussed in Chapter 2. In line with the scope of the current analysis, two classical modes of failure described by this method are essential: fatigue cracking at base of the asphalt layer and permanent deformation at the top of the subgrade. According to this design approach, strains measured at these locations are used to determine the critical life due to fatigue and permanent deformation experienced within a pavement structure. The two different configurations used for the pavement analysis, i.e. LE analysis model and *Model 2*, are demonstrated in Figure 5.3.6a. The difference in interlayer bonding is highlighted in this figure where interlayer friction was set to represent bonding (Figure 5.3.6a left) at two interfaces or interlayers. For *Model 2*, a tack coat region was incorporated into the model and relative information was included in the analysis.

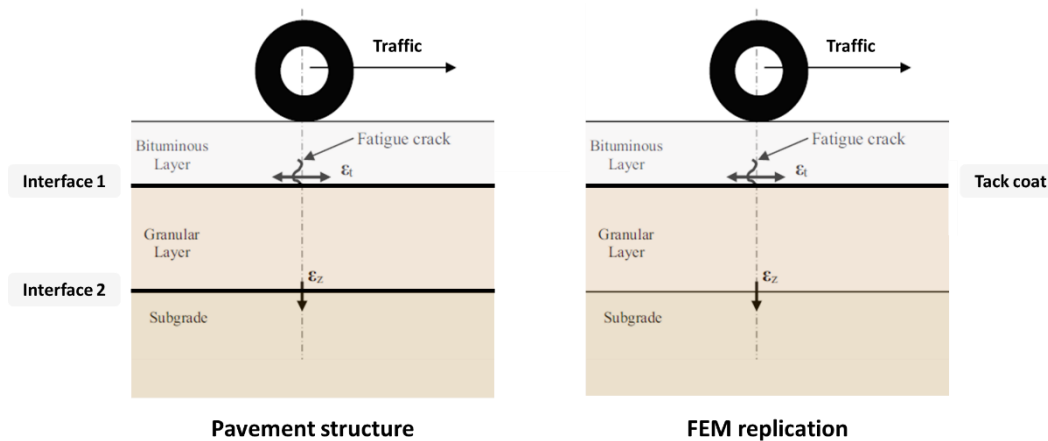


**Figure 5.3.6a:** Critical strains for SAMDM approach for LE analysis and Model 2 (After Sutanto, 2009)

The estimations of the strains required to predict pavement life in terms of the fatigue and serviceability were completed by using the stresses measured within the three-dimensional modelling space for *Model 2*.

**5.3.6.1 Fatigue Life of Asphalt**

The horizontal strains in Section 5.3.4 were used to estimate the Fatigue Life according to each of the structures *Case 1* to *4*. These estimations were carried out similar to preliminary research in Chapter 3 by means of Shell nomographs expressed by Equation 3.2.7.2a.

The derived function is based on a standard 50/70 Bitumen Type at 15°C. These strains are shown in Figure 5.3.6.1a. The estimates are indicated in the number of load repetitions.

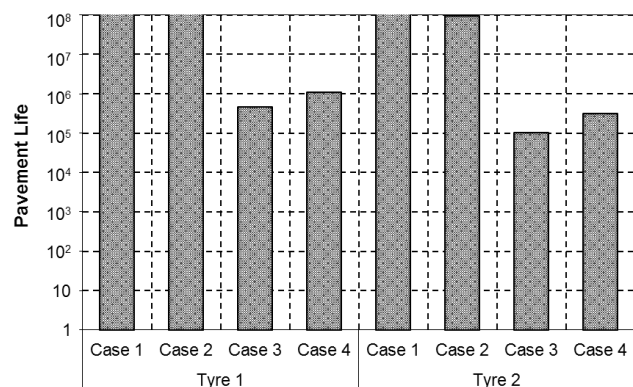


**Figure 5.3.6.1a:** Model 2 fatigue life

With regards to these estimates, the following aspects are noticeable when studying the results in this figure:

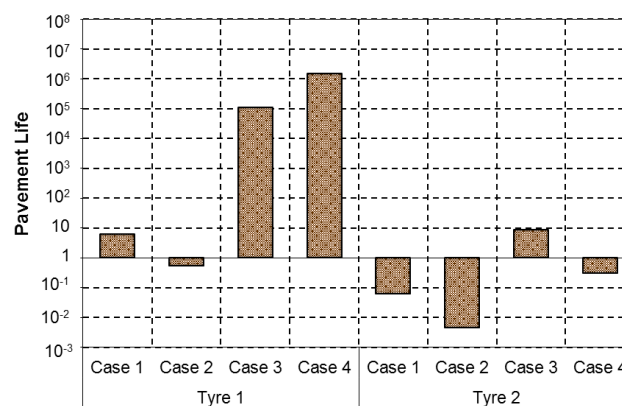
1. The fatigue life ranges between 0.1 to 1927MESAs (equivalent of  $1 \times 10^5$  to  $1.9 \times 10^9$  load repetitions).
2. Maximum Fatigue Life:
  - a. Studying in line with the horizontal strains in Figure 5.3.4.1a, it is apparent that the increase in strains leads to a reduction in fatigue life.
  - b. In accordance with a, the more critical loading condition, *T2*, which produced higher strains, produces the shortest fatigue life span of structures compared to *T1*. Overall, *T1* produced estimates that are very significant relative to *T2* results.
    - i. For *T1* loading condition: fatigue life spans between 0.5 and 1927 MESAs
    - ii. For *T2* loading condition: fatigue life spans between 0.1 to 145MESAs
  - c. The variation of results due to the impact of the loading condition is expressed similar to Equation 5.2.4.1c. These results are shown in Figure E12 in Appendix E2, from which the following is concluded:
    - i. 92.5 to 93.7% change in result for *Case 1* and *2*
    - ii. For *Case 3* and *4*, a smaller variation of approximately 78 and 71% was achieved.
    - iii. The observation highlights that variation of results is contributed to a combination of change in parameters. However, it appears that  $t_{\text{Asphalt}}$  was the most critical parameter.
3. The influence of change in  $E_{\text{base}}$  and  $t_{\text{Asphalt}}$ :
  - a. The variance in results in accordance with these two parameters are indicated in Figure E13 in Appendix E2 as required in similar manner than Equation 5.2.4.1c.
    - i. Change in  $E_{\text{base}}$ : 12 and 36% decrease in fatigue for *Case 1* and *2*, but a 59 and 48% increase for *Case 3* and *4*. This indicates the impact of the change in  $t_{\text{Asphalt}}$ .
    - ii. Change in  $t_{\text{Asphalt}}$ : a change of approximately 99 and exceeding 100% is achieved in fatigue when considering
  - b. The combination of increase in  $E_{\text{base}}$  and  $t_{\text{Asphalt}}$  with the increase in loading has a significant impact on the results leading to a variation of increase and decrease in the results with the change in these parameters.
  - c. From inspection of these results,  $t_{\text{Asphalt}}$  was most critical parameter concerning fatigue life of the pavement structures. For aforementioned parameter, variation up to 100% is noticeable whereas for change in  $E_{\text{base}}$ , results vary only between 36 up to 59%.
4. The results indicate that *Case 3* and *4* pavement structures are the most critical and will experience fatigue failure before *Case 1* and *2* pavement structures. First-mentioned are both composed with a thicker asphalt layer of 100mm.
5. A comparison of FEM results with the preliminary research is given in Table 5.3.6.1a. Common trends in results are noticeable when comparing the results – increase in horizontal strains causes a reduction in fatigue life of a pavement structure.

**Table 5.3.6.1a:** LE Analysis versus replicated model for fatigue life

Analyses	LE Analysis	FEM
<b>Magnitude</b>	Ranges between 0.01 and 0.72MESAs	Ranges between 0.1 and 1927MESAs
<b>Increase in <math>E_{base}</math></b>	<b>T1 loading</b>	
	Decrease in fatigue for <i>Case 1</i> and 2	✘
	Decrease in fatigue for <i>Case 3</i> and 4	✓
	<b>T2 loading</b>	
	Decrease in fatigue for <i>Case 1</i> and 2	✘
	Decrease in fatigue for <i>Case 3</i> and 4	✓
<b>Increase in <math>t_{Asphalt}</math></b>	<b>T1 loading</b>	
	Decrease in fatigue for <i>Case 1</i> and 3	✘
	Increase in fatigue for <i>Case 2</i> and 4	✓
	<b>T2 loading</b>	
	Increase in fatigue for <i>Case 1</i> to 4	✓

### 5.3.6.2 Serviceability Life

The vertical strains in Section 5.3.5 were used to estimate Serviceability Life of *Case 1* to 4 pavement structures under the different testing conditions. The estimates are completed following transfer function used for preliminary research Serviceability Life estimates in Chapter 3. The transfer function used is represented by Equation 3.2.7.3a. The serviceability results are given in Figure 5.3.6.2a.

**Figure 5.3.6.2a:** Model 2 serviceability life

From the estimated serviceability, subsequent listed elements are observed whilst studying these results:

1. The serviceability life ranges between less than 0.004 load repetitions up to 1.54MESAs (equivalent of  $1.54 \times 10^6$  load repetitions).
2. Maximum Serviceability Life:
  - a. Studying in line with the vertical strains in Figure 5.3.5.1a, a reduction in serviceability life is apparent.
  - b. The range of the serviceability relates to the vertical strains which demonstrated the influence of the properties of upper layers i.e. surfacing, tack coat and base on the behaviour of the subgrade within the pavement structure. The impact from the bonding in the pavement

## 5.3 Pavement Analysis Model

- significantly impacts the pavement structure starting from the base layer carried through to the subgrade. The increase in  $t_{\text{Asphalt}}$  is beneficial although the increase in the loading condition to T2, significantly impacts the serviceability life showing a reduction in pavement life from  $1.54 \times 10^6$  to 0.004 load repetitions.
- c. In accordance with a, T2, the more critical loading condition, produced higher strains leading to the shortest serviceability life span in comparison with T1 results. With the exception of Case 1, T1 produced more significant estimates for serviceability.
    - i. For T1 loading condition: serviceability life ranges between 0.5 load repetitions and 0.11 MESAs (equivalent of  $5.4 \times 10^{-1}$  and  $1.1 \times 10^5$  load repetitions).
    - ii. For T2 loading condition: serviceability life ranges between 0.005 load repetitions to 1.54MESAs (equivalent of  $4.6 \times 10^{-3}$  and  $1.5 \times 10^6$  load repetitions).
  - d. The variation of results due to the impact of the loading condition is expressed similar to Equation 5.2.4.1c. These results are shown in Figure E14 in Appendix E2 and indicates a significant impact on results with a 99 and 100% change in the results. This would suggest that the loading condition plays a more significant role for the serviceability compared to the fatigue life of the pavement structures.
3. The influence of change in  $E_{\text{base}}$  and  $t_{\text{Asphalt}}$ :
    - a. The variance in results in accordance with these two parameters are indicated in Figure E15 in Appendix E2 acquired with Equation 5.2.4.1c.
      - i. Change in  $E_{\text{base}}$ : 92 and 93% decrease in fatigue for Case 1 and 2, but a 92 and 97% increase for Case 3 and 4. This indicates the impact of the change in the loading condition.
      - ii. Change in  $t_{\text{Asphalt}}$ : a change of 100% is achieved in fatigue when considering all combinations for T1. However, a slightly smaller change ranging between 93 and 98.5% is obtained for T2 results set. This could imply that loading plays a less important role with the change in  $t_{\text{Asphalt}}$ .
    - b. In this instance, the combination of increase in  $E_{\text{base}}$  and  $t_{\text{Asphalt}}$  with the increase in loading has a remarkable effect on the results were changes in results range from 92% up to 100% whereas for fatigue results,  $t_{\text{Asphalt}}$  individually had the most significant impact on the results.
  4. The results indicate that Case 1 and 2 are the most critical under both loading conditions with the exception experiencing serviceability failure with the exception of Case 3 and 4. Last-mentioned is also prone to serviceability failure when subjected to the critical loading, T2.
  5. A comparison of FEM results with the preliminary research is given in Table 5.3.6.2a. Common trends in results are noticeable when comparing the results – increase in vertical strains causes a reduction in serviceability life of a pavement structure.

**Table 5.3.6.2a:** LE Analysis versus replicated model for serviceability life

Analyses	LE Analysis	FEM
<b>Magnitude</b>	Ranges between 0.01 and 461MESAs	Ranges between <0.1 and 1.54MESAs
<b>Increase in <math>E_{base}</math></b>	<b>T1 loading</b>	
	Increase in serviceability for <i>Case 1</i> and <i>2</i>	✘
	Increase in serviceability for <i>Case 3</i> and <i>4</i>	✓
	<b>T2 loading</b>	
	Increase in serviceability for <i>Case 1</i> and <i>2</i>	✘
	Increase in serviceability for <i>Case 3</i> and <i>4</i>	✘
<b>Increase in <math>t_{Asphalt}</math></b>	<b>T1 loading</b>	
	Increase in serviceability for <i>Case 1</i> and <i>3</i>	✓
	Increase in serviceability for <i>Case 2</i> and <i>4</i>	✓
	<b>T2 loading</b>	
	Increase in serviceability for <i>Case 1</i> to <i>4</i>	✓

### 5.3.7 Conclusion

In general, a significant change in the results are observed in the different capacities of the analyses i.e. shear stresses and strains as discussed in Sections 5.3.2 to 5.3.6. For the FE model, less realistic results were acquired under most circumstances such as the shear stresses and horizontal strains measured comparing to results obtained during preliminary research. However, it should be noted, that the replicated model did not exactly replicate pavement conditions which take external factors into consideration such as climate, change in material loading and the variation of traffic on the pavement surface. This would correspond to preliminary research where these factors were also note taken into consideration.

The most significant factor which differed between the two approaches is the bonding element. For preliminary research, states of bonding were evaluated whereas the FE model considered a tack coat with specific properties and its contribution of the pavement behaviour when subject to different conditions. Hence, last-mentioned is the critical factor as to why results differ to such a significant extent.

### 5.3.8 Model 2 versus preliminary laboratory work

The preliminary laboratory results in 5.2.8.2 will be used to evaluate the difference in results relative to *Model 2*. This will focus on comparing the interface shear stress achieved within the tack coat layer. This serves as a mere comparison of the shear stresses concerning its magnitude. The extent of differences between these stresses is mostly attributed to the different properties between the two testing methods. A comparison of these properties are provided in Table 5.3.8a.

## 5.4 Finite Element Model Comparison: Model 1 versus Model 2

Table 5.3.8a: Comparison of testing properties

	Trial field testing	Model 2
Model composition	<b>Two layered system</b> with tack coat layer: <ul style="list-style-type: none"> <li>• Asphalt wearing course: 45.6mm</li> <li>• Asphalt base: 60mm</li> <li>• Equivalent tack coat thickness: 0.15mm</li> </ul>	<b>Three layered system</b> with tack coat layer: <ul style="list-style-type: none"> <li>• Asphalt surfacing: 50mm or 100mm</li> <li>• Base layer: 200mm</li> <li>• Subgrade: 1000mm</li> <li>• Tack coat thickness: 0.5mm</li> </ul>
	Two asphalt layers with variance in stiffness, but given its material composition, significantly influence the shear stress development and magnitude of shear stresses.	The variability in material properties results in a contradictive stress distribution pattern, producing significant different behaviours concerning shear development.
Loading	Test set-up: Leutner measures load of failure (at 17.8kN). Continuous increase in load is applied until failure.	Two half-axle loadings: 40kN ( <i>T1</i> ) and 70kN ( <i>T2</i> ). The equivalent pressures as opposed to concentrated loads were used in the analysis (750kPa for <i>T1</i> and 900kPa for <i>T2</i> )

Significantly small shear stresses were measured at the interface for *Model 2* as indicated per Figure 5.3.2.1a. For the trial field testing results used, the average of the shear stresses was 1.74MPa. This signifies a difference of approximately 99.9% when determined as a ratio of the average shear stress from trial field testing.

It should be noted that these results signify a difference in shear stress to such an extent with a tack coat that is twice the thickness of the tack coat in the core sample used for laboratory testing. In addition, it describes the extent of change in material composition, which is a very important factor influencing the stress development as explained in Table 5.3.8a. Another major influence would be the different testing approaches used for the acquisition of shear stress results.

Given the contrasting scope of these two projects, both did conclude that the type of results obtained is significantly influenced by the testing conditions. In contrast with *Model 2*, the preliminary laboratory work carried out by Pisa University highlighted the impact of tack coat application on the bonding strength. *Model 2* gives an indication of the overall behaviour of a pavement structure with a tack coat. Furthermore, providing an understanding of how the bonding layer contributes to the strength of the pavement structure when subjected to loading simulating actual road conditions.

## 5.4 Finite Element Model Comparison: Model 1 versus Model 2

### 5.4.1 Introduction

Sections 5.2 and 5.3 investigated and discussed the results obtained for the two FE models. In addition, both sections also studied these results in compared to the preliminary research completed and discussed in Chapter 3. For the purpose of the discussion in Sections 5.2 and 5.3, the preliminary LE-analysis by Stellenbosch University and laboratory work carried out by Pisa University was used.

## 5.4 Finite Element Model Comparison: Model 1 versus Model 2

The golden throughout the discussion was the influence of different defined conditions on the output of these analyses. Section 5.4 will compare *Model 1* and *Model 2* discussed in Sections 5.2 and 5.3 respectively. Analyses will be evaluated according to relative criteria involving the study of different testing conditions. As the focus of the current study is on bonding, this section will also compare the bonding results acquired for each model.

## 5.4.2 Testing conditions

The testing conditions of the two models are compared according to each of the elements designated to each of the models as set out in the appropriate section of the *Methodology* chapter – Chapter 3. The model set-up was discussed elaborately with respect to the different components required to “build” a finite element method model in Chapter 4. A summary of the key characteristics of the two models is given in parallel for comparison purposes, in Table 5.4.2a.

Table 5.4.2a: Model 1 versus Model 2 testing conditions

	Model 1	Model 2
Parts	<p><b>Part 1:</b> <i>Shear ring</i> (excl. from comparison)</p> <p><b>Part 2:</b> <i>Core sample</i> Two layered system with tack coat layer:</p> <ul style="list-style-type: none"> <li>• Wearing course</li> <li>• Tack coat</li> <li>• Base</li> </ul>	<p><b>Part:</b> <i>Pavement structure</i> Three layered system with tack coat layer:</p> <ul style="list-style-type: none"> <li>• Asphalt surface</li> <li>• Tack coat</li> <li>• Base</li> <li>• Subgrade</li> </ul>
Properties	<p><b>Wearing course</b> <i>Material:</i> Asphalt <i>Stiffness:</i> 2500MPa <i>Thickness (<math>T_{WC}</math>):</i> 30mm, 50mm and 100mm</p> <p><b>Tack coat</b> <i>Material:</i> Bitumen Emulsion <i>Stiffness:</i> 0.21MPa and 1MPa <i>Thickness (<math>T_{TC}</math>):</i> 0.2mm, 0.5mm and 1mm</p> <p><b>Base</b> <i>Material:</i> Asphalt <i>Stiffness:</i> 1000MPa and 2500MPa (MR = 2.5 and MR = 1) <i>Thickness:</i> 60mm</p>	<p><b>Asphalt surface</b> <i>Material:</i> Asphalt <i>Stiffness:</i> 2500MPa <i>Thickness (<math>t_{Asphalt}</math>):</i> 50mm, 100mm</p> <p><b>Tack coat</b> <i>Material:</i> Bitumen Emulsion <i>Stiffness:</i> 1MPa <i>Thickness (<math>T_{TC}</math>):</i> 0.5mm</p> <p><b>Base</b> <i>Material:</i> Granular <i>Stiffness:</i> 400MPa and 1500MPa (MR = 6.25 and MR = 1.67) <i>Thickness:</i> 200mm</p> <p><b>Subgrade</b> <i>Material:</i> Granular <i>Stiffness:</i> 150MPa <i>Thickness:</i> 1000mm (Infinite thickness in reality)</p>

## 5.4 Finite Element Model Comparison: Model 1 versus Model 2

<b>Boundary conditions</b>	Boundary conditions and restrains at selected points on model (reference points) i.e. RP1 to RP3. Constraints were also defined at these points.	<ul style="list-style-type: none"> <li>• <i>Base of the subgrade layer: Fixed</i></li> <li>• <i>Outer surface of the pavement structure: constraint against rotation about x-, y- and z-axis.</i></li> </ul>
<b>Loading</b>	Not applicable. Shear load (axial load) was measured from shear stress results.	<i>Tyre pressure 1 (T1): 750kPa</i> <i>Tyre pressure 2 (T2): 900kPa</i>
<b>Analysis</b>	Results obtained as average values of two element sets consisting on series of nodes (68 or 102 nodes depending on layer thickness)	Results obtained at selected depth along pavement structure by defining a path along the model at the point where loading is initiated

## 5.4.3 Shear stresses

This section scrutinizes the shear stresses measured at the interface for both FEM models, attributed to the fact that the bonding layer was incorporated in a similar manner. For both the models, the tack properties were included during the model set-up and analyses were performed accordingly. The extent of the difference between analysis results is expressed by similar “difference” parameter, similar to Equation 5.2.4.1c, i.e.  $\Delta_{Model}$ . The parameter is determined as the change in model results proportional to the *Model 1* result. This parameter is represented by Equation 5.4.3a.

$$\Delta_{Model} = \frac{x_{Model2} - x_{Model1}}{x_{Model1}} \times 100 \quad (5.4.3a)$$

Where:

- $\Delta_{Model}$  = Difference of analysis results (%)
- $x_{Model1}$  = Leutner model result
- $x_{Model2}$  = Pavement analysis model result

The interpretation of the results for *Model 2* was completed in Section 5.3 in parallel with the findings made from the preliminary LE analysis results. *Model 2* produced shear stress from approximately 1 and 2kPa suggesting that the tack coat barely has an influence on the stress development. However, similar to the strains, it should be kept in mind that these results do not portray actual stresses. Thus, it does not necessarily provided an accurate description of the shear stress distribution in the pavement structures modelled and analysed. The shear stresses obtained for the Leutner model, *Model 1*, were completed in Section 5.2.

Equation 5.4.3a is used to express the difference in the results in correlation with the different input parameters. A reduction in the number of analysis combinations is completed using results of models with corresponding properties. The analysis will mainly include the properties of the tack coat, such as its thickness and material stiffness,  $T_{TC}$  and  $E_{TC}$ . The approach will provide a fair comparison of the results obtained between the two models. Subsequently, models comprising of corresponding properties are shown in Table 5.4.3a and are considered for the estimations with Equation 5.4.3a.

**Table 5.4.3a:** Model 1 versus Model 2 testing conditions

Requirement	Model 1	Model 2
Asphalt surface of 100mm	$T_{WC2}$ (100mm)	Case 3 and 4
Tack coat thickness of 0.5mm	$T_{TC2}$ (0.5mm)	Case 1 - 4
Tack coat stiffness of 1MPa	$E_{TC2}$ (1MPa)	Case 1 -4

According to the summarised information in Table 5.4.3a, *Case 3* and *4* are the only two combinations of *Model 2* that comply with the desired criteria to enable fair comparison of the results. *Model 1* incorporated the two modular ratios, *MR1* and *MR2* according to the increase in  $E_{base}$ , while *Case 3* and *4* from *Model 2* analysis are each composed of a different  $E_{base}$ . For this reason, the difference will be determined for both MR values as shown in Figure 5.4.3a.

For the *MR1* value of the particular combination, a shear stress of 2.12MPa was obtained and 2.34MPa for *MR2* value. The estimates were repeated for both loading conditions, *T1* and *T2*, of *Model 2*. The determined values with Equation 5.4.3a are also indicated in Figure 5.4.3a. The two dashed lines each represent a results relative to one of the loading conditions, *T1* and *T2*.

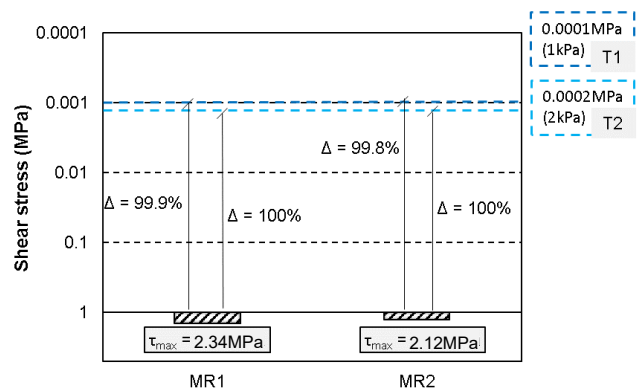
For *Case 3* and *4* modular ratios of 6.25 and 1.67 were specified while *MR1* and *MR2* represented modular ratios of 1 and 2.5 respectively. Given the significant difference, values estimated for the  $\Delta_{Model}$  parameter varied between 99.8% and 100% which is a very small window for variation, despite the 20% increase in loading magnitude.

All comparative analyses have shown a relationship between the loading, layer thickness and modular ratio (material layer stiffness) and suggested a gradual change in the extent of influence. The motivation for this type of behaviour can be justified based on the Burmister theory described in Appendix F.

## 5.5 Synthesis of Results Interpretation

It was reported that different combinations of prescribed testing conditions are influential concerning the type of results obtained from the specific analyses. The preliminary linear-elastic research conducted and discussed in Section 3.2 has been studied and compared with both the FEM models simulated in Abaqus. Furthermore, a brief comparative analysis was undertaken for the two FEM models, relative to preliminary laboratory work executed by Pisa University in Sections 5.2.8 and 5.3.8.

The defined conditions illustrated similar behaviours, even though in certain circumstances findings were found to be insufficient, given the limited information available to enable a fair comparison of the influence of the different conditions on the results. This observation justifies the “limited” conclusions and motivation for behaviours demonstrated. The findings gathered are made prominent in line with



**Note:** Vertical axis values in this figure are shown in reverse order and results in this figure

**Figure 5.4.3a:** Model 1 versus Model 2 shear stress comparison

### 5.5 Synthesis of Results Interpretation

the Burmister theory. The use of the method illustrates the relation between the three criteria graphically, according to which results were examined. The estimations performed in accordance with this method illustrated the influence of the top layer thickness, stiffness of layers (modular ratio) and the loading. The loading was incorporated into the graphs, using the tyre pressure and defined load radius.

The results for *Model 2* indicates the impact of shear stresses on the pavement life in terms of fatigue and serviceability. Firstly, horizontal strains showed similar trends regarding increase and decrease relative to the different testing conditions for *Case 1* to *4*. As increase in strain occurs leading to a reduction in fatigue, fatigue shows contrasting behaviour to shear stress results. This suggests that where shear stresses increase, the fatigue life is reduced. Secondly, for the vertical strains, opposite trends are noticeable when compared to the horizontal strains. Consequently, the variation in serviceability is similar to the variation observed for shear stresses.

## CHAPTER 6: CONCLUSIONS AND RECOMMENDATIONS

---

*Phase 1* consisted of preliminary research conducted by Stellenbosch University in conjunction with, and parallel to, Pisa University. Both academic institutions completed a linear-elastic analysis with prescribed conditions for a series of pavement structures in order to evaluate a series of factors contributing to the durability of the pavement. The analyses allowed for the prediction of pavement life in terms of serviceability and fatigue. Pisa University also conducted a series of laboratory tests, motivated by the findings made during the preliminary linear-elastic analyses.

The findings from the preliminary research conducted for *Phase 1* of the research project created the opportunity for extended research by means of finite element modelling, which would enhance the understanding of the various mechanisms influencing the performance observed in *Phase 1*. Two material models were simulated in Abaqus, i.e. *Leutner Shear Test* and a *Pavement Analysis* model as a *Phase 2* component of the research. These models were replicated according to the preliminary laboratory work by Pisa University, which comprised of a series of Leutner (shear) testing. In addition, the *Pavement Analysis* model was modelled in association with the preliminary linear-elastic analysis.

The two-phase project was undertaken to evaluate the effect of interlayer bonding by means of tack coat application using Spray Jet technology. It included studying shear development in respective pavement layers. The research also included the evaluation of certain pavement conditions and their impact on pavement durability. This chapter provides a summary of the conclusions drawn from the study according to the two phases of the project. A summary of the findings from preliminary research in *Phase 1* is presented in Section 6.1, followed by the conclusions drawn from the two simulated FEM models. Section 6.2 provides recommendations, further study and improvement of testing conditions of analyses to extend understanding of the limited results in the current study.

### 6.1 Conclusions

#### 6.1.1 Preliminary Research

The pavement life was established for four different combinations by means of Mechanistic Empirical Linear Elastic Modelling, considering a series of conditions as described in Chapter 3. The extent of impact of the attributes on pavement life and shear resistance by Spray Jet, was evaluated and the following conclusions were made:

1. Observations from results proved that interface conditions, represented by the three different friction conditions, together with other variables such as loading condition and material stiffness, contribute to stress and strain generation in the pavement structures.
  - a. Shear stresses:
    - High Friction: 0.1 to 0.6MPa for *Tyre 1*; 0.1 to 0.8MPa for *Tyre 2*
    - Medium Friction: 0.2 to 1.1MPa for *Tyre 1*; 0.3 to 1.3MPa for *Tyre 2*
    - Low Friction: 0.2 to 1.2MPa for *Tyre 1*; 0.3 to 1.4MPa for *Tyre 2*
  - b. Horizontal strains:
    - High Friction: 9 to 267 $\mu\epsilon$  for *Tyre 1*; 31 to 351 $\mu\epsilon$  a for *Tyre 2*
    - Medium Friction: 183 to 496 for *Tyre 1*; 225 to 597 $\mu\epsilon$  a for *Tyre 2*
    - Low Friction: 196 to 521 $\mu\epsilon$  for *Tyre 1*; 244 to 623 $\mu\epsilon$  a for *Tyre 2*

- c. Vertical strains:
- High Friction: 312 to 946 $\mu\epsilon$  for *Tyre 1*; 487 to 1505 $\mu\epsilon$  a for *Tyre 2*
  - Medium Friction: 285 to 599 $\mu\epsilon$  for *Tyre 1*; 436 to 947 $\mu\epsilon$  a for *Tyre 2*
  - Low Friction: 261 to 581 $\mu\epsilon$  for *Tyre 1*; 400 to 921 $\mu\epsilon$  a for *Tyre 2*
- d. Fatigue Life:
- High Friction: 0.36 to >100MESAs for *Tyre 1*; 0.1 to 115MESAs for *Tyre 2*
  - Medium Friction: 0.02 to 1MESAs for *Tyre 1*; 0.01 to 0.5MESAs for *Tyre 2*
  - Low Friction: 0.02 to 0.7MESAs for *Tyre 1*; 0.01 to 0.3MESAs for *Tyre 2*
- e. Serviceability Life:
- High Friction: <0.1 to 64MESAs for *Tyre 1*; <0.1 to 0.4MESAs for *Tyre 2*
  - Medium Friction: 0.8 to 182MESAs for *Tyre 1*; <0.01 to 1.5MESAs for *Tyre 2*
  - Low Friction: 1.2 to 461MESAs for *Tyre 1*; 0.01 to 3.8MESAs for *Tyre 2*
2. Results obtained in terms of extended pavement life suggest that the bonding condition has a pronounced impact on the Fatigue Life. It was found that from a semi bonding state (50%) and higher i.e. full bond state, the Fatigue Life increases significantly. It increases from 0.4 and exceeding 100MESAs using *Case 2 Tyre 2* results as an example.
  3. The results from the analyses are considered preliminary, as broader understanding, which would confirm and justify observed aspects, is to be provided through FEM analyses.
  4. Despite the difference in testing conditions, research by Pisa University showed similar trends with some discrepancies, which is significantly attributed to the theory applied by the various analysis software used. Pisa University used analysis software which depends on the Burmister Theorem.
  5. Analyses from Pisa University confirmed that favourable results propose tack coat applied by Spray Jet technology.
  6. From the variety of variables evaluated, it was found that the change in physical properties, i.e. base layer stiffness and asphalt layer thickness, had the largest influence on the results, which in turn contributed towards the effect of friction (bonding) and loading conditions on the results achieved. However, between these two parameters, the base layer stiffness was identified as the most critical parameter, showing the most signification change in results.
  7. A study comparing the influence of change in  $E_{base}$  and  $t_{Asphalt}$  was carried out for the three different bonding conditions *HF*, *MF* and *LF* in Section 3.2.4 and illustrated in Figures 3.2.4d to relative to the two loading conditions, *Tyre 1* and *Tyre 2*. According to the differently grouped pavement structures analysed i.e. *Case 1* to 4.
    - a. High Friction
      - $E_{base}$ : 56 and 73% decrease in shear stress for *Tyre 1*; 61 and 81% decrease in shear stress for *Tyre 2*
      - $t_{Asphalt}$ : 7% decrease (*Case 1/3*) and 50.1% increase (*Case 2/4*) in shear stress for *Tyre 1*; 14 and 134% increase in shear stress for *Tyre 2*

## b. Medium Friction

- $E_{base}$ : 46% and 27% decrease in shear stress for *Tyre 1*; 48 and 30% decrease in shear stress for *Tyre 2*
- $t_{Asphalt}$ : 19% decrease (*Case 1/3*) and 10% increase (*Case 2/4*) in shear stress for *Tyre 1*; 5% decrease (*Case 1/3*) and 27% increase (*Case 2/4*) in shear stress for *Tyre 2*

## c. Low Friction

- $E_{base}$ : 46% and 27% decrease in shear stress for *Tyre 1*; 47 and 30% decrease in shear stress for *Tyre 2*
- $t_{Asphalt}$ : 19% decrease (*Case 1/3*) and 9% increase (*Case 2/4*) in shear stress for *Tyre 1*; 6% decrease (*Case 1/3*) and 25% increase (*Case 2/4*) in shear stress for *Tyre 2*

**6.1.2 Laboratory study**

Differently composed samples were tested with the Leutner Shear Test Method to evaluate interlayer shear strength (ISS). Two different types of samples were considered: samples with tack coat application by means of Spray Jet Technology and those subjected to tack coat application by conventional methods, i.e. emulsion tank. The listed aspects were observed from the laboratory and the trial test completed. The following observations were made:

1. The samples composed of tack coat application with Spray Jet application showed favourable results (significant interlayer shear strength) and showed more potential compared to those composed of tack application with emulsion tanks.
2. The results showed that a smaller quantity of bitumen emulsion is required for construction (for Spray Jet) to achieve the same performance as application by emulsion tanks.
3. Although overall favourable results were recorded for tack coat application by means of Spray Jet technology, more testing is required to motivate the reason for the high interlayer strength values achieved during laboratory testing. From the laboratory testing, from trial-field samples, application with Spray Jet technology showed a 62.7 and 20.7% increase in bond strength compared to application with an emulsion tanker. The results were found for tack coats applied at two different emulsion rates i.e. 0.31 and 0.83/m<sup>2</sup>.
4. Despite results showing favourable trends, more tests are required to provide a comprehensive understanding of the advantages of using the new technology.

**6.1.3 Leutner Shear Test Model**

The shear stress development in the model was shown to be impacted to a large extent by tack coat properties, i.e. stiffness and thickness. The analyses yielded the following findings:

1. In general, the results from the replicated Leutner Shear Test also favoured tack coat application and its contribution to strength within the pavement.
2. The asphalt materials (with largest material stiffness) provide significant increase in shear stress development. This is also associated with the modular ratio, as the increase in stiffness for the base layer affects the shear distribution, together with the magnitude of these stresses. The material stiffness is identified as one of the parameters which has the most impact on results achieved from the analyses performed, as it is responsible for describing the material's ability to distribute stresses which are generated, to subsequent layers.

3. The thickness of the wearing course layer contributes to the stress distribution within the specific layer, which in turn impacts the shear distribution, or development, within the tack coat layer, which is transferred to subsequent layers.
4. The material stiffness of the tack coat was one of the factors identified having a bigger impact on results than other properties such as modular ratio and wearing course layer thickness. Furthermore, the tack coat thickness also showed to be very influential. Hence, in this analyses, it was apparent that the properties of tack coat has the most impact on the results obtained from the analyses. For the change in material stiffness, a change of 34 to 54% was noticeable in the results. In addition, a change in tack coat thickness produced results with a variation of 60% up to a double (100%) increase in the shear stress results obtained.
5. Comparing shear stress results with Interlayer Shear Strength (ISS) results from laboratory testing completed by Pisa University, variation of 57 to 61% is observable for change in wearing course thickness. The change in tack coat thickness showed variation of 30 and 61% in shear stresses.
6. For the FEM model, it was found that the change in wearing course thickness results in variation of shear stress results ranging from 3.3 to 16% only. In addition, the change in the base layer stiffness, modular ratio, produced shear stresses that varies between  $\approx 0$  to 17%. The difference are significantly lower compared to the change in shear stress due to tack coat properties as listed in point 5.
7. Results used for comparative purpose in point 5 is results of laboratory tests completed for samples of which tack coats were applied with Spray Jet technology. The average shear ISS was recorded as 1.74MPa. The average shear stress measured for the FEM model is 1.7MPa in very close proximity. Average ISS results from samples where tack coats (with same material characteristics) apply by emulsion tanker were measured at 1.6MPa. Shear strengths obtained for the FEM model are in close approximation to the laboratory results, which were the maximum shear results during laboratory testing. Hence, motivating the use of Spray Jet technology for the application of tack coats.

#### 6.1.4 Pavement Modelling using FEM

The results from the model were compared to the results from preliminary results, of which the following aspects were observed:

1. The FEM model provided contradictive trends when compared to the findings of the preliminary linear-elastic (LE) analysis. Differences were noted for the shear stresses and strains. Significant strains were measured within the subgrade layer, suggesting that the majority of the pavement structures would fail in the subgrade layer, resulting in immediate failure of these structures.
  - a. Shear stresses:
    - i. There are 2 instances where observations between two analyses where in contrast. However, the order of shear stresses where of main concern as there was a significant difference in this regard.
    - ii. The preliminary LE analysis produced shear stresses ranging from 0.2 to 1.2MPa where FEM model produced significantly smaller shear stresses between 0.8 and 2.3kPa only.
    - iii. Main reason for significant changes attributed to change in incorporation of the bonding element.

- Preliminary research incorporated bonding with a shear spring compliance which is proportional to the load area. Furthermore, this approach replicated different states of bonding i.e. high, medium and low which would illustrate tack coats where one has good, average or poor bonding.
  - In contrast, the FE model incorporated the material properties of the tack coat. Thus, the results obtained illustrates the contribution of the tack coat to the overall pavement performance under specified conditions.
- b. Horizontal strains:
- i. For the majority of elements compared, observations were in agreement with two exceptions where contrasting trends are observable. Similar to shear stresses, the order of the results obtained for the two analyses were seemingly different.
  - ii. The preliminary LE analysis produced horizontal strains ranging from 232 to 623 $\mu\epsilon$  where FE model produced significantly smaller shear stresses between 48 and 344 $\mu\epsilon$  only.
  - iii. The change in results is not as significant compared to shear stress results although there is also some variation in the range of results obtained. Hence, highlighting the important role that the different defined conditions plays in the analysis.
  - iv. The less severe impact observed also contributes to the argument that the main contributing component lies within the interface suggesting the bonding component is the influential element in this case.
- c. Vertical strains:
- i. For the majority of elements compared, observations for the LE and FEM analyses were in agreement with a few exceptions where contrasting observations were made. Similar to shear stresses, the order of the results obtained for the two analyses were significantly different.
  - ii. The strains obtained from the FEM analyses do not reflect realistic strains where extreme values of 564 up to 4014 $\mu\epsilon$  were recorded. The preliminary LE analysis produced smaller horizontal strains ranging from 319 to 921 $\mu\epsilon$ .
  - iii. The contribution of the subgrade to the pavement structure is fundamental where upper layers play an important role. A change in the upper layer e.g. the tack coat leads to a change in the overall pavement performance which is evident in this case.
    - It is noticeable that these results measured at the top of the subgrade layer were impacted to a significant extent. At this location, strains 4 times of those obtained for the preliminary LE analysis were achieved.
    - The change of the bonding condition influences the stress and strain regime in the structure and is carried through the upper layers to the subgrade layer. Even though upper layers did not illustrate any critical differences, the effect of change in the regime was made visible through the results obtained in the subgrade layer.
2. Similar to preliminary research (Section 6.1.2), it is evident that the base layer stiffness and asphalt layer thickness are two parameters that play a significant role in stresses and strains generated and distributed within the pavement structure. The results for structures with an increase in

these two parameters have shown more potential for carrying these stresses and strains when subjected to loading.

3. The observation concerning the stress and strain regime with pavement structures, described in the previous point, also leads to favourable results concerning pavement life predictions. The results showed that the pavement structures with increased asphalt layer thickness and base layer stiffness will deteriorate more slowly, allowing an extended pavement life of the specific structure, compared to structures composed of a weaker base layer and thinner asphalt layer.
4. In contradiction with the preliminary research, the change in asphalt layer thickness and loading conditions subjected to the pavement structure, played a larger role on results compared to the base layer stiffness. The results obtained with regard to the change in these two parameters, produced a considerable variation in the results i.e. strains and pavement life (serviceability and fatigue), than for change in base layer stiffness.
5. Given the relationship between Fatigue Life and the asphalt surfacing, as anticipated, the most significant change in results occurred for Fatigue Life, highlighting the significant extent to which the change in the asphalt surfacing influences the durability of the pavement structure under specific loading conditions.
6. The shear stress results from the model shows that asphalt layer thickness and loading condition has a significantly higher influence than factors regarding the tack coat. The results reveal that the degree of compaction and the subgrade quality will provide a pavement structure with a good foundation. Hence, the structure will be able to withstand certain loading conditions.

## 6.2 Recommendations

The limited capabilities of the analysis software used for preliminary research led to extended investigation with FEM modelling. However, to reduce the scope concerning the number of variables to be considered, analysis conditions were simplified for both material models. Hence, recommendations are provided for the two material models in Sections 6.2.1 and 6.2.2. In addition, recommendations for further laboratory testing is provided in Section 6.2.3.

### 6.2.1 Leutner Shear Model

1. Perform analyses with same loading conditions to include external factors such as loading frequency, i.e. displacement rate of the test (50.8mm/min).
2. Investigate development of strain through dynamic loading, together with evaluation of Fatigue Life.
3. Include a damage parameter that will allow the measurement of the shear stress at failure. The element can only be implemented when dynamic loading conditions are applied.
4. The use of symmetry in the model to shorten computation time of the analyses, is recommended.
5. Incorporation of attributes of tack coat, such as the application rate and the quantity of material used is recommended. This will allow for a more accurate representation for the material model.
6. Incorporation of bonding state through a friction coefficient which represents the different bonding conditions i.e. good, poor or average, that is provided by tack coat in pavement structure.

### 6.2.2 Pavement Analysis Model

1. Perform analyses with same loading conditions to include external factors such as loading frequency.
2. Investigate development of strain through dynamic loading, together with evaluation of Fatigue Life, to signify actual road conditions.
3. Extend analysis to incorporate non-linear (plastic) regime of materials.
4. Addition of pavement layers to the model to avoid high subgrade values
5. Expand analysis to include additional loading conditions

### 6.2.3 Expanded Laboratory Testing

1. Expand laboratory testing to enhance understanding of shear development and distribution, together with the contribution of shear supplied by tack coats in overall.
2. The experimental plan adhered to by Pisa University can be expanded to include a broader range of samples with various properties, subjected to a series of different conditions composed of tack coats applied by different technologies.

## REFERENCES

- Abaqus Inc., 2017. Abaqus 2017.
- Afsar, J., 2012. Properties Comparison of Emulsion and Cutbacks. , 29–31. [Online]. Available: <http://www.engineeringintro.com/transportation/binding-materials/properties-comparison-of-emulsion-and-cutbacks/> [2018, June 29].
- Akzo Nobel, 2010. Bitumen emulsion - Technical Bulletin. [Online]. Available: [https://sc.akzonobel.com/en/asphalt/Documents/AN\\_Asphalt\\_Emulsion\\_TB\\_eng.pdf](https://sc.akzonobel.com/en/asphalt/Documents/AN_Asphalt_Emulsion_TB_eng.pdf).
- Al-Qadi, I.L. et al., 2012. Best Practices for Implementation of Tack Coat: Field Study. *Best practices for Implementation of Tack Coat Part 2*, (12), 26.
- Anagnos, J.N. & Kennedy, T.W., 1972. *Practical method of conducting the indirect tensile test*, Austin Texas, United States. [Online]. Available: <http://library.ctr.utexas.edu/digitized/texasarchive/phase1/98-10-chr.pdf>.
- ArrMaz, 2012. Bonded HMA Overlays – a matter of tack materials & method of application.
- Asphalt Institute & Asphalt Emulsion Manufacturers Association, 2008. *Basic Asphalt Emulsion Manual* 4th ed., Lexington, Ky: Asphalt Institute.
- Asphalt Institute & Federal Highway Administration, 2016. Tack Coat Best Practices. FHWA Cooperative Agreement Subtask.
- Bae, A. et al., 2010. Effects of Temperature on Interface Shear Strength of Emulsified Tack Coats and Its Relationship to Rheological Properties. *Transportation Research Record: Journal of the Transportation Research Board*, 2180, 102-109. [Online]. Available: <http://trrjournalonline.trb.org/doi/10.3141/2180-12>.
- Barna A. Szabó, 2015. *Finite Element Modeling*, St. Louis. [Online]. Available: <https://linkinghub.elsevier.com/retrieve/pii/B9780080983370000102>.
- Di Benedetto, H. et al., 2013. *Advances in Interlaboratory Testing and Evaluation of Bituminous Material State-of-the-Art Report of the RILEM Technical Committee 206-ATB* M. N. Partl et al., eds., Springer Netherlands.
- Bianchi, L., 2018. *Benefits of SprayJet Technology*, Italy.
- Bianchi, L., Marradi, A. & Garofalo, M., 2018a. *Ideas and Suggestions for Additional Laboratory or In-Situ Tests*, Italy.
- Bianchi, L., Marradi, A. & Garofalo, M., 2018b. *Influence in Pavement Life of an Innovative Technology for Tack Coat Applications*, Italy.
- Bianchi, L., Marradi, A., Jenkins, K.J., et al., 2018. Influence in Pavement Life of Spray Paver Technology. , (Dici).
- BSM Laboratories, 2016. Test procedure. Determination of the indirect tensile strength (ITS) of bitumen stabilised material (BSM). , (August), 1–8.
- Canestrari, F. et al., 2005. Advanced Testing and Characterization of Interlayer Shear Resistance. *Transportation Research Record: Journal of the Transportation Research Board*, 1929(January), 69–78. [Online]. Available: <http://trrjournalonline.trb.org/doi/10.3141/1929-09>.
- Canestrari, F. & Santagata, E., 2005. Temperature effects on the shear behaviour of tack coat emulsions used in flexible pavements. *International Journal of Pavement Engineering*, 6(1), 39–46.
- CEEC Trucks Industry, 2001. Intelligent Asphalt Distributor Truck User's Manual. , 1–29.

- Chen, J.-S. & Huang, C.-C., 2010. Effect of Surface Characteristics on Bonding Properties of Bituminous Tack Coat. *Transportation Research Record: Journal of the Transportation Research Board*, 2180, 142–149. [Online]. Available: <http://trrjournalonline.trb.org/doi/10.3141/2180-16>.
- Collop, A.C. et al., 2009. Shear bond strength between asphalt layers for laboratory prepared samples and field cores. *Construction and Building Materials*, 23(6), 2251–2258. [Online]. Available: <http://dx.doi.org/10.1016/j.conbuildmat.2008.11.017>.
- Committee of State Road Authorities, 1994a. The Use of Bitumen Emulsions in the Construction and Maintenance of Roads. *Technical Recommendations for Highways*, 7, 1–72.
- Committee of State Road Authorities, 1994b. TRH7 (Draft). The Use of Bitumen Emulsions in the Construction and Maintenance of Roads. *Technical Recommendations for Highways*, 39–40.
- Croney, P. & Croney, D., 1998. *The Design and Performance of Road Pavements* 3rd ed., New York, N.Y.: McGraw-Hill.
- CSIR, 2007. Implementing employment intensive road works. *Manual 4 Bituminous Pavement Seals*, 94.
- D’Andrea, A. & Tozzo, C., 2012. Interlayer Shear Failure Evolution with Different Test Equipments. In *Procedia - Social and Behavioral Sciences*. Elsevier B.V., pp. 556-567. [Online]. Available: <http://linkinghub.elsevier.com/retrieve/pii/S1877042812043686>.
- Dassault Systèmes Simulia, 2014a. *Abaqus 6.14. Analysis User’s Guide. Volume II: Analysis*, Providence, RI. [Online]. Available: <http://abaqus.software.polimi.it/v6.14/index.html>.
- Dassault Systèmes Simulia, 2014b. *Abaqus 6.14. Analysis User’s Guide. Volume III: Materials*, Providence, RI.
- Dassault Systèmes Simulia, 2014c. *Abaqus 6.14. Analysis User’s Guide. Volume IV: Elements*, Providence, RI.
- Dassault Systèmes Simulia, 2014d. *Abaqus 6.14. Analysis User’s Guide. Volume V: Prescribed Conditions, Constraints and Interactions*, Providence, RI. [Online]. Available: <http://abaqus.software.polimi.it/v6.14/index.html>.
- Dassault Systèmes Simulia, 2014e. *Abaqus 6.14. Getting Started with Abaqus: Keyword Edition*, Providence, RI. [Online]. Available: <http://abaqusdoc.ucalgary.ca/books/gsk/default.htm>.
- Dassault Systèmes Simulia, 2014f. *Abaqus 6.14 CAE User Guide*, Providence, RI.
- Dassault Systèmes Simulia, 2016a. Controlling mesh characteristics. *Abaqus Online Documentation*. [Online]. Available: <http://ivt-abaqusdoc.ivt.ntnu.no:2080/v2016/books/usi/default.htm> [2018, October 11].
- Dassault Systèmes Simulia, 2016b. Creating cohesive sections. *Abaqus Online Documentation*. [Online]. Available: <http://130.149.89.49:2080/v2016/books/usi/default.htm?startat=pt03ch12s13h1b12.html> [2018, June 25].
- Dassault Systèmes Simulia, 2016c. The Incrementation Tab. *Abaqus Online Documentation*. [Online]. Available: <http://ivt-abaqusdoc.ivt.ntnu.no:2080/v2016/books/usi/default.htm?startat=pt03ch14s03s01.html> [2016, April 16].
- Dassault Systèmes Simulia, 2016d. The Step Editor. *Abaqus Online Documentation*. [Online]. Available: <http://ivt-abaqusdoc.ivt.ntnu.no:2080/v2016/books/usi/default.htm?startat=pt03ch14s03s01.html> [2018, October 8].
- Destrée, A. et al., 2015. Field Study to Investigate the Impact of Conditions of Application of Tack Coats on the Interlayer Bond Strength. In *Development of Specifications and Guidelines for Hot in-Place Recycling in Finland — Outline and Framework*. pp. 347–358.

- Diakhaté, M. et al., 2011. Experimental investigation of tack coat fatigue performance: Towards an improved lifetime assessment of pavement structure interfaces. *Construction and Building Materials*, 25(2), 1123–1133.
- Dillard, P., 2015. Asphalt materials. [Online]. Available: <http://slideplayer.com/slide/3868209/> [2018, June 27].
- Ergon Asphalt and Emulsions, 2006. *Field Guide to Emulsions* 5th ed.,
- Federal Highway Administration, 2016. Tack Coat Best Practices - Technical Brief. , (April), 1–17.
- Fontes, L.P.T.L. et al., 2006. Improvement of the Functional Pavement Quality with Asphalt Rubber Mixtures. , (April). [Online]. Available: [http://www.civil.uminho.pt/transportinfra/publications/2006\\_\(AR2006\)\\_Liseane\\_Pais\\_Pereira\\_Triches\\_A.pdf](http://www.civil.uminho.pt/transportinfra/publications/2006_(AR2006)_Liseane_Pais_Pereira_Triches_A.pdf).
- For Construction Pros, 2014. How Tack Coat Improves Your Asphalt Paving. [Online]. Available: <https://www.forconstructionpros.com/asphalt/article/11408541/how-tack-coat-improves-your-asphalt-paving> [2018, July 4].
- Ghaly, N.F. et al., 2014. Tack coats for asphalt paving. *Egyptian Journal of Petroleum*, 23(1), 61–65. [Online]. Available: <http://dx.doi.org/10.1016/j.ejpe.2014.02.009>.
- Gierhart, D. & Johnson, D.R., 2017. *NCHRP Synthesis 516. Tack Coat Specifications, Materials, and Construction Practices*, Washington D.C, USA: The National Academies Press. [Online]. Available: <https://www.nap.edu/catalog/25122>.
- Hakimzadeh, S. et al., 2012. Development of Fracture-Energy Based Interface Bond Test for Asphalt Concrete. In *Association of Asphalt Paving Technologists Annual Meeting*. Austin Texas, United States.
- Hu, X. et al., 2017. Effect of tack coat dosage and temperature on the interface shear properties of asphalt layers bonded with emulsified asphalt binders. *Construction and Building Materials*, 141, 86–93. [Online]. Available: <http://dx.doi.org/10.1016/j.conbuildmat.2017.02.157>.
- Huang, W. et al., 2015. Effects of Tack Coat Type and Surface Characteristics on Interface Bond Strength. In L. Sun et al., eds. *New Frontiers in Road and Airport Engineering - Selected Papers from the 2015 International Symposium on Frontiers of Road and Airport Engineering*. Shanghai, China: American Society of Civil Engineers, pp. 25–36.
- Jaskula, P. & Rys, D., 2017. Effect of Interlayer Bonding Quality of Asphalt Layers on Pavement Performance. In *IOP Conference Series: Materials Science and Engineering*. p. 8.
- Jenkins, K.J., 2018. Hitchhikers Guide to Pavement Engineering Postgrad Chapters 5-10.
- Jenkins, K.J., 2000. *Mix Design Considerations for Cold and Half-Warm Bituminous Mixes with Emphasis on Foamed Bitumen*. Stellenbosch University.
- Jenkins, K.J. & Rudman, C.E., 2018a. Hitchhikers guide to Pavement Engineering. *Transportation 434 Course Notes Chapters 5 to 9*, 156–201.
- Jenkins, K.J. & Rudman, C.E., 2018b. Hitchhikers Guide to Pavement Engineering. *Transportation 434 Course Notes Chapters 1 to 4*, 19–22, 96.
- Johnson, D., 2018a. An Introduction to Asphalt Emulsions. *Asphalt magazine*. [Online]. Available: <http://asphaltmagazine.com/an-introduction-to-asphalt-emulsions/> [2018, June 26].
- Johnson, D., 2018b. Tackling Tack Coats. *Asphalt magazine*. [Online]. Available: <http://asphaltmagazine.com/tackling-tack-coats/> [2018, June 26].

- Kim, H. et al., 2011. Numerical and Experimental Analysis for the Interlayer Behavior of Double-Layered Asphalt Pavement Specimens. *Journal of Materials in Civil Engineering*, 23(1), 12–20. [Online]. Available: <http://ascelibrary.org/doi/10.1061/%28ASCE%29MT.1943-5533.0000003>.
- Krishma Rao, K. V., *Two-layer Systems Variation of Subgrade Stress with Modular Ratio*,
- Leng, Z. et al., 2008. Interface Bonding between Hot-Mix Asphalt and Various Portland Cement Concrete Surfaces: Laboratory Assessment. *Transportation Research Record*, 2057, 1, 46–53.
- Leutner, R., 1979. Investigation of the Adhesion of Bituminous Pavements [Untersuchungen des Schichtenverbunds beim Bituminösen Oberbau]. *Bitumen*, 3, 84–91.
- Malicki, K. & Górszczyk, J., 2012. Influence of the Tack Coat Material on Interlayer Bonding Properties in Asphalt Layers System. In *Proceedings of the 4th European Pavement and Asset Management Conference EPAM 2012*.
- Mathew, T. V. & Rao, K.V.K., 2007. Pavement Materials: Bitumen. In *Introduction to Transportation Engineering*. [Online]. Available: <http://nptel.ac.in/courses/105101087/23-Ltexhtml/p4/p.html>.
- Mohammad, L. et al., 2011. Effects of Shear Bond Characteristics of Tack Coats on Pavement Performance at the Interface. *Transportation Research Record: Journal of the Transportation Research Board*, 2209, 1–8. [Online]. Available: <http://trrjournalonline.trb.org/doi/10.3141/2209-01>.
- Mohammad, L. et al., 2002. Influence of Asphalt Tack Coat Materials on Interface Shear Strength. *Transportation Research Record: Journal of the Transportation Research Board*, 1789(January), 56–65. [Online]. Available: <http://trrjournalonline.trb.org/doi/10.3141/1789-06>.
- Mohammad, L. et al., 2008. Worldwide State of Practice on the Use of Tack Coats: A Survey. *Journal of the Association of Asphalt Paving Technologists*, 77, 1–34.
- Mohammad, L.N. et al., 2012. *NCHRP Report 712. Optimization of Tack Coat for HMA Placement*, Washington D.C, USA. [Online]. Available: <http://www.nap.edu/catalog/13652>.
- Molenaar, P. et al., 2009. The Development and Performance of a New Ultra Thin Friction Course for OR Tambo International Airport in South Africa. *CROW 2nd European Airport Pavement Workshop*, 1–17.
- nuroil, 2014. Performance Grade. *Types of bitumen*, 9-10. [Online]. Available: <http://www.nuroil.com/bitumen-performance-grade.aspx> [2018, July 9].
- Panda, M. et al., 2013. An Experimental Study on Assessment of Pavement Interlayer Bond Strength. *International Journal of Transportation Science and Technology*, 2(2), 141–148. [Online]. Available: <http://multi-science.atypon.com/doi/10.1260/2046-0430.2.2.141>.
- Papagiannakis, A.T. & Tashman, L., 2006. Evaluation of the Influence of Tack Coat Construction Factors on the Bond Strength Between Pavement Layers. *Washington Center for Asphalt Technology*, (September 2015).
- Pavement Interactive, 2012. Cutback Asphalt. [Online]. Available: <http://www.pavementinteractive.org/cutback-asphalt> [2018, June 26].
- Pavement Interactive, 2011. Tack Coats. [Online]. Available: <http://www.pavementinteractive.org/tack-coats/> [2018, January 26].
- Pavement Interactive, 2013. The Right Tack to Take. [Online]. Available: <https://www.pavementinteractive.org/the-right-tack-to-take/> [2019, July 2].
- Pavement Preservation and Recycling Alliance, 2018. Tack Coat Equipment Variations. [Online]. Available: [https://roadresource.org/treatment\\_resources/tack\\_coat?page=about\\_process](https://roadresource.org/treatment_resources/tack_coat?page=about_process) [2019, July 2].

- Petersen, B. & Knipe, M., 2009. Hand-laid Hot-mix Asphalt : , (April), 1–36.
- Portland Cement Association, 2018. Cement-Treated Base (CTB). [Online]. Available: [http://www.cement.org/cement-concrete-applications/paving/cement-treated-base-\(ctb\)](http://www.cement.org/cement-concrete-applications/paving/cement-treated-base-(ctb)) [2018, May 22].
- Raab, C. et al., 2010. Effect of Gap Width on Interlayer Shear Bond Results. *International Journal of Pavement Research and Technology*, 3(2), 79–85.
- Raab, C. & Partl, M.N., 2004. Effect of Tack Coats on Interlayer Shear Bond of Pavements. *8th Conference On Asphalt Pavements For Southern Africa*, (September), 9.
- Raab, C. & Partl, M.N., 2009. Interlayer bonding of binder, base and subbase layers of asphalt pavements: Long-term performance. *Construction and Building Materials*, 23(8), 2926–2931. [Online]. Available: <http://dx.doi.org/10.1016/j.conbuildmat.2009.02.025>.
- RAHA Bitumen, 2016a. Bitumen Emulsion. [Online]. Available: <http://rahabitumen.com/bitumen-emulsion/> [2018, June 29].
- RAHA Bitumen, 2016b. Bitumen Emulsion Advantages Compared to Cutback Bitumen. [Online]. Available: <http://rahabitumen.com/bitumen-emulsion-advantages/> [2018, June 29].
- RAHA Bitumen, 2016c. Cutback Bitumen. [Online]. Available: <http://rahabitumen.com/cutback-bitumen/> [2018, June 29].
- RAHA Bitumen, 2016d. How Tack Coat Improves Your Asphalt Paving. [Online]. Available: <http://rahabitumen.com/tack-coat-improves-asphalt-paving/> [2018, June 29].
- Rahman, A. et al., 2017. State-of-the-art review of interface bond testing devices for pavement layers: toward the standardization procedure. *Journal of Adhesion Science and Technology*, 31(2), 109–126. [Online]. Available: <http://dx.doi.org/10.1080/01694243.2016.1205240>.
- Raposeiras, A.C. et al., 2012. Influence of surface macro-texture and binder dosage on the adhesion between bituminous pavement layers. *Construction and Building Materials*, 28(1), 187–192. [Online]. Available: <http://dx.doi.org/10.1016/j.conbuildmat.2011.08.029>.
- Raposeiras, A.C. et al., 2013. Test methods and influential factors for analysis of bonding between bituminous pavement layers. *Construction and Building Materials*, 43, 372–381.
- RoadTec, 2008. Spray Paver SP-200.
- Romanoschi, S., 1999. *Characterization of pavement layer interfaces*. Louisiana State University and Agricultural and Mechanical College.
- Romanoschi, S.A. & Metcalf, J.B., 2001. Characterization of asphalt concrete layer interfaces. *Transportation Research Record No. 1778*, 132–139.
- Santagata, F.A. et al., 2009. Statistical investigation of two different interlayer shear test methods. *Materials and Structures/Materiaux et Constructions*, 42(6), 705–714.
- Serigos, P.A., 2013. The Contribution of Micro- and Macro-texture to the Skid Resistance of Pavements. In *European Conference of Transport Research Institutes. Young Researchers Seminar 2013*. Lyon, France, p. 25.
- Shell, 1998. Bisar 3.0 User Manual. , 1–47.
- Sholar, G.A. et al., 2004. Preliminary Investigation of a Test Method to Evaluate Bond Strength of Bituminous Tack Coats. *Journal of the Association of Asphalt Paving Technologists*, 73, 771–806.
- South African Bitumen Association, 2011. *Manual 30: A guide to the selection of bituminous binders for road construction*,
- Surface King, 2015. Tack & Prime Coat Applications With Asphalt Emulsions. [Online]. Available: <https://www.surfaceking.com/prime-tack-coat.htm> [2018, January 26].

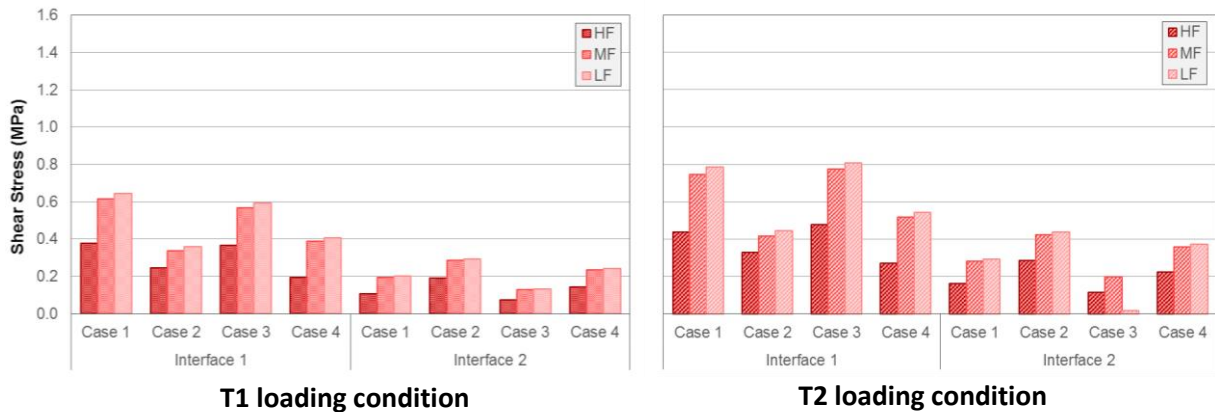
- Sutanto, M.H., 2009. *Assessment of bond between asphalt layers*. United Kingdom: University of Nottingham.
- Sutanto, M.H., 2011. Development of Automatic Torque Bond Test. *Journal of Transportation Engineering*, 11(3), 191–200.
- Texas Department of Transportation, 2015. *Asphalt Materials and Uses*. , 3–9.
- The Constructor, 2017. Different Types of Bitumen, their Properties and Uses. [Online]. Available: <https://theconstructor.org/transportation/types-of-bitumen-properties-uses/15709> [2018, June 29].
- Theyse, H. et al., 2011. Interim revision of the South African Mechanistic-Empirical pavement design method for flexible pavements. , 1-20. [Online]. Available: <http://researchspace.csir.co.za/dspace/handle/10204/5242>.
- Theyse, H.L. et al., 1996. Overview of South African Mechanistic Pavement Design Method. *Transportation Research Record*, (1), 6–17.
- Theyse, H.L. et al., 2007. Revision of the South African Flexible Pavement Design Method: Mechanistic-Empirical Component. In *9th Conference on Asphalt Pavements for Southern Africa*. pp. 256–292.
- Thom, N.H., 2014. Design Against Cracking - Asphalt Pavements. In *Principles of Pavement Engineering*. ICE Publishing.
- Tosas, 2018. In-situ Engineering Technology Solutions. Soil stabiliser and dust control palliative with Nano polymer. [Online]. Available: <https://www.tosas.co.za/wp-content/uploads/2018/07/IETS-General-Product-Information-Sheet.pdf> [2019, March 25].
- Tosas, 2019. Elasto-Tack UTFC Bonding Solution Brochure. [Online]. Available: <https://www.tosas.co.za/wp-content/uploads/2018/05/TOSAS-Elasto-Tack-Digital-Brochure.pdf> [2019, March 25].
- Tschegg, E.K. et al., 1995. Investigation of Bonding between Asphalt Layers on Road Construction. *Journal of Transportation Engineering*, 121(4), 309–316. [Online]. Available: <http://www.scopus.com/inward/record.url?eid=2-s2.0-0029345840&partnerID=tZOtx3y1>.
- University of Cambridge, 2011. Abaqus Analysis. [Online]. Available: <http://www-h.eng.cam.ac.uk/help/programs/fe/abaqus/faq68/abaqusf10.html> [2018, October 8].
- Uzan, J. et al., 1978. Investigation of adhesion properties between asphaltic-concrete layers. In *Asphalt Paving Technologist Proceedings*. pp. 495–521.
- van de Ven, M.F.C. et al., 2004. Concepts Used for Development of Bitumen Specifications. *Polymer*, (September).
- Vögele, J., 2018. SprayJet versus Conventional Paving with Pre-Spraying of Emulsion. [Online]. Available: [https://www.voegele.info/en/technologies/applications-technology/sprayjet\\_contra\\_klass.html](https://www.voegele.info/en/technologies/applications-technology/sprayjet_contra_klass.html) [2018, June 25].
- Vögele Wirtgen Group, 2017. *Technical Note (Draft). Spray Jet demo and testing campaign, Italy*.
- Vögele Wirtgen Group, 2018. The Super 1800-3i SprayJet Tracked Paver.
- Walubita, L. & Van de Ven, M., 2000. Stresses and strains in asphalt-surfacing pavements. *Satc 2000*, 3(12), 412–421. [Online]. Available: <http://137.215.9.22/handle/2263/8338>.
- Wan, J. et al., 2018. Using interface shear characteristics to evaluate the residual performance of asphalt pavements. *Journal of Adhesion Science and Technology*, 32(18), 2070–2082. [Online]. Available: <https://doi.org/10.1080/01694243.2018.1462948>.

- Wang, J. et al., 2017. Application of Tack Coat in Pavement Engineering. *Construction and Building Materials*, 152, 856-871. [Online]. Available: <http://dx.doi.org/10.1016/j.conbuildmat.2017.07.056>.
- Wang, X. et al., 2017. Shear fatigue between asphalt pavement layers and its application in design. *Construction and Building Materials*, 135, 297-305. [Online]. Available: <http://dx.doi.org/10.1016/j.conbuildmat.2016.12.151>.
- Wei, X. et al., 2015. Investigation into Influence Factors on Shear Properties between Layers of Asphalt Pavement. In L. Sun et al., eds. *New Frontiers in Road and Airport Engineering - Selected Papers from the 2015 International Symposium on Frontiers of Road and Airport Engineering*. Shanghai, China: American Society of Civil Engineers, pp. 132–142.
- Wheat, M., 2007. *Evaluation of Bond Strength at Asphalt Interfaces*. Kansas State University.
- Wirtgen Group, 2017. Technical note: Spray Jet demo and testing campaign DRAFT.
- Yaacob, H. et al., 2013. Bitumen Emulsion in Malaysia - A Conspectus. *Jurnal Teknologi (Sciences and Engineering)*, 65(3), 97–104.
- Yaacob, H. et al., 2014. Information for the Malaysian Asphalt Industry towards Better Pavement Interlayer Bonding (Maklumat kepada Industri Asfalt Malaysia ke Arah Lekatan Lapisan Turapan yang Lebih Baik). *Sains Malaysiana*, 43(3), 467-474. [Online]. Available: [http://www.ukm.my/jsm/pdf\\_files/SM-PDF-43-3-2014/18 Haryati Yaacob.pdf](http://www.ukm.my/jsm/pdf_files/SM-PDF-43-3-2014/18%20Haryati%20Yaacob.pdf).
- Zhang, W., 2017. Effect of tack coat application on interlayer shear strength of asphalt pavement: A state-of-the-art review based on application in the United States. *International Journal of Pavement Research and Technology*, 10(5), 434-445. [Online]. Available: <http://dx.doi.org/10.1016/j.ijprt.2017.07.003>.
- van Zyl, G., 2018. Construction of Surface. *Unpublished Class notes. Pavement Construction Course 2018*.
- van Zyl, S., 2018. *Bituminous Binder in South Africa and the Fatigue Performance*. Stellenbosch: University of Stellenbosch.

## **APPENDICES**

# **Appendix A: Stellenbosch Preliminary Analysis Results**

## Appendix A1: Shear Stresses



**Note:** Interface 1 = Asphalt/Base, Interface 2 = Base/ Subgrade. Case 1 and 2: Interface 1 at 0.05m, Interface 2 at 0.25m. Case 3 and 4: Interface 1 at 0.1m, Interface 2 at 0.3m

**Figure A1:** Shear stress results measured at Edge

**Table A1:** Shear stresses at Edge location for Case 1

Point	Depth (m)	T1 loading			T2 loading		
		HF	MF	LF	HF	MF	LF
1/2	0	340.1	352.4	346.7	445	436.4	426
3/4	0.05	377.3	613.6	644.4	438.3	746	786.8
5/6	0.05	207.3	39.08	40.48	274.4	61.93	64.13
7/8	0.15	140.9	167.3	168.3	203.5	235.7	236.6
9/11	0.25	108.1	193.7	201	160.6	282	291.4
10/12	0.25	60.19	19.29	16.84	91.79	28.29	24.99

**Note:** T1 loading = Tyre pressure of 750kPa and half-axle load of 40kN, T2 loading = Tyre pressure of 900kPa and half-axle load of 70kN.

**Table A2:** Shear stresses at Edge location for Case 2

Point	Depth (m)	T1 loading			T2 loading		
		HF	MF	LF	HF	MF	LF
1/2	0	146.1	47.84	38.11	236.6	76.48	60.97
3/4	0.05	246.2	339.3	360.1	330.2	415.8	445.3
5/6	0.05	247.8	136.9	149.1	328.7	220.7	237.2
7/8	0.15	180.1	226.6	228.1	264.2	326	327.9
9/11	0.25	190.4	285.2	295.2	286.2	424.2	438.5
10/12	0.25	35.15	18.6	15.02	54.57	27.51	22.26

**Table A3:** Shear stresses at Edge location for Case 3

Point	Depth (m)	T1 loading			T2 loading		
		HF	MF	LF	HF	MF	LF
1/2	0	253.3	336.8	342.7	366.8	483.4	490.3
3/4	0.1	365.5	568.9	593.6	476.1	774.6	809
5/6	0.1	135.8	21.16	17.83	193.3	29.39	31.43
7/8	0.2	88.43	93.01	92.51	135.3	139.2	138.2
9/11	0.3	74.65	129.6	134.5	116.2	198.7	205.2
10/12	0.3	40.38	13.96	12.09	64.11	21.19	18.56

**Table A4:** Shear stresses at Edge location for Case 4

Point	Depth (m)	T1 loading			T2 loading		
		HF	MF	LF	HF	MF	LF
1/2	0	95.95	125.8	126	166.3	195.1	194.5
3/4	0.1	195.5	387	406.6	270	516.5	544.4
5/6	0.1	193.3	103.5	116.8	270.1	173.6	192
7/8	0.2	130.5	156.7	157.4	198.9	236.5	237.5
9/11	0.3	144.6	233.8	242.9	223.9	357.5	370.6
10/12	0.3	25.85	16	13.02	41.11	24.12	19.66

**Table A5:** Case 1 difference ( $\Delta\%$ ) for shear stress results (%)

Point	Depth (m)	T1 loading				T2 loading			
		Below Wheel		Edge		Below Wheel		Edge	
1/2	0	8.5	↓	1.6	↓	2.6	↓	4.6	↑
3/4	0.05	80.9	↓	72.0	↓	50.5 (*)	↓	80.8	↓
5/6	0.05	99.1	↑	80.3	↑	89.9	↑	76.5	↑
7/8	0.15	16.6	↓	19.6	↓	13.0	↓	16.3	↓
9/11	0.25	50.1 (*)	↓	86.9	↓	98.3	↓	82.2	↓
10/12	0.25	72.6	↑	72.6	↑	73.2	↑	73.2	↑

**Note:** Increasing shear stress is indicated with arrow pointing in upward direction and describes results with increase in friction i.e. from low friction (full slip) to high friction (full friction)

(\*) For values exceeding 100%, Equation 3.2.3a adjusted: high friction (HF) relative to low friction (LF) as ratio of LF

**Table A6:** Case 2 difference ( $\Delta\%$ ) for shear stress results (%)

Point	Depth (m)	T1 loading				T2 loading			
		Below Wheel		Edge		Below Wheel		Edge	
1/2	0	69.1	↑	73.9	↑	77.7	↑	75.2	↑
3/4	0.05	71.9 (*)	↓	47.5	↓	81.8 (*)	↓	36.1	↓
5/6	0.05	21.3	↑	39.1	↑	57.6	↓	27.2	↑
7/8	0.15	10.1	↓	26.8	↓	1.7	↓	24.2	↓
9/11	0.25	62.2	↓	55.8	↓	60.5	↓	53.9	↓
10/12	0.25	59.5	↑	58.8	↑	61.3	↑	60.6	↑

**Table A7:** Case 3 difference ( $\Delta\%$ ) for shear stress results (%)

Point	Depth (m)	T1 loading				T2 loading			
		Below Wheel		Edge		Below Wheel		Edge	
1/2	0	33.6	↓	35.6	↓	33.5	↓	33.9	↓
3/4	0.1	57.0	↓	63.4	↓	65.9	↓	70.9	↓
5/6	0.1	99.1	↑	86.6	↑	94.2	↑	83.5	↑
7/8	0.2	4.3	↓	4.5	↓	1.8	↓	2.0	↓
9/11	0.3	91.4	↓	81.0	↓	90.2	↓	77.3	↓
10/12	0.3	70.7	↑	70.7	↑	71.6	↑	71.6	↑

**Note:** Increasing shear stress is indicated with arrow pointing in upward direction and describes results with increase in friction i.e. from low friction (full slip) to high friction (full friction)

(\*) For values exceeding 100%, Equation 3.2.3a adjusted: high friction (HF) relative to low friction (LF) as ratio of LF

**Table A8:** Case 4 difference ( $\Delta\%$ ) for shear stress results (%)

Point	Depth (m)	T1 loading				T2 loading			
		Below Wheel		Edge		Below Wheel		Edge	
1/2	0	49.3	↓	31.3	↓	34.4	↓	16.8	↓
3/4	0.1	61.3 (*)	↓	52.3 (*)	↓	66.0 (*)	↓	50.7 (*)	↓
5/6	0.1	45.4	↑	38.6	↑	18.0	↑	28.0	↑
7/8	0.2	0.2	↓	20.7	↓	6.1	↑	19.5	↓
9/11	0.3	76.2	↓	68.9	↓	74.9	↓	66.4	↓
10/12	0.3	51.9	↑	51.4	↑	54.3	↑	53.8	↑

## Appendix A2: Normal Stresses

**Table A9:** Deviator stresses for High Friction condition (kPa)

Analysis conditions	T1 loading		T2 loading	
	Below Wheel	Edge	Below Wheel	Edge
Case 1	-329.8	-161.1	-473.0	-208.0
Case 2	-363.7	-167.5	-504.0	-218.8
Case 3	-201.5	-126.9	-313.2	-179.2
Case 4	-277.1	-160.4	-417.9	-223.5

**Note:** T1 loading = Tyre pressure of 750kPa and half-axle load of 40kN, T2 loading = Tyre pressure of 900kPa and half-axle load of 70kN.

**Table A10:** Deviator stresses for Medium Friction condition (kPa)

Analysis conditions	T1 loading		T2 loading	
	Below Wheel	Edge	Below Wheel	Edge
Case 1	-382.5	-176.9	-532.8	-228.5
Case 2	-399.8	-153.6	-512.5	-192.2
Case 3	-211.6	-128.9	-321.5	-181.4
Case 4	-279.4	-136.3	-395.1	-178.1

**Table A11:** Deviator stresses for Low Friction condition (kPa)

Analysis conditions	T1 loading		T2 loading	
	Below Wheel	Edge	Below Wheel	Edge
Case 1	-384.6	-177.1	-534.4	-228.4
Case 2	-400.4	-153.3	-512.8	-191.9
Case 3	-210.2	-127.3	-318.8	-178.9
Case 4	-277.6	-134.1	-392.2	-175.2

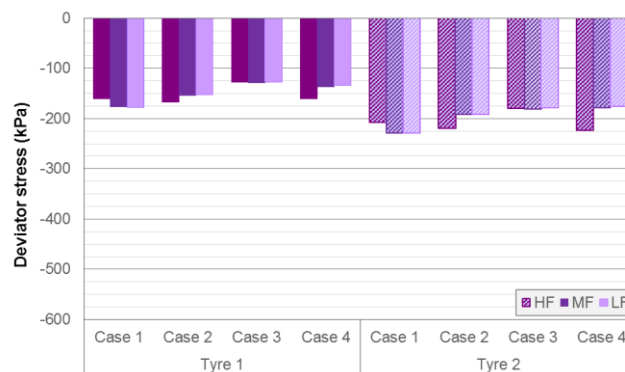


**Figure A2:** Deviator stress results measured at Edge

**Table A12:** Difference ( $\Delta\%$ ) for deviator stress results (%) for Below Wheel

<b>Analyses</b>	<b>T1 loading</b>		<b>T2 loading</b>		<b>Change</b>
<b>Case 1</b>	16.6	↑	13	↑	3.6 ↓
<b>Case 2</b>	10.1	↑	1.8	↑	8.4 ↓
<b>Case 3</b>	4.3	↑	1.8	↑	2.5 ↓
<b>Case 4</b>	0.2	↑	6.1	↓	-

**Table A13:** Difference ( $\Delta\%$ ) for deviator stress results (%) for Edge

<b>Analyses</b>	<b>T1 loading</b>		<b>T2 loading</b>		<b>Change</b>
<b>Case 1</b>	10.0	↑	9.8	↑	0.2 ↓
<b>Case 2</b>	-8.5	↓	-12.3	↓	3.8 ↓
<b>Case 3</b>	0.29	↑	-0.2	↑	-
<b>Case 4</b>	-16.4	↓	-21.6	↓	5.2 ↓

## Appendix A3: Strains

**Table A14:** Case 1 to 4 Horizontal strains for High Friction condition (Microstrain)

Analysis conditions	T1 loading		T2 loading	
	Below Wheel	Edge	Below Wheel	Edge
Case 1	257	190.4	262	206.7
Case 2	9	-53.68	-31.1	-79.64
Case 3	266.9	195.9	351.1	256
Case 4	78	51.4	84.3	56.12

**Note:** T1 loading = Tyre pressure of 750kPa and half-axle load of 40kN, T2 loading = Tyre pressure of 900kPa and half-axle load of 70kN. Negative strains = compressive strains, Positive strains = tensile strains.

**Table A15:** Case 1 to 4 Horizontal strains for Medium Friction condition (Microstrain)

Analysis conditions	T1 loading		T2 loading	
	Below Wheel	Edge	Below Wheel	Edge
Case 1	496.4	373.6	588.2	460.1
Case 2	218.1	183.1	250.2	224.9
Case 3	426.1	324.1	597.3	450.1
Case 4	275.3	206.4	371	281.4

**Table A16:** Case 1 to 4 Horizontal strains for Low Friction condition (Microstrain)

Analysis conditions	T1 loading		T2 loading	
	Below Wheel	Edge	Below Wheel	Edge
Case 1	521.1	394.1	621.7	487.4
Case 2	232.9	196.3	271.3	243.6
Case 3	444.2	340	623.3	472.3
Case 4	289	218.7	390.7	298.9

**Table A17:** Case 1 to 4 difference results ( $\Delta\%$ ) for horizontal strains (%)

Analysis conditions	T1 loading				T2 loading			
	Below Wheel		Edge		Below Wheel		Edge	
Case 1	50.7	↓	51.7	↓	57.9	↓	57.6	↓
Case 2	96.1	↓	72.7 [*]	↓	88.5 [*]	↓	67.3 [*]	↓
Case 3	66.4 (*)	↓	73.6 (*)	↓	77.5 (*)	↓	84.5 (*)	↓
Case 4	73	↓	76.5	↓	78.4	↓	81.2	↓

**Note:** Estimations obtained from Equation 3.2.3a adjusted: high friction (HF) relative to low friction (LF) as ratio of LF

(\*) Estimations with Equation 3.2.3a (unadjusted)

[\*] Where compressive strains were obtained. Equation 3.2.3a estimates performed based on the absolute values of the strains measured at these locations

**Table A18:** Case 1 to 4 Vertical strains for High Friction condition (Microstrain)

Analysis conditions	T1 loading		T2 loading	
	Below Wheel	Edge	Below Wheel	Edge
Case 1	-945.5	-676.2	-1505	-990.9
Case 2	-550.5	-415.3	-886.8	-630.8
Case 3	-600.1	-478.7	-988.3	-737.6
Case 4	-388.5	-312.4	-639.8	-487

*Note: Negative strains = compressive strains, Positive strains = tensile strains.*

**Table A19:** Case 1 to 4 Vertical strains for Medium Friction condition (Microstrain)

Analysis conditions	T1 loading		T2 loading	
	Below Wheel	Edge	Below Wheel	Edge
Case 1	-599	-435.3	-946.7	-636.5
Case 2	-424.3	-329.5	-669.5	-493.5
Case 3	-397.5	-319	-648.7	-488.3
Case 4	-349.9	-285.4	-563.8	-436.4

**Table A20:** Case 1 to 4 Vertical strains for Low Friction condition (Microstrain)

Analysis conditions	T1 loading		T2 loading	
	Below Wheel	Edge	Below Wheel	Edge
Case 1	-580.5	-420.3	-920.7	-616.3
Case 2	-383.6	-298.4	-608.5	-449.2
Case 3	-385.5	-308.6	-631.5	-475.4
Case 4	-318.9	-260.7	-515.9	-400.1

**Table A21:** Case 1 to 4 difference results ( $\Delta\%$ ) for vertical strains (%)

Analysis conditions	T1 loading				T2 loading			
	Below Wheel		Edge		Below Wheel		Edge	
Case 1	38.6	↓	37.8	↓	38.8	↓	37.8	↓
Case 2	30.3	↓	28.1	↓	31.4	↓	28.8	↓
Case 3	35.8	↓	35.5	↓	36.1	↓	35.5	↓
Case 4	17.9	↓	16.5	↓	19.4	↓	17.8	↓

## Appendix A4: Pavement Life

**Table A22:** Fatigue Life results for Edge location (MESAs)

Analysis conditions	T1 loading			T2 loading		
	HF	MF	LF	HF	MF	LF
Case 1	1.97	0.07	0.05	1.30	0.02	0.02
Case 2	-	>100	>100	-	>100	>100
Case 3	1.71	17.62	11.82	>100	8.61	5.50
Case 4	>100	1.31	0.98	>100	0.28	0.21

**Note:** T1 loading = Tyre pressure of 750kPa and half-axle load of 40kN, T2 loading = Tyre pressure of 900kPa and half-axle load of 70kN.

**Table A23:** Case 1 to 4 difference results ( $\Delta\%$ ) for Fatigue Life (%)

Analysis conditions	T1 loading				T2 loading			
	Below Wheel		Edge		Below Wheel		Edge	
Case 1	97.1	↑	97.4	↑	98.7	↑	98.6	↑
Case 2	100.0	↑	-	-	-	-	-	-
Case 3	92	↑	85.6 (*)	↓	94.3	↑	99.7	↑
Case 4	99.9	↑	99.9	↑	100.0	↑	100.0	↑

**Note:** Absence of pavement life as indicated in Table 3.2.7.2a

(\*) For values exceeding 100%, Equation 3.2.3a adjusted: high friction (HF) relative to low friction (LF) as ratio of LF

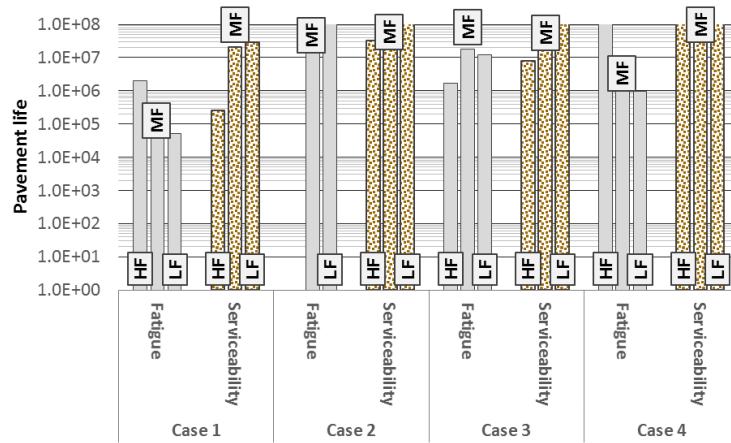
**Table A24:** Serviceability Life results for Edge location (MESAs)

Analysis conditions	T1 loading			T2 loading		
	HF	MF	LF	HF	MF	LF
Case 1	0.25	20.52	29.13	0.01	0.46	0.63
Case 2	32.84	>100	>100	0.5	5.85	14.98
Case 3	7.93	>100	>100	0.11	6.5	8.5
Case 4	>100	>100	>100	6.68	20.01	47.68

**Table A25:** Case 1 to 4 difference results ( $\Delta\%$ ) for Serviceability Life (%)

Analysis conditions	T1 loading				T2 loading			
	Below Wheel		Edge		Below Wheel		Edge	
Case 1	99.2	↓	99.1	↓	99.3	↓	99.1	↓
Case 2	97.3	↓	96.3	↓	97.7	↓	96.6	↓
Case 3	98.8	↓	98.8	↓	98.9	↓	98.8	↓
Case 4	86.1	↓	83.6	↓	88.4	↓	86	↓

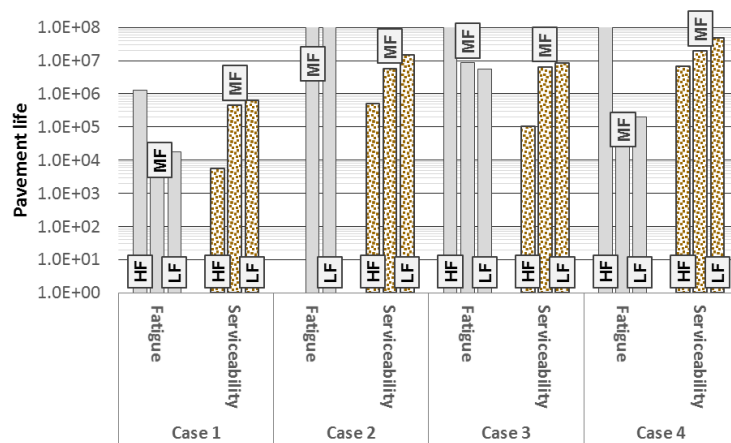
**Note:** All estimates were completed with adjusted Equation 3.2.3a: high friction (HF) relative to low friction (LF) as ratio of LF



**Note:** T1 = Tyre pressure of 750kPa and half-axle load of 40kN

**Note:** Pavement life values are capped at 100 MESAs as this is considered an upper limit for long life

**Figure A3:** T1 Pavement life Edge estimates



**Note:** T2 = Tyre pressure of 900kPa and half-axle load of 70kN

**Note:** Pavement life values are capped at 100 MESAs as this is considered an upper limit for long life

**Figure A4:** T2 Pavement life Edge estimates

## **Appendix B: Pisa Preliminary Analysis Results**

## Appendix B1: Preliminary laboratory and field-testing results

**Table B1:** Laboratory testing results (After Bianchi, 2018)

Series	Specimen	Normal load (kN)	Displacement (mm)	Avg displacement (mm)	ISS (MPa)	Average ISS (MPa)
A1	A	3.59	0.64	0.58	0.35	0.51
	B	8.88	0.51		0.87	
	C	4.16	0.63		0.41	
	D	4.14	0.55		0.41	
A2	A	9.19	0.97	1.01	0.90	0.87
	B	8.18	1.01		0.80	
	C	8.69	1.02		0.85	
	D	9.33	1.05		0.91	
B1	A	13.74	1.01	0.85	1.35	1.62
	B	16.37	0.6		1.60	
	C	19.27	0.89		1.89	
	D	16.58	0.89		1.63	
B2	A	11.28	1.4	1.05	1.11	1.10
	B	13.31	0.99		1.30	
	C	10.44	0.86		1.02	
	D	9.94	0.93		0.97	
D1	A	10.27	0.5	1.12	1.01	0.83
	B	8.48	1.02		0.83	
	C	7.21	1.08		0.71	
	D	7.88	1.87		0.77	
D2	A	11.44	0.85	1.05	1.12	1.04
	B	13.64	1.12		1.34	
	C	7.25	1.03		0.71	
	D	10.33	1.2		1.01	

**Table B2:** Field testing results (After Bianchi, 2018)

Series	Specimen	Normal load (kN)	Displacement (mm)	Avg displacement (mm)	ISS (MPa)	Average ISS (MPa)	Technology
I	A	19.70	2.90	2.99	1.93	1.74	Spray Jet
	B	15.37	2.19		1.51		
	C	16.59	2.69		1.63		
	D	17.99	3.69		1.76		
	E	17.52	3.37		1.72		
	F	19.56	3.13		1.92		
II	A	16.73	2.82	2.84	1.64	1.59	Emulsion tank
	B	15.64	3.10		1.53		
	C	18.23	3.52		1.79		
	D	15.46	2.45		1.52		
	E	15.05	2.29		1.48		
III	A	18.37	2.35	2.28	1.80	1.74	Emulsion tank
	B	15.94	1.65		1.56		
	C	20.18	2.97		1.98		
	D	17.86	2.49		1.75		
	E	16.51	1.96		1.62		
IV	A	9.98	1.02	2.17	0.98	1.46	Emulsion tank
	B	12.69	1.71		1.24		
	C	13.67	2.20		1.34		
	D	17.02	2.18		1.67		
	E	no data	no data		no data		
	F	21.30	3.76		2.09		
V	A	19.81	2.37	2.59	1.94	1.82	Emulsion tank
	B	17.94	2.38		1.76		
	C	18.08	2.54		1.77		
	D	14.84	2.12		1.45		
	E	19.14	2.24		1.88		
	F	21.83	3.91		2.14		

## Appendix B2: Linear-Elastic Analysis Results

**Table B3:** Case 1 to 4 difference results ( $\Delta\%$ ) for Pisa University shear stresses (%)

Analyses	Side points		Centre points	
Case 1	11.1	↓	11.8	↓
Case 2	<b>102.2</b>	↓	<b>124.2</b>	↓
Case 3	13.8	↓	14.3	↓
Case 4	29.8	↓	36.2	↓

**Note:** Values exceeding 100 are indicated in bold

**Table B4:** Case 1 to 4 difference results ( $\Delta\%$ ) for Pisa University horizontal strains (%)

Analyses	Side points		Centre points	
Case 1	13.2	↓	13.8	↓
Case 2	<b>129.9</b>	↓	53.6	↑
Case 3	16.0	↓	16.9	↓
Case 4	33.6	↓	81.7	↑

**Note:** Values exceeding 100 are indicated in bold

**Table B5:** Case 1 to 4 difference results ( $\Delta\%$ ) for Pisa University vertical strains (%)

Analyses	Side points		Centre points	
Case 1	59.2	↑	59.3	↑
Case 2	35.9	↑	36.0	↑
Case 3	54.7	↑	55.2	↑
Case 4	45.3	↑	<b>81.6 (*)</b>	↑

(\*) For values exceeding 100%, Equation 3.2.3a adjusted: high friction (HF) relative to low friction (LF) as ratio of LF

## **Appendix C: Preliminary Comparative Analysis**

## Appendix C1: Experimental Frameworks

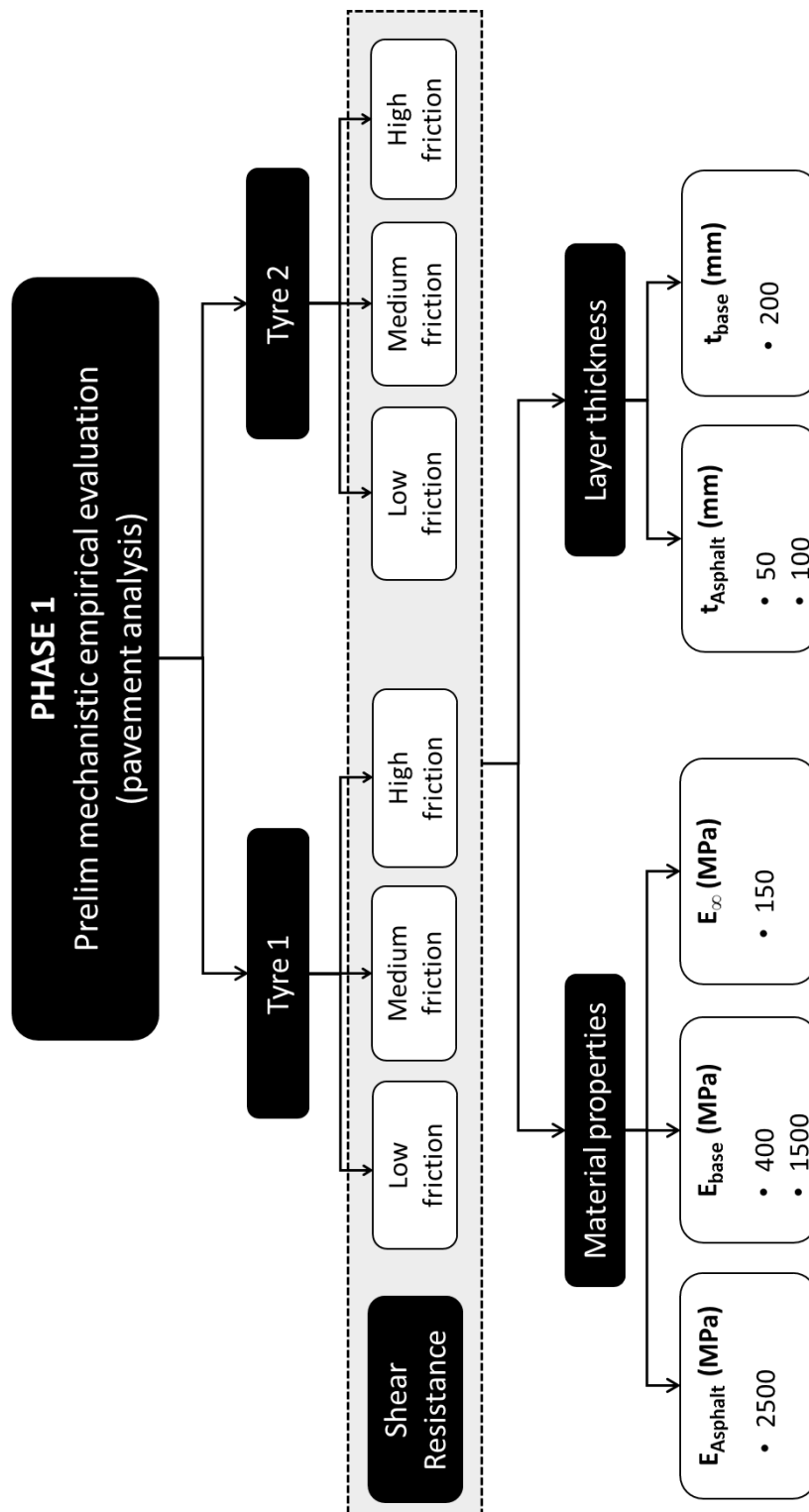


Figure C1: Experimental design for Stellenbosch University

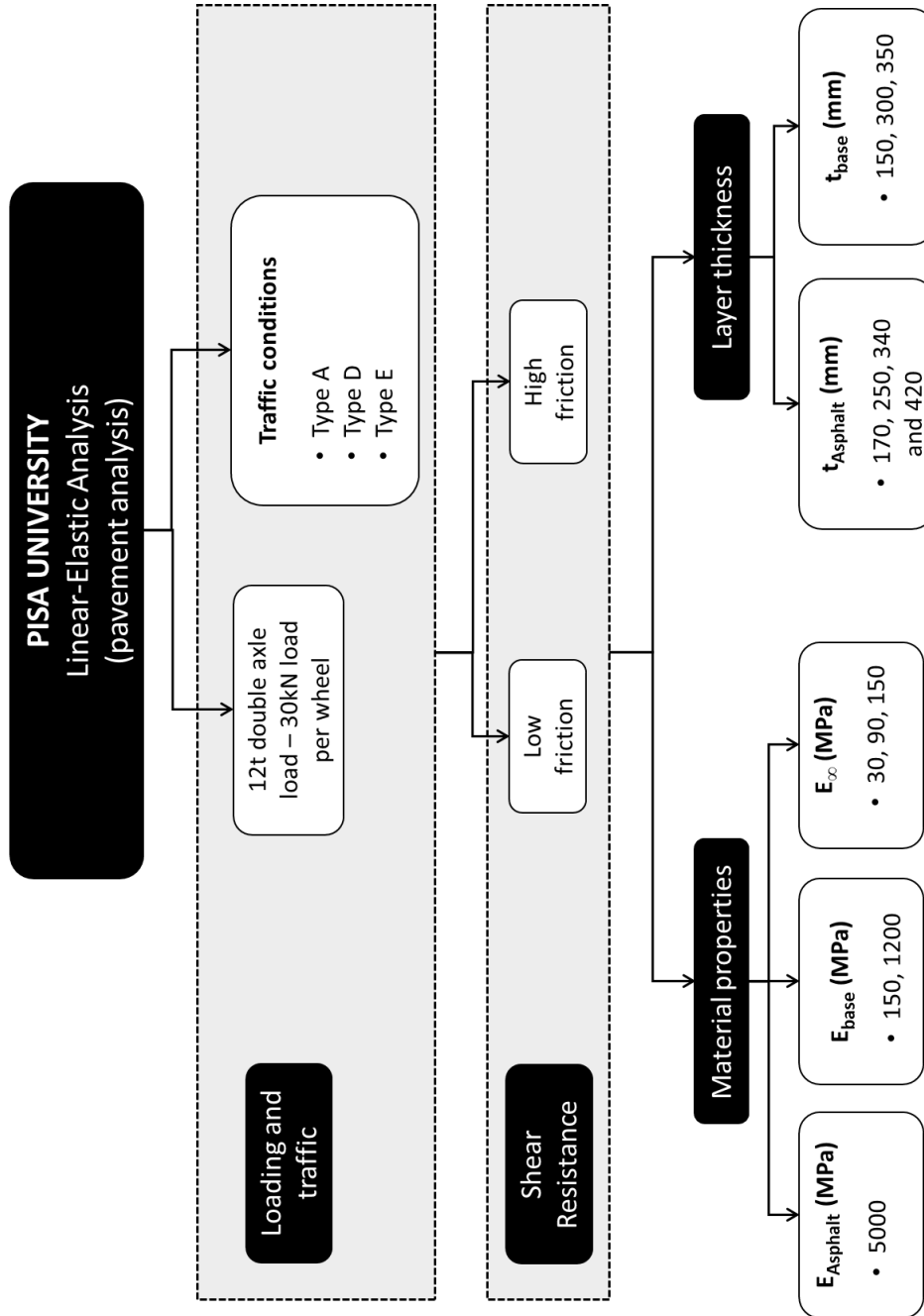


Figure C2: Experimental design for Pisa University

## Appendix C2: Sensitivity Analysis

**Table C1:** Sensitivity analysis for asphalt fatigue Pisa University results

Analyses	$\epsilon_h$	TF1 result	TF2 result	Difference	$\Delta_{Life}$	
Case 1	35.9	$8.25 \times 10^9$	$3.57 \times 10^8$	$7.89 \times 10^9$	95.7%	↓
Case 2	69.2	$3.10 \times 10^8$	$2.15 \times 10^7$	$2.89 \times 10^8$	93.1%	↓
Case 3	56.6	$8.47 \times 10^8$	$5.07 \times 10^7$	$7.96 \times 10^8$	94.0%	↓
Case 4	187	$2.15 \times 10^6$	$3.07 \times 10^5$	$1.84 \times 10^6$	85.7%	↓

**Note:** TF1 input strains as measured. TF2 input strains in microstrain.

**Table C2:** Sensitivity analysis for subgrade failure Pisa University results

Analyses	$\epsilon_v$	TF3 result	TF4 result	Difference	$\Delta_{Life}$	
Case 1	122	$6.86 \times 10^{12}$	$2.62 \times 10^9$	$6.86 \times 10^{12}$	100.0%	↓
Case 2	134	$2.69 \times 10^{12}$	$1.69 \times 10^9$	$2.68 \times 10^{12}$	99.9%	↓
Case 3	175	$1.86 \times 10^{11}$	$4.76 \times 10^8$	$1.86 \times 10^{11}$	99.7%	↓
Case 4	603	$7.89 \times 10^5$	$1.60 \times 10^6$	$8.11 \times 10^5$	50.7% (*)	↑

**Note:** TF3 input strains in microstrain. TF4 input strains as measured.

(\*) Estimations based on adjusted Equation 3.4.4.4a: PU relative to SU as ratio of PU

**Table C3:** SU and Pisa University  $\Delta_{Life}$  behaviours

		SU	Pisa University																				
$\Delta_{Life}$ Range		66 to 81% for <b>asphalt fatigue</b>  56 to 96% (lowest at 56 with sporadic jump to 93% with gradual increase here-after) for <b>subgrade failure</b>	86 to 96% for <b>asphalt fatigue</b>  99.7 to 100% (small margin of estimates) for <b>subgrade failure</b>																				
		Higher $\Delta_{Life}$ for Pisa University given the substantial increase in stiffness moduli and layer asphalt layer thickness. Pisa University defined conditions are approximately 200% increased relative to SU research conditions i.e. $t_{Asphalt}$ and $E_{Asphalt}$ specifically																					
Asphalt fatigue	$t_{Asphalt}$	<b>MR = 6.25</b> Case 1 to 3: 0.06% increase in $\Delta_{Life}$  <b>MR = 1.67</b> Case 2 to 4: 5.7% increase in $\Delta_{Life}$  Increasing difference in $\Delta_{Life}$ 5.6% difference in results with 200% increase in $t_{Asphalt}$	From $t_{Asphalt} = 170\text{mm}$ to 420mm: <table border="1" style="margin-left: auto; margin-right: auto;"> <thead> <tr> <th></th> <th></th> <th><math>\Delta t_{Asphalt}</math></th> <th>%</th> </tr> </thead> <tbody> <tr> <td>1</td> <td>Case 4 to 2</td> <td>80mm</td> <td>47%</td> </tr> <tr> <td>2</td> <td>Case 2 to 3</td> <td>90mm</td> <td>36%</td> </tr> <tr> <td>3</td> <td>Case 3 to 1</td> <td>80mm</td> <td>235%</td> </tr> <tr> <td>4</td> <td>Case 4 to 1</td> <td>250mm</td> <td>147%</td> </tr> </tbody> </table>			$\Delta t_{Asphalt}$	%	1	Case 4 to 2	80mm	47%	2	Case 2 to 3	90mm	36%	3	Case 3 to 1	80mm	235%	4	Case 4 to 1	250mm	147%
			$\Delta t_{Asphalt}$	%																			
1	Case 4 to 2	80mm	47%																				
2	Case 2 to 3	90mm	36%																				
3	Case 3 to 1	80mm	235%																				
4	Case 4 to 1	250mm	147%																				
MR	6.25 to 1.67 (73% decrease in MR for Case 1 to 2 and Case 3 to 4)	Variation between 4.2 and 33.3 (87.4% decrease or >100% increase)																					

Asphalt fatigue	MR	<p><b>t<sub>Asphalt</sub> = 50mm</b> Case 1 to 2: 15.5% increase in <math>\Delta_{Life}</math></p> <p><b>t<sub>Asphalt</sub> = 100mm</b> Case 3 to 4: 9.9% increase in <math>\Delta_{Life}</math></p> <p>Smaller difference in <math>\Delta_{Life}</math> with 73% decrease in MR producing results varying with 5.6%</p>	<p>Variance in MR between 4.2 and 33.3:</p> <table border="1"> <thead> <tr> <th></th> <th></th> <th><math>\Delta t_{Asphalt}</math></th> <th>MR</th> </tr> </thead> <tbody> <tr> <td>1</td> <td>Case 4 to 2</td> <td>80mm</td> <td>33 → 4.2</td> </tr> <tr> <td>2</td> <td>Case 2 to 3</td> <td>90mm</td> <td>4.2 → 33</td> </tr> <tr> <td>3</td> <td>Case 3 to 1</td> <td>80mm</td> <td>33</td> </tr> <tr> <td>4</td> <td>Case 4 to 1</td> <td>250mm</td> <td>33</td> </tr> </tbody> </table> <p>1. 7.3% increase in <math>\Delta_{Life}</math> 2. 1% increase in <math>\Delta_{Life}</math> 3. 1.7% increase in <math>\Delta_{Life}</math> 4. 9.9% increase in <math>\Delta_{Life}</math></p> <p>Variance in difference of <math>\Delta_{Life}</math>. Does not show consistency in terms of increase/decrease of the parameter</p>			$\Delta t_{Asphalt}$	MR	1	Case 4 to 2	80mm	33 → 4.2	2	Case 2 to 3	90mm	4.2 → 33	3	Case 3 to 1	80mm	33	4	Case 4 to 1	250mm	33
			$\Delta t_{Asphalt}$	MR																			
1	Case 4 to 2	80mm	33 → 4.2																				
2	Case 2 to 3	90mm	4.2 → 33																				
3	Case 3 to 1	80mm	33																				
4	Case 4 to 1	250mm	33																				
Subgrade failure	t <sub>Asphalt</sub>	<p><b>MR = 6.25</b> Case 1 to 3: 0.06% increase in <math>\Delta_{Life}</math></p> <p><b>MR = 1.67</b> Case 2 to 4: 5.7% increase in <math>\Delta_{Life}</math></p> <p>Increasing difference in <math>\Delta_{Life}</math></p> <p>5.6% difference in results with 200% increase in t<sub>Asphalt</sub></p>	<p><i>Refer to two previous tables used for Asphalt fatigue</i></p> <p>1. Varies with 102.9% decrease for Case 4 in <math>\Delta_{Life}</math> and Case 2 shows 99.9% increase in <math>\Delta_{Life}</math></p> <p>2. 0.2% decrease in <math>\Delta_{Life}</math></p> <p>3. 0.2% decrease in <math>\Delta_{Life}</math></p> <p>4. 9.9% decrease in <math>\Delta_{Life}</math></p>																				
	MR	<p><b>t<sub>Asphalt</sub> = 50mm</b> Case 1 to 2: 4.1% increase in <math>\Delta_{Life}</math></p> <p><b>t<sub>Asphalt</sub> = 100mm</b> Case 3 to 4: 36.4% increase in <math>\Delta_{Life}</math></p> <p>Increase in <math>\Delta_{Life}</math> with increase in t<sub>Asphalt</sub></p> <p>73% decrease in MR producing results varying with 32.4%</p>																					
General remarks		<ul style="list-style-type: none"> <li>Decrease in <math>\Delta_{Life}</math> for asphalt fatigue</li> <li>Increase in <math>\Delta_{Life}</math> for subgrade failure</li> </ul>	Variation in $\Delta_{Life}$ for both asphalt fatigue and subgrade failure																				
		<ul style="list-style-type: none"> <li>Gradual increase/ decrease of results attributed to manner of selection of pavement structures to be analysed</li> <li>Greatest variation in results exist for subgrade failure</li> </ul>	<ul style="list-style-type: none"> <li>Variance in results attributed to variety of pavement structures selected for analyses</li> <li>Asphalt fatigue produced results in close approximation with a variation occurring in subgrade failure estimates</li> </ul>																				

## **Appendix D: Finite Element Model Set Up**

## Appendix D1: Creation of Model 1

### Modelling space

According to Dassault Systèmes Simulia (2014f), a modelling space describes the space in which the part is embedded, as opposed to the topology of the part. Firstly, when a part is created, the modelling space in which the part resides, is specified. Three types of modelling spaces can be defined in Abaqus: three-dimensional (3D), two-dimensional (2D) planar and axisymmetric. These two models (Figure D1) describe models in a two-dimensional plane (X-Y plane) which can only contain a combination of planar shell and wire features. Axisymmetric embeds the X-Y plane with the Y axis, indicating the axis of revolution (represented by shaded area in Figure D1).

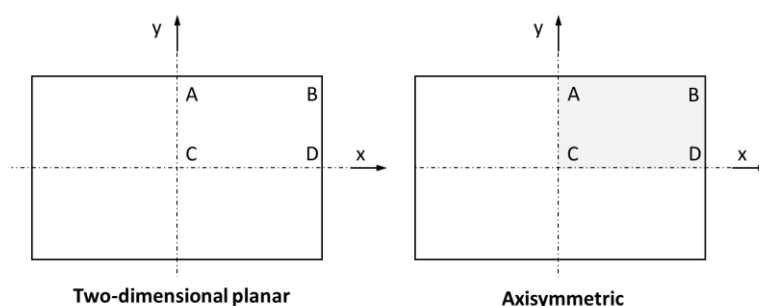


**Figure D1:** Two-dimensional plane in modelling space

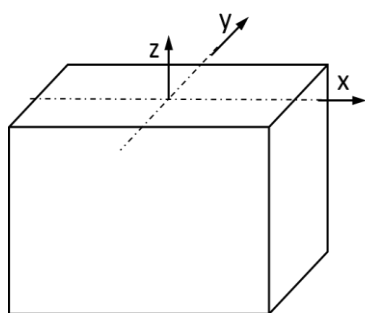


**Figure D2:** Three-dimensional plane in modelling space

A three-dimensional model (Figure D2) embeds the part in the X, Y and Z coordinate system and can contain any combination of solid, shell, wire, cut and other features. It will provide a more accurate distribution of stresses and strains in all directions, compared to a 2D model which provides limited information in this regard. It also shows enhanced information of these critical parameters at various locations within the model. The phenomenon is highlighted from the linear-elastic analysis performed in BISAR analysis, which provided limited information in terms of stresses. Hence, the part is created as a 3D FEM model.

### Part type

The possible types of parts are shown in Figure 4.2.3.2b. The function of the core part specifically is to experience stresses and strains during the analysis, when subjected to deformation due to loading. This attribute is best described by a *deformable* type part which represents deformation under loading, of which the loading can be mechanical, thermal or electrical. The other three options each involves parts which are not deformable when subjected to a type of loading under certain conditions.

However, if a model were to comprise of rigid part capabilities, reference points (RPs) can be allocated where rigid motion behaviour of a specific part (or section of model) can be assigned boundary conditions that would resemble rigid-like behaviour. The described behaviour is achieved by means of constraints added to the model. For the current model, this type of behaviour is expected at the sample support section represented by *Part E* in the schematic, shown in Figure 4.2.3.1a. These conditions are replicated in this section for the core sample part. The technicalities of this type of set-up is discussed in 4.2.6.3.

### Base feature

The base feature of the part is described in specifying the properties, i.e. shape and type. The shape of the part indicates the basic topology of the feature where it can be classified as either a solid, shell, wire or point. The type describes the method used to generate the base feature. The base feature type options are dependent on the type of shape the part is composed of. Based on the type modelling space used (3D), an *extrusion* type base feature is deemed appropriate, as it allows the feature profile to be extruded through a specified distance, i.e. it is assigned a certain layer thickness (height of the core sample) as illustrated in Figure D3.

### Part size

Another option provided in the definition of a part, is the approximate size (also defined in Figure 4.3.2b). The size which is defined, sets the size of the sketch plane and the spacing of its grid. It is set to the approximate size of the part to match the largest dimension of the finished part. This is where the relative part is sketched according to the preferred dimensions. After completing the sketch of the specific part, the thickness of the part can be selected (extruded as explained in the *base feature* section). The geometry of the part is (by default) sketched on the X-Y plane (shown in Figure D4) and assigned a thickness relative to the Z-direction. The type of part can be allocated, given that the part has been categorised as a solid element or part.

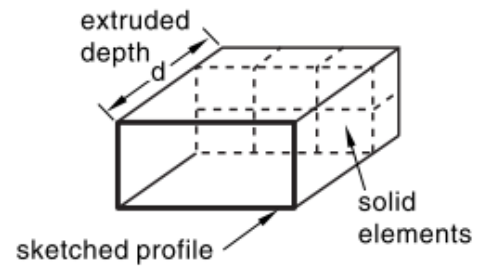


**Figure D3:** Extruded solid feature  
(Dassault Systèmes Simulia, 2014f)

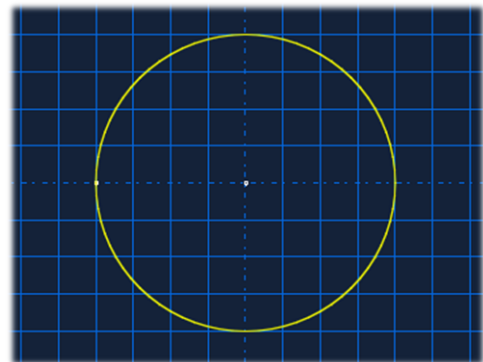


**Figure D4:** Sketch of geometry of part  
(Abaqus Inc., 2017)

## Appendix D2: Analysis Steps for Model 1

For each step, an analysis procedure (Figure 4.2.6.1a) is defined. Abaqus distinguishes between two procedure types for analysis steps, i.e. *General* and *Linear Perturbation* steps. This feature describes the type of analysis performed during the specific step. The first-mentioned (*General* analysis steps), are used to analyse linear or non-linear responses, whereas linear perturbations are used to only analyse linear problems. Given the description of the Leutner Test (Chapter 2), it is apparent that the test is representative of non-linear behaviour. Hence, a *General* type procedure is appropriate for this FEM model.

The *General* analysis procedure is broken down into different subcategories of this type of procedure, i.e. dynamic, soil, static etc. A *Static, General* (Figure 4.2.6.1a and Figure D5) category is used when inertia effects are neglected and when time-dependant material effects such as creeping, swelling and viscoelasticity is ignored (Dassault Systèmes Simulia, 2014a). Compared to the testing conditions of the Leutner shear test, for simplification of the analyses, time-dependant material effects were ignored, making the *Static, General* approach suitable for the current analysis.

### Step configuration of model

The type of procedure (*General*), would allow the specific configuration with the aid of tabbed pages, namely *Basic*, *Incrementation* and *Other* (Figures D5 and D6). The settings configured with these tabbed pages include the time period of the analysis (for the specific step), maximum number of increments, increment size and whether to account for geometric nonlinearity. Only one step (in addition to the initial step) is defined for the current analysis and will be named "LOAD". The analysis step is applicable to the boundary conditions applied as discussed per 4.2.6.2. The time period selected for the analysis was set to 3 seconds which, together with the incrementation conditions (Figure D6), will provide sufficient time for an appropriate number of iterations for the analysis to achieve convergence successfully.

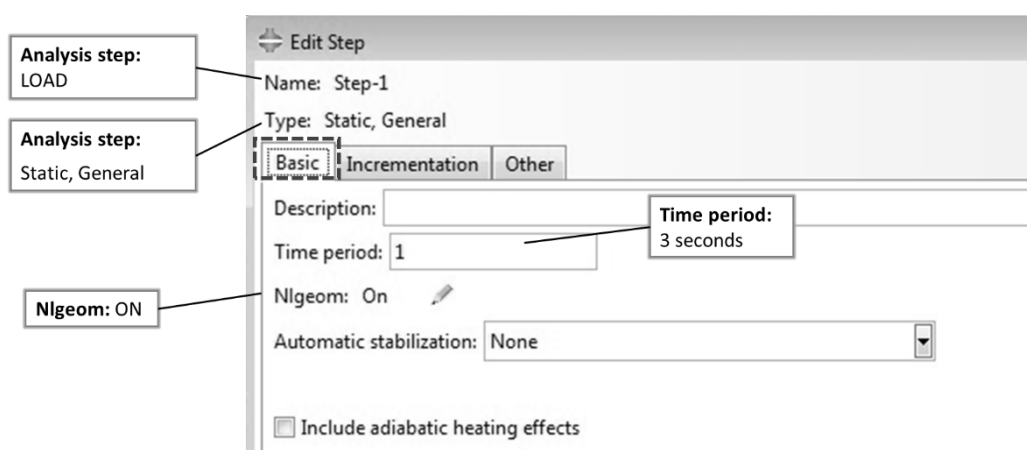
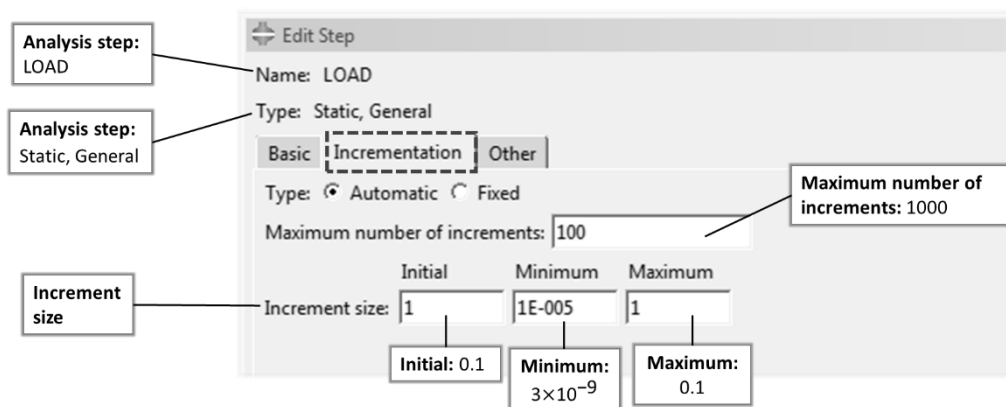


Figure D5: Analysis step basic tab for Model 1 (Abaqus Inc., 2017)

For each step (only one in this case), in this part of the set-up in the *Step* module (*Step Manager*), it is also indicated whether Abaqus accounts for non-linear effects due to large displacements and deformations. Large displacements and deformations are expected within the core sample with shear testing. Hence, the nonlinear geometric (Nlgeom) effects can become important. Going forward, in compliance with Dassault Systèmes Simulia (2016d), geometric nonlinearity is referred to as Nlgeom for discussion

purposes. The Nlgeom setting determines whether accommodation is made for this component. For the shear ring and core sample assembly the Nlgeom setting is toggled on as indicated in Figure D5. The *Basic* tabbed page is succeeded by the *Incrementation* tabbed page.

The *General* analysis procedures can adhere to two different approaches to control incrementation (Figure D6) – *Automatic* control or *Fixed* (or direct user control). For *Automatic* control, tolerances and error measures are specified, after which Abaqus automatically selects the increment size as it develops the response in the step. The *Fixed* approach provides control of increment size where the incrementation scheme is specified. The scheme is deemed “usable” by Dassault Systèmes Simulia (2014a), in repetitive analyses where convergence behaviour can be perceived easily. However, Dassault Systèmes Simulia (2016b) shows concern for the *Fixed* approach as it may prevent the solution from converging.



**Figure D6:** Analysis step incrementation tab for Model 1 (Abaqus Inc., 2017)

In contrast, nonlinear problems such as the FEM model replicated for the current analysis, proves to be a challenge when acquiring a convergent solution whilst minimizing computational time. Therefore, *Automatic* control is recommended by Dassault Systèmes Simulia (2014a). The use of this approach for the time increment is considered more efficient as the software can react to nonlinear responses, which cannot be predicted ahead of time. Incrementation commences by using the value entered for the initial increment size. When the automatic time stepping is used, the program will choose the largest time increment on efficiency and other grounds (University of Cambridge, 2011).

The size of the subsequent (time) increments is adjusted, based on how quick the solution converges. The number of increments in a step is limited to the maximum increment size selected. If the step exceeds the chosen number of increments, the analysis stops, and diagnostic information is reported to the *Job* module. A default value of the maximum number of increments is 100. To allow a suitable number of iterations in the given time of the analysis period (3 seconds), 1 000 increments were considered appropriate.

The analysis is started with the initial increment size defined. The minimum increment size is only verified during the analysis when *Automatic* control approach is used. If a smaller time increment than the specified value is required to reach a convergent solution, the analysis is terminated. Furthermore, the maximum increment size is only verified when the analysis is performed conforming to the *Automatic* control approach (Dassault Systèmes Simulia, 2016c). The increment size is not increased beyond the specified value during the analysis. With reference to Figure D5 (for the current analysis), the minimum

and maximum time increment is 0.1. These parameters serve as limits and are a means of controlling what happens in a defined step of the analysis. The maximum increment may not be exceeded in any increment in this step. The procedure is repeated until convergence is reached in a given increment. If a reduction in the time step (to a value less than the minimum time step) is deemed necessary, the analysis will abort. Additionally, when any of the defined limits of the increment size is reached, the step is terminated (aborts) irrespective of which of these limits are reached first.

The program takes the initial increment (Figure D5), goes through a series of iterations by means of Newton integration. During the analysis, Abaqus evaluates whether the model converges to a solution in first increment of the load. If the number for iterations is exhausted and a solution is not reached, the non-convergence is attributed to the initial and minimum increment sizes. Given that the initial increment did not converge to a solution, it automatically divides this increment by 2 and repeats the iteration process until a minimum increment value is reached. In an instance where the minimum defined value is reached, but non-convergence is still experienced, the analysis will abort.

The configuration of the *Step* module is completed. The model was built in the *Part* module and assigned its material properties in the *Property* module, after which the part instances of the model parts were used to assemble the Leutner test. Subsequently, the *Step* module was used where information with regard to the analysis (duration and increment size boundaries) was stated (Figure D7). Hereafter, more physical characteristics of the test can be replicated to illustrate the actual behaviour of the test. The phenomenon is achieved through boundary conditions (*Load* module) and constraints (*Interaction* module) added to the model in order for the assembled model to behave similar to the actual testing device.

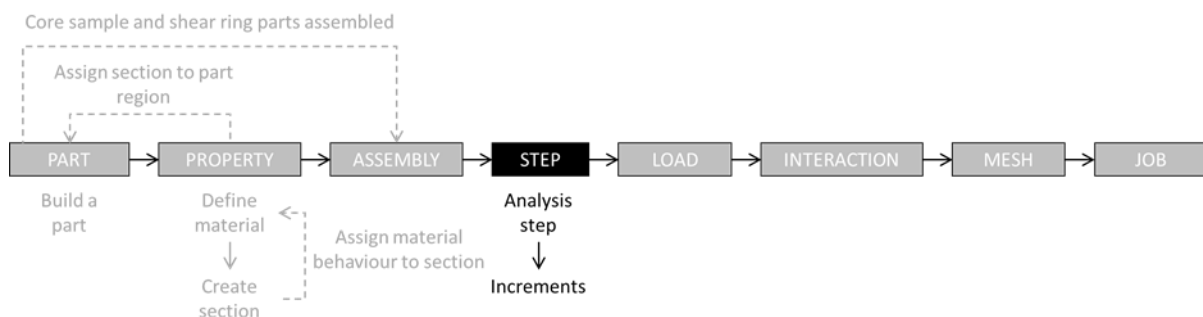


**Figure D7:** Model set-up procedure for Model 1 – Step module

## Appendix D3: Boundary Conditions and Constraints for Model 1

### Boundary Conditions

Similar to the components completed in the previous modules (*Part*, *Property*, *Assembly* and *Step* modules), these conditions are defined in an editor menu similar to the one portrayed in Figure D8 (left). The information required includes a name to recognise the particular boundary conditions (named *RP1* to *RP3*), step of the analysis – specified analysis step (“LOAD”), a category and types of conditions available in the specific category.

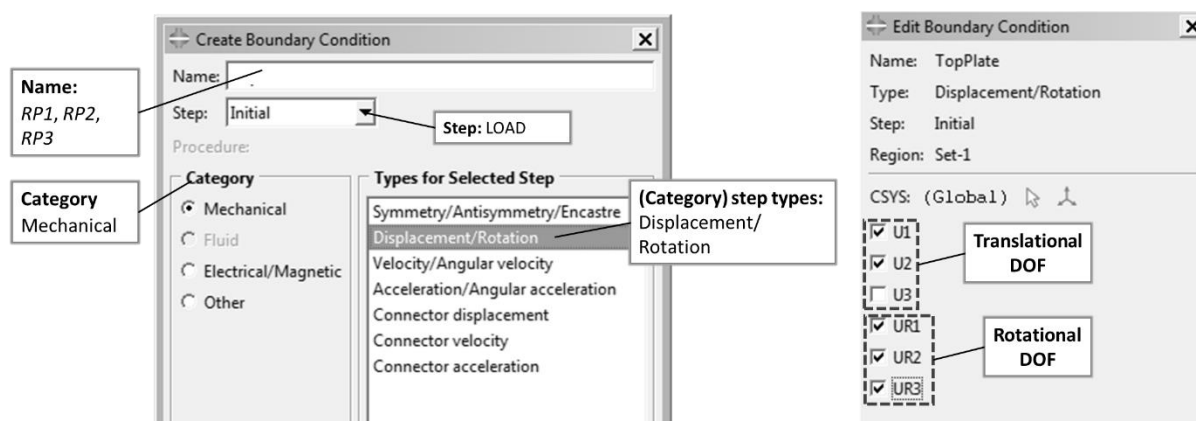


**Figure D8:** Definition of boundary conditions (Abaqus Inc., 2017)

The boundary conditions are used from the *Mechanical* category for which the *Displacement/Rotation* boundary condition is used to describe the constraint of movement in selected degrees of freedom to zero, or to prescribe the displacements or rotation for each selected degree of freedom. The boundary conditions summarised in Table 4.2.6.2b are entered and specified for each reference point shown in Figure D8 (right). Once the definition of the boundary conditions is complete, interaction of the model elements will be incorporated into the FEM model.

### Constraints

#### *Tie constraints*

Either element– or node-based surfaces can be used as the *slave* surface where any type of surface type can be used as the *master* surface. However, it is required that some surface restriction be taken into consideration, depending on the tie formulation used. According to Dassault Systèmes Simulia (2014d), only a few restrictions apply to the surface-to-surface formulation. It does not allow for a mixture of rigid and deformable portions of a surface and the *master* surface must not contain T-intersection. For this type of formulation, any nodes shared between the *slave* and *master* surface will not be considered.

Abaqus uses criteria to establish which *slave* nodes will be tied to the *master* surface. By default, the rotational degrees of freedom (dof4 to dof6) are constrained when they exist on both the slave and master surfaces (Figure D9). These components do not have to be incorporated in the tie constraint. Subsequently, constraints are formed between nodes of these two surfaces. From a mathematical perspective, tie coefficients are used to interpolate quantities from master nodes to the tie point. The objective is achieved by means of two approaches i.e. *surface-to-surface* or *node-to-surface* approach.

The first-mentioned approach (*surface-to-surface*) minimizes numerical noise for tied interfaces comprising of different meshes. It enforces constraints in an average sense over a finite region as opposed to discrete points compared to the other approach. In general, the approach involves more master nodes per constraint than the *node-to-surface* approach, resulting in an increase in solution cost with the increase in solver bandwidth. Despite the occurrence, Dassault Systèmes Simulia (2014d), found these additional costs to be fairly small and may become significant only in some instances. The factors influential of the type of behaviour described, include models that are composed of a large fraction of tied nodes, or when the *master* surface is more refined than the *slave* surface. The *node-to-surface* approach is not applicable to the current model. Reference can be made to Dassault Systèmes Simulia (2014d) in this regard.

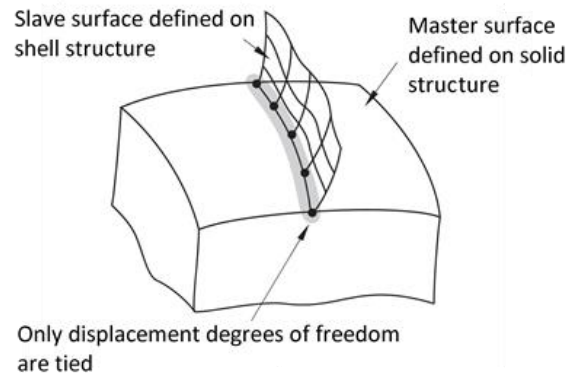


**Figure D9:** Surface-based tie algorithm (After Dassault Systèmes Simulia, 2014d)

### Rigid body constraints

The rigid body constraints are created (one for each reference point). In the constraint editor (Figure 4.2.6.3f), the information of the different attributes of the constraint type is set. Information entered includes the region type and the selection of the region where the desired constraint is to be applied. Information, such as the name of the constraint and type of constraint, is also indicated in the constraint editor.

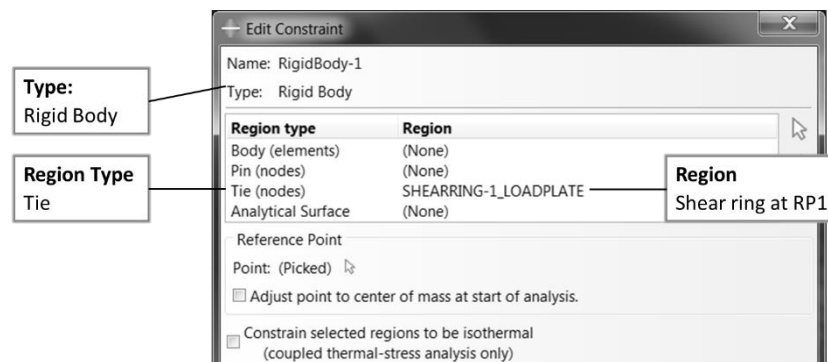


**Figure D10:** Definition of rigid body in constraint editor (Abaqus Inc., 2017)

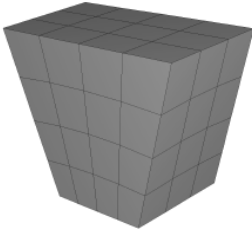
The region type selected is dependent on the DOFs associated with the particular region. Four types of regions are available within Abaqus namely *Body*, *Pin*, *Tie* and *Analytical Surface*. The *Body* region type is selected when elements of a geometric region or orphan elements in the rigid body are to be used. The *Pin* region type includes nodes with only translation DOF, while *Tie* region type includes both translational and rotational DOF associated with the rigid body. The final region type, *Analytical Surface*, is selected when an analytical surface in the rigid body is to be included. With the motions of these points described previously in 4.2.6.2, and summarised in Table 4.2.6.2b, the region types used for this model would be the *Tie* region type.

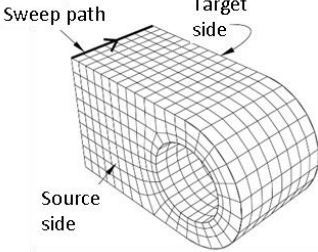
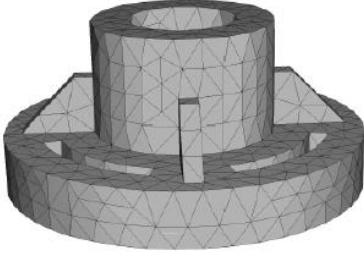
## Appendix D4: Meshing an Mesh Controls for Model 1

*Top-down* meshing techniques generate a mesh by working down from the geometry of a part or region to the individual mesh nodes and elements. The technique can be used to mesh any geometry (one-, two-, or three-dimensional) using any element type (available in the analysis software). The mesh produced by this technique conforms to the original geometry. The meshing technique is deemed difficult when a mesh is to be generated for regions composed of complex shapes (Dassault Systèmes Simulia, 2014f). The technique relies on the geometry of a part to define the outer bounds of the mesh. It matches the geometry to produce a high-quality mesh. In some instances, this method may not be allowable to mesh regions with a specific element type.

Three types of *top-down* techniques exist, i.e. *structured*, *swept* and *free* meshing (Figure 4.2.7.2c). Their geometry requirements are well-defined, and loads and boundary conditions applied are associated with the generated mesh (Dassault Systèmes Simulia, 2014f). A summary of the different *top-down* meshing techniques is given in Table D1, where the characteristics of each of the types of top-down techniques are covered together with illustrations. The descriptions of these different types and the illustrations provided for each, are a compilation of these aspects discussed in Dassault Systèmes Simulia (2014f). Abaqus uses different colours to indicate the meshing technique currently assigned to a region. Hence, the description of the colour representing the technique is also indicated in Table D1.

**Table D1:** Summary and illustration of top-down meshing techniques

Meshing techniques	Description	Code
<b>Structured</b>	<ol style="list-style-type: none"> <li>1. <i>Top-down</i> meshing technique that gives most control over mesh because it applies pre-established mesh patterns to particular model topologies</li> <li>2. Most unpartitioned solid models are too complex to be meshed using pre-established mesh patterns</li> </ol> <div style="text-align: center;">  <p><b>Figure D11:</b> Structured mesh</p> </div>	

<b>Swept</b>	<ol style="list-style-type: none"> <li>1. Created by initially generating mesh on edge or face and then sweep mesh along a sweep path (Figure D12)</li> <li>2. Results in two-dimensional mesh created from edge or three-dimensional mesh created from a face</li> <li>3. Limited to models with specific topologies and geometries</li> </ol> <div style="text-align: center;">  <p><b>Figure D12: Swept mesh</b></p> </div>	
<b>Free</b>	<ol style="list-style-type: none"> <li>1. Most flexible <i>top-down</i> meshing technique</li> <li>2. Uses pre-established mesh patterns and can be applied to almost any model shape</li> <li>3. Provides least control over mesh as there is no method that exists to predict the mesh pattern</li> </ol> <div style="text-align: center;">  <p><b>Figure D13: Free mesh generated with tetrahedral elements</b></p> </div>	

The *Bottom-up* meshing technique generates a mesh by working up from the two-dimensional entities (geometric and element faces or two-dimensional elements) in order to create a mesh that is three-dimensional. In contrast with *top-down* meshing, it can only be used for solid three-dimensional geometry, using hexahedral elements. According to Dassault Systèmes Simulia (2014f), the techniques involve a manual process whereby the mesh produced may vary significantly from the original geometry. In turn, the variation in geometry may result in a high quality hexahedral mesh on regions with complex shapes (Dassault Systèmes Simulia, 2014f).

The *bottom-up* meshing technique uses the part geometry as a guideline for the outer bounds of the mesh; however, the mesh is not required to conform to the geometry. Compared to *top-down* meshing, removing the restriction of geometry conformation, greater control is gained over the mesh. This occurrence allows the creation of hexahedral or hexahedral-dominated mesh (Table D4). Loads and boundary conditions are applied to the geometry. Contrary to *top-down meshing*, the *bottom-up* meshing may not be fully associated with geometry. Therefore, Dassault Systèmes Simulia (2014f) recommends that mesh associativity should be carried out to verify whether mesh is correctly associated with the geometry of the model in areas where loads or boundary conditions are applied. A similar summary as for *top-down* meshing is provided for *bottom-up* meshing in Table D2.

**Table D2:** Summary and illustration of bottom-up meshing techniques

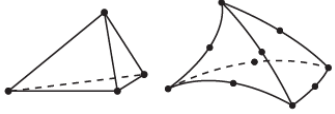
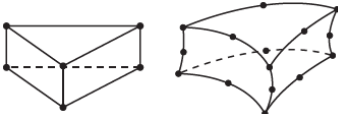
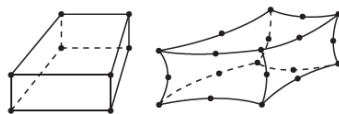
Description	Code
<p>1. To mesh a single <i>bottom-up</i> region, several successive bottom-up meshes may be required – an extruded bottom-up mesh can be used to generate part of a region and then used the element faces of the extruded mesh as a starting point to generate a swept mesh for features that the extruded mesh excluded.</p> <p>2. Figure 4.2.7.2f shows an example where the part requires two regions and four <i>bottom-up</i> meshes to completely mesh the part.</p> <p>3. <i>Bottom-up</i> regions are displayed using a mixture of region geometry colour (light tan) and the mesh colour (light blue) to indicate the fact that the geometry and mesh may not be associated.</p> <div data-bbox="502 750 997 1030" style="text-align: center;"> </div> <p><b>Figure D14:</b> Bottom-up hexahedral meshed part (After Dassault Systèmes Simulia, 2014f)</p>	

**Mesh elements and element types**

The meshes are generated by meshing techniques in Tables D1 and D2, containing element types summarised and illustrated in Table D3. Most of the elements correspond to one of the shapes listed and illustrated subsequently. By default, every mesh region has one or more element type assigned to it. It corresponds to an element shape that can be used in the particular region.

**Table D3:** Element types (After Dassault Systèmes Simulia, 2014f)

Dimension	Element types	
1D	Lines	
2D	Triangles	Quadrilaterals

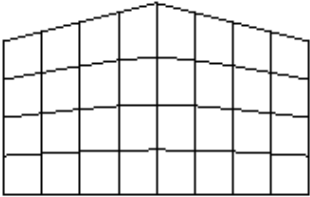
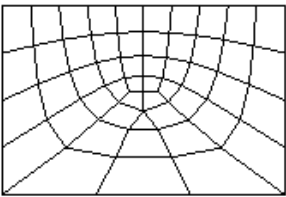
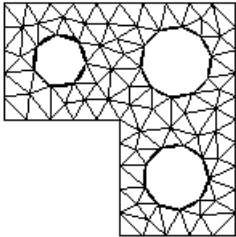
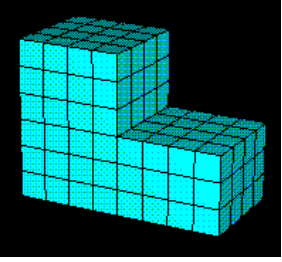
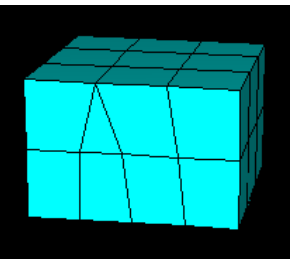
	Tetrahedra	Triangular prisms (wedges)	Hexahedra
3D			

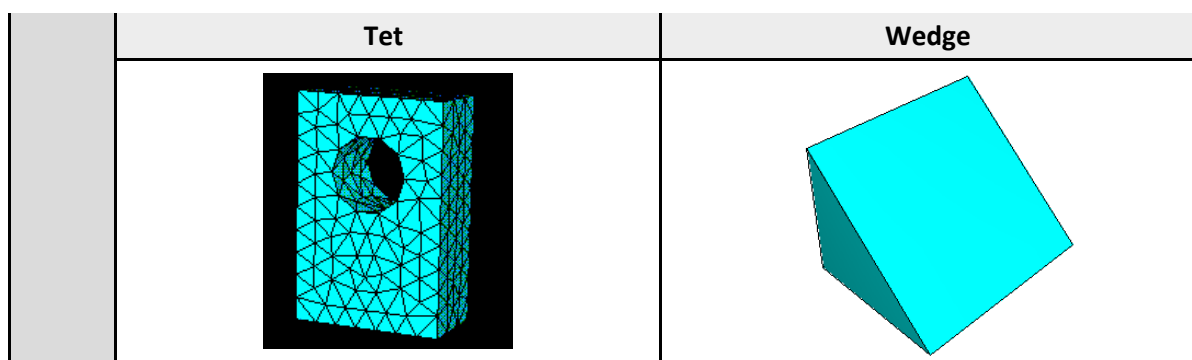
The element shapes available in Abaqus are listed as the following (illustration in Table D4):

5. *Quad* – Use of quadrilateral elements only;
6. *Quad-dominated* – Primary use of quadrilateral elements, but allows for triangles in transition regions;
7. *Tri* – Exclusive use of triangular elements which can only be used when mesh controls are applied to faces of solid regions;
8. *Hex* – Use of hexahedral elements only;
9. *Hex-dominated* - Primary use of hexahedral elements, but allows for triangular prisms (wedges) in transition regions;
10. *Tet* – Use of tetrahedral elements only;
11. *Wedge* – Use of wedges elements only.

Table D4 shows examples of each of the element shapes which can be used to mesh a model region. Studying the illustrations shown in the table, it is noticeable that the element shape used depends on the type of model: two-dimensional versus three-dimensional. The first three figures shown (shapes listed in points 1 to 3), can be used when generating a mesh for two-dimensional elements – *quad*, *quad-dominated* and *tri*. Alternatively, when a three-dimensional region is to be meshed, shapes listed in points 4 to 7 can be used – *hex*, *hex-dominated*, *tet* or *wedge*.

**Table D4:** Illustration of element shapes (Dassault Systèmes Simulia, 2016a)

Element shapes			
	Quad	Quad-dominated	Tri
2D			
3D	Hex		Hex-dominated
			



## Application of different meshing techniques

### ***Swept meshing technique***

The *swept* meshing technique is used to mesh complex solid and surface regions (Figure 4.2.7.3c). The technique involves two phases, where phase one entails the mesh on one side of the region (*source* side). The second phase involves the copy of nodes of *source* side mesh, one element layer at a time, until the final side (*target* side) is reached. Reference can be made to Figure 4.2.7.2e for demonstration of these regions relative to a model. The nodes are copied along the edge which is referred to as a *sweep* path. The path can be of any type of edge. When the sweep path is a straight edge (Figure D15), the resulting mesh is referred to as an *extruded* swept mesh.

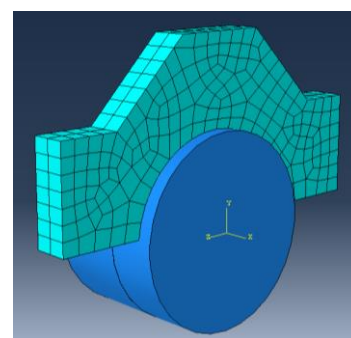


**Figure D15:** Mesh generation (Abaqus Inc., 2017)

Apart from the meshing technique, the meshing algorithm is another feature required in the *Mesh Controls* dialog box (Figure 4.2.7.3a). As shown in the dialog box, either *medial axis* or *advancing front* meshing algorithms can be selected when a solid region with hexahedral (hex) elements and *swept* meshing are used. For the current model, *advancing front* was selected. This approach is more favourable as it generates elements at the boundary of the region and continues to generate elements as it moves systematically to the interior of the region (Dassault Systèmes Simulia, 2014f).

### ***Bottom-up meshing technique***

Previously, it has been described that this meshing technique involves a manual, incremental meshing process which will allow building a hexahedral mesh in any solid region. The meshing generated for the top layer of the core sample and the steel shear ring (*swept* meshing) belongs to the *top-down* meshing technique family. Studying Figure D15, it is noticeable that this meshing technique is directly tied to the geometry in such a way that it “fills” the geometry. In contrast, the *bottom-up* meshing technique used for the cohesive layer and the subsequent layer of the core sample relaxes the constraint that ties the mesh to the geometry of the region; in other words it ignores geometric features (Dassault Systèmes Simulia, 2014f). Generating the preferred mesh requires multiple applications of the *bottom-up* meshing technique. Each *bottom-up* mesh becomes a building block for the next mesh until the mesh for the region is completed. Each application of this technique involves four phases (refer to Figure D16).

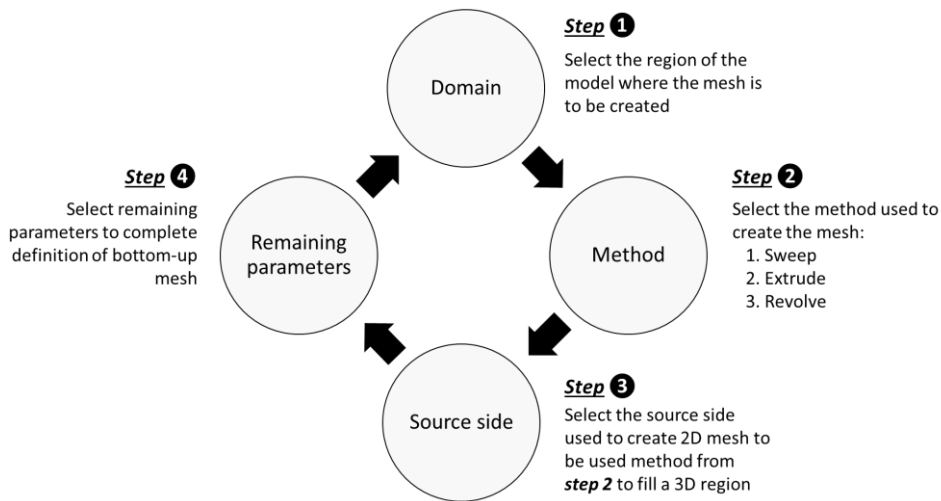


**Figure D16:** Four phases of bottom-up meshing technique (After Dassault Systèmes Simulia, 2014f)

The incorporation of the four phases shown in Figure D16 is provided subsequently in Figure D17 (left), where an illustration of the application relative to the model is demonstrated in Figure D17 (right). The bottom-up mesh technique will be used for the bottom and tack layer (Figure 4.2.7.3c). The same procedure is carried out to generate the mesh of these two regions. Once the bottom-up mesh is completed for the one, step one to four in Figures D16 and D17 are repeated to generate the meshing for the tack coat layer.

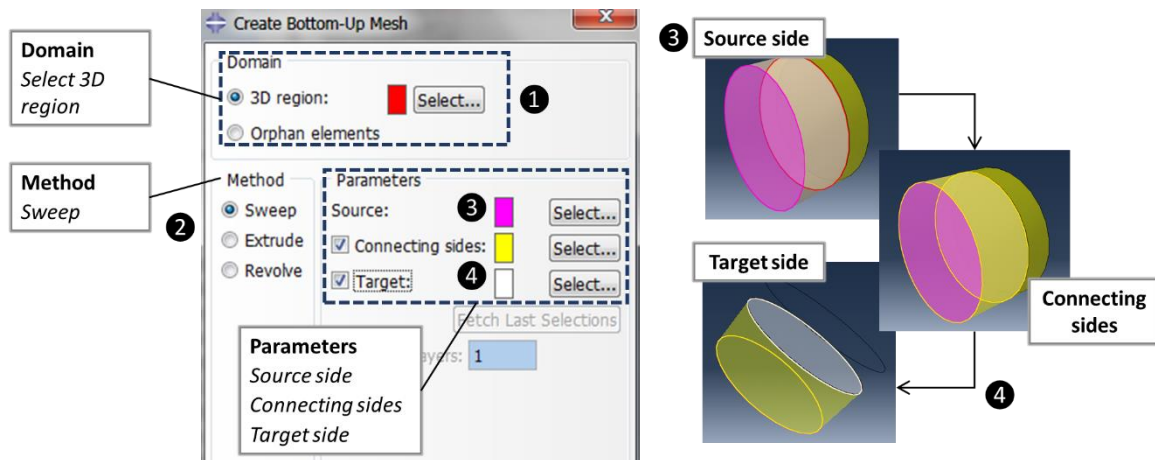


**Figure D17:** Mesh generation (Abaqus Inc., 2017)

To create the meshing for the region, the first requirement is to define the domain in which the mesh will be created (*Step 1* in D16 and D17). The domain will determine whether the *bottom-up* mesh is created as a native mesh or as a collection of orphan nodes and elements. Hence, the bottom layer of the core layer sample part instance is selected. When repeating the procedure, the tack coat region of the core sample will be selected. The selection of a three-dimensional region as the domain, suggests full *bottom-up* mesh associativity with geometry (Dassault Systèmes Simulia, 2014f). The association between mesh and geometry is deemed fundamental for the transfer of loads, boundary conditions and other information from the geometry of the mesh.

After the domain is selected, the *bottom-up* method, to be used for meshing, is required (Step 2 in Figures D16 and D17). Three methods can be used, i.e. *sweep*, *extrude*, and *revolve*. An example of the first two methods is provided in Figure D18. Only the *sweep* method is of relevance for the model created, and is the only method of interest for the current analysis. Reference can be made to Dassault Systèmes Simulia (2014f) for detailed information with regard to these three methods.

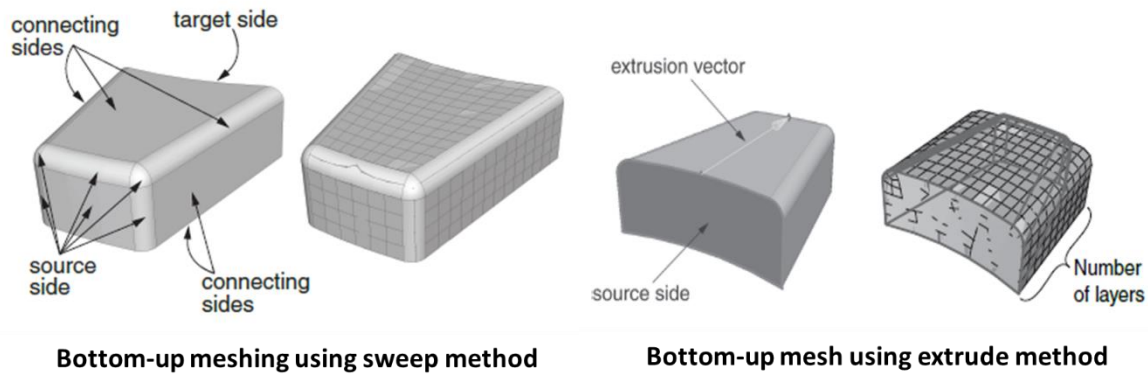


**Figure D18:** Bottom-up meshing methods (After Dassault Systèmes Simulia, 2014f)

The *sweep* method adhered to, is similar to the *Sweep* meshing technique discussed previously – a three-dimensional mesh is created by moving a two-dimensional mesh along a sweep path. The sweep method (Figure D17 left), was used to mesh both the bottom and tack coat layer of the sample, as demonstrated per Figure D17. Steps 3 and 4 conclude the selection of the surfaces, illustrated in Figure D17, represented by three respective colours, viz. magenta, yellow and white. The *source* side is selected first, which defines the faces on which the two-dimensional mesh will be created. On the replicated model, the bottom of the core sample is the *source* side (magenta surface in Figure D17). When the procedure is repeated for the tack coat, the bottom of the tack coat layer is the *source* side. The source side can be any combination of geometric or element faces or even two-dimensional elements.

After the *source* is selected, the *connecting* sides are defined. As stated in its name, it is a side which connects the *source* and *target* side, i.e. it is the sweep path followed to create the mesh. These surfaces are indicated in yellow in Figure D17. The sides that are selected in both instances, will conform closely to the geometry or mesh along the selected sides. In addition, a *target* side was specified. The *target* side is a single face used to end the mesh. These faces are represented by the surface indicated in white in Figure D17. Once the *source*, *connecting*, and *target* sides are selected, Abaqus sweeps the two-dimensional mesh from the *source* side into the volume of the solid region to produce a mesh for the two layers of the core sample as portrayed in Figure D19.

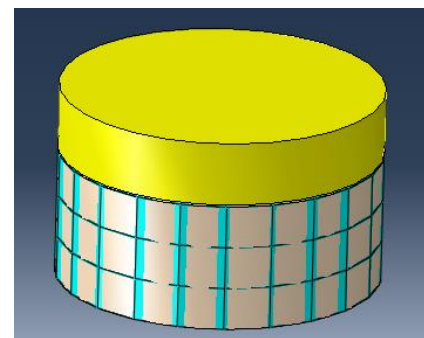


**Figure D19:** Bottom-up meshing (Abaqus Inc., 2017)

### **Meshing of multiple three-dimensional solid regions**

The different meshing techniques used to generate mesh for different regions of the modelled assembly (Figure D20) were addressed previously. It is important to note that, due to the assembly consisting of two parts, compatible meshes should be created. A compatible mesh could not be created generated over the entire part instance of the Leutner model replicated, by using available meshing techniques. If the *bottom-up* meshing was not used initially, starting from the bottom of the sample towards to the shear ring, a mismatch would occur between the nodes of the regions of the core sample and the steel shear ring and the opposite of the phenomenon demonstrated in Figure D20 (indicated in orange). If a mismatch were to be observed between the nodes of the generated mesh of each part instance, it would introduce the additional stress points in the model, which could have a dramatic impact on the result acquired from the analysis. This section concludes the mesh controls component of the *Mesh* module.

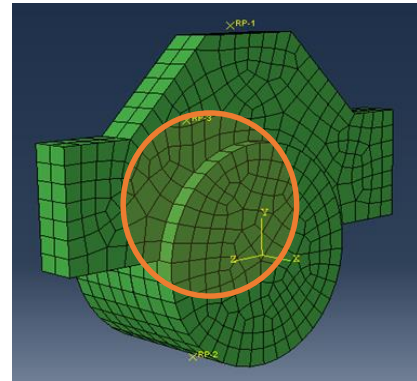


**Figure D20:** Compatible mesh  
(Abaqus Inc., 2017)

## Appendix D5: Element Types for Model 1

Element types can be assigned to a region or a set referring to a region from geometry-based parts or part instances. All the different types of regions to be assigned an element type, have default element types assigned to them. Similar to previous additions to the model, the element type associated with model region is added using the *Element Type* dialog box (Figure D21).

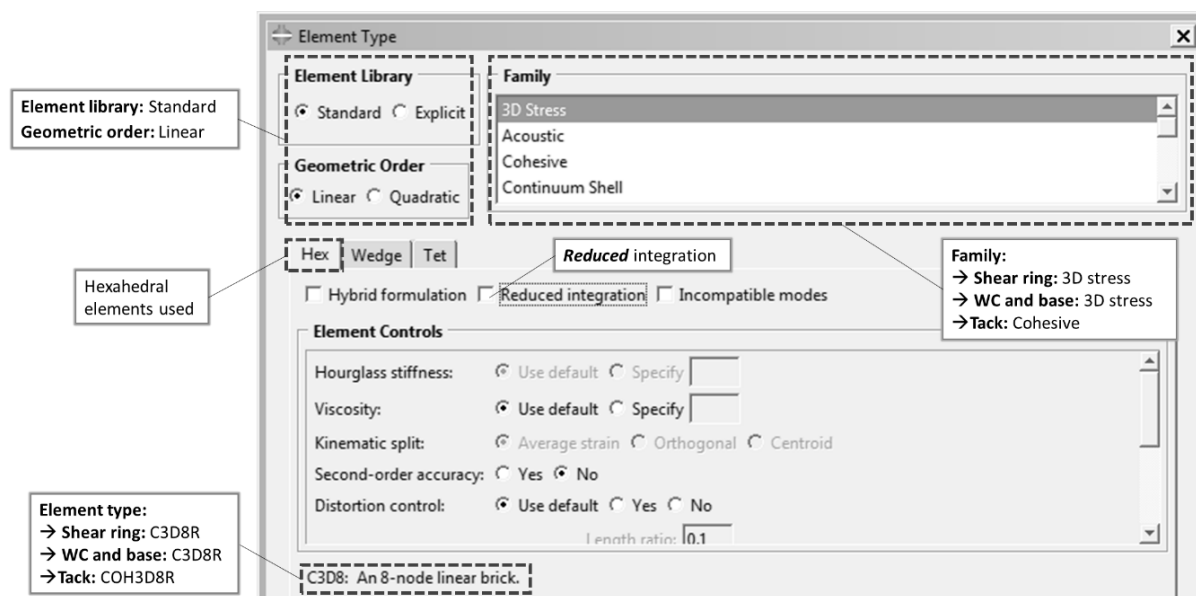


Figure D21: Element Type dialog box for Model 1 (Abaqus Inc., 2017)

### **Element library and geometric order**

At the top part of the dialog box shown in Figure D21, the preferences for the element library, geometric order and family are entered into the model. The settings, as indicated in the figure, are appropriate for the current analysis – the element library of Abaqus *Standard* will be used and linear (first-order) analysis will be used as opposed to a quadratic (second-order) analysis. For the first order analysis, the strain operator provides constant volumetric strains throughout the element. It prevents mesh “locking” when the material response is “incompressible”. Second-order, however, provides higher accuracy than first-order elements for smooth problems and other advantages featured in Dassault Systèmes Simulia, (2014c). This is not a cause for concern in the current analysis; hence, a linear analysis is deemed sufficient for the purpose of the research.

### **Full integration versus reduced integration**

Concerning the mathematical approach of this stage of the model set-up, a selection is considered, whether to apply full integration or reduced integration. Full integration refers to the number of Gauss points required to integrate the polynomial terms in an element’s matrix exactly when the element has a “regular” shape. In the case of this model, *regular shape*, for hexahedral elements, would require straight edges which meet at right angles, and any edge nodes are at the midpoint of the edge. Fully integrated (linear) elements use two integration points in each direction, meaning that for a three-dimensional element an array of eight integration points are within the element (Dassault Systèmes Simulia, 2014e).

Reduced integration can only be used for quadrilateral and hexahedral elements. These elements are one integration point fewer in each direction, in comparison with fully integrated elements. Reduced integration (linear) elements have a single integration point located at the centroid (Dassault Systèmes Simulia, 2014e). A visual representation of the integration application is provided in both instances in Figures D22 and D23 for a quadrilateral (two-dimensional) element. According to (Dassault Systèmes Simulia (2014e), the first-order elements in Abaqus use a more accurate uniform strain formulation, where average values of strain components are computed for the elements. For this reason, it was decided to perform a first-order analysis by means of *reduced* integration.

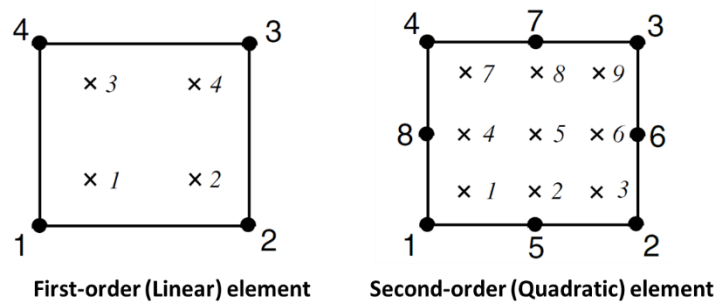


**Figure D22:** Fully integrated integration points for quadrilateral elements (After Dassault Systèmes Simulia, 2014e)

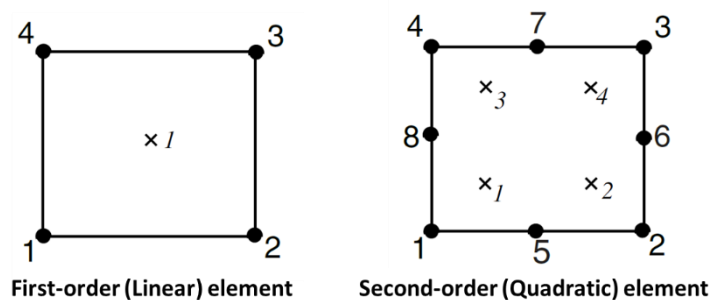


**Figure D23:** Integration points for quadrilateral elements with reduced integration (After Dassault Systèmes Simulia, 2014e)

The bottom half of the dialog box specifies the element type by clicking on the tabs (*Hex*, *Wedge* or *Tet*). Also, with this dialog box, the element type is dependent on the dimensionality of the model. For a model with a different dimensionality, i.e. 2-D, other options like *Quad* and *Tri* would have been available for selection. Given that hexahedral elements were used (4.2.7.3) for the three-dimensional assembly, the tab currently selected in the figure is of relevance to the current model.

### **Family and element types**

Certain elements are associated with specific mesh regions. Furthermore, considering the different part instances of the FEM model assembly, it should be evident that the model is composed of two types of sections and, therefore, comprises of two different element types. In the physical setup of the model, addressed in Section 4.2.4, especially, a *solid* (homogeneous) and *cohesive* section was assigned to relative regions of the model. Each of these elements belong to an element family. In the context of the discussion of the element types in the two subsequent sections, the sections are referred to as continuum (solid section) and special purpose (cohesive section) elements respectively.

### Solid (Continuum) elements

Solid or continuum elements are used on both linear and complex nonlinear analyses involving contact (such as interlayer bonding), plasticity and large deformations. In turn, these elements can be classified for stress, electromagnetic and a variety of other analyses. The elements used for the purpose of these analyses are known as stress/ displacement elements. Given the nature of the current analysis, stress is a critical parameter to be evaluated from the results acquired. From the dialog box provided in Figure D21, these elements are categorised by certain features such as interpolation elements (based on analysis order), the method of integration and element shapes used for the interpolation to obtain results from the analysis. The elements' shapes were introduced in Appendix D4 where a brief description was given of each of the different available element shapes and will therefore not be covered in this section.

The naming convention for solid elements depends on the dimensionality of the element, i.e. C3D8R (solid elements used for the replicate FEM model) is composed of the type of element ("C"), the modelling space, in Section 4.2.3, ("3D"), number of nodes based on interpolation method ("8"). The addition of the "R" indicates that *reduced* integration is used. If *full* integration were to be used, the previous notation would change to C3D8. Keeping the naming convention in mind, the analysis is composed of continuum elements in the 3D modelling space where an eight-node hexahedral (brick) element is used with reduced integration (Figure D24). For cohesive sections, the prefix of "C" is replaced with "COH".

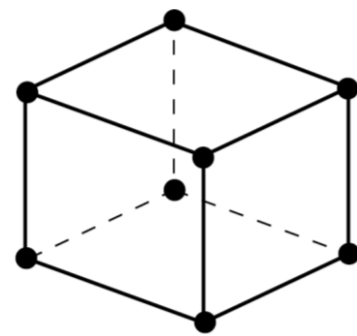


**Figure D24:** Linear element  
(Dassault Systèmes Simulia, 2014c)

### Cohesive elements

Cohesive elements are especially useful in modelling bonded interfaces (i.e. tack coat). The constitutive response of these elements depends on its application based on certain assumptions about the deformation and stress states appropriate for the application. The key geometrical features used to define cohesive elements are demonstrated in Figure D25 (left). In addition, Figure D25 (right) shows the different deformation modes of a cohesive element.

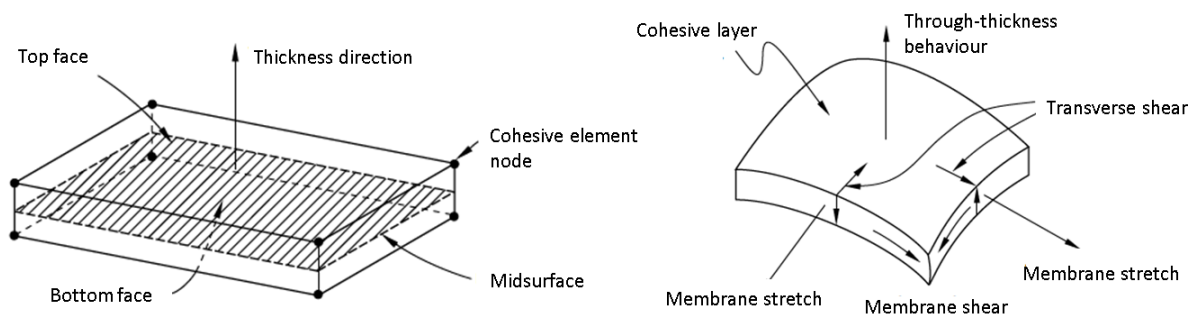


**Figure D25:** Geometrical features and deformation mode of cohesive element (Dassault Systèmes Simulia, 2014c)

The connectivity of cohesive elements can be compared to that of continuum elements, except that Dassault Systèmes Simulia (2014c) describes these elements as a composition of two faces separated by a thickness. The relative motion of the two faces is measured relative to the local 3-direction (Figure 4.2.6.2b) or z-direction. The change in position of the bottom and top faces in the plane orthogonal to the thickness direction quantifies the transverse shear behaviour. Furthermore, the "stretching" and

“shearing” of the element mid-surface are associated with membrane strains in the cohesive elements. It is important to note that Abaqus assumes that the cohesive elements do not generate any stresses in a pure membrane response (Dassault Systèmes Simulia, 2014c).

For this model, the cohesive zone represents an adhesive material (tack coat – bitumen emulsion) with a finite thickness ( $t_{TC}$ ), and the continuum macroscopic properties of the material are used for modelling the constitutive response of the cohesive zone. The function of tack coat was made prominent in Section 2.2 of the literature review (Chapter 2). In short, it acts as a type of glue between two layers (in this case the asphalt wearing course and base layers). In context of the FEM model, the top and bottom faces of the cohesive element are constrained to another component (the other two layers). A variety of approaches exists to incorporate this component in the model. Due to the functionality of the tack coat layer in the model, and the outcome preference, it was found convenient to have the cohesive element share nodes with the elements on the surfaces of the adjacent components. No interaction was created between the cohesive elements and other components.

When cohesive elements and neighbouring parts have matched meshes, it is convenient to connect the cohesive elements to other components in a model by sharing nodes (Figure D26). A replication of this phenomenon, in reference to the Leutner test (cores sample), is also provided in this figure. In this instance part was created to represent the core sample and the different layers are represented by sections which describe the different material characteristics of the three different layers of the sample through partitions. This approach was used as opposed to a composite model, as this approach would result in “weaker” elements and not a functional model (representation).

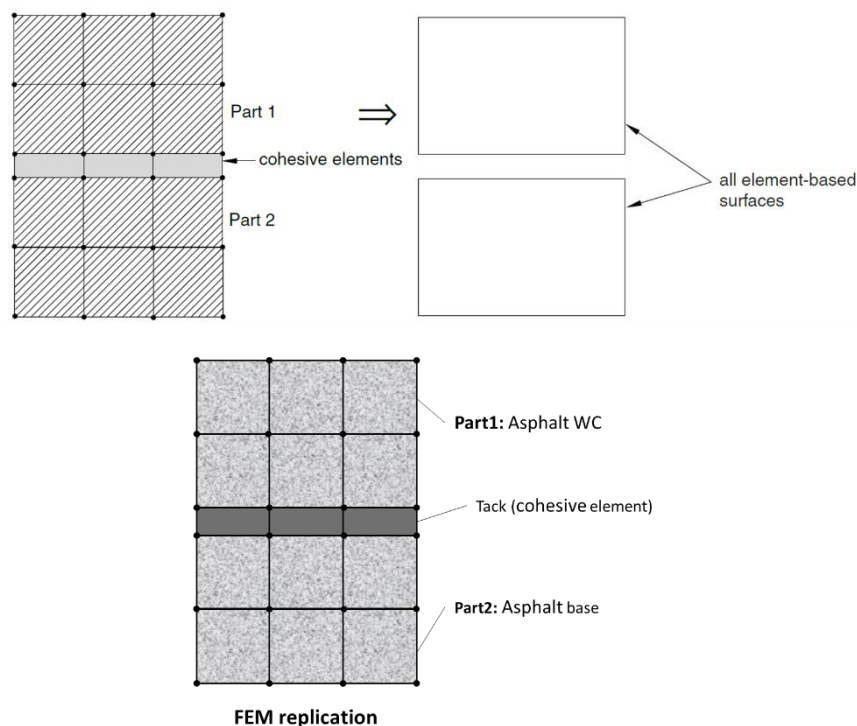


**Figure D26:** Cohesive elements sharing nodes with other elements (After Dassault Systèmes Simulia, 2014c)

In the *Property* module (Section 4.2.4) the material for this element was defined where it was described that the cohesive behaviour of this element is linear-elastic, and shows traction separation behaviour. Other features, such as the material response and the geometry of the part, were also covered in this section. Abaqus computes default local directions at each integration point (where results are obtained). The local 3-direction for three-dimensional cohesive elements corresponds to the thickness direction where the other two directions are normal to the thickness direction. The convention used to indicate these directions is in line with the convention shown previously in Figure 4.2.6.2b. The local directions for a three-dimensional cohesive element are shown in Figure D27.

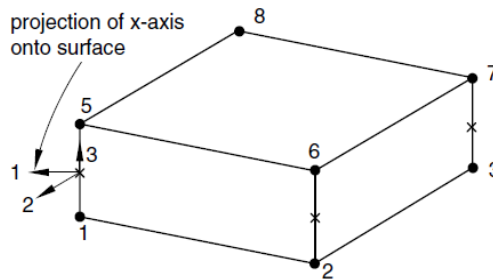


**Figure D27:** Local directions for 3D cohesive elements (Dassault Systèmes Simulia, 2014c)

## Appendix D6: Boundary Conditions for Model 2

The first boundary condition includes “fixed” boundary conditions. This type of boundary condition fixes a degree of freedom in place. For the model, the boundary conditions are applied to the subgrade layer which, according to Croney & Croney (1998), acts as a type of foundation for the pavement structure. Consequently, failure of this layer could (most likely) result in the failure of the entire pavement structure. At this location, a “fixed” boundary condition (Figure 4.3.4.2b left) is used to describe this phenomenon. All six degrees of freedom are thus fixed for example  $U1 = UR2 = U3 = 0$  and  $UR1 = UR2 = UR3$  (when the *Displacement/Rotation* option were to be used in Figure D28). A simpler method is to apply a *Symmetry/Axisymmetry/Encastre* type of boundary condition in Figure D29 (left). This provides a variety of options, such as fixed degrees of freedom, as opposed to setting the degrees of freedom individually. This would be the case if the *Displacement/Rotation* option was used.

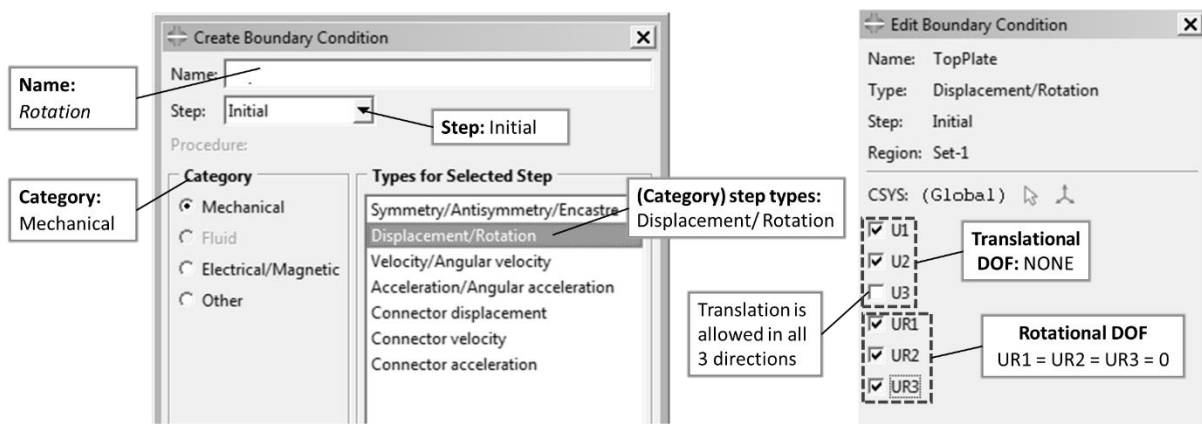


Figure D28: Sketch of geometry of part (Abaqus Inc., 2017)

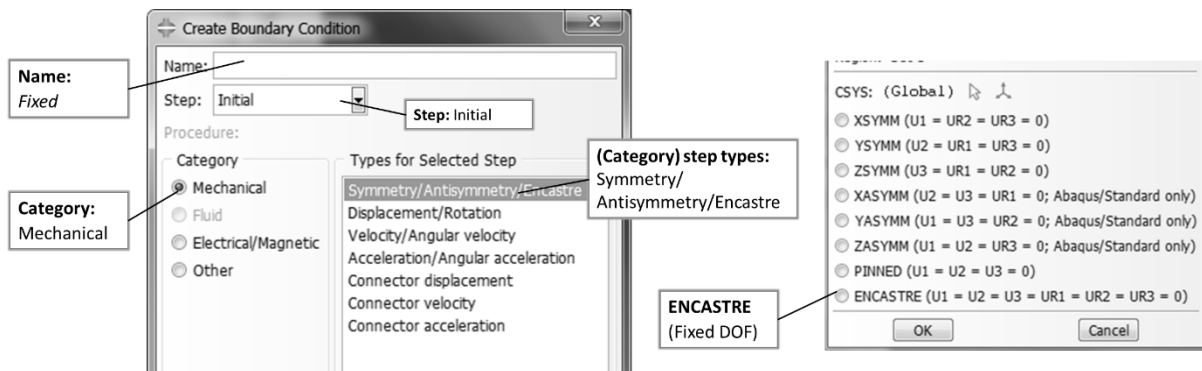
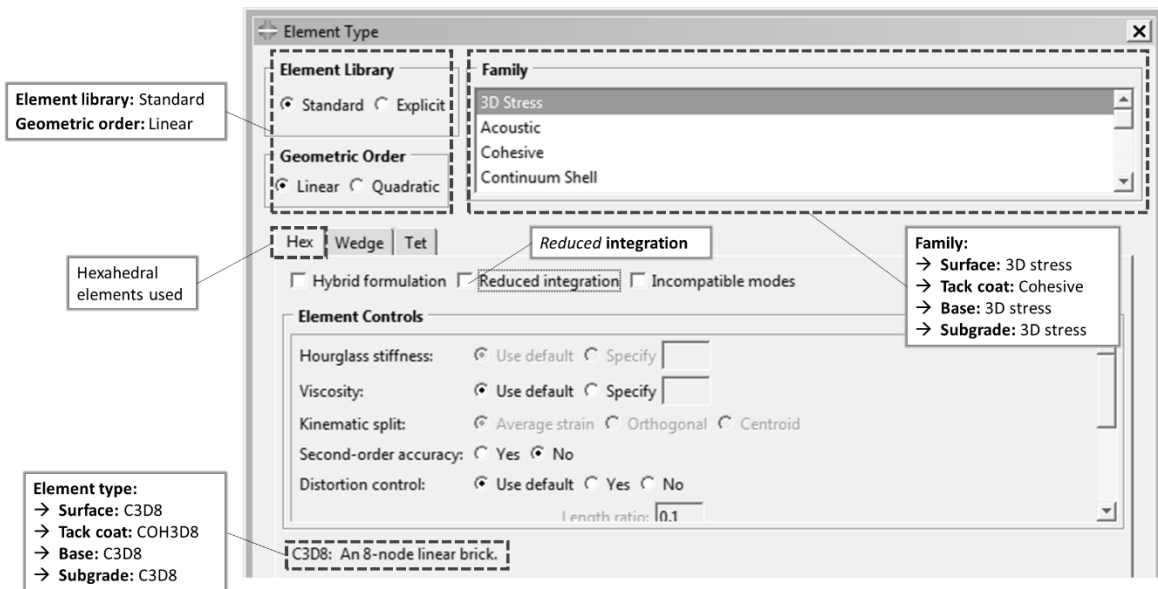


Figure D29: Sketch of geometry of part (Abaqus Inc., 2017)

The objectives of these analyses are to evaluate strains specifically to eventually estimate pavement life in terms of serviceability, and fatigue life for these models. Relative to the depth of the pavement structure (exposed areas of the pavement layers), translation (deformation) is allowed in the respective three directions (x, y and z) while rotational degrees of freedom are restrained at this location Figure D28 (right).

## Appendix D7: Element Types for Model 2

Information about the *element library* and *geometric order* is kept the same. In summary, the element type information of the replicated pavement structures is shown in Figure D30. The *Mesh* module finalizes the set-up of the model in preparation for the analysis by dividing the model into small finite elements to be analysed.



**Figure D30:** Element Type dialog box for Model 2 (Abaqus Inc., 2017)

The procedures carried out from Section 4.3.2 to 4.3.5 conclude the set-up of the model until preparation for analysis (meshing). Hereafter the model is submitted for analysis in the *Job* module. The different criteria required in this model, to set a job to be submitted for analysis, was discussed in Section 4.2.8. The same characteristics set in the *Job* editor (dialog box) shown in Figure 4.2.8b are also applicable for this material model. Once the job is created for the analysis, the model is submitted for analysis. The results obtained from the analysis can be obtained in the *Visualisation* Module.

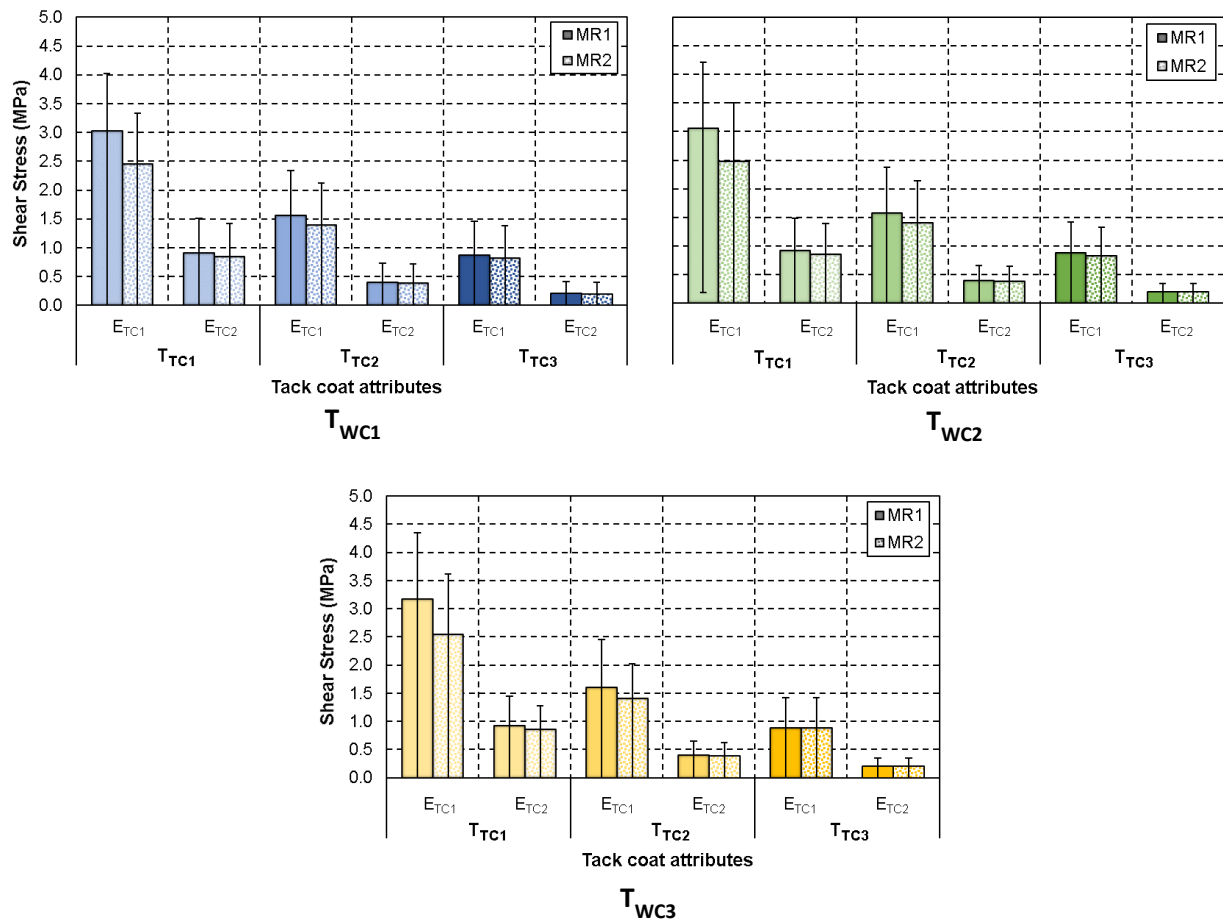
## **Appendix E: Finite Element Analysis**

## Appendix E1: Leutner Shear Model

**Note:**

$T_{wc}$  = Wearing course thickness,  $T_{TC}$  = Tack coat stiffness,  $E_{TC}$  = Tack coat material stiffness, **MR** = Modular ratio.  
Refer to Section 5.2.1 for detailed description of different attributes

### Interface bonding



$T_{WC1} = 30mm$ ,  $T_{WC2} = 50mm$  and  $T_{WC3} = 100mm$ ,  $T_{TC1} = 0.2mm$ ,  $T_{TC2} = 0.5mm$  and  $T_{TC3} = 1mm$ ,  $E_{TC1} = 1MPa$  and  $E_{TC2} = 0.21MPa$ ,  $MR1 = 1$  ( $E_{base} = 2500MPa$ ) and  $MR2 = 2.5$  ( $E_{base} = 1000MPa$ )

**Figure E1:** Minimum, Average and Maximum shear stress results for increase in  $T_{WC1}$

**Table E1:** Shear stress results (in MPa) for wearing course thickness of 30mm ( $T_{WC1}$ )

Material Properties		$E_{TC1}$			$E_{TC2}$		
		$\tau_{min}$	$\tau_{Avg}$	$\tau_{max}$	$\tau_{min}$	$\tau_{Avg}$	$\tau_{max}$
MR1	$T_{TC1}$	< 0.1	3.03	4.03	< 0.1	0.91	1.52
	$T_{TC2}$	< 0.1	1.56	2.34	< 0.1	0.40	0.74
	$T_{TC3}$	< 0.1	0.87	1.46	< 0.1	0.21	0.41
MR2	$T_{TC1}$	< 0.1	2.46	3.33	< 0.1	0.85	1.43
	$T_{TC2}$	< 0.1	1.39	2.12	< 0.1	0.39	0.72
	$T_{TC3}$	< 0.1	0.82	1.38	< 0.1	0.20	0.40

**Table E2:** Shear stress results (in MPa) for wearing course thickness of 50mm ( $T_{WC2}$ )

Material Properties		$E_{TC1}$			$E_{TC2}$		
		$\tau_{min}$	$\tau_{Avg}$	$\tau_{max}$	$\tau_{min}$	$\tau_{Avg}$	$\tau_{max}$
MR1	$T_{TC1}$	0.19	3.06	4.21	< 0.1	0.92	1.48
	$T_{TC2}$	< 0.1	1.58	2.38	< 0.1	0.40	0.66
	$T_{TC3}$	< 0.1	0.88	1.41	< 0.1	0.20	0.35
MR2	$T_{TC1}$	< 0.1	2.48	3.50	< 0.1	0.86	1.39
	$T_{TC2}$	< 0.1	1.41	2.15	< 0.1	0.39	0.64
	$T_{TC3}$	< 0.1	0.82	1.33	< 0.1	0.20	0.34

**Table E3:** Shear stress results (in MPa) for wearing course thickness of 100mm ( $T_{WC3}$ )

Material Properties		$E_{TC1}$			$E_{TC2}$		
		$\tau_{min}$	$\tau_{Avg}$	$\tau_{max}$	$\tau_{min}$	$\tau_{Avg}$	$\tau_{max}$
MR1	$T_{TC1}$	< 0.1	3.17	4.35	< 0.1	0.93	1.45
	$T_{TC2}$	< 0.1	1.61	2.45	< 0.1	0.40	0.66
	$T_{TC3}$	< 0.1	0.89	1.43	< 0.1	0.21	0.34
MR2	$T_{TC1}$	< 0.1	2.55	3.62	< 0.1	0.85	1.27
	$T_{TC2}$	< 0.1	1.41	2.02	< 0.1	0.38	0.62
	$T_{TC3}$	< 0.1	0.89	1.43	< 0.1	0.21	0.34

**Table E4:** Axial force (in kN) results for wearing course thickness of 30mm ( $T_{WC1}$ )

Material Properties		$E_{TC1}$			$E_{TC2}$		
		$V_{min}$	$V_{avg}$	$V_{max}$	$V_{min}$	$V_{avg}$	$V_{max}$
MR1	$T_{TC1}$	0.1	53.5	71.2	< 0.1	16.1	26.8
	$T_{TC2}$	< 0.1	27.5	41.4	< 0.1	7.0	13.0
	$T_{TC3}$	< 0.1	15.4	25.8	< 0.1	3.6	7.2
MR2	$T_{TC1}$	< 0.1	43.4	58.8	< 0.1	15.0	25.2
	$T_{TC2}$	< 0.1	24.6	37.4	< 0.1	6.8	12.7
	$T_{TC3}$	< 0.1	14.4	24.4	< 0.1	3.6	7.1

**Table E5:** Axial force (in kN) results for wearing course thickness of 50mm ( $T_{WC2}$ )

Material Properties		$E_{TC1}$			$E_{TC2}$		
		$V_{min}$	$V_{avg}$	$V_{max}$	$V_{min}$	$V_{avg}$	$V_{max}$
MR1	$T_{TC1}$	3.3	54.0	74.5	< 0.1	16.2	26.1
	$T_{TC2}$	< 0.1	27.8	42.0	< 0.1	7.0	11.7
	$T_{TC3}$	< 0.1	15.5	25.0	< 0.1	3.6	6.2
MR2	$T_{TC1}$	< 0.1	43.8	61.8	< 0.1	15.2	24.6
	$T_{TC2}$	< 0.1	24.9	37.9	< 0.1	6.8	11.4
	$T_{TC3}$	< 0.1	14.6	23.6	< 0.1	3.6	6.1

**Table E6:** Axial force (in kN) results for wearing course thickness of 100mm ( $T_{WC3}$ )

Material Properties		$E_{TC1}$			$E_{TC2}$		
		$V_{min}$	$V_{avg}$	$V_{max}$	$V_{min}$	$V_{avg}$	$V_{max}$
MR1	$T_{TC1}$	< 0.1	56.0	76.9	< 0.1	16.4	25.6
	$T_{TC2}$	< 0.1	28.4	43.3	< 0.1	7.1	11.6
	$T_{TC3}$	< 0.1	15.7	25.2	0.01	3.6	6.1
MR2	$T_{TC1}$	< 0.1	45.0	64.0	< 0.1	15.1	22.5
	$T_{TC2}$	< 0.1	24.9	35.6	< 0.1	6.8	11.0
	$T_{TC3}$	< 0.1	15.7	25.2	0.01	3.6	6.1

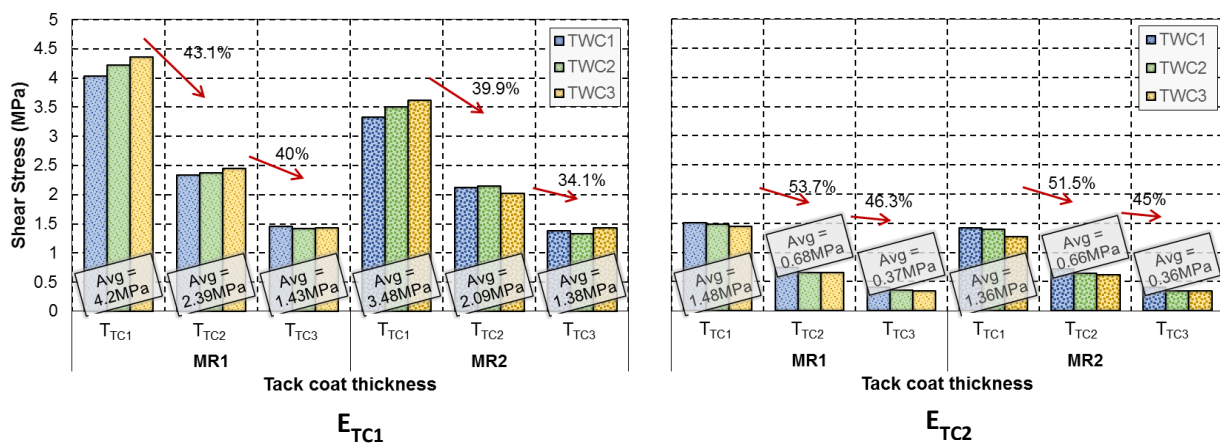


**Figure E2:** Progressive shear stress change according to wearing course thickness ( $T_{WC}$ )

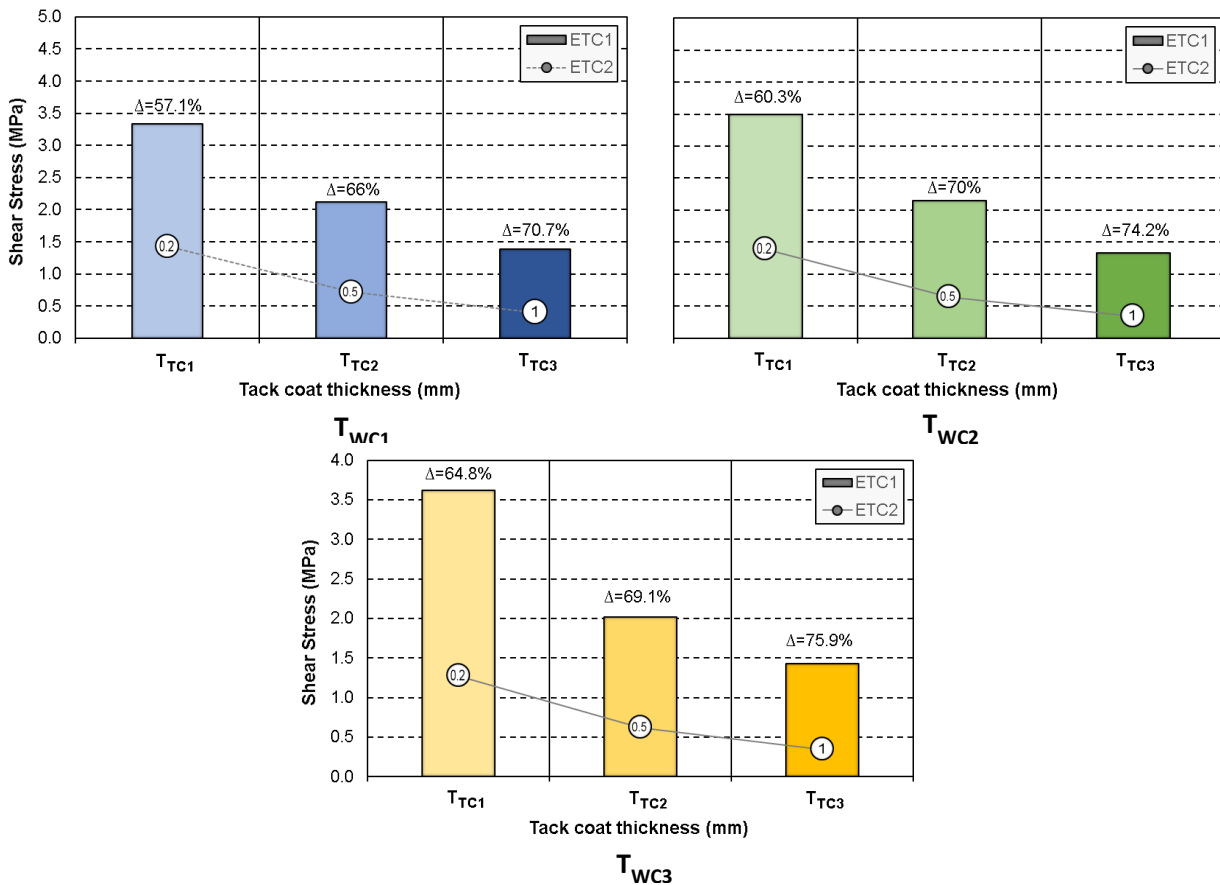


**Figure E3:** Tack coat stiffness influence for wearing course thickness for MR2

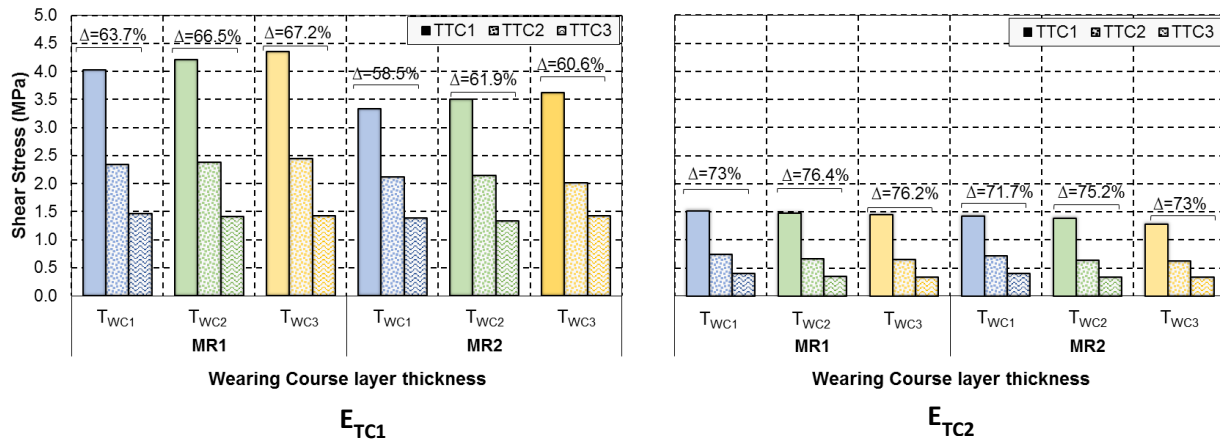


Figure E4: Shear stress variation in tack coat thickness (%)

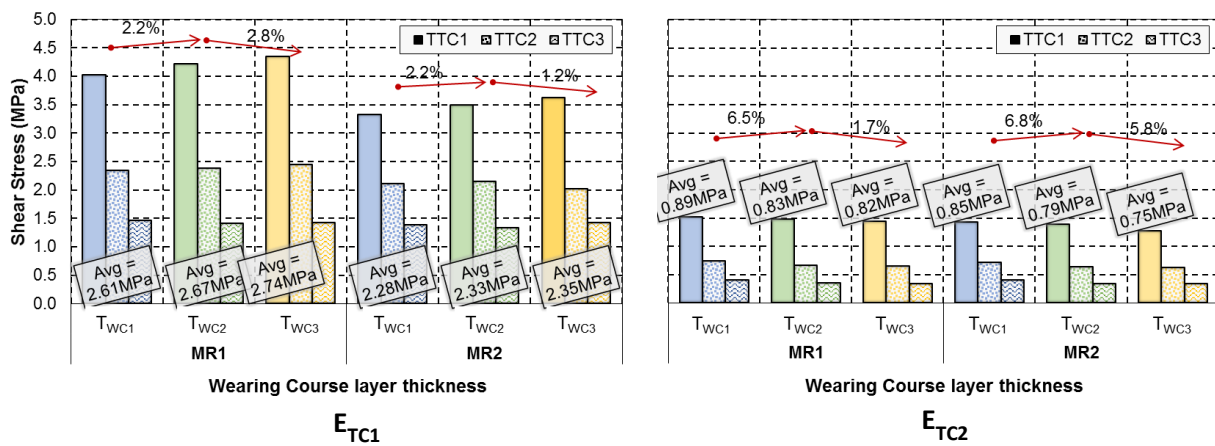


Figure E5: Tack coat thickness influence for  $E_{TC1}$  and  $E_{TC2}$  (%)

### Model 1 versus Linear-Elastic Analysis

The formula (Equation E1) is adjusted to accommodate the parameter representing the results from the preliminary analysis, replacing the  $x_{lab}$  parameter with this value from the linear-elastic (LE) analysis ( $x_{LE}$ ), as represented by Equation E1.

$$\Delta_{Analysis} = \frac{x_{LE} - x_{Model1}}{x_{Model1}} \quad (E1)$$

Where:

$x_{LE}$  = Results from preliminary linear-elastic analysis

The calculations for this equation are completed by adhering to the following listed guidelines (examples provided in Tables E7 to E9):

1. The average results of  $E_{TC1}$  combination of a specific wearing course was used i.e. for  $T_{WC1}$  combinations, these average of the tack coat thickness ( $T_{TC1}$  to  $T_{TC3}$ ) were used per MR condition (MR1 and MR2). For this condition, the average shear stress for the three defined tack coat thickness are 2.7MPa (for MR1) and 2.3 MPa (for MR2) respectively.

Example:

**Table E7:** Average estimation of modular ratio for  $T_{WC1}$  combinations

	MR1	MR2
$T_{TC1}$	4.3	3.3
$T_{TC2}$	2.3	2.1
$T_{TC3}$	1.5	1.4
<b>Average:</b>	2.7	2.3

2. The average estimated values acquired in point 1 are compared with every combination covering all the different testing conditions specified, such as the friction conditions (high, medium and low) and the two loading conditions ( $T1$  and  $T2$ ). Reference can be made to Section 3.2 of the *Preliminary Research* chapter (Chapter 3) for the details regarding these parameters. The shear stresses measured at the interface (*Interface 1*) were used for comparison purposes.

Example:

**Table E8:** Interface shear stress from LE analysis for  $T1$  loading condition (MPa)

Analyses	HF	MF	LF
<b>Case 1</b>	0.64	1.1	1.2
<b>Case 2</b>	0.18	0.6	0.63
<b>Case 3</b>	0.59	0.9	0.93
<b>Case 4</b>	0.26	0.65	0.68

3. The steps explained in points 1 and 2 are repeated for all three the wearing course thicknesses ( $T_{WC1}$  to  $T_{WC3}$ ). To reduce the number of combinations to be evaluated, the set of results for only one stiffness modulus ( $E_{TC1}$ ) was used. The stiffness selected was the lowest stiffness providing the most conservative results using the model composed of a “less stiff” tack coat material.

Example:

**Table E9:** Estimations for HF condition for  $T_{WC1}$  (%)

	Calculations for MR1			Calculation for MR2		
<b>Case 1</b>	$\frac{(0.64) - (2.7)}{(2.7)}$	76.3%	↓	$\frac{(0.64) - (2.3)}{(2.3)}$	72.2%	↓
<b>Case 2</b>	$\frac{(0.18) - (2.7)}{(2.7)}$	93.3%	↓	$\frac{(0.18) - (2.3)}{(2.3)}$	92.2%	↓
<b>Case 3</b>	$\frac{(0.59) - (2.7)}{(2.7)}$	78.1%	↓	$\frac{(0.59) - (2.3)}{(2.3)}$	74.3%	↓
<b>Case 4</b>	$\frac{(0.26) - (2.7)}{(2.7)}$	90.4%	↓	$\frac{(0.26) - (2.3)}{(2.3)}$	88.7%	↓

## Appendix E2: Pavement Analysis Model

### Shear Stresses

**Table E10:** Shear stress results for Model 2 i.e. Pavement Structure (in kPa)

Analyses	T1 loading	T2 loading
Case 1	1	1.7
Case 2	0.9	2.2
Case 3	2.3	0.9
Case 4	1.7	0.8

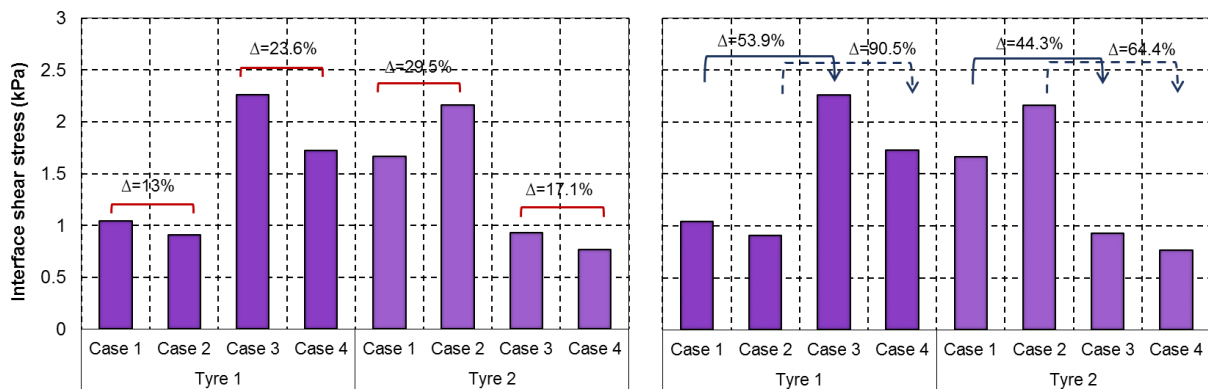


**Figure E6:** Property differences measured for Model 2 interface shear stress



**Figure E7:** Loading condition differences measured for Model 2 interface shear stress

### Horizontal Strains

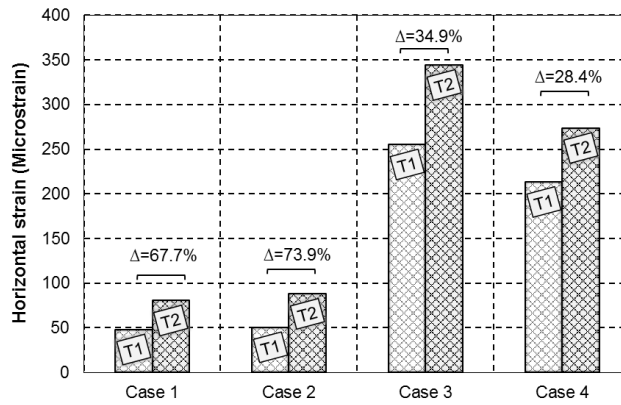
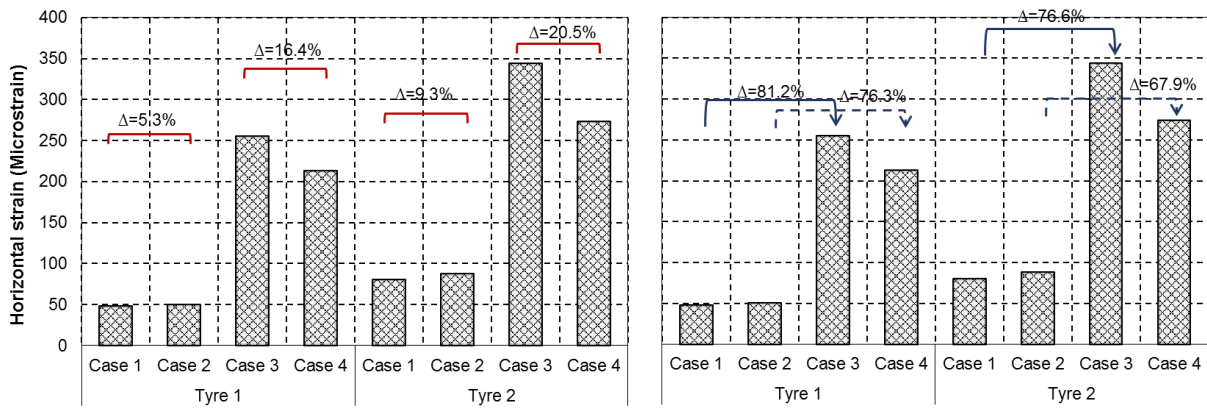


Figure E8: Loading condition differences measured for Model 2 horizontal strain



Note: Red = change in  $E_{base}$ , blue = change in  $t_{Asphalt}$

Figure E9: Property differences measured for Model 2 horizontal strain

### Vertical Strains

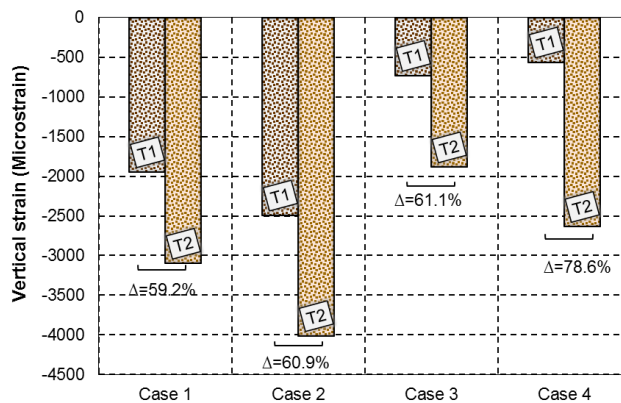
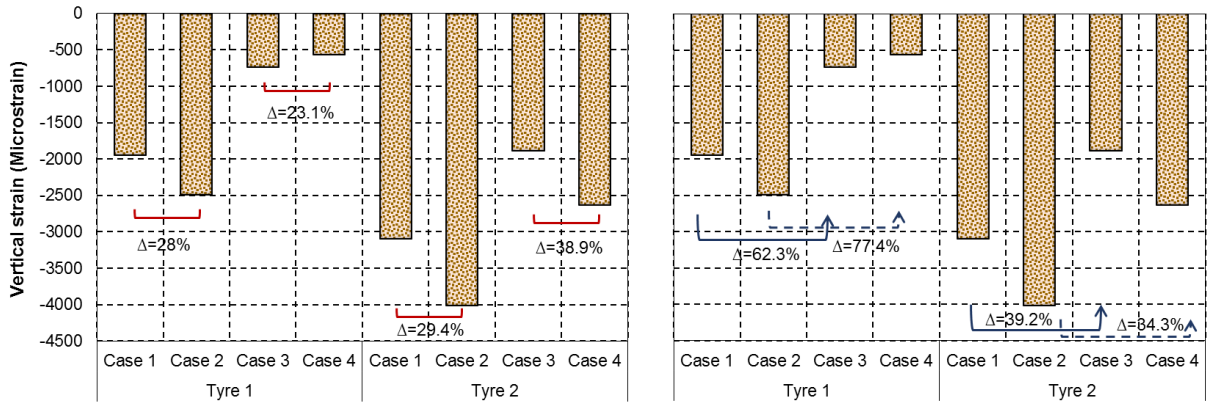


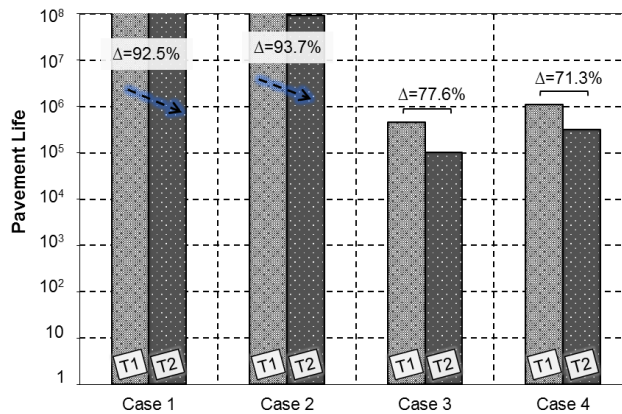
Figure E10: Loading condition differences measured for Model 2 vertical strain



Note: Red = change in  $E_{base}$ , blue = change in  $t_{Asphalt}$

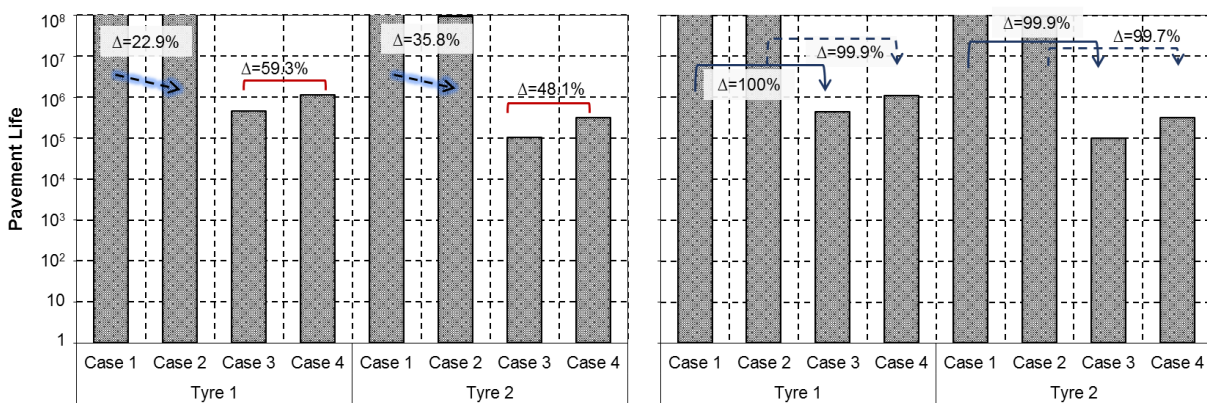
Figure E11: Property differences measured for Model 2 vertical strain

Fatigue Life



Note: Results indicated in number of load repetitions

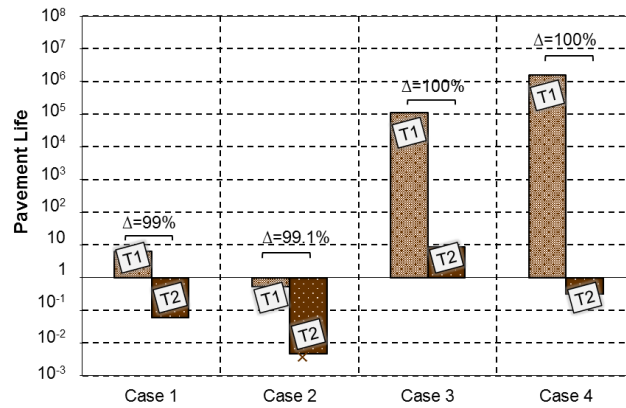
Figure E12: Loading condition differences measured for Model 2 fatigue life



Note: Red = change in  $E_{base}$ , blue = change in  $t_{Asphalt}$ , results indicated in number of load repetitions

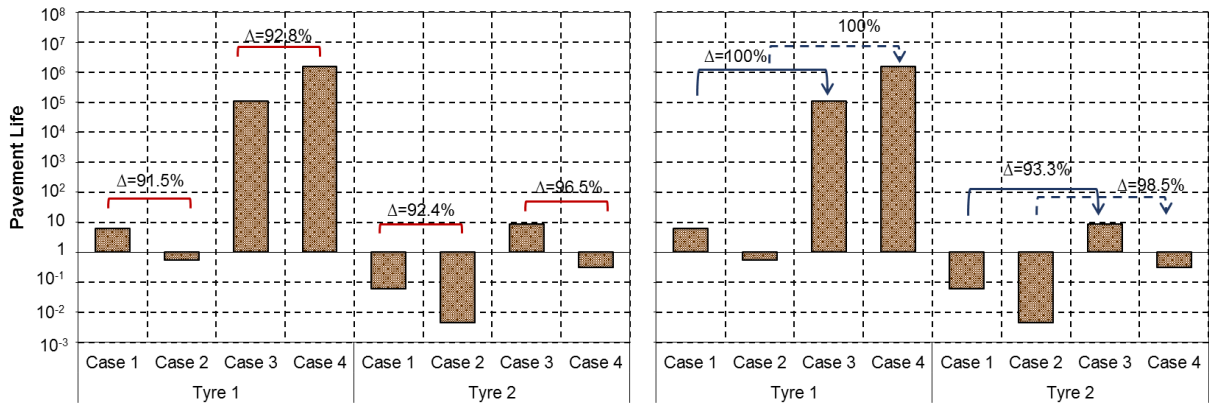
Figure E13: Property differences measured for Model 2 fatigue life

**Serviceability Life**



**Note:** Results indicated in number of load repetitions

**Figure E14:** Loading condition differences measured for Model 2 serviceability life



**Note:** Red = change in  $E_{base}$ , blue = change in  $t_{Asphalt}$ , results indicated in number of load repetitions

**Figure E15:** Property differences measured for Model 2 serviceability life

## **Appendix F: Stress distribution in pavements with Burmister Theory**

### Stress distribution in pavements

Stress distribution within pavement layers is complex, motivating the development of a single layered system approach to a multilayer analysis in order to determine these stresses and strains in respective layers. These methods are based on a variety of theorems developed by Boussinesq and Odemark. Another method was developed by Burmister in which solutions were obtained for a two-layer problem by means of using strains continuity equations (Krishma Rao, n.d.). This method entails determination of stress conditions at certain points and their relationship with stresses generated in laboratory tests which are used for evaluation of material characteristics and specification (Jenkins & Rudman, 2018a).

The method involves a series of graphs generated to estimate the stresses which are composed according to two Poisson ratios ( $\nu$  of 0.25 and 0.5) for instances where the height of the top layer ( $h$ ) is equal to the load radius ( $a$ ) i.e.  $h = a$ , or where the height of the top layer is the equivalent of half of the load radius, i.e.  $h = a/2$ . Thus, the thickness of the top layer and load radius are two of the three input parameters required for the graphs developed by Burmister, as illustrated in Figures F1 and F2. In addition, as seen in the interpretation of the results, stresses are dependent on the modular ratio as the stresses decrease with the increase in this critical parameter. Hence, the third required input parameter comprised of the material stiffness of the two layers ( $E_1$  and  $E_2$ ) to first establish the modular ratio. In these figures, the graph for vertical stress is shown first followed by horizontal stresses.

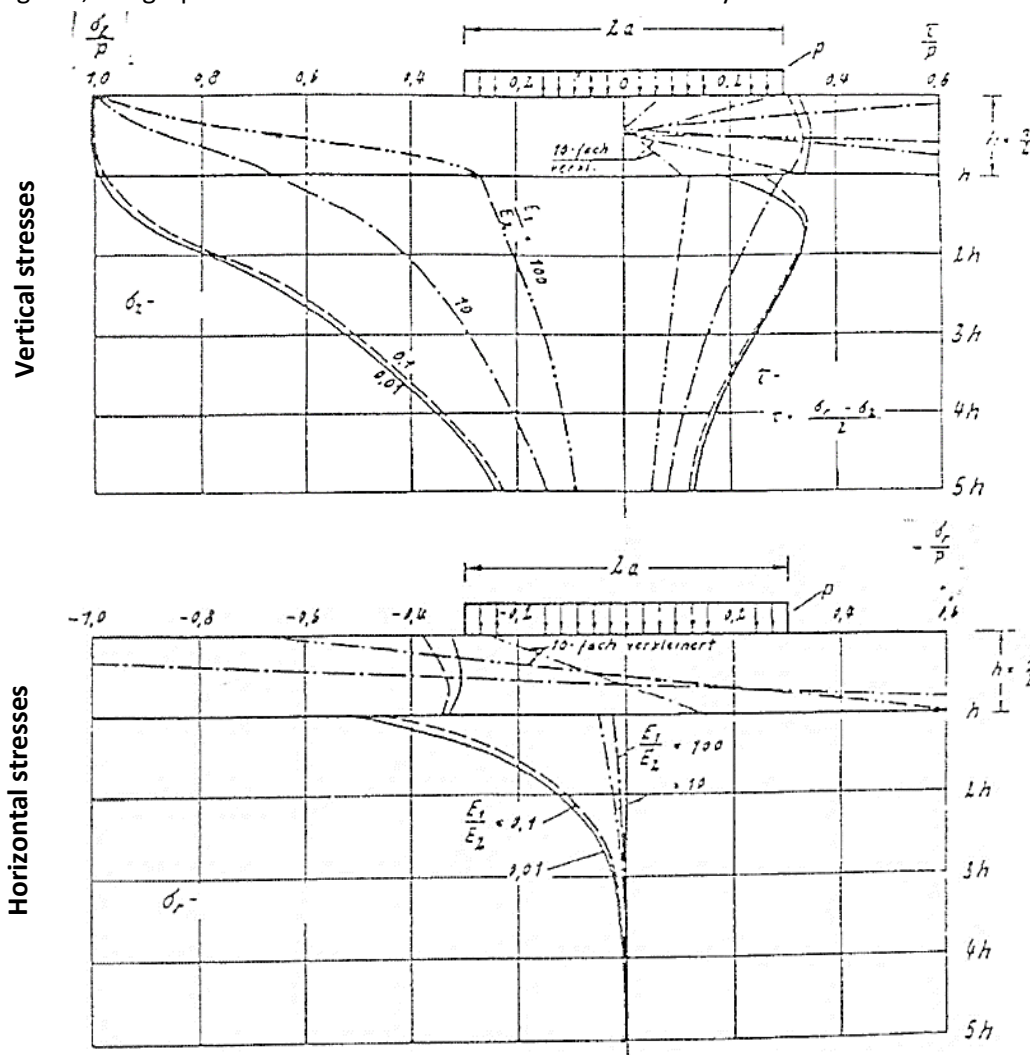


**Figure F1:** Burmister Graph (Vertical and Horizontal Stresses) for Poisson Ratio of 0.25 and Layer Thickness of  $h=a/2$  (Jenkins & Rudman, 2018a)

Both sets of graphs illustrated in F1 and F2 are used to calculate both the vertical ( $\sigma_z$ ) and horizontal stresses ( $\sigma_r$ ) within the depth through the layers. The first graph illustrated in Figures F1 and F2 includes a horizontal axis with a scale between 1 and 0 and again up to 0.6. The vertical stresses are estimated on the left hand side by means of the  $\sigma_z/p$  ratio (ratio of vertical stresses to tyre pressure) whilst the right hand side is used for estimation of shear stresses ( $\tau/p$ ). The vertical axis line indicates the depth into the layer and the vertical stresses can be determined at any depth within the two layered systems. In addition, contours in these figures represent the stiffness ratio (modular ratio) ranging from 100 to 0.01. The sign convention used in these figures is: compressive stresses denoted as positive and tensile as negative. This would imply that all vertical stresses will have a positive value (Jenkins & Rudman, 2018a).

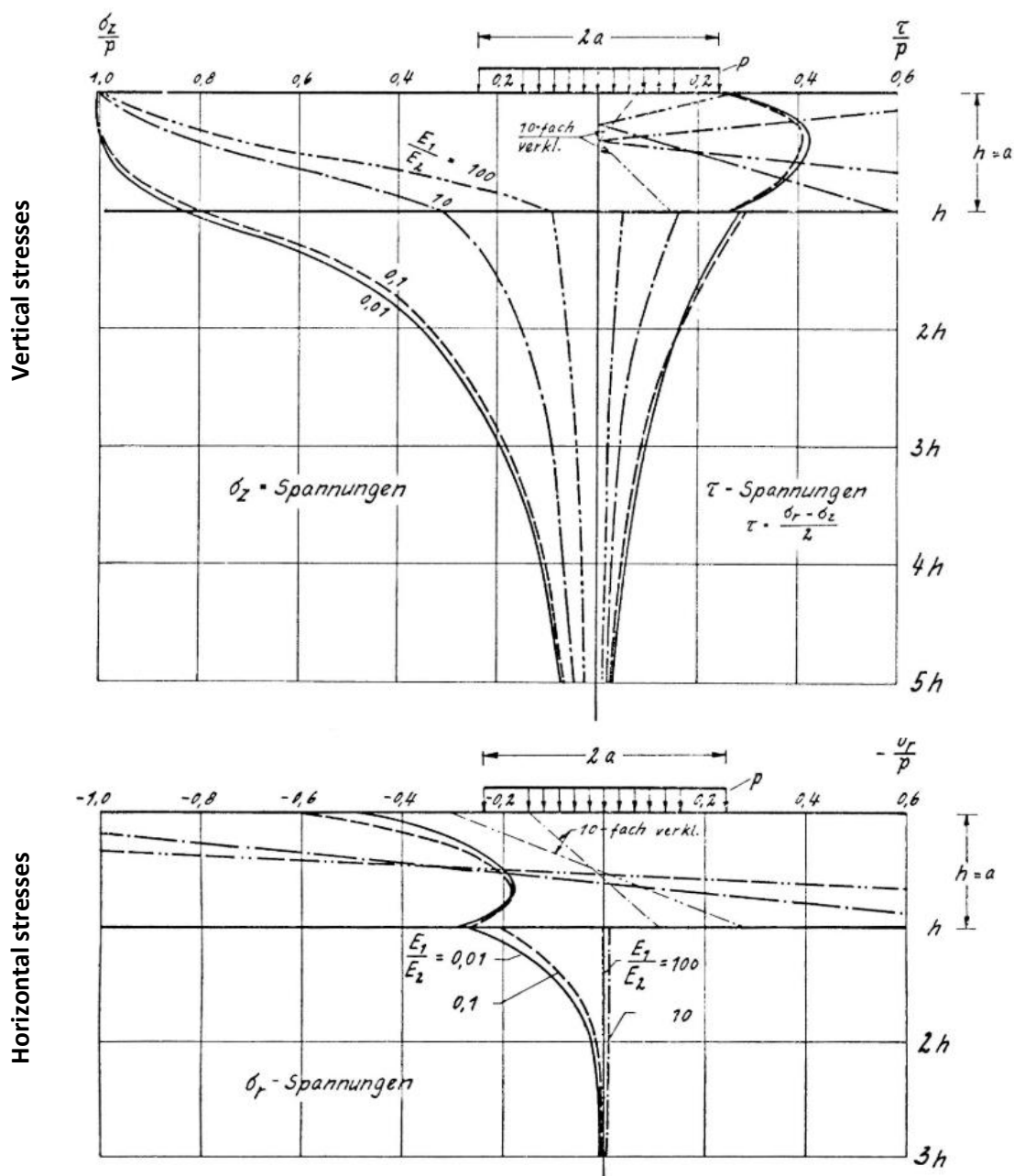


**Figure F2:** Burmister Graph (Vertical and Horizontal Stresses) for Poisson Ratio of 0.25 and Layer Thickness of  $h=a$  (Jenkins & Rudman, 2018a)

Concerning the horizontal stresses, the values of the stresses can be either negative or positive. For these graphs, the horizontal axis at the top of the graph starts at -1 to 0 and again to 0.6. In this instance, both the left and right-hand side are used to estimate horizontal stresses. Furthermore, a change in stress distribution occurs between the top and bottom layer. The change implies that the layer system produces a different value for the horizontal stress at the bottom of the top layer and the top of the bottom layer (Jenkins & Rudman, 2018a). It is also crucial to note that stresses in the top layer must be multiplied with a factor of 10 to acquire the correct stress value for the relative stiffness ratio(s).

The estimated values from these graphs were completed for both  $h=a$  and  $h=a/2$  instances and completed for both loading conditions considered in the current study, i.e.  $T1$  (750kPa) and  $T2$  (900kPa). Stresses were measured as indicated in Figure F3. The results generated from these estimations are shown in Tables F1 (for  $T1$ ) and F2 (for  $T2$ ). For the estimations, *Case 1* and *3* had a stiffness ratio of 6.25, and for *Case 2* and *4* a stiffness ratio of 1.67.

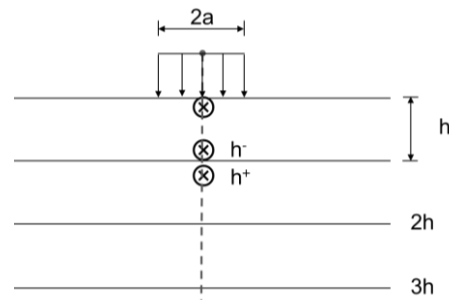


**Figure F3:** Illustration of stress locations of interest

**Table F1:** Burmister graph estimations for stresses for T1 loading condition (kPa)

Analyses	Depth	$h = a/2$		$h = a$	
		$\sigma_z$	$\sigma_r$	$\sigma_z$	$\sigma_r$
Case 1 and Case 3	0	750	1125	750	750
	$h^-$	562.5	-600	300	-450
	$h^+$	547.5	-15	300	-75
Case 2 and Case 4	0	750	750	825	375
	$h^-$	660	-375	570	-112.5
	$h^+$	645	-7.5	570	-112.5

**Note:** For Case 1 and 2  $h/a = 0.38$  ( $h = 100\text{mm}$ ), Case 3 and 3  $h/a = 0.77$  ( $h = 100\text{mm}$ ) with load radius ( $a$ ) of 130mm for T1 loading condition

**Table F2:** Burmister graph estimations for stresses for T2 loading condition (kPa)

Analyses	Depth	$h = a/2$		$h = a$	
		$\sigma_z$	$\sigma_r$	$\sigma_z$	$\sigma_r$
Case 1 and Case 3	0	900	1350	900	900
	$h^-$	675	-720	360	-540
	$h^+$	657	-18	360	-90
Case 2 and Case 4	0	750	900	990	450
	$h^-$	792	-375	684	-135
	$h^+$	774	-7.5	684	-135

**Note:** For Case 1 and 2  $h/a = 0.38$  ( $h = 100\text{mm}$ ), Case 3 and 3  $h/a = 0.77$  ( $h = 100\text{mm}$ ) with load radius ( $a$ ) of 130mm for T1 loading condition

The ratio results from the graphs used to estimate the stresses, shown in these tables, are compiled in in Tables F3 and F4. These results are also summarised according to each loading conditions for T1 and T2 loading conditions respectively.

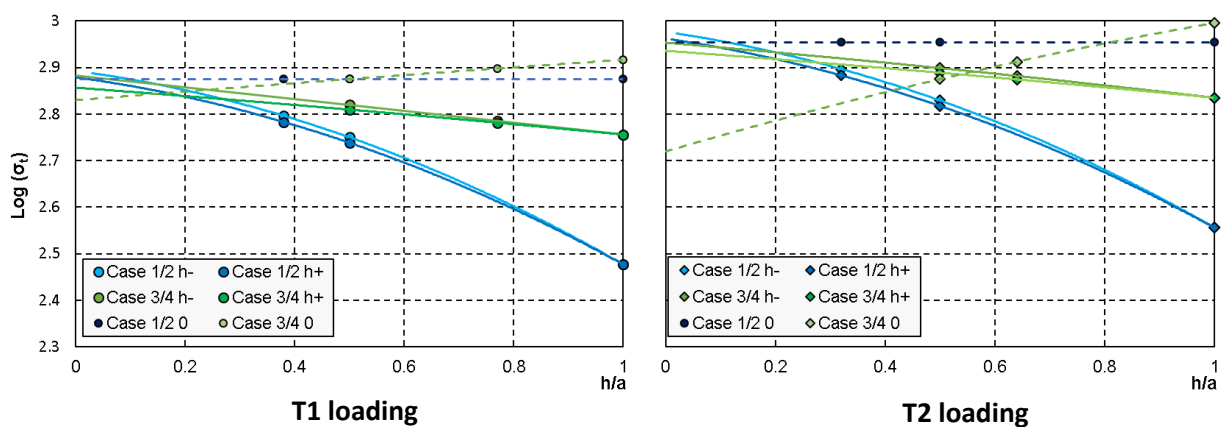
**Table F3:** Burmister graph results for T1 loading condition

Analyses	Depth	h = a/2				h = a			
		$\frac{\sigma_z}{p}$	$\sigma_z$	$\frac{-\sigma_r}{p}$	$\sigma_r$	$\frac{\sigma_z}{p}$	$\sigma_z$	$\frac{-\sigma_r}{p}$	$\sigma_r$
Case 1 and Case 3	0	1	750	-0.15×10	1125	1	750	-0.1×10	750
	h <sup>-</sup>	0.75	562.5	0.08×10	-600	0.4	300	0.06×10	-450
	h <sup>+</sup>	0.73	547.5	0.1	-15	0.4	300	0.1	-75
Case 2 and Case 4	0	1	750	0.1×10	750	1.1	825	-0.05×10	375
	h <sup>-</sup>	0.88	660	0.05×10	-375	0.76	570	0.015×10	-112.5
	h <sup>+</sup>	0.86	645	0.01	-7.5	0.76	570	0.05	-112.5

**Table F4:** Burmister graph results for T2 loading condition

Analyses	Depth	h = a/2				h = a			
		$\frac{\sigma_z}{p}$	$\sigma_z$	$\frac{-\sigma_r}{p}$	$\sigma_r$	$\frac{\sigma_z}{p}$	$\sigma_z$	$\frac{-\sigma_r}{p}$	$\sigma_r$
Case 1 and Case 3	0	1	900	-0.15×10	1350	1	900	-0.1×10	900
	h <sup>-</sup>	0.75	675	0.08×10	-720	0.4	360	0.06×10	-540
	h <sup>+</sup>	0.73	657	0.02	-18	0.4	360	0.02	-90
Case 2 and Case 4	0	1	750	0.1×10	900	1.1	990	-0.05×10	450
	h <sup>-</sup>	0.88	792	0.05×10	-375	0.76	684	0.015×10	-135
	h <sup>+</sup>	0.86	774	0.01	-7.5	0.76	684	0.05	-135

Following the summary of the results at selected points, an illustration of the results is provided in Figures F4 and F5 for the vertical and horizontal stresses measured for both the loading conditions. The stresses at the specific h/a ratio were obtained for each analysis combination (Case 1 to 4) by means of interpolation of the results relative to h = a/2 (h/a = 0.5) and h = a (h/a = 1).



**Note:** For Figures F4 and F5 stresses shown as (absolute) log values

**Figure F4:** Vertical stresses for analyses combinations (kPa)

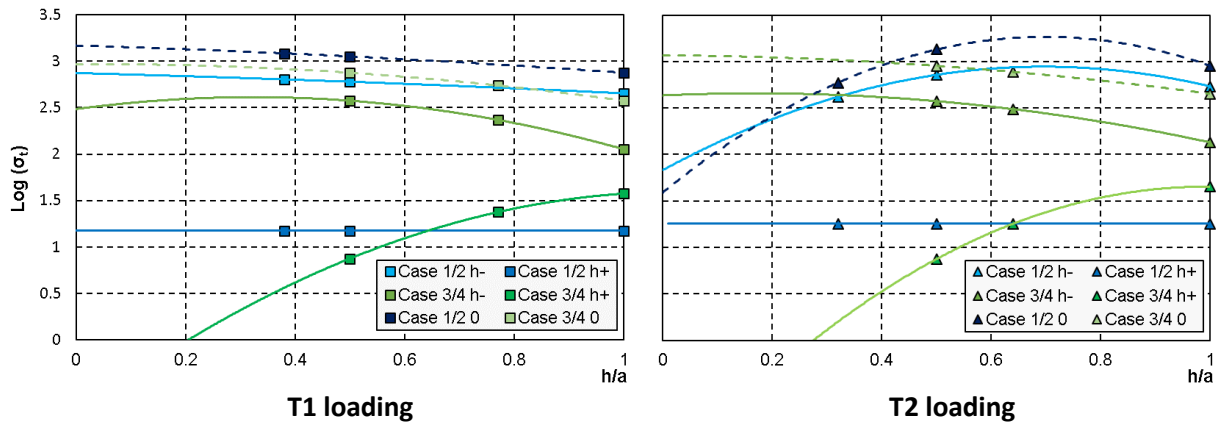


**Figure F5:** Horizontal stresses for analyses combinations (kPa)

These graphs emphasise the influence of three critical criteria, stiffness ratio, layer thickness and loading condition (incorporated in Burmister by the relative load radius,  $a$  and the tyre pressure,  $p$ ). It also points out the exponential change in these parameters as they are increased/ decreased in magnitude.